

***Synthesis, Reactivity, Structural, and
Computational Studies of $[\text{C}_6\text{F}_5\text{Xe}]^+$ and
 $[\text{C}_6\text{F}_5\text{XeF}_2]^+$ Salts.***

Vom Fachbereich Chemie
der Universität Duisburg-Essen

zur Erlangung des akademischen Grades eines
Doktors der Naturwissenschaften

genehmigte Dissertation

von
Karsten Koppe
aus Marl

Referent: Prof. Dr. Dr.(h.c.) Hermann-Josef Frohn
Korreferent: Prof. Dr. Gary John Schrobilgen, F.R.S.C.
Tag der mündlichen Prüfung: 19.10.2005

*Die experimentellen Arbeiten wurden in der Zeit von
Januar 2002 bis September 2004
unter Anleitung von
Herrn Prof. Dr. Dr (h.c.) H.-J. Frohn
im Fach Anorganische Chemie der Universität Duisburg-Essen (Campus Duisburg)
und
Herrn Prof. Dr. Gary J. Schrobilgen, F.R.S.C.
im Department of Chemistry der McMaster Universität in Hamilton, Ontario, Kanada
durchgeführt*

ERKLÄRUNG

Hiermit erkläre ich, dass ich die vorliegende Arbeit selbstständig verfasst habe. Die verwendeten Quellen sowie die verwendeten Hilfsmittel sind vollständig angegeben.

Duisburg Unterschrift

Acknowledgements

I sincerely thank both, Prof. Dr. Dr. (*h.c.*) Hermann-Josef Frohn and Prof. Dr. Gary John Schrobilgen (F.R.S.C.), for the excellent supervision and for the very interesting research projects, they provided me with. Both are thanked also for their enormous help, the financial and scientific support, and for the interesting and fruitful discussions without this Thesis wouldn't have been possible.

I especially thank Dr. H el ene P. A. Mercier (Schrobilgen) for the immeasurable help she gave even in her busiest times and for her support in all fields of life.

I am also very thankful to my friends Hermann Kampermann, Christoph Breitenstein and Michael Mastalerz for the nice time we spent during the whole studies, their interesting and fruitful discussions and their friendship.

I thank all the people who have offered their friendship, support and assistance throughout my studies at the Universit at Duisburg-Essen and the McMaster University, especially the members of both workgroups, namely Michael Gerken, Bernard E. Pointner, John F. Lehmann, Matthew D. Moran, Oliver Brehm, Michael Theissen, Petra Fritzen, Peter Barthen, Alina Bauer, Vural Bilir, Andr e Wenda, Christoph Steinberg, Anwar Abo-Amer, Markus Hirschberg, Dietmar Jansen, Vadim Bardin, and Nikolay Adonin.

I am also thankful to all the students, who have performed their advanced inorganic laboratory course under my guidance, for their contribution of some very useful results.

I also acknowledge the faculty members from both universities for the support in all technical belongings and for keeping the instruments in good shape. In particular, thanks are expressed to Brian G. Sayer (McMaster, NMR facility), Donald W. Hughes (McMaster, NMR facility), James F. Britten (McMaster, X-ray diffraction Lab), Manfred Z ahres (Duisburg, NMR facility) and Beate R omer (Duisburg, NMR facility).

My utmost thanks are expressed to my parents and grandparents for their emotional and financial support, love, trust and encouragement throughout my whole life. The biggest thanks, however, goes to my wife, Daniela, for covering my back in all belongings, for her love, trust and support. It wouldn't have been possible without her understanding for the frequent absence while working in Canada during the whole studies.

... Was nicht passt, wird passend gemacht.

Im Andenken an meine Oma,

Anna Rausch,

die mich durch Ihre Liebe und ihren unglaublichen Stolz
zu immer höheren Zielen ermutigt hat. Ihr Geist und
Ihre stetig ermunternden Worte werden alle Zeit mit mir sein.

LIST OF ABBREVIATIONS AND SYMBOLS

- In alphabetical order -

ϵ	Dielectric constant
δ	Chemical shift
$\Delta v_{1/2}$	Full width at half maximum
Δ	Difference
μ	Absorption coefficient
λ	Wavelength
ν	Stretching mode
δ	In-plane bend
ρ_w	Wagging mode
ρ_r	Rocking mode
ρ_t	Twisting mode
ax	Axial
BB	4.5 mm copper plated steel spheres (air rifle brass balls)
BO	Bond order
c-C₆F₈-1,4	1,2,3,3,4,5,6,6-octafluorocyclohex-1,4-diene
c-C₆F₁₀	Decafluorocyclohexene
CCD	Charge-coupled device
c.d.	Cross diameter
conc.	Concentrated
DCE	1,2-Dichloroethane
DFT	Density Functional Theory
DSC	Differential Scanning Calorimetry
ELF	Electron localization function
eq	Equatorial
eV	Electron volt
FID	Free-induction decay
h	Hours
HF	Hartree Fock Theory
I	Nuclear spin quantum number
i.d.	Inner diameter

IP	Ionization potential
i.p.	In plane
J	Scalar coupling constant in Hz
Kel-F	1-Chloro-1,2,2-trifluoroethylene polymer, $(-\text{CClFCF}_2)_n$
min	Minutes
Monel	Trade name for a copper-nickel alloy (~ 30% Cu, ~ 66% Ni)
MP2	Møller-Plesset, second order
NAO	Natural atomic orbital
NBO	Natural bond orbital
NMR	Nuclear magnetic resonance
n.o.	Not observed
o.d.	Outer diameter
o.o.p	Out of plane
PFB	1,1,1,3,3-pentafluorobutane, $\text{CF}_3\text{CH}_2\text{CF}_2\text{CH}_3$
PFP	1,1,1,3,3-pentafluoropropene, $\text{CF}_3\text{CH}_2\text{CF}_2\text{H}$
PFPE	Fomblin oil, perfluorinated polyether oil
PP	Polypropylene
ppm	Parts per million
RT	Room temperature
SAE	Society of Automotive Engineers
SERF	SE lective ReF okussing (2D NMR selective experiment)
SR	Standard reference
SET	Single electron transfer
Teflon® FEP	Tetrafluoroethylene and hexafluoropropylene block-co-polymer $[-(\text{CF}_2\text{CF}_2)_n-(\text{CF}_2-\text{CF}(\text{CF}_3))_m]_x$
Teflon® PCTFE	1-Chloro-1,2,2-trifluoroethylene polymer, $(-\text{CClFCF}_2)_n$ (Kel-F)
Teflon® PTFE	Poly(tetrafluoroethylene), $(-\text{CF}_2\text{CF}_2)_n$
Teflon® PFA	Poly(perfluoroalkoxytrifluoroethylen), $(-\text{CFR}\text{CF}_2)_n$
TMS	Tetramethylsilane, $\text{Si}(\text{CH}_3)_4$
Nd:YAG	Neodymium: Yttrium-aluminum-garnet

Table of Contents

I	INTRODUCTION	1
I.1	Brief Historical Overview	1
I.2	Xenon-Carbon Chemistry	4
II	OBJECTIVES OF THIS WORK	9
II.1	The $[\text{C}_6\text{F}_5\text{Xe}]^+$ Cation	9
II.2	The $[\text{C}_6\text{F}_5\text{XeF}_2]^+$ Cation	10
III	DISCUSSION	12
III.1	The $[\text{C}_6\text{F}_5\text{Xe}]^+$ Cation: Preparation, Structural and Computational Study, Decomposition and Reactivity	12
III.1.1	Preparation of $[\text{C}_6\text{F}_5\text{Xe}]^+$ Salts	12
III.1.1.1	Preparation of $[\text{C}_6\text{F}_5\text{Xe}][\text{BF}_4]$	12
III.1.1.2	Metatheses Leading to New $[\text{C}_6\text{F}_5\text{Xe}]^+$ Salts with Weakly Coordinating Anions	13
III.1.2	Characterization of $[\text{C}_6\text{F}_5\text{Xe}]^+$ Salts	14
III.1.2.1	Characterization of $[\text{C}_6\text{F}_5\text{Xe}][\text{BY}_4]$ (Y = F, CF_3 , CN, OTeF_5 , and C_6F_5) by Multi-NMR Spectroscopy	14
III.1.2.2	Characterization of $[\text{C}_6\text{F}_5\text{Xe}\cdot\text{NCCH}_3][\text{B}(\text{CF}_3)_4]$, $[\text{C}_6\text{F}_5\text{Xe}][\text{B}(\text{CF}_3)_4]$, $[\text{C}_6\text{F}_5\text{Xe}][\text{B}(\text{CN})_4]$, and $[\text{C}_6\text{F}_5\text{Xe}\cdot\text{NCCH}_3][\text{B}(\text{C}_6\text{F}_5)_4]$ by X-Ray Crystallography	23
III.1.2.3	Characterization by Low-Temperature Raman Spectroscopy	31
III.1.3	Computational Results	45
III.1.4	Behaviour of $[\text{C}_6\text{F}_5\text{Xe}][\text{BY}_4]$ (Y = F, CF_3 , C_6F_5 , OTeF_5 , and CN) in Solution	49
III.1.4.1	Behaviour of $[\text{C}_6\text{F}_5\text{Xe}][\text{BF}_4]$ in CH_3CN	55
III.1.4.2	Behaviour of $[\text{C}_6\text{F}_5\text{Xe}][\text{B}(\text{CN})_4]$ in CH_3CN	57

Contents		X
III.1.4.3	Behaviour of $[\text{C}_6\text{F}_5\text{Xe}][\text{B}(\text{CF}_3)_4]$ in CH_3CN	58
III.1.4.4	Behaviour of $[\text{C}_6\text{F}_5\text{Xe}][\text{B}(\text{OTeF}_5)_4]$ in CH_3CN	60
III.1.4.5	Behaviour of $[\text{C}_6\text{F}_5\text{Xe}][\text{B}(\text{C}_6\text{F}_5)_4]$ in CH_3CN	61
III.1.4.6	Behaviour of $[\text{C}_6\text{F}_5\text{Xe}][\text{BF}_4]$ in aHF	62
III.1.4.7	Behaviour of $[\text{C}_6\text{F}_5\text{Xe}][\text{B}(\text{CF}_3)_4]$ and $[\text{C}_6\text{F}_5\text{Xe}][\text{B}(\text{OTeF}_5)_4]$ in CH_2Cl_2	64
III.1.4.8	Behaviour of $[\text{C}_6\text{F}_5\text{Xe}][\text{BY}_4]$ ($\text{Y} = \text{F}, \text{CF}_3, \text{C}_6\text{F}_5,$ and CN) in the Solid State	66
III.1.5	Reaction of $[\text{C}_6\text{F}_5\text{Xe}][\text{BY}_4]$ ($\text{Y} = \text{F}, \text{CF}_3, \text{CN},$ and C_6F_5) and $[\text{C}_6\text{F}_5\text{Xe}][\text{AsF}_6]$ with $\text{C}_6\text{H}_5\text{F}$	67
III.1.5.1	Reaction of $[\text{C}_6\text{F}_5\text{Xe}][\text{BY}_4]$ ($\text{Y} = \text{C}_6\text{F}_5$ and CF_3) with $\text{C}_6\text{H}_5\text{F}$ in CH_2Cl_2	74
III.1.5.2	Reaction of $[\text{C}_6\text{F}_5\text{Xe}][\text{B}(\text{C}_6\text{F}_5)_4]$ with $\text{C}_6\text{H}_5\text{F}$ in the Presence of $[\text{N}(\text{CH}_3)_4]\text{F}$ and Reaction of $\text{C}_6\text{F}_5\text{XeF}$ with $\text{C}_6\text{H}_5\text{F}$ in CH_2Cl_2	75
III.1.5.3	Modified Preparation of $\text{C}_6\text{F}_5\text{XeF}$	77
III.2	THE $[\text{C}_6\text{F}_5\text{XeF}_2]^+$ SALT: PREPARATION, STRUCTURAL, AND COMPUTATIONAL STUDY, STABILITY AND REACTIVITY	79
III.2.1	Preparation of $[\text{C}_6\text{F}_5\text{XeF}_2]^+$ Salts	79
III.2.1.1	Preparation of $[\text{C}_6\text{F}_5\text{XeF}_2][\text{BF}_4]$	79
III.2.1.2	Metathesis Leading to $[\text{C}_6\text{F}_5\text{XeF}_2][\text{B}(\text{CF}_3)_4]$	80
III.2.2	Characterization of $[\text{C}_6\text{F}_5\text{XeF}_2]^+$ Salts	81
III.2.2.1	Characterization of $[\text{C}_6\text{F}_5\text{XeF}_2][\text{BF}_4]$ by ^{11}B , ^{19}F , and ^{129}Xe Multi-NMR Spectroscopy	81
III.2.2.2	Characterization of $[\text{C}_6\text{F}_5\text{XeF}_2][\text{BF}_4]$ and $[\text{C}_6\text{F}_5\text{XeF}_2 \cdot (\text{NCCH}_3)_{1.5}][\text{BF}_4]$ by X-Ray Crystallography	85
III.2.2.3	Characterization by Low-Temperature Raman Spectroscopy	97
III.2.3	Computational Results	104
III.2.3.1	Geometries of $[\text{C}_6\text{F}_5\text{XeF}_2]^+$, $[\text{C}_6\text{F}_5\text{XeF}_2 \cdot \text{NCCH}_3]^+$, $[\text{C}_6\text{F}_5\text{XeF}_2 \cdot (\text{NCCH}_3)_2]^+$ and $\text{C}_6\text{F}_5\text{IF}_2$	104
III.2.4	Behaviour of $[\text{C}_6\text{F}_5\text{XeF}_2]^+$ Salts in Solution and in Suspension	109
III.2.4.1	Behaviour of $[\text{C}_6\text{F}_5\text{XeF}_2][\text{BF}_4]$ in aHF Solution in the Presence of KF	120
III.2.4.2	Behaviour of $[\text{C}_6\text{F}_5\text{XeF}_2][\text{BF}_4]$ in aHF Solution in the Presence of $\text{K}[\text{C}_6\text{F}_5\text{BF}_3]$	121

Contents		XI
III.2.4.3	Behaviour of $[\text{C}_6\text{F}_5\text{XeF}_2][\text{BF}_4]$ in CH_3CN Solution in the Presence of $\text{K}[\text{C}_6\text{F}_5\text{BF}_3]$	123
III.2.5	Reactivity of the $[\text{C}_6\text{F}_5\text{XeF}_2]^+$ Cation in Solution	125
III.2.5.1	Reaction of $[\text{C}_6\text{F}_5\text{XeF}_2][\text{BF}_4]$ with $\text{C}_6\text{F}_5\text{Hal}$ (Hal = I, Br) in CH_3CN and aHF	125
III.2.5.2	Reaction of $[\text{C}_6\text{F}_5\text{XeF}_2][\text{BF}_4]$ with $\text{Pn}(\text{C}_6\text{F}_5)_3$ (Pn = P, As, and Bi) in CH_3CN and aHF at $-40\text{ }^\circ\text{C}$	127
IV	EXPERIMENTAL SECTION	131
IV.1	Applied Techniques	131
IV.2	Multi-NMR Spectroscopy	134
IV.3	Raman Spectroscopy and Raman Sample Preparation	136
IV.4	X-ray Crystallography	137
IV.4.1	Low-Temperature Crystal Growth	137
IV.4.2	Crystal Mounting, Collection of X-ray Data, Solution and Structure Refinement	139
IV.5	Differential Scanning Calorimetry (DSC)	140
IV.6	Calculations	140
IV.7	Chemicals	141
IV.7.1	Laboratory Inventory	141
IV.7.2	Commercially Available Chemicals	141
IV.8	Solvents and Other Starting Materials	142
IV.8.1	Solvents	142
IV.9	Solid Starting Materials	144
IV.9.1	Tetramethylammonium Fluoride, $[\text{N}(\text{CH}_3)_4]\text{F}$	144
IV.9.2	Xenon Difluoride, XeF_2	145
IV.9.2.1	Reaction of XeF_2 with C_6F_6 in CH_3CN at 0°C and $-40\text{ }^\circ\text{C}$ with and without Addition of aHF	146

Contents		XII
IV.9.3	Xenon Tetrafluoride, XeF ₄	148
IV.9.3.1	The Solubility of XeF ₄ in CH ₂ Cl ₂	149
IV.9.4	Pentafluorophenyl(dihydroxy)borane, C ₆ F ₅ B(OH) ₂	149
IV.9.4.1	Solubility of C ₆ F ₅ B(OH) ₂ in Selected Solvents at RT	150
IV.9.4.2	Solvolysis of C ₆ F ₅ B(OH) ₂ in CH ₃ OH at RT	150
IV.9.5	Potassium Pentafluorophenyltrifluoroborate, K[C ₆ F ₅ BF ₃]	151
IV.9.5.1	Solubility of K[C ₆ F ₅ BF ₃] in Selected Solvents at RT	152
IV.9.5.2	Behaviour of K[C ₆ F ₅ BF ₃] in Boiling CH ₃ CN and H ₂ O/CH ₃ CN	152
IV.9.5.3	Behaviour of K[C ₆ F ₅ BF ₃] in aHF at -40 °C and Comparison with K[BF ₄]	153
IV.9.6	Pentafluorophenyldifluoroborane, C ₆ F ₅ BF ₂	154
IV.9.7	Tris(pentafluorophenyl)borane, B(C ₆ F ₅) ₃	155
IV.9.8	Cesium Tetrakis(pentafluorophenyl)borate, Cs[B(C ₆ F ₅) ₄]	156
IV.9.8.1	Solubility of Cs[B(C ₆ F ₅) ₄] in Selected Solvents at RT	158
IV.9.9	Teflic Acid, HOTeF ₅ (Optimized Preparation Procedure)	158
IV.9.10	Cesium Pentafluorooxotellurate, CsOTeF ₅	160
IV.9.11	Tris(pentafluorooxotellurato)borane, B(OTeF ₅) ₃	161
IV.9.12	Cesium Tetrakis(pentafluorooxotellurato)borate, Cs[B(OTeF ₅) ₄]	163
IV.10	Pentafluorophenylxenon(II) Compounds: Preparation, Characterization, and Physical Properties	164
IV.10.1	Preparation of [C ₆ F ₅ Xe][BY ₄] (Y = F, CF ₃ , CN, C ₆ F ₅ , and OTeF ₅)	164
IV.10.2	Pentafluorophenylxenon(II)tetrafluoroborate, [C ₆ F ₅ Xe][BF ₄]	165
IV.10.2.1	NMR Characterization	165
IV.10.2.2	Raman Spectroscopic Characterization	166
IV.10.2.3	Attempt to Crystallize [C ₆ F ₅ Xe][BF ₄] from CH ₃ CN and CH ₃ CN/CH ₂ Cl ₂	166
IV.10.2.4	Thermo-analytical Measurements of [C ₆ F ₅ Xe][BF ₄] in the Solid State (DSC)	167
IV.10.2.4.1	Proof of the Reversibility of the Melting Point of [C ₆ F ₅ Xe][BF ₄]	167
IV.10.2.5	Solubility of [C ₆ F ₅ Xe][BF ₄] in Selected Solvents at RT	168
IV.10.2.6	Thermal Stability of [C ₆ F ₅ Xe][BF ₄] in CH ₃ CN and aHF at RT	169
IV.10.3	Pentafluorophenylxenon(II)tetrakis(trifluoromethyl)borate, [C ₆ F ₅ Xe][B(CF ₃) ₄]	170
IV.10.3.1	NMR Characterization	170

Contents	XIII
IV.10.3.2 Raman Spectroscopic Characterization	172
IV.10.3.3 Crystal Growth and Structure Refinement	172
IV.10.3.4 Thermo-analytical Measurements of $[\text{C}_6\text{F}_5\text{Xe}][\text{B}(\text{CF}_3)_4]$ in the Solid State (DSC)	173
IV.10.3.5 Solubility of $[\text{C}_6\text{F}_5\text{Xe}][\text{B}(\text{CF}_3)_4]$ in Selected Solvents at RT	173
IV.10.3.6 Solubility of $\text{K}[\text{B}(\text{CF}_3)_4]$ in CH_2Cl_2 at RT	174
IV.10.3.7 Thermal Stability of $[\text{C}_6\text{F}_5\text{Xe}][\text{B}(\text{CF}_3)_4]$	174
IV.10.3.8 Reaction of $[\text{C}_6\text{F}_5\text{Xe}][\text{B}(\text{CF}_3)_4]$ with $[\text{N}(\text{C}_4\text{H}_9)_4][\text{BF}_4]$ in CD_2Cl_2 at RT	176
IV.10.3.9 Reaction of $[\text{C}_6\text{F}_5\text{Xe}][\text{B}(\text{CF}_3)_4]$ with $[\text{N}(\text{C}_4\text{H}_9)_4][\text{BF}_4]$ in CD_3CN at RT	177
IV.10.4 Pentafluorophenylxenon(II)tetrakis(pentafluoro-oxotellurato)borate, $[\text{C}_6\text{F}_5\text{Xe}][\text{B}(\text{OTeF}_5)_4]$	178
IV.10.4.1 NMR Characterization	178
IV.10.4.2 Attempts to Crystallize $[\text{C}_6\text{F}_5\text{Xe}][\text{B}(\text{OTeF}_5)_4]$ from PFB/ CH_3CN at Low Temperatures	179
IV.10.4.3 Thermal Stability of $[\text{C}_6\text{F}_5\text{Xe}][\text{B}(\text{OTeF}_5)_4]$	179
IV.10.5 Pentafluorophenylxenon(II)tetracyanoborate, $[\text{C}_6\text{F}_5\text{Xe}][\text{B}(\text{CN})_4]$	182
IV.10.5.1 NMR Characterization	182
IV.10.5.2 Raman Spectroscopic Characterization	182
IV.10.5.3 Crystal Growth and Structure Refinement	182
IV.10.5.4 Thermo-analytical Measurements of $[\text{C}_6\text{F}_5\text{Xe}][\text{B}(\text{CN})_4]$ in the Solid State (DSC)	183
IV.10.5.5 Solubility of $[\text{C}_6\text{F}_5\text{Xe}][\text{B}(\text{CN})_4]$ at RT	183
IV.10.5.6 Thermal Stability of $[\text{C}_6\text{F}_5\text{Xe}][\text{B}(\text{CN})_4]$	184
IV.10.6 Pentafluorophenylxenon(II)tetrakis(pentafluorophenyl)borate, $[\text{C}_6\text{F}_5\text{Xe}][\text{B}(\text{C}_6\text{F}_5)_4]$	185
IV.10.6.1 NMR Characterization	185
IV.10.6.2 Raman Spectroscopic Characterization	185
IV.10.6.3 Crystal Growth and Structure Refinement	186
IV.10.6.4 Thermo-analytical Measurements of $[\text{C}_6\text{F}_5\text{Xe}][\text{B}(\text{C}_6\text{F}_5)_4]$ in the Solid State (DSC)	186
IV.10.6.5 Solubility of $[\text{C}_6\text{F}_5\text{Xe}][\text{B}(\text{C}_6\text{F}_5)_4]$ in Selected Solvents at RT	187
IV.10.6.6 Thermal Stability of $[\text{C}_6\text{F}_5\text{Xe}][\text{B}(\text{C}_6\text{F}_5)_4]$ in Solution	187
IV.10.6.7 Coordination Ability of CH_3CN to $[\text{C}_6\text{F}_5\text{Xe}][\text{B}(\text{C}_6\text{F}_5)_4]$	189
IV.10.7 Pentafluorophenylxenon(II)hexafluoroarsenate, $[\text{C}_6\text{F}_5\text{Xe}][\text{AsF}_6]$	190

Contents	XIV
IV.10.7.1	Thermo-analytical Measurements of $[\text{C}_6\text{F}_5\text{Xe}][\text{AsF}_6]$ in the Solid State (DSC) 190
IV.11	Reaction of $[\text{C}_6\text{F}_5\text{Xe}][\text{BY}_4]$ ($\text{Y} = \text{F}, \text{CF}_3, \text{CN}$ and C_6F_5) and $[\text{C}_6\text{F}_5\text{Xe}][\text{AsF}_6]$ with $\text{C}_6\text{H}_5\text{F}$ 190
IV.11.1	The Reaction of $[\text{C}_6\text{F}_5\text{Xe}][\text{BY}_4]$ ($\text{Y} = \text{F}, \text{CF}_3,$ and C_6F_5) and $[\text{C}_6\text{F}_5\text{Xe}][\text{AsF}_6]$ with $\text{C}_6\text{H}_5\text{F}$ (1.2-Fold Molar Excess) in CH_3CN at RT 191
IV.11.2	Reaction of $[\text{C}_6\text{F}_5\text{Xe}][\text{B}(\text{CF}_3)_4]$ with $\text{C}_6\text{H}_5\text{F}$ (1.2-Fold Molar Excess) in CH_2Cl_2 at RT 194
IV.11.3	Reaction of $[\text{C}_6\text{F}_5\text{Xe}][\text{BY}_4]$ ($\text{Y} = \text{F}, \text{CF}_3,$ and C_6F_5) and $[\text{C}_6\text{F}_5\text{Xe}][\text{AsF}_6]$ with Dried (P_4O_{10}) $\text{C}_6\text{H}_5\text{F}$ (20-Fold Molar Excess) in CH_3CN at RT 195
IV.11.4	Reaction of $[\text{C}_6\text{F}_5\text{Xe}][\text{BY}_4]$ ($\text{Y} = \text{F}, \text{CN}$) and $[\text{C}_6\text{F}_5\text{Xe}][\text{AsF}_6]$ with Dried (P_4O_{10}) $\text{C}_6\text{H}_5\text{F}$ (20-Fold Molar Excess) in CH_3CN at RT 197
IV.11.5	Reaction of $[\text{C}_6\text{F}_5\text{Xe}][\text{BY}_4]$ ($\text{Y} = \text{F}, \text{C}_6\text{F}_5,$ and CN) with Dried (P_4O_{10}) $\text{C}_6\text{H}_5\text{F}$ (20-Fold Molar Excess) in CH_3CN at RT 200
IV.11.6	Reaction of $[\text{C}_6\text{F}_5\text{Xe}][\text{B}(\text{C}_6\text{F}_5)_4]$ and $[\text{C}_6\text{F}_5\text{Xe}][\text{B}(\text{CF}_3)_4]$ with Neat $\text{C}_6\text{H}_5\text{F}$ at RT 202
IV.11.7	Reaction of $[\text{C}_6\text{F}_5\text{Xe}][\text{B}(\text{C}_6\text{F}_5)_4]$ in the Presence of $[\text{N}(\text{CH}_3)_4]\text{F}$ with $\text{C}_6\text{H}_5\text{F}$ (20-Fold Molar Excess) in CH_2Cl_2 at $-55\text{ }^\circ\text{C}$ 204
IV.11.8	Reaction of $[\text{C}_6\text{F}_5\text{Xe}][\text{BF}_4]$ and $[\text{C}_6\text{F}_5\text{Xe}][\text{AsF}_6]$ with $\text{C}_6\text{H}_5\text{F}$ (20-Fold Molar Excess) in CH_3CN : The Influence of Water (1 and 20 Equivalents) at RT 204
IV.11.9	Preparation of $\text{C}_6\text{F}_5\text{XeF}$ from $[\text{C}_6\text{F}_5\text{Xe}][\text{B}(\text{C}_6\text{F}_5)_4]$ and $[\text{N}(\text{CH}_3)_4]\text{F}$ in CH_2Cl_2 at $-80\text{ }^\circ\text{C}$ 207
IV.11.10	Reaction of $\text{C}_6\text{F}_5\text{XeF}$ with $\text{C}_6\text{H}_5\text{F}$ (20-Fold Molar Excess) in CH_2Cl_2 at $-40\text{ }^\circ\text{C}$ 208
IV.12	Reaction of $[\text{C}_6\text{F}_5\text{Xe}][\text{BY}_4]$ ($\text{Y} = \text{F}, \text{C}_6\text{F}_5$) with CX_4 ($\text{X} = \text{Cl}, \text{Br},$ and I) and $\text{C}_6\text{F}_5\text{Z}$ ($\text{Z} = \text{Br}, \text{I}$) 209
IV.12.1	Attempts to React $[\text{C}_6\text{F}_5\text{Xe}][\text{BF}_4]$ with CX_4 ($\text{X} = \text{Cl}, \text{Br}$) in the Melt ($95 - 100\text{ }^\circ\text{C}$) 209
IV.12.2	Reaction of Molten $[\text{C}_6\text{F}_5\text{Xe}][\text{BF}_4]$ with $\text{C}_6\text{F}_5\text{I}$ at $140\text{ }^\circ\text{C}$ 210
IV.13	Difluoropentafluorophenylxenon(IV) Compounds: Preparation, Characterization, and Physical Properties 211

Contents		XV
IV.13.1	Difluoropentafluorophenylxenon(IV)tetrafluoroborate, [C ₆ F ₅ XeF ₂][BF ₄]	211
IV.13.1.1	Preparation of [C ₆ F ₅ XeF ₂][BF ₄]	211
IV.13.1.2	NMR Characterization	212
IV.13.1.3	Analysis of the p-C ₆ F ₅ Signal of [C ₆ F ₅ XeF ₂][BF ₄] in aHF at –80 °C Using 2D NMR Spectroscopy (SERF)	212
IV.13.1.4	Thermal Stability of [C ₆ F ₅ XeF ₂][BF ₄] in Solution and Suspension	213
IV.13.2	Difluoropentafluorophenylxenon(IV) tetrakis(trifluoromethyl)borate, [C ₆ F ₅ XeF ₂][B(CF ₃) ₄]	220
IV.13.2.1	Metathesis	220
IV.13.2.2	Thermal Stability of [C ₆ F ₅ XeF ₂][B(CF ₃) ₄] in Solution	221
IV.13.3	Reaction of [C ₆ F ₅ XeF ₂][BF ₄] with [N(CH ₃) ₄]F in CH ₂ Cl ₂ at –80 °C and CH ₂ Cl ₂ /CH ₃ CN at –40 °C	222
IV.13.4	Reaction of [C ₆ F ₅ XeF ₂][BF ₄] with KF (3-Fold Molar Excess) in aHF at –30 and –40 °C	223
IV.13.5	Reaction of [C ₆ F ₅ XeF ₂][BF ₄] with K[C ₆ F ₅ BF ₃] in aHF at –40 °C	225
IV.13.6	Reaction of [C ₆ F ₅ XeF ₂][BF ₄] with K[C ₆ F ₅ BF ₃] in CH ₃ CN at –40 °C	227
IV.13.7	Reaction of [C ₆ F ₅ XeF ₂][BF ₄] with C ₆ F ₅ Br in aHF at –20 °C	229
IV.13.8	Reaction of [C ₆ F ₅ XeF ₂][BF ₄] with C ₆ F ₅ Br in CH ₃ CN at –40	230
IV.13.9	Reaction of [C ₆ F ₅ XeF ₂][BF ₄] with C ₆ F ₅ Br and C ₆ F ₅ I in aHF at –45 °C	232
IV.13.10	Analysis of the NMR Signals of C ₆ F ₅ IF ₂ in aHF Using 2D NMR Spectroscopy (SERF)	234
IV.13.11	Reaction of [C ₆ F ₅ XeF ₂][BF ₄] with M(C ₆ F ₅) ₃ (M = P, As) in aHF at –40 °C	235
IV.13.12	Reaction of [C ₆ F ₅ XeF ₂][BF ₄] with Bi(C ₆ F ₅) ₃ in aHF at –40	238
IV.13.13	Reaction of [C ₆ F ₅ XeF ₂][BF ₄] with Bi(C ₆ F ₅) ₃ in CH ₃ CN at –40 °C	239
IV.13.14	Reaction of [C ₆ F ₅ XeF ₂][BF ₄] with M(C ₆ F ₅) ₃ (M = P, As) in CH ₃ CN at –40 °C	241
IV.13.15	Reaction of [C ₆ F ₅ XeF ₂][BF ₄] and C ₆ H ₅ F in CH ₃ CN at –40 °C	244
V	SUMMARY	247
VI	APPENDIX	261
VI.1	Extended Crystallographic Information	266

Contents		XVI
VI.1.1	$[\text{C}_6\text{F}_5\text{XeF}_2][\text{BF}_4]$	267
VI.1.2	$[\text{C}_6\text{F}_5\text{XeF}_2 \cdot (\text{NCCH}_3)_{1.5}][\text{BF}_4]$	270
VI.1.3	$[\text{C}_6\text{F}_5\text{Xe} \cdot \text{NCCH}_3][\text{B}(\text{CF}_3)_4]$	277
VI.1.4	$[\text{C}_6\text{F}_5\text{Xe}][\text{B}(\text{CF}_3)_4]$	280
VI.1.5	$[\text{C}_6\text{F}_5\text{Xe} \cdot \text{NCCH}_3][\text{B}(\text{C}_6\text{F}_5)_4]$	284
VI.1.6	$[\text{C}_6\text{F}_5\text{Xe}][\text{B}(\text{CN})_4]$	289
VI.2	Extended Calculated Natural Atomic Charges	293
VI.3	Raman Spectra of Selected Materials	294

I Introduction

I.1 Brief Historical Overview

No attempt is made here to provide a comprehensive review of noble-gas chemistry as there are a number of excellent reviews available describing the developments in this field.^[1-14]

Early failed attempts to react the noble gases with other elements lead to the assumption of chemical inertness of the noble-gases.^[13] Prior to the discovery of noble gas reactivity, the noble gases were only known to form clathrate compounds with water, hydroquinone, and phenol, e.g., $[\text{C}_6\text{H}_4(\text{OH})_2]\text{Ng}$, where Ng is argon, krypton or xenon. It was on the evening of March 23rd, 1962 that Neil Bartlett discovered noble-gas reactivity. He had assembled a glass and quartz apparatus containing xenon gas and gaseous platinum hexafluoride separated by a glass break seal. After breaking the seal he immediately observed a reaction. The deep red-brown PtF_6 vapour reacted instantaneously with colourless xenon gas yielding a yellow-orange solid, which was initially described as $\text{Xe}[\text{PtF}_6]$.^[15] A recent review by Bartlett *et al.* discusses the nature of the reaction between Xe and PtF_6 in more detail. The initially discovered compound was not the simple product, $\text{Xe}[\text{PtF}_6]$, but a non-stoichiometric compound, $\text{Xe}[(\text{PtF}_6)_n]$, with $1 \leq n \leq 2$, whose stoichiometry depended upon the relative amounts of xenon and platinum hexafluoride that were employed in the reaction.^[16]

Within a few months of this discovery, xenon tetrafluoride^[17] and xenon difluoride^[18] were prepared. Other compounds of xenon, as well as krypton difluoride and radon difluoride followed soon thereafter.^[7]

The positive oxidation states of noble-gases have, until now, been stabilized in compounds with bonds to highly electronegative elements such as fluorine and oxygen and, more rarely, in compounds with bonds to nitrogen, carbon and chlorine. To date only Kr-F, Kr-O, and Kr-N bonds of Kr(II) are known. The chemistry most extensively developed is that of xenon, where the oxidation states of xenon range from $+1/2$ in the Xe_2^+ cation to +8 in XeO_4 . However, only Xe(II) exhibits bonds to F, O, N, and C whereas Xe(IV) forms F, O, and C bonds and Xe(VI) forms F and O bonds.

All binary fluorides of xenon are known except xenon octafluoride, XeF₈. The xenon fluorides, xenon difluoride, XeF₂, xenon tetrafluoride, XeF₄, and xenon hexafluoride, XeF₆, as well as xenon oxide tetrafluoride, XeOF₄, are thermodynamically stable with respect to the elements and are used as starting materials for the preparation of other xenon compounds. Xenon fluorides are colourless, crystalline solids which can be sublimed under vacuum at 24 °C. Xenon hexafluoride is yellow-green as a liquid or gas and colourless as a solid. Xenon difluoride is a symmetrical linear molecule having a Xe-F distance of 197.73(15) pm,^[19] and XeF₄ is a square planar molecule (Xe-F, 195.3(4) pm).^[20] Xenon hexafluoride has a distorted octahedral structure arising from the presence of the nonbonding electron lone pair in the xenon valence shell.^[21] All xenon fluorides can be obtained by reacting xenon gas directly with fluorine under elevated pressures and temperatures. Because of their thermochemical instabilities, no neutral halides other than the binary fluorides have been prepared in macroscopic amounts. Xenon dichloride, xenon chloride fluoride, xenon dibromide and xenon tetrachloride have been obtained in low-temperature matrix^[22, 23] or Mössbauer studies.^[24-26]

All xenon fluorides act as fluoride ion donors with the donor strength decreasing in the sequence XeF₆ > XeF₂ >> XeF₄. Xenon difluoride is a much better fluoride ion donor than xenon tetrafluoride and forms compounds with various fluoride ion acceptors according to eq. 1.^[4, 27]



M = Nb, Ta, Ru, Os, Ir, Pt, As, Sb, Bi, *etc.*

Xenon difluoride also interacts with weak fluoride ion acceptors, such as the metal fluorides of the MF₄ type (M = Cr, Mo, W), MoOF₄ and WOF₄.^[28, 29] Reaction with fluoride acceptors in the presence of an excess of XeF₂ yield the V-shaped cation [(XeF)₂F]⁺.^[4] Single crystal X-ray diffraction studies of those products revealed that the degree of ionicity of the “adducts” is largely dependent on the Lewis acid strength of the parent pentafluoride.^[9, 30, 31]

Xenon difluoride has not been shown to behave as an ion acceptor. However, a ¹⁹F NMR spectroscopic study by Schrobilgen and co-workers^[32] has demonstrated that [N(CH₃)₄]F undergoes ion exchange with XeF₂ under rigorously anhydrous and HF-free

conditions, having likely the intermediate $[\text{XeF}_3]^-$. Attempts to prepare salts of the $[\text{XeF}_3]^-$ anion with fluoride donors, such as CsF and $[\text{N}(\text{CH}_3)_4]\text{F}$ have been unsuccessful.

Xenon difluoride can also function as a ligand, as was shown first in 1991 by Bartlett *et al.*,^[33] who synthesized a compound where XeF_2 was directly bonded to a metal ion, namely $[\text{Ag}(\text{XeF}_2)_2][\text{AsF}_6]$. Recently, Žemva and co-workers synthesized an entire series of compounds of the type $[\text{M}_x(\text{XeF}_2)_n](\text{EF}_6)_x$ by reacting the $\text{M}_x(\text{EF}_6)_x$ salt with different stoichiometric amounts of XeF_2 in aHF at RT, namely $[\text{Ag}(\text{XeF}_2)_3][\text{PF}_6]$,^[34] $[\text{Ln}(\text{XeF}_2)_3][(\text{AsF}_6)_3]$ (Ln = La, Nd, Sm, Eu, Gd; E = As, Bi),^[35] $[\text{Nd}(\text{XeF}_2)_{2.5}][(\text{AsF}_6)_3]$,^[36] $[\text{M}(\text{XeF}_2)_3][(\text{AsF}_6)_2]$ (M = Pb, Sr),^[37] $[\text{Cd}(\text{XeF}_2)_4][(\text{AsF}_6)_2]$,^[38] $[\text{Cd}(\text{XeF}_2)][(\text{BF}_4)_2]$,^[39] $[\text{Ca}(\text{XeF}_2)_n][(\text{AsF}_6)_2]$ (n = 2.5, 4),^[40] $[\text{Mg}(\text{XeF}_2)_n][(\text{AsF}_6)_2]$ (n = 2, 4),^[41] and $[\text{Ba}(\text{XeF}_2)_5][(\text{SbF}_6)_2]$.^[42] The majority of those salts were also characterized by X-ray crystallography.

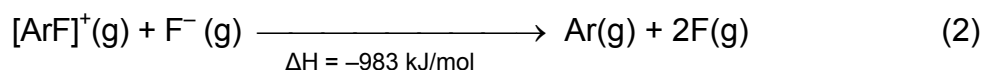
Xenon tetrafluoride only forms stable complexes with the strongest fluoride ion acceptors, such as SbF_5 in $[\text{XeF}_3][\text{SbF}_6]$ ^[43] and $[\text{XeF}_3][\text{Sb}_2\text{F}_{11}]$ ^[44] or BiF_5 in $[\text{XeF}_3][\text{BiF}_6]$.^[45] Xenon tetrafluoride has also been shown to behave as a weak ion acceptor, forming adducts with strong nucleophiles, such as $[\text{N}(\text{CH}_3)_4]\text{F}$ and $[\text{N}(\text{CH}_3)_4]\text{CN}$ to give two of the rare known pentagonal planar anions $[\text{XeF}_5]^-$ ^[46] and $[\text{XeF}_4\text{CN}]^-$.^[47] Additionally an entire series of $\text{M}[\text{XeF}_5]$ (M = Na, K, Cs, Rb, and $\text{N}(\text{CH}_3)_4$) salts have been prepared from XeF_4 and MF (M = Na, K, Cs, and Rb) at 190 °C in the melt and XeF_4 and $[\text{N}(\text{CH}_3)_4]\text{F}$ in CH_3CN solution at RT and has been fully characterized by NMR, Raman, IR, and X-ray crystallography.^[46]

The $[\text{IF}_5]^{2-}$ ^[48] anion has also been synthesized as its $[\text{N}(\text{CH}_3)_4]^+$ salt from $[\text{N}(\text{CH}_3)_4][\text{IF}_4]$ and $[\text{N}(\text{CH}_3)_4]\text{F}$ in CH_3CN solution and is isoelectronic and isostructural with $[\text{XeF}_5]^-$.

Xenon hexafluoride has the strongest donor-acceptor properties of all the binary xenon fluorides. It reacts, for example, with fluoride ion donors to give the $[\text{XeF}_7]^-$ and $[\text{XeF}_8]^{2-}$ anions and with fluoride ion acceptors to form salts of $[\text{XeF}_5]^+$ and $[(\text{XeF}_5)_2\text{F}]^+$ cations.^[4, 49] The propensity of $[\text{XeF}_n]^+$ cations to form strong contacts to their counteranions in the solid state reflects their substantial Lewis acid characters.^[1, 4]

While the heavier noble gases, krypton, xenon and radon, were shown to react with fluorine to yield fluorides on the preparative scale, no such compounds are known for the lighter noble gases – helium and neon. The reason can be explained by comparing the ionization potentials of the noble gases (Rn (10.2 eV), Xe (12.1

eV), Kr (14.0 eV), Ar (15.8 eV), Ne (21.6 eV), and He (24.6 eV).^[50] A successful reaction with radon can be achieved by use of comparatively weak oxidizers. It is not surprising that compounds of neon and helium do not exist because of their very high ionization potentials. Binary argon compounds with the most electronegative element fluorine seem to mark the borderline of existence. Theoretical calculations indicate that argon difluoride will be unstable but the $[\text{ArF}]^+$ cation is known in the gas phase from experiments performed by Berkowitz^[51] in 1970 and it is suggested to be stable in the presence of a suitable oxidatively resistant anion. Any synthesis of an $[\text{ArF}]^+$ salt apparently cannot rely upon synthesis from the difluoride precursor because ArF_2 is expected to be unbound.



The best counteranions to stabilize $[\text{ArF}]^+$ salts with respect to fluoride abstraction and withstanding the high oxidative power of the $[\text{ArF}]^+$ cation appear to be $[\text{ArF}][\text{AuF}_6]$ or $[\text{ArF}][\text{SbF}_6]$.^[51, 52] However, the synthesis has to go through either $[\text{ArF}]^+$ or F^+ precursor which has not been realized. Calculations also suggest that $[\text{HC}\equiv\text{N}-\text{ArF}]^+$ may be stable.^[53] The corresponding $[\text{HeF}]^+$ and $[\text{NeF}]^+$ cations are predicted to be unstable.^[52]

In addition to $[\text{ArF}]^+$ in the gas phase, HArF , is known which has been formed by HF photolysis in a solid argon matrix and characterized by IR spectroscopy.^[54] This investigation has extended the understanding of the formation of lighter noble gas compounds. Calculations suggest that the helium and neon analogues, HHeF and HNeF , are metastable and unstable, respectively.^[55]

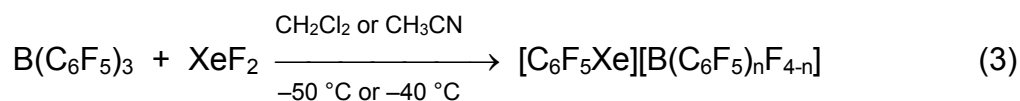
1.2 Xenon-Carbon Chemistry

Because only preparative scale chemistry is emphasized, xenon-carbon chemistry in the gas phase and in matrices is excluded in this introduction, as well as the formation of C-Xe species by radiochemical methods (β^- decay of $\text{C}-^{131}\text{I}$ compounds).

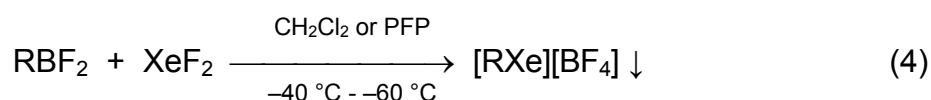
The first published xenon(II)-carbon compound, bis(trifluoromethyl)xenon(II), $\text{Xe}(\text{CF}_3)_2$, was described in 1979 by Lagow *et al.*^[56] The compound was reported to be a waxy white solid having a half-life of ca. 30 minutes at room temperature. The

reaction of XeF₂ in a trifluoromethyl-plasma was not independently confirmed and is therefore still controversial. In 1980, Schmeisser, Walter, and Naumann^[57] reported unsuccessful attempts to synthesize Xe(CF₃)₂ in a glow discharge reaction of CF₃• radicals and xenon gas.

The first communication on the preparation of a confirmed xenon-carbon bonded compound was published independently by the groups of D. Naumann and H.-J. Frohn in 1989. The pentafluorophenylxenon(II) salts, [C₆F₅Xe][Y] [Y] = (C₆F₅)₃BF,^[58] (C₆F₅)₂BF₂,^[59] and C₆F₅BF₃,^[60] were obtained by the direct reaction of XeF₂ with the aryl transfer reagent B(C₆F₅)₃ in CH₃CN or CH₂Cl₂ at low temperature according to equation 3.

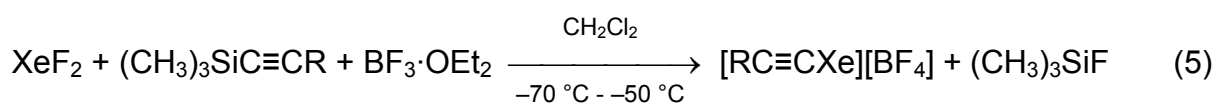


To successfully introduce organic groups into XeF₂, it is necessary to overcome the low electrophilicity of XeF₂ which is a result of the high symmetry of XeF₂. The dipole moment can be induced by interaction with a suitable Lewis acid. In case of xenodeboration, Lewis acidic organoboranes have been used which polarize the XeF₂ molecule. Today numerous arylxenon(II) salts have been isolated in which the aryl group always contains electron withdrawing substituents such as F, Cl, CF₃, and NO₂. Room-temperature stable salts have been prepared by metatheses with perfluoro-anions such as [AsF₆]⁻ and [BF₄]⁻. Pure [C₆F₅Xe][BF₄] can be readily prepared in quantitative yield by homogeneous reaction of stoichiometric amounts of C₆F₅BF₂ and XeF₂ in the weakly coordinating solvent CH₂Cl₂ at temperatures between -40 and -50 °C. Precipitation of pale yellow to white [C₆F₅Xe][BF₄] is the driving force in this reaction. Xenodeboration was later also extended to hydrogen-containing aryl transfer reagents such as BAr₃ (Ar = 2-C₆H₄F,^[61] 3-C₆H₄F,^[62] 4-C₆H₄F,^[61-63] 2,6-C₆H₃F₂,^[61, 64] 2,4,6-C₆H₂F₃,^[65] 4-C₆H₅Cl,^[65, 66] 2,6-C₆H₃Cl₂,^[65, 66] 2,4,6-C₆H₂Cl₃,^[65, 66] 3-C₆H₄CF₃,^[62, 63] and 4-C₆H₄CF₃^[62]). Access to fluorinated alkenyl- and alkynylxenon(II) compounds using xenodeboration was first achieved in 1999 when Frohn and Bardin developed a general preparative method to synthesize organoboranes, RBF₂, where R was CF₂=CX (X = H, F, and CF₃),^[67, 68] CFX=CF (X = F, *trans*-H, *cis*-Cl, *trans*-Cl, *cis*-CF₃, and *cis*-C₂F₅)^[69] and later where R was CF₃C≡C.^[70]



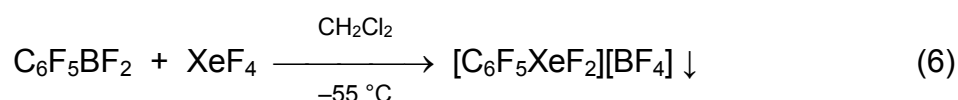
R = CF₂=CX (X = H, F, and CF₃), CFX=CF (X = F, *trans*-H, *cis*-Cl, *trans*-Cl, *cis*-CF₃, and *cis*-C₂F₅) and CF₃C≡C

A different reaction path to alkynylxenon(II) compounds had already been achieved in 1992 by Zhdankin *et al.*^[71] who reacted XeF₂ with (CH₃)₃SiC≡CR (R = C₂H₅, C₃H₇, t-Bu, and Si(CH₃)₃) in the presence of BF₃·OEt₂ and characterized the resulting [RC≡CXe]⁺ cation by NMR spectroscopy but could not isolate the cation as a salt.



R = C₂H₅, C₃H₇, t-Bu, and Si(CH₃)₃

The only example of a C-Xe bond where xenon has a higher oxidation state than +2 was described in 2000 by Frohn *et al.*,^[72] namely, difluoro(pentafluorophenyl)xenon(IV) tetrafluoroborate, [C₆F₅XeF₂][BF₄]. They successfully extended xenodeboration, developed for the organoxenon(II) chemistry, to organoxenon(IV) chemistry. Stoichiometric amounts of XeF₄ and C₆F₅BF₂ were reacted in CH₂Cl₂ at -55 °C and [C₆F₅XeF₂][BF₄] was obtained as yellow solid according to equation 6.

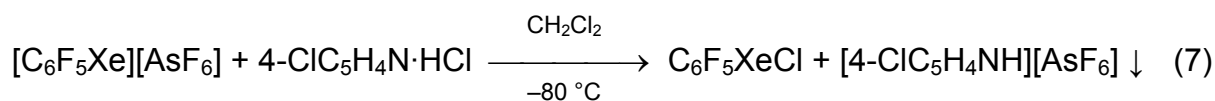


In 2000, this C-Xe(IV) compound was also observed in the laboratory of G. J. Schrobilgen as a by-product in the reaction of XeF₆ with C₆F₅BF₂ in SO₂ClF at -100 °C.^[73]

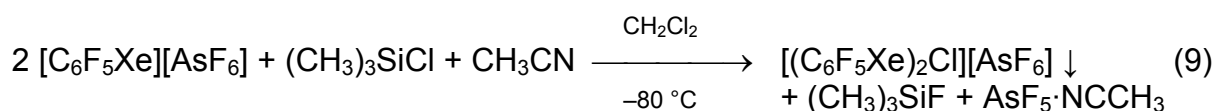
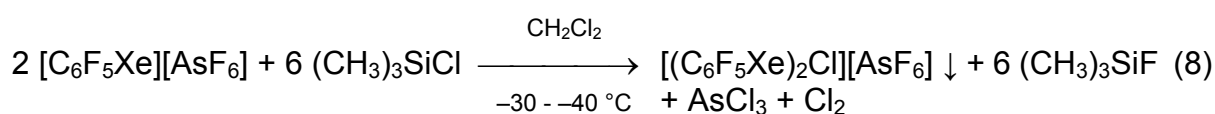
Besides the organoxenon(II) and organoxenon(IV) salts, only a few examples of neutral Xe(II) compounds have been prepared. The first neutral C-Xe(II) bonded compound, C₆F₅XeOC(O)C₆F₅ was obtained by reaction of Cs[OC(O)C₆F₅] and [C₆F₅Xe][AsF₆] in 1993 by Frohn and Klose.^[74]

The formation of C₆F₅XeCl was achieved six years later by Frohn and Schroer^[75] by reaction of the electrophilic [C₆F₅Xe]⁺ cation with chloride sources of moderate

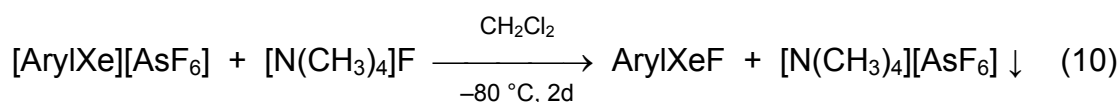
nucleophilicity. Pentafluorophenylxenon(II) chloride was obtained in 85% yield by reaction of $[\text{C}_6\text{F}_5\text{Xe}][\text{AsF}_6]$ with $4\text{-ClC}_5\text{H}_4\text{N}\cdot\text{HCl}$ in CH_2Cl_2 at $-80\text{ }^\circ\text{C}$.



Reaction of $[\text{C}_6\text{F}_5\text{Xe}][\text{AsF}_6]$ with a three-fold excess of $(\text{CH}_3)_3\text{SiCl}$ in CH_2Cl_2 at -40 to $-30\text{ }^\circ\text{C}$ (equation 8) or with stoichiometric amounts of $(\text{CH}_3)_3\text{SiCl}$ in the presence of CH_3CN (equation 9) yielded the V-shaped chlorine-bridged $[(\text{C}_6\text{F}_5\text{Xe})_2\text{Cl}]^+$ cation.^[75]

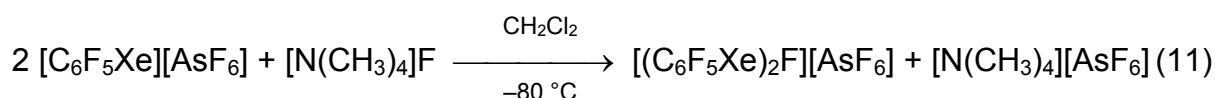


More recently, other neutral arylxenon(II) bonded species have been prepared, namely $\text{C}_6\text{F}_5\text{XeF}$ and $2,4,6\text{-C}_6\text{H}_2\text{F}_3\text{XeF}$. Frohn and Theißen^[76, 77] reacted stoichiometric amounts of $[\text{C}_6\text{F}_5\text{Xe}][\text{AsF}_6]$ and $[\text{N}(\text{CH}_3)_4]\text{F}$ in CH_2Cl_2 at $-80\text{ }^\circ\text{C}$ and obtained $\text{C}_6\text{F}_5\text{XeF}$ after two days according to equation 10.

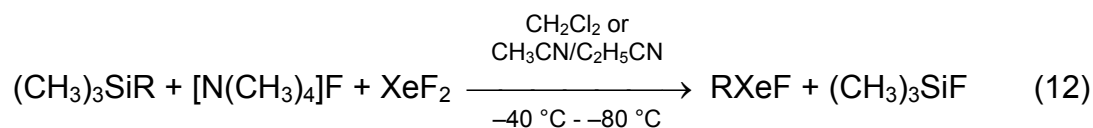


Aryl = C_6F_5 and $2,4,6\text{-C}_6\text{H}_2\text{F}_3$

A similar reaction with a two-fold molar excess of $[\text{C}_6\text{F}_5\text{Xe}][\text{AsF}_6]$ yielded the F^- -bridged $[(\text{C}_6\text{F}_5\text{Xe})_2\text{F}]^+$ cation (equation 11).^[76]



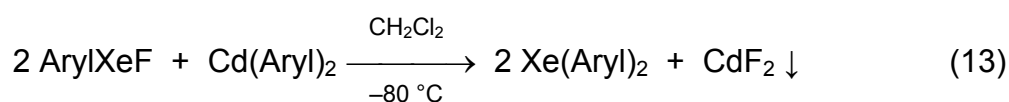
Naumann and Maggiorosa^[78] obtained $\text{C}_6\text{F}_5\text{XeF}$ as an intermediate in the reaction of $(\text{CH}_3)_3\text{SiC}_6\text{F}_5$ and XeF_2 in the presence of $[\text{N}(\text{CH}_3)_4]\text{F}$ in CH_3CN , $\text{C}_2\text{H}_5\text{CN}$, $\text{CH}_3\text{CN}/\text{C}_2\text{H}_5\text{CN}$ or CH_2Cl_2 at -40 or $-60\text{ }^\circ\text{C}$, respectively.



R = C₆F₅, C₆H₅C≡C, CH₃C≡C, and n-C₄H₉C≡C

In 2004, the same strategy had lead to the successful preparation of alkynylxenon(II) fluorides, RC≡CXeF (R = C₆H₅, CH₃, and n-C₄H₉), which were characterized by NMR spectroscopy but could not be isolated because they were thermally unstable.^[79] Thus far, these compounds are the only organoxenon(II) fluorides having an acyclic organo group bonded to the xenon(II) center. It has been shown that organoxenon(II) fluorides, such as C₆F₅XeF are useful starting materials for the introduction of a second organo group, especially an aryl group. In 2000, the reaction of stoichiometric amounts of (CH₃)₃SiC₆F₅ and XeF₂ in the presence of [N(CH₃)₄]F in CH₃CN, C₂H₅CN, CH₃CN/C₂H₅CN or CH₂Cl₂ at -40 or -60 °C, respectively,^[78] or of stoichiometric amounts of C₆F₅XeF and Cd(C₆F₅)₂ in CH₂Cl₂ at -80 °C^[76] yielded the first diorganoxenon(II) compound, Xe(C₆F₅)₂. This compound was characterized by ¹⁹F, ¹³C, and ¹²⁹Xe NMR spectroscopy and two years later by powder X-ray diffraction.^[76, 80, 81]

More recently other symmetric and asymmetric diorganoxenon(II) compounds followed, namely 2,4,6-C₆H₂F₃XeC₆F₅, Xe(2,4,6-C₆H₂F₃)₂, using Cd(Aryl)₂ as the arylation agent.^[76]



Aryl = C₆F₅ and 2,4,6-C₆H₂F₃

Despite the higher polarity of the Xe-F bond in ArylXeF compared to XeF₂, (CH₃)₃SiC₆F₅ was shown not to be a suitable C₆F₅ transfer reagent when used without [N(CH₃)₄]F.^[77] On the contrary, the analogous reaction of C₆F₅XeF and (CH₃)₃SiCN in CH₂Cl₂ at -80 °C yielded C₆F₅XeCN spontaneously.^[76] Attempts to prepare C₆F₅XeCF₃ and C₆F₅XeCF=CF₂ by reaction of C₆F₅XeF with either (CH₃)₃SiCF₃ and Cd(CF₃)₂ or (CH₃)₃SiCF=CF₂, respectively, failed. In the first case, only the coupling product C₆F₅CF₃ was obtained, whereas the second case yielded CF₂=CFH, C₆F₅H, (C₆F₅)₂, and (CH₃)₃SiF.^[82]

II Objectives of This work

To date, the field of organoxenon-chemistry includes the preparation of ArXe(II), alkenylxenon(II) and alkynylxenon(II) compounds, but only one example of an organoxenon(IV) species, namely difluoro(pentafluorophenyl)xenon(IV) tetrafluoroborate, $[\text{C}_6\text{F}_5\text{XeF}_2][\text{BF}_4]$.

II.1 The $[\text{C}_6\text{F}_5\text{Xe}]^+$ Cation

The $[\text{C}_6\text{F}_5\text{Xe}]^+$ cation has been a subject of interest since its discovery in 1989.^[58-60] In the following years, numerous $[\text{C}_6\text{F}_5\text{Xe}]^+$ salts have been isolated, most of which had binary perfluoro-anions, $[\text{EF}_n]^-$ (E = H, B, P, Si, As, and Sb; n = 2, 4, 5, and 6), $[\text{B}(\text{C}_6\text{F}_5)_n\text{F}_{4-n}]^-$ (n = 1 – 4), and $[\text{C}(\text{SO}_2\text{CF}_3)_3]^-$ as their counteranions. All these salts are very soluble in coordinating solvents such as CH_3CN , $\text{C}_2\text{H}_5\text{CN}$ or aHF, but only two candidates, $[\text{C}_6\text{F}_5\text{Xe}][\text{B}(\text{C}_6\text{F}_5)_3\text{F}]$ and $[\text{C}_6\text{F}_5\text{Xe}][\text{B}(\text{C}_6\text{F}_5)_4]$, are soluble in the more weakly coordinating solvent CH_2Cl_2 . However, CH_2Cl_2 solutions of both $[\text{C}_6\text{F}_5\text{Xe}]^+$ salts are unstable at ambient temperature and decompose very rapidly.

The $[\text{C}_6\text{F}_5\text{Xe}]^+$ salts which are soluble in CH_2Cl_2 are of great interest because they provide examples of the weakly coordinated and electrophilic $[\text{C}_6\text{F}_5\text{Xe}]^+$ cation, allowing its chemistry to be examined. One goal of the present work was to synthesize new $[\text{C}_6\text{F}_5\text{Xe}]^+$ salts with weakly coordinating borate anions that are comparably or even more stable than $[\text{C}_6\text{F}_5\text{Xe}][\text{B}(\text{C}_6\text{F}_5)_4]$. Such salts should provide interesting structural and spectroscopic information and would open up new synthetic possibilities.

Accordingly, such $[\text{C}_6\text{F}_5\text{Xe}]^+$ salts have to be fully characterized by multi-NMR and Raman spectroscopy and X-ray crystallography. The spectroscopic and physical measurements should be accompanied by computational studies to aid the assignments of the vibrational modes obtained in the Raman spectra and to facilitate the interpretation of the structural results. The paramount target was the comparison of the geometry, the vibrational modes of weakly coordinated $[\text{C}_6\text{F}_5\text{Xe}]^+$ and of the $[\text{C}_6\text{F}_5\text{Xe}\cdot\text{NCCH}_3]^+$ adduct and their reactivities.

The absence of completely assigned vibrational spectra of the $[\text{C}_6\text{F}_5\text{Xe}]^+$ cation and the $[\text{C}_6\text{F}_5\text{Xe}\cdot\text{NCCH}_3]^+$ adduct motivated us to determine and assign the full vibrational spectra of the $[\text{C}_6\text{F}_5\text{Xe}]^+$ salts.

The decomposition of the $[\text{C}_6\text{F}_5\text{Xe}]^+$ salts as pure solids and in solution had to be examined. The analysis of decomposition products was used to get insight into their decomposition pathways.

It had been shown by Frohn *et al.*^[83] that $[\text{C}_6\text{F}_5\text{Xe}][\text{AsF}_6]$ reacts with aromatic compounds, such as $\text{C}_6\text{H}_5\text{R}$ ($\text{R} = \text{CH}_3, \text{F}, \text{CF}_3, \text{NO}_2, \text{and CN}$) with the formation of isomeric mixtures of polyfluorobiphenyls, $x\text{-RC}_6\text{H}_4\text{C}_6\text{F}_5$ ($x = 2, 3, 4, \text{R} = \text{CH}_3, \text{F}, \text{CN}, \text{CF}_3, \text{NO}_2$) in CH_3CN at ambient temperature. The influence of the anion, the solvent as well as of the substrates was unknown. Therefore, experiments with $[\text{C}_6\text{F}_5\text{Xe}]^+$ salts having counteranions of different nucleophilicity and defined substrates were carried out to determine their influences on the product distributions and the reaction pathways.

II.2 *The $[\text{C}_6\text{F}_5\text{XeF}_2]^+$ Cation*

The only organoxenon(IV) compound presently known, $[\text{C}_6\text{F}_5\text{XeF}_2][\text{BF}_4]$, was synthesized in 2000 by Frohn *et al.*^[72] and had only been characterized by low-temperature NMR spectroscopy in CH_3CN at -40°C . Descriptions of the parameters that influenced the preparation and purity of $[\text{C}_6\text{F}_5\text{XeF}_2][\text{BF}_4]$ were very limited and motivated us to more fully characterize the $[\text{C}_6\text{F}_5\text{XeF}_2]^+$ cation and to optimize the syntheses of $[\text{C}_6\text{F}_5\text{XeF}_2]^+$ salts. This included the full characterization of the cations by multi-NMR and Raman spectroscopy and by X-ray crystallography accompanied by computational studies. Vibrational and structural investigations in the solid state had to be undertaken to complete the characterization of $[\text{C}_6\text{F}_5\text{XeF}_2][\text{BF}_4]$ and to help understand the bonding and interionic contacts in the solid state. The computational study had to be performed to assign the Raman frequencies and to obtain the optimized gas-phase geometry of the $[\text{C}_6\text{F}_5\text{XeF}_2]^+$ cation as well as possible CH_3CN -adducts, $[\text{C}_6\text{F}_5\text{XeF}_2\cdot\text{NCCH}_3]^+$ and $[\text{C}_6\text{F}_5\text{XeF}_2\cdot(\text{NCCH}_3)_n]^+$.

Another goal was to synthesize new $[\text{C}_6\text{F}_5\text{XeF}_2]^+$ salts having more weakly coordinating anions. It is assumed that a more weakly coordinating anion would increase the solubility in weakly coordinating solvents and, consequently, open new

synthetic possibilities. It would provide useful information about the “uncoordinated” $[\text{C}_6\text{F}_5\text{XeF}_2]^+$ cation in solution and its reactivity.

Samples of high-purity $[\text{C}_6\text{F}_5\text{XeF}_2][\text{BF}_4]$ should be investigated as a pure solid as well as in different solvents to determine its stability. The analyses of the decomposition products should then be used to establish possible decomposition pathways. The mixtures of decomposition products obtained in the course of the preparation of $[\text{C}_6\text{F}_5\text{XeF}_2][\text{BF}_4]$ shows the necessity of a thorough examination of the parameters which influence the extent of decomposition and the decomposition pathway.

Previous investigations have shown that $[\text{C}_6\text{F}_5\text{XeF}_2][\text{BF}_4]$ is able to fluorinate I_2 to IF_5 , $\text{C}_6\text{F}_5\text{I}$ to $\text{C}_6\text{F}_5\text{IF}_2$ and $\text{P}(\text{C}_6\text{F}_5)_3$ to $\text{P}(\text{C}_6\text{F}_5)_3\text{F}_2$ in homogeneous reactions in CH_3CN at $-40\text{ }^\circ\text{C}$.^[72] These first experiments have provided a brief introduction to the reactivity of the $[\text{C}_6\text{F}_5\text{XeF}_2]^+$ cation under specific conditions (coordinating solvent) and with easy-to-fluorinate compounds. To incorporate the $[\text{C}_6\text{F}_5\text{XeF}_2]^+$ cation into the family of oxidatively fluorinating agents and to evaluate its oxidation strength, a systematic study was performed on tris(pentafluorophenyl)pnictogen(III) compounds ($\text{Pn} = \text{P}, \text{As}, \text{Bi}$) and halogenopentafluorobenzenes ($\text{Hal} = \text{Br}, \text{I}$) in basic (CH_3CN) and super acidic media (aHF)

III Discussion

III.1 The [C₆F₅Xe]⁺ Cation: Preparation, Structural and Computational Study, Decomposition and Reactivity

III.1.1 Preparation of [C₆F₅Xe]⁺ Salts

III.1.1.1 Preparation of [C₆F₅Xe][BF₄]

The synthesis of the [C₆F₅Xe][BF₄] salt was developed and optimized by Frohn and co-workers in 1999 using the pentafluorophenylation reagent, C₆F₅BF₂. The main advantage of C₆F₅BF₂ when compared with the original reagent, B(C₆F₅)₃, is the ability to transfer only one C₆F₅ group to XeF₂ with the formation of the tetrafluoroborate anion which contains no C-nucleophile.



Reactions with B(C₆F₅)₃ yielded the first [C₆F₅Xe][Y] salts, [Y] = C₆F₅BF₃,^[60] (C₆F₅)₂BF₂,^[59] (C₆F₅)₃BF.^[58] All of these salts were soluble in CH₃CN and (C₆F₅)₃BF as well as in CH₂Cl₂ but decomposed rapidly at ambient temperature. Reactions of stoichiometric amounts of XeF₂ with C₆F₅BF₂ in CH₂Cl₂ at -50 °C yielded, quantitatively and in high purity, [C₆F₅Xe][BF₄]. This salt is stable at ambient temperature and can be stored in the inert atmosphere of a drybox for indefinite period of time.

The first synthesis of C₆F₅BF₂ by reaction of (CH₃)₃SnC₆F₅ with BF₃ (eq. 15) or C₆F₅BCl₂ with SbF₃ (eq. 16) was reported by Chambers and Chivers.^[84-86]



In 2000, Frohn and co-workers^[87] reacted dihalogenopentafluorophenylboranes with aHF in CH₂Cl₂ yielding C₆F₅BF₂ in a two-phase reaction where Hal was chlorine and bromine.



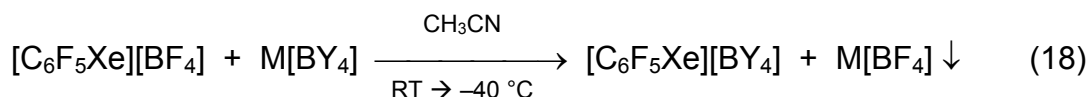
The above synthetic approach is, however, problematic, because it requires hydrolytically sensitive, toxic and ecologically critical reactants. A further problem was the shelf life of the borane which has to be prepared immediately before use.

Frohn and co-workers^[87] developed a new synthetic route to C₆F₅BF₂ in which the borane was isolated from the reaction suspension starting from the corresponding K[C₆F₅BF₃] salt and BF₃ in CH₂Cl₂ at -50 °C. The use of K[C₆F₅BF₃] has important advantages. It can be prepared in high quality on a 30 g scale and can be stored at ambient temperature without decomposition. This heterogeneous solid-gas reaction was further optimized. By varying the reaction temperature, time and rate of BF₃ addition, the BF₃ degassing step, and the washing process of the co-product, K[BF₄], it was possible to obtain quantitative conversion to C₆F₅BF₂ without the formation of C₆F₅H.^[88] The optimized synthesis of C₆F₅BF₂ was of importance because it is a frequently used arylation reagent for compounds of the F-E-F type (E = electrophilic center).

Contrary to previous reports by Chambers and Chivers^[84] who reported a rearrangement of 40 mol-% C₆F₅BF₂ to (C₆F₅)₂BF and BF₃ within one month at RT, no conversion of C₆F₅BF₂ was observed in CH₂Cl₂ at RT over a period of two months.

III.1.1.2 *Metatheses Leading to New [C₆F₅Xe]⁺ Salts with Weakly Coordinating Anions*

The syntheses of the hitherto unknown salts, [C₆F₅Xe][B(CF₃)₄], [C₆F₅Xe][B(CN)₄], [C₆F₅Xe][B(OTeF₅)₄], and [C₆F₅Xe][B(C₆F₅)₄], were achieved in quantitative yields and in high purities by metatheses of [C₆F₅Xe][BF₄] with the corresponding M[BY₄] salts (Y = CF₃, CN, OTeF₅, and C₆F₅; M = K and Cs) in CH₃CN at -40 °C.



Y = CF₃, CN, OTeF₅, and C₆F₅; M = K and Cs

The driving forces for the metatheses were the low solubilities of M[BF₄] (5 μmol/mL; M = K and Cs) in CH₃CN at RT, whereas the four salts, [C₆F₅Xe][BY₄] (Y = CF₃, CN, OTeF₅, and C₆F₅), and [C₆F₅Xe][BF₄] are soluble in CH₃CN. Even smallest amounts of M[BF₄] can be avoided when performing the metatheses at –40 °C and in high concentrations. Both, K[BF₄] and Cs[BF₄], are practically insoluble in CH₃CN at –40 °C. In a typical reaction M[BY₄] (0.3 – 0.5 mmol) was dissolved in CH₃CN (400 μL) and transferred to stoichiometric amounts of solid [C₆F₅Xe][BF₄] at RT. The separated solid reaction product was subsequently washed with CH₃CN (100 μL). The combined solutions were centrifuged (–40 °C) and the mother liquor was separated. The new salts were isolated as pale yellow to white solids by simply removing CH₃CN under dynamic vacuum at RT. The salts were thermally stable as solids at ambient temperatures for extended periods of time in the inert atmosphere of a drybox.

III.1.2 Characterization of [C₆F₅Xe]⁺ Salts

III.1.2.1 Characterization of [C₆F₅Xe][BY₄] (Y = F, CF₃, CN, OTeF₅, and C₆F₅) by Multi-NMR Spectroscopy

The [C₆F₅Xe]⁺ cation has been a subject of considerable interest in Prof. Frohn's group since its discovery in 1989. It was previously characterized in CH₃CN, C₂H₅CN, and aHF by low-field (1.4093 T or 1.8790 T) ¹⁹F, ¹³C, and ¹²⁹Xe NMR spectroscopy with the anions, [HF₂][–],^[89] [C(SO₂CF₃)₃][–],^[90] [SiF₅][–],^[91, 92] [PF₆][–],^[90] [AsF₆][–],^[60, 93] and [B(C₆F₅)_nF_{4–n}][–] (n = 0 – 4).^[58, 60, 90, 93, 94]

Progress in NMR spectroscopy and the availability of new [C₆F₅Xe][BY₄] (Y = F, CN, OTeF₅, C₆F₅, and CF₃) salts motivated us to characterize these salts by ¹⁹F, ¹¹B, and ¹²⁹Xe NMR spectroscopy in CH₃CN at 24 °C and to fully interpret the NMR spectra. The different salts allow one to measure the following NMR-active nuclei, ¹⁰B

($I = 3$, 19.58%), ^{11}B ($I = 3/2$, 80.42%), ^{13}C ($I = 1/2$, 1.11%), ^{14}N ($I = 1$, 99.64%), ^{15}N ($I = 1/2$, 0.37%), ^{19}F ($I = 1/2$, 100%), ^{123}Te ($I = 1/2$, 0.87%), ^{125}Te ($I = 1/2$, 6.99%), ^{129}Xe ($I = 1/2$, 26.44%) and ^{131}Xe ($I = 3/2$, 21.18%).

The ^{19}F NMR spectrum (figures 1 and 2) of the $[\text{C}_6\text{F}_5\text{Xe}]^+$ cation shows the three resonances characteristic of the C_6F_5 group which are slightly shifted depending on their counteranions. A summary of the chemical shifts of $[\text{C}_6\text{F}_5\text{Xe}]^+$ salts is provided in Table 1.

Table 1 ^{19}F NMR Data for Selected $[\text{C}_6\text{F}_5\text{Xe}]^+$ Salts in CH_3CN Solution

Compound	^{19}F NMR spectroscopic data								Anion [ppm]	Temp
	<i>o</i> - C_6F_5 [ppm]	$^3J(^{19}\text{F}-^{129}\text{Xe})$ [Hz]	<i>p</i> - C_6F_5 [ppm]	$^3J(^{19}\text{F}-^{19}\text{F})$ [Hz]	$^4J(^{19}\text{F}-^{19}\text{F})$ [Hz]	$^5J(^{19}\text{F}-^{129}\text{Xe})$ [Hz]	<i>m</i> - C_6F_5 [ppm]	$^4J(^{19}\text{F}-^{129}\text{Xe})$ [Hz]		
$[\text{C}_6\text{F}_5\text{Xe}][\text{B}(\text{CN})_4]^{[95]}$	-124.7	68	-141.0	20	6	4	-153.9	9	---	24 °C
$[\text{C}_6\text{F}_5\text{Xe}][\text{C}(\text{SO}_2\text{CF}_3)_3]^{[90]}$	-124.7	70	-141.0	20	n.o.	n.o.	-154.1	n.o.	-76.0	35 °C
$[\text{C}_6\text{F}_5\text{Xe}][\text{SbF}_6]^{[91, 92]}$	-124.7	68	-141.1	20	5	n.o.	-154.0	n.o.	-122.3	?
$[\text{C}_6\text{F}_5\text{Xe}][\text{B}(\text{CF}_3)_4]^{[95]}$	-125.0	68	-141.2	20	6	2	-154.3	9	-62.6	24 °C
$[\text{C}_6\text{F}_5\text{Xe}][\text{AsF}_6]^{[90, 96]}$	-124.8	68	-141.3	20	5	n.o.	-154.2	n.o.	-64.2	24 °C
$[\text{C}_6\text{F}_5\text{Xe}][\text{PF}_6]^{[90]}$	-124.8	67	-141.3	20	6	n.o.	-154.2	n.o.	-71.3	24 °C
$[\text{C}_6\text{F}_5\text{Xe}][\text{B}(\text{C}_6\text{F}_5)_4]^{[95]}$	-125.2	69	-141.5	20	6	4	-154.5	9	-132.4, -162.8, -167.8	24 °C
$[\text{C}_6\text{F}_5\text{Xe}][(\text{C}_6\text{F}_5)_3\text{BF}]^{[94]}$	-125.3	n.o.	-141.5	20	5	4	-154.2	16*	-135.2, -160.8, -165.7, -176.5	-30 °C
$[\text{C}_6\text{F}_5\text{Xe}][\text{C}_6\text{F}_5\text{BF}_3]^{[60, 94]}$	-125.1	69	-141.6	20	5	4	-154.3	16*	-132.3, -135.3, -160.5, -164.9	-30 °C
$[\text{C}_6\text{F}_5\text{Xe}][\text{BF}_4]^{[90]}$	-125.1	68	-141.7	20	6	n.o.	-154.5	n.o.	-148.5	-30 °C

Table 1 (continued...)

$[\text{C}_6\text{F}_5\text{Xe}][\text{AsF}_6]^{[93]}$	-125.4	69	-141.7	20	5	n.o.	-154.8	n.o.	-64.4	-40 °C
$[\text{C}_6\text{F}_5\text{Xe}][\text{BF}_4]^{[90]}$	-125.0	68	-141.8	20	6	n.o.	-154.6	n.o.	-148.8	24 °C
$[\text{C}_6\text{F}_5\text{Xe}][\text{B}(\text{OTeF}_5)_4]^{[95]}$	-125.5	68	-141.8	20	6	n.o.	-154.7	n.o.	-38.8, -45.4	24 °C
$[\text{C}_6\text{F}_5\text{Xe}][(\text{C}_6\text{F}_5)_2\text{BF}_2]^{[94]}$	-125.2	69	-142.0	20	5	4	-154.7	16*	-136.5, -144.6, -160.5, -165.4	-30 °C
$[\text{C}_6\text{F}_5\text{Xe}][\text{B}(\text{C}_6\text{F}_5)_4]^{[96]}$	-125.6	68	-142.0	20	n.o.	n.o.	-154.7	n.o.	-132.8, -162.1, -166.7	-40 °C
$[\text{C}_6\text{F}_5\text{Xe}][\text{BF}_4]^{[95]}$	-125.4	66	-142.8	20	5	n.o.	-155.5	8	-149.0	24 °C
$[\text{C}_6\text{F}_5\text{Xe}][\text{SiF}_5]^{[91, 92]}$	-126.8	70	-143.0	?	?	n.o.	-154.9	n.o.	?	?
$[\text{C}_6\text{F}_5\text{Xe}][\text{HF}_2]^{[89, 96]}$	-127.1	73	-144.6	20	5	n.o.	-156.1	n.o.	-142.4	-40 °C

n.o. not observed

The ^{19}F spectra of the $[\text{C}_6\text{F}_5\text{Xe}]^+$ salts are well-resolved at 7.0463 T exhibiting multiplet structures for the *o*- and *m*- C_6F_5 fluorine resonances and a triplet of triplets for the *p*- C_6F_5 fluorine resonance. All C_6F_5 resonances are accompanied by ^{129}Xe satellites ($I = \frac{1}{2}$, 26.44%) arising from 3-bond, $^3J(^{19}\text{F}-^{129}\text{Xe})$, 4-bond, $^4J(^{19}\text{F}-^{129}\text{Xe})$, and 5-bond, $^5J(^{19}\text{F}-^{129}\text{Xe})$, spin-spin couplings between ^{129}Xe and the *o*-, *m*-, and *p*- C_6F_5 ^{19}F nuclei, respectively.

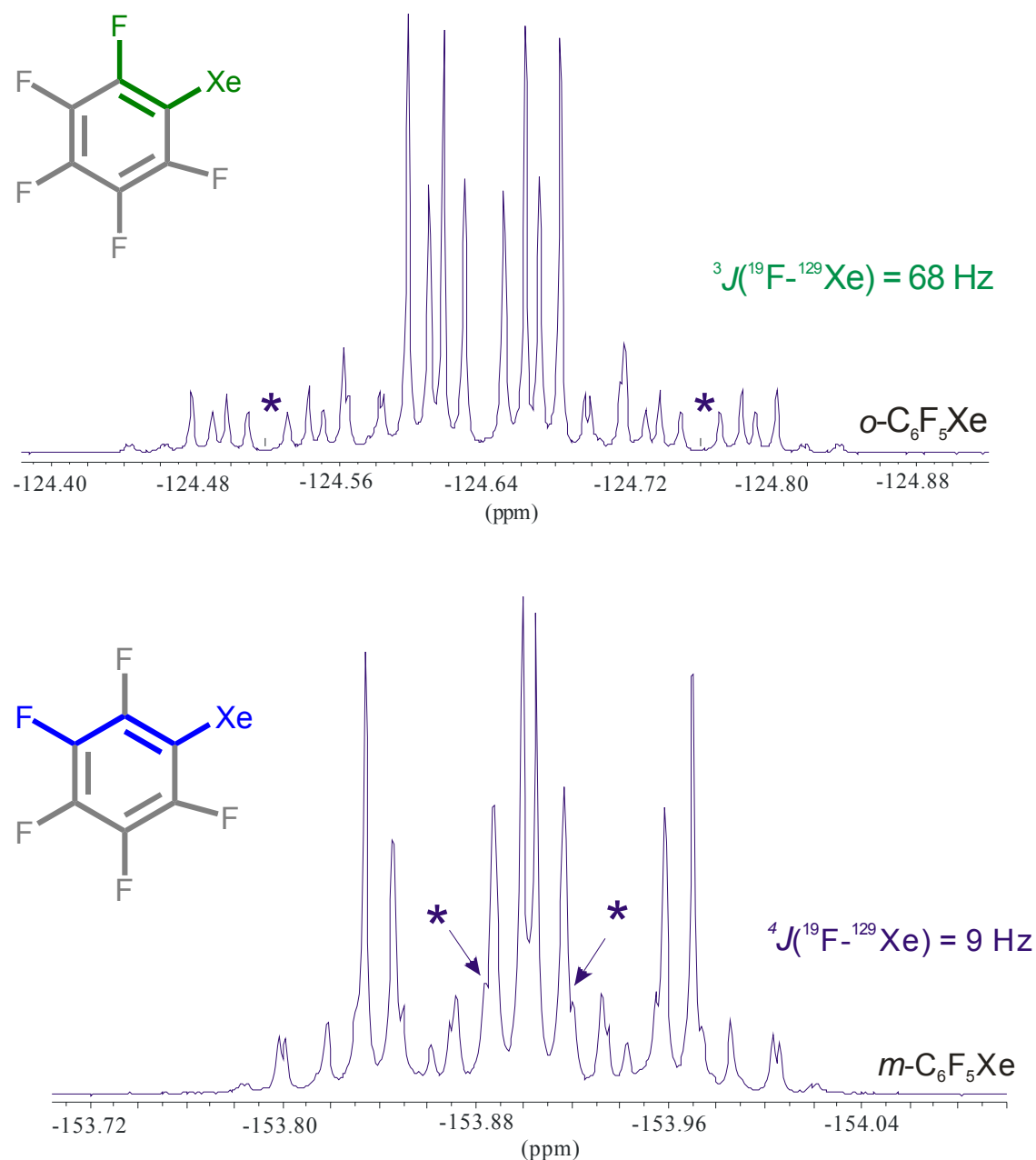


Figure 1 Typical *o*- and *m*- C_6F_5 fluorine resonances of the $[\text{C}_6\text{F}_5\text{Xe}]^+$ cation (in $[\text{C}_6\text{F}_5\text{Xe}][\text{B}(\text{CN})_4]$ salt) in CH_3CN at 24 °C. Asterisks denote ^{129}Xe satellites.

The $p\text{-C}_6\text{F}_5$ fluorine resonance exhibits a triplet of triplets attributed to a 3-bond and 4-bond $^{19}\text{F}\text{-}^{19}\text{F}$ spin coupling having a coupling constant in CH_3CN solution of 20 Hz and 5 Hz, respectively. The ^{129}Xe satellites arising from the 5-bond spin-spin coupling, $^5J(^{19}\text{F}\text{-}^{129}\text{Xe})$, of 4 Hz were also observed.

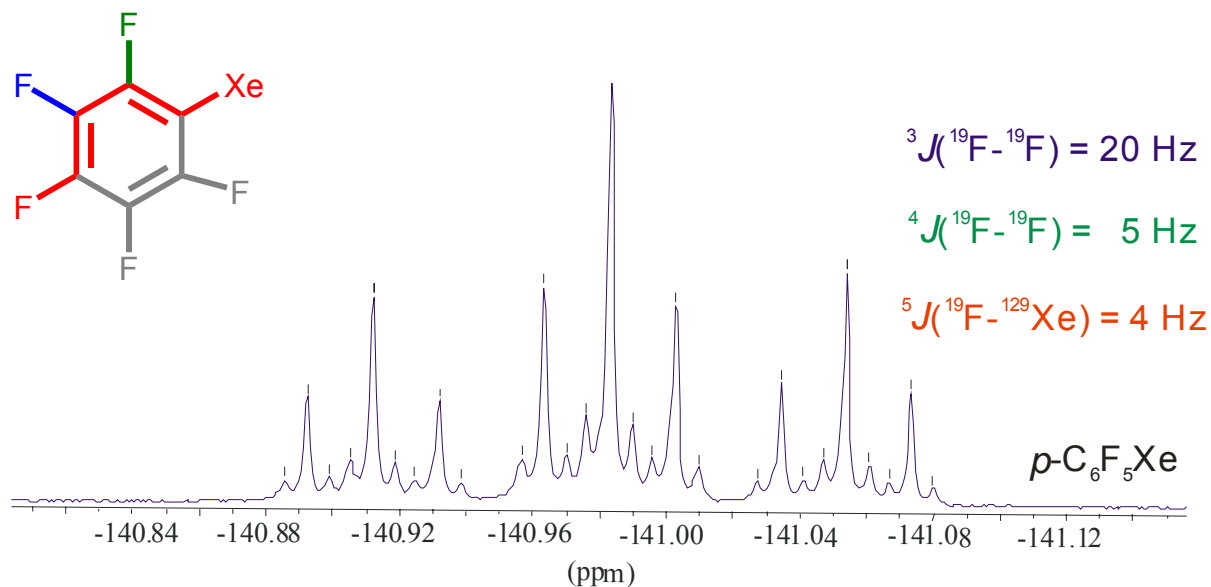


Figure 2 A typical $p\text{-C}_6\text{F}_5$ fluorine resonance of the $[\text{C}_6\text{F}_5\text{Xe}]^+$ cation (in $[\text{C}_6\text{F}_5\text{Xe}][\text{B}(\text{CN})_4]$ salt) in CH_3CN solvent at 24 °C

All spin coupling constants have been previously published and all but the $^4J(^{19}\text{F}\text{-}^{129}\text{Xe})$ coupling are identical within experimental errors to those obtained in the present study. Prior to this study, the 4-bond spin-spin coupling constant has been erroneously assigned in a low-field (1.8790 T) NMR study from the ^{19}F NMR spectrum of the $m\text{-C}_6\text{F}_5$ fluorine resonance. The $^4J(^{19}\text{F}\text{-}^{129}\text{Xe})$ coupling was reported to be 16 – 17 Hz^[58-60, 62] and has now been corrected to 9 Hz.

The lack of well-resolved ^{129}Xe NMR spectra at ≥ 7.0463 T only allowed the $^3J(^{19}\text{F}\text{-}^{129}\text{Xe})$ spin-spin coupling to be measured. The 4J and 5J couplings were only accessible from the ^{19}F NMR spectra. In this study it was possible to obtain fully resolved ^{129}Xe NMR spectra at 7.0463 T of the $[\text{C}_6\text{F}_5\text{Xe}]^+$ cation showing all of the expected $^{19}\text{F}\text{-}^{129}\text{Xe}$ spin-spin couplings in the form of a triplet of triplets of doublets which are attributed to the 3-bond, 4-bond, and 5-bond spin coupling between ^{129}Xe nucleus and the o -, p -, and $m\text{-C}_6\text{F}_5$ ^{19}F nuclei, respectively. The $^4J(^{129}\text{Xe}\text{-}^{19}\text{F})$ coupling constant is directly measurable in the ^{129}Xe NMR spectrum at 9 Hz but can

barely be revealed in the ^{19}F NMR spectrum at 7.0463 T. This coupling manifests itself as shoulders of the central pseudo-quartet of the *m*- C_6F_5 fluorine resonance (Figure 1).

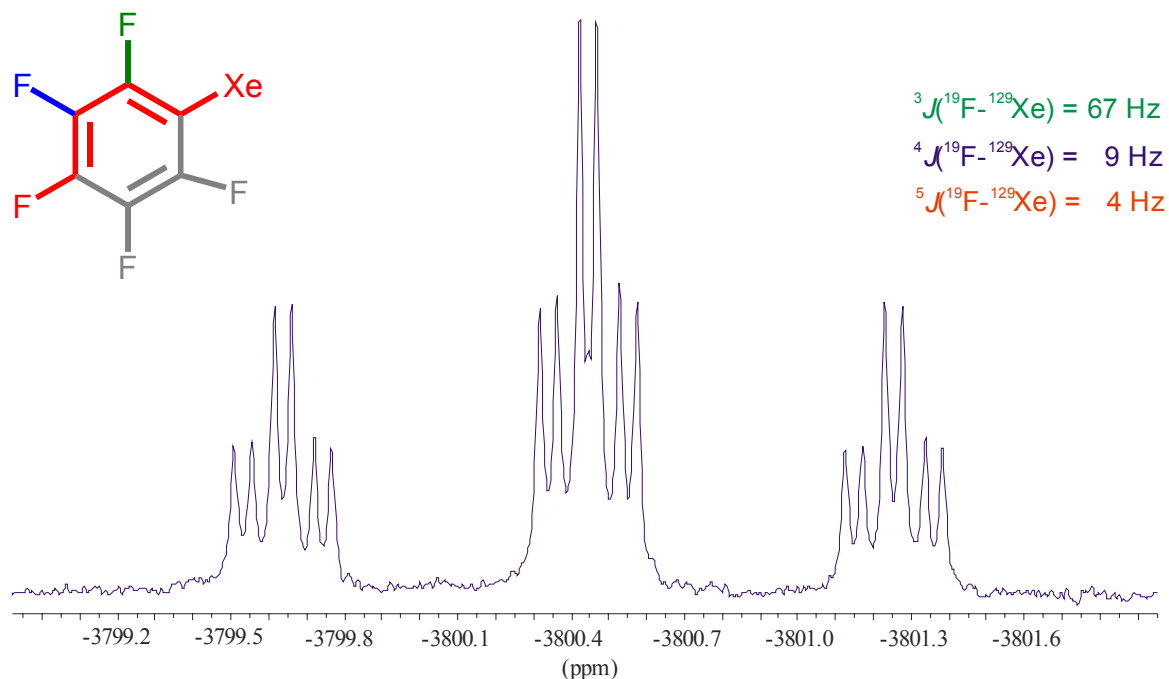


Figure 3 The ^{129}Xe NMR spectrum of $[\text{C}_6\text{F}_5\text{Xe}\cdots\text{NCCH}_3]^+$ (in $[\text{C}_6\text{F}_5\text{Xe}][\text{B}(\text{CF}_3)_4]$), in CH_3CN at 24 °C

It was found that the chemical shifts of the C_6F_5 resonances in different $[\text{C}_6\text{F}_5\text{Xe}]^+$ salts are dependent on the nucleophilicity of both the solvent (table 1 and 2) and the counteranion. The solvent and counteranions compete for coordination to the positively charged xenon(II) center. To simplify the interpretation of those chemical shifts two cases have to be distinguished: (1) salts with counteranions of weaker nucleophilicity than CH_3CN and (2) counteranions of higher nucleophilicity than CH_3CN . The first case always provides comparable ^{19}F resonances for the C_6F_5 ring fluorines indicative of the formation of a $[\text{C}_6\text{F}_5\text{Xe}\cdot(\text{NCCH}_3)_n]^+$ adduct which was always obtained for $[\text{C}_6\text{F}_5\text{Xe}]^+$ salts with weakly coordinating anions (Table 1).

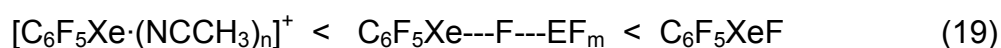
The second case results in a small shift to low frequency, especially for the *p*- C_6F_5 resonance, which occurs as a result of the stronger coordination of the counteranions to the positively charged xenon center than to the solvent. The shift increases with higher nucleophilicity of the counteranion and is indicative of the strength of the interaction. The low frequency shift of the fluorine atom of the C_6F_5

group is a consequence of a higher electron density around the fluorine atoms which shield it from the applied magnetic field.

The chemical shifts of the C_6F_5 resonances of the $[C_6F_5Xe]^+$ cation in the $[C_6F_5Xe][BY_4]$ ($Y = F, CN, OTeF_5, C_6F_5,$ and CF_3) salts are of comparable magnitude because their counteranions are all weakly coordinating and less nucleophilic than the solvent, CH_3CN . The formation of a $[C_6F_5Xe \cdot (NCCH_3)_n]^+$ adduct occurs whose chemical shifts are only slightly or unaffected by different counteranions.

The group of $[C_6F_5Xe]^+$ salts having counteranions that are more weakly coordinating than CH_3CN is relatively large. Table 1 shows several compounds having comparable chemical shifts for the C_6F_5 fluorine resonances in CH_3CN solution at 24 °C being -125.0 ± 0.3 ppm for the *o*- C_6F_5 , -141.5 ± 0.5 ppm for the *p*- C_6F_5 , and -154.4 ± 0.3 ppm for the *m*- C_6F_5 resonances. Only two salts having stronger nucleophilic anions, $[SiF_5]^-$ and $[HF_2]^-$, show lower frequency shifts for the C_6F_5 fluorine resonances ($\Delta\delta$ ($[SiF_5]^-$) = 1.8 ppm (*o*- C_6F_5), 1.5 ppm (*p*- C_6F_5), 0.5 ppm (*m*- C_6F_5); $\Delta\delta$ ($[HF_2]^-$) = 2.1 ppm (*o*- C_6F_5), 2.1 ppm (*p*- C_6F_5), 1.7 ppm (*m*- C_6F_5)).

The same trend was also obtained for the ${}^3J({}^{19}F-{}^{129}Xe)$ coupling constants obtained from the *o*- C_6F_5 resonances which are 68 ± 1 Hz for the $[C_6F_5Xe \cdot (NCCH_3)_n]^+$ adduct and 70 Hz and 73 Hz for the $C_6F_5Xe \cdots F \cdots SiF_4$ and $C_6F_5Xe \cdots F \cdots HF$, respectively. The extreme for coordination occurs for fluoride ions and is given by the neutral C_6F_5XeF molecule where the fluorine atom is bonded by means of an asymmetric semiionic 3c-4e bond.



E = H, Si; m = 3 and 5

The ${}^{19}F$ chemical shifts of C_6F_5XeF in CH_2Cl_2 at -80 °C, -129.6 ppm (*o*- C_6F_5), -147.0 ppm (*p*- C_6F_5), and -157.2 ppm (*m*- C_6F_5), are most shielded and have, as expected, the largest ${}^3J({}^{19}F-{}^{129}Xe)$ coupling constant (80 Hz). Different solvents, such as CH_2Cl_2 , PFB or CH_3CN and temperatures do not influence the chemical shift of C_6F_5XeF remarkably because the coordination sphere of the xenon(II) center is occupied by the fluoride ion so that coordination of further solvent molecules may be assumed to be negligible.

The ${}^{129}Xe$ NMR chemical shifts are not available for all $[C_6F_5Xe]^+$ salts but for all those considered in this study, namely $[C_6F_5Xe][BY_4]$ ($Y = F, CN, OTeF_5, C_6F_5,$

and CF_3) and $\text{C}_6\text{F}_5\text{XeF}$. The comparison of those chemical shifts differ only slightly, ranging in CH_3CN at 24 °C from -3795.2 ppm to -3813.3 ppm and having average spin-spin coupling constants of ${}^3J({}^{19}\text{F}-{}^{129}\text{Xe}) = 68 \pm 1$ Hz, ${}^4J({}^{19}\text{F}-{}^{129}\text{Xe}) = 9 \pm 0$ Hz, and ${}^5J({}^{19}\text{F}-{}^{129}\text{Xe}) = 3 \pm 1$ Hz. The slight deviation is most likely the result of different concentrations and/or temperatures. Even the ${}^{129}\text{Xe}$ -NMR chemical shift of neutral $\text{C}_6\text{F}_5\text{XeF}$, -3793.4 ppm, is just slightly shifted to higher frequency when compared with the above mentioned $[\text{C}_6\text{F}_5\text{Xe}]^+$ salts. All of the new salts have moderately to weakly coordinating anions. The comparable chemical shifts in both the ${}^{19}\text{F}$ and ${}^{129}\text{Xe}$ NMR spectra are indicative of a $[\text{C}_6\text{F}_5\text{Xe} \cdot (\text{NCCH}_3)_n]^+$ adduct.

The chemical shifts of the counteranions were not affected by the $[\text{C}_6\text{F}_5\text{Xe} \cdot (\text{NCCH}_3)_n]^+$ adduct and are comparable to those previously reported so that they do not need to be discussed in detail.

With access to CH_2Cl_2 -soluble $[\text{C}_6\text{F}_5\text{Xe}]^+$ salts, it was possible to examine the properties of a more weakly coordinated $[\text{C}_6\text{F}_5\text{Xe}]^+$ cation. Only salts containing very weakly coordinating anions such as $[\text{B}(\text{CF}_3)_4]^-$, $[\text{B}(\text{OTeF}_5)_4]^-$ and $[\text{B}(\text{C}_6\text{F}_5)_4]^-$ are soluble in weakly coordinating solvents such as CH_2Cl_2 , SO_2ClF , and $\text{CF}_3\text{CH}_2\text{CF}_2\text{CH}_3$, whereas $[\text{BF}_4]^-$ and $[\text{B}(\text{CN})_4]^-$ salts are insoluble. Only solutions of $[\text{C}_6\text{F}_5\text{Xe}][\text{B}(\text{CF}_3)_4]$ in CH_2Cl_2 and $\text{CF}_3\text{CH}_2\text{CF}_2\text{CH}_3$ are stable at RT for more than 3 and 5 days, respectively, contrasting with CH_2Cl_2 solutions of $[\text{C}_6\text{F}_5\text{Xe}][\text{B}(\text{C}_6\text{F}_5)_4]$ and $[\text{C}_6\text{F}_5\text{Xe}][\text{B}(\text{OTeF}_5)_4]$ which must be maintained at temperatures below -40 °C to avoid rapid decomposition.

A comparison of the ${}^{19}\text{F}$ NMR chemical shifts was undertaken using $[\text{C}_6\text{F}_5\text{Xe}][\text{B}(\text{CF}_3)_4]$ in basic CH_3CN and in CH_2Cl_2 at ambient temperature. It was found that the C_6F_5 fluorine resonances were shifted to higher frequencies (~ 5 ppm; *m*- and *p*- C_6F_5), indicative of a more weakly coordinated $[\text{C}_6\text{F}_5\text{Xe}]^+$ cation.

Table 2 The ${}^{19}\text{F}$ -NMR chemical shifts of $[\text{C}_6\text{F}_5\text{Xe}][\text{B}(\text{CF}_3)_4]$ in different solvents recorded at 24 °C

${}^{19}\text{F}$ NMR data recorded at 24 °C						
Solvent	<i>o</i> - C_6F_5 [ppm]	<i>p</i> - C_6F_5 [ppm]	${}^3J({}^{19}\text{F}-{}^{19}\text{F})$ [Hz]	${}^4J({}^{19}\text{F}-{}^{19}\text{F})$ [Hz]	<i>m</i> - C_6F_5 [ppm]	$[\text{B}(\text{CF}_3)_4]^-$ [ppm]
<i>CH</i>₃<i>CN</i>	-125.0	-141.2	20	6	-154.3	-61.4
<i>PFB</i>	-124.3	-138.9	19	6	-152.3	-60.2
<i>CH</i>₂<i>Cl</i>₂	-124.1	-136.6	20	6	-150.6	-61.4

Another approach to forming a weakly coordinated $[\text{C}_6\text{F}_5\text{Xe}]^+$ cation was by dissolution of $[\text{C}_6\text{F}_5\text{Xe}][\text{BF}_4]$ in the superacid, aHF, at $-40\text{ }^\circ\text{C}$. The resulting ^{19}F NMR chemical shifts, -123.3 ppm (*o*- C_6F_5), -138.2 ppm (*p*- C_6F_5), and -152.1 ppm (*m*- C_6F_5) are comparable to those obtained in PFB solution at $24\text{ }^\circ\text{C}$ and are indicative of a weakly coordinated $[\text{C}_6\text{F}_5\text{Xe}]^+$ cation. Anhydrous HF is a very weak nucleophile but it is assumed to be able to weakly coordinate to the positively charged Xe(IV) center through fluorine. Anhydrous HF predominantly solvates the anion, resulting in a much larger $[\text{BF}_4\cdot(\text{HF})_n]^-$ anion which disperses the negative charge over more fluorine atoms making it less nucleophilic. The $[\text{BF}_4\cdot(\text{HF})_n]^-$ anion exhibits a quartet splitting in the ^{19}F spectrum at -148.6 ppm attributed to ^{11}B coupling and a quintet splitting in the ^{11}B spectrum at -1.3 ppm attributed to ^{19}F coupling. The resolved signals confirm the presence of a highly symmetric arrangement on the NMR time scale. It is clear that the solvated $[\text{BF}_4\cdot(\text{HF})_n]^-$ anion is a member of the class of weakly coordinating anions.

III.1.2.2 Characterization of $[\text{C}_6\text{F}_5\text{Xe}\cdot\text{NCCH}_3][\text{B}(\text{CF}_3)_4]$, $[\text{C}_6\text{F}_5\text{Xe}][\text{B}(\text{CF}_3)_4]$, $[\text{C}_6\text{F}_5\text{Xe}][\text{B}(\text{CN})_4]$, and $[\text{C}_6\text{F}_5\text{Xe}\cdot\text{NCCH}_3][\text{B}(\text{C}_6\text{F}_5)_4]$ by X-Ray Crystallography

A summary of the refinement results and other crystallographic information are given in Table 3. Important bond lengths and bond angles are listed in Table 4 along with calculated values of $[\text{C}_6\text{F}_5\text{Xe}]^+$ in the gas phase.

Table 3 Crystallographic Data for [C₆F₅Xe·NCCH₃][B(CF₃)₄], [C₆F₅Xe][B(CF₃)₄], [C₆F₅Xe·NCCH₃][B(C₆F₅)₄], and [C₆F₅Xe][B(CN)₄]

	[C ₆ F ₅ Xe·NCCH ₃][B(CF ₃) ₄]	[C ₆ F ₅ Xe][B(CF ₃) ₄]	[C ₆ F ₅ Xe·NCCH ₃][B(C ₆ F ₅) ₄]	[C ₆ F ₅ Xe][B(CN) ₄]
Chem. formula	C ₁₂ H ₃ F ₁₇ BNXe	C ₁₀ F ₁₇ BXe	C ₃₂ F ₂₅ H ₃ BNXe	C ₁₀ F ₅ BN ₄ Xe
space group	<i>Pca</i> 2 ₁	<i>P</i> 2 ₁ / <i>c</i>	<i>P</i> 2 ₁ / <i>c</i>	<i>Pbca</i>
<i>a</i> (Å)	18.903(8)	6.751(2)	10.606(2)	9.919(2)
<i>b</i> (Å)	7.472(4)	15.950(5)	22.458(4)	16.269(4)
<i>c</i> (Å)	12.801(6)	14.715(4)	13.835(2)	16.783(4)
<i>α</i> (°)	90	90	90	90
<i>β</i> (°)	90	99.740(5)	94.775(5)	90
<i>γ</i> (°)	90	90	90	90
<i>V</i> (Å³)	1808.14	1561.52	3284.07	2708.12
molecules/unit cell	4	4	4	8
mol wt (g·mol⁻¹)	2505.06	2340.84	4073.86	3306.00
calc. density (g·cm⁻³)	2.284	2.489	2.060	2.027
T (°C)	-173	-173	-173	-173
<i>μ</i> (mm⁻¹)	2.08	2.39	1.22	2.60
<i>R</i>₁^a	0.0354	0.0445	0.0594	0.0363
<i>wR</i>₂^b	0.0531	0.1131	0.1776	0.0543

$${}^a R_1 = \frac{\sum \left(|F_0| - |F_c| \right)}{\sum |F_0|} \text{ for } l > 2\sigma(l); \quad {}^b wR_2 = \sqrt{\frac{\sum w \cdot \left(|F_0|^2 - |F_c|^2 \right)^2}{\sum w \cdot \left(|F_0|^2 \right)^2}} \text{ for } l > 2\sigma(l)$$

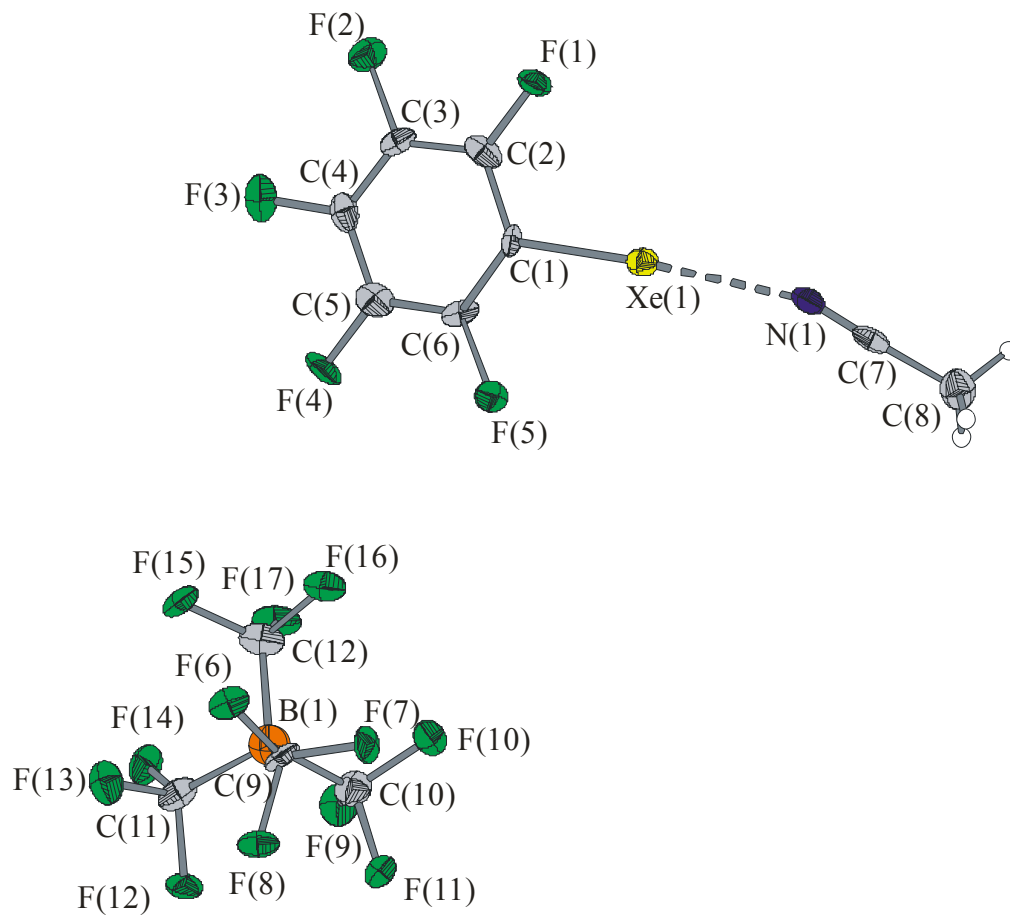


Figure 4 Crystal structure of $[\text{C}_6\text{F}_5\text{Xe}\cdot\text{NCCH}_3][\text{B}(\text{CF}_3)_4]$. Thermal ellipsoids are shown at the 50% probability level.

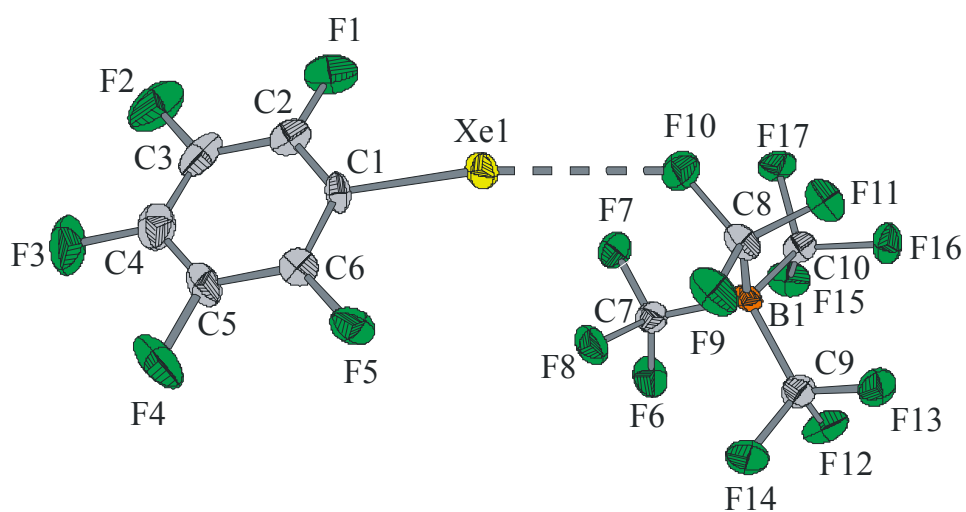


Figure 5 Crystal structure of $[\text{C}_6\text{F}_5\text{Xe}][\text{B}(\text{CF}_3)_4]$. Thermal ellipsoids are shown at the 50% probability level.

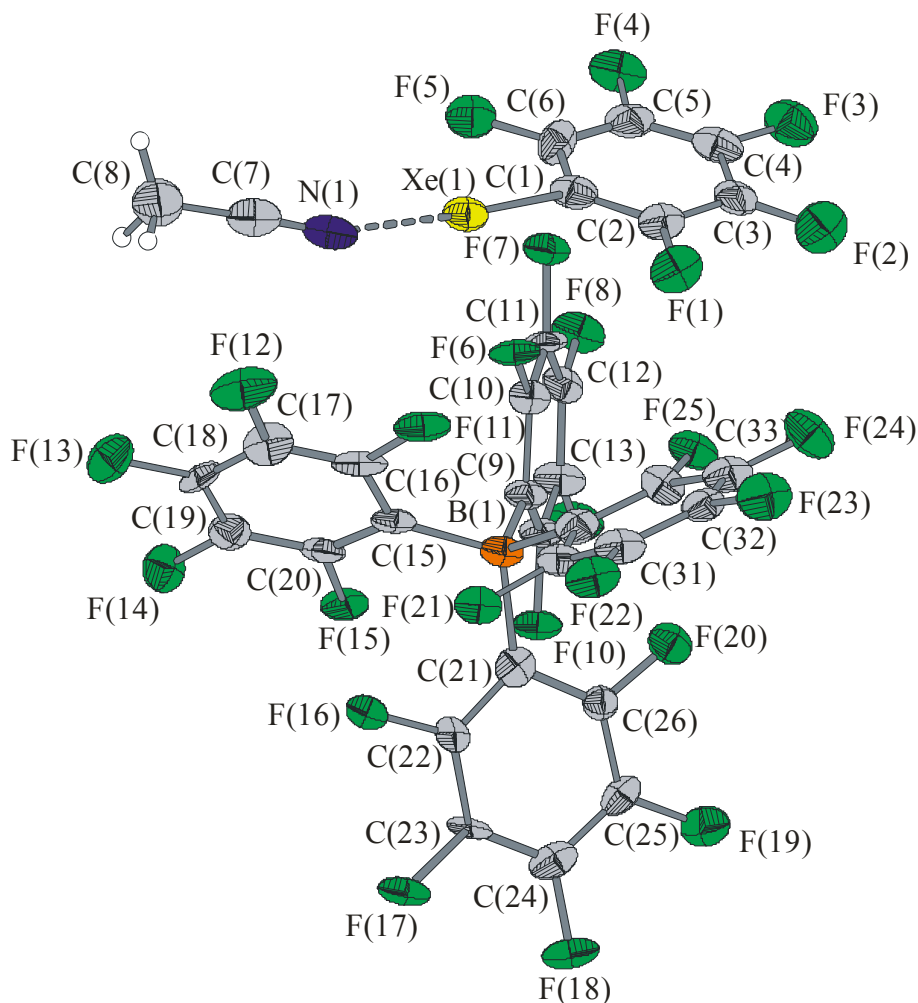


Figure 6 Crystal structure of $[C_6F_5Xe \cdot NCCH_3][B(C_6F_5)_4]$. Thermal ellipsoids are shown at the 50% probability level.

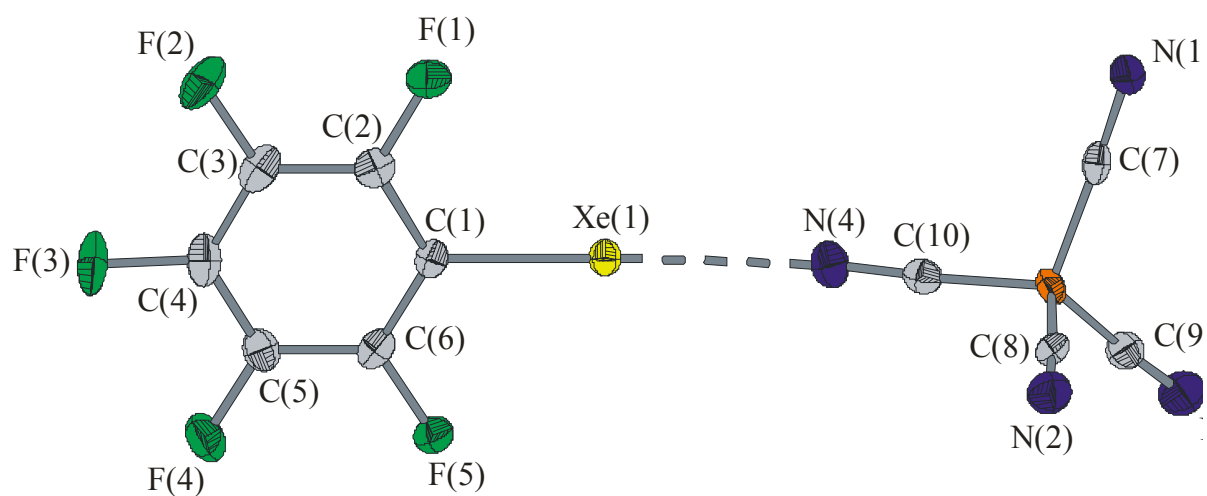


Figure 7 Crystal structure of $[C_6F_5Xe][B(CN)_4]$. Thermal ellipsoids are shown at the 50% probability level.

Table 4 Experimental Geometrical Parameters for $[\text{C}_6\text{F}_5\text{Xe}][\text{B}(\text{CF}_3)_4]$, $[\text{C}_6\text{F}_5\text{Xe}\cdot\text{NCCH}_3][\text{B}(\text{CF}_3)_4]$, $[\text{C}_6\text{F}_5\text{Xe}\cdot\text{NCCH}_3][\text{B}(\text{C}_6\text{F}_5)_4]$, $[\text{C}_6\text{F}_5\text{Xe}][\text{B}(\text{CN})_4]$, and Calculated Geometrical Parameters for $[\text{C}_6\text{F}_5\text{Xe}]^+$, $[\text{C}_6\text{F}_5\text{Xe}\cdot\text{NCCH}_3]^+$, $[\text{B}(\text{C}_6\text{F}_5)_4]^-$, $[\text{B}(\text{CF}_3)_4]^-$, and $[\text{B}(\text{CN})_4]^-$

	$[\text{B}(\text{CF}_3)_4]^-$ salt		$[\text{B}(\text{C}_6\text{F}_5)_4]^-$ salt	$[\text{B}(\text{CN})_4]^-$ salt	calc ^a	
	$[\text{C}_6\text{F}_5\text{Xe}]^+$	$[\text{C}_6\text{F}_5\text{Xe}\cdot\text{NCCH}_3]^+$	$[\text{C}_6\text{F}_5\text{Xe}\cdot\text{NCCH}_3]^+$	$[\text{C}_6\text{F}_5\text{Xe}]^+$	$[\text{C}_6\text{F}_5\text{Xe}]^+$	$[\text{C}_6\text{F}_5\text{Xe}\cdot\text{NCCH}_3]^+$
Xe(1)-C(1) (Å)	2.104(6)	2.099(6)	2.099(13)	2.082(3)	2.095	2.104
C(1)-C(2) (Å)	1.380(8)	1.396(9)	1.363(19)	1.375(4)	1.380	1.379
C(2)-F(1) (Å)	1.330(7)	1.319(9)	1.345(14)	1.334(4)	1.308	1.315
C(2)-C(3) (Å)	1.364(9)	1.387(15)	1.388(19)	1.378(4)	1.387	1.385
C(3)-F(2) (Å)	1.337(7)	1.369(11)	1.330(16)	1.337(4)	1.303	1.307
C(3)-C(4) (Å)	1.374(10)	1.348(15)	1.399(20)	1.378(5)	1.391	1.389
C(4)-F(3) (Å)	1.335(8)	1.335(9)	1.337(16)	1.341(4)	1.300	1.304
C(4)-C(5) (Å)	1.383(8)	1.383(8)	1.350(20)	1.378(4)	1.391	1.389
C(5)-F(4) (Å)	1.336(7)	1.309(8)	1.337(16)	1.337(4)	1.303	1.307
C(5)-C(6) (Å)	1.366(9)	1.377(9)	1.365(20)	1.379(4)	1.387	1.385
C(6)-F(5) (Å)	1.334(6)	1.336(7)	1.338(15)	1.340(4)	1.308	1.315
C(6)-C(1) (Å)	1.364(8)	1.349(9)	1.375(19)	1.378(5)	1.380	1.379
Xe(1)---N(1) (Å)		2.637(7)	2.613(15)			2.557
N(1)-C(7) (Å)		1.096(9)	1.157(19)			1.153
C(7)-C(8) (Å)		1.479(10)	1.438(24)			1.423
C(2)-C(1)-C(6)	123.5(6)	122.7 (6)	121.7(13)	121.3 (3)	124.3	122.3
C(1)-Xe(1)-N(1) (°)		174.8(2)	177.1(4)			179.9
Xe(1)-N(1)-C(7) (°)		164.2(5)	149.2(12)			180.0
N(1)-C(7)-C(8) (°)		178.1(9)	177.2(17)			180.0
Xe(1)---N(4) (Å)	-	-	-	2.716(3)		
Xe(1)---F(10) (Å)	2.913(4)	-	-	-		

Table 4 (continued...)

[C₆F₅Xe][B(CN)₄]		[C₆F₅Xe][B(CF₃)₄]		[C₆F₅Xe][B(CF₃)₄]·NCCH₃		[C₆F₅Xe][B(C₆F₅)₄]·NCCH₃	
B-C (Å)	1.593(5) - 1.609(5)	B-C (Å)	1.590(9) - 1.617(8)	B-C (Å)	1.589(10) - 1.629(11)	B-C (Å)	1.649(22) - 1.682(19)
C-N (Å)	1.132(4) - 1.144(4)	C-F (Å)	1.354(6) - 1.372(7)	C-F (Å)	1.334(8) - 1.347(9)	C-C (Å)	1.357(18) - 1.407(18)
						C-F (Å)	1.324(16) - 1.389(16)
C-B-C (°)	106.8(3) - 112.2(3)	C-B-C (°)	107.5(5) - 111.2(5)	C-B-C (°)	108.4(7) - 111.0(6)	C-B-C (°)	100.7(10) - 113.8(11)
B-C-N (°)	174.6(4) - 178.3(4)	B-C-F (°)	113.0(5) - 115.1(5)	B-C-F (°)	111.4(6) - 115.7(7)	B-C-C (°)	119.5(11) - 129.2(12)
		F-C-F (°)	103.5(4) - 105.8(5)	F-C-F (°)	103.0(6) - 106.7(6)	C-C-C (°)	119.0(12) - 126.0(13)
						C-C-F (°)	113.3(12) - 122.6(12)

^a Calculated using the SVWN/(SDB-)cc-pVTZ level.

The crystal structures of the $[\text{B}(\text{CF}_3)_4]^{-[97]}$ and $[\text{B}(\text{C}_6\text{F}_5)_4]^-$ anions have been previously reported. The structural parameters obtained in this study are in good agreement with the published parameters, and therefore require no further comment. The structure of the $[\text{B}(\text{CN})_4]^-$ anion has also been previously determined in $\text{Li}[\text{B}(\text{CN})_4]$ and $\text{K}[\text{B}(\text{CN})_4]^{[98]}$ and in $(\text{CH}_3)_3\text{Si}\cdot\text{NCB}(\text{CN})_3^{[99]}$ where the silicon atom interacts with one of the nitrogen atoms (1.872(2) Å). The geometrical parameters of the $[\text{B}(\text{CN})_4]^-$ anion are comparable to those in the literature.^[98] The distance between one nitrogen atom and the xenon atom is 2.716(3) Å in the structure of the $[\text{C}_6\text{F}_5\text{Xe}][\text{B}(\text{CN})_4]$ salt, which is significantly shorter than the sum of the xenon (2.16 Å)^[100] and nitrogen (1.55 Å)^[100] van der Waals radii (3.71 Å), suggesting a significant cation-anion interaction. This interaction, however, does not seem to affect the geometry of the $[\text{B}(\text{CN})_4]^-$ anion, with the C-N bond that is involved in the contact being equal, within $\pm 3\sigma$, to the other three C-N bonds, and the angles around boron being tetrahedral, within $\pm 3\sigma$.

The $[\text{C}_6\text{F}_5\text{Xe}]^+$ cation has previously been isolated in the solid state as adduct-cations in $[\text{C}_6\text{F}_5\text{Xe}\cdot\text{NCCH}_3][(\text{C}_6\text{F}_5)_2\text{BF}_2]^{[59]}$, $[\text{C}_6\text{F}_5\text{Xe}\cdot\text{NC}_5\text{H}_3\text{F}_2][\text{AsF}_6]^{[83]}$ as an ion pair in $[\text{C}_6\text{F}_5\text{Xe}][\text{AsF}_6]^{[93]}$ and as a rather covalent compound in $\text{C}_6\text{F}_5\text{Xe}\cdot\text{OC}(\text{O})\text{C}_6\text{F}_5^{[101]}$. The present Thesis reports further examples of the $[\text{C}_6\text{F}_5\text{Xe}\cdot\text{NCCH}_3]^+$ adduct-cation in the $[\text{B}(\text{CF}_3)_4]^-$ and $[\text{B}(\text{C}_6\text{F}_5)_4]^-$ salts where the adduct-cation structure is essentially identical to that published earlier in the $[(\text{C}_6\text{F}_5)_2\text{BF}_2]^-$ salt.^[59] In both cases, the adduct is well separated from the $[\text{B}(\text{CF}_3)_4]^-$ and $[\text{B}(\text{C}_6\text{F}_5)_4]^-$ anions. The structure of $[\text{C}_6\text{F}_5\text{Xe}]^+$ is also reported here in the $[\text{C}_6\text{F}_5\text{Xe}][\text{B}(\text{CN})_4]$ and $[\text{C}_6\text{F}_5\text{Xe}][\text{B}(\text{CF}_3)_4]$ salts. In the $[\text{C}_6\text{F}_5\text{Xe}][\text{B}(\text{CN})_4]$ salt, the Xe---N distance is 2.716(3) Å (*vide supra*), which is comparable to the Xe---F distance in $[\text{C}_6\text{F}_5\text{Xe}][\text{AsF}_6]$ (2.714(5) and 2.672(5) Å). Unlike $[\text{C}_6\text{F}_5\text{Xe}][\text{AsF}_6]$, it seems to be not appropriate to describe the present salt as an ion pair because $[\text{B}(\text{CN})_4]^-$ has T_d symmetry without one CN group being significantly elongated upon coordination. The ion-pair interaction seems stronger with $[\text{AsF}_6]^-$, giving rise to the expected elongation of the more ionic As-F bridge bond, whereas the covalent C≡N bond is little affected in the $[\text{B}(\text{CN})_4]^-$ salt. In the $[\text{C}_6\text{F}_5\text{Xe}][\text{B}(\text{CF}_3)_4]$ salt, the interaction is even weaker with an Xe---F distance of 2.913(4) Å.

The geometrical parameters of $[\text{C}_6\text{F}_5\text{Xe}]^+$ in the free cation and in the adducts are equal within experimental error (Table 4) and are comparable to those derived from the crystal structure of $[\text{C}_6\text{F}_5\text{Xe}][\text{AsF}_6]$. In particular, the C-Xe distances are

equal, in agreement with the $\nu(\text{Xe-C})$ stretches that are also observed to be the same (vide infra).

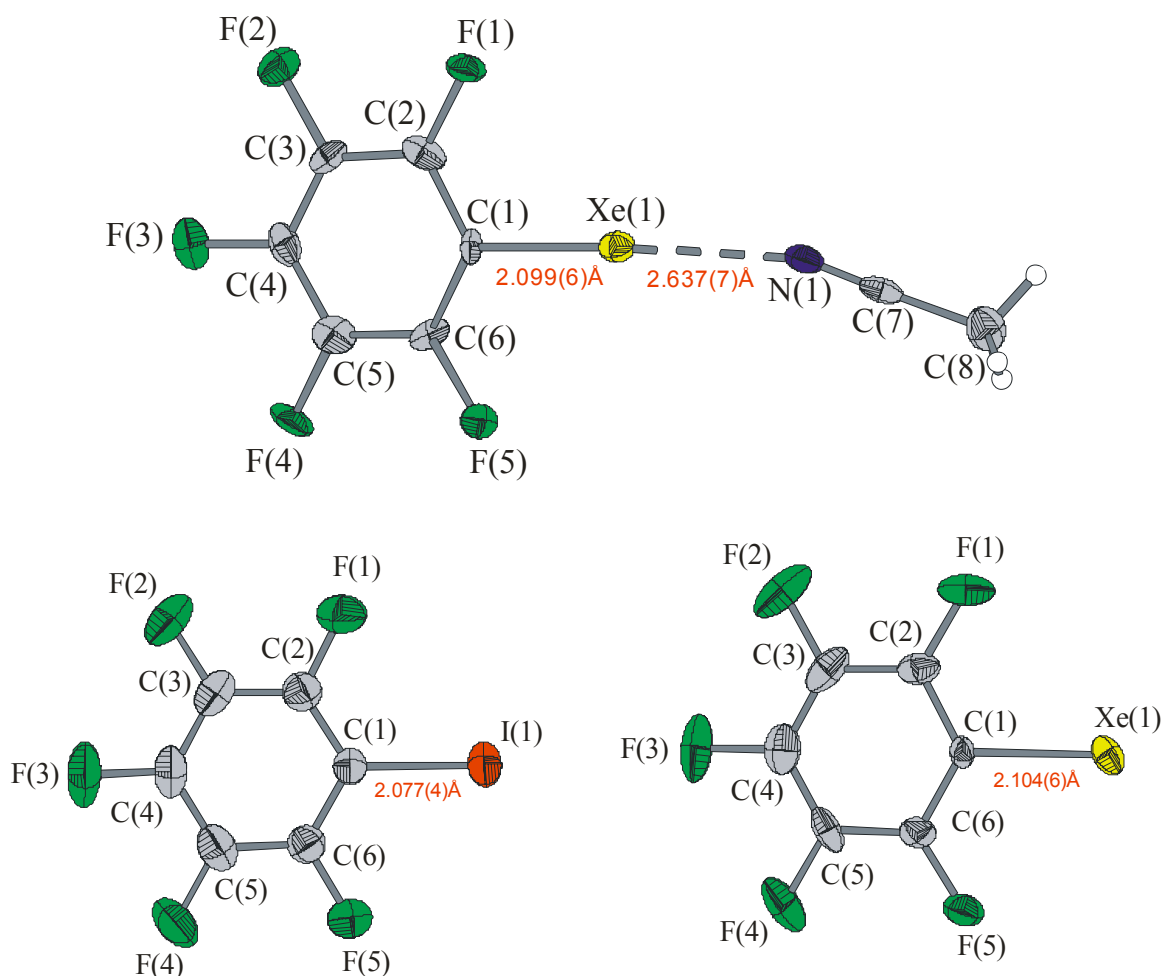


Figure 8 Comparison of the crystal structures of $[\text{C}_6\text{F}_5\text{Xe}]^+$, $[\text{C}_6\text{F}_5\text{Xe}\cdot\text{NCCH}_3]^+$ (both in $[\text{C}_6\text{F}_5\text{Xe}][\text{B}(\text{CF}_3)_4]$), and $\text{C}_6\text{F}_5\text{I}$.^[102] Thermal ellipsoids are shown at the 50% probability level.

The only previous example showing a C-Xe bond lengthening is that of $\text{C}_6\text{F}_5\text{Xe}\cdot\text{OC}(\text{O})\text{C}_6\text{F}_5$ with a C-Xe bond of 2.122(4) Å. In that case however, the Xe---O distance was found to be correspondingly shorter than all the present Xe---N distances. As expected, the C-Xe bond lengths are comparable to the C-I bond in $\text{C}_6\text{F}_5\text{I}$ (2.077(4) Å) (table 8).^[102] The experimental C-N bond lengths of the adducts are equal within $\pm 3\sigma$ to that observed in neat CH_3CN . This is in agreement with the Raman spectra which show only a small complexation shift for the CN stretching

frequency (*vide infra*). It is worth noting that this shift is much smaller than, for example, in $[\text{FXe} \cdots \text{NCCH}_3]^+$ where the C-N and Xe \cdots N distances are 1.120(11) and 2.179(7) Å, respectively. These experimental results are in agreement with $[\text{XeF}]^+$ being a much stronger Lewis acid than $[\text{C}_6\text{F}_5\text{Xe}]^+$ and therefore gives rise to stronger interactions that will show a greater effect on the geometrical parameters.

The C-Xe \cdots N angles are 174.8(2) and 177.1(4)° in the $[\text{B}(\text{CF}_3)_4]^-$ and the $[\text{B}(\text{CN})_4]^-$ salts, respectively, and are comparable to those observed in the $[(\text{C}_6\text{F}_5)_2\text{BF}_2]^-$ salt (174.5(3)°). The deviation of the C-Xe \cdots N angle from linearity in the $[\text{C}_6\text{F}_5\text{Xe} \cdot \text{NCCH}_3]^+$ adduct shows that this angle is susceptible to intermolecular contacts. This deviation from linearity has also been observed in $[\text{C}_6\text{F}_5\text{Xe}][\text{AsF}_6]$ where the C-Xe \cdots F angles were 170.5(3) and 174.2(3)°. ^[93]

III.1.2.3 Characterization by Low-Temperature Raman Spectroscopy

The observed frequencies for the low-temperature solid-state Raman spectra of $[\text{C}_6\text{F}_5\text{Xe}][\text{BF}_4]$, $[\text{C}_6\text{F}_5\text{Xe}][\text{B}(\text{CN})_4]$, $[\text{C}_6\text{F}_5\text{Xe} \cdot \text{NCCH}_3][\text{B}(\text{CF}_3)_4]$, and $[\text{C}_6\text{F}_5\text{Xe} \cdot \text{NCCH}_3][\text{B}(\text{C}_6\text{F}_5)_4]$ are summarized in Tables 5 and 6. The spectral assignments are based upon those of the isolated $[\text{C}_6\text{F}_5\text{Xe}]^+$ cation or $[\text{C}_6\text{F}_5\text{Xe} \cdot \text{NCCH}_3]^+$ adduct-cation and those of the respective anions. The 30 vibrational modes of the $[\text{C}_6\text{F}_5\text{Xe}]^+$ cation under C_{2v} point symmetry belong to the irreducible representation $11 A_1 + 3 A_2 + 6 B_1 + 10 B_2$, which are all Raman and infrared active. The highest symmetry possible for all borate counteranions is the T_d point symmetry having the following vibrational modes: 9 vibrational modes for the $[\text{BF}_4]^-$ anion belong to the irreducible representations $A_1 + E + 2T_2$, the 21 vibrational modes of the $[\text{B}(\text{CN})_4]^-$ anion belong to the irreducible representations $2 A_1 + 2 E + 1 T_1 + 4 T_2$, the 45 vibrational modes of the $[\text{B}(\text{CF}_3)_4]^-$ anion belong to the irreducible representations $3 A_1 + 1 A_2 + 4 E + 4 T_1 + 7 T_2$, and the 129 vibrational modes of the $[\text{B}(\text{C}_6\text{F}_5)_4]^-$ anion belong to the irreducible representations $7 A_1 + 4 A_2 + 11 E + 14 T_1 + 18 T_2$.

The frequencies observed for the $[\text{BF}_4]^-$, ^[99] $[\text{B}(\text{CF}_3)_4]^-$, ^[97] and $[\text{B}(\text{CN})_4]^-$ ^[98] anions are of less symmetry and are in agreement with those reported earlier; and therefore their assignments have been made by comparison with the published assignments and require no further discussion (Table 5 and 6, footnote b).

There are no frequency assignments published for the free $[\text{C}_6\text{F}_5\text{Xe}]^+$ cation or the $[\text{C}_6\text{F}_5\text{Xe} \cdot \text{NCCH}_3]^+$ adduct-cation, and only a list of unassigned infrared

frequencies were provided for $\text{C}_6\text{F}_5\text{Xe}\cdot\text{OC}(\text{O})\text{C}_6\text{F}_5$ ^[101] and $[\text{C}_6\text{F}_5\text{Xe}\cdot\text{NCCH}_3][(\text{C}_6\text{F}_5)_2\text{BF}_2]$ ^[59]. The frequency assignments for $[\text{C}_6\text{F}_5\text{Xe}]^+$ and $[\text{C}_6\text{F}_5\text{Xe}\cdot\text{NCCH}_3]^+$ were made by comparison with the assignments calculated in the present study. The calculations were carried out at the HF and DFT levels of theory using the Stuttgart and (SDB-)cc-pVTZ basis sets but only the best DFT/(SDB-)cc-pVTZ results are reported in Tables 5 and 6 (*vide infra*). The frequencies of the isoelectronic C_6F_5 ^[103] compound and of $\text{C}_6\text{F}_5\text{Cl}$ and $\text{C}_6\text{F}_5\text{Br}$ ^[104, 105] were also calculated at the same level but only the values from $\text{C}_6\text{F}_5\text{I}$ are reported (Table 9), allowing valid comparisons to be made based on the new assignments.

Table 5 Experimental^a Raman Vibrational Frequencies and Intensities for [C₆F₅Xe][B(CN)₄] and [C₆F₅Xe][BF₄] and Calculated Vibrational Frequencies and Infrared Intensities for [C₆F₅Xe]⁺

[C ₆ F ₅ Xe][B(CN) ₄] exp. ^b	[C ₆ F ₅ Xe][BF ₄] exp. ^c	[C ₆ F ₅ Xe] ⁺ calc. ^d	Assignments ^e
1651(5)	1659(10)	1671(5) [5]	} ν(C–C)
1632(7)	1637(15)	1620(13) [6]	
	1523(9)	1565(452) [<<1]	} ν(C–C) + ν(C–F)
1435(5)		1559(295) [1]	
		1467(5) [2]	} ν(C–C)
		1376(35) [1]	
1289(5)	1286(9)	1331(7) [3]	} ν(C–C) + ν(C–F)
1166(6)	1163(12)	1225(1) [3]	
1096(10)			δ(CCC) i.p. + small (ν(C–C) + ν(C–F))
1093(14)		1123(58) [2]	
924(13)	957(12)	1033(127) [<1]	} ν(C–C) + ν(C–F)
794(18)	795(14)	772(87) [<1]	
			δ(CCC) i.p. + small (ν(C–C) + ν(C–F)) δ(CCC) i.p.
753(5)		752(<1) [<<1]	
711(4)	709(8)	695(<1) [<<1]	} δ(CCC) o.o.p.
		646(0) [<<1]	
605(5)	605(10)	591(1) [2]	} δ(CCC) i.p.
587(32)	588(61)	587(5) [14]	
511(5)			} δ(CCC) i.p.
500(8)		489(6) [10]	
492(62)	494(76)		} δ(CCF) i.p.
438(19)	440(35)	425(0) [3]	
376(24)	382(32)		} δ(CCF) o.o.p.
355(17)	374(12)	344(2) [3]	
351(30)		302(3) [<1]	} δ(CCC) o.o.p.
		299(0) [3]	
		296(1) [0]	} δ(CCF) i.p.
276(12)	277(20)	263(0) [<1]	
		256(0) [<<1]	} δ(CCF) o.o.p.
		197(1) [<1]	
201(80)	205(100)	188(1) [5]	ν(Xe–C) + ν(CCF) i.p.
173(13)			} δ(CCF) o.o.p.
164(25)		160(0) [0]	
152(13)	142(13)		} δ(CCF) i.p.
137(15)		129(0) [<<1]	
126(12)			} δ(CCF) o.o.p.
122(13)	119(12)	112(0) [<1]	
	106(15)		} δ(CCF) o.o.p.
85(26)		77(0) [<<1]	
55(4)	59(9)		lattice modes
47(4)			

Table 5 (continued...)

- ^a The Raman spectra were recorded at $-150\text{ }^{\circ}\text{C}$ in a heat-sealed glass NMR tube (Wilmad 507). Frequencies are given in cm^{-1} .
- ^b Bands at 2245(100) ($\nu_1(\text{A}_1)$), 2240(54), 2234(41), 2227(44) ($\nu_6(\text{T}_2)$), 951(6), 944(6) ($\nu_7(\text{T}_2)$), 526(16), 524(13) ($\nu_3(\text{E})$), 486(10) ($\nu_2(\text{A}_1)$), 329(5) ($\nu_5(\text{T}_1)$), and 143(14) ($\nu_9(\text{T}_2)$) cm^{-1} were assigned to $[\text{B}(\text{CN})_4]^-$ by comparison with previous assignments.^[98, 99] The three Bands, $\nu_6(\text{T}_2)$, clearly indicate a side symmetry lowering.
- ^c Bands at 1107(11) ($\nu_3(\text{T}_2)$), 760(32) ($\nu_1(\text{A}_1)$), 524(10), 518(9) ($\nu_4(\text{T}_2)$) and 363(14), 354(59) ($\nu_2(\text{E})$) cm^{-1} were assigned to $[\text{BF}_4]^-$ by comparison with previous assignments.^[99]
- ^d SVWN/(SDB-)cc-pVTZ; calculated infrared intensities, in $\text{kJ}\cdot\text{mol}^{-1}$, are given in parentheses and calculated Raman intensities, in $\text{\AA}^4\cdot\text{amu}^{-1}$, are given in square brackets.
- ^e The deformation modes of the C_6F_5 ring are denoted by the general symbol δ and are relative to the plane containing the C_6F_5 ring; i.p. and o.o.p denote in-plane and out-of-plane, respectively.

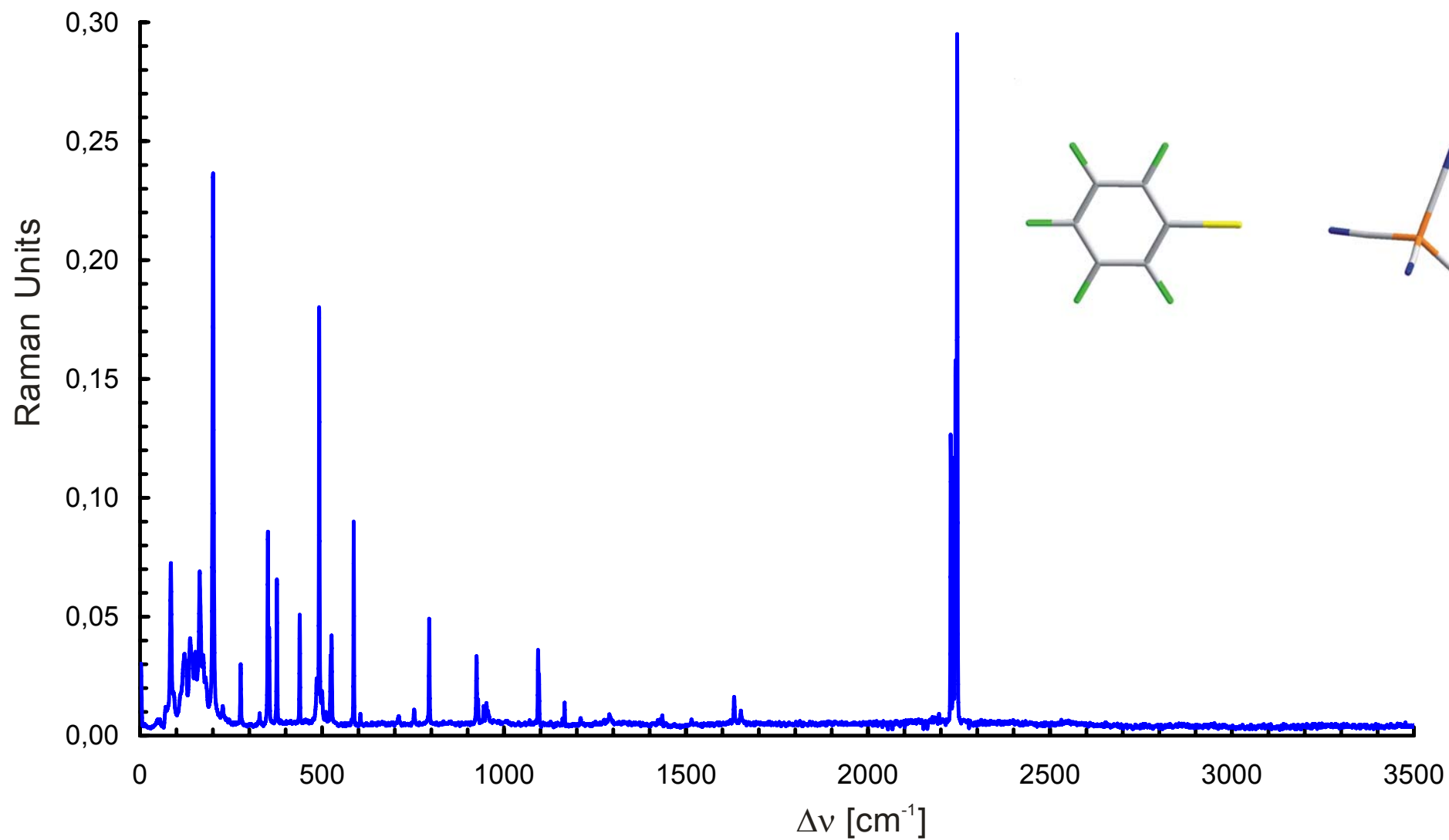


Figure 9 Raman spectrum of solid $[\text{C}_6\text{F}_5\text{Xe}][\text{B}(\text{CN})_4]$ at $-150\text{ }^\circ\text{C}$

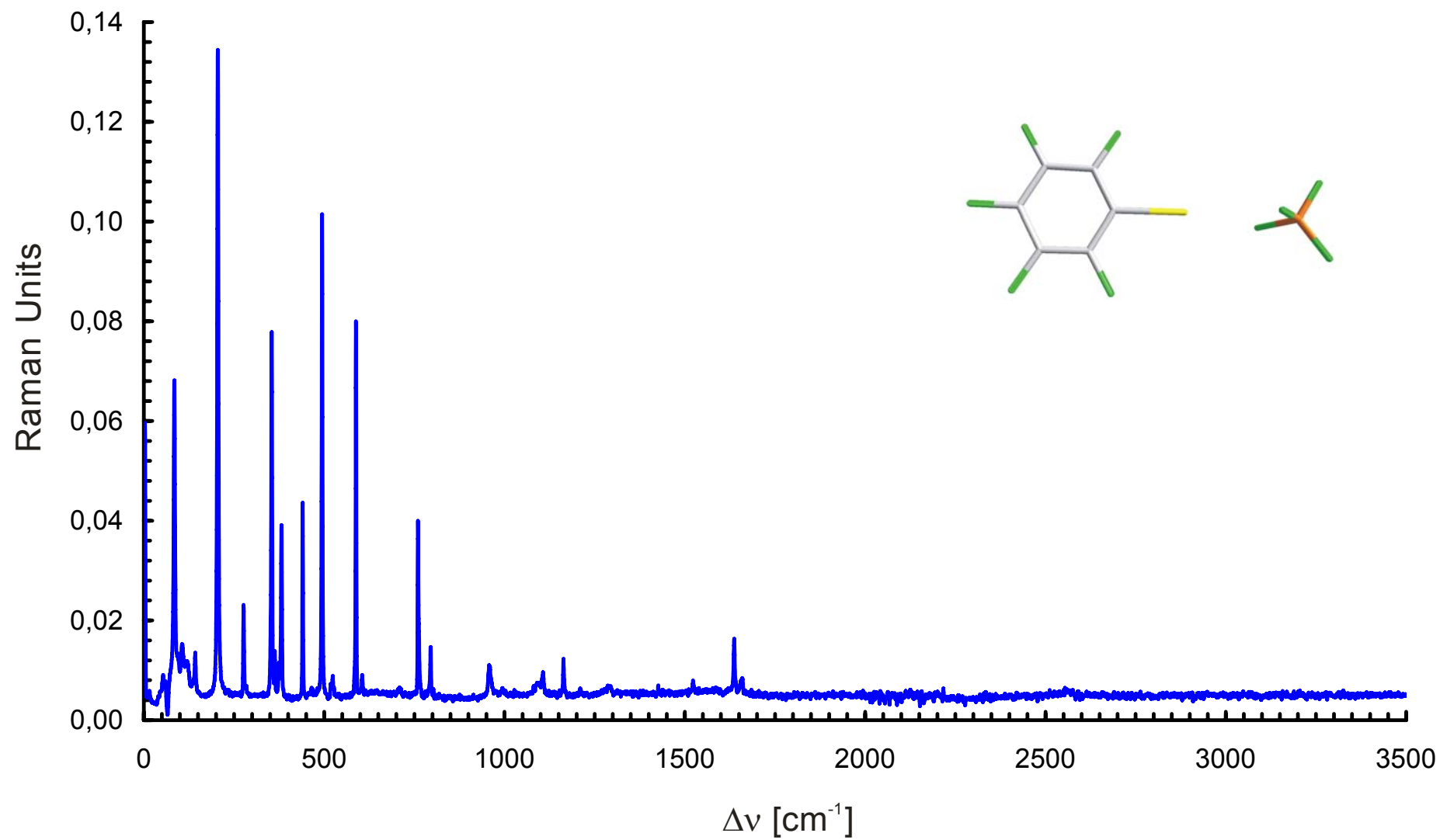


Figure 10 Raman spectrum of solid $[\text{C}_6\text{F}_5\text{Xe}][\text{BF}_4]$ at $-150\text{ }^\circ\text{C}$

Table 6 Observed Raman Frequencies for $[\text{C}_6\text{F}_5\text{Xe}\cdot\text{NCCH}_3]^+$ in $[\text{C}_6\text{F}_5\text{Xe}\cdot\text{NCCH}_3][\text{B}(\text{CF}_3)_4]$ and $[\text{C}_6\text{F}_5\text{Xe}\cdot\text{NCCH}_3][\text{B}(\text{C}_6\text{F}_5)_4]$ and Calculated Frequencies for $[\text{C}_6\text{F}_5\text{Xe}\cdot\text{NCCH}_3]^+$ and CH_3CN

$[\text{C}_6\text{F}_5\text{Xe}\cdot\text{NCCH}_3]^+$ exp. ^a		exp. ^a	calc. ^c		assignments ^d
$[\text{B}(\text{CF}_3)_4]^-$ ^b	$[\text{B}(\text{C}_6\text{F}_5)_4]^-$	CH_3CN	$[\text{C}_6\text{F}_5\text{Xe}\cdot\text{NCCH}_3]^+$	CH_3CN	
3014(10)		3000(38)	3064(15) 3061(15)	3063	} $\nu_{\text{as}}(\text{CH}_3)$
2951(40)	2947(47) ^e	2938(94)	2978(33)	2982	
2309(28)	2303(21)				$\nu(\text{C}\equiv\text{N})$
2278(79)	2273(48)	2248(100)	2342(244)	2332	} $\nu(\text{C}-\text{C})$
1654(9)	1660(26)		1666(<1)		
1636(11)			1635(9)		} $\nu(\text{C}-\text{C}) + \nu(\text{C}-\text{F})$
1516(8)			1558(450)		
1433(9)			1557(341)		} $\nu(\text{C}-\text{C})$
			1456(15)		
			1387(18)	1391	} CH_3 def. as
			1371(18)		
1377(13)	1376(20)	1376(17)	1370(18)		} CH_3 def. s + small ($\nu(\text{C}-\text{C}) + \nu(\text{C}-\text{F})$)
			1331(2)	1335	
			1330(8)		CH_3 def. s
1168(12)			1215(1)		$\nu(\text{C}-\text{C}) + \nu(\text{C}-\text{F})$
1121(10)			1123(100)		$\delta(\text{CCC})$ i.p. + small ($\nu(\text{C}-\text{C}) + \nu(\text{C}-\text{F})$)
1090(14)	1091(19)		1027(142)		$\nu(\text{C}-\text{C}) + \nu(\text{C}-\text{F})$
			989(9)	999	$\rho_{\text{r}}(\text{CH}_3)$
			988(10)		
930(23)	930(23)	922(23)	982(17)	959	$\nu(\text{C}-\text{C})$
795(23)	796(20)		791(34)		$\delta(\text{CCC})$ i.p. + small ($\nu(\text{C}-\text{C}) + \nu(\text{C}-\text{F})$)
			753(0)		

Table 6 (continued...)

			697(<1)			}	$\delta(\text{CCC})$ o.o.p.
			650(0)				
609(9)			608(1)			}	
587(34)	584		586(5)				
493(92)	490(37)		490(0)			}	$\delta(\text{CCC})$ i.p.
438(32)	438(22)		430(0)				
389(15)	390(29)	387(15)	399(0)	377		}	$\delta(\text{CCF})$ i.p.
385(23)			398(<1)				
357(29)	358(24)		347(0)			}	$\delta(\text{CCN})$
350(28)	349(26)		345(0)				
			331(3)			}	$\delta(\text{CCF})$ o.o.p.
			298(1)				
			262(2)			}	$\delta(\text{CCF})$ i.p.
			256(0)				
			204(1)			}	$\delta(\text{CCF})$ o.o.p.
202(100)	203(34)		202(57)				
161(9)	164(19)		166(<1)			}	$\nu(\text{Xe-C}) + \delta(\text{CCF})$ i.p.
144(12)			153(10)				
			141(3)			}	$\delta(\text{CCF})$ o.o.p. + $\delta(\text{CXeN})$
			130(0)				
			120(6)			}	$\nu(\text{Xe-N})$
			85(5)				
			70(3)			}	$\delta(\text{CCF})$ i.p. + $\delta(\text{CXeN})$
			24(1)				
			23(3)			}	$\delta(\text{CCF})$ o.o.p.
			22(2)				
						}	$\delta(\text{XeNC})$ o.o.p. + small $\delta(\text{CCF})$ o.o.p.
						}	$\delta(\text{XeNC})$ i.p. + small $\delta(\text{CCF})$ i.p.
						}	$\delta(\text{XeNC})$ o.o.p. + small $\delta(\text{CCF})$ o.o.p.
						}	$\rho_t(\text{CH}_3)$
						}	$\delta(\text{NCC})$ o.o.p.
						}	$\rho_t(\text{CH}_3)$

Table 6 (continued...)

- ^a The Raman spectra were recorded at $-150\text{ }^{\circ}\text{C}$ in a heat-sealed glass NMR tube (Wilmad 507). Frequencies are given in cm^{-1} .
- ^b Bands at 1279(15) ($\nu_1(\text{A})$ & $\nu_9(\text{T})$), 1110(11) ($\nu_5(\text{E})$), 724(65) ($\nu_2(\text{A})$), 696(8) ($\nu_3(\text{T})$), 318(21) ($\nu_7(\text{E})$), 298(14) ($\nu_{16}(\text{T})$), 226(9) ($\nu_{17}(\text{T})$) and 52(9) ($\nu_{19}(\text{T})$) cm^{-1} were assigned to $[\text{B}(\text{CF}_3)_4]^-$ by comparison with previous assignments.^[97, 106]
- ^c SVWN/(SDB-)cc-pVTZ; infrared intensities, in $\text{kJ}\cdot\text{mol}^{-1}$, are given in parentheses.
- ^d The deformation modes of the C_6F_5 ring are denoted by the general symbol δ and are relative to the plane containing the C_6F_5 ring; i.p. and o.o.p denote in-plane and out-of-plane, respectively.
- ^e Modes of the anion and cation overlap.
- .

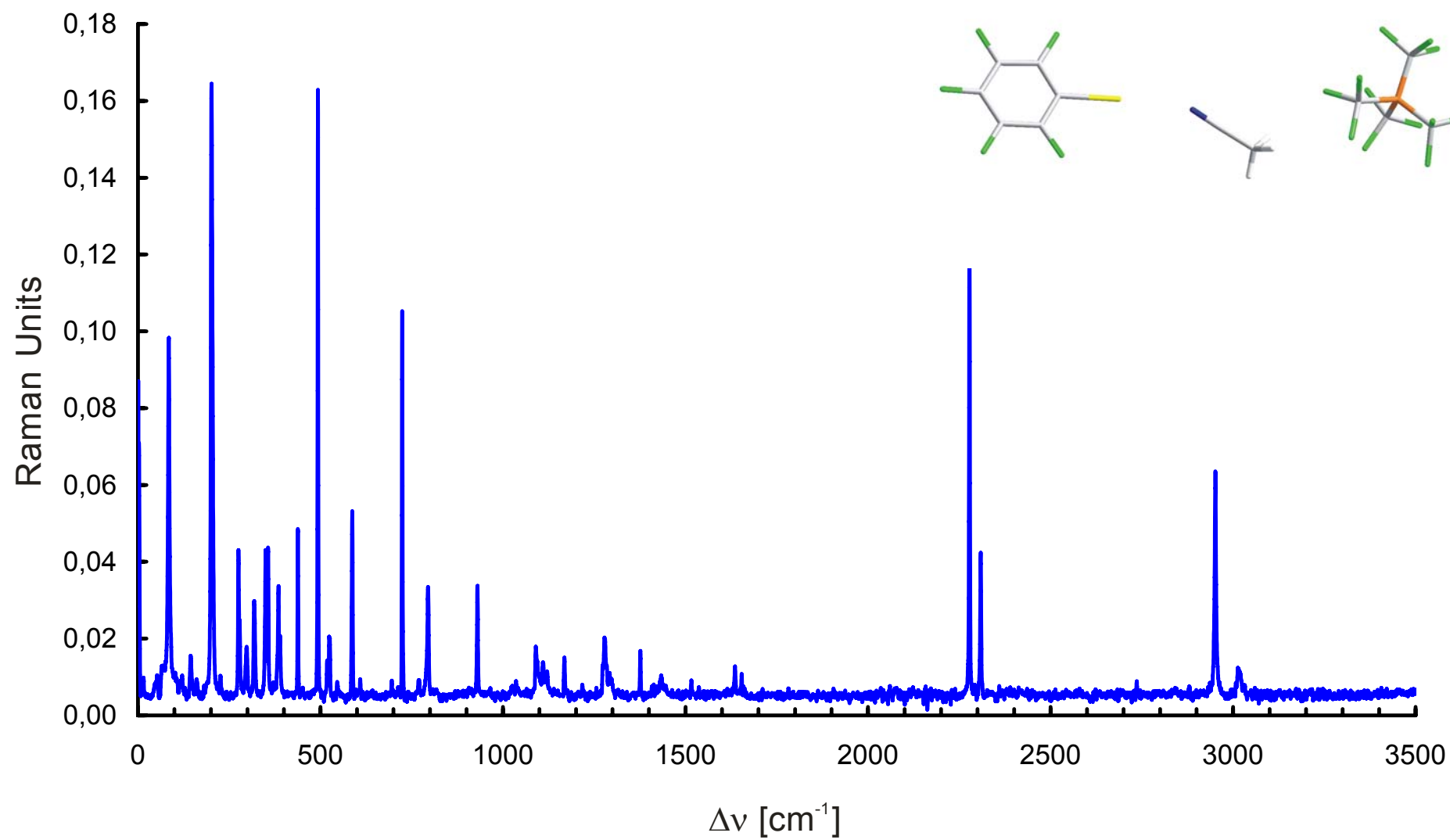


Figure 11 Raman spectrum of solid $[\text{C}_6\text{F}_5\text{Xe}][\text{B}(\text{CF}_3)_4]$ at $-150\text{ }^\circ\text{C}$

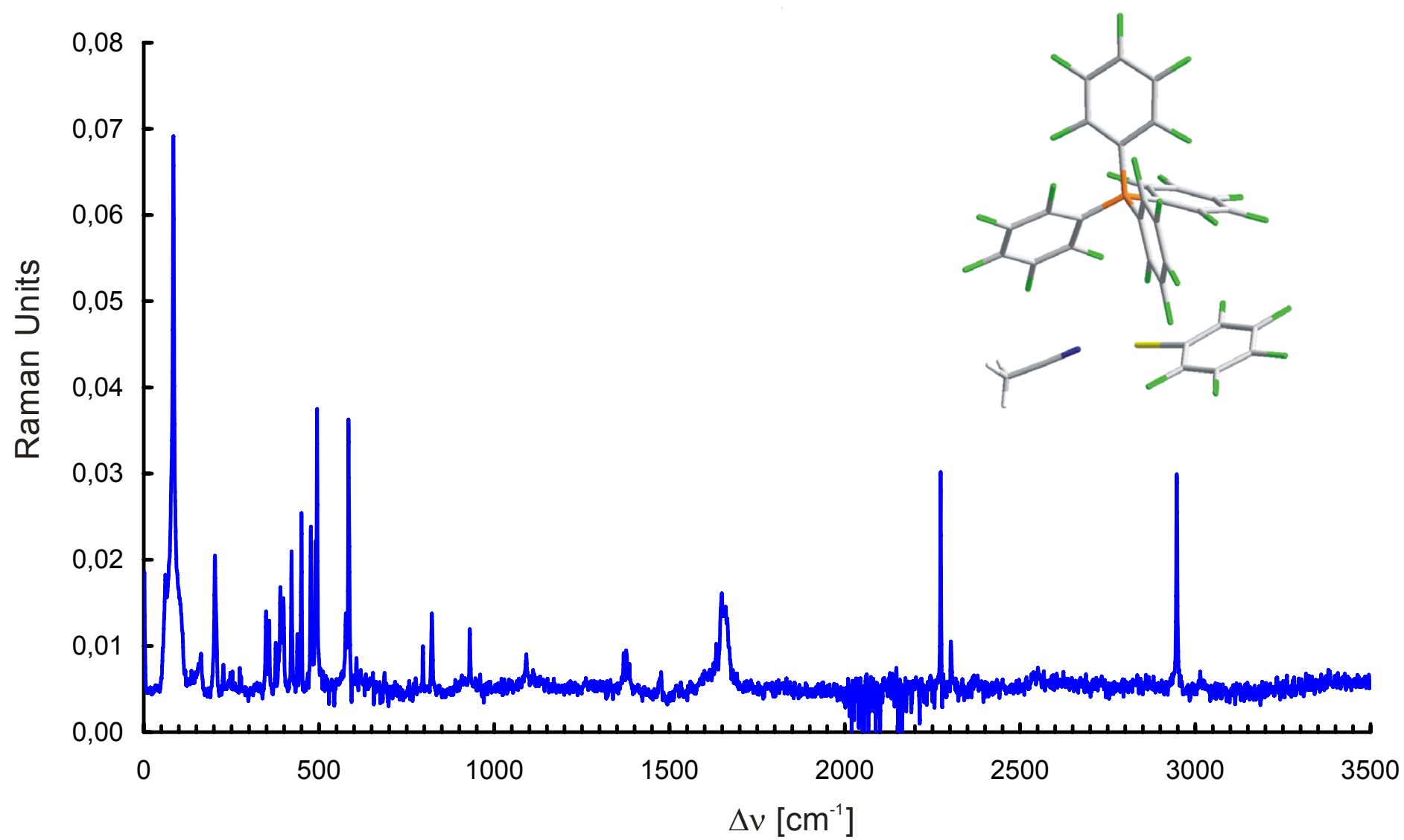


Figure 12 Raman spectrum of solid $[\text{C}_6\text{F}_5\text{Xe}][\text{B}(\text{C}_6\text{F}_5)_4]$ at $-150\text{ }^\circ\text{C}$

Table 7 Observed Raman Frequencies for $[\text{B}(\text{C}_6\text{F}_5)_4]^-$ in $\text{Cs}[\text{B}(\text{C}_6\text{F}_5)_4]$ and $[\text{C}_6\text{F}_5\text{Xe}\cdot\text{NCCH}_3][\text{B}(\text{C}_6\text{F}_5)_4]$

$\text{Cs}[\text{B}(\text{C}_6\text{F}_5)_4]^a$	$[\text{C}_6\text{F}_5\text{Xe}][\text{B}(\text{C}_6\text{F}_5)_4]^a$	assignments
2948(9)	2947(47) ^c	?
2552(10)		
1647(28)		$\nu(\text{C}-\text{C})$
	1476(16)	} $\nu(\text{C}-\text{C}) + \nu(\text{C}-\text{F})$
1387(16)	1385(17)	
1377(17)	1376(20)	
	1369(19)	
824(34)	822(25)	$\nu_s(\text{B}-\text{C})$
776(15)		
769(12)		
758(15)		
684(10)		
662(10)		
582(100)		} $\delta(\text{CCC})$
574(33)		
495(48)	494(57)	
478(54)	477(39)	
450(63)	450(41)	$\delta(\text{CBC})$
422(61)	422(35)	
400(28)	398(28)	
393(66)	390(29)	
376(12)	376(21)	
358(17)		$\delta(\text{CCF})$ i.p.
343(11)		$\delta(\text{CCF})$ i.p.
242(20)		
162(19)		$\delta(\text{CCF})$ o.o.p.
158(21)		$\delta(\text{CCF})$ o.o.p.
85(56)		
70(31)		
57(13)	61(31)	$\delta(\text{CCF})$ o.o.p.

^a The Raman spectra were recorded at $-150\text{ }^\circ\text{C}$ in a heat-sealed glass NMR tube (Wilmad 507). Frequencies are given in cm^{-1} .

^b The deformation modes of the C_6F_5 ring are denoted by the general symbol δ and are relative to the plane containing the C_6F_5 ring; i.p. and o.o.p denote in-plane and out-of-plane, respectively.

^c Modes of the anion and cation overlap.

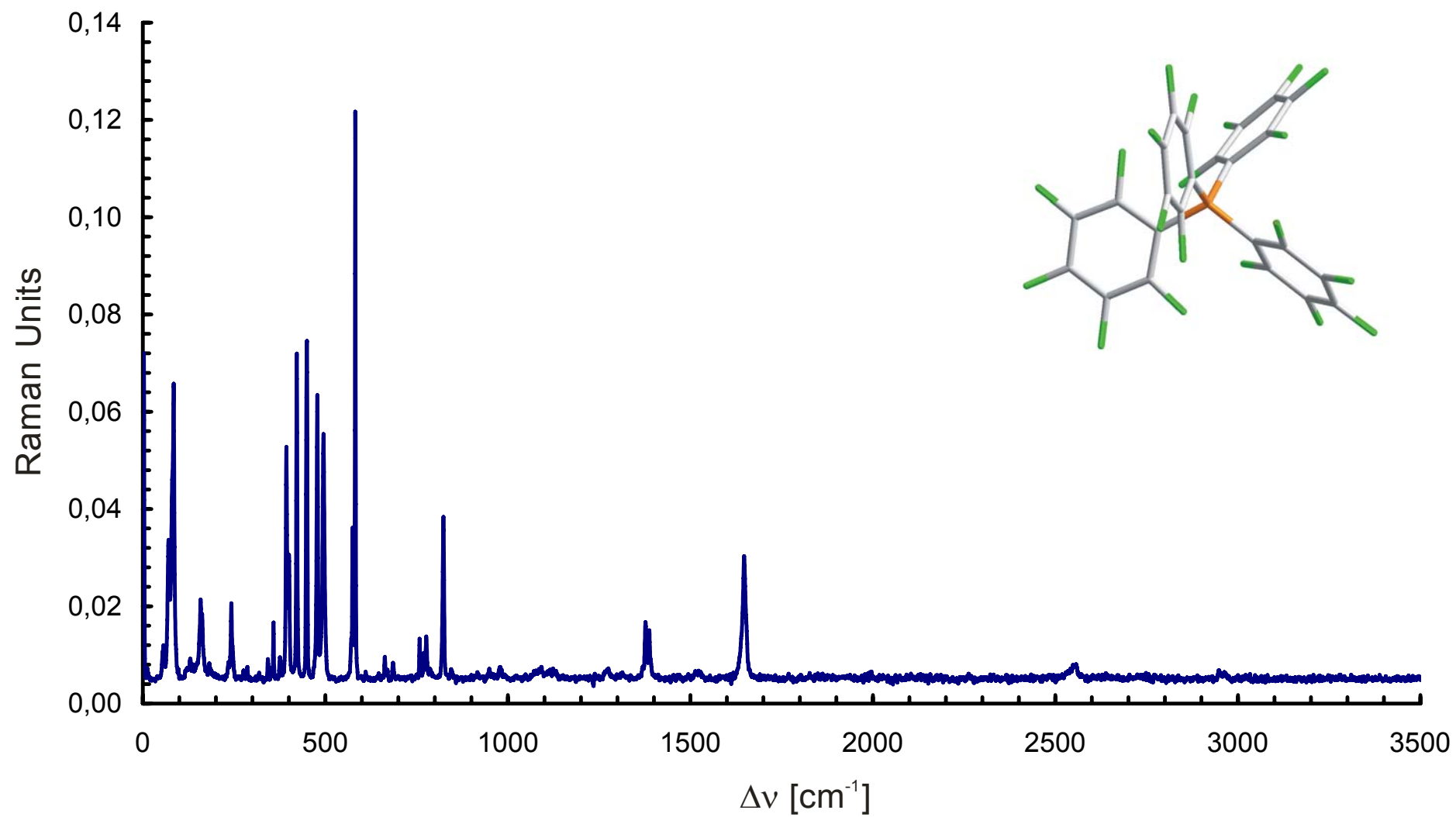


Figure 13 Raman spectrum of solid Cs[B(C₆F₅)₄] at -150 °C

There is overall good agreement between the observed and calculated frequencies for the $[\text{C}_6\text{F}_5\text{Xe}]^+$ cation, the $[\text{C}_6\text{F}_5\text{Xe}\cdot\text{NCCH}_3]^+$ adduct-cation and for $\text{C}_6\text{F}_5\text{I}$. All modes involving $\nu(\text{C-F})$ and/or $\nu(\text{C-C})$ stretches are slightly overestimated while the deformation modes are underestimated. The $\nu(\text{Y-C})$ mode ($\text{Y} = \text{Xe}, \text{I}$) is coupled to the deformation mode $\delta(\text{CCF})$ i.p. and is underestimated. The C_6F_5 ring modes are comparable to those observed in other systems containing C_6F_5 groups,^[103-105, 107] and it is only at low frequencies in the adduct that some changes are observed with some deformation modes being coupled with $\delta(\text{XeNC})$. The medium intensity mode observed at 794 (Xe) and 808 (I) cm^{-1} is assigned to the CCC deformation mode where the central carbon is coordinated to Xe or I, and was calculated at 772 and 818 cm^{-1} , respectively, and was predicted to be rather intense in the infrared spectra. This mode was previously reported for $\text{C}_6\text{F}_5\text{I}$ as well as for the Cl and Br analogues ($\text{C}_6\text{F}_5\text{Cl}$, 885 cm^{-1} ; $\text{C}_6\text{F}_5\text{Br}$, 836 cm^{-1})^[104, 105] and are mass dependent. The modes were, however, wrongly assigned in the prior study, most likely because of their strong intensities, to the C-Y ($\text{Y} = \text{Cl}, \text{Br}, \text{and I}$) stretches. The present study reveals that the C-Y stretches occur at much lower frequencies (Table 5, 6, and 9). The $\nu(\text{C-Xe})$ and $\nu(\text{C-I})$ modes were calculated at 188 and 203 cm^{-1} , respectively, and were predicted to be intense in the Raman spectra. The most intense mode of the $[\text{BF}_4]^-$ and $[\text{B}(\text{CN})_4]^-$ salts at 201 and 205 cm^{-1} and the very intense mode in $\text{C}_6\text{F}_5\text{I}$ at 204 cm^{-1} were assigned to the $\nu(\text{Xe-C})$ and $\nu(\text{I-C})$ modes. To the authors knowledge, there are no other published values for C-Xe(II) and C-I(I) stretching frequencies. The calculated and observed frequency provided in the present work follow the predicted trend $\nu(\text{C-Xe}) < \nu(\text{Xe-N})$ (330 cm^{-1} in $[\text{HCN}\cdots\text{XeF}]^+$)^[108] $< \nu(\text{Xe-O})$ (490 cm^{-1} in $[\text{XeOTeF}_5]^+$)^[109] $< \nu(\text{Xe-F})$ (610 cm^{-1} in $[\text{XeF}]^+$). The $\nu(\text{C-Xe})$ mode is predicted to shift to lower frequency by 14 cm^{-1} upon CH_3CN coordination, but, in practice, it is observed at ca. 200 cm^{-1} in both the free $[\text{C}_6\text{F}_5\text{Xe}]^+$ cation and in the $[\text{C}_6\text{F}_5\text{Xe}\cdot\text{NCCH}_3]^+$ adduct-cation. The insensitivity of this mode to coordination is in agreement with corresponding insensitivity in the geometrical parameters (*vide supra*). The $\nu(\text{C-N})$ stretch is expected to shift by 10 cm^{-1} upon coordination, which is in good agreement with the observed shift (CH_3CN , 2267 cm^{-1} ; adduct, 2278 and 2273 cm^{-1}) and is consistent with a weak donor-acceptor interaction. The weak interaction is also supported by the calculated low frequency for the $\nu(\text{Xe-N})$ stretch at 153 cm^{-1} . These frequencies are indeed much lower than those predicted in cases where a real Xe-N bond occurs (e.g. $[\text{F}_5\text{TeN}(\text{H})\text{Xe}]^+$, 430

cm^{-1} ; $[\text{HCN}\cdot\text{XeF}]^+$, 330 cm^{-1} ; $[\text{CH}_3\text{CN}\cdot\text{XeF}]^+$, 262 cm^{-1}). The frequency at 144 cm^{-1} is assigned to $\nu(\text{Xe-N})$. Because strong bands associated with CCF bending modes are also observed in this region, and because the $\nu(\text{Xe-N})$ stretch is expected to be very low in intensity, this mode could not be assigned with certainty in the experimental spectrum. The deformation mode $\delta(\text{CXe}\cdots\text{N})$ is expected at 141 and 166 cm^{-1} and is coupled with a $\delta(\text{CCF})$ deformation mode.

To the authors knowledge, and although the $[\text{B}(\text{C}_6\text{F}_5)_4]^-$ anion has been known for some time, no vibrational data are available for this anion. To assign the experimental spectrum of the $[\text{B}(\text{C}_6\text{F}_5)_4]^-$ anion, its structure was optimized at the HF level. There is very good agreement using a scaling factor of 0.89. The bands at 824 and 822 cm^{-1} are assigned to the symmetric $\nu(\text{B-C})$ stretch which is expected to be very intense in the Raman spectrum and predicted at 791 cm^{-1} . The asymmetric $\nu(\text{B-C})$ stretch is predicted at 872 cm^{-1} , but is not observed experimentally. This is in agreement with the expected very weak intensity. The bending mode $\delta(\text{CBC})$, is expected to be strong and at 526 cm^{-1} and is assigned to the band at 450 cm^{-1} .

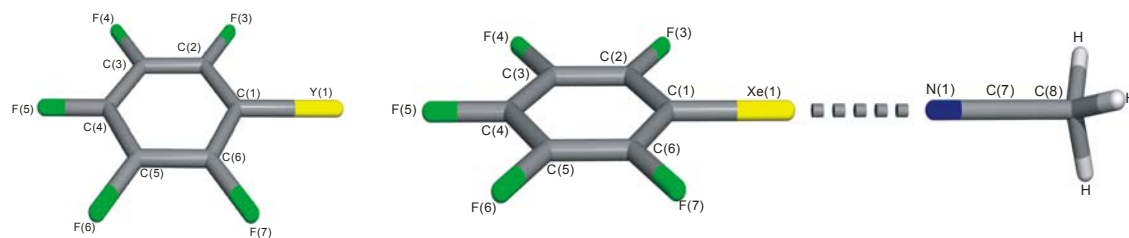
III.1.3 Computational Results

The electronic structures of the $[\text{C}_6\text{F}_5\text{Xe}]^+$ cation and the $[\text{C}_6\text{F}_5\text{Xe}\cdot\text{NCCH}_3]^+$ adduct-cation were calculated by using Hartree-Fock (HF) and pure density functional theory (DFT) methods with the Stuttgart and (SDB-)cc-pVTZ basis sets starting from C_s and C_1 symmetry, respectively. Both types of calculations resulted in stationary points with all frequencies real, with the DFT calculations giving overall better agreement with experimental geometries and vibrational frequencies (see Table 9). For this reason, only the DFT results are discussed. The $[\text{C}_6\text{F}_5\text{Xe}]^+$ cation^[93] and CH_3CN molecule had previously been the subject of theoretical calculations; they were, however, recalculated under the same conditions as of $[\text{C}_6\text{F}_5\text{Xe}\cdot\text{NCCH}_3]^+$ adduct-cation in order to confirm the experimental changes that were observed upon coordination of $[\text{C}_6\text{F}_5\text{Xe}]^+$ to CH_3CN . We also note that the basis sets used include semi-relativistic effects by employing semi-relativistic effective core potentials (RLC ECP). Key optimized metric parameters for $[\text{C}_6\text{F}_5\text{Xe}]^+$ (C_s) and $[\text{C}_6\text{F}_5\text{Xe}\cdot\text{NCCH}_3]^+$ (C_1) are listed in Table 4. The isoelectronic systems, $\text{C}_6\text{F}_5\text{Y}$ ($\text{Y} = \text{Cl}, \text{Br}, \text{I}$), were also calculated.

Overall, there is good agreement between the observed and the calculated bond lengths and bond angles. The calculations also show that the C-Xe bond is expected to elongate slightly upon coordination to nitrogen. The Xe---N contact is slightly underestimated. The largest deviation is for the C-Xe---N angle that is 179.9° even at the DFT level (C_1), and differ from the observed bent C-Xe---N angle (Table 4), suggesting that the angle distortion at the nitrogen arises from packing effects. Such deviations from the ideal 180° angle about Xe(II) have been encountered in other compounds. The deformability of this angle is also reflected in the calculated low frequency C-Xe---N bending (Table 6).

Upon complexation, the bond orders for Xe(1)-C(1) and N(1)-C(7) decrease slightly, while that of C(7)-C(8) increase accordingly. Coordination of CH₃CN to [C₆F₅Xe]⁺ has no significant effect on the C₆F₅ ring. The weakness of the donor-acceptor interaction is consistent with the small Xe(1)---N(1) bond order (0.114). Upon adduct formation, the Xe atom becomes more positive and the N atom becomes more negative. There are no significant changes on the C and F atoms, except for the C atom bonded to Xe which becomes more negative, and the C atom bonded to N, which becomes more positive. The valency on Xe increases only slightly and that of nitrogen decreases, in agreement with the formation of a weak covalent bond.

Table 8 Calculated ^a Natural Atomic Charges, Mayer Bond Orders, and Mayer Natural Atomic Orbital Valencies for $[\text{C}_6\text{F}_5\text{Xe}]^+$ and $[\text{C}_6\text{F}_5\text{Xe}\cdot\text{NCCH}_3]^+$



		$[\text{C}_6\text{F}_5\text{Xe}]^+$	$[\text{C}_6\text{F}_5\text{Xe}\cdot\text{NCCH}_3]^+$	NCCH_3
charge	Xe(1)	0.90	0.94	
	C(1)	-0.25	-0.31	
	F(3)	-0.24	-0.26	
	C(2)	0.29	0.30	
	F(4)	-0.22	-0.23	
	C(3)	0.30	0.29	
	F(5)	-0.22	-0.23	
	C(4)	0.32	0.31	
	F(6)	-0.22	-0.23	
	C(5)	0.30	0.29	
	F(7)	-0.24	-0.26	
	C(6)	0.29	0.30	
	N(1)		-0.46	-0.31
	C(7)		0.45	0.27
	C(8)		-0.80	-0.79
	H(1-3)		0.31 x 3	0.28 x 3
	valency	Xe(1)	0.71	0.78
C(1)		3.10	3.05	
F(3)		0.83	0.81	
C(2)		3.13	3.13	
F(4)		0.74	0.73	
C(3)		3.02	3.02	
F(5)		0.74	0.73	
C(4)		3.03	3.03	
F(6)		0.74	0.73	
C(5)		3.02	3.02	
F(7)		0.83	0.81	
C(6)		3.13	3.13	
N(1)			2.04	1.96
C(7)			3.01	3.01
C(8)			3.32	3.30
H(1-3)			0.79 x 3	0.79 x 3
bond order		Xe(1)–C(1)	0.72	0.68
	C(1)–C(2)	1.15	1.16	
	C(2)–F(3)	0.85	0.84	
	C(2)–C(3)	1.11	1.12	
	C(3)–F(4)	0.77	0.76	
	C(3)–C(4)	1.11	1.11	
	C(4)–F(5)	0.77	0.76	
	C(4)–C(5)	1.11	1.11	
	C(5)–F(6)	0.77	0.76	
	C(5)–C(6)	1.11	1.12	
	C(6)–F(7)	0.85	0.84	
	C(6)–C(1)	1.15	1.16	
	Xe(1)---N(1)		0.11	
	N(1)–C(7)		1.91	1.95
	C(7)–C(8)		1.04	1.01
	C(8)–H		0.76 x 3	0.76 x 3

Table 9 Experimental and Calculated (C_s) Infrared Frequencies and Intensities for C_6F_5I

Raman ^a	IR	calc	assignments
1633	1634	1653 (2)[4] 1652 (6) [35]	$\nu(C-C)$
1507	1512	1546 (276) [1] 1534(433) [$\ll 1$]	$\nu(C-C) + \nu(C-F)$
1406	1409	1448(1) [16] 1386(<1) [2]	$\nu(C-C)$
1296	1296	1310(<1) [1]	$\nu(C-C) \pm \nu(C-F)$
1268	1263	1192(2) [1]	
1147	1149	1116(82) [$\ll 1$]	$\delta(CCC)$ i.p. + small ($\nu(C-C) \pm \nu(C-F)$)
1082	1083	1014(157) [<1]	
1002	977		$\nu(C-C) \pm \nu(C-F)$
805	808	818(72) [6]	$\delta(CCC)$ i.p. + small ($\nu(C-C) \pm \nu(C-F)$)
	714	747(0) [<1]	$\delta(CCC)$ i.p.
696	694	696(1) [<1] 650(0) [$\ll 1$]	$\delta(CCC)$ o.o.p.
609	600	616(1) [1]	
581	581	585(<1) [17]	
489	489	493(1) [10]	$\delta(CCC)$ i.p.
438	442	436(<1) [4]	
381	385	371(0) [3]	$\delta(CCF)$ i.p.
349	350	354(<1) [2]	$\delta(CCF)$ o.o.p.
	349	336(1) [1]	$\delta(CCC)$ o.o.p.
	311	302(1) [$\ll 1$]	
278	280	267(<1) [<1] 257(<1) [$\ll 1$]	$\delta(CCF)$ i.p.
	215	204(1) [2]	$\delta(CCF)$ o.o.p.
204	205	203(1) [<1]	$\nu(I-C) + \delta(CCF)$ i.p.
	133	165(<1) [$\ll 1$]	$\delta(CCF)$ o.o.p.
	129	130(0) [0]	
	114	124(<1) [1]	$\delta(CCF)$ i.p.
	110	80($\ll 1$) [$\ll 1$]	$\delta(CCF)$ o.o.p.
			lattice modes

^a additional modes: 1954, m, 1908, vw, 1891, vw, 1862, m, 1844, vw, 1815, vw, 1773, w, 1760, w, 1729, s, 1695, w

III.1.4 Behaviour of $[C_6F_5Xe][BY_4]$ ($Y = F, CF_3, C_6F_5, OTeF_5,$ and CN) in Solution

Previous solution studies on $[C_6F_5Xe]^+$ salts were predominantly carried out in CH_3CN ; fewer were done in aHF and practically none in CH_2Cl_2 . The problems with performing reactions in CH_2Cl_2 were either the insolubility of the $[C_6F_5Xe]^+$ salt or its instability. The only examples of $[C_6F_5Xe]^+$ salts soluble in CH_2Cl_2 , $[C_6F_5Xe][BF_x(C_6F_5)_{4-x}]$ ($x = 0 - 1$)^[58, 60, 90, 93, 94] and $[C_6F_5Xe][O_2CC_6F_5]$,^[74, 110] are unstable and decompose rapidly in CH_2Cl_2 at ambient temperature. Salts of $[C_6F_5Xe]^+$ with the weakly coordinating anions, $[B(C_6F_5)_4]^-$, $[B(OTeF_5)_4]^-$, and $[B(CF_3)_4]^-$ are soluble in the weakly coordinating solvents CH_2Cl_2 , SO_2ClF , and $CF_3CH_2CF_2CH_3$, but salts with more nucleophilic and strongly coordinating anions such as $[BF_4]^-$ and $[B(CN)_4]^-$ salts are insoluble. Solutions of $[C_6F_5Xe][B(CF_3)_4]$ in CH_2Cl_2 and $CF_3CH_2CF_2CH_3$ are the only examples that are stable at ambient temperature for more than 3 and 5 days, respectively, contrasting with CH_2Cl_2 solutions of $[C_6F_5Xe][B(C_6F_5)_4]$ which must be maintained at temperatures below -40 °C to avoid decomposition. With access to CH_2Cl_2 -stable solutions of the $[C_6F_5Xe]^+$ salt, new synthetic possibilities arose including the optimized preparation of the neutral and key compound, C_6F_5XeF , which will be discussed later.

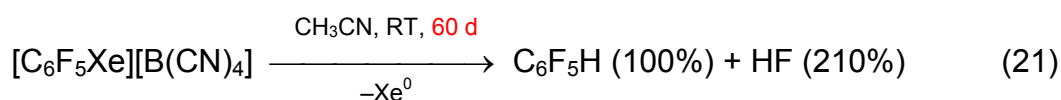
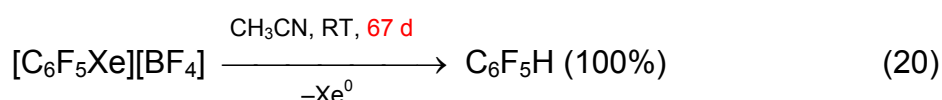
A high solubility was obtained for $[C_6F_5Xe][BF_4]$ in aHF but there are two reasons why aHF solutions are not suitable to investigate the decomposition of $[C_6F_5Xe]^+$ salts: (1) the high stability of the $[C_6F_5Xe]^+$ cation in aHF even at RT (15% conversion in 54 d) and (2) the ability of HF to coordinate to the counteranions buffers the influence of the anion on the decomposition making an interpretation more difficult. The decomposition of $[C_6F_5Xe][BF_4]$ in aHF and a comparison with the decompositions of hydrogen-containing organoxenon(II) compounds will be discussed in section III.1.4.6.

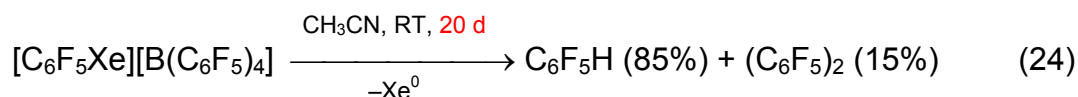
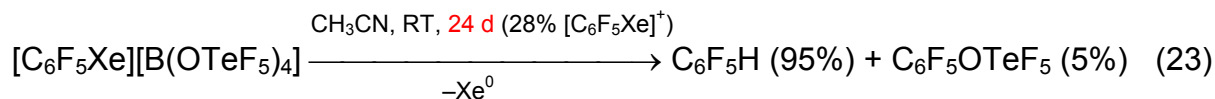
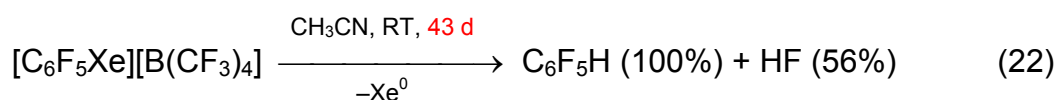
All $[C_6F_5Xe]^+$ salts that have been prepared thus far are soluble in CH_3CN and it was shown in the X-ray crystal structures of $[C_6F_5Xe---NCCH_3][A]$ ($A = BF_2(C_6F_5)_2$,^[59] $B(CF_3)_4$, and $B(C_6F_5)_4$), in the Raman spectra of solid $[C_6F_5Xe---NCCH_3][A]$ ($A = B(CF_3)_4$ and $B(C_6F_5)_4$) and in the NMR spectra of numerous $[C_6F_5Xe]^+$ salt solutions that CH_3CN is basic enough to interact to a significant extent with the cation. Cation-anion interactions are consequently reduced upon coordination of CH_3CN . The high solubilities of $[C_6F_5Xe]^+$ salts in CH_3CN and the

comparable interaction of CH₃CN with the [C₆F₅Xe]⁺ cation motivated to a detailed study of the decomposition in CH₃CN as a function of different counteranions. The stabilities of [C₆F₅Xe]⁺ salt solutions were monitored in FEP reaction tubes by ¹⁹F NMR spectroscopy at ambient temperatures. The samples were stored in glass traps protected by argon gas and in the absence of daylight. Details of the NMR spectroscopic changes with time are summarized in the Experimental Section.

The stability of a pure compound is expressed by its thermodynamic and kinetic stabilities. The presence of other compounds or impurities, even in traces, can affect the stability, in most cases as a consequence of kinetic effects. From repeated decomposition studies, it was found that the rate of decomposition and, to some extent the pattern of decomposition products be strongly dependent upon the purities of the [C₆F₅Xe]⁺ salts and solvents. Thus, individual preparations of several [C₆F₅Xe]⁺ salts provided slightly different decomposition results. It was possible, however, to point out the main trends and the important decomposition channels. A comparison with previous studies on [C₆F₅Xe][BF₄]^[90] and [C₆F₅Xe][AsF₆]^[93] is not particularly useful because of the reaction conditions, in most cases, are not well known. For example, a previous decomposition study on [C₆F₅Xe][BF₄], described by H. Franke^[90] had shown a decomposition rate in CH₃CN of 20% [C₆F₅Xe][BF₄] after 5 d at ambient temperature. It was reported that the decomposition products were C₆F₅H, C₆F₆ and BF₃·NCCH₃. In the present study, the decomposition rate for [C₆F₅Xe][BF₄] in CH₃CN was only 7% after 7 d and 32% after 30 d.

The following reaction schemes provide the product distributions and decomposition rates of [C₆F₅Xe]⁺ salts in CH₃CN solutions at ambient temperature. The decomposition was described as complete when no [C₆F₅Xe]⁺ cation could be detected by ¹⁹F NMR spectroscopy. All, but the study involving [C₆F₅Xe][B(OTeF₅)₄], were monitored until the [C₆F₅Xe]⁺ cation had been completely consumed. In the case of [C₆F₅Xe][B(OTeF₅)₄], the decomposition study had to be discontinued after 24 d (72% of the [C₆F₅Xe]⁺ had decomposed) because of NMR spectrometer problems.





The following decomposition sequence was obtained starting with the slowest decomposition:

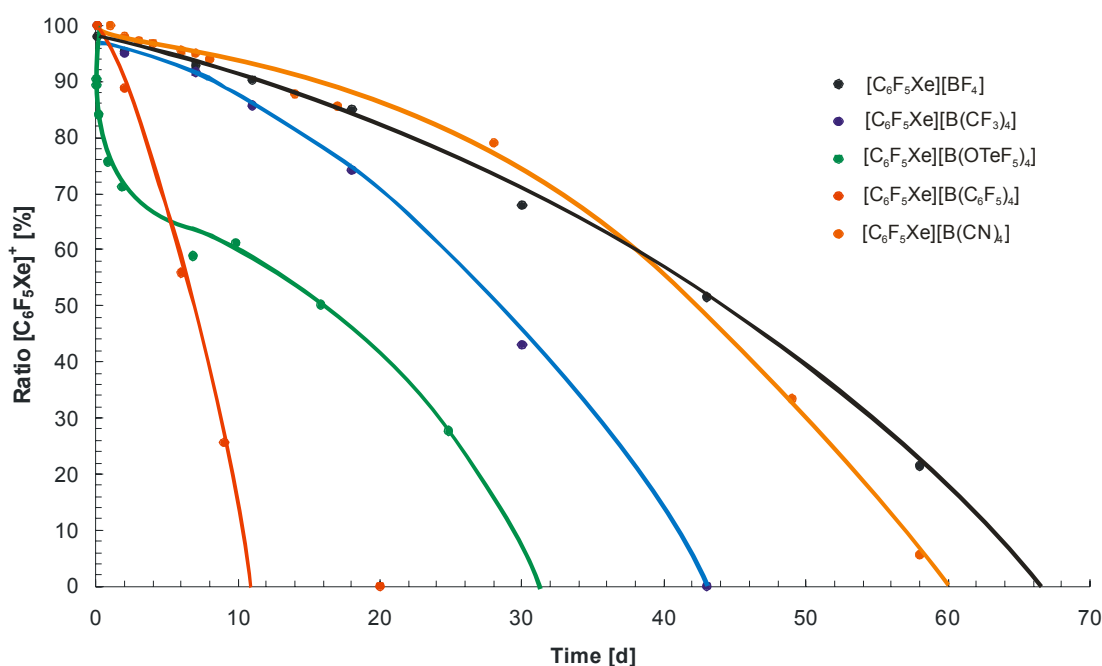
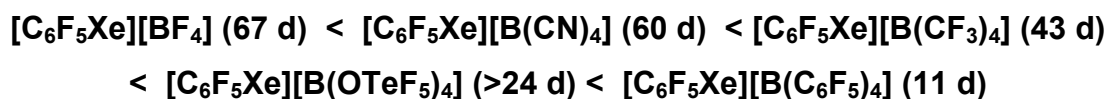
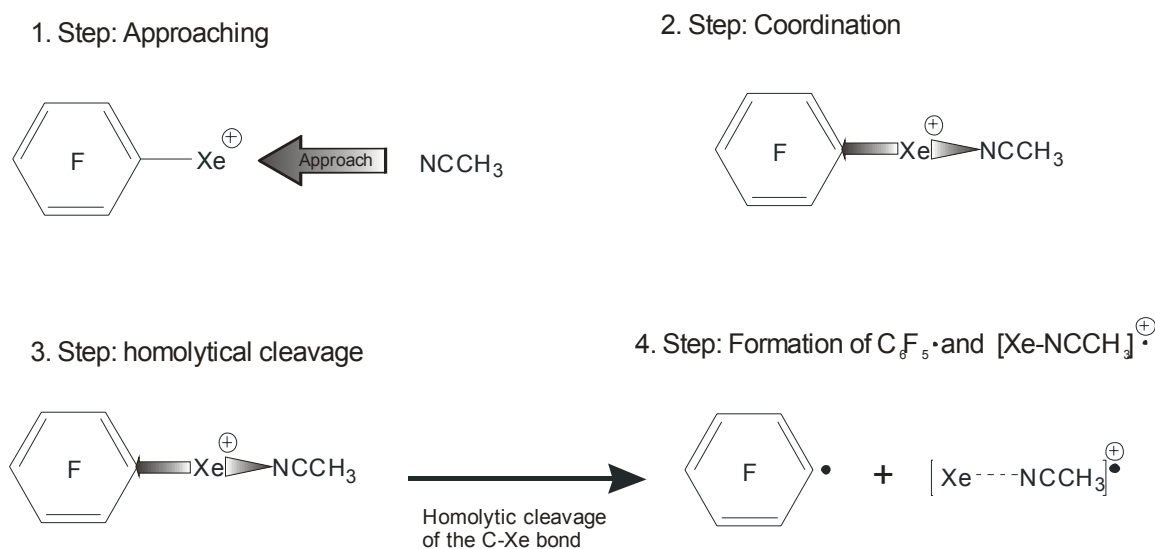
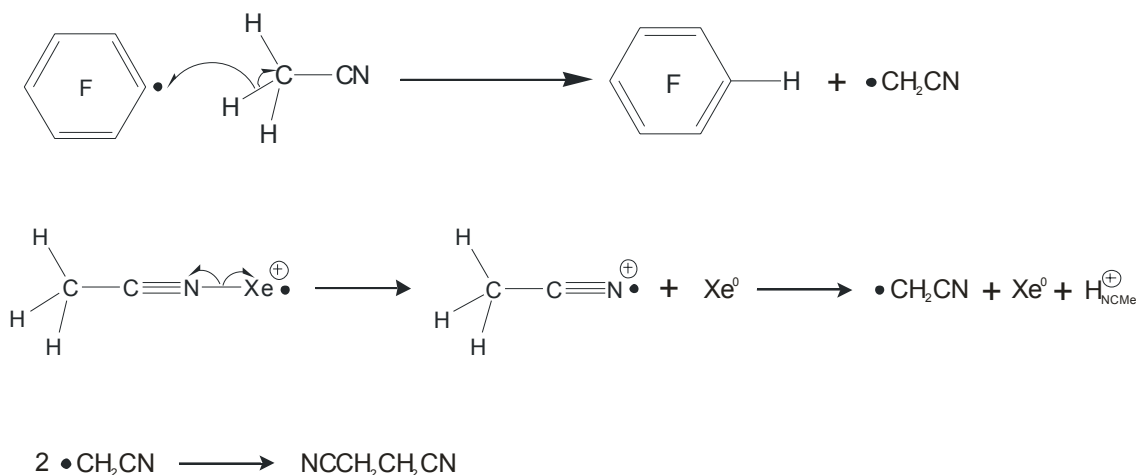


Figure 14 Decomposition of the $[\text{C}_6\text{F}_5\text{Xe}]^+$ cation in CH_3CN solutions of $[\text{C}_6\text{F}_5\text{Xe}][\text{BY}_4]$ salts ($\text{Y} = \text{F}, \text{CN}, \text{CF}_3, \text{OTeF}_5, \text{C}_6\text{F}_5$) at ambient temperatures.

It is apparent from those studies that C_6F_5H was the main, and in some cases, the only decomposition product. Pentafluorobenzene was formed after C-Xe bond cleavage by attack of CH_3CN by $C_6F_5\cdot$ radicals. The solvent plays a key role acting as proton source. The role of CH_3CN was confirmed by conducting decomposition studies in CD_3CN which yielded C_6F_5D as the main decomposition product. There are two major decomposition channels that are possible. Both channels include essentially the same four steps: approach of a nucleophile, coordination of a nucleophile to the positively charged xenon(II) center in $[C_6F_5Xe]^+$ followed by donation of electron density towards the C_6F_5 moiety and finally cleavage of the C-Xe bond with formation of $C_6F_5\cdot$ radicals and $[Xe-Nu]^+\cdot$ radical cations or $[Xe-Nu]\cdot$ radicals. The main decomposition channel is initiated by coordination of CH_3CN .



After coordination and homolytical cleavage of the C-Xe bond, the resulting $C_6F_5\cdot$ radical and $[Xe-NCCH_3]^+\cdot$ radical cation attack the solvent forming C_6F_5H , Xe^0 , and $\cdot CH_2CN$ and H^+ , respectively.



Two of the •CH₂CN radicals could, for example, recombine to form succinonitrile, N≡CCH₂CH₂C≡N. The second decomposition channel can be initiated at the counteranion. Both solvent and counteranion compete for the coordination to the positively charged Xe(II) center. In either case, the C-Xe bonding changes upon coordination from a 2c-2e bond (formal bond order = 1) in the “uncoordinated” [C₆F₅Xe]⁺ cation to an asymmetric 3c-4e bond (formal bond order 1 < x < 0.5) in the adduct cation, [C₆F₅Xe·(Nu)_n]⁺.

$$BO = BO_{C-Xe} + BO_{Xe-Nu} = 1 \quad (BO_{C-Xe} \neq BO_{Xe-Nu})$$

The approach of a nucleophile to the xenon center results in a donation of negative charge to the *ipso*-C atom of the C₆F₅ group. The positive charge on the xenon center was calculated to be comparable to that of the uncoordinated [C₆F₅Xe]⁺ cation, whereas the N atom of coordinated CH₃CN is more negatively charged than in “free” CH₃CN molecules (see Table 8). A useful tool to observe the interaction with CH₃CN in small amounts is the low-temperature Raman spectroscopy. The intense ν(CH₃) modes of CH₃CN at 3064, 3061, and 2978 cm⁻¹ can be observed at very low concentrations. The ν(Xe-C) mode of the [C₆F₅Xe·(NCCH₃)_n]⁺ adduct is also intense and was calculated to shift to lower frequency by 21 cm⁻¹ upon coordination, but in practice it is observed at 202 cm⁻¹ for the “uncoordinated” [C₆F₅Xe]⁺ cation and 205 cm⁻¹ for the [C₆F₅Xe·(NCCH₃)_n]⁺ adduct. The lack of a clear change of the frequencies upon coordination is in agreement with the lack of change in the geometrical parameters obtained from the X-ray crystal structures. The missing Raman spectra and single X-ray crystal structures of the corresponding Xe(C₆F₅)₂ or

C_6F_5XeF compounds did not permit further comparisons of the geometrical changes. Naumann *et al.*^[81] succeeded in obtaining $Xe(C_6F_5)_2$ as a microcrystalline powder. The molecular structure they obtained at $-223\text{ }^\circ\text{C}$ using a powder diffraction methods, C-Xe bond lengths to be 2.394(9) and 2.35(1) Å, which are 14 and 12% longer than the C-Xe bond lengths obtained for the $[C_6F_5Xe][A]$ salts ($A = AsF_6$ (2.079(6) Å),^[93] $BF_2(C_6F_5)_2$ (2.092(8) Å),^[59] $B(CN)_4$ (2.082(3) Å), $B(C_6F_5)_4$ (2.099(13) Å), and $B(CF_3)_4$ (2.099(6) Å)) and are 13% and 11% longer than the C-Xe bond lengths in the chlorine-bridged cation, $[(C_6F_5Xe)_2Cl]^+$ (2.111(2) and 2.116(9) Å),^[75] which is indicative of a reduced bond order. Comparable situations exist for the Xe-F bond lengths which were obtained in various reactions of fluoroorganic N-bases with the $[XeF]^+$ cation, including $[RC\equiv N-XeF]^+$ ($R = H, CH_3, C_2H_5, n-C_3F_7, (CH_3)_3C, CF_3, C_2F_5, n-C_3F_7$),^[108, 111-115] perfluoropyridines, $[x-CF_3-C_5F_4N-XeF]^+$ ($x = 2, 3$ and 4),^[113] $[C_5F_5N-XeF]^+$,^[115] perfluorinated diazines, $[C_4F_4NN-XeF]^+$,^[116-118] and trifluortriazine, $[s-C_3F_3N_2N-XeF]^+$.^[115] Most of the above listed compounds have been characterized in the solid state by low-temperature Raman spectroscopy, X-ray crystallography and in solution by NMR spectroscopy and show elongation and weakening of the Xe-F bond. The geometrically simplest example of CH_3CN coordination to xenon that has been investigated in the $[Xe-F]^+$ cation in form of the $[FXe---NCCH_3][AsF_6]$ adduct. The characteristic Raman frequency of the Xe-F bond in $[FXe---NCCH_3][AsF_6]$ (560 cm^{-1})^[111] was shifted 50 cm^{-1} to lower frequency when compared with the Xe-F bond in $[FXe][AsF_6]$ (610 cm^{-1}) indicating a weaker and longer Xe-F bond in the case of $[FXe---NCCH_3]^+$. The X-ray crystal structures of both of the above mentioned compounds have provided Xe-F bond lengths of 1.873(6) Å for $[FXe][AsF_6]$ ^[119] and 1.952(3) Å for $[FXe---NCCH_3][AsF_6]$.^[115] The elongation of 0.079 Å for the acid-base adduct in the crystal structures and the 50 cm^{-1} low frequency complexation shift in the Raman spectra arises from a weaker Xe-F bond when compared with that of $[XeF][AsF_6]$. Calculated frequencies showed that a comparable, but less pronounced effect of coordinated CH_3CN is predicted for the $[C_6F_5Xe]^+$ cation (complexation shift 21 cm^{-1}). The complexation shift is less because the C_6F_5 group is able to balance additional electron density by means of mesomeric effects. No such balancing is possible in the case of the $[XeF]^+$ cation, which results in a larger complexation shift.

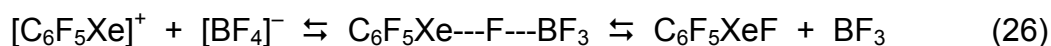
The behaviours of $[C_6F_5Xe]^+$ salts in CH_3CN solution were examined with respect to anion nucleophilicities. The decompositions of each $[C_6F_5Xe]^+$ salt is discussed separately:

III.1.4.1 Behaviour of $[\text{C}_6\text{F}_5\text{Xe}][\text{BF}_4]$ in CH_3CN

Perfluoro-anions such as $[\text{BF}_4]^-$, $[\text{PF}_6]^-$, and $[\text{AsF}_6]^-$ are widely used and are known to be moderately coordinating anions depending on the counter cation and the solvent. At first glance, it is astonishing that CH_3CN solutions of $[\text{C}_6\text{F}_5\text{Xe}][\text{BF}_4]$, are the most stable of all $[\text{C}_6\text{F}_5\text{Xe}]^+$ salts examined in this study.



The dynamic competition of solvent molecules and the $[\text{BF}_4]^-$ anion are the initial steps that lead to two possible decomposition pathways. The decomposition which is initiated by coordination of the anion to the xenon center is thought to be less important than the decomposition initiated by CH_3CN coordination.



Even though the four equivalent fluorine atoms of $[\text{BF}_4]^-$ carry approximately a quarter of the negative charge, the electron lone pairs of the fluorine ligands appear to be less available for coordination to the xenon center. The interaction of the anion is mainly electrostatic in nature and does not result in electron transfer from the anion to the cation. The electron donor strength of the anion is less when compared with that of CH_3CN . As a result, the C-Xe bond is stronger and the decomposition is slower. Coordination of the $[\text{BF}_4]^-$ anion is an exception when compared with the weakly coordinating $[\text{B}(\text{CF}_3)_4]^-$ and $[\text{B}(\text{C}_6\text{F}_5)_4]^-$ anions which result in an inner coordination sphere around the xenon center that is more highly populated with $[\text{BF}_4]^-$ anions than in the $[\text{B}(\text{C}_6\text{F}_5)_4]^-$ or $[\text{B}(\text{CF}_3)_4]^-$ cases. It is therefore not surprising that CH_3CN solutions of $[\text{C}_6\text{F}_5\text{Xe}][\text{BF}_4]$ are the most stable because there are fewer significant interactions with the solvent, the main initiator for the decomposition. The first step leading to decomposition results from coordination of CH_3CN to the positively charged xenon center. All influences resulting from anion interactions with CH_3CN , which are often used to explain decompositions of strong electrophiles having perfluoro-anions, $[\text{EF}_{n+1}]^-$, as the counterion, are regarded as negligible.



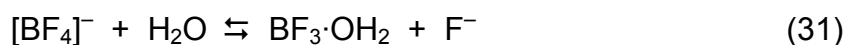
The equilibrium in the above equation is thought to strongly favour the $[\text{BF}_4]^-$ and CH_3CN side. Only small amounts of fluoride are formed which could interact with the xenon(II) center to yield neutral $\text{C}_6\text{F}_5\text{XeF}$. Previous experiments involving the interaction of $[\text{C}_6\text{F}_5\text{Xe}][\text{AsF}_6]$ with $[\text{N}(\text{CH}_3)_4]\text{F}$ in CH_3CN at -40°C demonstrated the fluoride nucleophilicity and immediately led to the evolution of gaseous xenon and the formation of $\text{C}_6\text{F}_5\text{H}$, C_6F_6 , HF and $(\text{C}_6\text{F}_5)_2$ as main decomposition products.^[120] The neutral molecule, $\text{C}_6\text{F}_5\text{XeF}$, has been known since 2000 and was first prepared by Frohn and Theißen.^[76] Solutions of $\text{C}_6\text{F}_5\text{XeF}$ were found to be thermally unstable at temperatures above -40°C , clearly showing the effect of a “coordinated” fluoride ion and the resulting asymmetric xenon(II) compounds. The simple homolytic cleavage of the C-Xe bond in $\text{C}_6\text{F}_5\text{XeF}$ yields $\text{C}_6\text{F}_5\cdot$ and $\cdot\text{XeF}$ radicals which can further react with the solvent to yield $\text{C}_6\text{F}_5\text{H}$, C_6F_6 , Xe^0 and HF according to the following schemes.



It is, however, very interesting to note that the only product obtained in the decomposition of $[\text{C}_6\text{F}_5\text{Xe}][\text{BF}_4]$ was $\text{C}_6\text{F}_5\text{H}$. The absence of HF and C_6F_6 clearly shows that the main decomposition channel arose from CH_3CN coordination and not from $[\text{BF}_4]^-$ anion coordination. The findings differ from those of H. Franke,^[90] who reported that $\text{C}_6\text{F}_5\text{H}$, C_6F_6 and $\text{BF}_3 \cdot \text{NCCH}_3$ are the main decomposition products but may be explainable if one considers that the material used in the previous study was not rigorously dry.

Frohn *et al.*^[93] reported that $[\text{C}_6\text{F}_5\text{Xe}][\text{AsF}_6]$ decomposed in H_2O within 72 h at ambient temperature which was 12 times faster than the decomposition rate reported for $[\text{C}_6\text{F}_5\text{Xe}][\text{AsF}_6]$ in CH_3CN (35 d). Water, which is a stronger base than CH_3CN , is in the first instance able to coordinate strongly to the $[\text{C}_6\text{F}_5\text{Xe}]^+$ cation. This would lead to a more rapid decomposition but to identical decomposition products. Water

can also interact more strongly with the $[\text{BF}_4]^-$ anion leading to a stable $\text{BF}_3 \cdot \text{OH}_2$ adduct. The equilibrium would then be shifted to favour “free” fluoride.

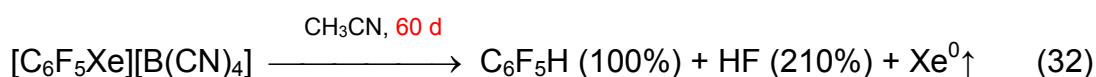


An increase in $\text{C}_6\text{F}_5\text{XeF}$ concentration would lead to a more rapid formation of $\text{C}_6\text{F}_5\cdot$ and $\cdot\text{Xe-F}$ radicals and a higher rate of formation of $\text{C}_6\text{F}_5\text{H}$, C_6F_6 , Xe^0 gas and HF. The HF formed in the decomposition can accept another fluoride yielding the $[\text{HF}_2]^-$ anion which is known to be a stronger coordinating anion than CH_3CN . The reaction of $[\text{C}_6\text{F}_5\text{Xe}][\text{AsF}_6]$ with $\text{Cs}[\text{HF}_2]$ or $[\text{N}(\text{CH}_3)_4][\text{HF}_2]$ was previously shown to lead to decomposition in CH_3CN at RT with the formation of $\text{C}_6\text{F}_5\text{H}$, C_6F_6 , $(\text{C}_6\text{F}_5)_2$, HF, and Xe^0 .^[120] Formation of C_6F_6 was also observed in the decomposition of CH_3CN solutions of $[\text{C}_6\text{F}_5\text{Xe}][\text{HF}_2]$ at ambient temperatures.^[96] The decomposition under “wet” conditions would therefore result in the formation of $\text{C}_6\text{F}_5\text{H}$, C_6F_6 , $\text{BF}_3 \cdot \text{OH}_2$, Xe^0 gas and HF which were exactly the products obtained by H. Franke.^[90]

III.1.4.2 Behaviour of $[\text{C}_6\text{F}_5\text{Xe}][\text{B}(\text{CN})_4]$ in CH_3CN

The $[\text{B}(\text{CN})_4]^-$ anion was first prepared by Willner and co-workers^[98] by reaction of $[\text{NBu}_4]\text{Hal}$ and BHal_3 (Hal = Cl and Br) with KCN under phase-transfer conditions in toluene at 130 – 160 °C. They obtained the $[\text{B}(\text{CN})_4]^-$ salt in 75% yield after one week. The anion has shown to be kinetically stable over several hours when reacted with H_2O or concentrated HCl under reflux conditions or in anhydrous HF at 50 °C for 1 h.

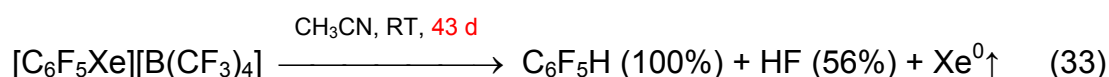
Solid state structure determination of the $[\text{B}(\text{CN})_4]^-$ anion indicated a rather strongly coordinating anion (similar to $[\text{BF}_4]^-$) in CH_3CN when compared with other anions examined in this study. It is therefore not surprising that the decomposition rate of $[\text{C}_6\text{F}_5\text{Xe}][\text{B}(\text{CN})_4]$ (5% $[\text{BF}_4]^-$) in CH_3CN at ambient temperature is the second slowest obtained. The salt, $[\text{C}_6\text{F}_5\text{Xe}][\text{B}(\text{CN})_4]$, decomposes within 60 d in CH_3CN at RT to $\text{C}_6\text{F}_5\text{H}$ (100%), HF (210%), and an unidentified species ($\delta = -144.9$ ppm (52%)).



The rate of decomposition is comparable to that of $[\text{C}_6\text{F}_5\text{Xe}][\text{BF}_4]$ and it is assumed that both decompositions follow similar pathways. There is one discrepancy in the decomposition of $[\text{C}_6\text{F}_5\text{Xe}][\text{B}(\text{CN})_4]$, the high amount of HF which can not obviously occur from anion destruction. A destruction of the C_6F_5 group by cleavage of one C-F bond does seem to be not very likely. Partially fluorinated benzenes should have been found. Thus the high content of HF can not be readily explained at present.

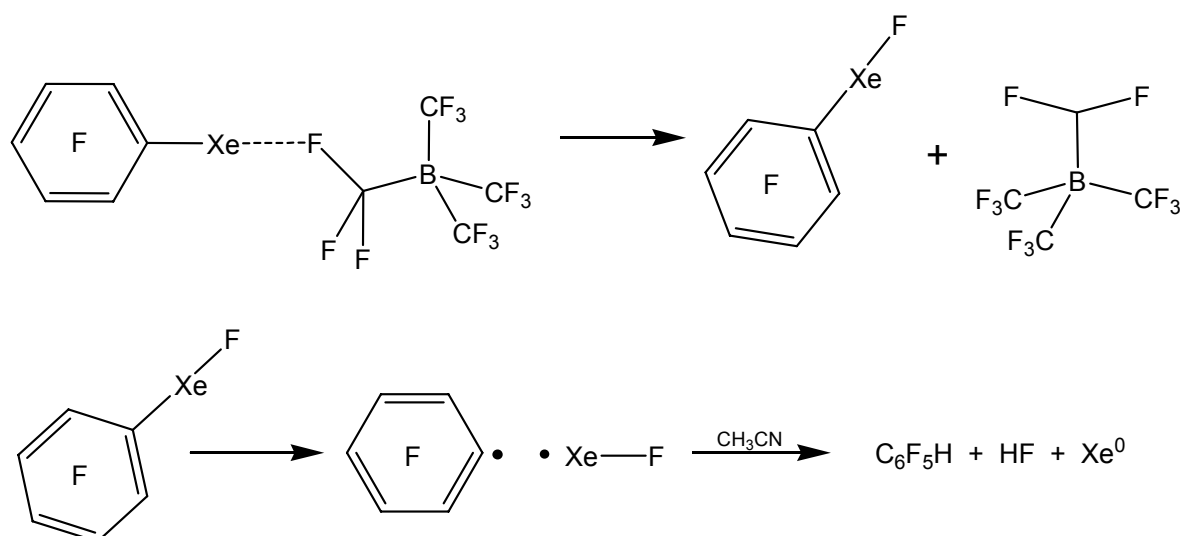
III.1.4.3 Behaviour of $[\text{C}_6\text{F}_5\text{Xe}][\text{B}(\text{CF}_3)_4]$ in CH_3CN

The decomposition of $[\text{C}_6\text{F}_5\text{Xe}][\text{B}(\text{CF}_3)_4]$ was first thought to be much slower than that of the perfluoro-anion salts, $[\text{C}_6\text{F}_5\text{Xe}][\text{EF}_{n+1}]^-$, because fluoride abstraction followed by elimination of difluorocarbene or attack by electrophilic reagents was reported to be kinetically hindered.^[121, 122] The formation of the intermediate, $\text{C}_6\text{F}_5\text{XeF}$, would not have been probable. It was, however, reported that the decomposition of the $[\text{B}(\text{CF}_3)_4]^-$ anion does occur in *conc.* H_2SO_4 . Fluoride abstraction followed by hydrolysis of the resulting carbene adduct leads to the main reaction products, $\text{B}(\text{CF}_3)_3\text{CF}_2$, $\text{B}(\text{CF}_3)_3\text{CO}$, and 3 HF. In the case of $[\text{C}_6\text{F}_5\text{Xe}][\text{B}(\text{CF}_3)_4]$ decomposition in CH_3CN at ambient temperature, the $[\text{C}_6\text{F}_5\text{Xe}]^+$ cation was completely consumed after 43 d which is 24 d more rapid than the decomposition rate of $[\text{C}_6\text{F}_5\text{Xe}][\text{BF}_4]$ (67 d).

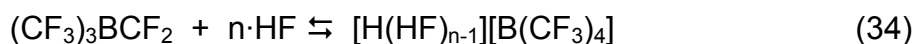


The products mainly consist of $\text{C}_6\text{F}_5\text{H}$ and HF leading to the assumption that the decomposition pathway is analogous to that described for *conc.* H_2SO_4 .

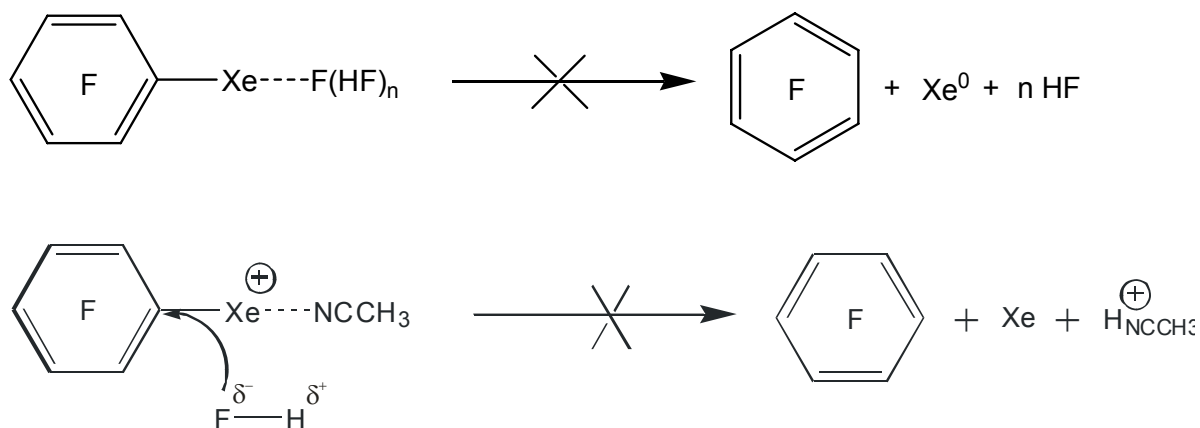
There are two possible pathways to abstraction of fluoride from the $[\text{B}(\text{CF}_3)_4]^-$ anion. One channel is initiated by cation-anion interaction. After coordination of the $[\text{B}(\text{CF}_3)_4]^-$ anion, a fluoride ion can be abstracted yielding $\text{C}_6\text{F}_5\text{XeF}$ and $\text{B}(\text{CF}_3)_3\text{CF}_2$. Homolytic cleavage of the C-Xe bond would yield $\text{C}_6\text{F}_5\text{H}$, Xe^0 and HF as previously described.



Resulting HF could subsequently react with the transient difluorocarbene complex, $(\text{CF}_3)_3\text{BCF}_2$, to yield the conjugated base, $[\text{B}(\text{CF}_3)_4]^-$.



The second, more probable decomposition pathway can be initiated by H^+ , which is basically the back reaction of equation 34 and was produced from the decomposition of a $[\text{C}_6\text{F}_5\text{Xe} \cdot (\text{NCCH}_3)_n]^+$ adduct as previously described. The HF can accept a fluoride ion yielding the $[\text{HF}_2]^-$ anion which functions as a strongly coordinating anion and coordinates to the $[\text{C}_6\text{F}_5\text{Xe}]^+$ cation. The known decomposition yields $\text{C}_6\text{F}_5\text{H}$, C_6F_6 , Xe^0 and, again, HF. The absence of C_6F_6 in the decomposition of $[\text{C}_6\text{F}_5\text{Xe}][\text{B}(\text{CF}_3)_4]$ in CH_3CN indicates that no attack of the C-Xe bond by HF or $[\text{F}(\text{HF})_n]^-$ had occurred.



Substitution of CF_2 by fluoride yielding the $[(\text{CF}_3)_3\text{BF}]^-$ anion is also possible but was reported to be difficult. *Ab initio* calculations, performed by Willner *et al.*,^[122] predicted a higher stability for $(\text{CF}_3)_3\text{BCF}_2$ with respect to loss of the neutral ligand than, for example, $(\text{CF}_3)_3\text{BCO}$. Unfortunately, none of the possible decomposition products, $[(\text{CF}_3)_3\text{BF}]^-$, $(\text{CF}_3)_3\text{BCF}_2$ or $(\text{CF}_3)_3\text{BNCCH}_3$, were detected in significant quantities but HF was obtained in 56% yield.

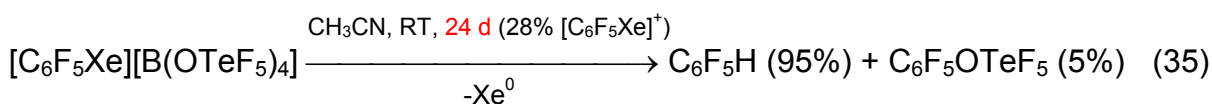
The main decomposition pathway most likely goes by means of CH_3CN coordination. Acetonitrile is assumed to coordinate preferentially to the positively charged Xe(II) center when compared to the more nucleophilic anions. It is speculated that the inner coordination sphere of xenon is mainly populated by CH_3CN molecules, resulting in an increased probability of decomposition when compared to the case in which the inner coordination sphere is populated by mainly counteranions.

Moreover, it was found by ^1H NMR and Raman spectroscopy that CH_3CN coordinates strongly and irreversibly to the xenon center of the $[\text{C}_6\text{F}_5\text{Xe}]^+$ cation in case of the $[\text{B}(\text{CF}_3)_4]^-$ and $[\text{B}(\text{C}_6\text{F}_5)_4]^-$ anions which is indicative of the low nucleophilicities of these anions and the increased Lewis acidity of the $[\text{C}_6\text{F}_5\text{Xe}]^+$ cation.

III.1.4.4 Behaviour of $[\text{C}_6\text{F}_5\text{Xe}][\text{B}(\text{OTeF}_5)_4]$ in CH_3CN

The weakly nucleophilic $[\text{B}(\text{OTeF}_5)_4]^-$ anion was first synthesized in 1981 by Sladky *et al.*^[123] The negative charge is distributed over 20 fluorine atoms. The relatively unshielded basic O atoms are likely sites for electrophilic attack. The propensity of this anion to dissociate to $[\text{OTeF}_5]^-$ and $\text{B}(\text{OTeF}_5)_3$ limits its use as a weakly coordinating anion for strong electrophiles. It has been shown by Strauss *et al.*^[124] that $[\text{SiPh}_3]^+$, $[\text{Fe}(\text{tetraphenylporphyrinate})]^+$ and Ag^+ are able to rapidly abstract a teflate group in CH_2Cl_2 or mesitylene with the formation of $\text{B}(\text{OTeF}_5)_3$ and $\text{Ph}_3\text{SiOTeF}_5$, $\text{Fe}(\text{tetraphenylporphyrinate})\text{OTeF}_5$, and AgOTeF_5 , respectively.

Decomposition of $[\text{C}_6\text{F}_5\text{Xe}][\text{B}(\text{OTeF}_5)_4]$ occurred in CH_3CN at RT with the formation of $\text{C}_6\text{F}_5\text{H}$ and $\text{C}_6\text{F}_5\text{OTeF}_5$. After 24 d, 72% of $[\text{C}_6\text{F}_5\text{Xe}]^+$ had decomposed.

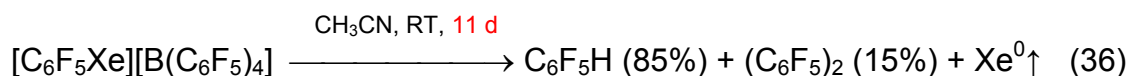


The decomposition products clearly show the conversion of the majority of $[\text{C}_6\text{F}_5\text{Xe}]^+$ to $\text{C}_6\text{F}_5\text{H}$. Only 5% of the $[\text{C}_6\text{F}_5\text{Xe}]^+$ decomposition product was found to be $\text{C}_6\text{F}_5\text{OTeF}_5$ in addition to some other unidentified OTeF_5 compounds which are indicative for OTeF_5 abstraction from the anion.

III.1.4.5 Behaviour of $[\text{C}_6\text{F}_5\text{Xe}][\text{B}(\text{C}_6\text{F}_5)_4]$ in CH_3CN

The $[\text{B}(\text{C}_6\text{F}_5)_4]^-$ anion belongs to the class of weakly coordinating anions and its salts are of importance in numerous organic reactions with homogeneous catalysts. They are classified as weakly coordinating anions distributing the negative charge over 25 fluorine atoms. The utility of this anion is limited by its relatively open tetrahedral geometry and rigid C_6F_5 groups. The four *ipso*-C atoms are readily accessible by small electrophiles which can, by analogy to the $[\text{B}(\text{OTeF}_5)_4]^-$ anion, dissociate to $[\text{C}_6\text{F}_5]^-$ and $\text{B}(\text{C}_6\text{F}_5)_3$. It has been previously shown that the $[\text{B}(\text{C}_6\text{F}_5)_4]^-$ anion decomposes in the presence of the counter cations $[\text{RZn}]^+$ or $[\text{AlR}_2]^+$ ($\text{R} = \text{CH}_3$ and C_2H_5) to yield $\text{Zn}(\text{C}_6\text{F}_5)_2$ and $[\text{BR}_4]^-$ or $\text{AlR}_n(\text{C}_6\text{F}_5)_{3-n}$ and $[\text{B}(\text{C}_6\text{F}_5)_{4-m}\text{R}_m]^-$ ($n = 0 - 2$; $m = 1 - 4$), respectively.^[125-127]

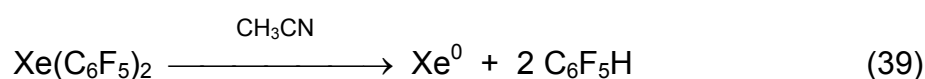
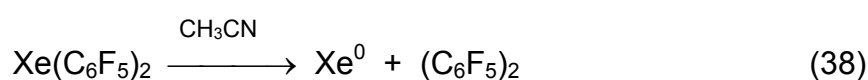
Complete decomposition of $[\text{C}_6\text{F}_5\text{Xe}][\text{B}(\text{C}_6\text{F}_5)_4]$ in CH_3CN at RT occurred within 11 d. The main decomposition products were $\text{C}_6\text{F}_5\text{H}$ (85%) and $(\text{C}_6\text{F}_5)_2$ (15%) according to scheme 36.



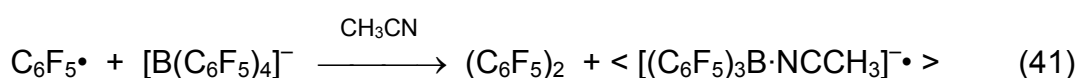
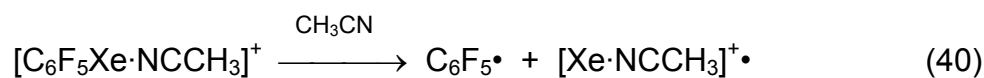
It is noteworthy that $[\text{C}_6\text{F}_5\text{Xe}]^+$ salts having C_6F_5 substituted anions such as $[(\text{C}_6\text{F}_5)_x\text{BF}_{4-x}]^-$ ($x = 1 - 4$) always decompose with the partial formation of decafluorobiphenyl, $(\text{C}_6\text{F}_5)_2$, whereas no $(\text{C}_6\text{F}_5)_2$ or only trace amounts were obtained in cases of salts having counteranions without C_6F_5 groups. The anion was most likely attacked by either the $[\text{C}_6\text{F}_5\text{Xe}]^+$ cation (A) or its decomposition product, the $\text{C}_6\text{F}_5^\bullet$ radical (B), yielding decafluorobiphenyl, $(\text{C}_6\text{F}_5)_2$. It is also possible that the $[\text{C}_6\text{F}_5\text{Xe}]^+$ cation abstracts a C_6F_5 group from the $[\text{B}(\text{C}_6\text{F}_5)_4]^-$ anion to form neutral bis(pentafluorophenyl)xenon(II), $\text{Xe}(\text{C}_6\text{F}_5)_2$. This compound was prepared independently by Frohn and Theißen^[76] and Naumann, Maggiorosa and Tyrra^[78, 128]

and was characterized by ^{19}F , ^{13}C , and ^{129}Xe NMR spectroscopy and by powder X-ray diffraction. Solutions of $\text{Xe}(\text{C}_6\text{F}_5)_2$ in CH_3CN were reported^[78] to decompose within 24 h at $-40\text{ }^\circ\text{C}$ to mainly $(\text{C}_6\text{F}_5)_2$ and trace amounts of $\text{C}_6\text{F}_5\text{H}$. The same products were obtained by Theißen when $\text{Xe}(\text{C}_6\text{F}_5)_2$ was prepared.^[129] The decomposition product distribution for $[\text{C}_6\text{F}_5\text{Xe}][\text{B}(\text{C}_6\text{F}_5)_4]$ contained of 15% $(\text{C}_6\text{F}_5)_2$ and 85% $\text{C}_6\text{F}_5\text{H}$. Two possible decomposition sequences are depicted below showing proposed reaction schemes which lead to the formation of $(\text{C}_6\text{F}_5)_2$.

(A)

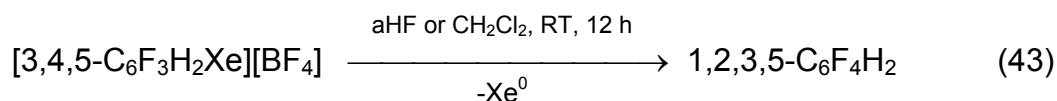


(B)



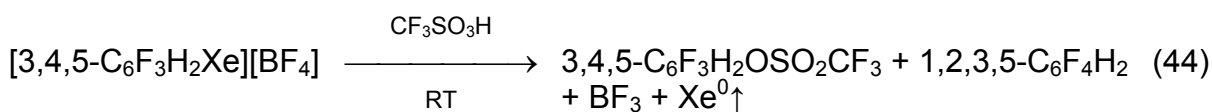
III.1.4.6 Behaviour of $[\text{C}_6\text{F}_5\text{Xe}][\text{BF}_4]$ in aHF

Studies of $[\text{C}_6\text{F}_5\text{Xe}][\text{BF}_4]$ in aHF have shown that the $[\text{C}_6\text{F}_5\text{Xe}]^+$ cation is stable for at least 2 d without decomposition and after 54 d at RT only ~15% of the original amount of $[\text{C}_6\text{F}_5\text{Xe}]^+$ was converted to C_6F_6 , the only decomposition product observed by ^{19}F NMR spectroscopy. The high stability can be explained in terms of a less negatively charged *ipso*-C atom. It is known that aHF solutions of hydrogen-containing arylxenon(II) compounds such as $[3,4,5\text{-C}_6\text{F}_3\text{H}_2\text{Xe}]^+$ and $[3,5\text{-C}_6\text{F}_3\text{H}_2\text{Xe}]^+$ are less stable than the isomeric arylxenon(II) compounds having two fluorine substituents in the *ortho*-positions such as in $[2,6\text{-C}_6\text{F}_2\text{H}_3\text{Xe}]^+$. Previous decomposition studies of hydrogen-containing arylxenon(II) compounds, namely $[3,5\text{-C}_6\text{F}_3\text{H}_2\text{Xe}]^+$ and $[3,4,5\text{-C}_6\text{F}_3\text{H}_2\text{Xe}]^+$ have shown that complete decomposition proceeded in aHF at RT within only 12 h.^[130]

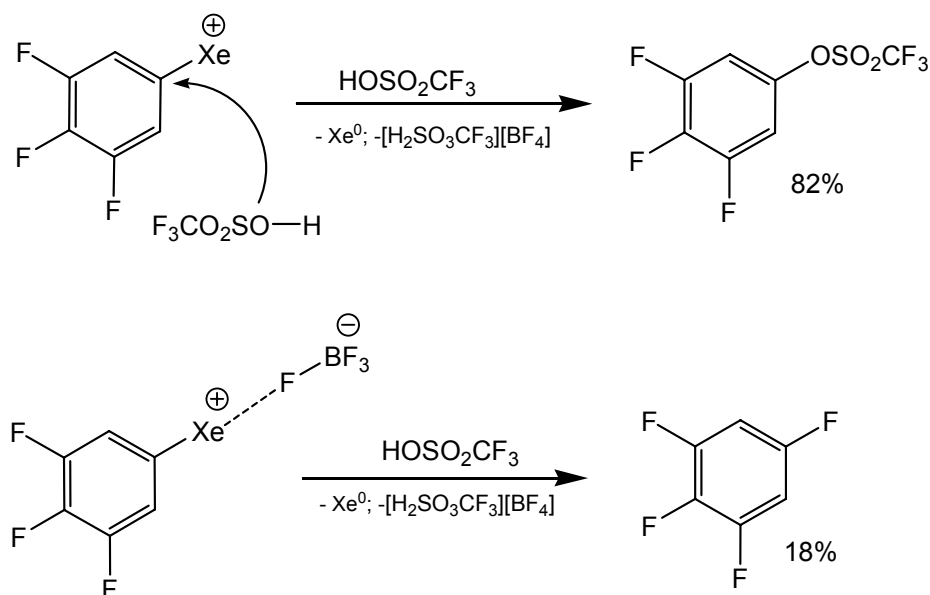


The positively charged Xe(II) center directly bonded to the *ipso*-C atom polarizes the C-Xe bond. As a result, the *ipso*-C atom becomes more positive than in the corresponding C₆F₅ group where the *ortho* fluorine atoms prevent strong polarization of the aryl group.

The dipolar HF molecule has the ability to interact with [C₆F₅Xe]⁺ in two different ways. It can coordinate to the positively charged Xe(II) center with the fluorine atom or it can attack the polar C-Xe bond with subsequent bond cleavage. Both interactions yield C₆F₆, Xe⁰ and [H(HF)_n][BF₄]. Previous decomposition studies on [3,4,5-C₆F₃H₂Xe][BF₄] in CF₃SO₃H at RT have verified the assumption that cleavage of the C-Xe bond results from solvent attack.^[130]



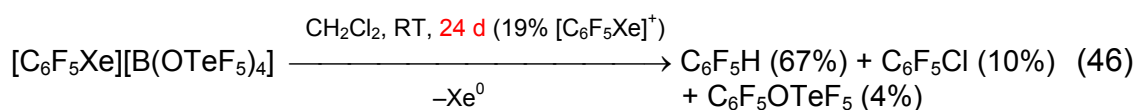
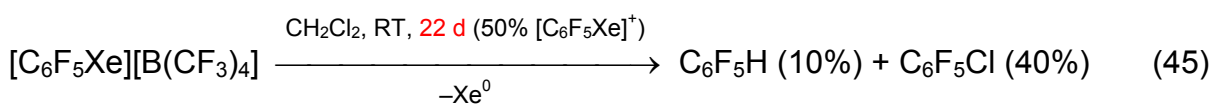
Decomposition in CF₃SO₃H, however, resulted in a mixture of 3,4,5-C₆F₃H₂OSO₂CF₃ (82%) and 1,2,3,5-C₆F₄H₂ (18%). In strong acidic media, a more naked [3,4,5-C₆F₃H₂Xe]⁺ cation is present. The absence of *ortho*-fluorine atoms results in a more polarized and destabilized C-Xe bond having a more electrophilic *ipso*-C atom. This *ipso*-C atom can be attacked by triflic acid yielding 3,4,5-C₆F₃H₂OSO₂CF₃. The additional formation of 1,2,3,5-C₆F₄H₂, however, clearly showed that not only the participation of weakly nucleophilic HF but also the [BF₄]⁻ anion or HF from its solvation had to be involved. The nucleophilic coordination of fluoride to the positively charged Xe(II) cation from the anion, [BF₄]⁻, results in the intermediate formation of 3,4,5-C₆F₃H₂XeF, which is assumed to be very unstable and would decompose to yield 1,2,3,5-C₆F₄H₂ and Xe⁰.



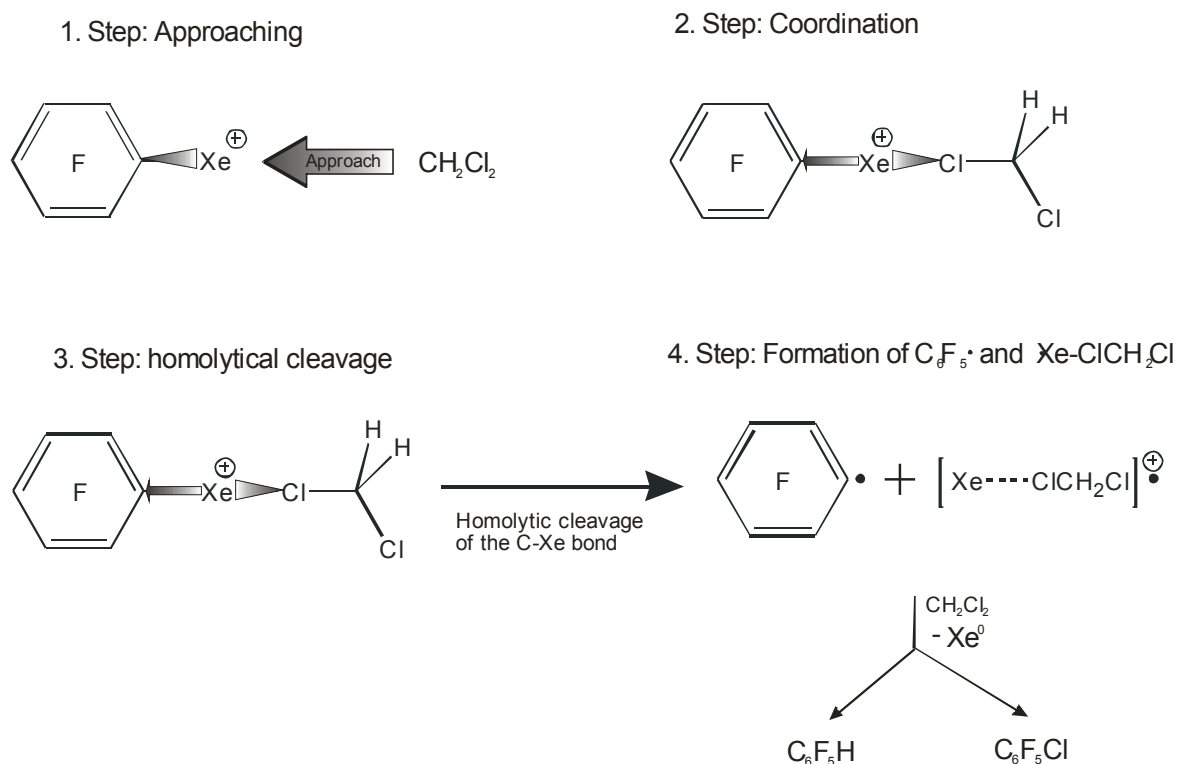
III.1.4.7 Behaviour of $[\text{C}_6\text{F}_5\text{Xe}][\text{B}(\text{CF}_3)_4]$ and $[\text{C}_6\text{F}_5\text{Xe}][\text{B}(\text{OTeF}_5)_4]$ in CH_2Cl_2

Three of the new $[\text{C}_6\text{F}_5\text{Xe}]^+$ salts are soluble in CH_2Cl_2 at $-40\text{ }^\circ\text{C}$ but only $[\text{C}_6\text{F}_5\text{Xe}][\text{B}(\text{CF}_3)_4]$ and $[\text{C}_6\text{F}_5\text{Xe}][\text{B}(\text{OTeF}_5)_4]$ are stable at ambient temperature whereas solutions of $[\text{C}_6\text{F}_5\text{Xe}][\text{B}(\text{C}_6\text{F}_5)_4]$ have to be maintained at temperatures below $-40\text{ }^\circ\text{C}$.

Decomposition studies of $[\text{C}_6\text{F}_5\text{Xe}][\text{B}(\text{CF}_3)_4]$ and $[\text{C}_6\text{F}_5\text{Xe}][\text{B}(\text{OTeF}_5)_4]$ in CH_2Cl_2 at ambient temperature give rise to $\text{C}_6\text{F}_5\text{H}$ and $\text{C}_6\text{F}_5\text{Cl}$ as the main decomposition products. Neither decomposition was followed to completion and was halted after 22 d and 24 d, respectively. The final product distribution was extrapolated to zero $[\text{C}_6\text{F}_5\text{Xe}]^+$ cation concentration.



The decomposition rate in CH_2Cl_2 is comparable to the rate obtained in CH_3CN solution at RT. The product distribution is different because $\text{C}_6\text{F}_5\text{Cl}$ was obtained as well as significant amounts of $\text{C}_6\text{F}_5\text{H}$. The $[\text{C}_6\text{F}_5\text{Xe}]^+$ cation is more weakly coordinating to CH_2Cl_2 , resulting in a higher electrophilicity of the positively charged xenon(II) center. The weakly coordinated cation has an increased oxidation potential when compared with that of the $[\text{C}_6\text{F}_5\text{Xe}\cdot\text{NCCH}_3]^+$ adduct. The decomposition sequence can be initiated by means of a solvent coordination and subsequent homolytic cleavage of the C-Xe bond.



The very weak and polar Lewis base, CH_2Cl_2 , is able to coordinate to strong electrophiles. The crystal structure of $[\text{Ag}(\text{CH}_2\text{Cl}_2)_2]_2[\text{Pd}(\text{OTeF}_5)_4]$ obtained by Strauss *et al.*^[131] from CH_2Cl_2 solution had shown that each Ag^+ ion in this centrosymmetric complex is coordinated to two bidentate dichloromethane ligands. The Ag-Cl bond distances ranged from 2.775(2) to 2.882(2) Å. Recently, Schrobilgen and Moran^[132] were able to obtain the crystal structure of $[\text{F}_5\text{TeOXe}\cdot\text{SO}_2\text{ClF}][\text{Sb}(\text{OTeF}_5)_6]$ in which the even weaker Lewis base SO_2ClF was coordinated to the $[\text{XeOTeF}_5]^+$ cation through an oxygen atom (Xe-O, 2.471(5) Å)

which clearly demonstrates that weakly coordinating solvents can coordinate to electrophilic xenon(II) cations.

There are two further significant decomposition channels that are discussable upon coordination of CH_2Cl_2 to xenon. One is the abstraction of a chloride ion from CH_2Cl_2 and formation of the unstable $\text{C}_6\text{F}_5\text{XeCl}$ molecule^[75] or decomposition of the $[\text{C}_6\text{F}_5\text{Xe}\cdot\text{Cl}\cdot\text{CH}_2\text{Cl}]^+$ adduct, which both tend to decompose by analogy with $\text{C}_6\text{F}_5\text{XeF}$ and $\text{C}_6\text{F}_5\text{Xe}\cdot\text{F}\cdot\text{HF}$, respectively. It is likely that in either case the same decomposition products would be obtained.

The high concentration of $\text{C}_6\text{F}_5\text{Cl}$ (80%) that results from the decomposition of $[\text{C}_6\text{F}_5\text{Xe}][\text{B}(\text{CF}_3)_4]$ in CH_2Cl_2 and can be explained by the very weak coordination of the counteranion, which are not able to diminish the positive charge on xenon. The increased Lewis acidity of the $[\text{C}_6\text{F}_5\text{Xe}]^+$ cation leads to solvent attack. Attack on chlorine is preferred because of the partial negative charge on the chlorine atom.

III.1.4.8 Behaviour of $[\text{C}_6\text{F}_5\text{Xe}][\text{BY}_4]$ ($Y = \text{F}, \text{CF}_3, \text{C}_6\text{F}_5,$ and CN) in the Solid State

It has been found by Frohn, Klose,^[133] and Scholten^[96] that $[\text{C}_6\text{F}_5\text{Xe}][\text{SbF}_6]$ and $[\text{C}_6\text{F}_5\text{Xe}][\text{AsF}_6]$ can be handled in melts without decomposition at temperatures of 95 and 98 °C, respectively, whereas $[\text{C}_6\text{F}_5\text{Xe}][\text{HF}_2]$ and $[\text{C}_6\text{F}_5\text{Xe}][\text{B}(\text{C}_6\text{F}_5)_4]$ decompose before melting at 25 and 66 °C.^[96]

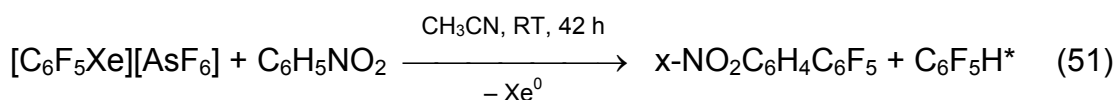
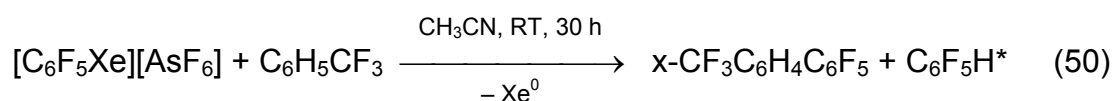
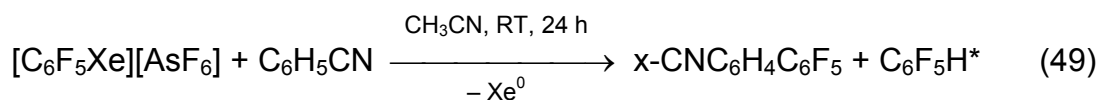
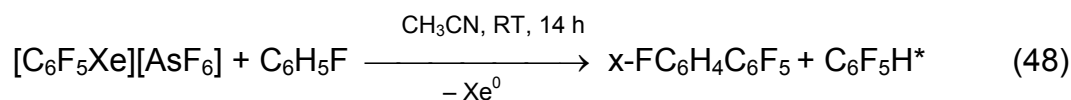
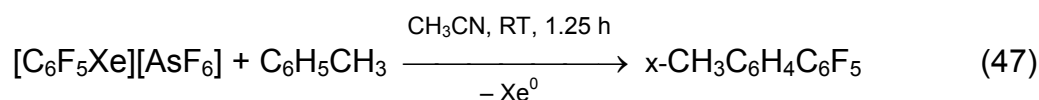
Thermo-analytical measurements of the solid salts, $[\text{C}_6\text{F}_5\text{Xe}][\text{Y}]$ ($Y = \text{BF}_4, \text{AsF}_6, \text{B}(\text{C}_6\text{F}_5)_4,$ and $\text{B}(\text{CN})_4$) prepared in this study, were thoroughly investigated by a systematic DSC study in the temperature range of 20 – 300 °C. It was found that only $[\text{C}_6\text{F}_5\text{Xe}][\text{BF}_4]$ and $[\text{C}_6\text{F}_5\text{Xe}][\text{AsF}_6]$ form stable melts at 80.5 and 110.0 °C, respectively. In the present studies the melting process was shown to be reversible without decomposition. The salts, $[\text{C}_6\text{F}_5\text{Xe}][\text{B}(\text{C}_6\text{F}_5)_4]$, $[\text{C}_6\text{F}_5\text{Xe}][\text{B}(\text{CF}_3)_4]$, $[\text{C}_6\text{F}_5\text{Xe}][\text{B}(\text{CN})_4]$, decompose without melting at 152.2, 117.2, and 85.2 °C, respectively. In the case of $[\text{C}_6\text{F}_5\text{Xe}][\text{B}(\text{CF}_3)_4]$ two additional exothermal local maxima were obtained indicating a stepwise decomposition. The melting and decomposition temperature ranges are summarized in Table 10. The decomposition temperature of $[\text{C}_6\text{F}_5\text{Xe}][\text{B}(\text{C}_6\text{F}_5)_4]$ prepared in this study was 19.2 °C higher than that previously noted by T. Schroer.^[96]

Table 10 Thermo-analytical properties of solid $[C_6F_5Xe][Y]$ ($Y = BF_4, AsF_6, B(CN)_4, B(C_6F_5)_4,$ and $B(CF_3)_4$)

Compound	Melting point		Decomposition	
	Endotherm		Exotherm	
	Onset	Maximum	Onset	Maximum
$[C_6F_5Xe][BF_4]$	80.9 °C	86.1 °C	158.4 °C	181.1 °C
$[C_6F_5Xe][AsF_6]$	110.0 °C	112.3 °C	156.9 °C	183.8 °C
$[C_6F_5Xe][B(CN)_4]$	---	---	152.2 °C	154.8 °C
$[C_6F_5Xe][B(C_6F_5)_4]$	---	---	85.2 °C	85.5 °C
$[C_6F_5Xe][B(CF_3)_4]$	---	---	(I) 117.2 °C	(I) 123.0 °C
			(II) 139.3 °C	(II) 140.9 °C
			(III) 148.8 °C	(III) 169.9 °C

III.1.5 Reaction of $[C_6F_5Xe][BY_4]$ ($Y = F, CF_3, CN,$ and C_6F_5) and $[C_6F_5Xe][AsF_6]$ with C_6H_5F

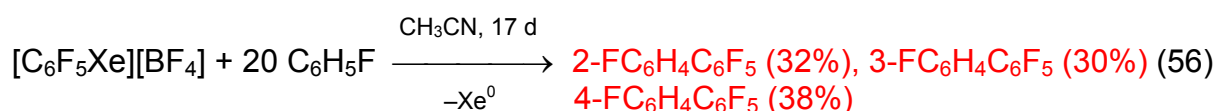
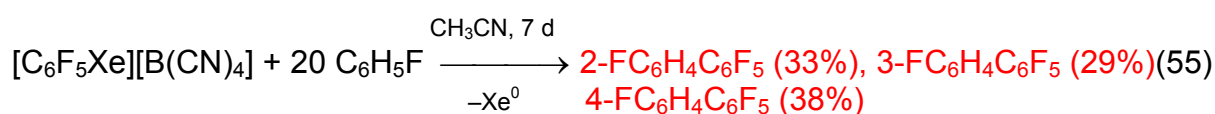
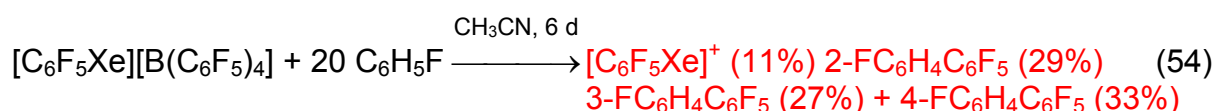
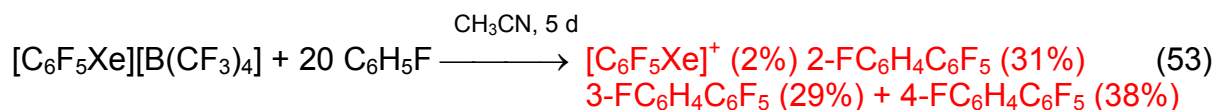
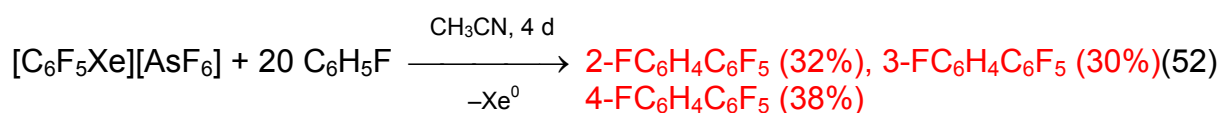
It had been shown by Frohn *et al.*^[83] that $[C_6F_5Xe][AsF_6]$ reacts with aromatic compounds, such as C_6H_5R ($R = CH_3, F, CF_3, NO_2,$ and CN) under formation of isomeric mixtures of polyfluorobiphenyls, $x-RC_6H_4C_6F_5$ ($x = 2, 3, 4, R = CH_3, F, CN, CF_3, NO_2$) in CH_3CN at ambient temperature. The rate of reaction had been found to be the faster the less electron withdrawing the nature of substituents R localized in the aromatic compound C_6H_5R . The following reactions had been previously published.



* traces or minor amounts

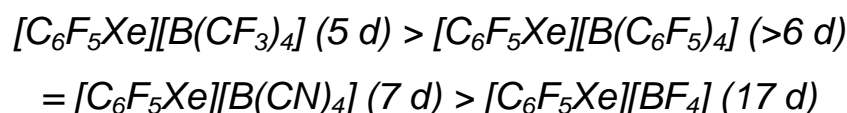
The arylation of $\text{C}_6\text{H}_5\text{R}$ compounds has been studied with electron-donating and -withdrawing substituents, R. The effect of the counteranions of organoxenon(II) salts had not yet been examined. One candidate of $\text{C}_6\text{H}_5\text{R}$ was chosen to investigate these influences. Fluorobenzene was chosen because it had shown moderate reactivity with $[\text{C}_6\text{F}_5\text{Xe}][\text{AsF}_6]$ (14 h until complete consumption of $[\text{C}_6\text{F}_5\text{Xe}]^+$) optimal for the planned investigations. Another advantage of $\text{C}_6\text{H}_5\text{F}$ was the easy determination of the products by ^{19}F NMR spectroscopy.

Four of the $[\text{C}_6\text{F}_5\text{Xe}][\text{BY}_4]$ ($\text{Y} = \text{F}, \text{CN}, \text{CF}_3,$ and C_6F_5) salts with borate anions and $[\text{C}_6\text{F}_5\text{Xe}][\text{AsF}_6]$ were reacted with $\text{C}_6\text{H}_5\text{F}$ in CH_3CN and additionally $[\text{C}_6\text{F}_5\text{Xe}][\text{BY}_4]$ ($\text{Y} = \text{CF}_3$ and C_6F_5) salts in CH_2Cl_2 at ambient temperature. The salts were reacted with 1.2 and 20 molar excess of dried (P_4O_{10}) and distilled $\text{C}_6\text{H}_5\text{F}$. All reactions yielded biphenyl isomers, $x\text{-FC}_6\text{H}_4\text{C}_6\text{F}_5$ ($x = 2, 3, 4$) as only detectable compounds. The reactions were monitored by ^{19}F NMR spectroscopy in the respective solvent at 24°C . The rate of consumption of the $[\text{C}_6\text{F}_5\text{Xe}]^+$ cation was used as primary indicator for the rate of reaction. The following schemes show the results of the reactions of the $[\text{C}_6\text{F}_5\text{Xe}]^+$ salts with $\text{C}_6\text{H}_5\text{F}$ (20 molar excess) in CH_3CN at ambient temperature.



$\Sigma\text{C}_6\text{F}_5$ groups and derivatives = 100 %

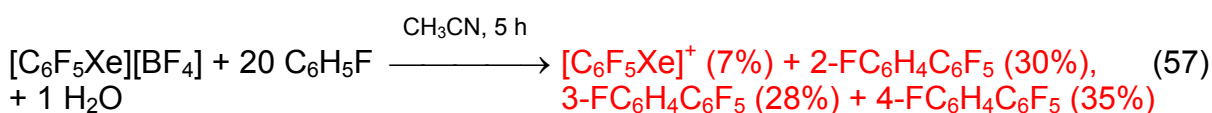
The product distribution was comparable for all $[\text{C}_6\text{F}_5\text{Xe}]^+$ salts. The only products detectable were $x\text{-FC}_6\text{H}_4\text{C}_6\text{F}_5$ ($x = 2, 3$ and 4). The only difference was the rate of $[\text{C}_6\text{F}_5\text{Xe}]^+$ consumption. The different rates provided a sequence dependent on the different counteranions:



The rate of reaction of $[\text{C}_6\text{F}_5\text{Xe}][\text{AsF}_6]$ with $\text{C}_6\text{H}_5\text{F}$ was compared with previous studies.^[83] It was shown that the reaction rate was not comparable to the previous study where $[\text{C}_6\text{F}_5\text{Xe}][\text{AsF}_6]$ reacted completely with $\text{C}_6\text{H}_5\text{F}$ within 14 h. The reaction performed in this Thesis showed only 53% conversion of $[\text{C}_6\text{F}_5\text{Xe}]^+$ after 31 h and 100% after 96 h. The difference can be explained by the different reaction conditions. The reaction was found to be very sensible towards moisture. Thus, the rate of consumption was increased in reactions where fluorobenzene was only distilled prior to use instead of additional drying with P_4O_{10} . The reaction of $[\text{C}_6\text{F}_5\text{Xe}][\text{BF}_4]$ with only distilled $\text{C}_6\text{H}_5\text{F}$ was completed after 10 d whereas reactions of $[\text{C}_6\text{F}_5\text{Xe}][\text{BF}_4]$ with dried (P_4O_{10}) and distilled $\text{C}_6\text{H}_5\text{F}$ were not completed until 17 d. To exclude the

possibility of large variation limits or high systematic uncertainties, a series of reproductions were performed with $[\text{C}_6\text{F}_5\text{Xe}][\text{BF}_4]$. Four repeated reactions of $[\text{C}_6\text{F}_5\text{Xe}][\text{BF}_4]$ with $\text{C}_6\text{H}_5\text{F}$ in CH_3CN at ambient temperature gave almost the same rates for the complete consumption (15 d, 17 d, 16 d and 17 d) showing that those examined experiments are reliable and reproducible. All mentioned experiments were performed under rigorously anhydrous conditions and all reactants and solvents were dried and distilled prior to use to provide equal initial conditions.

Experiments with additions of water (1 and 20 molar equivalents) were examined to show the influence of moisture in the reaction. Therefore, $[\text{C}_6\text{F}_5\text{Xe}][\text{BF}_4]$ was reacted with $\text{C}_6\text{H}_5\text{F}$ in the presence of 1 and 20 equivalents of H_2O in CH_3CN at ambient temperature. The reaction with 1 equivalents of H_2O was almost completed after 5 h (remaining $[\text{C}_6\text{F}_5\text{Xe}]^+ = 7\%$), with 20 equivalents of H_2O after less than 15 min., which was more than 60 and 950 times faster than without addition of water. A comparable trend was obtained for the rates of the reaction with $[\text{C}_6\text{F}_5\text{Xe}][\text{AsF}_6]$. Those two examples clearly show the enhanced reactivity of the $[\text{C}_6\text{F}_5\text{Xe}]^+$ cation in the presence of water. The product distribution was comparable for reactions with and without addition of water.

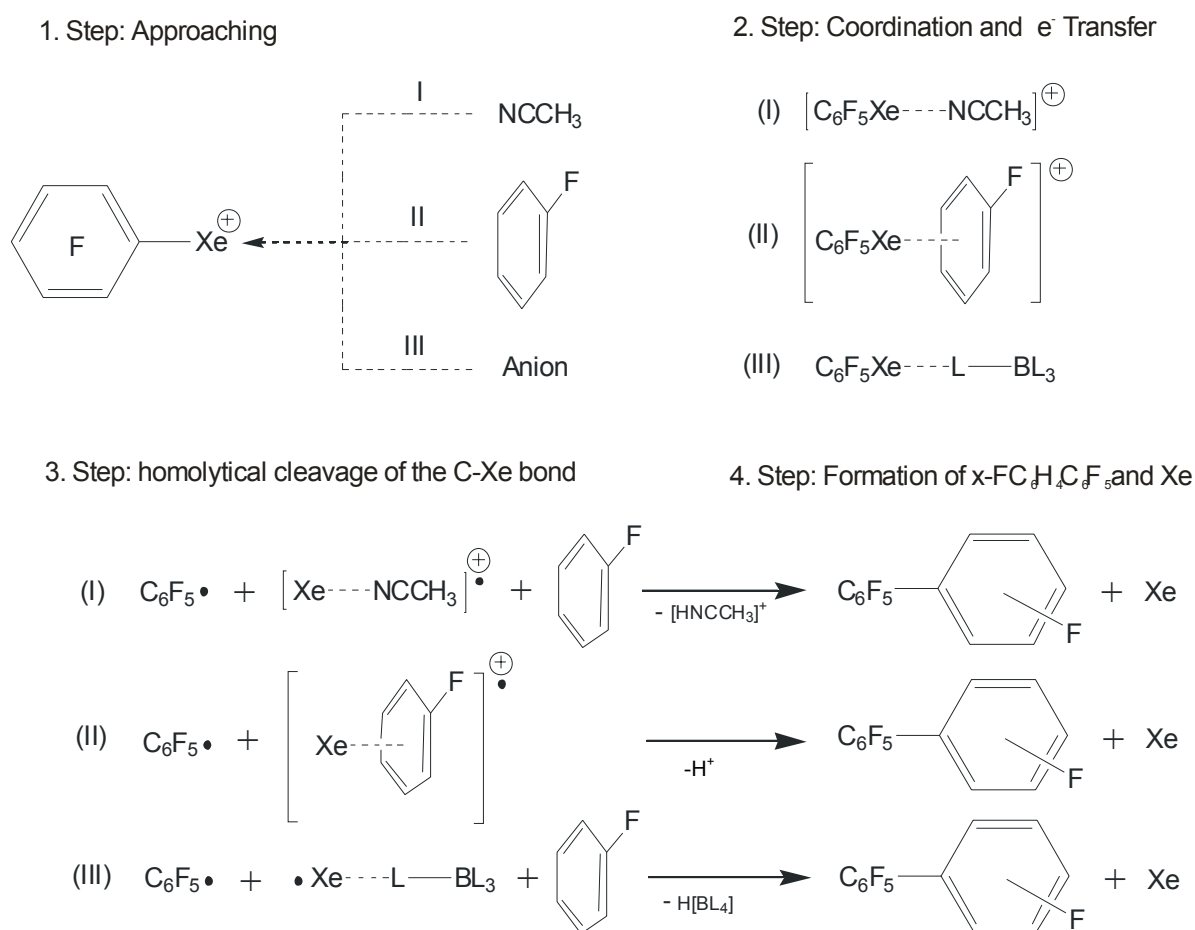


$\Sigma\text{C}_6\text{F}_5$ groups and derivatives = 100 %

The faster reaction rate in the presence of water may be explained by the predominate coordination of H_2O towards the positively charged xenon(II) center. The homolytical cleavage of the C-Xe bond would be facilitated and is a consequence of the higher basicity of water when compared to CH_3CN . It is, however, important to recognize that no $\text{C}_6\text{F}_5\text{H}$ was formed which leads to the assumption of a reaction pathway different to that described for the decompositions of the $[\text{C}_6\text{F}_5\text{Xe}]^+$ salts in coordinating solvents.

The formation of isomeric mixture of the biphenyls in all reactions of $[\text{C}_6\text{F}_5\text{Xe}]^+$ with $\text{C}_6\text{H}_5\text{F}$ may be a result of a radical substitution on the aromatic fluorobenzene.

The initial steps show similarities to those described for the decompositions of the $[\text{C}_6\text{F}_5\text{Xe}]^+$ salts and include principally comparable steps: approach of a nucleophile, coordination of the nucleophile towards the positively charged Xe(II) center and donation of electron density, homolytical cleavage of the C-Xe bond and subsequent radical substitution on fluorobenzene. The important difference to the decomposition was the consecutive interaction with fluorobenzene. It seems obvious from those reactions that the key step of the reaction of $[\text{C}_6\text{F}_5\text{Xe}]^+$ with $\text{C}_6\text{H}_5\text{F}$ follows a radical mechanism and could be as depicted in the following scheme.



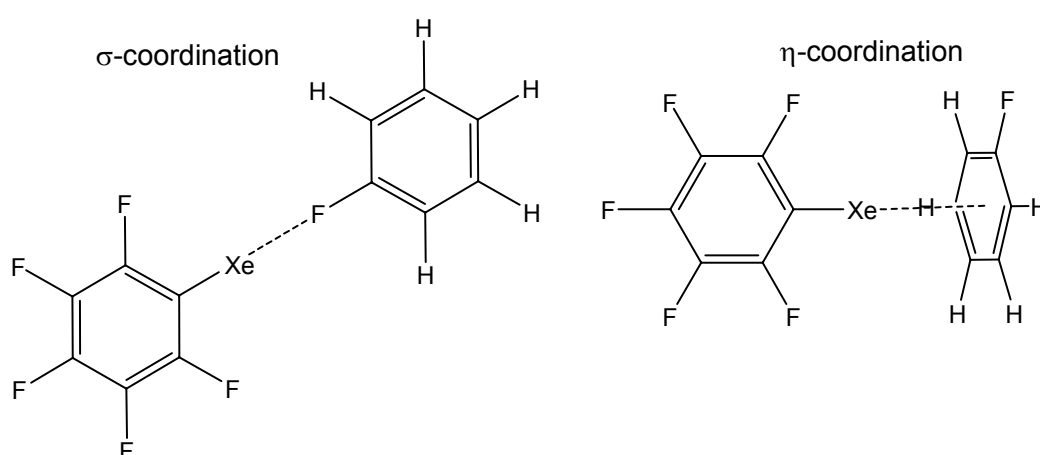
The initial step, the coordination of a nucleophile to the positively charged Xe(II) center can occur with basic solvent molecules, the counteranion of the $[\text{C}_6\text{F}_5\text{Xe}]^+$ salt or fluorobenzene. The coordination of CH_3CN (I) and $\text{C}_6\text{H}_5\text{F}$ (II) are cation-dipole interactions which lead to the donation of electron density or even of an electron transfer whereas the cation-anion interaction (III) belongs mainly in Coulomb interactions. The cases I and III, (coordination of CH_3CN or of the counteranion) are principally similar with the initial steps of the previously described decomposition

pathways of $[\text{C}_6\text{F}_5\text{Xe}]^+$ salts. The decompositions of all investigated salts were, however, much slower than the reaction with $\text{C}_6\text{H}_5\text{F}$ leading to the assumption that the reaction is mainly initiated by means of interaction with $\text{C}_6\text{H}_5\text{F}$.

Table 11 Comparison of the decomposition of $[\text{C}_6\text{F}_5\text{Xe}][\text{BY}_4]$ ($\text{Y} = \text{F}, \text{CN}, \text{C}_6\text{F}_5,$ and CF_3) versus their reaction with 20 molar excess $\text{C}_6\text{H}_5\text{F}$ in CH_3CN at ambient temperature

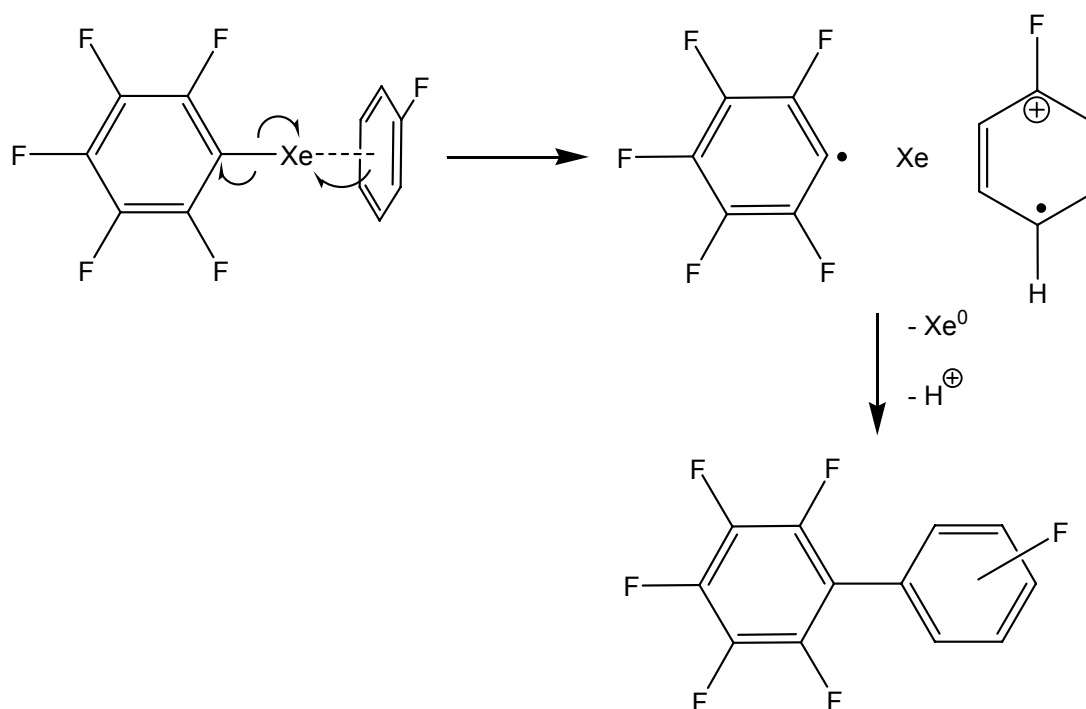
	Decomposition in CH_3CN at RT	Reaction with $\text{C}_6\text{H}_5\text{F}$ in CH_3CN at RT
$[\text{C}_6\text{F}_5\text{Xe}][\text{BF}_4]$	67 d	17 d
$[\text{C}_6\text{F}_5\text{Xe}][\text{B}(\text{CN})_4]$	60 d	7 d
$[\text{C}_6\text{F}_5\text{Xe}][\text{B}(\text{C}_6\text{F}_5)_4]$	20 d	6 d
$[\text{C}_6\text{F}_5\text{Xe}][\text{B}(\text{CF}_3)_4]$	43 d	5 d

The absence of $\text{C}_6\text{F}_5\text{H}$, the main decomposition product in the decomposition of $[\text{C}_6\text{F}_5\text{Xe}]^+$ in CH_3CN , in the reaction with $\text{C}_6\text{H}_5\text{F}$ indicates that the C-Xe bond cleavage is followed by the only interaction with fluorobenzene and not by CH_3CN . The coordination of fluorobenzene is assumed to be the main reaction channel and can principally occur by means of a η - or σ -coordination of $\text{C}_6\text{H}_5\text{R}$ to the xenon center of the $[\text{C}_6\text{F}_5\text{Xe}]^+$ cation.



A σ -coordination of fluorobenzene can however only occur by means of coordination with the R terminus of $\text{C}_6\text{H}_5\text{F}$ which is disfavoured. Neither the formation of $\text{C}_6\text{H}_5\text{CH}_2\text{C}_6\text{F}_5$ was detected nor would a σ -interaction explain the higher reactivity of

toluene over fluorobenzene. A η -coordination only involves π -interaction from the aromatic system and is assumed to be the favoured coordination. Toluene is a stronger π -basic ligand than fluorobenzene resulting in a better interaction and a faster reaction. A followed single electron transfer step would yield $C_6F_5\cdot$ radicals and $C_6H_5^+\cdot$ radical cations which may simply recombine to give the hexafluorobiphenyls.



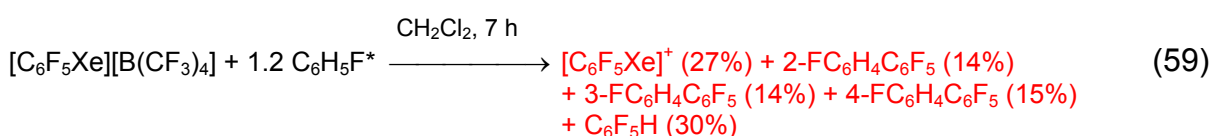
The absence of C_6F_5H implies a fast reaction of $C_6F_5\cdot$ radicals with fluorobenzene instead of reacting with CH_3CN . Long life $C_6F_5\cdot$ radicals react predominantly with CH_3CN to C_6F_5H because of the large excess of solvent molecules which was already demonstrated in the decomposition studies of the $[C_6F_5Xe]^+$ salts in CH_3CN . There has to be obviously a different reaction pathway to the hexafluorobiphenyls, $x-FC_6H_4C_6F_5$ ($x = 2, 3, 4$). A rapid release of Xe^0 , in a form of an inverted insertion, followed by recombination gives $x-FC_6H_4C_6F_5$ ($x = 2, 3, 4$). The absence of HF in either reaction of a $[C_6F_5Xe]^+$ salt, especially in the cases of $[C_6F_5Xe][B(CF_3)_4]$ is indicative that no fluoride ion is present or was abstracted from the counteranion.

The different rates of consumption could be explained by the different electrophilicity of the $[C_6F_5Xe]^+$ salts or in other words by the different nucleophilicity of the counteranions. Salts with weakly coordinating anions, such as $[C_6F_5Xe][B(CF_3)_4]$ and $[C_6F_5Xe][B(C_6F_5)_4]$, favours the contact of C_6H_5F over CH_3CN to the Xe center. The 4 times faster reaction of $[C_6F_5Xe][B(CF_3)_4]$ in CH_2Cl_2 solution,

when compared to the reaction in CH₃CN, occurred because of the better coordination of C₆H₅F. The fastest reaction was obtained for the [C₆F₅Xe][B(CF₃)₄] (5 d) followed by [C₆F₅Xe][B(C₆F₅)₄] (6 d). An astonishingly fast reaction was obtained for [C₆F₅Xe][B(CN)₄] with the moderately coordinating [B(CN)₄]⁻ anion whose rate of reaction was equal to that of the [B(C₆F₅)₄]⁻ anion. The slowest reaction was obtained for the [C₆F₅Xe][BF₄] salt (16 d) whose anion belongs to the stronger coordinating anions in these series.

III.1.5.1 Reaction of [C₆F₅Xe][BY₄] (Y = C₆F₅ and CF₃) with C₆H₅F in CH₂Cl₂

The reaction of [C₆F₅Xe][BY₄] (Y = C₆F₅ and CF₃) with fluorobenzene was also examined in the weakly coordinating solvent CH₂Cl₂ to further simplify the coordination situation. The competition to coordinate at the positively charged xenon center was therewith mainly reduced to the coordination of fluorobenzene. Only salts with weakly coordinating anions, such as [C₆F₅Xe][B(OTeF₅)₄], [C₆F₅Xe][B(C₆F₅)₄], and [C₆F₅Xe][B(CF₃)₄] are soluble in CH₂Cl₂. The solvent is also weakly nucleophilic so that the diminishing nucleophile was the π base, fluorobenzene. The reaction of [C₆F₅Xe][B(CF₃)₄] with C₆H₅F in CH₂Cl₂ at ambient temperatures showed already 73% conversion of [C₆F₅Xe]⁺ after 7 h. The complete product distribution is shown in scheme 59. The reaction was found to be ~8 times faster than in CH₃CN solution.



ΣC₆F₅ groups and derivatives = 100 %

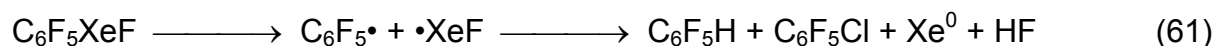
* distilled, without pre-drying (P₄O₁₀)

The product distribution of this reaction shows that not only reaction with C₆H₅F but also decomposition of the [C₆F₅Xe]⁺ cation occurs. After 7 h at ambient temperature 43% of the [C₆F₅Xe]⁺ cation have been successfully reacted to x-FC₆H₄C₆F₅ (x = 2, 3, 4). The formation of 30% of C₆F₅H clearly indicates that decomposition of the [C₆F₅Xe]⁺ cation occurred. The ¹⁹F NMR spectra showed not only the decomposition of the cation but also of the anion. The [B(CF₃)₄]⁻ anion was found to be not stable in CH₂Cl₂ at ambient temperature. After 7 h roughly 40% of the [B(CF₃)₄]⁻ anion

decomposed yielding an unidentified $[(CF_3)_3BX]^-$ anion ($\delta(^{19}F) = -59$ ppm, $\delta(^{11}B) = -14$ ppm), which represents a boron compound such as $[(CF_3)_3BCF_2Cl]^-$. Compounds such as $CHFC_2$ or CF_2Cl_2 were not obtained just as well as C_6F_6 or C_6F_5Cl . The reaction of $[C_6F_5Xe][B(CF_3)_4]$ with fluorobenzene in CH_2Cl_2 is the only reaction in which the $[B(CF_3)_4]^-$ was remarkably decomposed. No such compounds were obtained in the decomposition reaction of $[C_6F_5Xe][B(CF_3)_4]$ in CH_2Cl_2 indicating a different reaction pathway. The 30% of pentafluorobenzene obtained in the reaction can be explained by reaction of the $C_6F_5\cdot$ radicals with solvent molecules. It is, however, exceptional that the $C_6F_5\cdot$ radicals only reacted with the H terminus of CH_2Cl_2 . Decomposition studies in CH_2Cl_2 have shown that mainly the Cl terminus of CH_2Cl_2 was attacked from $C_6F_5\cdot$ radicals yielding C_6F_5Cl which was not obtained. It is more probable that the reaction with "only" distilled fluorobenzene might consist of small amounts of moisture which could react with the $[C_6F_5Xe]^+$ cation to yield C_6F_5H . The high rate of decomposition can be explained by the increased electrophilicity of the very weakly coordinated $[C_6F_5Xe]^+$ cation and the comparable strong π -basicity of the aromat, C_6H_5F .

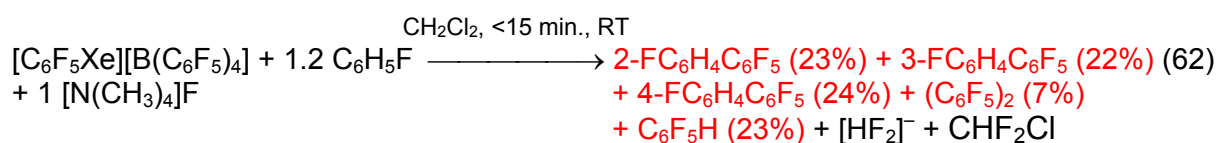
III.1.5.2 Reaction of $[C_6F_5Xe][B(C_6F_5)_4]$ with C_6H_5F in the Presence of $[N(CH_3)_4]F$ and Reaction of C_6F_5XeF with C_6H_5F in CH_2Cl_2

The initial step of reactions of $[C_6F_5Xe]^+$ salts containing perfluoro-anions, $[EF_{n+1}]^-$, such as $[BF_4]^-$ and $[AsF_6]^-$ with C_6H_5F was previously thought to be the coordination of a fluoride anion, formed by solvolysis of the $[EF_{n+1}]^-$ anion, towards the xenon(II) center. Neutral C_6F_5XeF was predicted to be the intermediate which decomposes at ambient temperature to yield the $C_6F_5\cdot$ radical.



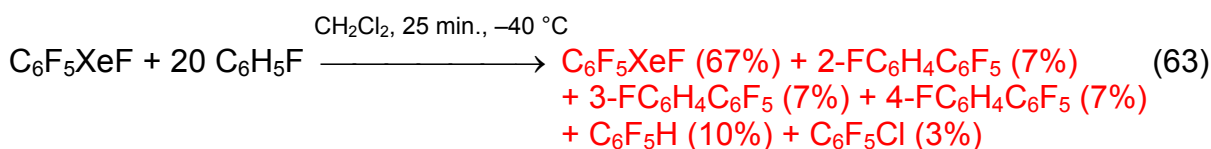
It has been shown that the coordination of the counteranion does not play the key role in the reaction with aromatic compounds. A reaction of $[C_6F_5Xe][B(C_6F_5)_4]$ with C_6H_5F in the presence of 1.2 equivalents of $[N(CH_3)_4]F$ in CH_2Cl_2 led immediately (<15 min.) to $x\text{-}FC_6H_4C_6F_5$ (~70.3%), $(C_6F_5)_2$ (6.5%), C_6F_5H (23.2%), CHF_2Cl and

$[\text{HF}_2]^-$. A comparable reaction of $[\text{C}_6\text{F}_5\text{Xe}][\text{B}(\text{C}_6\text{F}_5)_4]$ and $\text{C}_6\text{H}_5\text{F}$ showed only a small amount of $x\text{-FC}_6\text{H}_4\text{C}_6\text{F}_5$ and $(\text{C}_6\text{F}_5)_2$ after 3 h at RT.



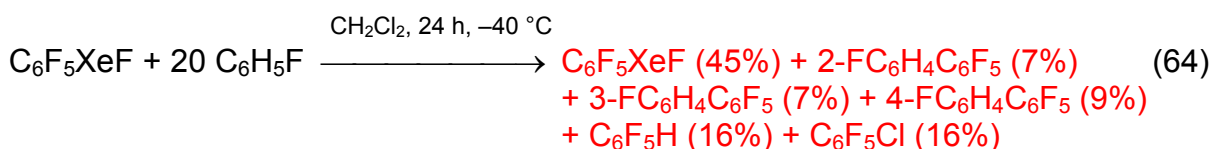
$\Sigma\text{C}_6\text{F}_5$ groups and derivatives = 100 %

The reaction was much faster than without addition of fluoride and was indicative for the reduced stability of intermediately formed $\text{C}_6\text{F}_5\text{XeF}$ and the rapid formation of reactive $\text{C}_6\text{F}_5^\bullet$ radicals. A reaction of freshly prepared $\text{C}_6\text{F}_5\text{XeF}$ (containing 9% of $[\text{C}_6\text{F}_5\text{Xe}][\text{B}(\text{C}_6\text{F}_5)_4]$) with $\text{C}_6\text{H}_5\text{F}$ in CH_2Cl_2 at -40°C was performed to elucidate the rate of a reaction between $\text{C}_6\text{F}_5\text{XeF}$ and $\text{C}_6\text{H}_5\text{F}$ within the thermal stability of $\text{C}_6\text{F}_5\text{XeF}$.



$\Sigma\text{C}_6\text{F}_5$ groups and derivatives = 100 %

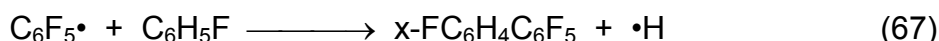
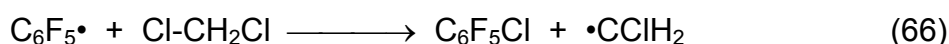
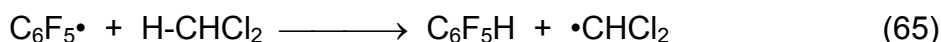
After 24 h still 45% of $\text{C}_6\text{F}_5\text{XeF}$ were detected showing a significantly slower reaction with $\text{C}_6\text{H}_5\text{F}$ compared to $[\text{C}_6\text{F}_5\text{Xe}]^+/\text{F}^-$.



$\Sigma\text{C}_6\text{F}_5$ groups and derivatives = 100 %

Both last experiments clearly show that only 22% of $\text{C}_6\text{F}_5\text{XeF}$ reacted with $\text{C}_6\text{H}_5\text{F}$ in CH_2Cl_2 at -40°C within 24 h which is more than 20 times slower than comparable reactions of $[\text{C}_6\text{F}_5\text{Xe}][\text{B}(\text{CF}_3)_4]$ in CH_2Cl_2 at ambient temperature (difference first and second measurement: $\Delta t = 1 \text{ h} \rightarrow 20\%$ consumption). The reaction was much slower because the positively charged xenon(II) center was already occupied by the fluoride ion. Coordination of fluorobenzene was therewith inhibited resulting in a slower reaction. The product distribution after 24 h clearly shows large amounts of $\text{C}_6\text{F}_5\text{H}$ (16%) and $\text{C}_6\text{F}_5\text{Cl}$ (16%) which is a consequence of the decomposition of $\text{C}_6\text{F}_5\text{XeF}$ in CH_2Cl_2 . A successful reaction of $\text{C}_6\text{F}_5\text{XeF}$ and $\text{C}_6\text{H}_5\text{F}$ is assumed to only occur upon

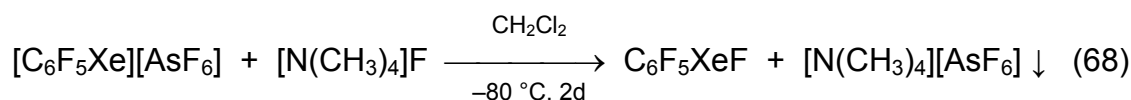
decomposition of neutral C_6F_5XeF . The neutral molecule, C_6F_5XeF , is thermally unstable at temperatures above $-40\text{ }^\circ\text{C}$ which explains the fast reaction of $[C_6F_5Xe][B(C_6F_5)_4]$ in the presence of $[N(CH_3)_4]F$ in CH_2Cl_2 at ambient temperature. The formation of isomeric hexafluorobiphenyls, $x\text{-}FC_6H_4C_6F_5$ (23%), C_6F_5H (16%), and C_6F_5Cl (16%) are the results of the reaction of $C_6F_5\cdot$ radicals with C_6H_5F and CH_2Cl_2 , respectively.



III.1.5.3 Modified Preparation of C_6F_5XeF

Until now only a limited number of neutral symmetric and asymmetric arylxenon(II)halogenides, -pseudohalogenids, and diarylxenon(II) compounds have been isolated. Recently, three examples of alkynylxenon(II) fluorides, namely $RC\equiv CXeF$ ($R = C_6H_5, CH_3,$ and $n\text{-}C_4H_9$), were characterized in solution by NMR spectroscopy but could not be isolated because of their thermal instability.^[78]

There are two general preparative methods to synthesize neutral organoxenon(II)fluorides. One method was developed by Naumann *et al.* who reacted XeF_2 with $(CH_3)_3SiC_6F_5$ in the presence of $[N(CH_3)_4]F$ in CH_3CN at -40 and $C_2H_5CN, CH_3CN/C_2H_5CN$ or CH_2Cl_2 at $-60\text{ }^\circ\text{C}$. However, C_6F_5XeF was only observed as intermediate and was not isolated. In a subsequent step, C_6F_5XeF reacted with $(CH_3)_3SiC_6F_5$ to yield the diarylxenon(II) compound, $(C_6F_5)_2Xe$. A synthetic strategy, in which C_6F_5XeF has been isolated, was developed by Frohn *et al.*^[76] who reacted $[C_6F_5Xe][AsF_6]$ with $[N(CH_3)_4]F$ in CH_2Cl_2 at $-80\text{ }^\circ\text{C}$ and obtained C_6F_5XeF after two days in 70% yield. Undesired co-products were $C_6F_5H, C_6F_5Cl,$ and $(C_6F_5)_2$. The long reaction time was accompanied by increased amounts of decomposition products. The driving force of the reaction of $[C_6F_5Xe][AsF_6]$ and $[N(CH_3)_4]F$ is the precipitation of $[N(CH_3)_4][AsF_6]$ which is insoluble in CH_2Cl_2 at $-80\text{ }^\circ\text{C}$.



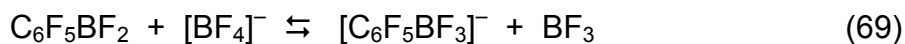
The insolubility of the $[\text{C}_6\text{F}_5\text{Xe}][\text{AsF}_6]$ salt in CH_2Cl_2 is responsible for the long reaction time of 2 days. The heterogeneous reaction takes place at the surface of the solid. With access to CH_2Cl_2 soluble $[\text{C}_6\text{F}_5\text{Xe}][\text{BY}_4]$ salts ($\text{Y} = \text{C}_6\text{F}_5$ and CF_3) it was possible to improve the preparation of $\text{C}_6\text{F}_5\text{XeF}$. Anion pure $[\text{C}_6\text{F}_5\text{Xe}][\text{B}(\text{C}_6\text{F}_5)_4]$ or $[\text{C}_6\text{F}_5\text{Xe}][\text{B}(\text{CF}_3)_4]$ were reacted with $[\text{N}(\text{CH}_3)_4]\text{F}$ in CH_2Cl_2 at $-80\text{ }^\circ\text{C}$ yielding $\text{C}_6\text{F}_5\text{XeF}$ (76%) after less than one hour. The by-products obtained were $[\text{N}(\text{CH}_3)_4][\text{B}(\text{C}_6\text{F}_5)_4]$ (9%), $(\text{C}_6\text{F}_5)_2$ (2%), $\text{C}_6\text{F}_5\text{H}$ (4%), $\text{C}_6\text{F}_5\text{Cl}$ (<1%), and some unidentified $\text{C}_6\text{F}_5\text{Y}$ compounds ($\Sigma 8\%$) which are the characteristic decomposition products of $\text{C}_6\text{F}_5\text{XeF}$. The by-products can mostly be removed by washing the solid product with cold ($-60\text{ }^\circ\text{C}$) *n*-pentane. The reaction rate in the homogenous system was fastened by factor 50.

III.2 The $[\text{C}_6\text{F}_5\text{XeF}_2]^+$ salt: Preparation, Structural, and Computational Study, Stability and Reactivity

III.2.1 Preparation of $[\text{C}_6\text{F}_5\text{XeF}_2]^+$ Salts

III.2.1.1 Preparation of $[\text{C}_6\text{F}_5\text{XeF}_2][\text{BF}_4]$

A preliminary report of $[\text{C}_6\text{F}_5\text{XeF}_2][\text{BF}_4]$ ^[72] showed that the xenodeboration reaction which had been successfully used for the formation of C-Xe(II) bonds could be extended to C-Xe(IV) bond formation. The $[\text{C}_6\text{F}_5\text{XeF}_2]^+$ cation is presently the only example of a C-Xe(IV) bond. In the present and previous work, the $[\text{BF}_4]^-$ salt was obtained by the reaction of stoichiometric amounts of $\text{C}_6\text{F}_5\text{BF}_2$ and XeF_4 in CH_2Cl_2 at $-55\text{ }^\circ\text{C}$ and the product, $[\text{C}_6\text{F}_5\text{XeF}_2][\text{BF}_4]$, is precipitated as a pale yellow solid. The reaction was studied in detail and it was found that the synthesis of high purity $[\text{C}_6\text{F}_5\text{XeF}_2][\text{BF}_4]$ in nearly quantitative yield requires specific conditions. Unlike the syntheses of organoxenon(II) compounds, a large amount of solvent has to be used because of the low solubility of XeF_4 in CH_2Cl_2 at $-55\text{ }^\circ\text{C}$ ($\sim 20\text{ }\mu\text{mol/mL}$) and because of the voluminous nature of the precipitated product. In typical reactions, XeF_4 ($\sim 1\text{ mmol}$) was suspended in cold CH_2Cl_2 ($-80\text{ }^\circ\text{C}$, 20 mL), so that approximately 40% of the XeF_4 crystals were dissolved at the beginning of the reaction. Freshly prepared $\text{C}_6\text{F}_5\text{BF}_2/\text{CH}_2\text{Cl}_2$ ($\sim 7\text{ mL}$) solution (free of $[\text{C}_6\text{F}_5\text{BF}_3]^-$) was added at $-80\text{ }^\circ\text{C}$ where the reaction rate was negligible. The reaction commenced at *ca.* $-60\text{ }^\circ\text{C}$ whereupon $[\text{C}_6\text{F}_5\text{XeF}_2][\text{BF}_4]$ rapidly precipitated as a voluminous yellow solid. The reaction was quantitative after 1 h at $-55\text{ }^\circ\text{C}$. Syntheses employing smaller quantities of solvent (1 – 5 mL) resulted in reduced yields ($<50\%$). In these cases, the separated and washed solid always contained admixtures containing up to 50 mol-% of XeF_4 , even when longer reaction times (3 h) were used. The combination of precisely equimolar amounts of XeF_4 and $\text{C}_6\text{F}_5\text{BF}_2$ was necessary for two reasons. (1) Excess $\text{C}_6\text{F}_5\text{BF}_2$ reacts with the $[\text{BF}_4]^-$ anion yielding $[\text{C}_6\text{F}_5\text{BF}_3]^-$ and BF_3 according to equation 69.

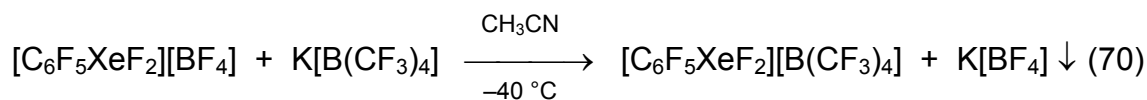


(2) The separation of admixtures with XeF_4 was not possible by multiple washing of the solid with cold CH_2Cl_2 ($-55\text{ }^\circ\text{C}$).

The pure, ochre coloured solid $[\text{C}_6\text{F}_5\text{XeF}_2][\text{BF}_4]$ was found to be very shock sensitive. The solid decomposed explosively and without any residue at $-80\text{ }^\circ\text{C}$ f.e. by dropping a piece of FEP rod ($\sim 3\text{ g}$) from a height of 6 cm onto the solid or by filling the reaction tube with argon gas at RT. Solids containing XeF_4 did not decompose explosively even when pulverizing the solid by knocking the sample tube with a wooden stick.

III.2.1.2 Metathesis Leading to $[\text{C}_6\text{F}_5\text{XeF}_2][\text{B}(\text{CF}_3)_4]$

The preparation of the new salt, $[\text{C}_6\text{F}_5\text{XeF}_2][\text{B}(\text{CF}_3)_4]$, was achieved by metathesis of $[\text{C}_6\text{F}_5\text{XeF}_2][\text{BF}_4]$ with $\text{K}[\text{B}(\text{CF}_3)_4]$ in CH_3CN at $-40\text{ }^\circ\text{C}$ according to equation 70.



The driving force for the metathesis was the insolubility of $\text{K}[\text{BF}_4]$ in CH_3CN at $-40\text{ }^\circ\text{C}$. Both, $[\text{C}_6\text{F}_5\text{XeF}_2][\text{BF}_4]$ and $[\text{C}_6\text{F}_5\text{XeF}_2][\text{B}(\text{CF}_3)_4]$, are very soluble in CH_3CN at $-40\text{ }^\circ\text{C}$. The $[\text{C}_6\text{F}_5\text{XeF}_2][\text{BF}_4]$ salt was always freshly prepared, isolated, dissolved in cold CH_3CN ($-40\text{ }^\circ\text{C}$) and transferred to solid, dried $\text{K}[\text{B}(\text{CF}_3)_4]$. Because of the detectable thermal instability of the $[\text{C}_6\text{F}_5\text{XeF}_2][\text{BF}_4]$ salt at even $-40\text{ }^\circ\text{C}$, it was impossible to determine the exact amount of $[\text{C}_6\text{F}_5\text{XeF}_2][\text{BF}_4]$ in the CH_3CN solution. Commonly used internal standards such as C_6F_6 , $\text{C}_6\text{H}_5\text{CF}_3$, 1,3,5- $\text{C}_6\text{F}_3\text{H}_3$, etc. could not be used because they were either attacked by the $[\text{C}_6\text{F}_5\text{XeF}_2]^+$ cation or they were among the decomposition products. To achieve complete conversion to $[\text{C}_6\text{F}_5\text{XeF}_2][\text{B}(\text{CF}_3)_4]$, an excess of $\text{K}[\text{B}(\text{CF}_3)_4]$ was always used. The new salt, $[\text{C}_6\text{F}_5\text{XeF}_2][\text{B}(\text{CF}_3)_4]$, was thermally unstable at temperatures above $-40\text{ }^\circ\text{C}$. Relatively rapid decomposition of the $[\text{C}_6\text{F}_5\text{XeF}_2]^+$ cation was found to occur in CH_3CN even at $-40\text{ }^\circ\text{C}$. Unfortunately, it was not possible to isolate the new salt as a solid because the decomposition rate is faster than the time needed to remove the CH_3CN under vacuum at $-40\text{ }^\circ\text{C}$.

III.2.2 Characterization of $[\text{C}_6\text{F}_5\text{XeF}_2]^+$ Salts

III.2.2.1 Characterization of $[\text{C}_6\text{F}_5\text{XeF}_2][\text{BF}_4]$ by ^{11}B , ^{19}F , and ^{129}Xe Multi-NMR Spectroscopy

The availability of pure $[\text{C}_6\text{F}_5\text{XeF}_2][\text{BF}_4]$ motivated us to characterize this salt by ^{19}F , ^{11}B , and ^{129}Xe NMR spectroscopy in CH_3CN at $-40\text{ }^\circ\text{C}$ and aHF at $-40\text{ }^\circ\text{C}$ and $-80\text{ }^\circ\text{C}$ to provide a more complete interpretation of the NMR spectra. The full NMR spectroscopic characterization was also required to study the detailed decomposition and reactivity of $[\text{C}_6\text{F}_5\text{XeF}_2][\text{BF}_4]$ in the above mentioned solvents. The following NMR active nuclei can, in principle, be measured for this salt: ^{10}B ($I = 3$, 19.58%), ^{11}B ($I = 3/2$, 80.42%), ^{13}C ($I = 1/2$, 1.11%), ^{19}F ($I = 1/2$, 100%), ^{129}Xe ($I = 1/2$, 26.44%) and ^{131}Xe ($I = 3/2$, 21.18%). The ^{11}B , ^{13}C , ^{19}F , and ^{129}Xe NMR spectra of $[\text{C}_6\text{F}_5\text{XeF}_2][\text{BF}_4]$ in CH_3CN at $-40\text{ }^\circ\text{C}$ have been previously reported but were not well-resolved, so that no ^{19}F - ^{19}F coupling constants could be reported.^[72] In this study, $[\text{C}_6\text{F}_5\text{XeF}_2][\text{BF}_4]$ was characterized by ^{11}B , ^{19}F , and ^{129}Xe NMR spectroscopy in the superacidic media aHF and in the basic solvent CH_3CN .

It is important to consider the influences of the $[\text{XeF}_2]^+$ substituent on the C_6F_5 group when accounting for the NMR spectroscopic results. The strong electrophilic character of the $[\text{XeF}_2]^+$ substituent resulted in polarization of the pentafluorophenyl group in a hypothetical uncoordinated $[\text{C}_6\text{F}_5\text{XeF}_2]^+$ cation. Both the electron density in the π system and the σ frame are shifted towards the *ipso*-carbon of the C_6F_5 group. The polarization of the π electrons is assumed to be stronger than those of the σ frame. The electron withdrawing character of the $[\text{XeF}_2]^+$ substituent depends on the partial positive charge on the xenon(IV) center and the C-Xe distance. Characteristic for the π electron density in C_6F_5 compounds is the alternation of charges from C(1) to C(4), which was calculated for the ring carbons in $\text{C}_6\text{F}_5\text{IF}_2$ and follows the sequence: $\text{C}(1) < \text{C}(3,5) < \text{C}(2,6) < \text{C}(4)$.^[107] The bonding situation in the $[\text{C}_6\text{F}_5\text{XeF}_2]^+$ cation can be described by means of a 3c-4e bond for the nearly linear F-Xe-F group and a classical 2c-2e bond for the C-Xe bond. The 3c-4e bond uses mainly a filled pure 5p orbital which overlaps in the linear arrangement with two orbitals (single occupied) of the fluorine ligands. The occupied non-bonding (first order

approximation) molecular orbital has mainly ligand character which explains the high electron density on the xenon bonded fluorine atoms in the $[\text{XeF}_2]^+$ substituent.

The $[\text{C}_6\text{F}_5\text{XeF}_2][\text{BF}_4]$ salt was only known to be soluble and relatively stable in CH_3CN solution. In CH_3CN solution, coordination of basic solvent molecules to the Xe(IV) center upon formation of an $[\text{C}_6\text{F}_5\text{XeF}_2 \cdot (\text{NCCH}_3)_n]^+$ adduct occurs which reduces the degree of polarization of the C_6F_5 group attributed to the reduced negative charge on C(1). The ^{19}F chemical shifts of the $[\text{C}_6\text{F}_5\text{XeF}_2]^+$ cation in CH_3CN at -40°C consist of four resonances, $\delta = -25.7$ ppm (XeF_2), -124.7 ppm (*o*- C_6F_5), -134.8 ppm (*p*- C_6F_5), and -152.2 ppm (*m*- C_6F_5) which are comparable to those previously reported. The chemical shifts of the C_6F_5 fluorines are shifted to higher frequencies in CH_3CN at -40°C when compared to the $[\text{C}_6\text{F}_5\text{Xe}]^+$ cation ($\Delta\delta(\textit{p}\text{-C}_6\text{F}_5) = 8.0$ ppm) or the isoelectronic neutral $\text{C}_6\text{F}_5\text{IF}_2$ ($\Delta\delta(\textit{p}\text{-C}_6\text{F}_5) = 9.7$ ppm), which clearly shows the influences of the highly electron withdrawing $[\text{XeF}_2]^+$ substituent. The xenon bonded fluorine resonance (-25.7 ppm) is shifted more than 134 ppm to higher frequency compared to the iodine bonded fluorines in $\text{C}_6\text{F}_5\text{IF}_2$ (-160.5 ppm). The iodine (+III) center is much less electronegative than the xenon (+IV) center of the cation. The charge on the xenon bonded fluorine atoms is expected to be more strongly shifted towards the center, consistent with the high frequency shift.

The situation in aHF was new and results in a less coordinated $[\text{C}_6\text{F}_5\text{XeF}_2]^+$ cation when compared with its solution in CH_3CN , where the $[\text{C}_6\text{F}_5\text{XeF}_2 \cdot (\text{NCCH}_3)_n]^+$ adduct is formed. The dipolar nature of the HF molecule opens the ability to coordinate to the $[\text{C}_6\text{F}_5\text{XeF}_2]^+$ cation in two different ways. It can coordinate to the fluorine atoms of the $[\text{XeF}_2]^+$ moiety by means of the H bonding or to the positively charged xenon(IV) center through fluorine. The first case withdraws electron density from the Xe(IV) center whereas the second would donate electron density to the Xe(IV) center. The coordination of HF to the Xe(IV) is supposedly weak when compared to H-bonding. This trend can clearly be deduced from the chemical shifts of the C_6F_5 fluorines.

The ^{19}F chemical shifts of the $[\text{C}_6\text{F}_5\text{XeF}_2]^+$ cation in aHF at -40°C consists of four resonances, $\delta = -33.0$ ppm (XeF_2), -123.5 ppm (*o*- C_6F_5), -129.1 ppm (*p*- C_6F_5), and -150.3 ppm (*m*- C_6F_5), which shows a high frequency shift ($\Delta\delta(\textit{p}\text{-C}_6\text{F}_5) = 5.7$ ppm) for the C_6F_5 fluorine resonances and a low frequency shift for the fluorine-on-xenon environment. The low frequency shift of the $[\text{XeF}_2]^+$ moiety ($\Delta\delta = 7.3$ ppm) is in agreement with the shift obtained for the isoelectronic $\text{C}_6\text{F}_5\text{IF}_2$ ($\Delta\delta = 16.9$ ppm) and

can be explained by the higher covalency of the M-F bonds resulting from the coordination of HF and withdrawal of electron density. The C₆F₅ fluorine atoms of C₆F₅IF₂ are deshielded in aHF ($\Delta\delta(\rho\text{-C}_6\text{F}_5) = 6.2$ ppm) and the fluorines-on-iodine are more shielded ($\Delta\delta = 16.9$ ppm) than in basic CH₃CN.

The *o*- and *m*-C₆F₅ fluorine resonances of the [C₆F₅XeF₂]⁺ cation exhibit multiplet structures in CH₃CN and aHF solution. No C₆F₅ resonance was well enough resolved at 7.0463 T and 11.7440 T to observe the ¹²⁹Xe satellites (*I* = 1/2, 26.44 %) arising from the ³*J*(¹⁹F-¹²⁹Xe), ⁴*J*(¹⁹F-¹²⁹Xe), and ⁵*J*(¹⁹F-¹²⁹Xe). The *p*-C₆F₅ fluorine resonance exhibits a nonet structure with a line distance of 9 Hz. 2D NMR SERF experiments were performed to analyze the pseudo nonet structure resulting from a triplet of triplet of triplets attributed to 3-bond, 4-bond, and 6-bond ¹⁹F-¹⁹F spin couplings. The spin couplings in aHF solutions at -80 °C were analyzed and shown to arise from ³*J*(¹⁹F-¹⁹F) = 18 Hz, ⁴*J*(¹⁹F-¹⁹F) = 9 Hz, and ⁶*J*(¹⁹F-¹⁹F) = 9 Hz. It is noteworthy that the ⁴*J*(¹⁹F-¹⁹F) and ⁶*J*(¹⁹F-¹⁹F) are of the same magnitude as the coupling constants of the *p*-C₆F₅ fluorine resonance in C₆F₅IF₂ (ttt, ³*J*(¹⁹F-¹⁹F) = 19 Hz, ⁴*J*(¹⁹F-¹⁹F) = 7 Hz, and ⁶*J*(¹⁹F-¹⁹F) = 7 Hz) which was also analyzed in the present work using the 2D NMR SERF experiments. The [XeF₂]⁺ moiety is a singlet in aHF at -80 °C with ¹²⁹Xe satellites, ¹*J*(¹⁹F-¹²⁹Xe), of 3912 Hz.

The chemical shift of the counteranion, [BF₄]⁻, is to a much lesser extent, solvent dependent being only shifted by 1.5 ppm to lower frequency from aHF solution (-148.6 ppm) to CH₃CN (-147.1 ppm) at -40 °C. Anhydrous HF predominantly solvates the [BF₄]⁻ anion. An effectively solvated [BF₄]⁻ anion is larger in size and disperses the negative charge over more fluorine atoms in the periphery making it less nucleophilic. The [BF₄·(HF)_{*n*}]⁻ exhibits a quartet splitting in the ¹⁹F spectrum at -148.6 ppm which is attributed to ¹¹B coupling and a quintet splitting in the ¹¹B spectrum at -1.3 ppm attributed to a 1-bond ¹¹B-¹⁹F coupling. The resolved fine structure confirms the presence of a highly symmetric environment around boron. The ¹⁰B-¹⁹F coupling in the ¹⁹F NMR spectrum was resolved at 7.0463 T as an equal intensity septet splitting shifted slightly to higher frequency of the ¹¹B quartet. The one-bond spin coupling, ¹*J*(¹⁰B-¹⁹F), was superimposed with the ¹¹B signal so that no coupling constant could be determined. The ¹*J*(¹¹B-¹⁹F) was 12 Hz. In CH₃CN an interaction of the base with the [BF₄]⁻ anion occurred upon fluoride substitution by CH₃CN according to equation 16.



This interaction is assumed to be fast when compared with the NMR time scale, so that the corresponding ^{11}B and ^{19}F NMR splittings collapse to a singlet. The ^{19}F chemical shift of $[\text{BF}_4]^-$ in CH_3CN was obtained at -147.1 ppm. The boron isotopic shift arising from interaction with ^{10}B was obtained as singlet shifted 18 Hz to lower frequency than the resonance of $[\text{BF}_4]^-$.

A comparison of the ^{19}F , ^{11}B , and ^{129}Xe chemical shifts of $[\text{C}_6\text{F}_5\text{XeF}_2][\text{BF}_4]$, $[\text{C}_6\text{F}_5\text{Xe}][\text{BF}_4]$, and $\text{C}_6\text{F}_5\text{IF}_2$ in CH_3CN and aHF at -40 °C or 24 °C, respectively, is summarized in Table 12.

Table 12 NMR chemical shifts of $[\text{C}_6\text{F}_5\text{XeF}_2][\text{BF}_4]$, $[\text{C}_6\text{F}_5\text{Xe}][\text{BF}_4]$, and $\text{C}_6\text{F}_5\text{IF}_2$ in CH_3CN and aHF at -40 °C, respectively.

Species	Chem. shift (δ) [ppm]						
	^{19}F					^{11}B	^{129}Xe
	$-\text{EF}_2$	$o\text{-C}_6\text{F}_5$	$p\text{-C}_6\text{F}_5$	$m\text{-C}_6\text{F}_5$	$[\text{BF}_4]^-$		
aHF/ -40 °C							
$[\text{C}_6\text{F}_5\text{XeF}_2][\text{BF}_4]$	-33.0	-123.5	-129.1	-150.3	-148.6	-1.3	-1765.9
$\text{C}_6\text{F}_5\text{IF}_2$	-177.4	-119.6	-138.3	-154.9	—	—	—
$[\text{C}_6\text{F}_5\text{Xe}][\text{BF}_4]$	—	-123.9	-138.5	-151.9	-148.6	-1.3	-3831.5
$\text{CH}_3\text{CN} / -40$ °C; 24 °C							
$[\text{C}_6\text{F}_5\text{XeF}_2][\text{BF}_4]$	-25.7	-124.7	-134.8	-152.2	-147.1	-0.6	-1701.3
$\text{C}_6\text{F}_5\text{IF}_2$	-160.5	-122.9	-144.5	-157.0	—	—	—
$[\text{C}_6\text{F}_5\text{Xe}][\text{BF}_4]$	—	-125.4	-142.8	-155.5	-148.0	-2.0	-3813.8

The lack of well-resolved ^{129}Xe NMR spectra at 7.0463 T only allowed a triplet attributed to a $^1J(^{19}\text{F}-^{129}\text{Xe})$ spin-spin coupling to be observed. The 3-bond, 4-bond, and 5-bond $^{19}\text{F}-^{129}\text{Xe}$ spin couplings were not resolved. The $^1J(^{19}\text{F}-^{129}\text{Xe})$ is slightly dependent on the temperature and varies in aHF solution from 3894 Hz at -40 °C to 3912 Hz at -80 °C ($\Delta = 18$ Hz). The coupling in CH_3CN at -40 °C is of the same magnitude (3920 Hz) as that in aHF.

III.2.2.2 Characterization of $[C_6F_5XeF_2][BF_4]$ and $[C_6F_5XeF_2 \cdot (NCCH_3)_{1.5}][BF_4]$ by X-Ray Crystallography

A summary of the refinement results and other crystallographic information is given in Table 13. Important bond lengths and bond angles are listed in Table 14. The structural parameters observed in this study for the $[BF_4]^-$ anions and the C_6F_5 rings of the $[C_6F_5XeF_2]^+$ cations of both structures are in good agreement with previously published values for C_6F_5 ^[103-105, 107] and $[BF_4]^-$ ^[99] and require no further comment. There may be a slight elongation of the B-F bonds when the fluorine ligands of the anions are involved in the contacts with xenon, but a better data set would be needed to confirm this interpretation.

The crystal structure of the $[C_6F_5XeF_2]^+$ cation represents the first crystallographic characterization of a C-Xe(IV) bond. A similar geometry has been previously reported for the X-ray crystal structure of the isoelectronic $C_6F_5IF_2$ molecule.^[107] The C-Xe(IV) bond length is comparable to the C-Xe(II) bonds in $[C_6F_5Xe]^+$ salts^[59] and is not significantly affected by the coordination around xenon or the higher positive charge on the central Xe(IV) atom.

Table 13 Crystallographic Data for [C₆F₅XeF₂][BF₄] and [C₆F₅XeF₂·(NCCH₃)_{1.5}][BF₄]

	[C ₆ F ₅ XeF ₂][BF ₄]	[C ₆ F ₅ XeF ₂ ·(NCCH ₃) _{1.5}][BF ₄]
Chem. formula	C ₆ F ₁₁ BXe	C ₉ H _{4.5} F ₁₁ BN _{1.5} Xe
space group	<i>P2₁/n</i>	<i>C2/c</i>
<i>a</i> (Å)	7.4740(7)	12.803(5)
<i>b</i> (Å)	19.195(2)	23.549(8)
<i>c</i> (Å)	7.7611(8)	19.439(6)
<i>α</i> (°)	90	90
<i>β</i> (°)	109.320(7)	103.08(3)
<i>γ</i> (°)	90	90
<i>V</i> (Å³)	1050.8	5708.6
molecules/unit cell	4	16
mol wt (g·mol⁻¹)	1692	7756
Calcd. density (g·cm⁻³)	2.675	2.256
<i>T</i> (°C)	-173	-173
<i>μ</i> (mm⁻¹)	3.42	2.54
<i>R</i>₁^a	0.0791	0.0818
<i>wR</i>₂^b	0.1539	0.1807

$${}^a R_1 = \frac{\sum \left\| |F_0| - |F_c| \right\|}{\sum |F_0|} \text{ for } l > 2\sigma(l); \quad {}^b wR_2 = \sqrt{\frac{\sum w \cdot \left(|F_0|^2 - |F_c|^2 \right)^2}{\sum w \cdot \left(|F_0|^2 \right)^2}} \text{ for } l > 2\sigma(l)$$

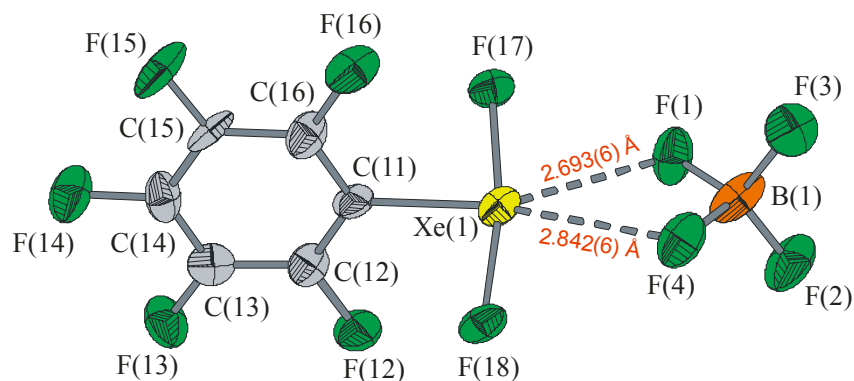


Figure 15 The crystal structure of [C₆F₅XeF₂][BF₄]. Thermal ellipsoids are shown at the 50 % probability level.

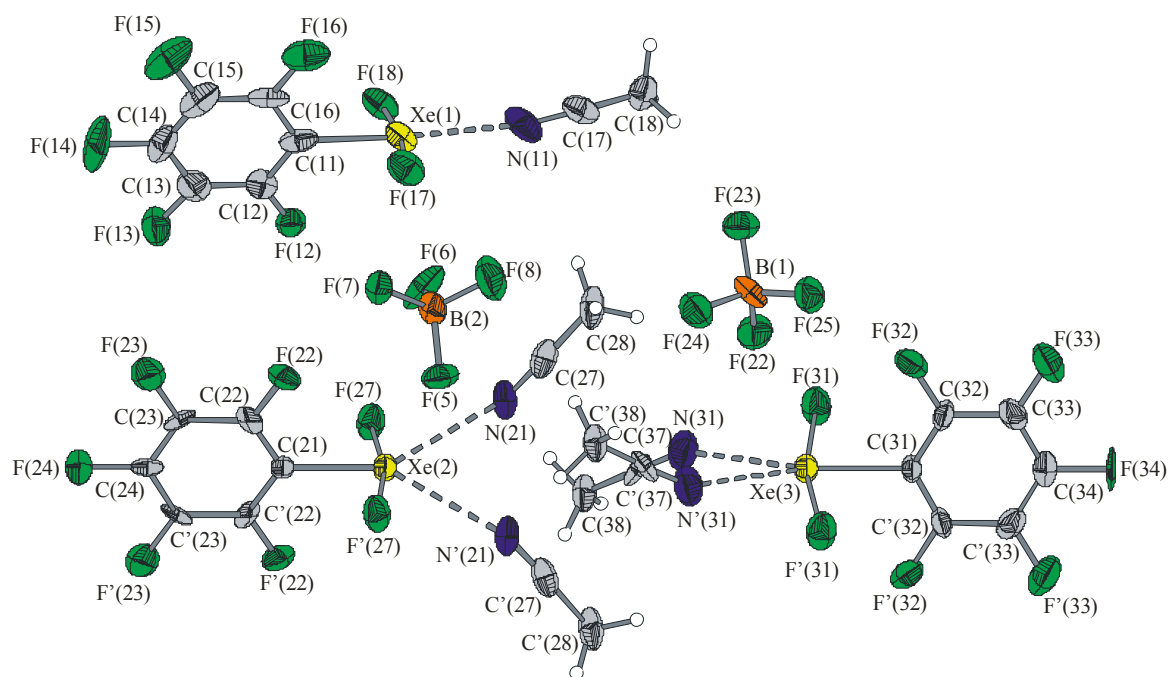


Figure 16 The crystal structure of [C₆F₅XeF₂·(NCCH₃)_{1.5}][BF₄]. Thermal ellipsoids are shown at the 50 % probability level.

Table 14 Experimental Geometrical Parameters for $[\text{C}_6\text{F}_5\text{XeF}_2][\text{BF}_4]$ and $[\text{C}_6\text{F}_5\text{XeF}_2(\text{NCCH}_3)_{1.5}][\text{BF}_4]$

$[\text{C}_6\text{F}_5\text{XeF}_2][\text{BF}_4]$		$[\text{C}_6\text{F}_5\text{XeF}_2(\text{NCCH}_3)_{1.5}][\text{BF}_4]$					
Bond Lengths (Å)		Bond Lengths (Å)					
C(11)-C(12)	1.37 (1)	C(11)-C(12)	1.38 (2)	C(21)-C(22)	1.40 (1)	C(31)-C(32)	1.35 (1)
C(12)-F(12)	1.34 (1)	C(12)-F(12)	1.29 (1)	C(22)-F(22)	1.31 (1)	C(32)-F(32)	1.33 (1)
C(12)-C(13)	1.38 (2)	C(12)-C(13)	1.36 (2)	C(22)-C(23)	1.40 (2)	C(32)-C(33)	1.39 (2)
C(13)-F(13)	1.31 (1)	C(13)-F(13)	1.33 (1)	C(23)-F(23)	1.33 (1)	C(33)-F(33)	1.33 (1)
C(13)-C(14)	1.38 (2)	C(13)-C(14)	1.41 (2)	C(23)-C(24)	1.34 (1)	C(33)-C(34)	1.38 (2)
C(14)-F(14)	1.32 (1)	C(14)-F(14)	1.31 (1)	C(24)-F(24)	1.36 (1)	C(34)-F(34)	1.32 (2)
C(14)-C(15)	1.41 (2)	C(14)-C(15)	1.36 (2)				
C(15)-F(15)	1.33 (1)	C(15)-F(15)	1.34 (2)				
C(15)-C(16)	1.37 (1)	C(15)-C(16)	1.37 (2)				
C(16)-F(16)	1.35 (1)	C(16)-F(16)	1.34 (1)				
C(16)-C(11)	1.34 (1)	C(16)-C(11)	1.42 (2)				
Xe(1)-C(11)	2.082(11)	Xe(1)-C(11)	2.05 (1)	Xe(2)-C(21)	2.05 (2)	Xe(3)-C(31)	2.10 (2)
Xe(1)-F(17)	1.942(6)	Xe(1)-F(17)	1.947(7)	Xe(2)-F(27)	1.934(6)	Xe(3)-F(37)	1.949(6)
Xe(1)-F(18)	1.927(6)	Xe(1)-F(18)	1.941(6)				
Xe(1)---F(1)	2.693(6)	Xe(1)---N(11)	2.76 (1)	Xe(2)---N(21)	2.86 (1)	Xe(3)---N(31)	2.83 (1)
Xe(1)---F(4)	2.842(6)	Xe(1)---F(3A)	3.061(7)			Xe(3)---F(X)	
Xe(1)---F(2A)	2.936(6)	Xe(1)---F(1A)	2.972(7)	Xe(2)---F(7)	3.04 (1)	Xe(3)---F(X)	
Xe(1)---F(3A)	3.076(7)	Xe(1)---F(5A)	3.053(7)			Xe(3)---F(X)	
Xe(1)---F(17A)	3.157(7)						
Bond Angles (°)		Bond Angles (°)					
C(11)-C(12)-C(13)	120 (1)	C(11)-C(12)-C(13)	118 (1)	C(21)-C(22)-C(23)	118 (1)	C(31)-C(32)-C(33)	117 (1)
C(12)-C(13)-C(14)	118 (1)	C(12)-C(13)-C(14)	121 (1)	C(22)-C(23)-C(24)	119 (1)	C(32)-C(33)-C(34)	118 (1)
C(13)-C(14)-C(15)	121 (1)	C(13)-C(14)-C(15)	120 (1)	C(23)-C(24)-C(23A)	124 (2)	C(33)-C(34)-C(33A)	123 (2)
C(14)-C(15)-C(16)	118.3(9)	C(14)-C(15)-C(16)	121 (1)				
C(15)-C(16)-C(11)	120 (1)	C(15)-C(16)-C(11)	118 (1)				
C(11)-C(12)-F(12)	120.5(9)	C(11)-C(12)-F(12)	120 (1)	C(21)-C(22)-F(22)	121 (1)	C(31)-C(32)-F(32)	123 (1)
F(12)-C(12)-C(13)	119 (1)	F(12)-C(12)-C(13)	121 (1)	F(22)-C(22)-C(23)	121 (1)	F(32)-C(32)-C(33)	120 (1)
C(12)-C(13)-F(13)	122 (1)	C(12)-C(13)-F(13)	120 (1)	C(22)-C(23)-F(23)	118 (1)	C(32)-C(33)-F(33)	121 (1)
F(13)-C(13)-C(14)	120 (1)	F(13)-C(13)-C(14)	119 (1)	F(23)-C(23)-C(24)	123 (1)	F(33)-C(33)-C(34)	120 (1)
C(13)-C(14)-F(14)	119 (1)	C(13)-C(14)-F(14)	119 (1)	C(23)-C(24)-F(24)	117.9(9)	C(33)-C(34)-F(34)	118.7(9)
F(14)-C(14)-C(15)	120 (1)	F(14)-C(14)-C(15)	121 (1)				
C(14)-C(15)-F(15)	119 (1)	C(14)-C(15)-F(15)	119 (1)				
F(15)-C(15)-C(16)	123 (1)	F(15)-C(15)-C(16)	120 (1)				
C(15)-C(16)-F(16)	118 (1)	C(15)-C(16)-F(16)	122 (1)				
F(16)-C(16)-C(11)	122 (1)	F(16)-C(16)-C(11)	120 (1)				

Table 14 (continued ...)

Xe(1)-C(11)-C(12)	117.9(7)	Xe(1)-C(11)-C(12)	120 (1)	Xe(2)-C(21)-C(22)	119.1(8)	Xe(3)-C(31)-C(32)	117.2(8)
Xe(1)-C(11)-C(16)	119.8(8)	Xe(1)-C(11)-C(16)	118 (1)	Xe(2)-C(21)-C(22A)	119.1(8)	Xe(3)-C(31)-C(32A)	117.2(8)
C(11)-Xe(1)-F(17)	83.9(4)	C(11)-Xe(1)-F(17)	86.8(4)	C(21)-Xe(2)-F(27)	83.4(2)	C(31)-Xe(3)-F(37)	82.5(2)
C(11)-Xe(1)-F(18)	85.9(4)	C(11)-Xe(1)-F(18)	83.7(4)	C(21)-Xe(2)-F(27A)	83.4(2)	C(31)-Xe(3)-F(37A)	82.5(2)
C(11)-Xe(1)---F(1)	153.3(3)	C(11)-Xe(1)---F(3A)	131.5(4)	C(21)-Xe(2)---N(21)	147.6(2)	C(31)-Xe(3)---N(31)	148.2(2)
C(11)-Xe(1)---F(4)	158.6(3)	C(11)-Xe(1)---N(11)	158.3(4)	C(21)-Xe(2)---N(21A)	147.6(2)	C(31)-Xe(3)---N(31A)	148.2(2)
C(11)-Xe(1)---F(2A)	112.0(3)	C(11)-Xe(1)---F(1A)	104.7(4)	C(21)-Xe(2)---F(7)	109.5(1)	C(31)-Xe(3)-F(4A)	110.3(1)
C(11)-Xe(1)---F(3A)	81.2(3)	C(11)-Xe(1)---F(5A)	79.2(4)	C(21)-Xe(2)---F(7A)	109.5(1)	C(31)-Xe(3)-F(4)	110.3(1)
F(17)-Xe(1)-F(18)	169.8(3)	F(17)-Xe(1)-F(18)	170.3(3)	F(27)-Xe(2)-F(27A)	166.7(4)	F(37)-Xe(3)-F(37A)	164.9(4)
F(17)-Xe(1)---F(1)	70.8(2)	F(17)-Xe(1)---F(3A)	71.3(2)	F(27)-Xe(2)---N(21)	69.8(3)	F(37)-Xe(3)---N(31)	69.2(3)
F(17)-Xe(1)---F(4)	112.5(2)	F(17)-Xe(1)---N(11)	114.5(3)	F(27)-Xe(2)---N(21A)	122.8(3)	F(37)-Xe(3)---N(31A)	125.3(3)
F(17)-Xe(1)---F(2A)	115.3(2)	F(17)-Xe(1)---F(1A)	102.7(3)	F(27)-Xe(2)---F(7)	113.2(3)	F(37)-Xe(3)---F(4A)	113.6(3)
F(17)-Xe(1)---F(3A)	113.1(2)	F(17)-Xe(1)---F(5A)	66.0(3)	F(27)-Xe(2)---F(7A)	113.2(3)	F(37)-Xe(3)---F(4)	72.0(3)
F(18)-Xe(1)---F(1)	119.1(2)	F(18)-Xe(1)---F(3A)	114.4(2)	F(27A)-Xe(2)---N(21)	122.8(3)	F(37A)-Xe(3)---N(31)	125.3(3)
F(18)-Xe(1)---F(4)	77.5(2)	F(18)-Xe(1)---N(11)	75.1(3)	F(27A)-Xe(2)---N(21A)	69.8(3)	F(37A)-Xe(3)---N(31A)	69.2(3)
F(18)-Xe(1)---F(2A)	68.2(2)	F(18)-Xe(1)---F(1A)	78.4(2)	F(27A)-Xe(2)---F(7)	71.6(3)	F(37A)-Xe(3)---F(4A)	72.0(3)
F(18)-Xe(1)---F(3A)	65.7(2)	F(18)-Xe(1)---F(5A)	113.4(2)	F(27A)-Xe(2)---F(7A)	113.2(3)	F(37A)-Xe(3)---F(4)	113.6(3)
F(1)---Xe(1)---F(4)	47.3(2)	F(3A)---Xe(1)---N(11)	63.7(3)	N(21)---Xe(2)---N(21A)	64.9(3)	N(31)-Xe(3)---N(31A)	63.6(3)
F(1)---Xe(1)---F(2A)	73.2(2)	F(3A)---Xe(1)---F(1A)	44.4(2)	N(21)---Xe(2)---F(7)	67.5(3)	N(31)-Xe(3)---F(4A)	70.6(3)
F(1)---Xe(1)---F(3A)	116.2(2)	F(3A)---Xe(1)---F(5A)	124.9(2)	N(21)---Xe(2)---F(7A)	79.5(3)	N(31)-Xe(3)---F(4)	75.0(3)
F(4)---Xe(1)---F(2A)	74.4(2)	N(11)---Xe(1)---F(1A)	75.6(3)	N(21A)---Xe(2)---F(7)	79.5(3)	N(31A)---Xe(3)---F(4A)	75.0(3)
F(4)---Xe(1)---F(3A)	79.8(2)	N(11)---Xe(1)---F(5A)	105.2(3)	N(21A)---Xe(2)---F(7A)	67.5(3)	N(31A)---Xe(3)---F(4)	70.6(3)
F(2A)---Xe(1)---F(3A)	130.8(2)	F(1A)---Xe(1)---F(5A)	168.1(2)	F(7)---Xe(2)---F(7A)	140.9(3)	F(4A)---Xe(3)---F(4)	139.3(3)

[BF₄]⁻

Bond Lengths (Å)		Bond Lengths (Å)	
B(1)-F(1)	1.41 (1)	B(1)-F(1)	1.40 (2)
B(1)-F(2)	1.36 (1)	B(1)-F(2)	1.39 (2)
B(1)-F(3)	1.37 (1)	B(1)-F(3)	1.40 (2)
B(1)-F(4)	1.40 (1)	B(1)-F(4)	1.37 (2)
Bond Angles (°)		Bond Angles (°)	
F(1)-B(1)-F(2)	110.7(9)	F(1)-B(1)-F(2)	109 (1)
F(1)-B(1)-F(3)	110 (1)	F(1)-B(1)-F(3)	109 (1)
F(1)-B(1)-F(4)	105 (1)	F(1)-B(1)-F(4)	111 (1)
F(2)-B(1)-F(3)	113 (1)	F(2)-B(1)-F(3)	109 (1)
F(2)-B(1)-F(4)	110 (1)	F(2)-B(1)-F(4)	111 (1)
F(3)-B(1)-F(4)	108.8(9)	F(3)-B(1)-F(4)	109 (1)
		B(2)-F(5)	1.38 (2)
		B(2)-F(6)	1.38 (1)
		B(2)-F(7)	1.37 (2)
		B(2)-F(8)	1.40 (2)
		F(5)-B(2)-F(6)	110 (1)
		F(5)-B(2)-F(7)	110 (1)
		F(5)-B(2)-F(8)	108 (1)
		F(6)-B(2)-F(7)	109 (1)
		F(6)-B(2)-F(8)	109 (1)
		F(7)-B(2)-F(8)	109 (1)

The Xe-F bond lengths (1.927(6) Å - 1.949(6) Å) are comparable to the axial bond lengths in $[\text{XeF}_3]^+$ 1.906(13) Å and 1.907(15) Å in the $[\text{SbF}_6]^-$ salt,^[27] 1.908(4) and 1.883(4) Å in the $[\text{Sb}_2\text{F}_{11}]^-$ salt^[134]) and XeF_4 (1.92(8) Å) but shorter than the I-F bonds in $\text{C}_6\text{F}_5\text{IF}_2$ (1.959(2) Å - 2.025(2) Å)^[107] which is a consequence of the higher positive charge on xenon(IV) when compared to iodine(III), giving rise to a more polar bonds. The $[\text{C}_6\text{F}_5\text{XeF}_2]^+$ cation is T-shaped, which is expected for an AX_2E_3 VSEPR arrangement of three bonding electron pairs and two electron lone pairs, with the more electronegative fluorine atoms (F_{ax}) in the axial positions and the less electronegative C_6F_5 ring and the two non-bonding electron pairs in the equatorial plane.

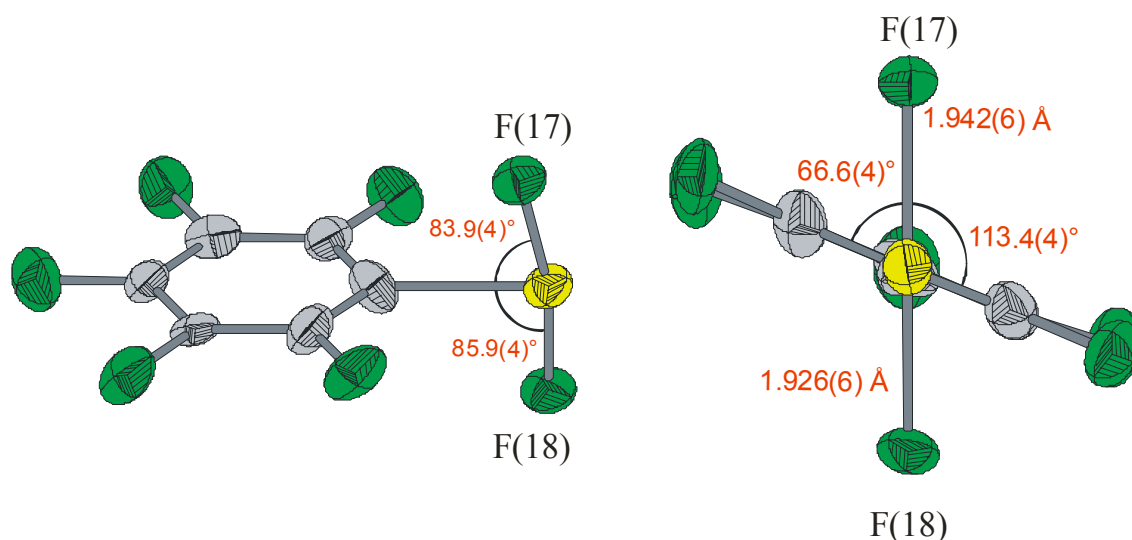


Figure 17 Geometry of the $[\text{C}_6\text{F}_5\text{XeF}_2]^+$ cation (in $[\text{C}_6\text{F}_5\text{XeF}_2][\text{BF}_4]$). Thermal ellipsoids are shown at the 50 % probability level.

The larger electron lone pair domains force the two fluorine atoms bonded to xenon to bend towards the C_6F_5 ring producing non-linear F-Xe-F angles of 169.8(4) to 170.3(3)°. The XeF_2 moieties are twisted out of the plane orthogonal to the C_6F_5 ring in both crystal structures with a twist angle of 23.4 and 26.2°. While the origins of the twist angles are not obvious, it is also reproduced in the calculated geometry of the gas-phase cation (see Table 16). Moreover, a similar structural arrangement has been found in $\text{C}_6\text{F}_5\text{IF}_2$, where the F-I-F angles are 170.46(10) and 171.59(9)° and the twist angles are 15.3 and 15.6°, respectively.

The xenon atom of $[\text{C}_6\text{F}_5\text{XeF}_2][\text{BF}_4]$ shows two contacts (Xe(1)---F(1), 2.693(6) Å and Xe(1)---F(4), 2.842(6) Å) with two fluorines belonging to the same $[\text{BF}_4]^-$ anion.

The Xe---F contacts are significantly less than the sum of the van der Waals radii of Xe and F (3.47 Å)^[100] and are somewhat shorter than the Xe---F contact observed in [C₆F₅Xe][B(CF₃)₄] (2.913(4) Å),^[135] indicating that the [BF₄]⁻ anion is not as weakly coordinated to the [C₆F₅XeF₂]⁺ cation. This interaction is comparable to the CH₃CN coordination to the xenon centers in [C₆F₅Xe]⁺ cation (Xe(II)-N, 2.637(7) and 2.613(15) Å (*vide supra*)) and the [C₆F₅XeF₂]⁺ cation (Xe(IV)-N, 2.828(12) and 2.858(12) Å (*vide infra*)). The two fluorine atoms, F(1) and F(4), are slightly above and below the Xe(1)C(11)F(17)F(18) plane. The geometry around the xenon atom can therefore be described as a distorted pentagonal planar arrangement with the two valence electron lone pairs perpendicular to the plane.

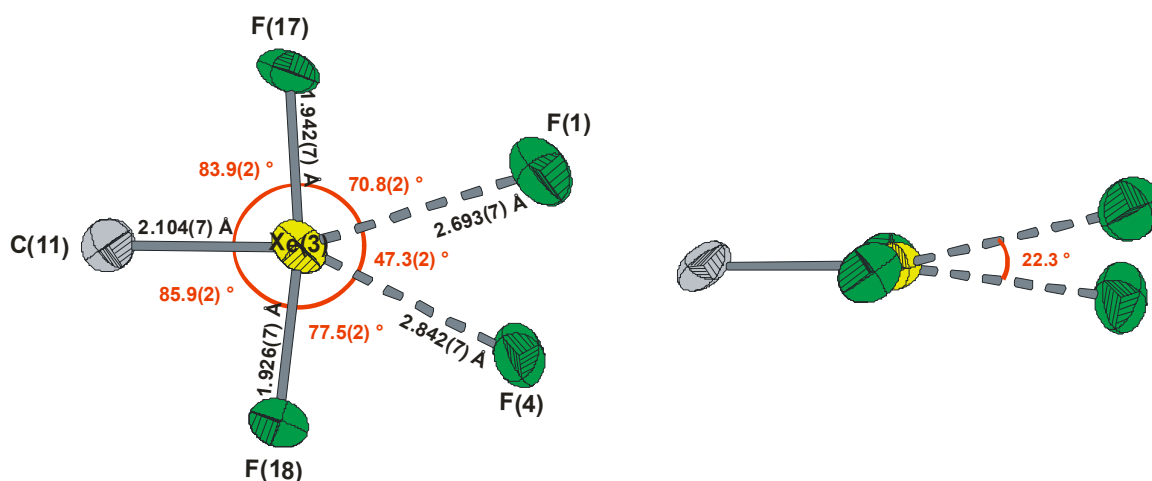


Figure 18 Pentagonal planar arrangement of the formal [C₆F₅XeF₂F₂]⁻ anion. Thermal ellipsoids are shown at the 50 % probability level.

The F(17)-Xe(1)---F(1) (70.8(2)°) and F(18)-Xe(1)---F(4) (77.5(2)°) angles within the plane are close to the ideal 72° value. The C(11)-Xe(1)-F(17) and C(11)-Xe(1)-F(18) angles are 83.9(4)° and 85.9(4)°, respectively, and are more open as a result of repulsion between the *ortho*-C₆F₅ fluorine atoms and the fluorine atoms bonded to xenon, while the F(1)---Xe(1)---F(4) angle (47.3(2)°) is closed. When the coordination sphere is enlarged to 3.5 Å, two additional long Xe(1)---F contacts with two different [BF₄]⁻ anions are found at 2.936(6) and 3.076(7) Å. These contacts occur on either side of the pentagonal plane and are directed away from the C₆F₅ ring, avoiding the free valence electron lone pairs on xenon. A similar pentagonal planar arrangement has previously been observed in the crystal structure of [XeF₅]⁻

,^[46] and $[\text{IF}_5]^{2-}$.^[48] Moreover, the long cation-anion contacts in $[\text{XeF}_3][\text{SbF}_6]$ also give rise to a distorted pentagonal planar arrangement around xenon.^[27]

A third $\text{Xe}(1)\cdots\text{F}_{\text{ax}}$ intermolecular long contact occurs at 3.157(6) Å with a second $[\text{C}_6\text{F}_5\text{XeF}_2]^+$ molecule. The weak contact results in a dimer formation between the $[\text{C}_6\text{F}_5\text{XeF}_2]^+$ cations which pack along the *a*-axis (Figure 20).

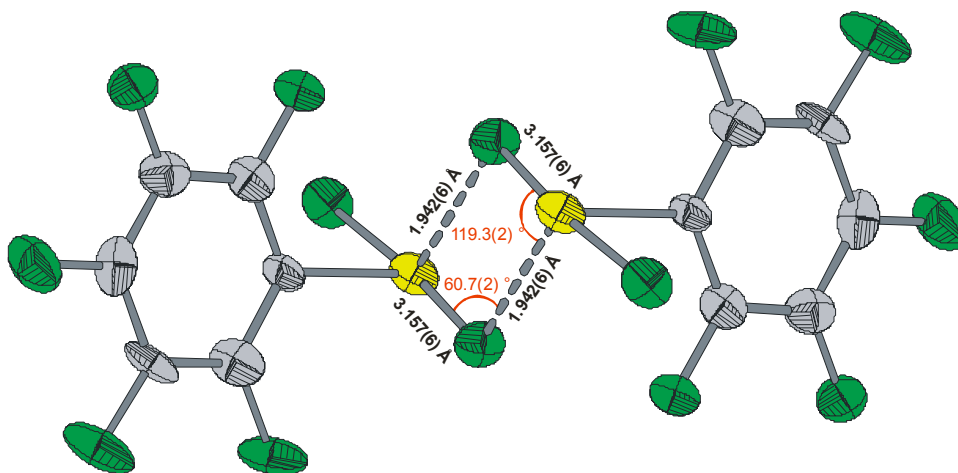


Figure 19 Dimer of $[\text{C}_6\text{F}_5\text{XeF}_2]_2$. Thermal ellipsoids are shown at the 50 % probability level.

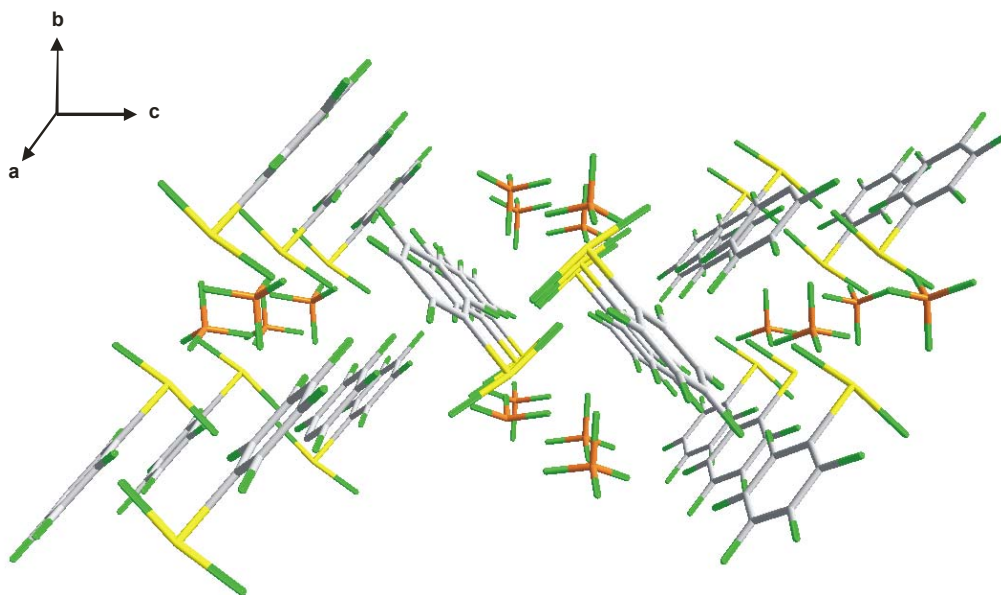


Figure 20 Crystal packing of [C₆F₅XeF₂][BF₄] along the a-axis.

The (XeF_{ax})₂ dimer units are separated by [BF₄]⁻ anions and are reminiscent of the (IF_{ax})₂ rhombohedrals found in C₆F₅IF₂.^[107] In the latter case, however, the (IF_{ax})₂ units are part of infinite chains. The [C₆F₅XeF₂]⁺ cations are packed along the a-axis so that the dimers form zigzag chains along the b-axis which are separated by a layer of [BF₄]⁻ anions.

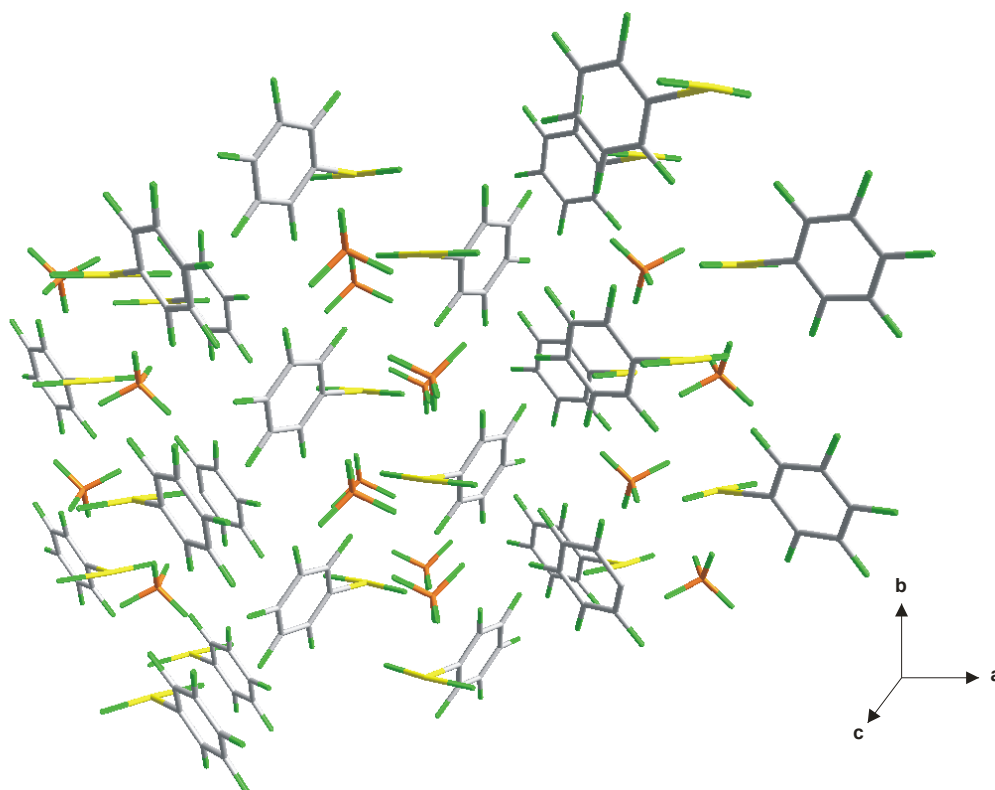


Figure 21 Crystal packing of $[\text{C}_6\text{F}_5\text{XeF}_2][\text{BF}_4]$ along the c-axis.

A similar coordination sphere occurs around xenon in the crystal structure of $[\text{C}_6\text{F}_5\text{XeF}_2 \cdot (\text{NCCH}_3)_{1.5}][\text{BF}_4]$ that is achieved through contacts with CH_3CN . Two of the $[\text{C}_6\text{F}_5\text{XeF}_2]^+$ cations have two $\text{Xe} \cdots \text{N}$ contacts with two symmetry-related CH_3CN molecules in which the geometries of the CH_3CN molecules are not noticeably affected by the coordination.

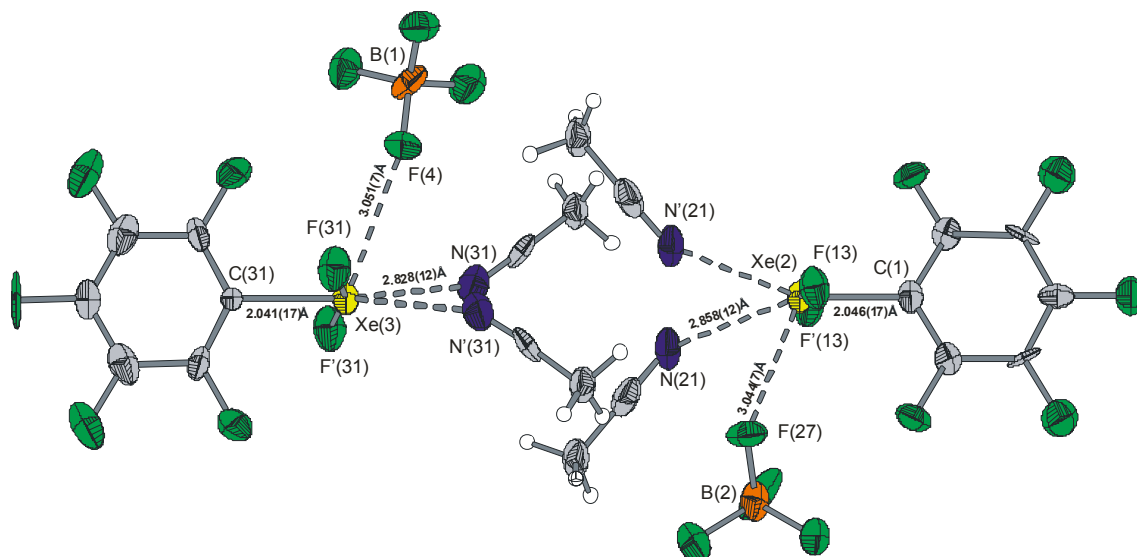


Figure 22 Two of the three non-equivalent molecules of the asymmetric cell of the crystal structure $[\text{C}_6\text{F}_5\text{XeF}_2 \cdot (\text{NCCH}_3)_{1.5}][\text{BF}_4]$. Thermal ellipsoids are shown at the 50 % probability level.

The Xe---N distances are 2.86(1) and 2.83(1) Å and are comparable to the Xe---F contact observed in the former structure, but are longer than the Xe---N distance in $[\text{C}_6\text{F}_5\text{Xe} \cdot \text{NCCH}_3]^+$ (2.613(15) and 2.637(7) Å).^[135] The angles subtended at the xenon atom are similar to those in $[\text{C}_6\text{F}_5\text{XeF}_2][\text{BF}_4]$ except for the angle involving the two bridging atoms which is now more open (N---Xe---N, 64.9(5) and 63.3(5)°). Although the angles are closer to what is expected for a pentagonal planar arrangement, the nitrogen atoms are now further from the $\text{XeCF}_{\text{ax}}\text{F}_{\text{ax}}$ plane giving rise to a much more distorted pentagonal environment around xenon.

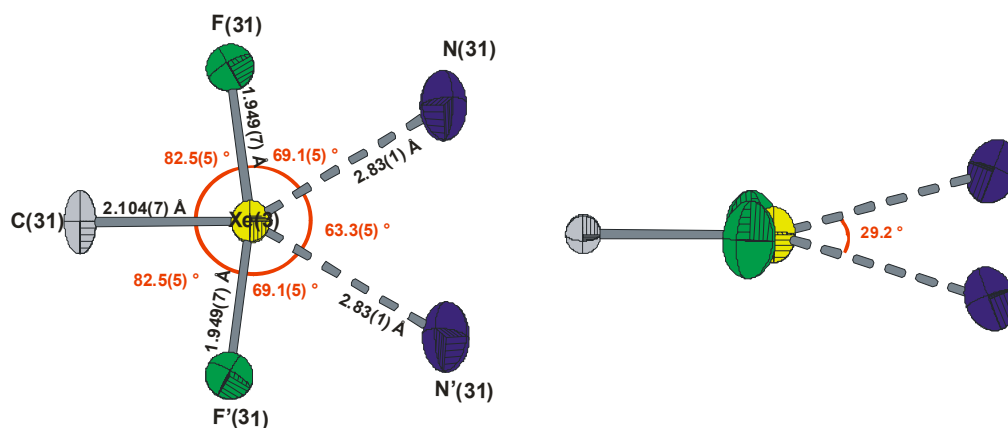


Figure 23 Pentagonal planar arrangement of the formal $\text{C}_6\text{F}_5\text{XeF}_2\text{N}_2$ arrangement. Thermal ellipsoids are shown at the 50 % probability level.

The third $[\text{C}_6\text{F}_5\text{XeF}_2]^+$ cation from the asymmetric cell of the crystal structure $[\text{C}_6\text{F}_5\text{XeF}_2 \cdot (\text{NCCH}_3)_{1.5}][\text{BF}_4]$ has one Xe---N contact (2.76(1) Å) with a CH_3CN molecule and this contact is 2.76(1) Å from the $\text{CXeF}_{\text{ax}}\text{F}_{\text{ax}}$ plane.

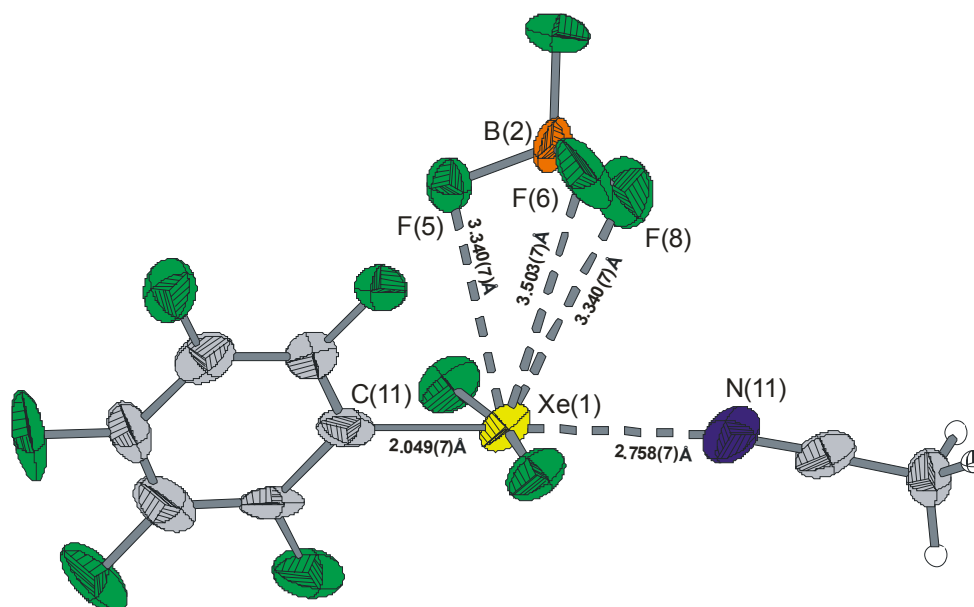


Figure 24 The third of the three non-equivalent molecules of the asymmetric cell of the crystal structure $[\text{C}_6\text{F}_5\text{XeF}_2 \cdot (\text{NCCH}_3)_{1.5}][\text{BF}_4]$. Thermal ellipsoids are shown at the 50 % probability level.

The next shortest contact is at 3.061(7) Å to a fluorine of a $[\text{BF}_4]^-$ anion, and it is slightly longer than those observed in $[\text{C}_6\text{F}_5\text{XeF}_2][\text{BF}_4]$. In all three cases, there are two additional long contacts between $[\text{BF}_4]^-$ anions and the $[\text{C}_6\text{F}_5\text{XeF}_2]^+$ cation as observed in $[\text{C}_6\text{F}_5\text{XeF}_2][\text{BF}_4]$ (Table 14). The C-Xe---N angles of both $[\text{C}_6\text{F}_5\text{XeF}_2 \cdot (\text{NCCH}_3)_2]^+$ (147.6(2)° and 148.2(2)°) and $[\text{C}_6\text{F}_5\text{XeF}_2 \cdot \text{NCCH}_3]^+$ (158.3(4)°) are much more bent than those in $[\text{C}_6\text{F}_5\text{Xe} \cdot \text{NCCH}_3][\text{B}(\text{CF}_3)_4]$ (174.8(2)°), $[\text{C}_6\text{F}_5\text{Xe} \cdot \text{NCCH}_3][\text{B}(\text{C}_6\text{F}_5)_2\text{F}_2]$ (174.5(3)°), $[\text{C}_6\text{F}_5\text{Xe} \cdot \text{NCCH}_3][\text{B}(\text{C}_6\text{F}_5)_4]$ (177.1(4)°), and $\text{C}_6\text{F}_5\text{Xe} \cdots \text{NCB}(\text{CN})_3$ (175.9(1)°), which may arise from additional long contacts with the $[\text{BF}_4]^-$ anions.

III.2.2.3 Characterization by Low-Temperature Raman Spectroscopy

The 36 vibrational modes of the $[\text{C}_6\text{F}_5\text{XeF}_2]^+$ cation under C_1 point symmetry belong to the irreducible representation 36A, which are all Raman and infrared active and the 9 vibrational modes of the $[\text{BF}_4]^-$ anion under T_d point symmetry belong to the irreducible representations $A_1 + E + 2T_2$.

The observed frequencies for the low-temperature solid-state Raman spectrum of $[\text{C}_6\text{F}_5\text{XeF}_2][\text{BF}_4]$ are summarized in Table 15.

Table 15 Experimental and Calculated Vibrational Frequencies for $[\text{C}_6\text{F}_5\text{XeF}_2][\text{BF}_4]$ and $\text{C}_6\text{F}_5\text{IF}_2$

$\text{C}_6\text{F}_5\text{XeF}_2^+$		$\text{C}_6\text{F}_5\text{IF}_2$			$\text{C}_6\text{F}_5\text{YF}_2^{+/0}$ (Y = Xe/I)	
expt ^a	SVWN ^b	expt ^{c,d}	expt ^{c,e}	SVWN ^b	assignments (C_1) ^f	
1630(10)	1641(<1)[1]	1636(10)	1637, m	1657(<1)[4]	v(C–C)	
	1630(17)[13]			1651(24)[20]		
1513(6)	1570(487)[1]	1512(3)	1521, vs	1549(254)[2]	v(C–C ₂) + v(C–F)	
	1554(465)[60]			1543(445)[<1]		
1431(5)	1447(5)[3]	1408(3)	1409, m	1449(3)[10]		
1427(7)						
	1393(34)[3]		1376, m	1391(7)[1]	v(C–C)	
	1330(11)[7]		1346, m			
	1233(2)[2]	1153(3)	1296, m	1317(5)[<1]	v(C–C ₂) + v(C–F)	
	1132(104)[6]	1090(2)	1154, m			
			1100, s	1201(2)[1]	$\delta(\text{CCC})$ i.p.small + v(C–C) ± v(C–F)	
			1047, w	1125(122)[1]		
	1035(124)[<1]		1013, m	1019(154)[1]	v(C–C ₂)v(C–F)	
789(7)	784(8)[4]	812(3)	989, vs	821(27)[3]	$\delta(\text{CCC})$ i.p.small + v(C–C ₂) + v(C–F)	
	754(<1)[<1]		813, s	751(<1)[<1]		$\delta(\text{CCC})$ i.p.
	696(<1)[<<1]			695(1)[<<1]		$\delta(\text{CCC})$ o.o.p.
	648(0)[<<1]			651(<1)[<<1]		$\delta(\text{CCC})$ o.o.p.
	609(139)[1]		547, sh	574(179)[<1]	v _{as} (YF ₂) ^g	
	588(9)[5]		541, s			
589(23)	587(2)[9]	625(1)	625, m	622(2)[1]	$\delta(\text{CCC})$ o.o.p. ^h	
535(69)		586(22)	585, w	587(<1)[13]	$\delta(\text{CCC})$ i.p.	
530(100)	514(39)[132]	533(100)	532, s	537(4)[19]	v _s (YF ₂)	

Table 15 (continued...)

494(14)	491(<1)[9]	496(29), 478(2)	487, sh 479, s 472, s	}	494(<1)[9]	$\delta(\text{CCC})$ i.p.
438(18)	423(<1)[4]	441(49)	446, s 437, s		}	434(<1)[4]
348(5)	338(3)[<<1] 319(0)[3]	386(21)	393, s 387, s	}		364(2)[1] 367(<1)[4]
343(6)	342(<<1)[2] 299(1)[<<1]	354(10)	352, m		}	350(<1)[2] 302(1)[<<1]
278(6)	263(2)[1] 257(<<1)[<<1]	281(5)		}		266(3)[1] 258(<1)[<<1]
237(7)	224(1)[2] 208(37)[1] 192(10)[0] 169(<<1)[<1]	241(10)			}	223(<1)[1] 225(31)[<<1] 204(12)[<<1] 178(<1)[<1]
188(19) 162(8)	151(10)[5]	174(25)		}		168(6)[3]
137(8)	127(0)[<<1]	150(4)			}	133(<1)[<<1] 142(<1)[1]
127(6)	125(1)[1]	130(8)		}		115(<1)[<1] 61(<1)[1]
116(5)	110(<1)[1] 52(<<1)[2] 25(0)[3]	96(47)			}	47(<1)[2]

Table 15 (continued...)

- ^a The Raman spectra were recorded at $-150\text{ }^{\circ}\text{C}$ in a heat-sealed glass NMR tube (Wilmad 507). Frequencies are given in cm^{-1} . Bands at 765(12) ($\nu_1(\text{A}_1)$), 368(11), 361(10) and 351(6) ($\nu_2(\text{E})$) cm^{-1} were assigned to $[\text{BF}_4]^-$ by comparison with previous assignments.^[99] Other combination bands have also been observed at 2948(4) and 1180(6) cm^{-1} .
- ^b SVWN/(SDB-)cc-pVTZ; infrared intensities, in $\text{kJ}\cdot\text{mol}^{-1}$, are given in parentheses and Raman intensities, in $\text{\AA}^4\cdot\text{amu}^{-1}$, are given in square brackets.
- ^c From ref.^[107]
- ^d Raman frequencies and intensities.
- ^e Infrared frequencies and intensities.
- ^f The deformation modes of the C_6F_5 ring are denoted by the general symbol δ and are relative to the plane containing the C_6F_5 ring; i.p. and o.o.p denote in-plane and out-of-plane, respectively. The deformation modes of the XeF_2 moiety are relative to a plane passing by the XeF_2 moiety and the *ipso*-C atom. In that case δ denotes a bend, ρ_w a wag, ρ_r a rock, and ρ_t a twist.
- ^g In the Xe case, there is also a small contribution from $\delta(\text{CCC})$ o.o.p.
- ^h In the Xe case, there is also a small contribution from $\nu_{\text{as}}(\text{YF}_2)$

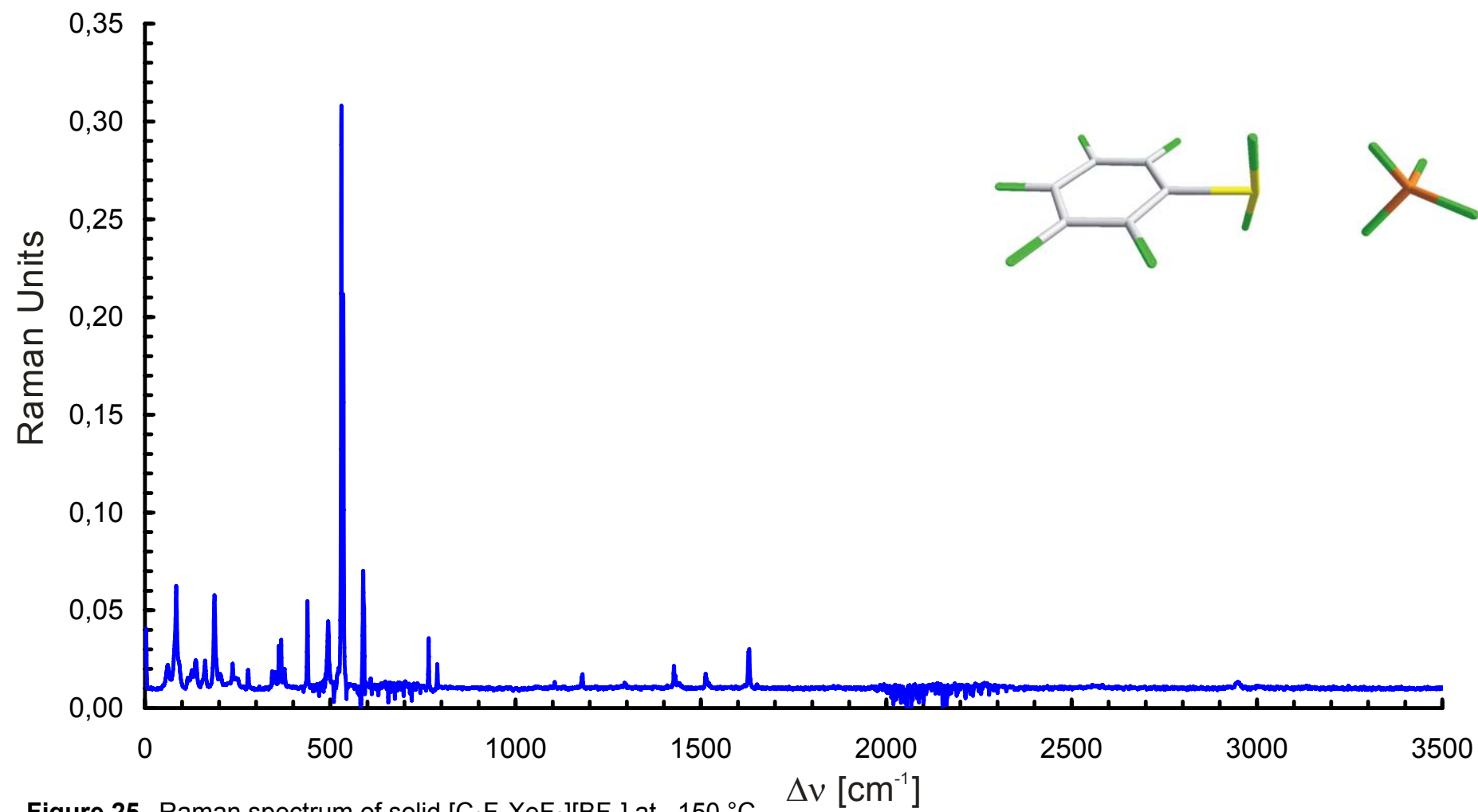


Figure 25 Raman spectrum of solid $[\text{C}_6\text{F}_5\text{XeF}_2][\text{BF}_4]$ at $-150\text{ }^\circ\text{C}$

Although the structure reveals several anion-cation contacts, the Raman spectrum can be analyzed in terms of isolated $[\text{C}_6\text{F}_5\text{XeF}_2]^+$ cations and $[\text{BF}_4]^-$ anions, the latter having frequencies that are in agreement with those reported earlier.^[99] Thus, the anion assignments require no further comment (Table 15, footnote a).

The frequency assignments for $[\text{C}_6\text{F}_5\text{XeF}_2]^+$ were aided by the calculated frequencies and calculated Raman intensities and previous vibrational assignments for $[\text{C}_6\text{F}_5\text{Xe}]^{+[135]}$ and the C_6F_5 group.^[103-105] The calculations were carried out using HF and DFT methods, and Stuttgart and SVWN/(SDB-)cc-pVTZ basis sets. The DFT results are in better agreement with the experimental spectra and are reported in Table 15. The experimental frequencies for the isoelectronic $\text{C}_6\text{F}_5\text{IF}_2$ compound have been reported earlier, but were not assigned. This Thesis also provides a complete assignment of the vibrational spectrum of $\text{C}_6\text{F}_5\text{IF}_2$, allowing a direct comparison of its vibrational frequencies with those of the $[\text{C}_6\text{F}_5\text{XeF}_2]^+$ cation (Table 15).

There is a good agreement between calculated and observed frequencies in Table 15. The stretching modes are all slightly overestimated, except for the $\nu(\text{Y-C})$ stretch ($\text{Y} = \text{Xe}, \text{I}$), but these modes are actually coupled to two deformation modes, which overall tend to be underestimated. Most modes associated with the C_6F_5 ring are essentially identical in both $[\text{C}_6\text{F}_5\text{XeF}_2]^+$ and $\text{C}_6\text{F}_5\text{IF}_2$. They are comparable to those observed in the $[\text{C}_6\text{F}_5\text{Xe}]^{+[135]}$ $\text{C}_6\text{F}_5\text{I}^{[103]}$ and other systems containing C_6F_5 groups.^[104, 105] The mode that is the most affected by the nature of Y is the bending mode, $\delta(\text{CCC})$ (the central C atom is bonded to Y) is shifted to higher frequency by 40 cm^{-1} when going from Xe to I for the calculated values (784 and 821 cm^{-1}) and by 23 cm^{-1} for the experimental values (789 and 812 cm^{-1}). A similar pattern for this mode has been observed in $[\text{C}_6\text{F}_5\text{Xe}]^{+}$ and $\text{C}_6\text{F}_5\text{I}$ (exptl.: 795 and 808 cm^{-1} ; calcd.: 772 and 818 cm^{-1}).^[103] The C-Xe(IV) stretch is calculated at slightly lower frequency (208 cm^{-1}) than the C-I(III) stretch (225 cm^{-1}), and they are both strongly coupled to two deformation modes, $\delta(\text{YF}_2)$ and $\delta(\text{CCF})$ i.p., which may account for the expected low intensity of this mode. As expected, the C-Xe(IV) and C-I(III) stretching frequencies are both about 20 cm^{-1} higher than the C-Xe(II) and C-I(I) stretching frequencies in $[\text{C}_6\text{F}_5\text{Xe}]^{+}$ (188 cm^{-1}) and $\text{C}_6\text{F}_5\text{I}$ (203 cm^{-1}).^[103] In practice, the $\nu(\text{Y-C})$ modes were proposed to be contributors to the modes at 237 and 241 cm^{-1} , respectively, which are 40 cm^{-1} higher in frequency than the experimental C-Xe(II) and C-I(I) stretching frequencies in $[\text{C}_6\text{F}_5\text{Xe}]^{+}$ ($201 - 205 \text{ cm}^{-1}$) and $\text{C}_6\text{F}_5\text{I}$ ($204 - 205 \text{ cm}^{-1}$).^[103] These experimental modes were not, however, solely

assigned to stretches because they occurred as medium intensity bands, and were consequently also assigned to the strongly coupled deformation mode $\delta(\text{CCF})$ o.o.p. + $\rho_r(\text{YF}_2)$ which is expected to have a medium intensity. It is worth noting that a significant increase in the $\nu(\text{Xe(IV)-F})$ versus $\nu(\text{Xe(II)-F})$ stretching frequencies has been observed in XeF_4 (554 cm^{-1}) and XeF_2 (496 cm^{-1}).^[136] The frequencies of the $\nu_{\text{as}}(\text{XeF}_2)$ and $\nu_{\text{s}}(\text{XeF}_2)$ modes in the $[\text{C}_6\text{F}_5\text{XeF}_2]^+$ cation are calculated at 609 and 514 cm^{-1} , respectively, and the $\nu_{\text{s}}(\text{XeF}_2)$ band is predicted to be the most intense band in the Raman spectrum of the $[\text{C}_6\text{F}_5\text{XeF}_2]^+$ cation; it was therefore assigned to the most intense bands at 535 and 530 cm^{-1} . The $\nu_{\text{as}}(\text{XeF}_2)$ band is predicted to be very weak because of the near-centrosymmetric XeF_2 moiety, and was not observed in the experimental Raman spectrum. Both frequencies are comparable to the $\nu_{\text{as}}(\text{XeF}_{2a})$ (608 cm^{-1}) and $\nu_{\text{s}}(\text{XeF}_{2a})$ (570 cm^{-1}) stretches in $[\text{XeF}_3]^+$ ^[9] and the $\nu_{\text{s}}(\text{XeF}_4)$ (586 cm^{-1}) and $\nu_{\text{as}}(\text{XeF}_4)$ (543 cm^{-1}) stretches in XeF_4 . The frequency of $\nu_{\text{s}}(\text{IF}_2)$ in $\text{C}_6\text{F}_5\text{IF}_2$ is expected to be only 40 cm^{-1} lower than that of $\nu_{\text{as}}(\text{IF}_2)$ with both values being intermediate between the ν_{as} and ν_{s} frequencies in $[\text{C}_6\text{F}_5\text{XeF}_2]^+$. As is the case for $[\text{C}_6\text{F}_5\text{XeF}_2]^+$, only the symmetric stretch of $\text{C}_6\text{F}_5\text{IF}_2$ is observed in the Raman spectrum, where it is also the most intense band; the asymmetric stretch could be observed as a very intense band in the infrared spectrum at 541 cm^{-1} . The frequency of $\nu_{\text{s}}(\text{IF}_2)$ in $\text{C}_6\text{F}_5\text{IF}_2$ is comparable to that of $\nu_{\text{s}}(\text{IF}_2)$ (550 cm^{-1}) in IF_3 .^[137, 138] The deformation modes, $\rho_w(\text{XeF}_2)$ and $\rho_w(\text{IF}_2)$, which are predicted to occur at 192 and 204 cm^{-1} , respectively, and to be very weak in the Raman spectrum, were not observed. The seven modes below 192 (Xe) and 204 (I) cm^{-1} are all deformation modes. Two are deformations within the C_6F_5 ring and are comparable to those calculated for $[\text{C}_6\text{F}_5\text{Xe}]^+$ or $\text{C}_6\text{F}_5\text{I}$.^[103] The remaining eight modes include pure XeF_2 or IF_2 bending modes or modes where both deformation motions of the C_6F_5 ring and XeF_2 or IF_2 are coupled. The $\delta(\text{XeF}_2)$ and $\delta(\text{IF}_2)$ modes are calculated at 151 and 168 cm^{-1} and are predicted to be rather intense in the Raman spectrum. They were assigned to the medium intensity bands observed at $162/188$ and 174 cm^{-1} , respectively. These frequencies are significantly lower than $\delta(\text{XeF}_{2a})$ in $[\text{XeF}_3]^+$ (209 cm^{-1}),^[9] $\delta(\text{FXeF})$ in XeF_4 (235 cm^{-1}) and $\delta(\text{IF}_{2a})$ in IF_3 (211 cm^{-1})^[137, 138] where the central Xe/I atom coordination is more congested.

III.2.3 Computational Results

III.2.3.1 Geometries of $[C_6F_5XeF_2]^+$, $[C_6F_5XeF_2 \cdot NCCH_3]^+$, $[C_6F_5XeF_2 \cdot (NCCH_3)_2]^+$ and $C_6F_5IF_2$

The electronic structures of the $[C_6F_5XeF_2]^+$ cation, the $[C_6F_5XeF_2 \cdot NCCH_3]^+$ and $[C_6F_5XeF_2 \cdot (NCCH_3)_2]^+$ adducts and $C_6F_5IF_2$ were calculated using Hartree-Fock (HF) and pure density function theory (DFT) with the Stuttgart and (SDB-)cc-pVTZ basis sets starting from C_1 symmetry. Both types of calculations resulted in stationary points with all frequencies real, with the DFT calculations giving better agreement with the experimental geometries (see Table 16) and vibrational frequencies (see Table 15). For this reason, only the DFT results are reported. The basis sets used employ semi-relativistic effective core potentials (RLC ECP), consequently, the calculated values for $C_6F_5IF_2$ are improved when compared with the previously reported values.^[107]

The calculations show that the F-Xe-C-C and F-I-C-C dihedral angles vary significantly depending on the level of the calculation and on the basis set used. While $C_6F_5IF_2$ gave an energy-minimized geometry having a F-I-C-C dihedral angle of 32.7° (Table 16), the energy-minimized geometry of $[C_6F_5XeF_2]^+$ had essentially C_s symmetry with the XeF_2 -moiety orientated perpendicular to the C_6F_5 ring at the SVWN level for $[C_6F_5XeF_2]^+$. It is worth noting that the cation also gives rise to a local minimum using C_s symmetry that has an energy that is only $16 \text{ KJ} \cdot \text{mol}^{-1}$ lower than that obtained in the C_1 structure. It is difficult to account for the difference in calculated twist angles in view of the longer or larger calculated Xe-F bond lengths and F-Xe-F and F-Xe-C bond angles relative to the analogous geometric parameters in $C_6F_5IF_2$. The differences between observed and experimental twist angles are likely accounted for by the existence of various intermolecular contacts in the experimental structures (*vide infra*).

Table 16 Calculated ^a (*C₇*) Geometrical Parameters for [C₆F₅XeF₂]⁺, [C₆F₅XeF₂·NCCH₃]⁺, [C₆F₅XeF₂·(NCCH₃)₂]⁺ and C₆F₅IF₂

Bond Lengths (Å)	[C ₆ F ₅ XeF ₂] ⁺	[C ₆ F ₅ XeF ₂ ·NCCH ₃] ⁺	[C ₆ F ₅ XeF ₂ ·(NCCH ₃) ₂] ⁺	C ₆ F ₅ IF ₂
C(1)-C(2)	1.389	1.386	1.379	1.382
C(2)-F(2)	1.305	1.310	1.313	1.315
C(2)-C(3)	1.382	1.381	1.383	1.383
C(3)-F(3)	1.300	1.304	1.308	1.316
C(3)-C(4)	1.395	1.393	1.390	1.385
C(4)-F(4)	1.295	1.299	1.305	1.314
C(4)-C(5)	1.395	1.393	1.390	1.385
C(5)-F(5)	1.300	1.304	1.308	1.316
C(5)-C(6)	1.382	1.381	1.383	1.383
C(6)-F(6)	1.305	1.310	1.313	1.315
C(6)-C(1)	1.389	1.386	1.380	1.382
Xe(1)-C(1)	2.038	2.056	2.086	2.048
Xe(1)-F(11)	1.966	1.983	1.990	1.960
Xe(1)-F(12)	1.966	1.976	1.990	1.960
Xe(1)---N(1)		2.567	2.570	
Xe(1)---N(2)			2.570	
N(1)-C(7)		1.153	1.152	
C(7)-C(8)		1.422	1.425	
C(8)-H x3		1.100	1.100	
N(2)-C(9)			1.152	
C(9)-C(10)			1.425	
C(10)-H x3			1.100	
Bond Angles (°)				
C(1)-C(2)-C(3)	117.3	118.3	118.4	120.0
C(2)-C(3)-C(4)	119.5	119.3	119.5	119.5
C(3)-C(4)-C(5)	121.9	121.7	121.2	120.6
C(4)-C(5)-C(6)	119.5	119.3	119.5	119.5

Table 16 (continued...)

C(5)-C(6)-C(1)	117.2	118.3	118.4	120.0
C(1)-C(2)-F(2)	121.1	120.8	120.9	120.9
C(2)-C(1)-F(6)				
F(2)-C(2)-C(3)	121.6	120.9	120.7	119.1
C(2)-C(3)-F(3)	120.5	120.7	120.5	120.6
F(3)-C(3)-C(4)	120.0	120.0	120.1	119.9
C(3)-C(4)-F(4)	119.0	119.2	121.2	119.7
F(4)-C(4)-C(5)	119.0	119.2	119.4	119.7
C(4)-C(5)-F(5)	120.0	120.0	120.1	119.9
F(5)-C(5)-C(6)	120.5	120.7	120.5	120.6
C(5)-C(6)-F(6)	121.6	120.9	120.7	119.1
F(6)-C(6)-C(1)	121.1	120.8	120.9	120.9
Xe(1)-C(1)-C(2)	117.7	118.4	118.4	119.8
Xe(1)-C(1)-C(6)	117.7	118.4	118.4	119.8
F(11)-Xe(1)-F(12)	178.6	176.5	158.4	170.2
F(11)-Xe(1)-C(1)	89.3	88.6	79.2	85.1
F(12)-Xe(1)-C(1)	89.3	87.9	79.2	85.1
F(11)-Xe(1)---N(1)		102.2	67.8	
F(11)-Xe(1)---N(2)			133.8	
F(12)-Xe(1)---N(1)		81.3	133.8	
F(12)-Xe(1)---N(2)			67.8	
N(1)---Xe(1)---N(2)			66.0	
C(1)-Xe(1)---N(1)		169.3	147.0	
C(1)-Xe(1)---N(2)			147.0	
Xe(1)---N(1)-C(7)		176.3	165.2	
Xe(1)---N(2)-C(9)			165.2	
N(1)-C(7)-C(8)		179.9	179.9	
N(2)-C(9)-C(10)			179.9	
C(2)-C(1)-Xe(1)-F(11)		-89.9	-113.4	-122.7
C(2)-C(1)-Xe(1)-F(11)		90.1	66.6	57.3

Table 16 (continued...)

Dihedral Angles (°)				
C(2)-C(1)-Xe(1)-F(11)	90	-89.9	-113.4	-122.7
C(2)-C(1)-Xe(1)-F(12)	90	90.1	66.6	57.3

^a SVWN/SDB-cc-pVTZ using C_1 symmetry.

The calculations reproduce the XeF₂ and IF₂ angles which are bent towards their respective C₆F₅ rings. While the calculated F-I-F angle is 170.2° when compared with the experimental value of 171.59(9)°, the calculated F-Xe-F angle of 178.6° is much more open than in the crystal structures (164.9(4) – 170.3(3)°). The smaller F-I-F angle (170.2°) is in agreement with the larger more diffuse lone pairs in C₆F₅IF₂, while the wider F-Xe-F angle (178.6°) accounts for the more contracted lone pairs in the [C₆F₅XeF₂]⁺ cation. The difference between experimental and calculated values for the xenon compound may be associated with the additional intermolecular contacts to xenon (*vide supra*).

As already noted, Xe-F bond lengths and F-Xe-F and F-Xe-C bond angles of [C₆F₅XeF₂]⁺ are all calculated to be slightly larger than the analogous I-F, F-I-F and F-I-C parameters, which differs from experiment where all of these parameters are equal within experimental error.

The calculated structure of [C₆F₅XeF₂·NCCH₃]⁺ shows that the XeF₂-moiety is no longer perpendicular to the C₆F₅ ring, showing only a small dihedral angle of -9.86° (90 – 99.86) with respect to the plane perpendicular to the C₆F₅ ring.

The calculated structure of [C₆F₅XeF₂·(NCCH₃)₂]⁺ is in good agreement with the experimental structure and even reproduces the dihedral angle of the F-Xe-F moiety relative to the plane of the C₆F₅ ring. The Xe---N contacts lie in the XeF₂ plane with the C₆F₅ ring subtending an angle of 23.4° (90 - 66.6°) with the XeF₂N₂-plane, slightly larger than what is observed experimentally. It is worth noting that as the coordination number of xenon increases, the F-Xe-F angle decreases while the twist angle increases. The Xe-F bonds also elongate upon coordination of two CH₃CN ligands. Experimentally, there is no change in the Xe-F, F-Xe-F and F-Xe-C parameters because all cases are “di-adducts” with two CH₃CN in two molecules, one CH₃CN and one [BF₄]⁻ in another and finally two [BF₄]⁻. In all cases, the F-Xe-F angles are smaller with the smallest angles being observed for coordination of two CH₃CN molecules. As observed in the experimental structure, the CH₃ groups are pushed away from one another and the Xe-N-C angle is 165.2°. The differences between the experimental and calculated structures most likely arise from packing effects that allow the CH₃CN groups and [BF₄]⁻ anions to twist away from their “ideal” gas-phase positions. The two fluorine ligands bonded to xenon also bend toward the

C₆F₅ ring with a F-Xe-F angle of 158.7°. The N---Xe---N angle is 65.3°, in good agreement with experiment.

III.2.4 *Behaviour of [C₆F₅XeF₂]⁺ Salts in Solution and in Suspension*

The stability of [C₆F₅XeF₂][BF₄] in solution was less compared to those of the organoxenon(II) salts and strongly dependent on its purity, thus smallest amounts of reducing agents, such as moisture, resulted in a faster decomposition of [C₆F₅XeF₂][BF₄]. Every sample of [C₆F₅XeF₂][BF₄] had a slightly different distribution of decomposition products. Nevertheless, it was possible to optimize the preparation of [C₆F₅XeF₂][BF₄] in nearly quantitative yield (ca. 90 – 98%).

The pale ochre solid, [C₆F₅XeF₂][BF₄], was insoluble in weakly coordinating solvents such as CH₂Cl₂, SO₂ClF, and PFB consistent with the assumption of a strong cation-anion interaction in the solid state. Methylene chloride suspensions of [C₆F₅XeF₂][BF₄] were handled at temperatures below –40 °C but the solvent was attacked by the [C₆F₅XeF₂]⁺ cation at temperatures higher than –40 °C. A black coloration and gas evolution were observed when warming a [C₆F₅XeF₂][BF₄]/CH₂Cl₂ suspension to ambient temperature, yielding, almost immediately, the following decomposition products: C₆F₅H (59%), C₆F₅Cl (11%), C₆F₆ (30%), CHF₃ (7%), CH₂ClF (33%), CH₂F₂ (78%), and HF (75%). No precipitation and no reduced xenon compounds, such as [C₆F₅Xe]⁺ or XeF₂ were obtained in the mother liquor. The ¹⁹F NMR spectra of the mother liquor clearly showed that the solvent was attacked by the [C₆F₅XeF₂]⁺ cation. The rapid gas evolution and the absence of xenon-containing compounds lead to the assumption that xenon gas had evolved. The sum of the C₆F₅-containing compounds was normalized to 100% and compounds not containing C₆F₅ were calculated relative to 100% C₆F₅. The excess of fluorine compounds (85%) in the decomposition products might be caused by anion decomposition under fluoride abstraction yielding F[–] and BF₃ and/or evolution of volatile C₆F₅ compounds such as C₆F₅H, C₆F₆, and BF₃.

The salt, [C₆F₅XeF₂][BF₄], has a very high solubility in the basic solvent CH₃CN at –40 °C and in aHF solvent at –80 °C. Both solutions are intensive yellow in colour. The dipolar nature of the HF molecule is capable of coordinating to the [C₆F₅XeF₂]⁺ cation in two different ways. It can coordinate to the fluorine atoms of the

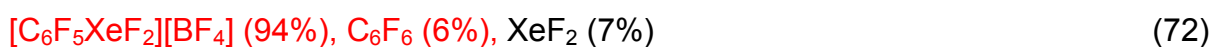
$[\text{XeF}_2]^+$ moiety by means of the H-bonding or to the positively charged xenon(IV) center by means of fluorine bridge formation.



The HF molecule is known to be a very weak nucleophile making the second coordination path less likely. The coordination to a fluorine on xenon withdraws electron density from the $[\text{XeF}_2]^+$ unit and increases the positive charge on the xenon center. The higher positive charge on xenon polarizes the C_6F_5 group and, more importantly for the decomposition, the C-Xe bond by withdrawing electron density through the σ frame. The *ipso*-C atom becomes more positive and can be attacked by nucleophiles. This decomposition pathway will be discussed later in detail as solvolysis.

Detailed decomposition studies of the salt, $[\text{C}_6\text{F}_5\text{XeF}_2][\text{BF}_4]$, in aHF showed an astonishing stability between -80 and -40 °C. The solution can be stored without decomposition over a period of more than 18 d in a FEP reaction tube protected by argon gas in the dark. Slow decomposition was obtained in aHF solution at -40 °C (complete consumption of $[\text{C}_6\text{F}_5\text{XeF}_2]^+$ within 88 d), whereas faster decomposition was detected at -30 °C (complete consumption of $[\text{C}_6\text{F}_5\text{XeF}_2]^+$ within 4 d). At ambient temperatures, rapid decomposition under gas evolution was observed. The following schemes show the product distributions at different temperatures. The initial purity of the sample of $[\text{C}_6\text{F}_5\text{XeF}_2][\text{BF}_4]$ dissolved in aHF at -40 °C is also reported.

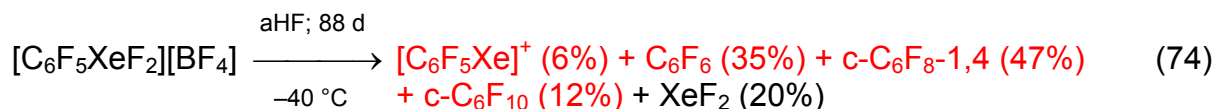
Purity of the starting material used to study the decomposition in aHF at -40 °C and at RT



Purity of the starting material used to study the decomposition in aHF at -30 °C

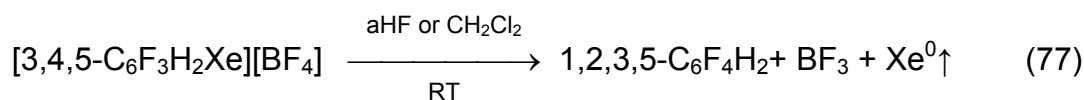


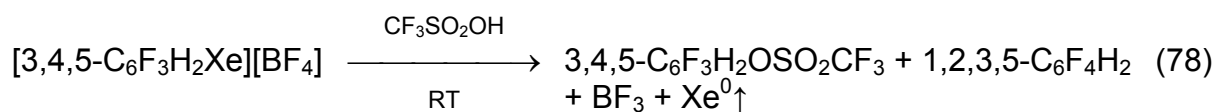
Product distribution resulting from the decomposition of $[\text{C}_6\text{F}_5\text{XeF}_2][\text{BF}_4]$ in aHF at -40 , -30 °C, and RT.



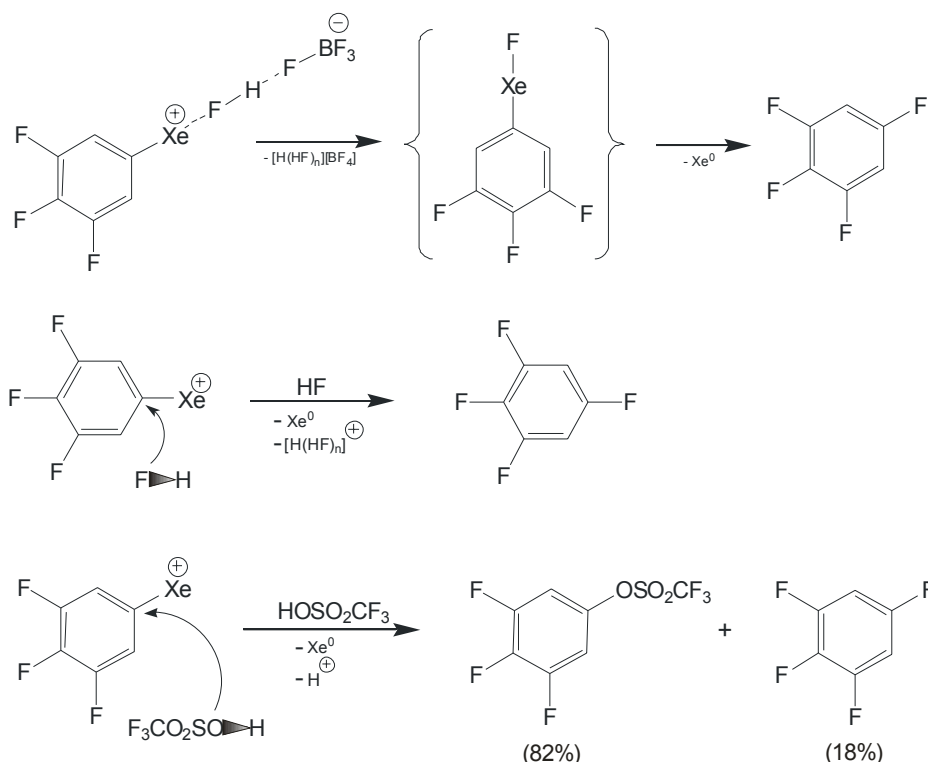
$\Sigma\text{C}_6\text{F}_5$ groups and derivatives = 100%

The main decomposition products for all decomposition studies of $[\text{C}_6\text{F}_5\text{XeF}_2][\text{BF}_4]$ in aHF were C_6F_6 or its oxidation products, namely c- $\text{C}_6\text{F}_8\text{-1,4}$ and c- C_6F_{10} . However, the product distribution differs for the “slow” decomposition reactions (≤ -40 °C) and the “fast” decomposition reactions (≥ -30 °C). The decomposition pathways can be explained by the following mechanisms. One mechanism involves nucleophilic attack of the polar Lewis acidic solvent at the polar C-Xe bond. Comparable behaviour was previously observed for hydrogen-containing arylxenon(II) compounds. It has been found that hydrogen-containing arylxenon(II) compounds, such as $[\text{3,4,5-C}_6\text{F}_3\text{H}_2\text{Xe}]^+$ and $[\text{3,5-C}_6\text{F}_3\text{H}_2\text{Xe}]^+$, were less stable towards solvolysis than the analogous arylxenon compounds having fluorine substituents in *ortho*-position such as $[\text{2,6-C}_6\text{F}_2\text{H}_3\text{Xe}]^+$ and $[\text{C}_6\text{F}_5\text{Xe}]^+$. The decomposition studies in aHF at RT have shown that $[\text{C}_6\text{F}_5\text{Xe}][\text{BF}_4]$ was stable for 2 d without any decomposition whereas after 54 d at RT only ~15% of $[\text{C}_6\text{F}_5\text{Xe}]^+$ was converted to C_6F_6 , the only detectable decomposition product. Comparable decomposition studies from Frohn, Franke, and Bardin^[130] have shown that the *ortho*-hydrogen-containing arylxenon compounds decompose completely in aHF at RT within only 12 h.



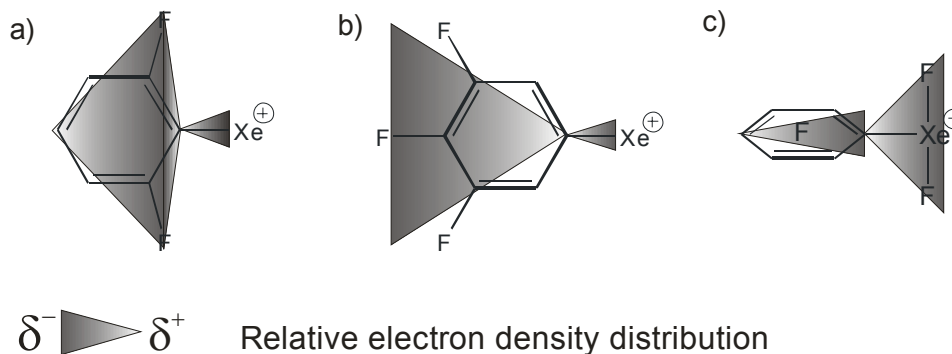


The decomposition yielded 1,2,3,5-C₆F₄H₂ besides BF₃ and Xe⁰, indicative of solvolysis of the C-Xe bond by HF. Decompositions in CF₃SO₂OH resulted in a mixture of 3,4,5-C₆F₃H₂OSO₂CF₃ (82%) and 1,2,3,5-C₆F₄H₂ (18%) which clearly shows participation of the solvent. The mixture in scheme 78 and the decomposition in CH₂Cl₂ (equation 77), however, indicates that not only solvolysis of the C-Xe bond but also coordination of the [BF₄]⁻ anion and formation of an intermediate, C₆F₃H₂XeF, might have initiated the decomposition of the organoxenon(II) cation. The following schemes illustrate three decomposition pathways in polar Lewis acidic solvents.

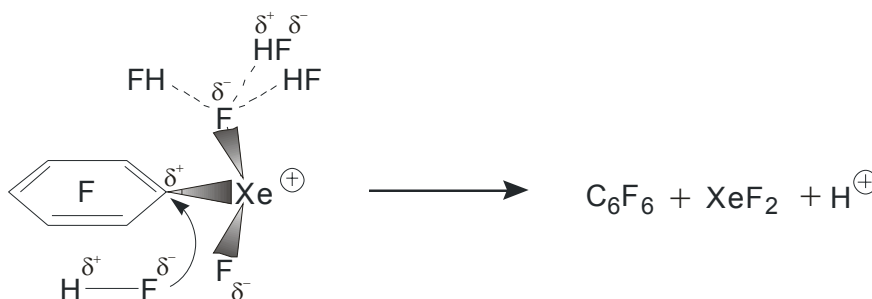


The three fluorine atoms in 3,4,5-C₆F₃H₂Xe (b) are able to strongly polarize their adjacent C-atoms and, in addition, the Xe(II) substituent polarizes the C-Xe bond more strongly than in the cases where the fluorine atoms are at the *ortho*-positions

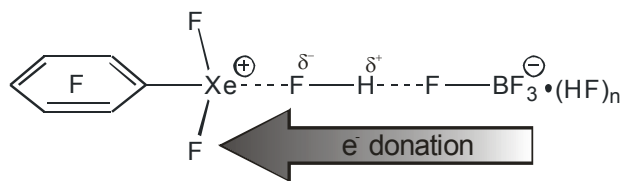
(a). The high polarity of the C-Xe bond is responsible for the facile solvolysis of this bond by polar solvents resulting in a faster decomposition with the formation of 3,4,5- $C_6F_3H_2A$ (A = corresponding base of the solvent).



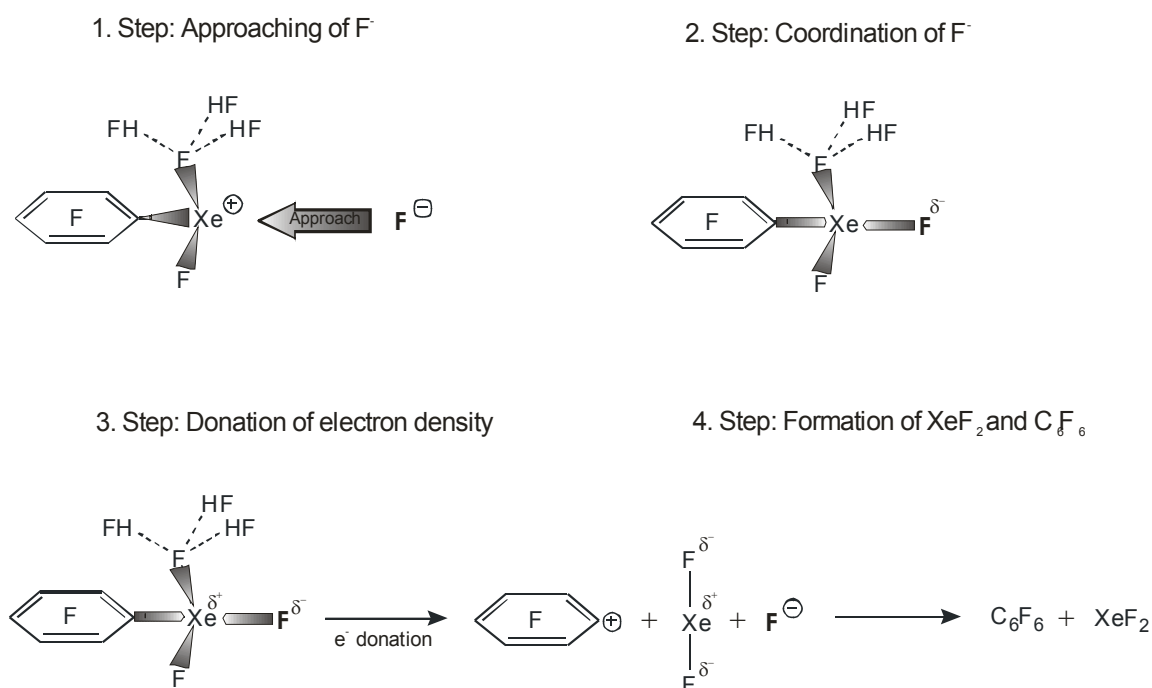
The C-Xe bond in $[C_6F_5XeF_2]^+$ is assumed to be even more polarized because of the strongly electron withdrawing effect of the $[XeF_2]^+$ substituent. The solvolysis of the C-Xe bond occurs in the case of $[C_6F_5XeF_2][BF_4]$ in aHF at $-40^\circ C$ but not for $[C_6F_5Xe][BF_4]$.



The product of the solvolysis of the C-Xe bond is, in the case of $[C_6F_5XeF_2]^+$, C_6F_6 and XeF_2 . The formation of H^+ means acidification of HF ($[H_2F]^+$) which reinforces the previously described interactions of the $[C_6F_5XeF_2]^+$ cation. The same products could be formed in a second possible pathway which involves the nucleophilic coordination of fluoride to the positively charged xenon(IV) center. This nucleophile might be a solvated anion, $[BF_4 \cdot (HF)_n]^-$, which carries a partial negative charge.

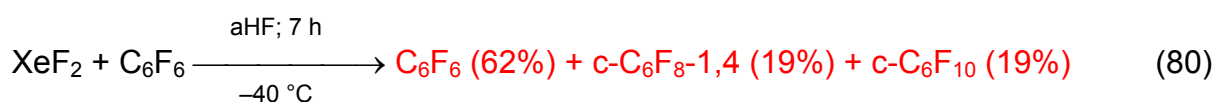
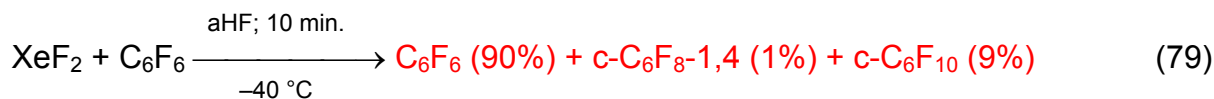


The fluoro nucleophile approaches the $[\text{C}_6\text{F}_5\text{XeF}_2]^+$ cation whereby the electronic environment around xenon changes. Donation of electron density into the Xe(IV) valence shell weakens the C-Xe bond such that the cationic presentation of the $[\text{C}_6\text{F}_5\text{XeF}_2]^+$ cation is reduced. The borderline description of this interaction, the neutral $\text{C}_6\text{F}_5\text{XeF}_3$ molecule, decomposes yielding C_6F_6 and XeF_2 . Whether this decomposition proceeds by means of the neutral $\text{C}_6\text{F}_5\text{XeF}_3$ molecule or its precursor and whether the cleavage of the C-Xe bond functions heterolytically with the formation of $[\text{C}_6\text{F}_5]^+$ and $[\text{XeF}_3]^-$ or even homolytically with the formation of $\text{C}_6\text{F}_5\cdot$ and $\cdot\text{XeF}_3$ radicals cannot be deduced from the experimental results. The proposed decomposition pathway is illustrated in the following Figure.



The product distribution shows significant amounts of XeF_2 in the “slow” decomposition reactions at $-40\text{ }^\circ\text{C}$ whereas no XeF_2 was detected in the faster decomposition reactions above $-30\text{ }^\circ\text{C}$. But with increasing temperature larger

amounts of *c*-C₆F_{8-1,4} and *c*-C₆F₁₀ ($\Sigma = >50\%$) were detected. The oxidative fluorination of C₆F₆ can occur with XeF₂ and/or with the [C₆F₅XeF₂]⁺ cation.



$\Sigma\text{C}_6\text{F}_5$ groups and derivatives = 100 %

Independent experiments with XeF₂ and C₆F₆ were performed and have shown that XeF₂ is able to fluorinate C₆F₆ in aHF at –40 °C. Stoichiometric amounts of XeF₂ and C₆F₆ were reacted in aHF at –40 °C yielding *c*-C₆F₁₀ (9%) after 10 minutes and *c*-C₆F_{8-1,4} (19%) and *c*-C₆F₁₀ (19%) after 7 h. The fact that XeF₂ was present in the decomposition of [C₆F₅XeF₂][BF₄] after 88 d in aHF at –40 °C is indicative that the decomposition of the [C₆F₅XeF₂]⁺ cation in C₆F₆ and XeF₂ has to be the rate determining step in the reaction sequence.

The oxidative fluorination of C₆F₆ to *c*-C₆F_{8-1,4} and subsequently to *c*-C₆F₁₀ was mainly due to XeF₂. The direct oxidative fluorination of C₆F₆ by [C₆F₅XeF₂]⁺ was significantly less as can be deduced from the relatively small amount of [C₆F₅Xe]⁺ (6%).

It is obvious that the solvolysis of the [C₆F₅XeF₂]⁺ cation was faster at temperatures above –30 °C and was followed by rapid consumption of XeF₂ by the fluorination of C₆F₆ to *c*-C₆F_{8-1,4}. In the decomposition studies at ≥ -30 °C no XeF₂ was present. At this elevated temperature, a higher content of [C₆F₅Xe]⁺ (25 – 36%) was obtained which is indicative of the oxidative fluorination of C₆F₆ by the [C₆F₅XeF₂]⁺ cation. It is noteworthy that the fluorination of *c*-C₆F_{8-1,4} to *c*-C₆F₁₀ was only detected at –40 °C.

It was shown in the X-ray crystal structure of [C₆F₅XeF₂·(NCCH₃)_{1.5}][BF₄] from crystals obtained from CH₂Cl₂/CH₃CN solution that coordination of CH₃CN molecules to the positively charged xenon(IV) center of the [C₆F₅XeF₂]⁺ cation occurs through nitrogen. Surprisingly, not only a single, but two molecules CH₃CN coordinate to xenon(IV) in the solid state. The coordinated N-base donates electron density to the [C₆F₅XeF₂]⁺ cation resulting in a less positive xenon center. The increased electron

density on the Xe(IV) of the adduct, $[\text{C}_6\text{F}_5\text{XeF}_2 \cdot (\text{NCCH}_3)_n]^+$ weakens both the Xe-F and the C-Xe bonds.

Detailed decomposition studies of CH_3CN solutions of $[\text{C}_6\text{F}_5\text{XeF}_2][\text{BF}_4]$ have shown that such solutions can be handled at $-40\text{ }^\circ\text{C}$ neglecting the initial slow decomposition of the $[\text{C}_6\text{F}_5\text{XeF}_2]^+$ cation (see decomposition trend in Figure 26). The cation was completely decomposed at $-40\text{ }^\circ\text{C}$ after 58 d according to scheme 82.

Purity of the starting material used to study the decomposition in CH_3CN at $-40\text{ }^\circ\text{C}$
 $[\text{C}_6\text{F}_5\text{XeF}_2][\text{BF}_4]$ (92%), $[\text{C}_6\text{F}_5\text{Xe}][\text{BF}_4]$ (7%), C_6F_6 (1%), XeF_2 (3%), HF (6%) (81)

Product distribution resulting from the decomposition of $[\text{C}_6\text{F}_5\text{XeF}_2][\text{BF}_4]$ in CH_3CN at $-40\text{ }^\circ\text{C}$



$\Sigma\text{C}_6\text{F}_5$ groups and derivatives = 100%

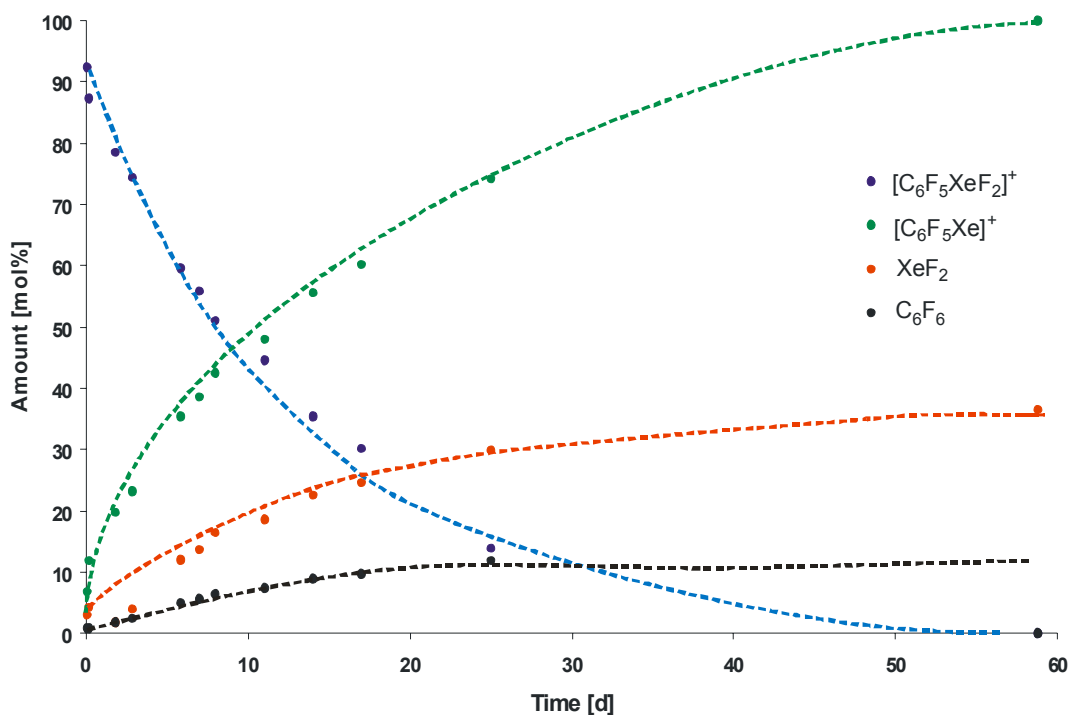
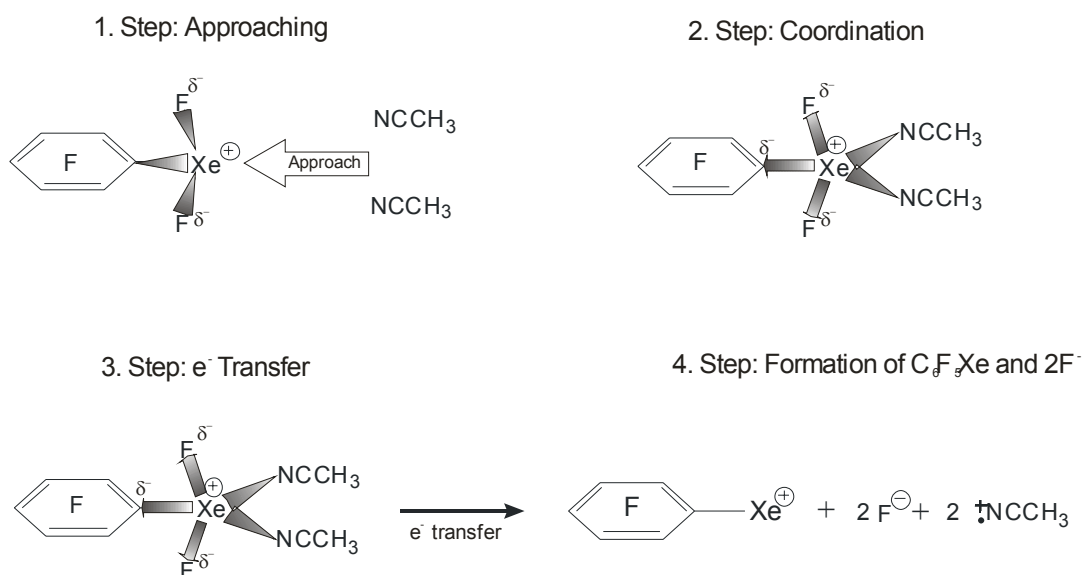


Figure 26 Decomposition trend of $[\text{C}_6\text{F}_5\text{XeF}_2][\text{BF}_4]$ in CH_3CN at $-40\text{ }^\circ\text{C}$

It is apparent from these studies that the main decomposition product in CH₃CN at -40 °C is [C₆F₅Xe][BF₄] (83%) besides significant amounts of XeF₂ (36%) and HF (46%). Only small amounts of C₆F₆ (13%) and its fluorinated product, c-C₆F_{8-1,4} (4%), and no c-C₆F₁₀ were detected in the CH₃CN solutions by ¹⁹F NMR spectroscopy. Repeated decomposition experiments in CH₃CN solution at -40 °C have demonstrated that CH₃CN solutions of [C₆F₅XeF₂][BF₄], which require 58 d to go to completion, yielding that the [C₆F₅XeF₂]⁺ cation is less stable in CH₃CN than in aHF solution (88 d) at -40 °C.

One decomposition channel in CH₃CN solution is assumed to occur in three steps: approach of CH₃CN, coordination of CH₃CN and subsequent electron transfer of two electrons and formation of [C₆F₅Xe]⁺, 2 F⁻, and 2 CH₃CN•.



It can not be proven that either Xe-F bonds were heterolytically cleaved with the formation of [C₆F₅Xe]⁺ and 2 F⁻ or homolytically with the formation of [C₆F₅Xe]⁺ and 2 F•, but it is obvious that the abstracted fluorine atoms (ions or radicals) were observed mainly as HF. The formation of significant amounts of HF is indicative of fluoride attack on the solvent because CH₃CN is the only proton source in the reaction medium and is therefore the only source for hydrogen atoms. The small amount of C₆F₆, which was detected, can be explained by intramolecular decomposition of the C₆F₅XeF₃ intermediate.



The fluoride ion, required for the formation of $C_6F_5XeF_3$ could be formed by interaction of CH_3CN with the $[BF_4]^-$ anion. It is known that fluoride anions can be substituted in fluoro complexes by neutral bases according to equation 84.



In this case, an equilibrium occurs which favours the adducts. However, trapping of the fluoride ion by an electrophile, such as $[C_6F_5XeF_2]^+$ cation, could yield neutral $C_6F_5XeF_3$ as an unstable intermediate. Neutral $C_6F_5XeF_3$ is assumed to decompose by intramolecular fluoride transfer to the *ipso*-C atom which yields C_6F_6 and XeF_2 . A discrepancy in the product distribution is either the too small ratio of C_6F_6 or the high ratio of XeF_2 . Such deviations are often observed when the compounds used for comparison are volatile such as C_6F_6 , C_6F_5H or HF . Such volatile compounds are able to penetrate through the FEP walls of the reaction tubes.

The decomposition of the new salt, $[C_6F_5XeF_2][B(CF_3)_4]$, in CH_3CN at $-40\text{ }^\circ\text{C}$ was also studied to determine the influence of coordinated CH_3CN towards the $[C_6F_5XeF_2]^+$ cation. The use of $[B(CF_3)_4]^-$ as a counteranion eliminates fluoride ion participation from the decomposition mechanism. The interaction of the $[C_6F_5XeF_2]^+$ cation with the $[B(CF_3)_4]^-$ anion is supposed to be negligible because the tetrakis(trifluoromethyl)borate anion belongs to the class of weakly nucleophilic anions. The only significant coordination to the $[C_6F_5XeF_2]^+$ cation is therefore assumed to be that of CH_3CN molecules. The influence of coordinated CH_3CN on the decomposition of the $[C_6F_5XeF_2]^+$ cation was examined. In this study it was found that $[C_6F_5XeF_2][B(CF_3)_4]$ was apparently less stable in CH_3CN at $-40\text{ }^\circ\text{C}$ than its $[BF_4]^-$ analogue. After 1.5 h only 21% of the $[C_6F_5XeF_2]^+$ cation was detected. Complete decomposition of $[C_6F_5XeF_2]^+$ in CH_3CN at $-40\text{ }^\circ\text{C}$ was obtained after 3 d according to scheme 85.

Purity of the material after metathesis (1.5 h)

$[C_6F_5XeF_2]^+$ (21%), $[C_6F_5Xe]^+$ (54%), C_6F_5H (10%), $C_6F_5CF_3$ (8%), C_6F_6 (7%), XeF_2 (24%)

Product distribution resulting from the decomposition of $[\text{C}_6\text{F}_5\text{XeF}_2][\text{B}(\text{CF}_3)_4]$ in CH_3CN at $-40\text{ }^\circ\text{C}$



$\Sigma\text{C}_6\text{F}_5$ groups and derivatives = 100%

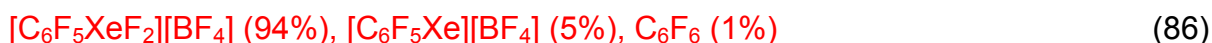
The most difficult step in the preparation of $[\text{C}_6\text{F}_5\text{XeF}_2][\text{B}(\text{CF}_3)_4]$ is the metathesis of $[\text{C}_6\text{F}_5\text{XeF}_2][\text{BF}_4]$ with $\text{K}[\text{B}(\text{CF}_3)_4]$ in CH_3CN at $-40\text{ }^\circ\text{C}$. The isolation and characterization time was too long to allow $[\text{C}_6\text{F}_5\text{XeF}_2][\text{B}(\text{CF}_3)_4]$ to be obtained in acceptable purity. Attempts to isolate $[\text{C}_6\text{F}_5\text{XeF}_2][\text{B}(\text{CF}_3)_4]$ as a solid failed because the time to remove the solvent, CH_3CN , is longer than the complete decomposition time.

The faster decomposition of $[\text{C}_6\text{F}_5\text{XeF}_2][\text{B}(\text{CF}_3)_4]$ when compared with that of $[\text{C}_6\text{F}_5\text{XeF}_2][\text{BF}_4]$ in CH_3CN at $-40\text{ }^\circ\text{C}$ parallels that of the more weakly coordinated anion and therewith a favoured coordination of CH_3CN . The donation of electron density from CH_3CN to the $\text{Xe}(\text{IV})$ center weakens both $\text{Xe}-\text{F}$ bonds as previously described. After formation of $[\text{C}_6\text{F}_5\text{Xe}\cdot(\text{NCCH}_3)_n]^+$ electron transfer occurs, the product distribution shows mainly the formation of the $[\text{C}_6\text{F}_5\text{Xe}]^+$ cation besides a significant amount of XeF_2 which is in agreement with the results obtained in the decomposition studies of $[\text{C}_6\text{F}_5\text{XeF}_2][\text{BF}_4]$ in CH_3CN at $-40\text{ }^\circ\text{C}$. The small amount of $\text{C}_6\text{F}_5\text{H}$ was already obtained during the metathesis to $[\text{C}_6\text{F}_5\text{XeF}_2][\text{B}(\text{CF}_3)_4]$ and was a consequence of impurities in the $\text{K}[\text{B}(\text{CF}_3)_4]$ salt which were not removed by recrystallization and drying the salt under vacuum at RT. It is interesting to note that no HF was obtained during the decomposition. The large amount of XeF_2 might supposedly arise from reaction of the $[\text{C}_6\text{F}_5\text{XeF}_2]^+$ with the $[\text{BF}_4]^-$ during the metathesis. Unfortunately, fluoride abstraction from the anion was not detected in form of the carbene, $\text{B}(\text{CF}_3)_3\text{CF}_2$.

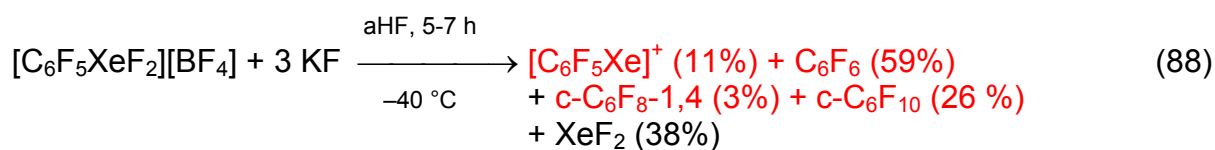
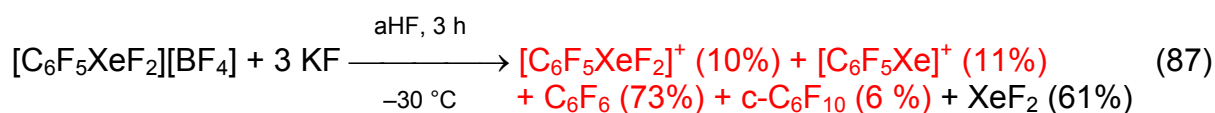
III.2.4.1 Behaviour of $[C_6F_5XeF_2][BF_4]$ in aHF Solution in the Presence of KF

The influence of the acidity of aHF solution on the stability of $[C_6F_5XeF_2][BF_4]$ was examined. A three-fold molar excess of spray-dried KF was dissolved in aHF and added to an aHF solution of $[C_6F_5XeF_2][BF_4]$ at $-80\text{ }^\circ\text{C}$. This study has shown a much faster consumption of the $[C_6F_5XeF_2]^+$ cation when compared with the decomposition in aHF at the same temperatures without addition of KF. In the presence of KF, the consumption rate was *ca.* 25 times faster at $-30\text{ }^\circ\text{C}$ and *ca.* 400 times faster at $-40\text{ }^\circ\text{C}$ than in the absence of KF. The sample with addition of KF reacted rapidly at $-40\text{ }^\circ\text{C}$, whereas no fast decomposition proceeded in the absence of fluoride. In the presence of KF storage at $-80\text{ }^\circ\text{C}$. Even at this temperature, decomposition of the salt occurred within 13 h. The molar percentage of the $[C_6F_5XeF_2]^+$ cation was reduced from 41% to 19% whereas the ratios of C_6F_6 (+14%), *c*- C_6F_{10} (+12%) and XeF_2 (+12%) increased by the molar percentages given in brackets. For comparison, aHF solutions of $[C_6F_5XeF_2][BF_4]$ at $-80\text{ }^\circ\text{C}$ were stable for more than 18 d without decomposition.

Purity of the starting material used to study the decomposition in aHF at -40 and $-30\text{ }^\circ\text{C}$



Product distribution resulting from the decomposition of $[C_6F_5XeF_2][BF_4]$ in aHF at -40 and $-30\text{ }^\circ\text{C}$ in the presence of KF.



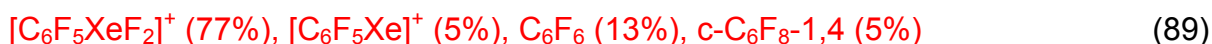
ΣC_6F_5 groups and derivatives = 100 %

The product distributions exhibit significant amounts of C₆F₆, c-C₆F_{8-1,4}, c-C₆F₁₀ and XeF₂ besides small amounts of [C₆F₅Xe]⁺. The product ratio is slightly different for the decompositions at –30 and –40 °C but both show the characteristic compounds formed by solvolysis of the C-Xe bond as previously described. The more rapid consumption of the [C₆F₅XeF₂]⁺ cation in the presence of KF can be explained in terms of the more basic HF solution. Dissolved KF supplies F[–] anions, which are efficiently solvated by HF molecules, [(HF)_nF][–], but are nevertheless more nucleophilic than neutral HF molecules. The polyhydrogenfluoride anion enables the cleavage of the polarized C-Xe bond more easily than with [BF₄·(HF)_n][–] with formation of C₆F₆ and XeF₂. The fluorination with the [C₆F₅XeF₂]⁺ cation seems to play a less important role as can be deduced from the small amount of [C₆F₅Xe][BF₄] found for both decomposition reactions.

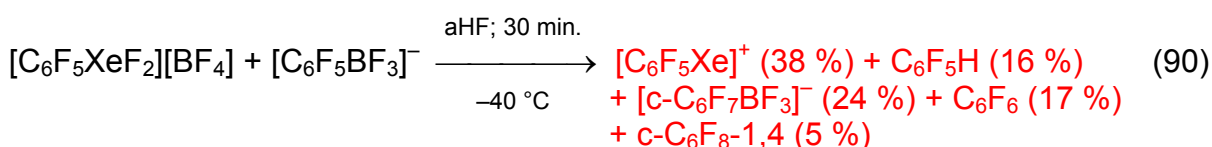
III.2.4.2 Behaviour of [C₆F₅XeF₂][BF₄] in aHF Solution in the Presence of K[C₆F₅BF₃]

The thermal stability of the [C₆F₅XeF₂]⁺ cation in aHF was significantly decreased in the presence of the K[C₆F₅BF₃] salt. Detailed decomposition studies have shown that all [C₆F₅XeF₂]⁺ was consumed in less than 30 min. The consumption at –40 °C is ca. 4250 times faster than the decomposition rate in the absence of K[C₆F₅BF₃] (88 d).

Purity of the starting material used to study the decomposition in aHF at –40 and –30 °C



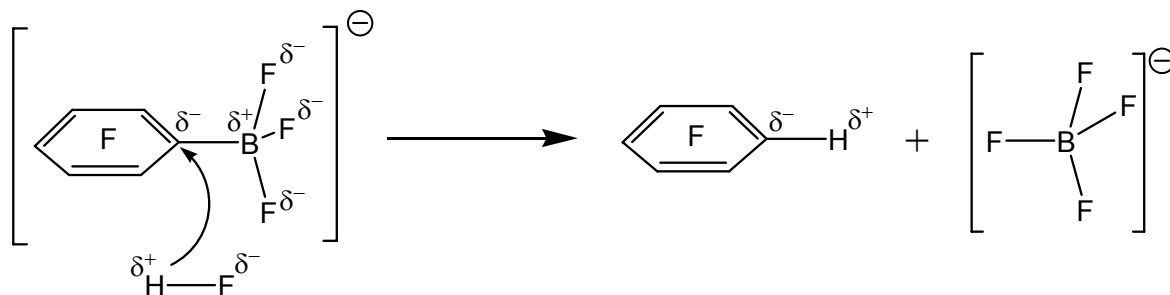
Product distribution resulting from the decomposition of [C₆F₅XeF₂][BF₄] in aHF at –40 and –30 °C in the presence of K[C₆F₅BF₃].



$\Sigma\text{C}_6\text{F}_5$ groups and derivatives = 100 %, The remaining amount of $\text{K}[\text{C}_6\text{F}_5\text{BF}_3]$ in the mother liquor was not given because the sample was a suspension with undissolved borate. The solubility of $\text{K}[\text{C}_6\text{F}_5\text{BF}_3]$ in aHF is very poor.

The product distribution at $-40\text{ }^\circ\text{C}$ exhibits significant amounts of the $[\text{C}_6\text{F}_5\text{Xe}]^+$ cation (38%) above average, $[\text{c-C}_6\text{F}_7\text{BF}_3]^-$ (24%) and smaller amounts of $\text{C}_6\text{F}_5\text{H}$ (16%), C_6F_6 (17%) and traces of $\text{c-C}_6\text{F}_8\text{-1,4}$ (5%) indicative for an ancillary solvolysis process and the more favourable direct fluorination with the $[\text{C}_6\text{F}_5\text{XeF}_2]^+$ cation. The fluorination of the $[\text{C}_6\text{F}_5\text{BF}_3]^-$ anion is favoured. The borate anion is negatively charged, providing a higher electron density in the C_6F_5 ring which allows it to be more easily fluorinated than for example C_6F_6 or $\text{c-C}_6\text{F}_8\text{-1,4}$. Another possibility for an enhanced decomposition rate may be the coordination of the borate anion to the positive xenon center, as described previously for CH_3CN , by means of terminal B-F bonds of the $[\text{C}_6\text{F}_5\text{BF}_3]^-$ anion. This mode of coordination should be preferred for the $[\text{C}_6\text{F}_5\text{BF}_3]^-$ anion compared to $[\text{BF}_4]^-$ because the F^- nucleophilic sites are favoured by the permanent dipole moment. The cleavage of the Xe-F bonds is aided as previously described.

The formation of $\text{C}_6\text{F}_5\text{H}$ (16%) was not observed in any other decomposition study with $[\text{C}_6\text{F}_5\text{XeF}_2][\text{BF}_4]$ and can only be formed by solvolysis of the C-B bond of the $[\text{C}_6\text{F}_5\text{BF}_3]^-$ anion according to scheme 90.



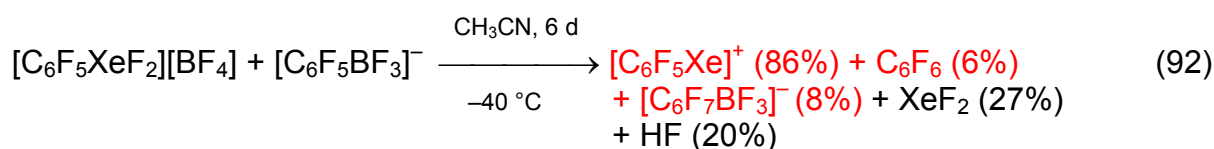
The absence of XeF_2 which parallels the detection of C_6F_6 is evident for a fast reaction of XeF_2 , most likely with $[\text{C}_6\text{F}_5\text{BF}_3]^-$ and/or C_6F_6 leading to the formation of $[\text{c-C}_6\text{F}_7\text{BF}_3]^-$ or/and $\text{c-C}_6\text{F}_8\text{-1,4}$, respectively. Xenon difluoride had to be formed because solvolysis of the C-Xe bond yields XeF_2 and C_6F_6 as described. Other decomposition channels that lead only to C_6F_6 formation were not obtained in either decomposition study.

III.2.4.3 Behaviour of $[C_6F_5XeF_2][BF_4]$ in CH_3CN Solution in the Presence of $K[C_6F_5BF_3]$

The main decomposition products obtained from the interaction of $[C_6F_5XeF_2][BF_4]$ with $[C_6F_5BF_3]^-$ in CH_3CN was $[C_6F_5Xe][BF_4]$ besides significant amounts of XeF_2 and HF. The latter are similar to the decomposition results obtained in the absence of $K[C_6F_5BF_3]$. The more rapid consumption of the $[C_6F_5XeF_2]^+$ cation in the presence of the $[C_6F_5BF_3]^-$ anion can be explained by the simple fluorination of $[C_6F_5BF_3]^-$ compared to C_6F_6 . The rate of $[C_6F_5XeF_2]^+$ cation consumption clearly shows an increase in decomposition rate (~10 times faster) in the presence of $[C_6F_5BF_3]^-$ in CH_3CN at $-40\text{ }^\circ\text{C}$.

Purity of the starting material used to study the decomposition in CH_3CN at $-40\text{ }^\circ\text{C}$
 $[C_6F_5XeF_2][BF_4]$ (86%), $[C_6F_5Xe][BF_4]$ (13%), C_6F_6 (1%) (91)

Product distribution resulting from the decomposition of $[C_6F_5XeF_2][BF_4]$ in CH_3CN at $-40\text{ }^\circ\text{C}$ in the presence of $[C_6F_5BF_3]^-$.



ΣC_6F_5 groups and derivatives = 100 %

The remaining amount of $K[C_6F_5BF_3]$ is not given because a large excess of borate was added. The majority of the borate remained in the insoluble solid.

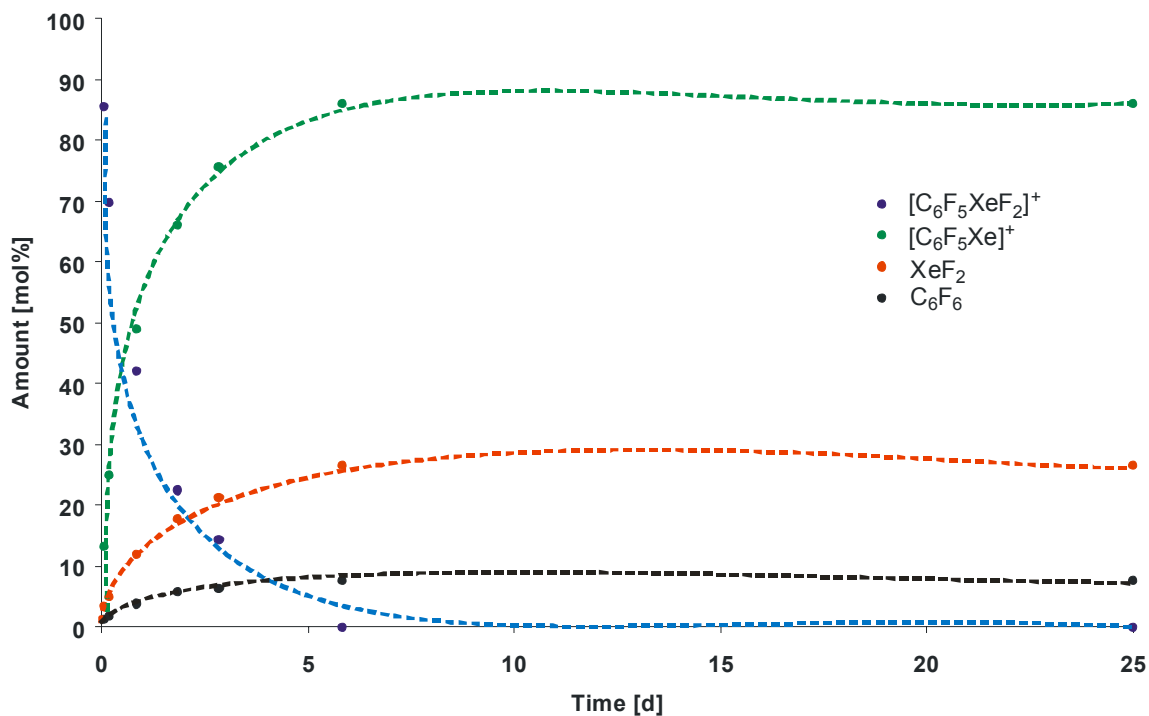


Figure 27 Decomposition trend of $[\text{C}_6\text{F}_5\text{XeF}_2][\text{BF}_4]$ in the presence of $\text{K}[\text{C}_6\text{F}_5\text{BF}_3]$ in CH_3CN at $-40\text{ }^\circ\text{C}$

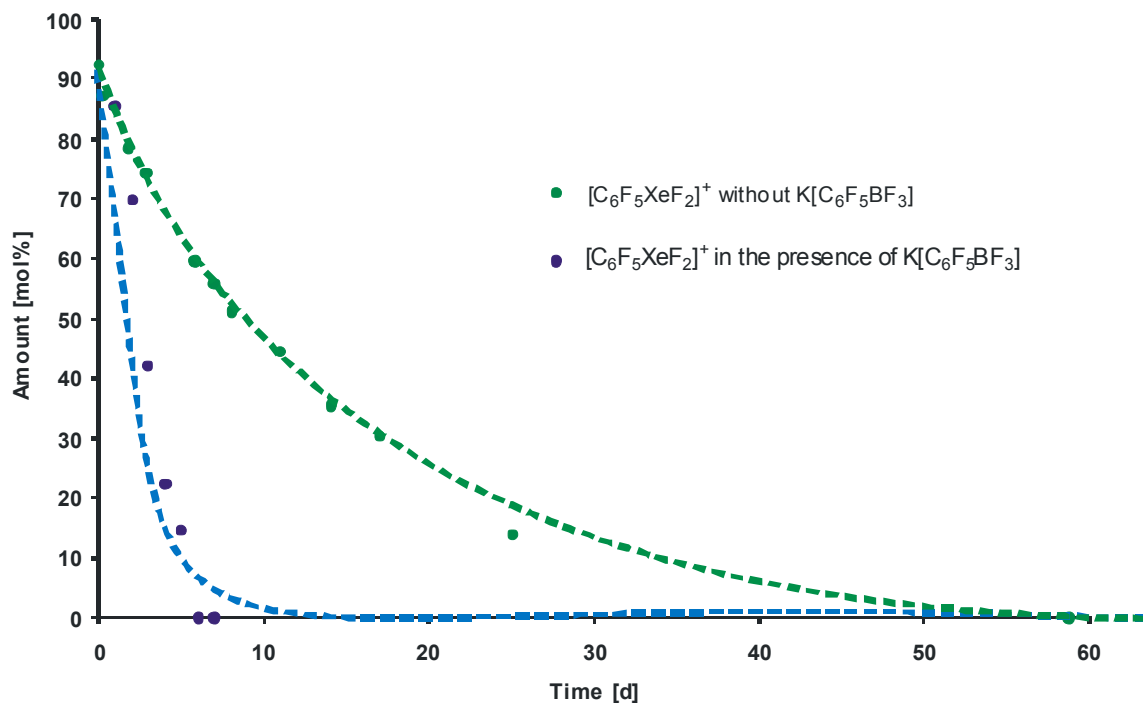


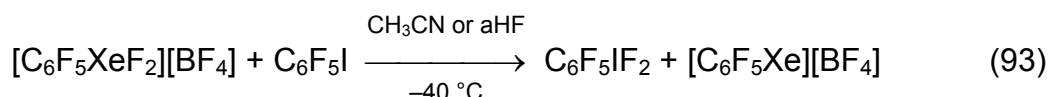
Figure 28 Comparison of the consumption rates of the $[\text{C}_6\text{F}_5\text{XeF}_2]^+$ cation in the presence and absence of $\text{K}[\text{C}_6\text{F}_5\text{BF}_3]$

III.2.5 Reactivity of the $[C_6F_5XeF_2]^+$ Cation in Solution

First investigations have shown that $[C_6F_5XeF_2][BF_4]$ is able to fluorinate I_2 to IF_5 , C_6F_5I to $C_6F_5IF_2$ and $P(C_6F_5)_3$ to $P(C_6F_5)_3F_2$ in homogenous reactions in CH_3CN at $-40\text{ }^\circ\text{C}$.^[72] These first experiments have given a short introduction in the reactivity of the $[C_6F_5XeF_2]^+$ cation under moderate conditions (coordinating solvent) and with easy-to-fluorinate compounds. To incorporate the $[C_6F_5XeF_2]^+$ cation into the family of oxidatively fluorinating agents and to evaluate its oxidation strength a systematic study was performed on tris(pentafluorophenyl)pnictogen(III) compounds ($Pn = P, As, Bi$) and halogenopentafluorobenzenes ($Hal = Br, I$) in basic (CH_3CN) and super acidic media (aHF).

III.2.5.1 Reaction of $[C_6F_5XeF_2][BF_4]$ with C_6F_5Hal ($Hal = I, Br$) in CH_3CN and aHF

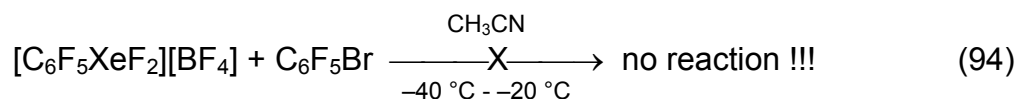
The salt, $[C_6F_5XeF_2][BF_4]$, was reacted with C_6F_5I and C_6F_5Br in CH_3CN and aHF at $-40\text{ }^\circ\text{C}$. The reaction of $[C_6F_5XeF_2][BF_4]$ with excess C_6F_5I yielded in a rapid reaction (15 – 30 minutes) independently of the media, CH_3CN and aHF , at $-40\text{ }^\circ\text{C}$ quantitatively $C_6F_5IF_2$.



The $[C_6F_5Xe]^+$ cation was the main product of reduction beside trace amounts of C_6F_6 and $c-C_6F_8-1,4$ resulting from $[C_6F_5XeF_2]^+$ decomposition.

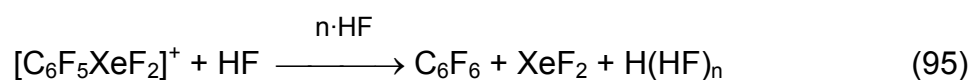
The reaction with C_6F_5Br was of interest because the only publication which reports of direct fluorination of bromine in C_6F_5Br with elemental fluorine to give $C_6F_5BrF_4$ is erroneous and therefore discussed controversially.^[139] Attempts to fluorinate bromine in C_6F_5Br with XeF_2 ,^[140] or ClF_3 ^[141] have been reported to be unsuccessful and had shown only fluorination of the C_6F_5 moiety.

The reaction of $[C_6F_5XeF_2][BF_4]$ with C_6F_5Br in CH_3CN at $-40\text{ }^\circ\text{C}$ did also not yield $C_6F_5BrF_2$. Even at elevated temperatures ($-20\text{ }^\circ\text{C}$) no oxidative addition at bromopentafluorobenzene was obtained.

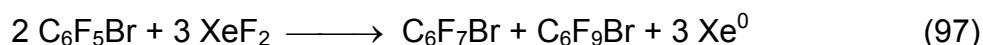
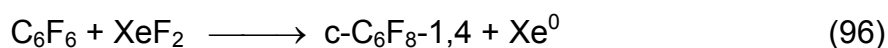


It seems that the oxidation potential of the $[\text{C}_6\text{F}_5\text{XeF}_2 \cdot (\text{NCCH}_3)_n]^+$ adduct is too small for the oxidation of $\text{C}_6\text{F}_5\text{Br}$.

The reaction was additionally performed in aHF solution because the oxidation potential of the $[\text{C}_6\text{F}_5\text{XeF}_2]^+$ cation is increased in Lewis acids. Freshly prepared $[\text{C}_6\text{F}_5\text{XeF}_2][\text{BF}_4]$ was reacted with $\text{C}_6\text{F}_5\text{Br}$ in aHF for 2 h at -40 °C and for 4 d at -80 °C without any reaction. It is noteworthy that the reactions with $\text{C}_6\text{F}_5\text{Br}$ or $\text{C}_6\text{F}_5\text{I}$ were limited to temperatures >-40 °C by the melting points of the $\text{C}_6\text{F}_5\text{Hal}$ compounds. It was found that $\text{C}_6\text{F}_5\text{Br}$ and $\text{C}_6\text{F}_5\text{I}$ had melting points of -31 °C and -35 °C, respectively. The general reaction procedure of $[\text{C}_6\text{F}_5\text{XeF}_2][\text{BF}_4]$ with $\text{C}_6\text{F}_5\text{Br}$ or $\text{C}_6\text{F}_5\text{I}$ at lower temperatures than -40 °C involved dissolution of $\text{C}_6\text{F}_5\text{Br}$ or $\text{C}_6\text{F}_5\text{I}$ in the solvent at <-30 °C. The transfer of the resulting suspension to a pre-cooled (-80 °C) aHF solution of $[\text{C}_6\text{F}_5\text{XeF}_2][\text{BF}_4]$ followed. The suspension was then allowed to warm to -40 °C and stirred for 10 min. before the mother liquor was separated from the frozen $\text{C}_6\text{F}_5\text{Hal}$. The reaction was controlled by low-temperature ^{19}F NMR spectroscopy at -40 °C. In experiments where $[\text{C}_6\text{F}_5\text{XeF}_2][\text{BF}_4]$ was reacted with $\text{C}_6\text{F}_5\text{Br}$ at -20 °C decomposition of the $[\text{C}_6\text{F}_5\text{XeF}_2]^+$ cation occurred. After 30 min. the following product distribution was obtained: $[\text{C}_6\text{F}_5\text{XeF}_2]^+$ (3%), $[\text{C}_6\text{F}_5\text{Xe}]^+$ (9%), $\text{C}_6\text{F}_5\text{Br}$ (26%), *c*- $\text{C}_6\text{F}_7\text{Br}$ (8%), *c*- $\text{C}_6\text{F}_9\text{Br}$ (8%), *c*- $\text{C}_6\text{F}_{8-1,4}$ (11%), *c*- C_6F_{10} (1%), $\text{C}_6\text{F}_5\text{Y}$ (14%), and C_6F_6 (21%), and XeF_2 (6%). The product distribution shows only a small amount of $[\text{C}_6\text{F}_5\text{Xe}]^+$ (9%) beside significant amounts of C_6F_6 (21%) and *c*- $\text{C}_6\text{F}_{8-1,4}$ (11%) which is indicative for the decomposition of the $[\text{C}_6\text{F}_5\text{XeF}_2]^+$ cation.



The small amount of XeF_2 (6%) relative to *c*- $\text{C}_6\text{F}_7\text{Br}$ (8%), *c*- $\text{C}_6\text{F}_9\text{Br}$ (8%), and *c*- $\text{C}_6\text{F}_{8-1,4}$ (11%) and the absence of expected amounts of $[\text{C}_6\text{F}_5\text{Xe}]^+$ leads to the assumption that XeF_2 might have fluorinated $\text{C}_6\text{F}_5\text{Br}$ and C_6F_6 , respectively.



The decomposition of the $[\text{C}_6\text{F}_5\text{XeF}_2]^+$ is assumed to be the initial step of the reaction followed by fluorination of $\text{C}_6\text{F}_5\text{Br}$ and C_6F_6 involving XeF_2 . Decomposition studies of $[\text{C}_6\text{F}_5\text{XeF}_2][\text{BF}_4]$ in aHF at $-30\text{ }^\circ\text{C}$ did show comparable products. In the first 2 d XeF_2 (49%) and C_6F_6 (46%) were detected. The complete consumption was obtained after 4 d and no XeF_2 and C_6F_6 were obtained but *c*- C_6F_8 -1,4 (56%).

III.2.5.2 Reaction of $[\text{C}_6\text{F}_5\text{XeF}_2][\text{BF}_4]$ with $\text{Pn}(\text{C}_6\text{F}_5)_3$ (Pn = P, As, and Bi) in CH_3CN and aHF at $-40\text{ }^\circ\text{C}$

The oxidative fluorination of pnictogen(III) compounds, $\text{Pn}(\text{C}_6\text{F}_5)_3$ (Pn = P, As, and Bi), to the corresponding pnictogen(V) compounds, $\text{Pn}(\text{C}_6\text{F}_5)_3\text{F}_2$ (Pn = P, As, and Bi), is strongly dependent on the kind of ligand. Electron withdrawing groups decrease the electron density at the central pnictogen which hampers the oxidative fluorination. Furthermore, it is generally described that the relativistic effect contracts the 6s electron pair of the heaviest pnictogen, bismuth, which results in a higher ionization potential.

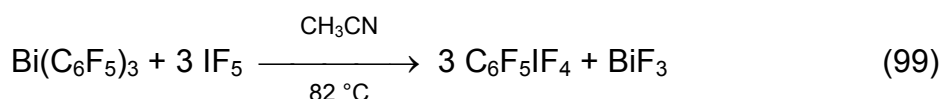
The difluoro tris(pentafluorophenyl)phosphorane, $(\text{C}_6\text{F}_5)_3\text{PF}_2$, is easily accessible from the phosphine, $\text{P}(\text{C}_6\text{F}_5)_3$, using moderately fluorinating agents.^[142] Stronger fluorination agents such as XeF_2 ,^[143] IF_5 ,^[144] or F_2 ^[145] had been shown to be additionally able to fluorinate $\text{Pn}(\text{C}_6\text{F}_5)_3$ (Pn = As, Sb) successfully to $(\text{C}_6\text{F}_5)_3\text{PnF}_2$. Frohn and Maurer^[144] performed the reaction of $\text{As}(\text{C}_6\text{F}_5)_3$ with IF_5 even under mild conditions (coordinating solvent CH_3CN) at $0\text{ }^\circ\text{C}$.



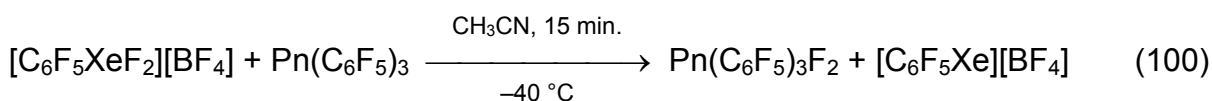
Pn = As and Sb

There are numerous arylbismuth(V) compounds known but only two examples of $(\text{C}_6\text{F}_5)_3\text{BiR}_2$, namely $(\text{C}_6\text{F}_5)_3\text{BiF}_2$ and $(\text{C}_6\text{F}_5)_3\text{Bi}(\text{OTeF}_5)_2$. The partially fluorinated triarylbiomuth(V) compounds, $\text{Bi}(2,6\text{-C}_6\text{F}_2\text{H}_3)_3$, has been oxidatively fluorinated directly with XeF_2 yielding $(2,6\text{-C}_6\text{F}_2\text{H}_3)_3\text{BiF}_2$.^[146] A comparable approach from Naumann *et al.*^[147] who reacted $\text{Bi}(\text{C}_6\text{F}_5)_3$ with XeF_2 or “[XeF]⁺ in CH_3CN (?)” at low temperature was reported to lead to the formation of $(\text{C}_6\text{F}_5)_3\text{BiF}_2$. The published results are, however, not completely interpreted and lead to questionable reaction

pathways. Hitherto, $(\text{C}_6\text{F}_5)_3\text{BiF}_2$, is the only derivative known for $(\text{C}_6\text{F}_5)_3\text{BiHal}_2$ (Hal = F, Cl, Br, I) compounds. The synthesis of pentafluorophenylbismuth(V) derivatives starting with $\text{Bi}(\text{C}_6\text{F}_5)_3$ and xenon oxo compounds were reported to give spectroscopic evidence for $(\text{C}_6\text{F}_5)_3\text{Bi}(\text{OTeF}_5)_2$.^[148, 149] Unfortunately, no reaction parameters were presented. Attempts of oxidative fluorination with IF_5 did not yield $(\text{C}_6\text{F}_5)_3\text{BiF}_2$ but $\text{C}_6\text{F}_5\text{IF}_4$ and BiF_3 . Instead of fluorination a ligand transfer reaction occurred.^[102]

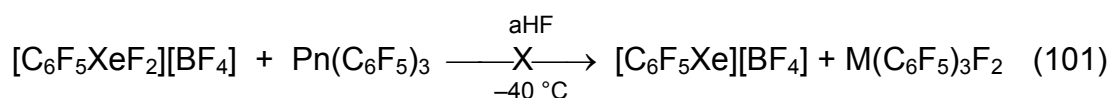


Reactions of freshly prepared $[\text{C}_6\text{F}_5\text{XeF}_2][\text{BF}_4]$ with $\text{Pn}(\text{C}_6\text{F}_5)_3$ (Pn = P, As, Bi) in a rapid reaction (15 minutes) even under moderate conditions (coordinating solvent CH_3CN) at -40°C yielded in all examined cases the corresponding $(\text{C}_6\text{F}_5)_3\text{PnF}_2$ (Pn = P, As, Bi).



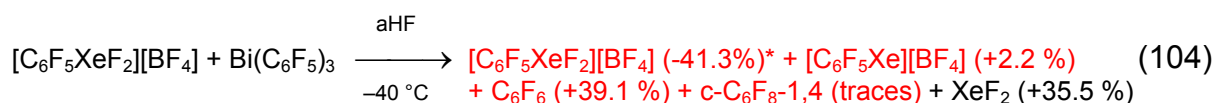
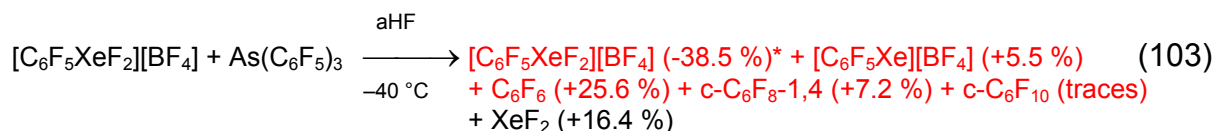
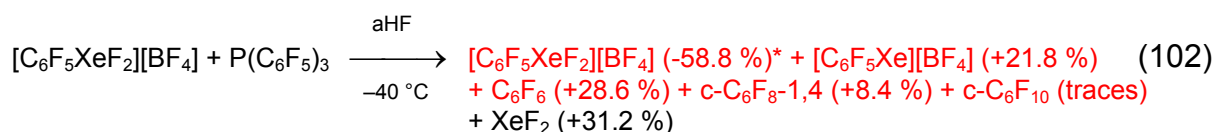
Pn = P, As, and Bi

The main by-product detected was $[\text{C}_6\text{F}_5\text{Xe}][\text{BF}_4]$. In all cases, reactions of $[\text{C}_6\text{F}_5\text{Xe}][\text{BF}_4]$ in aHF solutions did not lead to $(\text{C}_6\text{F}_5)_3\text{PnF}_2$ (Pn = P, As, Bi). The very poor solubility of $\text{P}(\text{C}_6\text{F}_5)_3$ and the insolubility of $\text{As}(\text{C}_6\text{F}_5)_3$ and $\text{Bi}(\text{C}_6\text{F}_5)_3$ in aHF at -40°C might be reasons for the unsuccessful attempts to $(\text{C}_6\text{F}_5)_3\text{PnF}_2$ (Pn = P, As, Bi). The following reaction schemes show the product distribution of the mother liquors of the reaction of $[\text{C}_6\text{F}_5\text{XeF}_2][\text{BF}_4]$ with more than equimolar amounts of $\text{Pn}(\text{C}_6\text{F}_5)_3$ (Pn = P, As, Bi) in aHF at -40°C .



Pn = P, As, and Bi

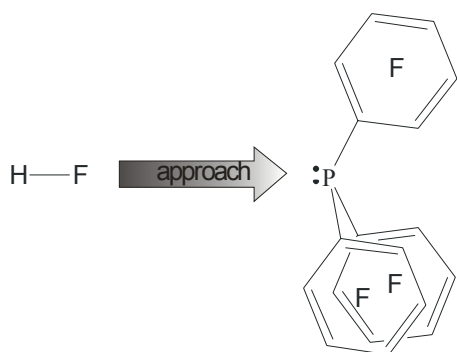
but



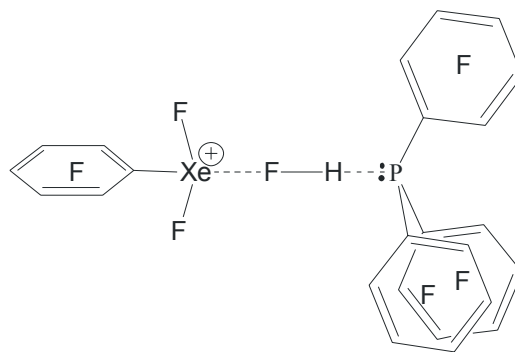
$\Sigma\text{C}_6\text{F}_5$ groups and derivatives = 100 %

The rate of reaction and the product distribution reflects a faster consumption of the $[\text{C}_6\text{F}_5\text{XeF}_2]^+$ cation in the presence of the pnictogen(III) compounds when compared to the decomposition of the neat $[\text{C}_6\text{F}_5\text{XeF}_2][\text{BF}_4]$ salt in aHF at $-40\text{ }^\circ\text{C}$. The formation of the Lewis acidic pnictogen(V) compounds, $(\text{C}_6\text{F}_5)_3\text{PnF}_2$, as intermediate species can not be excluded. Significant amounts of C_6F_6 (29%) and XeF_2 (31%) in the reaction with $\text{P}(\text{C}_6\text{F}_5)_3$ is indicative for the decomposition of the $[\text{C}_6\text{F}_5\text{XeF}_2]^+$ cation under solvolysis of the C-Xe bond. The additional detection of significant amounts of $[\text{C}_6\text{F}_5\text{Xe}]^+$ (22%) may be a hint for partial fluorination of $\text{P}(\text{C}_6\text{F}_5)_3$ to $(\text{C}_6\text{F}_5)_3\text{PF}_2$. The accelerated decomposition rate can generally be explained in analogy of the decomposition reaction in “basic” HF solution. The reaction pathway may include the same four steps: coordination of the nucleophile, $\text{P}(\text{C}_6\text{F}_5)_3$ or $\text{FHP}(\text{C}_6\text{F}_5)_3$, donation of electron density to the xenon center, cleavage of the *ipso*-C-Xe bond, and formation of XeF_2 and C_6F_6 .

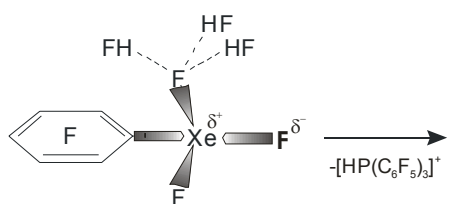
1. Step: Solvation of $\text{P}(\text{C}_6\text{F}_5)_3$ and approach



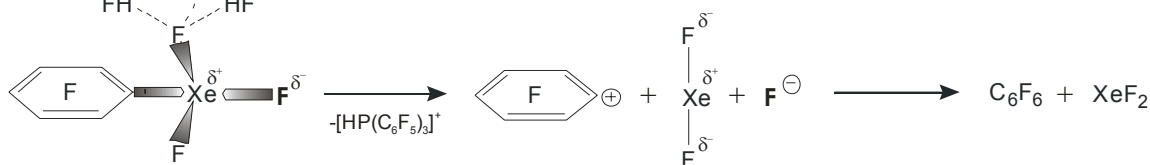
2. Step: Coordination of solvated F^-



3. Step: Donation of electron density



4. Step: Formation of XeF_2 and C_6F_6



The main reaction pathway is likely the decomposition of the $[\text{C}_6\text{F}_5\text{XeF}_2]^+$ cation indicative from the significant amounts of C_6F_6 (29%) and XeF_2 (31%). The consumption rate is comparable to the decomposition rate of $[\text{C}_6\text{F}_5\text{XeF}_2][\text{BF}_4]$ in aHF in the presence of KF or $\text{K}[\text{C}_6\text{F}_5\text{BF}_3]$ and can be explained in terms of more basic HF solution. The product ratio is slightly different for the reaction at -40°C but both, the decomposition in aHF in the presence of KF and the reaction with $\text{Pn}(\text{C}_6\text{F}_5)_3$ ($\text{Pn} = \text{P}, \text{As}, \text{Bi}$) show the characteristic compounds formed by solvolysis of the C-Xe bond as previously described. The relatively small amount of *c*- C_6F_8 -1,4 (8%) and *c*- C_6F_{10} (traces) are mainly a results of the relatively short reaction time of 30 min. (no complete consumption of the $[\text{C}_6\text{F}_5\text{XeF}_2]^+$ cation).

IV Experimental Section

IV.1 Applied Techniques

The moisture- and temperature-sensitive compounds in this work were handled under rigorously anhydrous conditions on glass and metal vacuum line systems or in the nitrogen or argon atmosphere of a drybox (Vacuum Atmospheres Model DLX, nitrogen atmosphere: oxygen and moisture < 0.1 ppm; Firma Braun, Gasreinigung MB 100 G, argon atmosphere: Ar 4.8 or 5.0).

In order to dissipate electrostatic charges arising inside the drybox, FEP and Teflon equipment was handled, either in the vicinity of an α -source consisting of a silver strip impregnated with $^{241}\text{Am}_2\text{O}_3$ (Amersham) having an activity of 2.4 mCi = 88.8 MBq or was treated at least 30 s with a de-ionization fan (Sartorius, YIB01-0DR) prior to weighing. Compounds were weighed inside the drybox in close proximity to the α -source on a Mettler AE 163 electronic balance equipped with a printer external to the drybox. Preparative work inside the drybox requiring low-temperature was accomplished using a metal dewar filled with 4.5 mm copper-plated spheres (air rifle BB's) that had previously been cooled to *ca.* $-140\text{ }^\circ\text{C}$ with liquid nitrogen inside a glass cryowell fitted to the drybox.

All synthetic work with reagents that attacked glass, were carried out in reaction vessels constructed from FEP, a block-co-polymer of tetrafluoroethylene and hexafluoropropylene, $[-(\text{CF}_2\text{CF}_2)_n-(\text{CF}_2-\text{C}(\text{CF}_3)\text{F})_m]_x$ or PFA, a block-co-polymer of tetrafluoroethylene and trifluoroalkoxyethylene, $(-\text{CF}_2\text{CF}(\text{OR}))_n$, having melting points of $260\text{ }^\circ\text{C}$ and $305\text{ }^\circ\text{C}$,^[150] respectively. The maximum working temperature of FEP and PFA are limited to *ca.* $205\text{ }^\circ\text{C}$ and $260\text{ }^\circ\text{C}$,^[150] respectively. Typical FEP reaction tubes were usually used in four sizes (o.d. = 4.10 mm, i.d. = 3.50 mm ("FEP reaction tube"); o.d. 6.3 mm; i.d. 5.0 mm; o.d. = 9.0 mm, i.d = 7.8 or 8.0 mm; o.d. = 25.4 mm, i.d. = 23.0 mm). Other equipment such as plugs, valves, connections and tubing were made from PTFE (Poly(tetrafluoroethylene), $(-\text{CF}_2\text{CF}_2)_n$) having a melting point of $327\text{ }^\circ\text{C}$.^[150] The maximum working temperatures ranging from *ca.* -270 to $260\text{ }^\circ\text{C}$ ^[150] or from Kel-F (PCTFE), a polymer of 1-Chloro-1,2,2-trifluoroethylene, $(-\text{CClF}\text{CF}_2)_n$, having a melting point of $240\text{ }^\circ\text{C}$ ^[150] and a working temperature range of *ca.* $-240\text{ }^\circ\text{C}$ to $180\text{ }^\circ\text{C}$.^[150]

Air- and moisture sensitive solutions and suspensions were transferred either by static distillation on vacuum line systems or by using a Teflon hose which connects two reaction tubes (source and target) as shown in Figure 29. The latter transfer technique allows a fast and complete transfer of moisture sensitive solutions and suspensions by argon pressure.

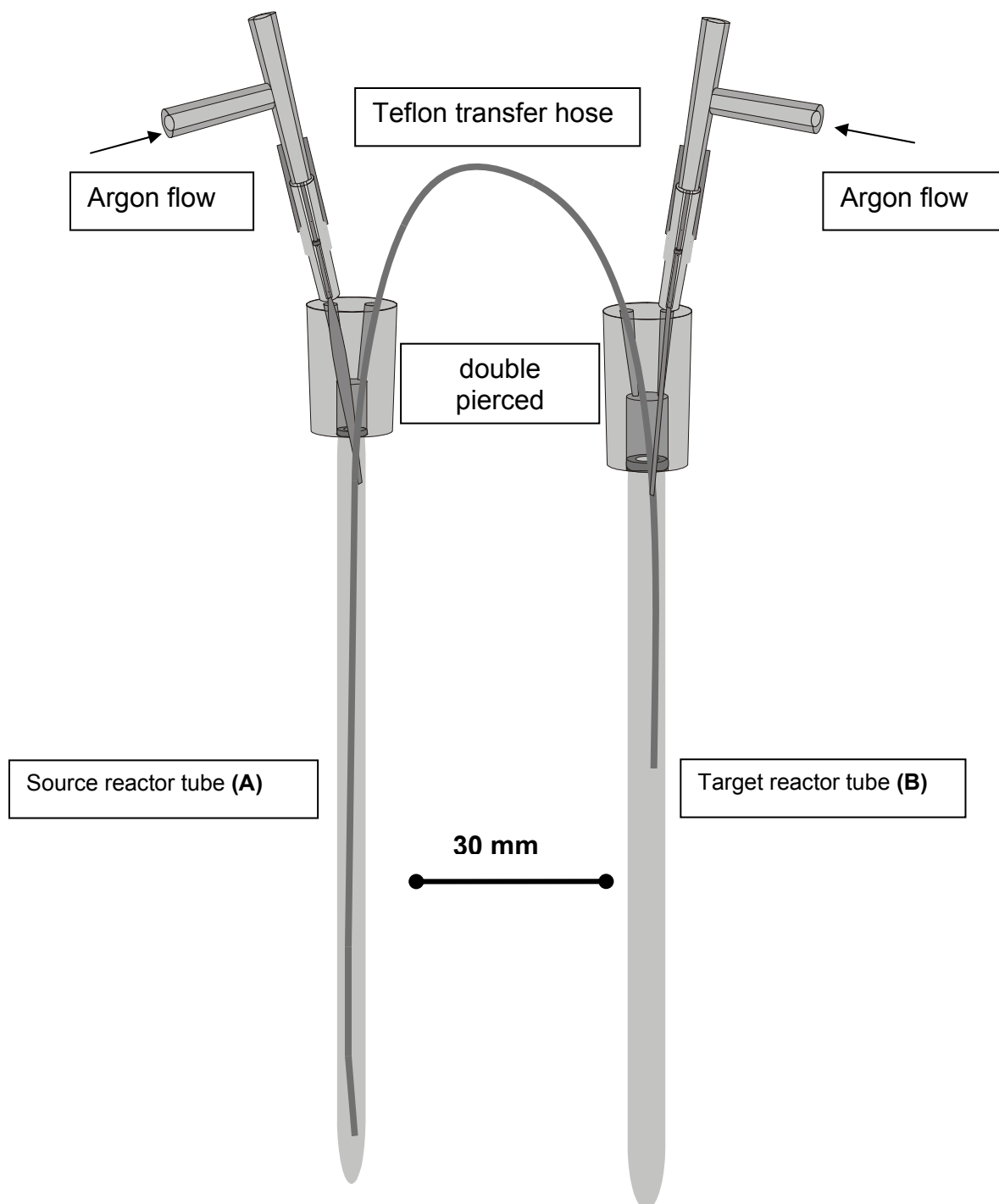


Figure 29 Transfer equipment for solutions and/or suspensions

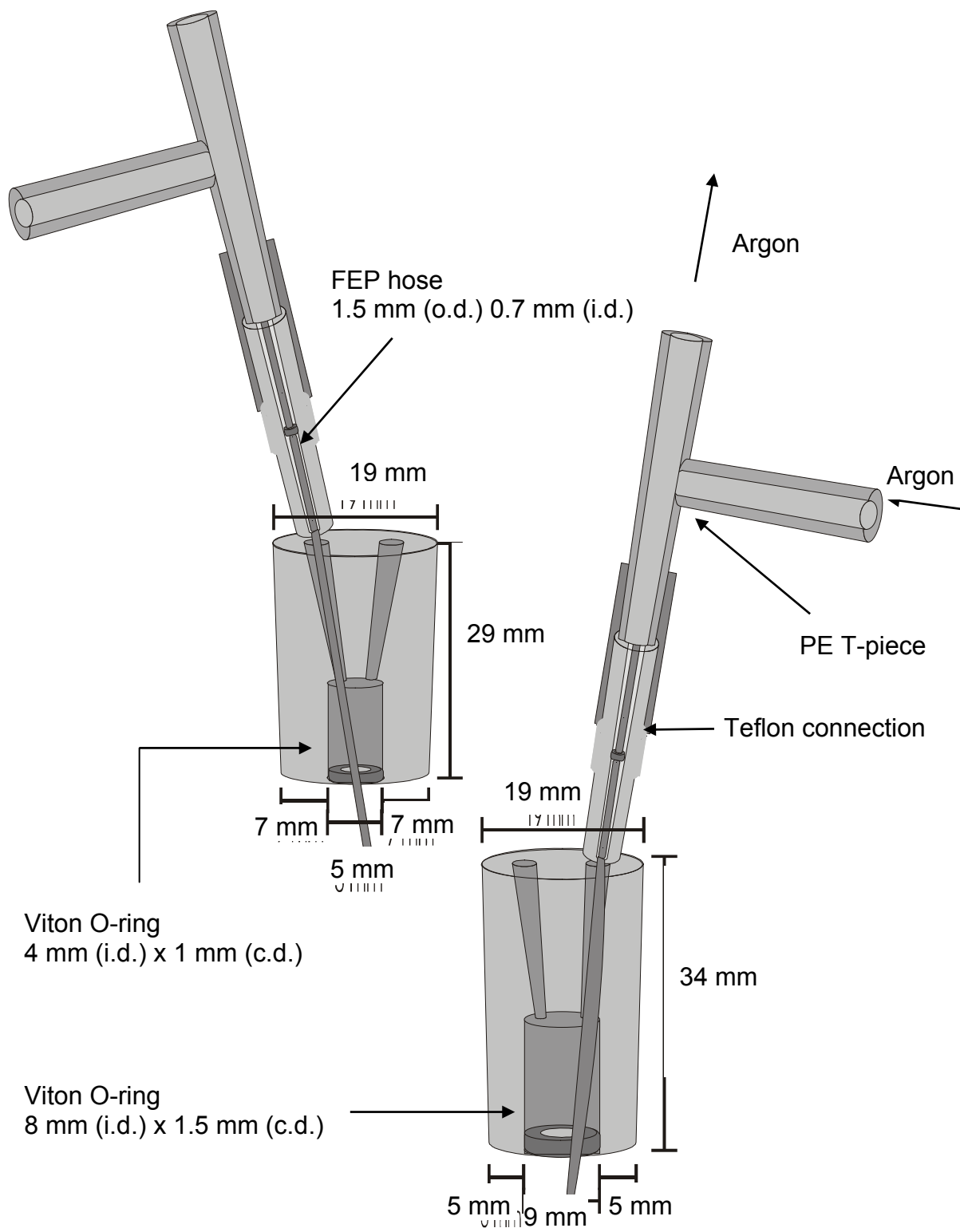


Figure 30 Double pierced Teflon plugs used in the transfer equipment.

Both the source and the target reaction tube were each equipped with a double pierced Teflon plug and connected by means of a Teflon tubing (o.d. = 1.5 mm or 1.55 mm, i.d. = 0.7 mm; o.d. = 2.0 mm, i.d. = 1.5 mm or o.d. = 3.0 mm; i.d. = 2.0 mm). By closing the exit of the T-piece, the source reaction tube (A) was pressurized with argon. Lowering the hose into the solution/suspension allowed the transfer of the liquid or suspension into the target reaction tube (B). To prevent moisture from entering the target reaction tube (B) a slow argon flow was applied.

Samples that were retained for long-term experiments were stored in the absence of daylight in glass traps with grounded necks and were protected by argon gas. The contents of the reaction and their relative molar percentage were determined summing up all C_6F_5 compounds. Non- C_6F_5 compounds were calculated on the base of the sum of all C_6F_5 compounds. Product distributions involving compounds with high vapour pressures such as C_6F_5H , C_6F_6 , and HF can be falsified. Some of those compounds diffuse through the FEP material so that a smaller amount of this compound may be found in solution and a larger relative molar percentage of the additional compounds may be calculated.

IV.2 *Multi-NMR Spectroscopy*

1H NMR spectroscopy

Frequencies: Bruker Avance 300 (BF1 = 300.13 MHz)
 Bruker Avance DRX 500 (BF1 = 500.13 MHz)

The chemical shifts are referenced with respect to TMS using the Bruker standard settings for the solvents. CH_2Cl_2 ($\delta = 5.3$ ppm); CH_3CN ($\delta = 1.9$ ppm); $CHCl_3$ ($\delta = 7.3$ ppm)

^{11}B NMR spectroscopy

Frequencies: Bruker Avance 300 (BF1 = 96.29 MHz)
 Bruker Avance DRX 500 (BF1 = 160.76 MHz)

The chemical shifts are referenced either externally to neat $BF_3 \cdot Et_2O$ at 24 °C ($\delta = 0$ ppm) or to a $BF_3 \cdot Et_2O/CD_3Cl$ solution (15%) at 24 °C ($\delta = 0$ ppm).

^{13}C NMR spectroscopy

Frequencies: Bruker Avance 300 (BF1 = 75.47 MHz)
 Bruker Avance DRX 500 (BF1 = 125.76 MHz)

The chemical shifts were referenced with respect to the TMS scale using one C-signal of the solvent: CD_2Cl_2 ($\delta = 53.5$ ppm) and CD_3CN ($\delta = 118.1$ ppm)

^{19}F NMR spectroscopy

Frequencies: Bruker Avance 300 (BF1 = 282.40 MHz)
 Bruker Avance DRX 500 (BF1 = 470.59 MHz)

The chemical shifts were referenced with respect to the CFCl_3 scale ($\delta(\text{CFCl}_3) = 0$ ppm) using either the internal standards hexafluorobenzene ($\delta = -162.9$ ppm) or benzotrifluoride ($\delta = -63.9$ ppm), respectively or are referenced externally to a neat trichlorofluoromethane reference sample at 24 °C.

^{31}P NMR spectroscopy

Frequencies: Bruker Avance 300 (BF1 = 121.44 MHz)
 Bruker Avance DRX 500 (BF1 = 202.40 MHz)

The chemical shifts were referenced externally to a H_3PO_4 (85%) sample at 24 °C.

^{125}Te NMR spectroscopy

Frequencies: Bruker Avance DRX 500 (BF1 = 157.70 MHz)

The chemical shifts were referenced externally to a $\text{Te}(\text{CH}_3)_2$ sample at 24 °C.

^{129}Xe NMR spectroscopy

Frequencies: Bruker Avance 300 (BF1 = 83.02 MHz)
 Bruker Avance DRX 500 (BF1 = 138.34 MHz)

The chemical shifts were referenced with respect to the XeOF_4 scale using a neat XeOF_4 reference sample or by taking the SR-value from a linear extrapolation of a $\text{XeF}_2/\text{CD}_3\text{CN}$ solution at 24 °C to the concentration 0, whose chemical shift (set to -1813.3 ppm) has been measured externally to XeOF_4 at 24 °C.

Chemical shifts at lower frequency than the standard are assigned by a negative sign. The multiplicities for NMR signals were denoted as follows:

s = singlet, d = doublet, t = triplet, q = quartet, qui = quintet, sex = sextet, sep = septet, etc. m = multiplet, br = broad, and/or unresolved signal, $\Delta\nu_{1/2}$ = line width [Hz]; J = coupling constant [Hz].

Both the chemical shift of signals in first order spectra and of more complex, symmetric signals were taken directly from the center of the signal, whereas chemical shifts from asymmetric signals were denoted in their local maximum position.

2D-NMR experiment SERF

The SERF (**SE**lective **ReF**okussing) experiment describes a 2D NMR method employing two or more selective shaped pulses yielding the desired selective coupling constant of a chosen spin pair without other passive spin couplings. The first pulse of the multiple pulse sequence excites the selected atom and develops a coupling to all other atoms. The second pulse (coherent pulse) suppresses unwanted coherence. The third selective pulse just acts on the chosen spin pair. The subsequently acquired FID is only modulated by the selected spin coupling. The coupling constant can then be taken directly out of the recorded spectrum.

IV.3 Raman Spectroscopy and Raman Sample Preparation

All low-temperature Raman spectra were recorded on a Bruker RFS 100 FT Raman spectrometer equipped with a quartz beam splitter, a liquid-nitrogen-cooled germanium diode detector and a low-temperature accessory. The backscattered (180 °C) radiation was sampled. The scanner velocity was 5 kHz and the wavelength range for acquisition ranged from 5500 to 10500 cm^{-1} when shifted relative to the laser line at 9394 cm^{-1} (1064.5 nm wavelength). The actual usable Stokes range was 50 – 3500 cm^{-1} with a spectral resolution of 2 (1) cm^{-1} . The Fourier transformation was carried out by using a Blackman Harris-4-term apodization and a zero-filling factor of 4 (2). The 1064-nm line of the YAG Laser (300 (400) mW maximum output) was used for excitation of the sample with a laser spot of ca. 0.2 mm (<0.1 mm) at the sample. Processing of the raw data was completed using the OPUS Version 4.0. [151]

The Raman spectra of samples which did not attack glass were measured in thin-walled glass NMR tube (Wilmad 507) fused to a ¼ inch o.d. length of glass tubing which was attached to a J. Young stopcock by means of a ¼ inch Cajon. To prevent a dispersion of the solid over the walls of the reaction tube, the solid material was loaded into the tube by using a self made solid syringe made out of 2.0 mm o.d. FEP tubing and a 1.5 mm o.d. metal rod as piston. After transfer of the solid the

reaction tube was connected to a glass vacuum line, cooled to $-196\text{ }^{\circ}\text{C}$ or dry ice ($-80\text{ }^{\circ}\text{C}$), pumped under dynamic vacuum and later heat sealed.

IV.4 ***X-ray Crystallography***

IV.4.1 *Low-Temperature Crystal Growth*

Crystals were grown in $\frac{1}{4}$ inch o.d. T- or h-shaped FEP reaction tubes equipped with a Kel-F valve (Figure 31). The arm containing the solution was inserted into a glass, vacuum jacketed dewar cooled by a flow of cold nitrogen gas. The dewar was maintained at the desired temperature by flowing cold, dry nitrogen gas along the outside of the FEP tube. The cold N_2 flow was derived by submersion of a nichrome resistance heater in a 50-L dewar of liquid N_2 . The flow was directed through the crystal growing dewar by means of an insulated rubber tubing and regulated by means of two variacs connected in series. The temperature near the FEP tube was measured with a copper-constantan thermocouple (error $\pm 0.2\text{ }^{\circ}\text{C}$). Crystals were isolated by decanting the mother liquor into the side arm of the T- or h-shaped FEP reaction tube, which was cooled to $-196\text{ }^{\circ}\text{C}$. The sample was then pumped under dynamic vacuum to completely dry the crystals before the sidearm was heat-sealed using a small diameter nichrome wire resistance furnace. The reaction tube containing the dry crystals was backfilled with dry nitrogen and stored at dry ice temperature until the crystals could be mounted on the X-ray diffractometer.

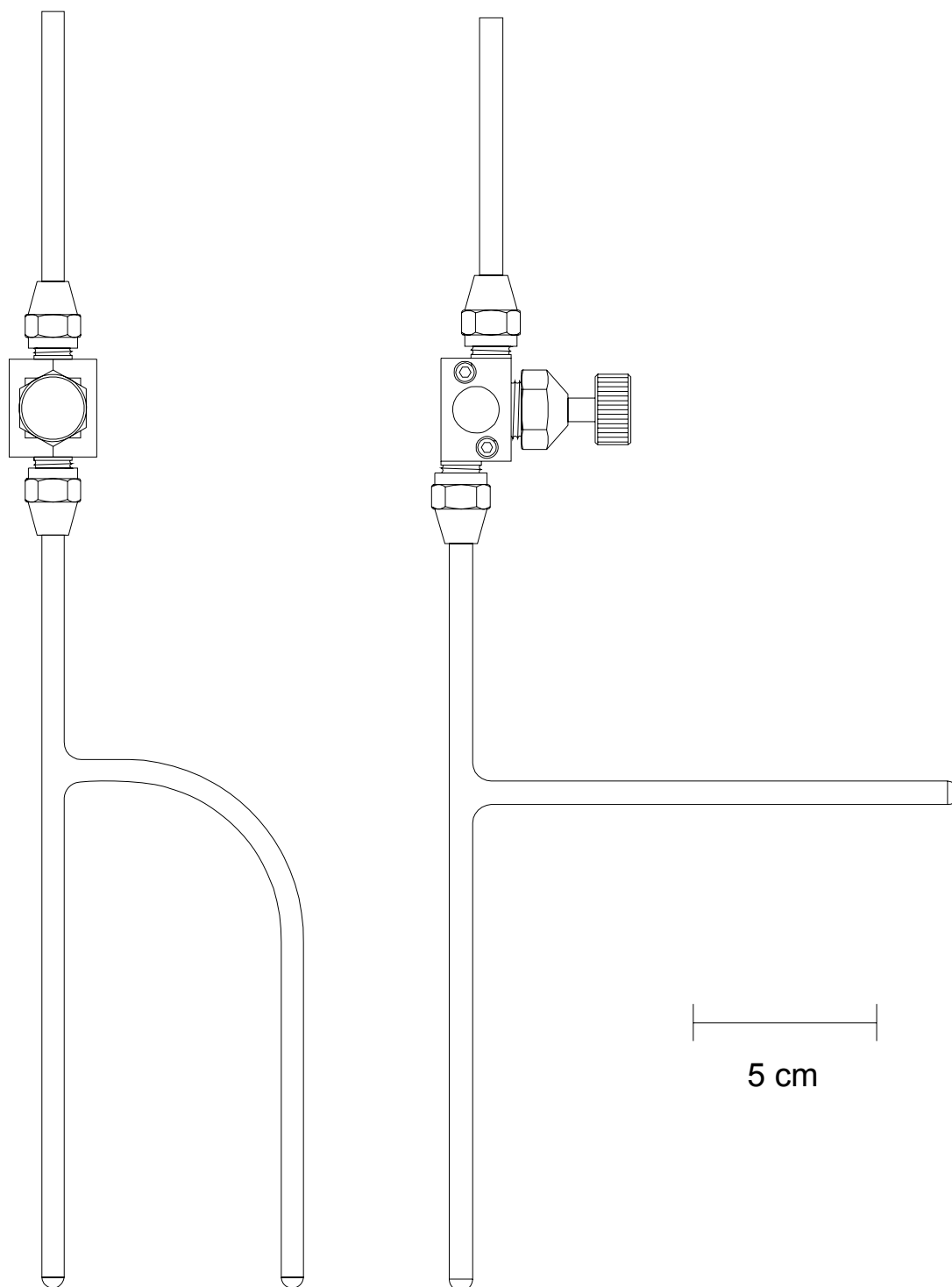


Figure 31 ¼ inch o.d. h- and T-shaped FEP reaction tubes equipped with a Kel-F valve

IV.4.2 Crystal Mounting, Collection of X-ray Data, Solution and Structure Refinement

A low-temperature crystal mounting technique was utilized for thermally unstable and/or moisture-sensitive crystals. The cold ($-80\text{ }^{\circ}\text{C}$) FEP reaction tube containing the crystals was opened by cutting below the Kel-F valve under a flow of dry nitrogen (RT). The crystals were quickly transferred from the chilled tube onto an aluminum trough cooled by passing a flow of dry nitrogen through a 5 L dewar of liquid nitrogen. The temperature of the trough, *ca.* $-100\text{ }^{\circ}\text{C}$ to $-110\text{ }^{\circ}\text{C}$ had been previously measured with a copper-constantan thermocouple inserted midway into the steam *ca.* 2 mm above the trough. Suitable crystals were selected under a stereomicroscope and mounted on a glass fibre using an inert perfluorinated polyether (Fomblin oil). The glass fibre, which had been attached to a metallic pin using epoxy that was, in turn, magnetically mounted on the magnetic interface of a $\frac{1}{4}$ -inch-steel wand for ease of handling. The perfluorinated polyethers used to attach crystals to the glass fibres were chosen based on their pour points and the trough temperature. The perfluorinated polyethers selected for crystal mounting were sufficiently viscous to adhere to the crystal, engulf it, and freeze quickly thereafter. The magnetic interface including the crystal was quickly (*ca.* $< 15\text{ s}$) transferred to the goniometer head of the X-ray instrument using a cryotongs, which had been chilled by liquid nitrogen prior to use, and attached by means of the magnetic interface. The crystals were then centered on a P4 Siemens diffractometer, equipped with a Siemens SMART 1K CCD area detector, controlled by SMART^[152] and a rotating anode emitting K_{α} radiation ($\lambda = 0.71073\text{ \AA}$) monochromated by a graphite crystal. The data collection was carried out in a 512 x 512 pixel mode using 2 x 2 pixel binning. Processing of the raw data was completed using SAINT PLUS,^[153] which applied Lorentz and polarization corrections to the three-dimensionally integrated diffraction spots. Scaling of the integrated data was completed with SADABS,^[154] which applies decay corrections and an empirical absorption correction on the basis of the intensity ratios of redundant reflections. The program XPREP^[155] was used to confirm the unit cell dimensions and crystal lattices. All atom positions, except for hydrogen, were identified in successive difference Fourier syntheses. Final refinements were obtained using data that had been corrected for absorption by introducing an extinction coefficient and optimized by using anisotropic thermal parameters.

IV.5 *Differential Scanning Calorimetry (DSC)*

The thermal analyses were performed using a NETZSCH 204 “Phoenix[®]” instrument equipped with a CC220 controller, a microprocessor system TASC414/3A and a personal computer. Reproducibility had been tested on standard materials and confirmed an error < 0.1 K. The baseline linearity was tested to be ± 0.2 mW in the range of $-150 - +700$ °C.

In a typical experiment, solid material (2 – 5 mg) was weighed into a cold-welded aluminium pan inside the drybox. The pan was closed by a pierced aluminium lid and the precise weight of the solid was measured on an analytical balance and the pan placed inside the furnace of the DSC instrument. An empty aluminium pan with pierced lid was used as a reference together with the sample. The furnace was closed by two gold-plated silver lids. A third lid closed the measuring cell. The complete cell was purged with dry nitrogen gas as a protection gas which also purged the furnace.

The temperature difference between the sample and the reference was measured using coupled heat capacity sensors. A temperature program was used to heat the furnace (usually 5 or 10 K/min).^[156] Processing of the raw data was completed using NETZSCH Proteus[®] Software Version 4.2.^[156]

IV.6 *Calculations*

Electronic structure calculations were carried out at the HF and SVWN (DFT) (for geometry optimizations and vibrational frequencies and intensities) levels of theory using the program Gaussian-98.^[157] The standard all-electron Stuttgart (2d) and cc-pVTZ basis sets, as implemented in the Gaussian program, were utilized for all elements except Xe, for which the semirelativistic large core (RLC) pseudopotential basis set SDB-cc-pVTZ was used. The combined use of cc-pVTZ and SDB-cc-pVTZ basis sets is indicated as (SDB-)cc-pVTZ. Natural orbital analyses were performed using HF or SVWN densities with the NBO program (versions 3.1 and 5.0).

IV.7 Chemicals

IV.7.1 Laboratory Inventory

XeF ₂	C ₆ F ₅ I ₂
XeF ₄	C ₆ F ₅ I ₄
P(C ₆ F ₅) ₃	K[B(CN) ₄]
As(C ₆ F ₅) ₃	M[B(CF ₃) ₄]; M = K, Cs
Bi(C ₆ F ₅) ₃	[C ₆ F ₅ Xe][AsF ₆]

IV.7.2 Commercially Available Chemicals

Ar	Messer Griesheim, Ar 4.8: moisture ≤ 5 Vol. ppm
BF ₃	BASF, ≥ 96.5 Vol.% (≤ 2 Vol.% SO ₂ , ≤ 1.5 Vol.% N ₂)
BCl ₃	Merck, ≥ 99.9%
B(OCH ₃) ₃	Merck Schuckhard, >99%, distilled with sodium
NaF	Riedel-de Häen
KF (spray-dried)	Riedel-de Häen, ≥ 99%
K[HF ₂]	Riedel-de Häen, ≥ 99%
MgSO ₄ (dry)	Riedel-de Häen
[N(C ₄ H ₉) ₄][BF ₄]	Fluka
CsF	ABCR
CsOH·H ₂ O	Fluka, ≥ 95.0%
CCl ₃ F (K11)	Solvay
(C ₂ H ₅) ₂ O	Fluka, ≥ 99%; Aluminum container; peroxide free
C ₆ F ₅ Br	Institute of Organic Chemistry, Novosibirsk, 99%
C ₆ F ₆	Bristol Organics Ltd.
C ₆ H ₅ CF ₃	Fluorochem Ltd.
C ₄ H ₉ Li (in hexanes)	Aldrich
Mg	Merck, Turnings, degreased with CH ₂ Cl ₂
CD ₃ CN	Deutero GmbH, 99.5 atom% D
CD ₂ Cl ₂	Deutero GmbH, 99.5 atom% D
SO ₂ ClF	Allied Chemical, Baker, and Adams Division
HF	Harshaw Chemical Co. or Bayer AG

IV.8 Solvents and Other Starting Materials

IV.8.1 Solvents

Molar Sieves (3 Å):

The molar sieves (3Å) were washed three times with boiling water before being dried for one day under atmospheric pressure at ~80 °C. The pre-dried sieves were loaded inside a glass trap which was subsequently connected to a glass vacuum line system. The trap with the sieves was warmed under dynamic vacuum (10^{-3} mbar) to 180 °C for 1 h and finally dried at 340 °C for 4 h using a block furnace. The sieves were stored inside a glass trap under argon protection.

Acetonitrile (CH₃CN)

Refluxed with KMnO₄ (5 g/L CH₃CN), distilled, repeatedly refluxed with P₄O₁₀ and distilled until the suspension was colorless, distilled again and stored over 3 Å molecular sieves.

Dichloromethane (CH₂Cl₂)

The CH₂Cl₂ was washed with *conc.* H₂SO₄, Na₂CO₃, and H₂O; refluxed with P₄O₁₀, distilled and stored over 3 Å molecular sieves.

Diethyl ether ((C₂H₅)₂O)

The (C₂H₅)₂O was used as was delivered and stored over sodium.

n-Pentane (C₅H₁₂)

The C₅H₁₂ was refluxed with P₄O₁₀, distilled and stored over 3 Å molar sieves.

n-Hexane (C₆H₁₄)

The C₆H₁₄ was refluxed with P₄O₁₀, distilled and stored over 3 Å molar sieves.

Toluene (C₆H₅CH₃)

The C₆H₅CH₃ was refluxed with sodium; distilled and stored over sodium.

Fluorobenzene (C₆H₅F)

The C₆H₅F was refluxed with P₄O₁₀, distilled and stored over 3 Å molar sieves.

1,2-Dichloroethane (C₂H₄Cl₂)

The C₂H₄Cl₂ was refluxed with P₄O₁₀, distilled and stored over 3 Å molar sieves.

1,1,1,3,3-Pentafluorobutane (CF₃CH₂CF₂CH₃)

The CF₃CH₂CF₂CH₃ was refluxed with P₄O₁₀, distilled and stored over 3 Å molecular sieves.

Sulfuryl chloride fluoride (SO₂ClF)

Sulfuryl chloride fluoride (Allied Chemical, Baker, and Adams Division) was purified by use of the literature method and stored over KF.^[158] The purity of the sample was assessed by ¹H, and ¹⁹F NMR spectroscopy of a neat sample recorded at -80 °C, in which trace amounts of SO₂F₂ (2.2%) were found. Transfers were performed using a glass vacuum line by vacuum distillation of SO₂ClF through a submanifold comprised of a Y-shaped glass connection to the reaction vessel.

Hydrogen Fluoride (aHF)

Anhydrous hydrogen fluoride, aHF (Harshaw Chemical Co.) was purified by treatment with 5 atm. of fluorine gas in a nickel can for a period of 1 month, converting residual water to HF and O₂ gas. The anhydrous HF was then vacuum-distilled into a dry Kel-F storage vessel equipped with a Kel-F valve and stored at room temperature until used.

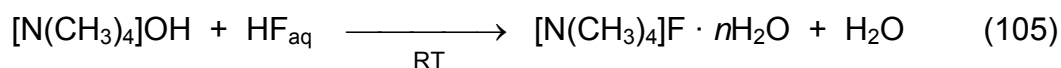
Another technique used to dry hydrogen fluoride was electrochemically in a cell with Ni-anodes described in the literature.^[159] Hydrogen fluoride was therein pre-electrolyzed at a cell voltage of 4.5 to 5.5 V and a current density of 0.20 to 0.35 A·dm⁻³ for 50 - 130 h before transferred into a PE or Teflon (FEP or PTFE) storage vessel and stored in a refrigerator at -18 °C until used.

Anhydrous hydrogen fluoride was transferred into reaction vessels by vacuum distillation on a metal vacuum line through connections constructed of PTFE, Kel-F and FEP or transferred through the previously described transfer technique.

IV.9 Solid Starting Materials

IV.9.1 Tetramethylammonium Fluoride, $[N(CH_3)_4]F$

Tetramethylammonium Fluoride, $[N(CH_3)_4]F$, was prepared analogue to the previously reported method.^[160]



An aqueous 25% solution of $[N(CH_3)_4]OH$ (200 mL; 0.6 mol) was transferred to a 400-mL polypropylene beaker and cooled using an ice bath. Aqueous HF (48%) (23.12 g; 0.55 mol) was added at 0 °C. The solution was slightly basic (pH = 8). A diluted HF solution (H_2O , 10 mL and 48% HF, 2 mL) was prepared and 2 mL was added to the reaction mixture. The solution was then slightly acidic (pH ~6). The clear, colourless solution was stirred for 30 min. before H_2O (may be small amounts of HF) was removed by distillation under dynamic vacuum using a distillation apparatus made out of Teflon at ~120 °C. The completion of the reaction was monitored by NMR spectroscopy. The distillation was stopped after approximately 20 h when most of the H_2O had been removed. The residual H_2O (~50 mL) was removed more efficiently on a glass vacuum line ($\sim 10^{-2}$ mbar) into a FEP U-trap equipped with two Kel-F valves which was cooled with liquid nitrogen (-196 °C). The viscose solution was transferred in portions of ~5 mL into an 11.7 mm i.d. PFA reaction tube and heated to 95 °C using an oil bath. The solvent was removed until solid, white $[N(CH_3)_4]F \cdot nH_2O$ was obtained at 95 °C (roughly after 1 h) under dynamic vacuum ($5 \cdot 10^{-3}$ mbar). The solid fractions were collected in a 23 mm i.d. FEP reaction tube.

Subsequently, small portions of the “crude” $[N(CH_3)_4]F \cdot nH_2O$ (3.3 g) were presented in a 23 mm i.d. FEP reaction tube and further dried under dynamic vacuum ($\sim 5 \cdot 10^{-3}$ mbar) for 2 h at 95 °C, 3 h at 110 °C and 2 h at 122 °C. The powder-like, bright white and easily dispersible solid $[N(CH_3)_4]F \cdot nH_2O$ was then dissolved in freshly dried 2-propanol (over Na followed by distillation) (20 mL).

The 2-propanol/ H_2O was then removed by azeotropic distillation under atmospheric pressure (bath temperature: 124 °C) under argon protection. After 6 h

some solvent (~7 mL) was removed. Residual solvent was then removed under vacuum at RT on a glass vacuum line (10^{-2} mbar). The resulting pre-dried $[\text{N}(\text{CH}_3)_4]\text{F}$ was further dried for 0.5 h at RT and 0.5 h at 80 °C under vacuum (10^{-3} mbar). The solid product was dissolved a second time in 2-propanol (20 mL), the solvent removed under vacuum at RT and the bright white $[\text{N}(\text{CH}_3)_4]\text{F}$ finally dried under vacuum for 6 h at 80 – 85 °C. A sample was dissolved in CD_2Cl_2 (500 μL) at –80 °C and checked by NMR spectroscopy at –40 °C. The spectrum showed the characteristic signals of $[\text{N}(\text{CH}_3)_4]\text{F}$ (98.8%) and trace amounts of $[\text{N}(\text{CH}_3)_4][\text{HF}_2]$ (1.2%).

$[\text{N}(\text{CH}_3)_4]\text{F}$ (dry) (admixture with $[\text{N}(\text{CH}_3)_4][\text{HF}_2]$)

^{19}F -NMR (282.40 MHz) in CD_2Cl_2 at –40 °C (SR = 67.81)

$[\text{N}(\text{CH}_3)_4]\text{F}$ $\delta = -97.8$ ppm (s, $\Delta\nu_{1/2} = 3$ Hz)

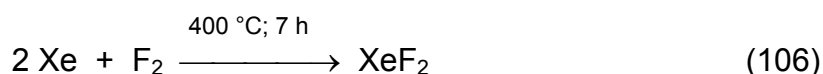
$[\text{N}(\text{CH}_3)_4][\text{HF}_2]$ $\delta = -151.0$ ppm (d, $^1J(^1\text{H}-^{19}\text{F}) = 121$ Hz)

^1H -NMR (300.13 MHz) in CD_2Cl_2 at –40 °C (SR = 0.0)

$[\text{N}(\text{CH}_3)_4]\text{F}$ $\delta = 3.4$ ppm (s, $\Delta\nu_{1/2} = 2$ Hz, 12 H)

IV.9.2 Xenon Difluoride, XeF_2

Xenon difluoride was prepared by the thermal method described in the literature.^[161] The preparation of XeF_2 has been carried out by using two parts xenon and one part of fluorine gas in a nickel reaction can.



Therefore, xenon gas (0.3544 mol) and fluorine (0.1772 mol) were reacted at 400 °C for at least 7 h in an electric furnace. The initial pressure in the can at 400 °C was calculated to be 122 atm. (124 bar) assuming ideal gas conditions and no reaction. After 9 h the reaction can was removed from the furnace and quenched in cold running water. The can and the contents were further cooled to –196 °C and the unreacted fluorine gas was removed under dynamic vacuum. After warming (–80 °C) excess of xenon gas was condensed into a nickel storage vessel at liquid nitrogen temperature for further use. Xenon difluoride was collected in a 3/4 inch o.d. FEP-U-

trap at $-196\text{ }^{\circ}\text{C}$ by sublimation under dynamic vacuum. To accelerate the sublimation, the reaction can was warmed to $30\text{ }^{\circ}\text{C}$. The purity of the white crystalline product was checked by low-temperature Raman spectroscopy.

IV.9.2.1 Reaction of XeF_2 with C_6F_6 in CH_3CN at 0°C and $-40\text{ }^{\circ}\text{C}$ with and without Addition of aHF

In the drybox, XeF_2 (**b**) 0.033 g; 0.20 mmol; **c**) 0.033 g; 0.20 mmol; **d**) 0.029 g; 0.17 mmol; **e**) 0.027 g; 0.16 mmol) was each loaded in a 3.5 mm i.d. FEP reaction tube and suspended in cold ($-40\text{ }^{\circ}\text{C}$) CH_3CN ($\sim 500\text{ }\mu\text{L}$). The mother liquors were each separated in 3.5 mm i.d. FEP reaction tubes (Samples **b**, **c**, **d** and **e**) before C_6F_6 ($5\text{ }\mu\text{L}$; 0,04 mmol) was added to each sample and cold ($-40\text{ }^{\circ}\text{C}$) aHF ($\sim 300\text{ }\mu\text{L}$) was added additionally to the samples **b** and **c**. Sample **b** was measured immediately by ^{19}F NMR spectroscopy at $-40\text{ }^{\circ}\text{C}$ to establish the initial composition. Sample **b** and **d** were then allowed to warm to $0\text{ }^{\circ}\text{C}$ and samples **c** und **e** were allowed to warm to $-40\text{ }^{\circ}\text{C}$. The samples were maintained at $0\text{ }^{\circ}\text{C}$ and $-40\text{ }^{\circ}\text{C}$ in an ice bath or cryostat, respectively, inside a glass trap protected by argon gas and were periodically monitored by ^{19}F NMR spectroscopy at $-40\text{ }^{\circ}\text{C}$.

Initial spectrum

^{19}F -NMR (282.40 MHz) in CH_3CN in the presence of HF at $-40\text{ }^{\circ}\text{C}$

C_6F_6 $\delta = -162.7\text{ ppm}$ (s, $\Delta\nu_{1/2} = 3\text{ Hz}$, 6F)

HF $\delta = -190.7\text{ ppm}$ (s, $\Delta\nu_{1/2} = 21\text{ Hz}$, 1F)

XeF_2 $\delta = -195.8\text{ ppm}$ (s, $\Delta\nu_{1/2} = 5\text{ Hz}$, $^1J(^{19}\text{F}-^{129}\text{Xe}) = 5650\text{ Hz}$, 2F)

C_6F_5 -balance^a: C_6F_6 (100%); XeF_2 (3726 %)

^a The total amount (mol-%) of all C_6F_5 compounds was normalized to 100%.

b) Composition of Reactants and Products Resulting from the Reaction of XeF₂ with C₆F₆ in CH₃CN in the presence of HF at 0 °C

Zeit [d]	C ₆ F ₆ ^a [mol-%]	XeF ₂ ^b [mol-%]	-144.7 ppm ^b [mol-%]
30 min.	100	372.6	0
3	100	203.7	126.8
7	100	49.8	95.7
21	100	0	95.5
29	100	0	107.1

^a The total amount (mol-%) of all C₆F₅ compounds was normalized to 100%.

^b XeF₂ and the unidentified compound at -144.7 ppm were calculated with regard to the sum of C₆F₅ compounds.

c) Composition of Reactants and Products Resulting from the Reaction of XeF₂ with C₆F₆ in CH₃CN in the Presence of HF at -40 °C

Zeit [d]	C ₆ F ₆ ^a [mol-%]	XeF ₂ ^a [mol-%]	-144.7 ppm ^a [mol-%]
30 min.	100	212.1	0
3	100	217.5	56.5
7	100	241.6	164.3
21	100	338.5	502.1
29	100	387.6	708.7

^a The total amount (mol-%) of all C₆F₅ compounds was normalized to 100%.

d) Composition of Reactants and Products Resulting from the Reaction of XeF₂ with C₆F₆ in CH₃CN in the Absence of HF at 0 °C

Zeit [d]	C ₆ F ₆ ^a [mol-%]	XeF ₂ ^a [mol-%]
30 min.	100	357
3	100	415.8
7	100	160.2
21	100	168.3
29	100	438.9

^a The total amount (mol-%) of all C₆F₅ compounds was normalized to 100%.

e) Composition of Reactants and Products Resulting from the Reaction of XeF₂ with C₆F₆ in CH₃CN in the Absence of HF at -40 °C

Zeit [d]	C ₆ F ₆ ^a [mol-%]	XeF ₂ ^a [mol-%]
30 min.	100	319.4
3	100	413.5
7	100	411.7
21	100	195.6
29	100	449.6 ^b

^a The total amount (mol-%) of all C₆F₅ compounds was normalized to 100%.

^b A white precipitate was observed.

IV.9.3 Xenon Tetrafluoride, XeF₄

Xenon tetrafluoride was prepared from xenon and excess of fluorine according to the methods described by Malm and Chernick.^[162] Xenon tetrafluoride was purified by heating with dry sodium fluoride as described by Sheft *et al.*^[163] The purity of the white crystalline compound was checked by low-temperature Raman spectroscopy.



IV.9.3.1 The Solubility of XeF₄ in CH₂Cl₂

In a 3.5 mm i.d. FEP reaction tube, XeF₄ (~25 mg) was suspended in cold (−80 °C) CH₂Cl₂ (700 μL) and benzotrifluoride (5.0 μL; 0.04 mmol) was added as internal standard. The suspension was maintained at −80 °C for 30 min. before being monitored by low-temperature NMR spectroscopy. The solubility of XeF₄ in CH₂Cl₂ at −80 °C was calculated to be 11 μmol/mL. The sample was then allowed to warm to −40 °C inside the NMR spectrometer. The sample was measured after 15 min. and 20 min. The solubility was calculated to be 15 and 17 μmol/mL, respectively. Reproducible measurements were obtained at −80, −55, and −40 °C showing solubilities ranging from 17 to 25 μmol/mL for every temperature mentioned. It can only be said that the solubility of XeF₄ in CH₂Cl₂ at low temperatures (−40 to −80 °C) was shown to be in the range of 21±4 μmol/mL.

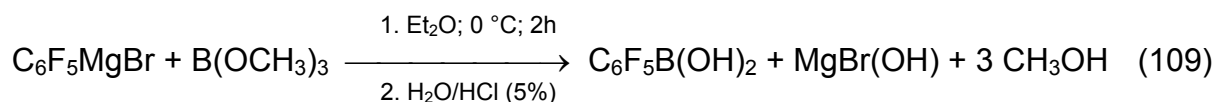
Characterization of XeF₄

¹⁹F NMR (282.40 MHz) in CH₂Cl₂ bei −80 °C

XeF₄ δ = −17.9 ppm (s, ¹²⁹Xe-satellites: ¹J(¹⁹F-¹²⁹Xe) = 3821 Hz, 4F)

IV.9.4 Pentafluorophenyl(dihydroxy)borane, C₆F₅B(OH)₂

Pentafluorophenyl(dihydroxy) borane was generally prepared analogue to the previously reported method.^[164]



Pentafluorophenylmagnesiumbromide was prepared in a 3-neck round bottom flask equipped with a reflux condenser and a dropping funnel. Bromopentafluorobenzene (20.35 g; 0.082 mol) was diluted with Et₂O (30 mL) and added drop wise to magnesium turnings (2.75 g; 0.11 mol) in dry Et₂O (50 mL) at refluxing temperature (~35 °C). The suspension was stirred for 1.5 h. After completion (monitored by ¹⁹F NMR spectroscopy) the reaction mixture was diluted

with additional Et₂O (70 mL) and cooled to 0 °C. In a second round bottom flask, B(OCH₃)₃ (19.36 g; 0.186 mol) in Et₂O (50 mL) was also cooled to 0 °C. The cold (0 °C) Grignard mother liquor was subsequently transferred to the cold B(OCH₃)₃/Et₂O solution by means of a Teflon tube (1.5 mm o.d.). Immediately after combining the solutions, a beige precipitate was obtained. The suspension was stirred for 2 h at 0 °C until it was hydrolysed with a 5% HCl/H₂O solution (200 mL). The organic layer was separated and the water layer extracted three times with Et₂O (50 mL). The combined Et₂O solutions were dried with MgSO₄. After removing MgSO₄ and Et₂O brownish-beige crude C₆F₅B(OH)₂ was obtained. Re-crystallization from (~110 °C) toluene (70 mL) yielded the white solid, C₆F₅B(OH)₂ (10.98 g; 51.83 mmol; 63%).

IV.9.4.1 Solubility of C₆F₅B(OH)₂ in Selected Solvents at RT

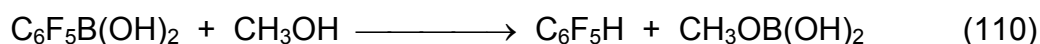
Small quantities of C₆F₅B(OH)₂ were suspended in the corresponding solvent at RT, stirred for 10 min. The mother liquor was separated and the internal standard, C₆H₅CF₃ (5 µL; 0.04 mmol) was added. The solution was measured by ¹⁹F NMR spectroscopy and the solubility calculated based on the internal standard.

Solubility in CH₃CN at RT = 2.02 mmol/mL

Solubility in CH₂Cl₂ at RT = 0.03 mmol/mL

Solubility in PFB at RT = 0.01 mmol/mL

IV.9.4.2 Solvolysis of C₆F₅B(OH)₂ in CH₃OH at RT



In a 8 mm i.d. FEP reaction tube, C₆F₅B(OH)₂ (100 mg; 0.5 mmol) was dissolved in CH₃OH (1.5 mL) at RT and the solution measured after ~30 min. by NMR spectroscopy.

¹⁹F NMR (282.40 MHz) in CH₃OH at 24 °C

C₆F₅B(OH)₂ δ = -132.1 ppm (m, *o*-C₆F₅, 2F); -153.6 ppm (t, ³J(¹⁹F-¹⁹F) = 19 Hz, *p*-C₆F₅, 1F); -162.3 ppm (m, *m*-C₆F₅, 2F)

C_6F_5H $\delta = -138.5$ ppm (m, *o*- C_6F_5 , 2F); -154.8 ppm (t, $^3J(^{19}F-^{19}F) = 19$ Hz, *p*- C_6F_5 , 1F); -162.7 ppm (m, *m*- C_6F_5 , 2F)

Molar ratio^a: $C_6F_5B(OH)_2$ (59.0%); C_6F_5H (41.0%)

^a All C_6F_5 compounds was normalized to 100%.

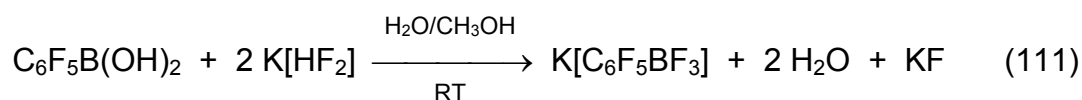
^{11}B -NMR (96.29 MHz) in CH_3OH at 24 °C

$C_6F_5B(OH)_2$ $\delta = 26.3$ ppm (s, $\Delta v_{1/2} = 84$ Hz)

$CH_3OB(OH)_2$ $\delta = 18.3$ ppm (s, $\Delta v_{1/2} = 35$ Hz)

IV.9.5 Potassium Pentafluorophenyltrifluoroborate, $K[C_6F_5BF_3]$

The salt, $K[C_6F_5BF_3]$, was prepared generally analogue to the previously reported method.^[87]



In a 100-mL polypropylene beaker, Pentafluorophenylboronic acid, $C_6F_5B(OH)_2$ (6.093 g; 29 mmol) was dissolved in CH_3OH (30 mL) at RT and quickly combined with a solution of $K[HF_2]$ (6.970 g; 89 mmol) in distilled water (30 mL). The resulting suspension was stirred overnight at RT before being filtrated. The solid was re-crystallized from boiling (~ 81.6 °C) CH_3CN (~ 100 mL). In a typical experiment white $K[C_6F_5BF_3]$ (6.776 g; 25 mmol; 86%) was obtained.

C_6F_5MgBr

^{19}F NMR (282.40 MHz) in Et_2O at 24 °C

C_6F_5MgBr : $\delta = -113.4$ ppm (m, *o*- C_6F_5 , 2F); -158.4 ppm (t, $^3J(^{19}F-^{19}F) = 19$ Hz, *p*- C_6F_5 , 1F); -162.3 ppm (m, *m*- C_6F_5 , 2F)

$Mg(C_6F_5)_2$: $\delta = -113.5$ ppm (m, *o*- C_6F_5 , 2F); -158.8 ppm (t, $^3J(^{19}F-^{19}F) = 19$ Hz, *p*- C_6F_5 , 1F); -162.3 ppm (m, *m*- C_6F_5 , 2F)

C₆F₅B(OH)₂¹⁹F NMR (282.40 MHz) in CH₃CN at 24 °C

C₆F₅B(OH)₂ δ = -132.1 ppm (m, *o*-C₆F₅, 2F); -153.2 ppm (tt, ³J(¹⁹F-¹⁹F) = 19 Hz, ⁴J(¹⁹F-¹⁹F) = 3 Hz, *p*-C₆F₅, 1F), -162.7 ppm (m, *m*-C₆F₅, 2F)

¹¹B NMR (96.29 MHz) in CH₃CN at 24 °C

C₆F₅B(OH)₂ δ = 26.5 (s, Δν_{1/2} = 81 Hz)

K[C₆F₅BF₃]¹⁹F NMR (282.40 MHz) in CH₃CN at 24 °C

[C₆F₅BF₃]⁻ δ = -133.3 ppm (qt, ¹J(¹¹B-¹⁹F) = 43 Hz, ⁴J(¹⁹F-¹⁹F) = 12 Hz, BF₃, 3F);
-135.1 ppm (m, *o*-C₆F₅, 2F); -160.9 ppm (t, ³J(¹⁹F-¹⁹F) = 19 Hz,
p-C₆F₅, 1F), -165.2 ppm (m, *m*-C₆F₅, 2F)

¹¹B NMR (96.29 MHz) in CH₃CN at 24 °C

[C₆F₅BF₃]⁻ δ = 1.6 ppm (q, ¹J(¹¹B-¹⁹F) = 43 Hz)

IV.9.5.1 Solubility of K[C₆F₅BF₃] in Selected Solvents at RT

Small quantities of K[C₆F₅BF₃] were suspended in the corresponding solvent at RT and stirred for 10 min. The mother liquor was separated and the internal standard, C₆H₅CF₃ (5 μL; 0.04 mmol), was added. The solution was measured by ¹⁹F NMR spectroscopy and the solubility calculated based on the internal standard.

Solubility in CH₃CN at RT = 0.14 mmol/mL

Solubility in CH₂Cl₂ at RT = insoluble

Solubility in PFB at RT = insoluble

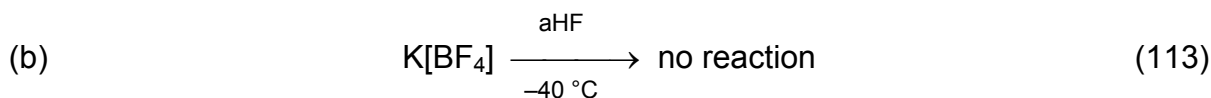
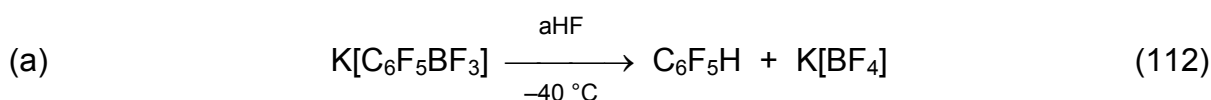
IV.9.5.2 Behaviour of K[C₆F₅BF₃] in Boiling CH₃CN and CH₃CN/H₂O

The compound, K[C₆F₅BF₃] (0.157 g; 0.6 mmol), was dissolved in CH₃CN (5 mL) and benzotrifluoride (10.0 μL; 0.08 mmol) was added as internal standard. The sample was monitored by ¹⁹F NMR spectroscopy. No additional signals were detected beside the characteristic ones of K[C₆F₅BF₃]. The solution was stirred under

reflux for 4 h. NMR spectra of the solution showed a small amount ($\sim 1 \mu\text{mol/mL}$) of $[\text{BF}_4]^-$ beside $\text{K}[\text{C}_6\text{F}_5\text{BF}_3]$. The solubility $\text{K}[\text{BF}_4]$ in CH_3CN at RT was independently determined to be $5 \mu\text{mol/mL}$. The observed amount of $\text{K}[\text{BF}_4]$ was not in the range for a saturated solution.

Distilled H_2O ($3.0 \mu\text{L}$; 0.17 mmol) was added and the solution stirred under reflux for another hour. The NMR spectra of the solution showed an insignificant rise in the $[\text{BF}_4]^-$ concentration ($1.6 \mu\text{mol/mL}$). The sample was stored at RT for 20 h without any additional decomposition. The solution was remained clear and colourless.

IV.9.5.3 Behaviour of $\text{K}[\text{C}_6\text{F}_5\text{BF}_3]$ in aHF at $-40 \text{ }^\circ\text{C}$ and Comparison with $\text{K}[\text{BF}_4]$



The compounds, $\text{K}[\text{C}_6\text{F}_5\text{BF}_3]$ and $\text{K}[\text{BF}_4]$, were each suspended in cold ($-80 \text{ }^\circ\text{C}$) aHF ($500 \mu\text{L}$). Both suspensions were allowed to warm to $\geq -40 \text{ }^\circ\text{C}$ and were maintained for 4 h (max. temperature was $-25 \text{ }^\circ\text{C}$). Both suspensions were finally monitored by low-temperature NMR spectroscopy.

$\text{K}[\text{C}_6\text{F}_5\text{BF}_3]$

^{19}F NMR (282.40 MHz) in aHF at $-40 \text{ }^\circ\text{C}$

$[\text{C}_6\text{F}_5\text{BF}_3]^-$ $\delta = -132.1 \text{ ppm}$ (s, BF_3 , 3F); -136.3 ppm (m, *o*- C_6F_5 , 2F); -155.3 ppm (t, $^3J(^{19}\text{F}-^{19}\text{F}) = 19 \text{ Hz}$, *p*- C_6F_5 , 1F); -163.3 ppm (m, *m*- C_6F_5 , 2F)

$[\text{BF}_4]^-$ $\delta = -148.4 \text{ ppm}$ (q, $^1J(^{11}\text{B}-^{19}\text{F}) = 12 \text{ Hz}$; sep, $^1J(^{10}\text{B}-^{19}\text{F}) = 4 \text{ Hz}$, 4F)

$\text{C}_6\text{F}_5\text{H}$ $\delta = -138.9 \text{ ppm}$ (m, *o*- C_6F_5 , 2F); -154.5 ppm (t, $^3J(^{19}\text{F}-^{19}\text{F}) = 19 \text{ Hz}$, *p*- C_6F_5 , 1F); -162.6 ppm (m, *m*- C_6F_5 , 2F)

aHF $\delta = -191.0 \text{ ppm}$ (s)

Molar ratios: $[\text{C}_6\text{F}_5\text{BF}_3]^-$ (95.3%); $[\text{BF}_4]^-$ (5.8%); $\text{C}_6\text{F}_5\text{H}$ (4.7%)

^{11}B NMR (96.29 MHz) in aHF at $-40\text{ }^\circ\text{C}$

$[\text{C}_6\text{F}_5\text{BF}_3]^-$ $\delta = 3.5$ ppm (s, $\Delta\nu_{1/2} = 55$ Hz)

$[\text{BF}_4]^-$ $\delta = -1.3$ ppm (qui, $^1J(^{10}\text{B}-^{19}\text{F}) = 12$ Hz)

K[BF₄]

^{19}F NMR (282.40 MHz) in aHF at $-40\text{ }^\circ\text{C}$

$[\text{BF}_4]^-$ $\delta = -148.4$ ppm (q, $^1J(^{11}\text{B}-^{19}\text{F}) = 12$ Hz)

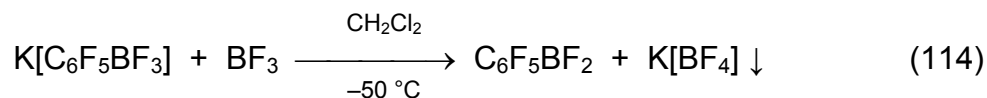
aHF $\delta = -191.1$ ppm (s)

^{11}B NMR (96.29 MHz) in aHF at $-40\text{ }^\circ\text{C}$

$[\text{BF}_4]^-$ $\delta = -1.2$ ppm (qui, $^1J(^{11}\text{B}-^{19}\text{F}) = 12$ Hz)

IV.9.6 Pentafluorophenyldifluoroborane, C₆F₅BF₂

The compound, $\text{C}_6\text{F}_5\text{BF}_2$, was mainly prepared by the method described in the literature.^[87]



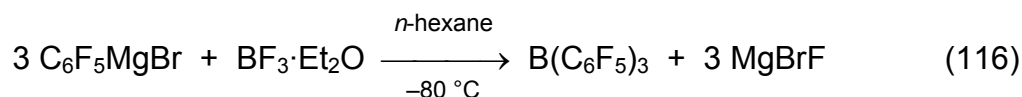
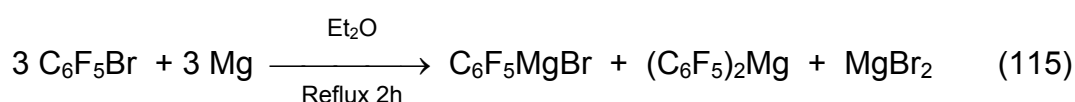
In a 23 mm i.d. FEP reaction tube, $\text{K}[\text{C}_6\text{F}_5\text{BF}_3]$ (1.620 g; 6 mmol) was suspended in CH_2Cl_2 (5 mL) and cooled to $-50\text{ }^\circ\text{C}$. On a metal line, BF_3 gas was passed through a $\text{NaF}/\text{CH}_2\text{Cl}_2$ suspension at RT before entering the reaction trap at $-50\text{ }^\circ\text{C}$. After slow addition (100 min.) of a five-fold molar excess of BF_3 gas (29.56 mmol) to the suspension, the reaction tube was closed and allowed to warm to RT. The reaction tube was pressurized by the excess of BF_3 . It was necessary to release the pressure several times. The suspension was subsequently stirred at RT for 1.5 h before dissolved BF_3 gas was removed by pumping under dynamic vacuum at $-80\text{ }^\circ\text{C}$ for 15 min. The suspension was centrifuged at RT, the CH_2Cl_2 mother liquor separated and $\text{C}_6\text{H}_5\text{CF}_3$ (5.0 μL ; 0.04 mmol) added as internal standard. The residual greyish solid, $\text{K}[\text{BF}_4]$ was extracted three times with CH_2Cl_2 (1000 μL) and the CH_2Cl_2 phases combined. The yield of $\text{C}_6\text{F}_5\text{BF}_2$ was 95% (2.8 mmol) based on the internal standard $\text{C}_6\text{H}_5\text{CF}_3$ (5.0 μL ; 0.04 mmol).

In CH₂Cl₂ solution at 24 °C¹⁹F NMR (282.40 MHz)

C₆F₅BF₂ δ = -74.4 ppm (s, Δv_{1/2} = 83 Hz, BF₂); -129.0 ppm (m, *o*-C₆F₅, 2F);
 -143.9 ppm (tt, ³J(¹⁹F-¹⁹F) = 20 Hz, ⁴J(¹⁹F-¹⁹F) = 7 Hz, *p*-C₆F₅, 1F);
 -161.3 ppm (m, *m*-C₆F₅, 2F)

¹¹B NMR (96.29 MHz)

C₆F₅BF₂ δ = 21.8 ppm (s, Δv_{1/2} = 114 Hz)

IV.9.7 *Tris(pentafluorophenyl)borane, B(C₆F₅)₃*

Pentafluorophenylmagnesiumbromide was prepared in a 250-mL 3-neck round bottom flask equipped with a reflux condenser and a dropping funnel. Bromopentafluorobenzene (25.46 g; 103 mmol) was diluted with Et₂O (40 mL) and added drop wise within 20 min. to magnesium turnings (3.40 g; 140 mmol) in dry Et₂O (60 mL) at the reflux temperature (~35 °C) and stirred for 70 min. The completion of the reaction was monitored by ¹⁹F NMR spectroscopy. In a second round bottom flask freshly distilled BF₃·Et₂O (4.8 g; 31 mmol) was diluted in Et₂O (10 mL), cooled to -80 °C and transferred to the cold (-80 °C) Grignard suspension within 5 – 10 min. via a 1.5 mm o.d. Teflon hose. The suspension was first stirred for 15 min. at -60 °C, 45 min. at 0 °C, and then allowed to warm to RT and stirred for 3.5 h until all C₆F₅MgBr had reacted yielding B(C₆F₅)₃. The completion of the reaction was monitored by NMR spectroscopy. The solvent was subsequently removed under dynamic vacuum. The crude, brown and gluey solid was extracted three times with boiling (69 °C) *n*-hexane (each 75 mL). The hexane solutions were combined and stored at RT. Over time, clear, colourless crystals (2 – 4 mm) of B(C₆F₅)₃ grew. The B(C₆F₅)₃ crystals (9.78 g; 19 mmol; 61.9%) were isolated and sublimed in dynamic

vacuum at 100 – 110 °C. The H₂O-cooled finger was dried and transferred to a drybox where bright white solid B(C₆F₅)₃ (6.73; 13 mmol; 42.6%) was recovered.

In CH₂Cl₂ solution at 24 °C

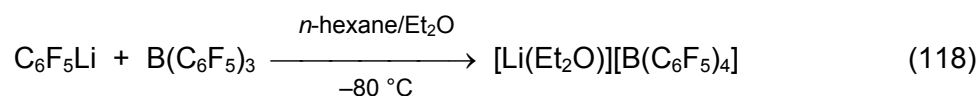
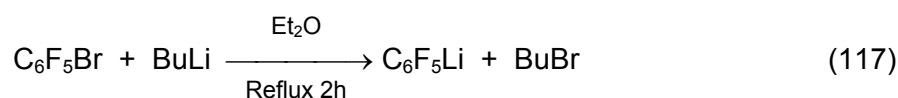
¹⁹F NMR (282.40 MHz)

B(C₆F₅)₃ δ = –129.6 ppm (m, *o*-C₆F₅, 2F); –146.6 ppm (s, *p*-C₆F₅, 1F); –161.5 ppm (m, *m*-C₆F₅, 2F)

¹¹B NMR (96.29 MHz)

B(C₆F₅)₃ δ = 59 ppm (s)

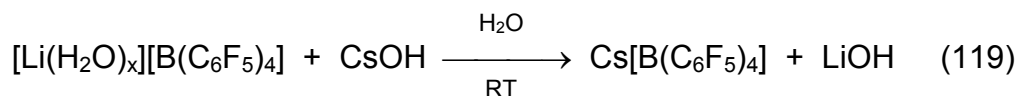
IV.9.8 Cesium Tetrakis(pentafluorophenyl)borate, Cs[B(C₆F₅)₄]



Bromopentafluorobenzene (1.783 g; 7 mmol) was diluted with Et₂O (25 mL) and cooled to –80 °C. Butyllithium/*n*-pentane solution (2.5 M; 5 mL; 7 mmol) was added dropwise at –80 °C and stirred for 2 h. The completion of the reaction was monitored by ¹⁹F NMR spectroscopy. A sample was hydrolysed with CH₃OH (250 μL) at –40 °C and the amount of pentafluorobenzene calculated based on the internal standard benzotrifluoride (10.0 μL; 0.08 mmol). Lithium pentafluorobenzene is unstable in Et₂O at temperatures higher than –20 °C and must be handled at low temperatures.

In a second round bottom flask bright white B(C₆F₅)₃ (2.896 g; 6 mmol) was suspended in *n*-pentane (50 mL) and cooled to –80 °C. The C₆F₅Li/Et₂O/*n*-pentane solution was transferred to the B(C₆F₅)₃/*n*-pentane suspension through a 1.5 mm o.d. Teflon tube and the mixture stirred for 15 min. at –60 °C, 60 min. at –40 °C and 30 min. at RT whereupon a white solid precipitated. The mother liquor was separated and the solid washed three times (20 mL each) with *n*-pentane. All solutions were combined and checked by NMR spectroscopy and showed no signals. The white solid, [Li(Et₂O)_x][B(C₆F₅)₄], was dried under vacuum for 8 h at RT. The solid was

dissolved in H₂O (30 mL) and the water was subsequently removed under vacuum. This treatment was repeated two times to remove coordinated ether. A dried (vacuum, RT, 2 h) solid of white [Li(H₂O)_x][B(C₆F₅)₄] (3.42 g; 5 mmol, yield 88% (calculated for one molecule of H₂O)) was isolated.



[Li(H₂O)][B(C₆F₅)₄] (3.02 g; 4 mmol) was dissolved in water (50 mL) (very exothermic) and combined with a saturated solution of cesium hydroxide monohydrate (1.8538 g; 11.00 mmol) in H₂O (40 mL). Immediately after combination a white precipitate was obtained. The suspension was stirred for 2 h at RT until the mother liquor was separated. The solid was washed with H₂O until the pH value was neutral. The white solid was dried under vacuum for 6 h at RT. Cesium tetrakis(pentafluorophenyl)borate (2.777 g; 3 mmol; yield 80%) was isolated as white solid.

[Li(Y)_x][B(C₆F₅)₄] (Y = H₂O and Et₂O) in D₂O solution at 24 °C

¹⁹F NMR (282.40 MHz)

[Li(Et₂O)_x][B(C₆F₅)₄] δ = -134.8 ppm (s, *v*_{1/2} = 45 Hz, *o*-C₆F₅, 2F); -165.1 ppm (s, Δ*v*_{1/2} = 52 Hz, *p*-C₆F₅, 1F); -169.0 ppm (s, Δ*v*_{1/2} = 49 Hz, *m*-C₆F₅, 2F)

¹¹B NMR (96.29 MHz)

[Li(Et₂O)_x][B(C₆F₅)₄] δ = -17.1 ppm (s, Δ*v*_{1/2} = 14 Hz)

¹⁹F NMR (282.40 MHz)

[Li(D₂O)_x][B(C₆F₅)₄] δ = -135.0 ppm (s, Δ*v*_{1/2} = 38 Hz, *o*-C₆F₅, 2F); -163.9 ppm (t, ³*J*(¹⁹F-¹⁹F) = 20 Hz, *p*-C₆F₅, 1F); -168.2 ppm (m, *m*-C₆F₅, 2 F)

¹¹B NMR (96.29 MHz)

[Li(D₂O)_x][B(C₆F₅)₄] δ = -17.0 ppm (s, Δ*v*_{1/2} = 22 Hz)

Cs[B(C₆F₅)₄] in acetone solution at 24 °C¹⁹F NMR (282.40 MHz)

Cs[B(C₆F₅)₄] δ = −131.0 ppm (s, Δv_{1/2} = 28 Hz, *o*-C₆F₅, 2F); −162.4 ppm (t, ³J(¹⁹F-¹⁹F) = 21 Hz, *p*-C₆F₅, 1F); −166.3 ppm (m, *m*-C₆F₅, 2F)

¹¹B NMR (96.29 MHz)

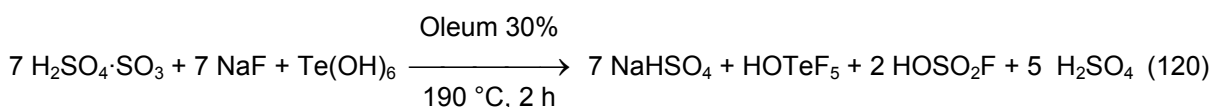
Cs[B(C₆F₅)₄] δ = −16.4 ppm (s, Δv_{1/2} = 20 Hz)

IV.9.8.1 Solubility of Cs[B(C₆F₅)₄] in Selected Solvents at RT

Small quantities of Cs[B(C₆F₅)₄] were suspended in the corresponding solvent at RT and stirred for 10 min. The mother liquor was separated and the internal standard, C₆H₅CF₃ (5 μL; 0.04 mmol) was added. The solution was measured by ¹⁹F NMR spectroscopy and the solubility calculated based on the internal standard.

Solubility in CH₃CN at RT = 1.5 mmol/mL

Solubility in CH₂Cl₂ at RT = insoluble

IV.9.9 Teflic Acid, HOTeF₅ (Optimized Preparation Procedure)

Fluorosulfuric acid, HOSO₂F was prepared in a 94 mm o.d. FEP vessel using oleum, H₂SO₄·SO₃ and NaF. The vessel was loaded with pre-dried (vacuum; 250 °C, ~10⁻⁴ mbar, 3 d) NaF (68.46 g; 1.63 mol), flushed with dry nitrogen and cooled to −80 °C. Pre cooled (−15 °C) oleum (27 – 33%) (500 g; 5.4 mol) was added portion wise. No reaction occurred at −15 °C. The mixture was subsequently allowed to warm to RT whereupon gas evolution and disappearance of solid NaF was observed. The reaction was exothermic and the temperature rose to ~40 °C. The suspension was transferred to a special designed glass-apparatus equipped with a reflux condenser, air cooled distillation bridge and a long cool-able inlet for inert gas connected directly to a 1000 mL round bottom flask (see photo).

Telluric acid, $\text{Te}(\text{OH})_6$ (53.30 g; 0.232 mol) was added at RT using a funnel. The suspension was heated to 140 – 160 °C and rigorously stirred for about 30 min. The mixture was finally refluxed for ~2 h (bath temperature: 190 – 200 °C). The cooling water in the condenser was turned off and the crude teflic acid, HOTeF_5 was distilled into a 16 mm i.d. FEP receiving tube equipped with a Kel-F valve. The distillation was performed directly at 240 °C where large amounts of teflic acid were obtained. Crude teflic acid, HOTeF_5 (36.70 g; 0.154 mol; 66.0% yield) was obtained as white crystalline solid. The crude teflic acid was stored at RT in the 16 mm i.d. FEP receiving vessel.

For the purification, concentrated sulfuric acid (95 – 97%) (200 mL) was transferred into a combined 500-mL round bottom flask with water cooled sublimation finger equipped with a Young stopcock. After transfer of the sulfuric acid, the flask was cooled to –80 °C. Crude teflic acid, HOTeF_5 , was condensed on top of the frozen sulfuric acid by using a warm water bath. The flask was allowed to warm to RT and completely mixed. The solution was frozen at dry ice temperature again and evacuated for 15 min. to degas the dissolved nitrogen (detected using a tesla coil). The reaction tube was closed and allowed to warm to RT. The reaction mixture was then further heated to 100 °C and refluxed under static vacuum for 12 h. At this temperature a strong reflux was observed at any time. After cooling the mixture to RT, teflic acid sublimed to the cold finger and on the walls building up a dense glassy coating. The apparatus was connected to a 63 mm o.d. glass vessel which functioned as a trap. This trap was cooled to –80 °C and teflic acid distilled under static vacuum at ~35 °C. At the end of the distillation the teflic acid, was melted into the bottom of the trap and the trap was pressurized with *ca.* 1 atm. of dry nitrogen. The HOTeF_5 was distilled into a 16 mm

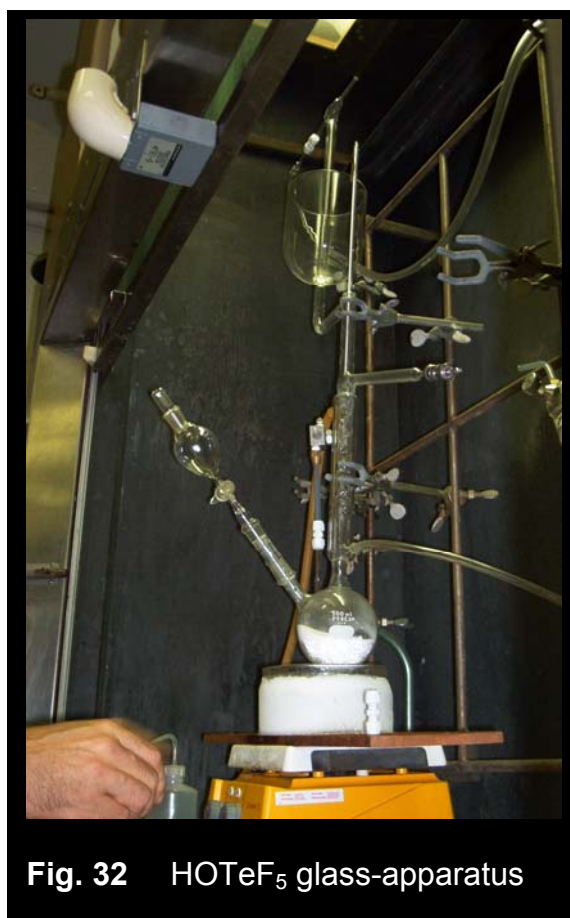


Fig. 32 HOTeF_5 glass-apparatus

i.d. FEP receiving tube. Teflic acid (~60 g) was purified yielding ~80% of the mass of the crude teflic acid. The over all yield of white solid HOTeF_5 was 51%.

HOTeF_5 in CH_3CN solution at 24 °C

^{19}F NMR (470.59 MHz)

HOTeF_5 $\delta = -41.0$ ppm (qui, 1F_{ax} ; ^{125}Te -satellites: $^1J(^{19}\text{F}_{\text{ax}}-^{125}\text{Te}) = 3340$ Hz);
 -47.8 ppm (d, $^2J(^{19}\text{F}_{\text{eq}}-^{19}\text{F}_{\text{ax}}) = 188$ Hz, 4F_{eq} ; ^{125}Te -satellites:
 $^1J(^{19}\text{F}_{\text{eq}}-^{125}\text{Te}) = 3550$ Hz; ^{123}Te -satellites: $^1J(^{19}\text{F}_{\text{eq}}-^{123}\text{Te}) = 2945$ Hz)

^{125}Te NMR (157.70 MHz)

HOTeF_5 $\delta = 604.9$ ppm (quid, $^1J(^{19}\text{F}_{\text{eq}}-^{125}\text{Te}) = 3550$ Hz, $^1J(^{19}\text{F}_{\text{ax}}-^{125}\text{Te}) = 3340$ Hz)

IV.9.10 Cesium Pentafluorooxotellurate, CsOTeF_5



Dry and powdered CsCl (624.87 mg; 3.71 mmol) was loaded into a ¼ inch o.d. FEP reaction tube equipped with a Kel-F valve. On a glass vacuum line, HOTeF_5 (4.3249 g; 5.5 mmol) was previously distilled into a ¼ inch o.d. FEP weighing vessel equipped with a Kel-F valve before distilling onto the frozen (-196 °C) CsCl under static vacuum. The reaction tube was pressurized with ca. 1 atm. of dry nitrogen and allowed to warm to RT. While warming, the teflic acid reacted on the surface with CsCl and HCl gas evolved. The reaction tube was then cooled to -80 °C to remove the HCl that had formed. This procedure was repeated until no further gas pressure was detected. An amount of HOTeF_5 (1.0235 g; 4.27 mmol) was distilled onto the resulting yellow solid at -196 °C. The sample was warmed to RT and maintained at this temperature for ~5 min. before the suspension was cooled to -80 °C and degassed. The reaction tube was then pressurized with ca. 1 atm. of dry nitrogen and maintained for ~3 h at RT. Excess of HOTeF_5 was back distilled and the yellow solid finally dried under dynamic vacuum for 4.5 h at RT. The solid was characterized by ^{19}F NMR spectroscopy and low-temperature Raman spectroscopy at -150 °C.

The yellow solid was purified by extraction with CH₃CN at RT. The yellow impurity is completely insoluble in CH₃CN at RT whereas CsOTeF₅ is well soluble (~0.7 mmol/mL). After removal of CH₃CN in vacuum at RT and drying of the resulting white solid no impurities were detected in its ¹⁹F NMR spectrum.

CsOTeF₅ in CH₃CN solution at 24 °C

¹⁹F NMR (282.40 MHz)

CsOTeF₅ δ = -30.3 ppm (qui, 1F_{ax}; ¹²⁵Te-satellites: ¹J(¹⁹F_{ax}-¹²⁵Te) = 3030 Hz);
 -43.6 ppm (dq, ²J(¹⁹F_{eq}-¹⁹F_{ax}) = 178 Hz, 4F_{eq}; ¹²⁵Te-satellites:
¹J(¹⁹F_{eq}-¹²⁵Te) = 3556 Hz; ¹²³Te-satellites: ¹J(¹⁹F_{eq}-¹²³Te) = 2960 Hz)

IV.9.11 *Tris(pentafluorooxotellurato)borane, B(OTeF₅)₃*



Teflic acid, HOTeF₅ (51.4732 g; 0.215 mol) was degassed and distilled in a 500-mL glass bulb equipped with a Young stopcock and cooled to -80 °C. Boron trichloride, BCl₃, was degassed and then condensed into an 8 mL volumetric vessel equipped with a Young stopcock under static vacuum. The volumetric vessel was cooled to -80 °C using a dry ice/acetone bath. An excess of BCl₃ (6.5 mL) was condensed in the cold volumetric vessel and allowed to be degassed. After warming to RT BCl₃ (7.7 mL) was measured into the volumetric vessel. Caution has to be exercised when warming BCl₃ because it tends to expand to a significant extent. The excess of BCl₃ was subsequently removed under dynamic vacuum at RT. The volumetric vessel was weighed using an analytical balance showing that BCl₃ (8.3905 g; 0.0716 mol) was condensed in. The volumetric vessel with BCl₃ and the 500-mL glass flask were connected to the vacuum line via a Y-piece and BCl₃ was condensed to HOTeF₅ in four portions of 1.5 to 2.0 mL to prevent high pressure from formed HCl. The 500-mL glass vessel was cooled to ca. -196 °C to minimize the vapor pressure of HCl and BCl₃. The maximum pressure inside the 500-mL vessel if the reaction would have been performed in one step would have been 10.47 bar calculated using the ideal gas equation. After each portion the vessel was allowed to warm to RT. The gas evolution, most likely arising from the reaction stopped even before all frozen material was molten, indicating a rapid reaction. The vessel was

then cooled to $-80\text{ }^{\circ}\text{C}$ and the resulting HCl was removed under vacuum. The chilled solution was subsequently allowed to warm to RT. This procedure was repeated four times until BCl_3 (8.3905 g; 0.0716 mol) had reacted completely with HOTeF_5 (51.4732g; 0.2150 mol). Because of the increasing amount of $\text{B}(\text{OTeF}_5)_3$ it was more difficult to melt the reaction mixture after each step. During the last addition the mixture had to be warmed by warm water ($\sim 40\text{ }^{\circ}\text{C}$). The 500-mL glass vessel was subsequently pressurized with ca. 1 atm. of dry nitrogen. White crystalline material of $\text{B}(\text{OTeF}_5)_3$ (51.9885 g; 0.0716 mol; 99.9% Yield) was obtained.



Fig. 33 Crystalline $\text{B}(\text{OTeF}_5)_3$

$\text{B}(\text{OTeF}_5)_3$ in CH_2Cl_2 solution at $24\text{ }^{\circ}\text{C}$

^{19}F NMR (282.40 MHz)

$\text{B}(\text{OTeF}_5)_3$ $\delta = -43.6$ ppm (d, $^2J(^{19}\text{F}_{\text{eq}}-^{19}\text{F}_{\text{ax}}) = 173$ Hz, 4F_{eq} ; ^{125}Te -satellites: $^1J(^{19}\text{F}_{\text{eq}}-^{125}\text{Te}) = 3681$ Hz; ^{123}Te -satellites: $^1J(^{19}\text{F}_{\text{eq}}-^{123}\text{Te}) = 3048$ Hz); -47.0 ppm (qui, 1F_{ax} ; ^{125}Te -satellites: $^1J(^{19}\text{F}_{\text{ax}}-^{125}\text{Te}) = 3665$ Hz)

^{11}B NMR (96.29 MHz)

$\text{B}(\text{OTeF}_5)_3$ $\delta = 12.8$ ppm (s, $\Delta\nu_{1/2} = 120$ Hz)

$\text{B}(\text{OTeF}_5)_3 \cdot \text{NCCH}_3$ in CH_3CN solution at $24\text{ }^{\circ}\text{C}$

^{19}F NMR (282.40 MHz)

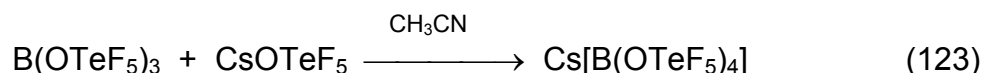
$\text{B}(\text{OTeF}_5)_3 \cdot \text{NCCH}_3$ $\delta = -40.4$ ppm (qui, 1F_{ax} ; ^{125}Te -satellites: $^1J(^{19}\text{F}_{\text{ax}}-^{125}\text{Te}) = 3432$ Hz); -44.2 ppm (d, $^2J(^{19}\text{F}_{\text{eq}}-^{19}\text{F}_{\text{ax}}) = 179$ Hz, 4F_{eq} ; ^{125}Te -satellites: $^1J(^{19}\text{F}_{\text{eq}}-^{125}\text{Te}) = 3558$ Hz; ^{123}Te -satellites: $^1J(^{19}\text{F}_{\text{eq}}-^{123}\text{Te}) = 2938$ Hz)

^{11}B NMR (96.29 MHz)

$\text{B}(\text{OTeF}_5)_3 \cdot \text{NCCH}_3$ $\delta = -3.4$ ppm (s, $\Delta\nu_{1/2} = 15$ Hz)

IV.9.12 *Cesium Tetrakis(pentafluorooxotellurato)borate*,
 $\text{Cs}[\text{B}(\text{OTeF}_5)_4]$

Cesium tetrakis(pentafluorooxotellurato)borate was prepared analogue to the previously reported method.^[123]



Tris(pentafluorooxotellurato)borane, $\text{B}(\text{OTeF}_5)_3$ (102.34 mg; 0.14 mmol) and cesium pentafluorooxotellurate, CsOTeF_5 (59.34 mg; 0.16 mmol) were each dissolved in CH_3CN (500 μL) and combined in a 8 mm i.d. FEP reaction tube at -40 °C. The solution was stirred for 30 min. at RT followed by removal of CH_3CN under dynamic vacuum. The resulting white solid was dried for 1 h at RT. Cesium tetrakis(pentafluorooxotellurato)borate, $\text{Cs}[\text{B}(\text{OTeF}_5)_4]$ (158.13 mg; 0.14 mmol; yield: 100%) was isolated.

$\text{Cs}[\text{B}(\text{OTeF}_5)_4]$ in CH_3CN solution at 24 °C

^{19}F NMR (282.40 MHz)

$\text{Cs}[\text{B}(\text{OTeF}_5)_4]$ $\delta = -38.4$ ppm (qui, 1F_{ax} ; ^{125}Te -satellites: $^1J(^{19}\text{F}_{\text{ax}}-^{125}\text{Te}) = 3325$ Hz);
 -45.4 ppm (d, $^2J(^{19}\text{F}_{\text{eq}}-^{19}\text{F}_{\text{ax}}) = 183$ Hz, 4F_{eq} ; ^{125}Te -satellites:
 $^1J(^{19}\text{F}_{\text{eq}}-^{125}\text{Te}) = 3017$ Hz; ^{123}Te -satellites: $^1J(^{19}\text{F}_{\text{eq}}-^{123}\text{Te}) = 2950$ Hz)

^{11}B NMR (96.29 MHz)

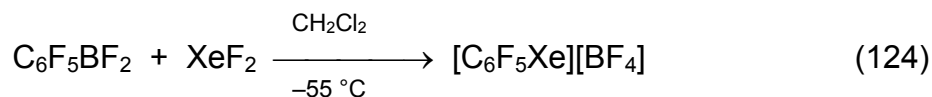
$\text{Cs}[\text{B}(\text{OTeF}_5)_4]$ $\delta = 0.1$ ppm (s, ^{125}Te -satellites: $^3J(^{11}\text{B}-^{125}\text{Te}) = 23$ Hz; ^{123}Te -satellites: $^2J(^{11}\text{B}-^{123}\text{Te}) = 46$ Hz)

IV.10 **Pentafluorophenylxenon(II) Compounds: Preparation, Characterization, and Physical Properties**

IV.10.1 *Preparation of [C₆F₅Xe][BY₄] (Y = F, CF₃, CN, C₆F₅, and OTeF₅)*

[C₆F₅Xe][BF₄]

The compound, [C₆F₅Xe][BF₄], was prepared analogue to the previously reported method.^[130]



Xenon difluoride (873.37 mg; 5.16 mmol) was suspended in cold (−40 °C) CH₂Cl₂ (25 mL) in a 23 mm i.d. FEP reaction tube with containing an adequate stir bar. Freshly prepared, cold (−80 °C) C₆F₅BF₂ solution (5.15 mmol) was transferred to the XeF₂ suspension at −60 °C. After 15 min., the temperature was raised to −40 °C. A pale yellow to white, fluffy solid precipitated. After 1.5 h of constant stirring, the suspension was quickly centrifuged at RT and the mother liquor separated. The almost white solid was dried under vacuum for at least 4 h at RT yielding [C₆F₅Xe][BF₄] (1.65 g; 4.28 mmol; yield: 83%).

[C₆F₅Xe][BY₄] (Y = CF₃, CN, C₆F₅, and OTeF₅)



The salts, [C₆F₅Xe][BY₄] (Y = CF₃, CN, C₆F₅, and OTeF₅) except [C₆F₅Xe][BF₄] were synthesized by metatheses of [C₆F₅Xe][BF₄] with stoichiometric amounts of either white Cs[BY₄] or K[BY₄]. Both reactants were separately dissolved in CH₃CN (300 μL) and combined at RT. The resulting yellow suspension was stirred for 15 min. at RT, centrifuged, and the CH₃CN mother liquor separated and the solid,

M[BF₄] (M = K, Cs), was washed with CH₃CN (300 μL). Remaining CH₃CN was subsequently removed under vacuum at RT. The resulting pale yellow solid, [C₆F₅Xe][BY₄], was dried under dynamic vacuum (~10⁻² mbar) for several hours at RT. In spite of the poor solubilities of K[BF₄] (4.8 μmol/mL) and Cs[BF₄] (5.0 μmol/mL) in CH₃CN at RT, small amounts (~5%) of [BF₄]⁻ were detected in the NMR spectra of the solution. To prevent small amounts of contamination with the co-product, M[BF₄], it was best to use the minimum amount of solvent and cool the reaction suspension to -40 °C. The amount of [BF₄]⁻ detectable by ¹⁹F NMR was negligible for all compounds. Thus, the salts, [C₆F₅Xe][B(CF₃)₄] and [C₆F₅Xe][B(C₆F₅)₄], which are somewhat soluble in CH₂Cl₂, could be prepared in high purity (≥98%). The co-products K[BF₄] and Cs[BF₄] are insoluble in CH₂Cl₂ at RT.

IV.10.2 Pentafluorophenylxenon(II)tetrafluoroborate, [C₆F₅Xe][BF₄]

IV.10.2.1 NMR Characterization

In CH₃CN solution at -40 °C

¹⁹F-NMR (282.40 MHz)

[C₆F₅Xe]⁺ δ = -124.1 ppm (m, ³J(¹⁹F-¹²⁹Xe) = 68 Hz, *o*-C₆F₅, 2F); -140.7 ppm (tt, ³J(¹⁹F-¹⁹F) = 21 Hz, ⁴J(¹⁹F-¹⁹F) = 5 Hz, *p*-C₆F₅, 1F); -153.5 ppm (m, *m*-C₆F₅, 2F)

[BF₄]⁻ δ = -147.5 ppm (s, Δν_{1/2} = 4 Hz, Δδ(¹¹B-¹⁰B) = 16 Hz, 4F)

In CH₃CN solution at 24 °C

¹⁹F NMR (282.40 MHz)

[C₆F₅Xe]⁺ δ = -125.4 ppm (m, *o*-C₆F₅, 2F); -142.8 ppm (tt, ³J(¹⁹F-¹⁹F) = 19 Hz, ⁴J(¹⁹F-¹⁹F) = 5 Hz, *p*-C₆F₅, 1F); -155.5 ppm (m, *m*-C₆F₅, 2F)

[BF₄]⁻ δ = -148.0 ppm (s, Δν_{1/2} = 24 Hz, 4F, Δδ(¹⁰B-¹¹B) = 16 Hz)

¹¹B NMR (96.29 MHz)

[BF₄]⁻ δ = -2.0 ppm (s, Δν_{1/2} = 2 Hz)

^{129}Xe NMR (83.02 MHz)

$[\text{C}_6\text{F}_5\text{Xe}]^+$ $\delta = -3813.8$ ppm (tt, $^3J(^{19}\text{F}-^{129}\text{Xe}) = 66$ Hz, $^4J(^{19}\text{F}-^{129}\text{Xe}) = 8$ Hz,
 $^5J(^{19}\text{F}-^{129}\text{Xe}) = 2$ Hz)

In aHF solution at -40 °C

^{19}F NMR (282.40 MHz)

$[\text{C}_6\text{F}_5\text{Xe}]^+$ $\delta = -123.6$ ppm (m, $^3J(^{19}\text{F}-^{129}\text{Xe}) = 59$ Hz, *o*- C_6F_5 , 2F); -138.2 ppm
(tt, $^3J(^{19}\text{F}-^{19}\text{F}) = 19$ Hz, $^4J(^{19}\text{F}-^{19}\text{F}) = 6$ Hz, *p*- C_6F_5 , 1F); -151.8 ppm
(m, *m*- C_6F_5 , 2F)

$[\text{BF}_4]^-$ $\delta = -148.6$ ppm (q, $^1J(^{11}\text{B}-^{19}\text{F}) = 12$ Hz, 4F)

HF $\delta = -191.0$ ppm (s)

^{11}B NMR (96.29 MHz)

$[\text{BF}_4]^-$ $\delta = -1.3$ ppm (qui, $^1J(^{11}\text{B}-^{19}\text{F}) = 12$ Hz)

^{129}Xe NMR (83.02 MHz)

$[\text{C}_6\text{F}_5\text{Xe}]^+$ $\delta = -3831.5$ ppm (t, $^3J(^{19}\text{F}-^{129}\text{Xe}) = 59$ Hz)

IV.10.2.2 Raman Spectroscopic Characterization

In the drybox, $[\text{C}_6\text{F}_5\text{Xe}][\text{BF}_4]$ (~50 – 100 mg), was transferred into a previously dried 5 mm glass NMR tube (Wilmad 507) which was heat sealed under dynamic vacuum ($\sim 10^{-3}$ mbar) at -196 °C as described before. A low-temperature (-150 °C) Raman spectrum was recorded using a laser power of 300 mW and a total of 1500 scans.

IV.10.2.3 Attempt to Crystallize $[\text{C}_6\text{F}_5\text{Xe}][\text{BF}_4]$ from CH_3CN and $\text{CH}_3\text{CN}/\text{CH}_2\text{Cl}_2$

In a $\frac{1}{4}$ inch o.d. T-shaped FEP reaction tube equipped with a Kel-F valve, $[\text{C}_6\text{F}_5\text{Xe}][\text{BF}_4]$ (39.20 mg; 0.10 mmol) was dissolved in CH_3CN (0.45 mL). The arm containing the pale yellow coloured solution was placed inside a glass dewar of the low-temperature crystal growing apparatus which had been pre-set to a temperature of -12.5 °C. As the temperature of the dewar was decreased to -45 °C within 2 h the

solvent began to freeze prior to crystallization of $[\text{C}_6\text{F}_5\text{Xe}][\text{BF}_4]$. After reducing the solvent from 450 μL ($c([\text{C}_6\text{F}_5\text{Xe}][\text{BF}_4]) = 0.23 \text{ mmol/mL}$) to 100 μL ($c([\text{C}_6\text{F}_5\text{Xe}][\text{BF}_4]) = 1.02 \text{ mmol/mL}$) under vacuum ($\sim 10^{-3} \text{ mbar}$) at RT no crystallization was observed even at $-40 \text{ }^\circ\text{C}$. Further removal resulted in a highly viscous oil.

Dry CH_2Cl_2 ($\sim 0.29 \text{ mL}$) was subsequently condensed on top of this solution to reduce the solubility of $[\text{C}_6\text{F}_5\text{Xe}][\text{BF}_4]$ in CH_3CN . The sample was cooled to $-80 \text{ }^\circ\text{C}$ overnight whereupon feather-like crystals of CH_3CN were observed. The reaction tube was pumped at $-60 \text{ }^\circ\text{C}$ under dynamic vacuum yielding a yellow oil which was then dried under dynamic vacuum for 5 h at RT.

A further attempt was made to crystallize $[\text{C}_6\text{F}_5\text{Xe}][\text{BF}_4]$ from a $\text{CH}_2\text{Cl}_2/\text{CH}_3\text{CN}$ solution was performed by suspending $[\text{C}_6\text{F}_5\text{Xe}][\text{BF}_4]$ (47.97 mg; 0.13 mmol) in CH_2Cl_2 ($\sim 400 \mu\text{L}$) in a $\frac{1}{4}$ inch o.d. T-shaped FEP reaction tube equipped with a Kel-F valve. Acetonitrile was added until nearly all solid material was dissolved at RT. Cooling the sample to $-80 \text{ }^\circ\text{C}$ did not result in crystallization but only a yellow oil resulted.

IV.10.2.4 Thermo-analytical Measurements of $[\text{C}_6\text{F}_5\text{Xe}][\text{BF}_4]$ in the Solid State (DSC)

In the drybox, pale yellow $[\text{C}_6\text{F}_5\text{Xe}][\text{BF}_4]$ (14.01 mg; 0.04 mmol) was loaded into a pierced aluminium pan. The sample was placed inside the DSC apparatus and heated to $310 \text{ }^\circ\text{C}$. The melting point was determined to $79.5 \text{ }^\circ\text{C}$ (onset) having its maximum at $85.8 \text{ }^\circ\text{C}$ and the decomposition at $156.6 \text{ }^\circ\text{C}$ (onset) reaching its maximum at $180.5 \text{ }^\circ\text{C}$.

IV.10.2.4.1 Proof of the Reversibility of the Melting Point of $[\text{C}_6\text{F}_5\text{Xe}][\text{BF}_4]$

In the drybox, pale yellow $[\text{C}_6\text{F}_5\text{Xe}][\text{BF}_4]$ (35.18 mg; 0.09 mmol) was loaded into a pierced aluminium pan. The sample was placed inside the DSC apparatus and heated according the followed temperature program:

No.	mode	T [°C]	Heat rate [K/min]	Erf.- rate [1/min]	Time [hh:mm]	Gas flow	Protection gas
---	START	25					
1	Dynamic	110	10.0	50.00	00:08		
2	Dynamic	60	5.0	30.00	00:10		
3	Isothermic	60	0.0	10.00	00:10	On	On
4	Dynamic	120	10.0	50.00	00:06		
5	Isothermic	300	10.0	50.00	01:00		
---	END	310					

The melting point was determined at 81.0 °C (onset) reaching its maximum at 86.1 °C. The melting process was found to be reversible. The subsequent decomposition started at 157.8 °C (onset) reaching its maximum at 181.1 °C.

IV.10.2.5 Solubility of $[C_6F_5Xe][BF_4]$ in Selected Solvents at RT

Small quantities of $[C_6F_5Xe][BF_4]$ were suspended in the corresponding solvent at RT, stirred for 10 min. The mother liquor was separated and the internal standard, $C_6H_5CF_3$ (5 μ L; 0.04 mmol), was added. The solution was measured by ^{19}F NMR spectroscopy and the solubility calculated related to the internal standard.

Solubility in CH_3CN at RT = ~4.8 mmol/mL

Solubility in CH_2Cl_2 at RT = insoluble

Solubility in PFB at RT = insoluble

Solubility in CCl_4 at RT = insoluble

Solubility in SO_2ClF at RT = insoluble

IV.10.2.6 Thermal Stability of $[C_6F_5Xe][BF_4]$ in CH_3CN and aHF at RT

In CH_3CN at RT

In the drybox, $[C_6F_5Xe][BF_4]$ (26.83 mg; 0.07 mmol), was dissolved in CH_3CN (300 μ L) at RT, stored in a 3.5 mm i.d. FEP reaction tube and monitored periodically by ^{19}F NMR spectroscopy.

Decomposition of $[C_6F_5Xe][BF_4]$ in CH_3CN at RT

time [d]	$[C_6F_5Xe]^+{}^a$ [mol-%]	$C_6F_5H^a$ [mol-%]	$[BF_4]^-{}^b$ [mol-%]	HF ^b [mol-%]
2 h	98.0	2.0	100	0.0
2	95.4	4.6	96.4	
7	92.8	7.2	98.7	
11	90.3	9.7	100.5	
18	85.0	15.0	103.3	
30	67.9	32.1	113.3	
43	51.6	48.4	131.5	
58	21.5	78.5	159.9	

rising traces

^a The total amount (mol-%) of all C_6F_5 compounds was normalized to 100%.

^b $[BF_4]^-$ anion and HF signal were calculated with regard to the sum of C_6F_5 compounds.

Over time, the $[BF_4]^-$ signal changed its shape and a shoulder developed at higher frequency ($\delta = -148.7$ ppm).

In aHF at RT

In a 3.5 mm i.d. FEP reaction tube, $[C_6F_5Xe][BF_4]$ (39.00 mg, 0.040 mmol), was dissolved in aHF (~500 μ L) at -40 °C. The sample was maintained inside a glass trap protected with argon at RT and was monitored periodically by ^{19}F NMR spectroscopy.

Decomposition of $[C_6F_5Xe][BF_4]$ in aHF at RT

time [d]	$[C_6F_5Xe]^+{}^a$	$C_6F_6{}^a$	$[BF_4]^-{}^b$
	l) C_6F_5 -bal. [mol-%]	l) C_6F_5 -bal. [mol-%]	l) C_6F_5 -bal. [mol-%]
12 h	100	Traces	103.5
2	98.5	1.5	103.4
5	96.4	3.6	103.8
8	95.4	4.6	106.3
11	94.4	5.6	108.2
16*	94.1	5.9	112.6
19*	92.6	7.4	110.6
26*	88.4	11.6	117.5
33*	88.2	11.8	127.5
40*	90.3	9.7	136.7
47*	87.3	12.7	139.9
54*	85.1	14.9	151.0

^a The total amount (mol-%) of all C_6F_5 compounds was normalized to 100%.

^b $[BF_4]^-$ anion signal was calculated with regard to the sum of C_6F_5 compounds.

* formation of a broad doublet at -165 ppm (d, $J = 485$ Hz)

IV.10.3 Pentafluorophenylxenon(II)tetrakis(trifluoromethyl)borate, $[C_6F_5Xe][B(CF_3)_4]$

IV.10.3.1 NMR Characterization

In CH_2Cl_2 solution at 24 °C

^{19}F NMR (282.40 MHz)

$[C_6F_5Xe]^+$ $\delta = -124.8$ ppm (m, *o*- C_6F_5 , 2F); -138.2 ppm (ttm, ${}^3J(^{19}F-^{19}F) = 20$ Hz, ${}^4J(^{19}F-^{19}F) = 6$ Hz, *p*- C_6F_5 , 1F); -152.1 ppm (m, *m*- C_6F_5 , 2F)

$[B(CF_3)_4]^-$ $\delta = -62.6$ ppm (q, ${}^2J(^{11}B-^{19}F) = 26$ Hz, sep, ${}^2J(^{10}B-^{19}F) = 9$ Hz, CF, 12F)

^{11}B NMR (96.29 MHz)

$[\text{B}(\text{CF}_3)_4]^-$ $\delta = -20.3$ ppm (tridec, $^2J(^{11}\text{B}-^{19}\text{F}) = 26$ Hz)

^{129}Xe NMR (83.02 MHz)

$[\text{C}_6\text{F}_5\text{Xe}]^+$ $\delta = -3813.3$ ppm (tt, $^3J(^{19}\text{F}-^{129}\text{Xe}) = 66$ Hz, $^4J(^{19}\text{F}-^{129}\text{Xe}) = 9$ Hz, $^5J(^{19}\text{F}-^{129}\text{Xe}) = 2$ Hz)

In CH_3CN solution at 24 °C

^{19}F NMR (282.40 MHz)

$[\text{C}_6\text{F}_5\text{Xe}]^+$ $\delta = -125.0$ ppm (m, $^3J(^{19}\text{F}-^{129}\text{Xe}) = 68$ Hz, *o*- C_6F_5 , 2F); -141.2 ppm (tt, $^3J(^{19}\text{F}-^{19}\text{F}) = 20$ Hz, $^4J(^{19}\text{F}-^{19}\text{F}) = 6$ Hz, *p*- C_6F_5 , 1F); -154.3 ppm (m, *m*- C_6F_5 , 2F)

$[\text{B}(\text{CF}_3)_4]^-$ $\delta = -62.6$ ppm (q, $^2J(^{11}\text{B}-^{19}\text{F}) = 26$ Hz, sep, $^2J(^{10}\text{B}-^{19}\text{F}) = 9$ Hz, CF, 12F)

^{11}B NMR (96.29 MHz)

$[\text{B}(\text{CF}_3)_4]^-$ $\delta = -19.3$ ppm (tridec, $^2J(^{11}\text{B}-^{19}\text{F}) = 26$ Hz)

^{129}Xe NMR (83.02 MHz)

$[\text{C}_6\text{F}_5\text{Xe}]^+$ $\delta = -3802.2$ ppm (tt, $^3J(^{19}\text{F}-^{129}\text{Xe}) = 68$ Hz, $^4J(^{19}\text{F}-^{129}\text{Xe}) = 9$ Hz, $^5J(^{19}\text{F}-^{129}\text{Xe}) = 2$ Hz)

In PFB solution at 24 °C

^{19}F NMR (282.40 MHz)

$[\text{C}_6\text{F}_5\text{Xe}]^+$ $\delta = -124.3$ ppm (m, $^3J(^{19}\text{F}-^{129}\text{Xe}) = 62$ Hz; *o*- C_6F_5 , 2F); -138.9 ppm (tt, $^3J(^{19}\text{F}-^{19}\text{F}) = 19$ Hz, $^4J(^{19}\text{F}-^{19}\text{F}) = 6$ Hz, *p*- C_6F_5 , 1F); -152.3 ppm (m, *m*- C_6F_5 , 2F)

$[\text{B}(\text{CF}_3)_4]^-$ $\delta = -60.2$ ppm (q, $^2J(^{11}\text{B}-^{19}\text{F}) = 26$ Hz; sep, $^2J(^{10}\text{B}-^{19}\text{F}) = 9$ Hz, CF, 12F)

^{11}B NMR (96.29 MHz)

$[\text{B}(\text{CF}_3)_4]^-$ $\delta = -19.7$ ppm (tridec, $^2J(^{11}\text{B}-^{19}\text{F}) = 26$ Hz)

^{129}Xe NMR (83.02 MHz)

$[\text{C}_6\text{F}_5\text{Xe}]^+$ $\delta = -3821.0$ ppm (t, $^3J(^{19}\text{F}-^{129}\text{Xe}) = 62$ Hz)

IV.10.3.2 Raman Spectroscopic Characterization

In the drybox, $[\text{C}_6\text{F}_5\text{Xe}][\text{B}(\text{CF}_3)_4]$ (~50 – 100 mg), was transferred into a previously dried 5 mm glass NMR tube (Wilmad 507) which was heat sealed under dynamic vacuum at -196 °C as described before. A low-temperature (-150 °C) Raman spectrum was recorded using a laser power of 300 mW and a total of 1500 scans. The spectra of $\text{K}[\text{B}(\text{CF}_3)_4]$, CH_3CN and CH_2Cl_2 were also measured at -150 °C. In addition, $\text{K}[\text{B}(\text{CF}_3)_4]$ was measured at ambient temperature for reference purposes.

IV.10.3.3 Crystal Growth and Structure Refinement

In the drybox, $[\text{C}_6\text{F}_5\text{Xe}][\text{B}(\text{CF}_3)_4]$ (61.69 mg; 0.01 mmol), was transferred into a $\frac{1}{4}$ inch o.d. T-shaped FEP reaction tube equipped with a Kel-F valve. The reaction tube was attached to a vacuum line and anhydrous CH_2Cl_2 (0.59 mL) was condensed into the reactor at ca. -196 °C. Acetonitrile was condensed at ca. -196 °C until most of the solid $[\text{C}_6\text{F}_5\text{Xe}][\text{B}(\text{CF}_3)_4]$ was dissolved. The reaction tube was pressurized with ca. 1 atm. of dry nitrogen and allowed to warm to RT. The arm containing the solution was subsequently placed inside the glass Dewar of a low-temperature crystal growing apparatus set at an initial temperature of -60 °C. After 10 h at -63 °C, clear, colorless, needle-shaped crystals formed throughout the solution. The sample was further cooled to -66 °C within 5 h. The still pale yellow solution was decanted into the side arm of the T-shaped reaction tube at -196 °C and heat sealed under dynamic vacuum. The remaining solvent was slowly (30 min.) removed under dynamic vacuum at -62 °C. The pale yellow needles were isolated and a single crystal was mounted at -173 °C on the X-ray diffractometer as previously described. The crystal used for the data acquisition had the dimensions $0.04 \times 0.04 \times 0.08$ mm³. Detailed information can be found in the Appendix.

In the drybox, $[\text{C}_6\text{F}_5\text{Xe}][\text{B}(\text{CF}_3)_4]$ (19.12 mg; 0.03 mmol), was transferred into a $\frac{1}{4}$ inch o.d. T-shaped FEP reaction tube equipped with a Kel-F valve. The reaction tube was then attached to a vacuum line where anhydrous CH_2Cl_2 (0.59 mL) was

condensed onto the sample at ca. $-196\text{ }^{\circ}\text{C}$. The sample was warmed to ca. $30\text{ }^{\circ}\text{C}$ to dissolve as much solute as possible. The resulting suspension was transferred into the sidearm B of the T-reactor and the mother liquor was decanted into the straight arm A of the T-reactor. The arm containing the solution was placed inside the glass dewar of a low-temperature crystal growing apparatus set at an initial temperature of $-38\text{ }^{\circ}\text{C}$. After several hours small seed crystals were observed. After 8 h, clear, yellow needles grew throughout the solution having a length of $\sim 10\text{ mm}$. The sample was maintained at $-40\text{ }^{\circ}\text{C}$ for 26 h before the pale solution was decanted into the side arm of the T-shaped reaction tube and then heat sealed under dynamic vacuum. The residual solution was slowly (30 min.) removed under dynamic vacuum at $-67\text{ }^{\circ}\text{C}$ to reduce the probability of pumping solvent out of the crystal lattice. Pale yellow needles were isolated and a single crystal was mounted at $-173\text{ }^{\circ}\text{C}$ on the X-ray diffractometer as previously described. The crystal used for the data acquisition had the dimensions $0.26 \times 0.16 \times 0.04\text{ mm}^3$. Detailed information can be found in the Appendix.

IV.10.3.4 Thermo-analytical Measurements of $[\text{C}_6\text{F}_5\text{Xe}][\text{B}(\text{CF}_3)_4]$ in the Solid State (DSC)

In the drybox, pale yellow $[\text{C}_6\text{F}_5\text{Xe}][\text{B}(\text{CF}_3)_4]$ (3.4 mg; $5.8\text{ }\mu\text{mol}$) was loaded into a pierced aluminium pan. The sample was placed inside the DSC apparatus and heated to $510\text{ }^{\circ}\text{C}$. The decomposition proceeded in three exothermic local maxima at 117.2 , 139.3 , and $148.8\text{ }^{\circ}\text{C}$ (onset) in the absence of a prior melting process.

IV.10.3.5 Solubility of $[\text{C}_6\text{F}_5\text{Xe}][\text{B}(\text{CF}_3)_4]$ in Selected Solvents at RT

Small quantities of $[\text{C}_6\text{F}_5\text{Xe}][\text{B}(\text{CF}_3)_4]$ were suspended in the corresponding solvent at RT, stirred for 10 min. The mother liquor was separated and the internal standard, $\text{C}_6\text{H}_5\text{CF}_3$ ($5\text{ }\mu\text{L}$; 0.04 mmol) was added. The solution was measured by ^{19}F NMR spectroscopy and the solubility calculated based on the internal standard.

Solubility in CH_3CN at RT = $> 4.5\text{ mmol/mL}$

Solubility in PFB at RT = $> 1.2\text{ mmol/mL}$

Solubility in CH_2Cl_2 at RT = $\sim 0.6\text{ mmol/mL}$

IV.10.3.6 Solubility of $K[B(CF_3)_4]$ in CH_2Cl_2 at RT

In CH_2Cl_2 at RT

Pre-dried (10^{-3} mbar, 1 h, RT) white $K[B(CF_3)_4]$ (90% purity) (35 mg; 0.11 mmol) was suspended in CH_2Cl_2 (1000 μ L) at RT. The insolubility of $K[B(CF_3)_4]$ in CH_2Cl_2 (1000 μ L) at RT was demonstrated by ^{19}F -NMR spectroscopy.

IV.10.3.7 Thermal Stability of $[C_6F_5Xe][B(CF_3)_4]$

In CH_3CN at RT

In a 3.5 mm i.d. FEP reaction tube, $[C_6F_5Xe][B(CF_3)_4]$ (22.00 mg; 0.04 mmol), was dissolved in CH_3CN (300 μ L) at RT and monitored periodically by ^{19}F NMR spectroscopy at 24 °C.

Decomposition of $[C_6F_5Xe][B(CF_3)_4]$ in CH_3CN at RT

time [d]	$[C_6F_5Xe]^+$ ^a [mol-%]	$[B(CF_3)_4]^-$ ^b [mol-%]	C_6F_5H ^a [mol-%]	HF ^b [mol-%]
2 h	100	103.1	0	0
2	95.0	100.0	5.0	0
7	91.7	104.2	8.3	0
11	85.7	109.9	14.3	Traces
18	74.2	107.5	25.8	Traces
30	43.1	138.9	56.9	44.4
43	0.0	181.8	100.0	56.4
58	0.0	200.0	100.0	Broad signal

^a The total amount (mol-%) of all C_6F_5 compounds was normalized to 100%.

^b The amount of the $[B(CF_3)_4]^-$ anion and the HF signal was calculated with regard to the sum of C_6F_5 compounds.

In CH_2Cl_2 at RT

In a 3.5 mm i.d. FEP reaction tube, $[C_6F_5Xe][B(CF_3)_4]$ (25.00 mg; 0.04 mmol), was dissolved in CH_2Cl_2 (500 μ L) at RT and monitored periodically by ^{19}F NMR spectroscopy at 24 °C.

Decomposition of $[\text{C}_6\text{F}_5\text{Xe}][\text{B}(\text{CF}_3)_4]$ in CH_2Cl_2 at RT

time [d]	$[\text{C}_6\text{F}_5\text{Xe}]^+{}^{\text{a}}$ [mol-%]	$\text{C}_6\text{F}_5\text{H}^{\text{a}}$ [mol-%]	$\text{C}_6\text{F}_5\text{Cl}^{\text{a}}$ [mol-%]
15 min.	100	0	0
3	96.2	0.0	3.8
13	72.3	5.9	21.8
17	60.2	9.7	30.1
22	50.4	9.7	39.9

^a The total amount (mol-%) of all C_6F_5 compounds was normalized to 100%.

In PFB at RT

In a 3.5 mm i.d. FEP reaction tube, $[\text{C}_6\text{F}_5\text{Xe}][\text{B}(\text{CF}_3)_4]$ (138 mg; 0.24 mmol), was dissolved in PFB (200 μL) at RT and the solution was monitored periodically by ^{19}F NMR spectroscopy. The solubility of $[\text{C}_6\text{F}_5\text{Xe}][\text{B}(\text{CF}_3)_4]$ in PFB at RT is higher than 1.19 mmol/mL.

Decomposition of $[\text{C}_6\text{F}_5\text{Xe}][\text{B}(\text{CF}_3)_4]$ in PFB at RT

time [d]	$[\text{C}_6\text{F}_5\text{Xe}]^+{}^{\text{a}}$ [mol-%]	$\text{C}_6\text{F}_6^{\text{a}}$ [mol-%]	1 ^a [mol-%]	2 ^a [mol-%]	3 ^a [mol-%]	$[\text{B}(\text{CF}_3)_4]^-{}^{\text{b}}$ [mol-%]
15 min	100.0	0	0	0	0	95.7
5	96.5	0.2	1.1	2.2	traces	95.9
6	95.2	0.3	1.6	2.9	traces	98.2
8	96.5	0.2	1.1	2.2	traces	95.9

^a The total amount (mol-%) of all C_6F_5 compounds was normalized to 100%.

^b The amount of the $[\text{B}(\text{CF}_3)_4]^-$ anion was calculated with regard to $[\text{C}_6\text{F}_5\text{Xe}]^+$.

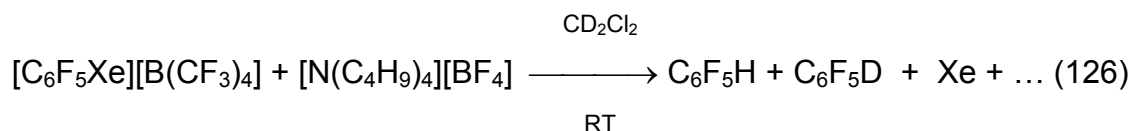
^{19}F NMR (282.40 MHz) in PFB at 24 °C

- 1** $\delta = -143.0$ ppm (m, *o*-C₆F₅, 2F); -154.7 ppm (t, $^3J(^{19}\text{F}-^{19}\text{F}) = 20$ Hz, *p*-C₆F₅, 1F); -163.1 ppm (m, *m*-C₆F₅, 2F)
- 2** $\delta = -143.1$ ppm (m, *o*-C₆F₅, 2F); -155.2 ppm (t, $^3J(^{19}\text{F}-^{19}\text{F}) = 19$ Hz, *p*-C₆F₅, 1F); -162.5 ppm (m, *m*-C₆F₅, 2F)
- 3** $\delta = -139.3$ ppm (m, *o*-C₆F₅, 2F); -155.2 ppm ? (t*, $^3J(^{19}\text{F}-^{19}\text{F}) = 20$ Hz, *p*-C₆F₅, 1F); -162.6 ppm* (m, *m*-C₆F₅, 2F)
- C₆F₆ $\delta = -162.9$ ppm (s, $\Delta\nu_{1/2} = 2$ Hz, 6F)

^{11}B NMR (96.29 MHz) in PFB at 24 °C

- [B(CF₃)₄]⁻ $\delta = -19.7$ ppm (tridec, $^2J(^{11}\text{B}-^{19}\text{F}) = 26$ Hz)
- 1** $\delta = -15.1$ ppm (s, $\Delta\nu_{1/2} = 142$ Hz)
- 2** $\delta = -7.4$ ppm (s, $\Delta\nu_{1/2} = 142$ Hz)
- 3** $\delta = -1.9$ ppm (s, $\Delta\nu_{1/2} = 6$ Hz)

IV.10.3.8 Reaction of [C₆F₅Xe][B(CF₃)₄] with [N(C₄H₉)₄][BF₄] in CD₂Cl₂ at RT



In a 3.5 mm i.d. FEP reaction tube, stoichiometric amounts of [C₆F₅Xe][B(CF₃)₄] (21.75 mg; 0.04 mmol) and [N(C₄H₉)₄][BF₄] (12.25 mg; 0.04 mmol) were dissolved separately in CD₂Cl₂ (each 150 μL) at RT. Both solutions were combined at RT and the mixture was monitored by ^{19}F NMR spectroscopy. Over time, [C₆F₅Xe][BF₄] deposited as a yellow oil.

**Composition of Reactants and Products Resulting from the Reaction of
[C₆F₅Xe][B(CF₃)₄] with [N(C₄H₉)₄][BF₄] in CD₂Cl₂ at RT**

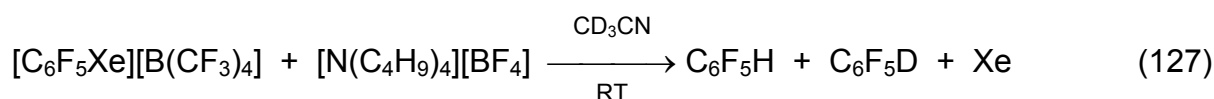
time [d]	[C ₆ F ₅ Xe] ^{+ a} [mol-%]	C ₆ F ₅ H /C ₆ F ₅ D ^a [mol-%]	(C ₆ F ₅) ₂ ^a [mol-%]	[BF ₄] ^{- b} [mol-%]	[B(CF ₃) ₄] ^{- b} [mol-%]
3 h	60.0 [C ₆ F ₅ Xe][B(CF ₃) ₄] 40.0 [C ₆ F ₅ Xe][BF ₄] (oil)	0.0 / 0.0	0.0	80.0	125.0
2	42.3 [C ₆ F ₅ Xe][B(CF ₃) ₄] 31.0 [C ₆ F ₅ Xe][BF ₄] (oil)	15.5 / 7.0	4.2	70.4	140.8
7	22.1 [C ₆ F ₅ Xe][B(CF ₃) ₄] 39.7 [C ₆ F ₅ Xe][BF ₄] (oil)	28.6 / 4.8	4.8	63.5	186.8
11	8.2 [C ₆ F ₅ Xe][B(CF ₃) ₄] 14.6 [C ₆ F ₅ Xe][BF ₄] (oil)	27.6 / 12.2	37.4	56.1	81.3
18	0.0 [C ₆ F ₅ Xe][B(CF ₃) ₄] 0.0 [C ₆ F ₅ Xe][BF ₄] (oil)	72.7 / 18.2	9.1	123.6	181.8

^a The total amount (mol-%) of all C₆F₅ compounds was normalized to 100%.

^b The amount of the [B(CF₃)₄]⁻ and [BF₄]⁻ anions were calculated with regard to the sum of C₆F₅ compounds.

^c The [BF₄]⁻ signal got broader with increasing reaction time.

IV.10.3.9 Reaction of [C₆F₅Xe][B(CF₃)₄] with [N(C₄H₉)₄][BF₄] in CD₃CN at RT



In the drybox, stoichiometric amounts of [C₆F₅Xe][B(CF₃)₄] (21.12 mg; 0.04 mmol) and [N(C₄H₉)₄][BF₄] (11.89 mg; 0.04 mmol) were dissolved separately in CD₃CN (each 150 μL) at RT. Both solutions were combined at RT and monitored by

NMR spectroscopy. It was shown by ^1H NMR spectroscopy that CD_3CN contained no detectable H_2O .

**Decomposition of $[\text{C}_6\text{F}_5\text{Xe}][\text{B}(\text{CF}_3)_4]$
in the presence of $[\text{N}(\text{CH}_3)_4][\text{BF}_4]$ in CD_3CN at RT**

time	$[\text{C}_6\text{F}_5\text{Xe}]^+$ ^a	$\text{C}_6\text{F}_5\text{H}/\text{C}_6\text{F}_5\text{D}^{\text{a}}$	$[\text{BF}_4]^-$ ^b	$[\text{B}(\text{CF}_3)_4]^-$ ^b
[d]	[mol-%]	[mol-%]	[mol-%]	[mol-%]
3 h	75.5	24.5 / 0.0	98.0	102.0
2	0.0	100.0 / traces	121.3	133.3

^a The total amount (mol-%) of all C_6F_5 compounds was normalized to 100%.

^b The amount of the $[\text{B}(\text{CF}_3)_4]^-$ and $[\text{BF}_4]^-$ anions were calculated with regard to the sum of C_6F_5 compounds.

IV.10.4 Pentafluorophenylxenon(II)tetrakis(pentafluoroxotellurato)borate, $[\text{C}_6\text{F}_5\text{Xe}][\text{B}(\text{OTeF}_5)_4]$

IV.10.4.1 NMR Characterization

In CH_3CN solution at 24 °C

^{19}F NMR (282.40 MHz)

$[\text{C}_6\text{F}_5\text{Xe}]^+$ $\delta = -125.5$ ppm (m, *o*- C_6F_5 , 2F); -141.8 ppm (tt, $^3J(^{19}\text{F}-^{19}\text{F}) = 20$ Hz, $^4J(^{19}\text{F}-^{19}\text{F}) = 6$ Hz, *p*- C_6F_5 , 1F); -154.7 ppm (m, *m*- C_6F_5 , 2F)

$[\text{B}(\text{OTeF}_5)_4]^-$ $\delta = -38.8$ ppm (qui, 1 F_{ax} ; ^{125}Te -satellites: $^1J(^{19}\text{F}_{\text{ax}}-^{125}\text{Te}) = 3336$ Hz); -45.4 ppm (d, $^2J(^{19}\text{F}_{\text{eq}}-^{19}\text{F}_{\text{ax}}) = 182$ Hz, 4 F_{eq} ; ^{125}Te -satellites: $^1J(^{19}\text{F}_{\text{eq}}-^{125}\text{Te}) = 3560$ Hz; ^{123}Te -satellites: $^1J(^{19}\text{F}_{\text{eq}}-^{123}\text{Te}) = 2978$ Hz)

^{11}B NMR (96.29 MHz)

$[\text{B}(\text{OTeF}_5)_4]^-$ $\delta = -0.2$ ppm (s, ^{125}Te -satellites: $^3J(^{11}\text{B}-^{125}\text{Te}) = 23$ Hz; ^{123}Te -satellites: $^3J(^{10}\text{B}-^{123}\text{Te}) = 46$ Hz)

^{129}Xe NMR (83.02 MHz)

$[\text{C}_6\text{F}_5\text{Xe}]^+$ $\delta = -3808.1$ ppm (t, $^3J(^{19}\text{F}-^{129}\text{Xe}) = 68$ Hz)

IV.10.4.2 Attempts to Crystallize $[C_6F_5Xe][B(OTeF_5)_4]$ from PFB/ CH_3CN at Low Temperatures

The compound, $[C_6F_5Xe][B(OTeF_5)_4]$, obtained as an oil (from the metathesis), was suspended in cold ($-42\text{ }^\circ\text{C}$) PFB (400 μL) until most of the material had dissolved or was emulsified. The suspension/emulsion was stirred for 60 min at $-41\text{ }^\circ\text{C}$ in a 8 mm i.d. FEP reaction tube whereupon a white solid precipitated. The suspension was rapidly centrifuged at RT, and the PFB mother liquor separated (< 1 min.). Residual PFB was removed under vacuum at $35\text{ }^\circ\text{C}$ (warm water bath) and the resulting orange oil was dried for 5 h under dynamic vacuum at RT. The still oily material was then dissolved in CH_3CN (500 μL) at RT and transferred into a $\frac{1}{4}$ inch o.d. T-shaped FEP reaction tube equipped with a Kel-F valve. A white fluffy solid immediately precipitated which was insoluble even when more CH_3CN (300 μL) was added. The yellow CH_3CN mother liquor was decanted and the remaining solid was dried under dynamic vacuum. As soon as the solvent was removed an oil formed. It was not possible to find conditions that produce crystalline $[C_6F_5Xe][B(OTeF_5)_4]$ from a PFB/ CH_3CN mixture at low temperatures.

IV.10.4.3 Thermal Stability of $[C_6F_5Xe][B(OTeF_5)_4]$

In CH_3CN at RT

Freshly prepared, deep yellow $[C_6F_5Xe][B(OTeF_5)_4]$ (~ 50 mg) was dissolved as an oil in CH_3CN (400 μL) and transferred to a 3.5 mm i.d. FEP reaction tube which was monitored periodically by ^{19}F NMR spectroscopy.

Decomposition of $[C_6F_5Xe][B(OTeF_5)_4]$ in CH_3CN at RT

time [h]	$[C_6F_5Xe]^+$ ^a [mol-%]	C_6F_5H ^a [mol-%]	$\Sigma[B(OTeF_5)_yX_{4-y}]^-$ [mol-%] ^{b,c}	Additional Compounds _{c,d}
15 min	89.3	9.7	100.0	I, II
30 min	90.4	9.6	102.2	I, II
4	84.1	15.9	104.8	I, II
20	75.7	24.3	103.0	I, II, III

Table (continued...)

44	71.2	28.8	98.5	I ↓, I →, II ↑
164	58.9	41.1	108.1	I ↓, II ↑, III ↑, V
236	61.2	38.8	123.8	I ↓, II →, III ↑, V ↑
380	50.2	49.8	121.0	I ↓, II →, III ↑, IV ↑, V ↑
596	27.7	68.3	134.2	I ↓, II →, III ↑, IV ↑, V ↑ 2 C ₆ F ₅ compounds (4%)

^a The total amount (mol-%) of all C₆F₅ compounds was normalized to 100%.

^b Molar amounts were calculated with regard to the sum of C₆F₅ compounds.

^c The total amount (mol-%) of all teflate-containing compounds were summarized and integrated as one. Separation was not possible due to superimposition. The calculation was based on 20 (max.) F-atoms per compound.

^d The arrows symbolize increasing ↑, decreasing ↓, or constant → amounts (mol-%) of the minor by-products.

Compound I $\delta = -45.4$ ppm (d, $^2J(^{19}\text{F}_{\text{eq}}-^{19}\text{F}_{\text{ax}}) = 183$ Hz, 4F_{eq}); -38.4 ppm (qui, 1F_{ax}) ([B(OTeF₅)₄]⁻)

Compound II: $\delta = -46.9$ ppm (d, $^2J(^{19}\text{F}_{\text{eq}}-^{19}\text{F}_{\text{ax}}) = 183$ Hz, 4F_{eq})

Compound III: $\delta = -46.6$ ppm (d, $^2J(^{19}\text{F}_{\text{eq}}-^{19}\text{F}_{\text{ax}}) = 183$ Hz, 4F_{eq}); -36.0 ppm (qui)

Compound IV: $\delta = -40.8$ ppm (d, 4F_{eq})

Compound V: $\delta = -130.6$ ppm (q, RBX_x); -136.6 ppm; -141.4 ppm; -162.7 ppm (*)
C₆F₅BX_y (?)

In CH₂Cl₂ at RT

Freshly prepared, deep yellow [C₆F₅Xe][B(OTeF₅)₄] (~50 mg) was suspended as an oil in CH₂Cl₂ (400 μ L) at RT, centrifuged, and the CH₂Cl₂ mother liquor separated in a 3.5 mm i.d. FEP reaction tube and monitored periodically by ¹⁹F NMR spectroscopy.

Decomposition of $[\text{C}_6\text{F}_5\text{Xe}][\text{B}(\text{OTeF}_5)_4]$ in CH_2Cl_2 at RT

time	$[\text{C}_6\text{F}_5\text{Xe}]^+ \text{ }^a$	$\text{C}_6\text{F}_5\text{H} \text{ }^a$	$\text{C}_6\text{F}_5\text{Cl} \text{ }^a$	Additional signals b
[h]	[mol-%]	[mol-%]	[mol-%]	
15'	100.0	0	0	I : II : III (7 : 11: 1) $\delta = -128,4$ ppm (s, br) (?) $\delta = -132,6$ ppm (s, br) (?)
30'	89.0	11.0	0	I : II (1: 1)
15.5	35.3	62.1	2.6	I ^c , II ^c , III, IV
40	33.6	58.6	4.1	I ^c , II ^c , III, IV \rightarrow , V (< 3%)
160	31.7	60.8	4.3	I ^c , II ^c , III, IV \uparrow , V (3.2%)
216	30.9	61.5	4.8	I ^c , II ^c , III, IV \rightarrow , V (2.8%)
360	28.8	61.5	6.9	III, IV \rightarrow V (2.8%)
576	18.7	65.9	10.6	III, IV \rightarrow V (4.8%)

^a The total amount (mol-%) of all C_6F_5 compounds was normalized to 100%.

^b molare amounts were calculated with regard to the sum of C_6F_5 compounds.

^c signals were superimposed

Compound I: $\delta = -46.3$ ppm (d, ${}^2J(^{19}\text{F}_{\text{eq}}-^{19}\text{F}_{\text{ax}}) = 183$ Hz, $4F_{\text{eq}}$); -38.4 ppm (qui, $1F_{\text{ax}})$ $[\text{B}(\text{OTeF}_5)_4]^-$

Compound II: $\delta = -46.9$ ppm (d, ${}^2J(^{19}\text{F}_{\text{eq}}-^{19}\text{F}_{\text{ax}}) = 183$ Hz, $4F_{\text{eq}}$); -39.8 ppm (qui, $1F_{\text{ax}})$

Compound III: $\delta = -47.1$ ppm (d, ${}^2J(^{19}\text{F}_{\text{eq}}-^{19}\text{F}_{\text{ax}}) = 183$ Hz, $4F_{\text{eq}}$)

Compound IV: $\delta = -81.1$ ppm (d, ${}^2J(^{19}\text{F}_{\text{eq}}-^{19}\text{F}_{\text{ax}}) = 53$ Hz, $4F_{\text{eq}}$)

Compound V: $\delta = -138.4$ ppm (*o*- C_6F_5); -151.3 ppm (*p*- C_6F_5); -161.8 ppm (*m*- C_6F_5)

In CH_3CN at -40 °C

The compound, $[\text{C}_6\text{F}_5\text{Xe}][\text{B}(\text{OTeF}_5)_4]$ (30.3 mg; 0.03 mmol), was dissolved in CH_3CN (400 μL) at -40 °C, stored in a 3.5 mm i.d. FEP reaction tube and was monitored periodically by ^{19}F NMR spectroscopy. No decomposition products were detected even after 168 h at -40 °C. Over time precipitation of $[\text{C}_6\text{F}_5\text{Xe}][\text{B}(\text{OTeF}_5)_4]$ resulted being responsible for a poor S/N ratios near the end of the study.

IV.10.5 Pentafluorophenylxenon(II)tetracyanoborate, [C₆F₅Xe][B(CN)₄]

IV.10.5.1 NMR Characterization

In CH₃CN solution at 24 °C

¹⁹F NMR (282.40 MHz)

[C₆F₅Xe]⁺ δ = -124.7 ppm (m, *o*-C₆F₅, 2F); -141.0 ppm (tt, ³J(¹⁹F-¹⁹F) = 20 Hz, ⁴J(¹⁹F-¹⁹F) = 6 Hz, *p*-C₆F₅, 1F); -153.9 ppm (m, *m*-C₆F₅, 2F)

¹¹B NMR (96.29 MHz)

[B(CN)₄]⁻ δ = -38.4 ppm (s, Δν_{1/2} = 1 Hz, ¹³C-satellites: ¹J(¹¹B-¹³C) = 72 Hz)

¹²⁹Xe NMR (83.02 MHz)

[C₆F₅Xe]⁺ δ = -3795.2 ppm (ttt, ³J(¹⁹F-¹²⁹Xe) = 68 Hz, ⁴J(¹⁹F-¹²⁹Xe) = 9 Hz, ⁵J(¹⁹F-¹²⁹Xe) = 4 Hz)

IV.10.5.2 Raman Spectroscopic Characterization

In the drybox, [C₆F₅Xe][B(CN)₄] (~50 – 100 mg) was loaded into a previously dried 5 mm glass NMR tube (Wilmad 507) which was heat sealed under dynamic vacuum at -196 °C as described before. A low-temperature (-150 °C) Raman spectrum was recorded using a laser power of 300 mW and a total of 1500 scans.

IV.10.5.3 Crystal Growth and Structure Refinement

In the drybox, [C₆F₅Xe][B(CN)₄] (40.56 mg; 0.10 mmol) was transferred into a ¼ inch o.d. T-shaped FEP reaction tube equipped with a Kel-F valve. The reaction tube was then attached to a vacuum line where anhydrous CH₂Cl₂ (0.29 mL) was condensed onto the sample at ca. -196 °C. Because of the insolubility of [C₆F₅Xe][B(CN)₄] in CH₂Cl₂, CH₃CN was also condensed onto the sample at ca. -196 °C until all of the yellow solid was dissolved at RT. The reaction tube was then pressurized with ca. 1 atm. of dry nitrogen. The arm containing the solution was

subsequently placed inside the glass Dewar of a low-temperature crystal growing apparatus set at an initial temperature of 0 °C. After cooling to –8 °C clear, colourless, square plates grew from the solution. The temperature was maintained at –8 °C for ca. 20 h. The sample was then cooled to –20 °C over a period of 2 h before the pale yellow mother liquor was decanted into the side arm B of the T-reaction tube. The sidearm B was then heat sealed under dynamic vacuum. The remaining solution was slowly removed under dynamic vacuum at –20 °C. The clear and colourless square plates were isolated and the crystal used for data acquisition had to be cut because of its large size ca. $3 \times 3 \times 1 \text{ mm}^3$. The crystal fragment had to be cut due to its dimensions. The crystal used for the data acquisition had the dimensions $0.22 \times 0.12 \times 0.05 \text{ mm}^3$. Detailed information can be found in the Appendix.

IV.10.5.4 Thermo-analytical Measurements of $[\text{C}_6\text{F}_5\text{Xe}][\text{B}(\text{CN})_4]$ in the Solid State (DSC)

In the drybox, pale yellow $[\text{C}_6\text{F}_5\text{Xe}][\text{B}(\text{CN})_4]$ (3.87 mg; 0.01 mmol) was loaded into a pierced aluminium pan. The sample was placed inside the DSC apparatus and heated to 310 °C. The decomposition proceeded at 152.2 °C (onset) in the absence of a prior melting process.

IV.10.5.5 Solubility of $[\text{C}_6\text{F}_5\text{Xe}][\text{B}(\text{CN})_4]$ at RT

Small quantities of $[\text{C}_6\text{F}_5\text{Xe}][\text{B}(\text{CN})_4]$ were suspended in the corresponding solvent at RT, stirred for 10 min. The mother liquor was separated and the internal standard, $\text{C}_6\text{H}_5\text{CF}_3$ (5 μL ; 0.04 mmol) was added. The solution was measured by ^{19}F NMR spectroscopy and the solubility calculated based on the internal standard.

Solubility in CH_3CN at RT = ~4.3 mmol/mL

Solubility in DCE at RT = insoluble

Solubility in CH_2Cl_2 at RT = insoluble

Solubility in PFB at RT = insoluble

Solubility in SO_2ClF at RT = insoluble

IV.10.5.6 Thermal Stability of $[C_6F_5Xe][B(CN)_4]$

In CH_3CN at RT

The salt, $[C_6F_5Xe][B(CN)_4]$, was stored in the drybox for almost a year and dried in dynamic vacuum for 8 h at RT prior to use. In the drybox, $[C_6F_5Xe][B(CN)_4]$ (40.80 mg; 0.10 mmol), was dissolved in CH_3CN (400 μ L) at RT, maintained in a 3.5 mm i.d. FEP reaction tube and monitored periodically by ^{19}F NMR spectroscopy.

^{19}F NMR (282.40 MHz) in CH_3CN

$[C_6F_5Xe][B(CN)_4]$ $\delta = -124.7$ ppm (m, *o*- C_6F_5 , 2F); -141.1 ppm (tt, $^3J(^{19}F-^{19}F) = 20$ Hz, $^4J(^{19}F-^{19}F) = 6$ Hz, *p*- C_6F_5 , 1F); -154.0 ppm (m, *m*- C_6F_5 , 2F)
 $[BF_4]^-$ $\delta = -146.9$ ppm (s, $\Delta\nu_{1/2} = 6.5$ Hz, $\Delta\delta(^{10}B-^{11}B) = 16$ Hz, 4F)

Decomposition $[C_6F_5Xe][B(CN)_4]$ in CH_3CN bei RT

time [d]	$[C_6F_5Xe]^+{}^a$ [mol-%]	$C_6F_5H^a$ [mol-%]	-144.9 ppm ^a [mol-%]	HF ^a [mol-%]
15 min	100	0	0	0
30 min	100	0	0	0
1 h	100	0	0	0
2 h	99.5	0.5	0	0
4 h	99.4	0.6	0	0
9 h	99.2	0.8	0	0
2	98.0	2.0	0	0
3	97.2	2.8	Traces	0
4	96.8	3.2	1.3	0
6	95.5	4.5	2.1	3.5
7	95.0	5.0	2.8	4.2
8	94.0	6.0	3.4	4.8
14	87.8	12.2	6.4	11.6
17	85.6	14.4	7.6	13.7
28*	79.0	21.0	11.5	23.4

Table (continued...)

49*	33.4	66.6	35.1	120.0
58*	5.6	94.4	48.2	178.0
71	0	100.0	52.0	210.0

^a The total amount (mol-%) of all C₆F₅ compounds was normalized to 100%.

* Additional decomposition products in the magnitude of 10 – 15 mol-% (based on C₆F₅)

IV.10.6 Pentafluorophenylxenon(II)tetrakis(pentafluorophenyl)borate, [C₆F₅Xe][B(C₆F₅)₄]

IV.10.6.1 NMR Characterization

In CH₃CN solution at 24 °C

¹⁹F NMR (282.40 MHz)

[C₆F₅Xe]⁺ δ = -125.2 ppm (m, *o*-C₆F₅, 2F); -141.5 ppm (tt, ³J(¹⁹F-¹⁹F) = 20 Hz, ⁴J(¹⁹F-¹⁹F) = 6 Hz, *p*-C₆F₅, 1F); -154.5 ppm (m, *m*-C₆F₅, 2F)

[B(C₆F₅)₄]⁻ δ = -132.4 ppm (m, *o*-C₆F₅, 8F); -162.8 ppm (t, ³J(¹⁹F-¹⁹F) = 20 Hz, *p*-C₆F₅, 4F); -167.8 ppm (m, *m*-C₆F₅, 8F)

¹¹B NMR (96.29 MHz)

[B(C₆F₅)₄]⁻ δ = -17.1 ppm (s, Δ_v^{1/2} = 21 Hz)

¹²⁹Xe NMR (83.02 MHz)

[C₆F₅Xe]⁺ δ = -3802.2 ppm (ttd, ³J(¹⁹F-¹²⁹Xe) = 69 Hz, ⁴J(¹⁹F-¹²⁹Xe) = 9 Hz, ⁵J(¹⁹F-¹²⁹Xe) = 4 Hz)

IV.10.6.2 Raman Spectroscopic Characterization

In the drybox, [C₆F₅Xe][B(C₆F₅)₄] (~50 – 100 mg) was loaded into a previously dried 5 mm glass NMR tube (Wilmad 507) which was heat sealed under dynamic vacuum at -196 °C as described before. A preliminary low-temperature (-150 °C) Raman spectrum was recorded using a laser power of 300 mW and a total of 1000 scans. Because of fluorescence, a second spectrum was recorded at -150 °C using

a reduced laser power of 100 mW and a total of 1500 Scans. The spectra of Cs[B(C₆F₅)₄], was also measured at –150 °C for reference purposes.

IV.10.6.3 Crystal Growth and Structure Refinement

In the drybox, [C₆F₅Xe][B(C₆F₅)₄] (43.87 mg; 0.04 mmol) was transferred into a ¼ inch o.d. T-shaped FEP reaction tube equipped with a Kel-F valve. The reaction tube was then connected to a vacuum line where dry CH₂Cl₂ (0.69 mL) was condensed onto the sample at *ca.* –196 °C. Because the solubility of [C₆F₅Xe][B(C₆F₅)₄] was poor in CH₂Cl₂, CH₃CN (some µL) was condensed onto the frozen CH₂Cl₂ suspension at *ca.* –196 °C to dissolve more salt. The reaction tube was then pressurized with *ca.* 1 atm. of dry nitrogen. The latter procedure was repeated until most of [C₆F₅Xe][B(C₆F₅)₄] was dissolved. The sample was finally warmed for several seconds to *ca.* 30 °C to dissolve as much solute as possible. The entire suspension was transferred into the sidearm B and the mother liquor decanted back into the straight arm A of the T-reactor to realize slowest crystal growth. The sample was warmed again (*ca.* 30 °C) to dissolve all solid material and subsequently placed inside the glass dewar of a low-temperature crystal growing apparatus set at an initial temperature of –25 °C. Over a period of 2 h, clear, colorless needles grew throughout the solution. The temperature was maintained at –25 °C for 8 h before the solution was decanted into the side arm of the T-shaped reaction tube. The sidearm was heat sealed under vacuum at –196 °C. The residual solvent adhering to the crystals was removed under dynamic vacuum (15 – 20 min.) at –75 °C. The crystal used for the data acquisition had the dimensions 0.2 × 0.1 × 0.02 mm³. Detailed information can be found in the Appendix.

IV.10.6.4 Thermo-analytical Measurements of [C₆F₅Xe][B(C₆F₅)₄] in the Solid State (DSC)

In the drybox, pale yellow [C₆F₅Xe][B(C₆F₅)₄] (3.50 mg; 0.004 mmol) was loaded into a pierced aluminium pan. The sample was placed inside the DSC apparatus and heated to 210 °C. The decomposition proceeded at 85.2 °C (onset) in the absence of a prior melting process.

IV.10.6.5 Solubility of $[C_6F_5Xe][B(C_6F_5)_4]$ in Selected Solvents at RT

Small quantities of $[C_6F_5Xe][B(C_6F_5)_4]$ were suspended in the corresponding solvent at RT and stirred for 10 min. The mother liquor was separated and the internal standard, $C_6H_5CF_3$ (5 μ L; 0.04 mmol), was added. The solution was measured by ^{19}F NMR spectroscopy and the solubility calculated based on the internal standard.

Solubility in CH_3CN at RT = \sim 0.5 mmol/mL

Solubility in DCE at RT = \sim 0.2 mmol/mL

Solubility in CH_2Cl_2 at RT = $<$ 0.05 mmol/mL

IV.10.6.6 Thermal Stability of $[C_6F_5Xe][B(C_6F_5)_4]$ in Solution

In CH_3CN at RT

In the drybox, $[C_6F_5Xe][B(C_6F_5)_4]$ (30.3 mg, 0.03 mmol) was presented in a 3.5 mm i.d. FEP reaction tube and dissolved in CH_3CN (400 μ L). The solution was periodically monitored by ^{19}F NMR spectroscopy.

Decomposition of $[C_6F_5Xe][B(C_6F_5)_4]$ in CH_3CN at RT

time [d]	$[C_6F_5Xe]^+$ ^a [mol-%]	C_6F_5H ^a [mol-%]	$(C_6F_5)_2$ ^a [mol-%]	$[B(C_6F_5)_4]^-$ ^b [mol-%]
2	88.8	11.2	0	87.6
6	55.9	34.9	9.2	67.7
9	25.6	57.5	16.9	87.6
20	0	84.7	15.3	46.7

^a The total amount (mol-%) of all C_6F_5 containing compounds excluding $[B(C_6F_5)_4]^-$ were calculated to 100%.

^b The amount of the $[B(C_6F_5)_4]^-$ anion was calculated with regard to the sum of C_6F_5

In CH₂Cl₂ at RT

The compound, [C₆F₅Xe][B(C₆F₅)₄] (35.8 mg, 0.04 mmol), was suspended in CH₂Cl₂ (800 μL) at RT. The yellow suspension turned to deep orange within several minutes. The suspension was subsequently centrifuged, the CH₂Cl₂ mother liquor was separated and the NMR spectra of the solution were recorded.

The characteristic signals of [C₆F₅Xe]⁺ disappeared after *ca.* 20 min. at RT. It was not possible to accurately integrate the C₆F₅ groups in the ¹⁹F NMR spectra because of the large number of decomposition products and their superimposition. The main decomposition product was C₆F₅H (~50%) in addition to (C₆F₅)₂, [(C₆F₅)₃BF]⁻, B(C₆F₅)₃, and [C₆F₅BF₃]⁻.

In CH₂Cl₂ at -40 and -80 °C

The compound, [C₆F₅Xe][B(C₆F₅)₄] (**A**: 22.41 mg; 0.02 mmol and **B**: 24.19 mg; 0.02 mmol), was suspended in cold (-40 °C) CH₂Cl₂ (500 μL). Sample **A** was maintained at -40 °C and sample **B** was cooled to -80 °C. Both samples were maintained at the set temperature for 15 min. before the CH₂Cl₂ mother liquor was separated and transferred into a pre-cooled (-40 °C) FEP reaction tube. Sample **A** was placed in a cryostat at -40 °C and sample **B** was placed in solid dry ice. Both pale yellow saturated solutions were monitored by low-temperature NMR spectroscopy over a period of 16 h and 72 h, respectively.

Decomposition of [C₆F₅Xe][B(C₆F₅)₄] in CH₂Cl₂ at -40 °C

time [h]	[C ₆ F ₅ Xe] ⁺ ^a [mol-%]	C ₆ F ₅ H ^a [mol-%]	[B(C ₆ F ₅) ₄] ⁻ ^b [mol-%]
45 min	100	0	128.4
2	99	1	131.1
16	96	4	133.3

^a The total amount (mol-%) of all C₆F₅ containing compounds excluding [B(C₆F₅)₄]⁻ were calculated to 100%.

^b The amount of the [B(C₆F₅)₄]⁻ anion was calculated with regard to the sum of C₆F₅

Decomposition of $[\text{C}_6\text{F}_5\text{Xe}][\text{B}(\text{C}_6\text{F}_5)_4]$ in CH_2Cl_2 at $-80\text{ }^\circ\text{C}$

time [h]	$[\text{C}_6\text{F}_5\text{Xe}]^+{}^{\text{a}}$ [mol-%]	$\text{C}_6\text{F}_5\text{H}^{\text{a}}$ [mol-%]	$[\text{B}(\text{C}_6\text{F}_5)_4]^-{}^{\text{b}}$ [mol-%]
0.9	100	0	138.8
2	97.5	2.5	126.6
72	97.6	2.4	119.0

^a The total amount (mol-%) of all C_6F_5 containing compounds excluding $[\text{B}(\text{C}_6\text{F}_5)_4]^-$ were calculated to 100%.

^b The amount of the $[\text{B}(\text{C}_6\text{F}_5)_4]^-$ anion was calculated with regard to the sum of C_6F_5

In 1,2-Dichloroethane (DCE) at RT

The compound, $[\text{C}_6\text{F}_5\text{Xe}][\text{B}(\text{C}_6\text{F}_5)_4]$ (18.20 mg; 1.86 mmol), was suspended in freshly dried (P_4O_{10}) and distilled DCE (300 μL) at RT. The yellow suspension was centrifuged, the DCE-mother liquor separated and monitored by NMR spectroscopy.

Decomposition of $[\text{C}_6\text{F}_5\text{Xe}][\text{B}(\text{C}_6\text{F}_5)_4]$ in DCE at RT

time [min]	$[\text{C}_6\text{F}_5\text{Xe}]^+{}^{\text{a}}$ [mol-%]	$\text{C}_6\text{F}_5\text{H}^{\text{a}}$ [mol-%]	$[\text{B}(\text{C}_6\text{F}_5)_4]^-{}^{\text{b}}$ [mol-%]
15	71.5	28.5	92.7
30	42.8	57.2	66.7
60	14.8	85.2	48.2

^a The total amount (mol-%) of all C_6F_5 containing compounds excluding $[\text{B}(\text{C}_6\text{F}_5)_4]^-$ were calculated to 100%.

^b The amount of the $[\text{B}(\text{C}_6\text{F}_5)_4]^-$ anion was calculated with regard to the sum of C_6F_5

IV.10.6.7 Coordination Ability of CH_3CN to $[\text{C}_6\text{F}_5\text{Xe}][\text{B}(\text{C}_6\text{F}_5)_4]$

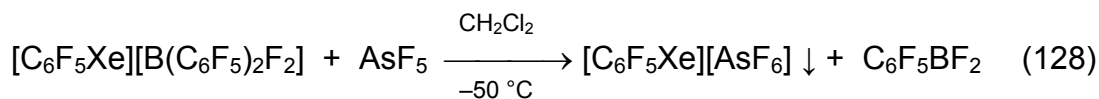
The compound, $[\text{C}_6\text{F}_5\text{Xe}][\text{B}(\text{C}_6\text{F}_5)_4]$, was loaded into a previously dried glass NMR tube (Wilmad 507) fused to a $\frac{1}{4}$ inch o.d. length of glass tubing which was attached to a J. Young stopcock by means of a $\frac{1}{4}$ inch Cajon using a self made solid

syringe made from 2.0 mm o.d. FEP tubing and a 1.5 mm o.d. metal rod as piston. The NMR tube was connected to a glass vacuum line and cooled to dry ice temperature. The tube was then heat sealed under dynamic vacuum and a low-temperature Raman spectrum was recorded at $-150\text{ }^{\circ}\text{C}$.

The salt, $[\text{C}_6\text{F}_5\text{Xe}][\text{B}(\text{C}_6\text{F}_5)_4]$, was subsequently dissolved in cold ($-80\text{ }^{\circ}\text{C}$) CH_2Cl_2 (1000 μL). After removal of CH_2Cl_2 solvent under vacuum at temperatures below $-50\text{ }^{\circ}\text{C}$ and drying the resulting pale yellow solid at RT, it was loaded into a similar glass NMR tube (Wilmad 507) and sealed in a similar fashion as described before.

IV.10.7 *Pentafluorophenylxenon(II)hexafluoroarsenate,* *$[\text{C}_6\text{F}_5\text{Xe}][\text{AsF}_6]$*

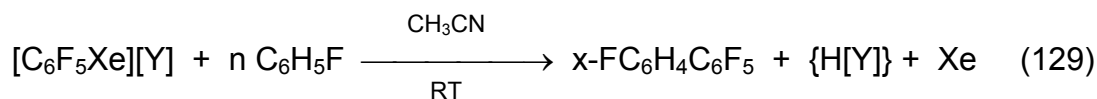
The salt, $[\text{C}_6\text{F}_5\text{Xe}][\text{AsF}_6]$, was previously prepared as described by Frohn and coworkers.^[59, 165]



IV.10.7.1 *Thermo-analytical Measurements of $[\text{C}_6\text{F}_5\text{Xe}][\text{AsF}_6]$ in the Solid State (DSC)*

In the drybox, pale yellow $[\text{C}_6\text{F}_5\text{Xe}][\text{AsF}_6]$ (7.70 mg; 0.02 mmol) was loaded into a pierced aluminium pan. The sample was placed inside the DSC apparatus and heated to $310\text{ }^{\circ}\text{C}$. The melting point was $109.8\text{ }^{\circ}\text{C}$ (onset) reaching its maximum at $112.2\text{ }^{\circ}\text{C}$ and the decomposition proceeded at $159.2\text{ }^{\circ}\text{C}$ (onset) reaching its maximum at $182.7\text{ }^{\circ}\text{C}$.

IV.11 *Reaction of $[\text{C}_6\text{F}_5\text{Xe}][\text{BY}_4]$ ($Y = \text{F}, \text{CF}_3, \text{CN}$ and C_6F_5) and $[\text{C}_6\text{F}_5\text{Xe}][\text{AsF}_6]$ with $\text{C}_6\text{H}_5\text{F}$*



($x = 2, 3, 4$; $Y = \text{BF}_4, \text{B}(\text{CN})_4, \text{B}(\text{CF}_3)_4, \text{B}(\text{C}_6\text{F}_5)_4$, and AsF_6 ; $n = 1.2, 20$)

IV.11.1 The Reaction of [C₆F₅Xe][BY₄] (Y = F, CF₃, and C₆F₅) and [C₆F₅Xe][AsF₆] with C₆H₅F (1.2-Fold Molar Excess) in CH₃CN at RT

The compounds, [C₆F₅Xe][BF₄] (24.36 mg; 0.06 mmol) (**a**), [C₆F₅Xe][B(CF₃)₄] (40.10 mg; 0.07 mmol) (**b**), [C₆F₅Xe][B(C₆F₅)₄] (68.28 mg; 0.07 mmol) (**c**), and [C₆F₅Xe][AsF₆] (33.40 mg; 0.07 mmol) (**d**), were each loaded in a 3.5 mm i.d. FEP reaction tube and dissolved in CH₃CN (500 μL) at RT. Freshly distilled fluorobenzene (1.2 equivalents; (**a**): 7.1 μL, 0.08 mmol; (**b**): 7.7 μL, 0.08 mmol; (**c**): 7.9 μL, 0.08 mmol; (**d**): 7.7 μL; 0.08 mmol) was added to the yellow C₆F₅-solutions using a Hamilton syringe. The FEP reaction tubes were shaken periodically and the reactions were monitored by ¹⁹F NMR spectroscopy at 24 °C.

¹⁹F NMR (282.40 MHz) in CH₃CN at 24 °C

C ₆ H ₅ F	δ = -113.8 ppm* (m, 1F)
2-FC ₆ H ₄ C ₆ F ₅	δ = -113.8 ppm* (m, 2-F, 1F); -143.2 ppm (m, <i>o</i> -C ₆ F ₅ , 2F); -154.9 ppm - -156.4 ppm (t, ³ J(¹⁹ F- ¹⁹ F) = 20 Hz, <i>p</i> -C ₆ F ₅ , 1F); -165 ppm* (m, <i>m</i> -C ₆ F ₅ , 2F)
3-FC ₆ H ₄ C ₆ F ₅	δ = -112.4 ppm (m, 3-F, 1F); -143.6 ppm (m, <i>o</i> -C ₆ F ₅ , 2F); -154.9 ppm - -156.4 ppm (t, ³ J(¹⁹ F- ¹⁹ F) = 20 Hz, <i>p</i> -C ₆ F ₅ , 1F); -165 ppm* (m, <i>m</i> -C ₆ F ₅ , 2F)
4-FC ₆ H ₄ C ₆ F ₅	δ = -111.6 ppm (m, 4-F, 1F); -141.0 ppm (m, <i>o</i> -C ₆ F ₅ , 2F); -154.9 ppm - -156.4 ppm (t, ³ J(¹⁹ F- ¹⁹ F) = 20 Hz, <i>p</i> -C ₆ F ₅ , 1F); -165 ppm* (m, <i>m</i> -C ₆ F ₅ , 2F)
C ₆ F ₅ H	δ = -139.1 ppm (m, <i>o</i> -C ₆ F ₅ , 2F); -155 ppm - -156 ppm* (<i>p</i> -C ₆ F ₅); -165 ppm* (<i>m</i> -C ₆ F ₅)

* superimposed signals

**Composition of Reactants and Products Resulting from the Reaction of
[C₆F₅Xe][BF₄] with 1.2 C₆H₅F in CH₃CN at RT**

time [h]	[C ₆ F ₅ Xe] ⁺ ^a [mol-%]	FC ₆ H ₄ C ₆ F ₅ ^a			C ₆ F ₅ H ^a [mol-%]
		2-FC ₆ H ₄ C ₆ F ₅ [mol-%]	3-FC ₆ H ₄ C ₆ F ₅ [mol-%]	4-FC ₆ H ₄ C ₆ F ₅ [mol-%]	
2	63.6	10.4	10.0	11.8	4.2
7	52.5	14.4	13.1	16.0	4.0
24	53.3	15.7	14.2	11.4	5.4
30	41.8	17.0	16.3	19.4	5.5
48	36.9	17.6	16.5	21.5	7.4
73	30.4	20.6	18.9	23.6	6.5
96	27.5	21.3	19.4	25.1	6.7
168	12.7	25.2	22.9	30.0	9.1
220	0.0	28.8	25.5	34.4	11.3

^a The total amount (mol-%) of all C₆F₅ compounds was normalized to 100%.

**Composition of Reactants and Products Resulting from the Reaction of
[C₆F₅Xe][B(CF₃)₄] with 1.2 C₆H₅F in CH₃CN at RT**

time [h]	[C ₆ F ₅ Xe] ⁺ ^a [mol-%]	FC ₆ H ₄ C ₆ F ₅ ^a			C ₆ F ₅ H ^a [mol-%]
		2-FC ₆ H ₄ C ₆ F ₅ [mol-%]	3-FC ₆ H ₄ C ₆ F ₅ [mol-%]	4-FC ₆ H ₄ C ₆ F ₅ [mol-%]	
2.5	81.6	5.9	5.2	7.3	0.0
7	56.0	9.7	10.5	12.7	11.0
24.5	0.0	31.6	29.4	38.0	1.0

^a The total amount (mol-%) of all C₆F₅ compounds was normalized to 100%.

**Composition of Reactants and Products Resulting from the Reaction of
[C₆F₅Xe][B(C₆F₅)₄] with 1.2 C₆H₅F in CH₃CN at RT**

time [h]	[C ₆ F ₅ Xe] ⁺ ^a [mol-%]	FC ₆ H ₄ C ₆ F ₅ ^a			C ₆ F ₅ H ^a [mol-%]
		2-FC ₆ H ₄ C ₆ F ₅ [mol-%]	3-FC ₆ H ₄ C ₆ F ₅ [mol-%]	4-FC ₆ H ₄ C ₆ F ₅ [mol-%]	
3	100.0	0.0	0.0	0.0	0.0
7	100.0	0.0	0.0	0.0	0.0
25	71.0	8.8	8.9	5.7	5.6
48	49.1	12.9	13.5	15.1	9.4
73	25.2	22.6	23.0	17.0	12.2
96	16.1	26.2	25.3	17.2	15.3
168	0.0	26.9	25.9	27.6	19.6

^a The total amount (mol-%) of all C₆F₅ containing compounds excluding [B(C₆F₅)₄] were calculated to 100%.

**Composition of Reactants and Products Resulting from the Reaction of
[C₆F₅Xe][AsF₆] with 1.2 C₆H₅F in CH₃CN at RT**

time [h]	[C ₆ F ₅ Xe] ⁺ ^a [mol-%]	FC ₆ H ₄ C ₆ F ₅ ^a			C ₆ F ₅ H ^a [mol-%]
		2-FC ₆ H ₄ C ₆ F ₅ [mol-%]	3-FC ₆ H ₄ C ₆ F ₅ [mol-%]	4-FC ₆ H ₄ C ₆ F ₅ [mol-%]	
0.5	78.6	5.8	5.8	7.7	7.7
2.5	51.8	14.5	13.3	16.2	4.2
8	20.7	26.2	22.9	22.3	7.8
11	14.6	22.7	21.5	28.1	13.0
24	0	28.4	26.3	33.2	12.0
96	0	28.4	26.3	33.2	12.0

^a The total amount (mol-%) of all C₆F₅ compounds was normalized to 100%.

IV.11.2 Reaction of $[\text{C}_6\text{F}_5\text{Xe}][\text{B}(\text{CF}_3)_4]$ with $\text{C}_6\text{H}_5\text{F}$ (1.2-Fold Molar Excess) in CH_2Cl_2 at RT

In the drybox, $[\text{C}_6\text{F}_5\text{Xe}][\text{B}(\text{CF}_3)_4]$ (37.18 mg; 0.06 mmol), was loaded in a 3.5 mm i.d. FEP reaction tube and suspended in CH_2Cl_2 (700 μL) at RT. The CH_2Cl_2 mother liquor was separated and undissolved $[\text{C}_6\text{F}_5\text{Xe}][\text{B}(\text{CF}_3)_4]$ (13.41 mg; 0.02 mmol) was dried under dynamic vacuum and weighed by difference. The solubility of $[\text{C}_6\text{F}_5\text{Xe}][\text{B}(\text{CF}_3)_4]$ in CH_2Cl_2 at RT was calculated to 33.9 mg/mL. Freshly dried (P_4O_{10}) and distilled fluorobenzene (1.2 equivalents; 3.8 μL ; 0.04 mmol) was added to the yellow solution using a Hamilton syringe. The FEP reaction tube was shaken periodically and the reaction periodically monitored by ^{19}F NMR spectroscopy.

Composition of Reactants and Products Resulting from the Reaction of $[\text{C}_6\text{F}_5\text{Xe}][\text{B}(\text{CF}_3)_4]$ with 1.2 $\text{C}_6\text{H}_5\text{F}$ in CH_2Cl_2 at RT

Time [h]	$[\text{C}_6\text{F}_5\text{Xe}]^+ \text{ }^a$ [mol-%]	$\text{FC}_6\text{H}_4\text{C}_6\text{F}_5 \text{ }^a$			$\text{C}_6\text{F}_5\text{H} \text{ }^a$ [mol-%]
		2- $\text{FC}_6\text{H}_4\text{C}_6\text{F}_5$ [mol-%]	3- $\text{FC}_6\text{H}_4\text{C}_6\text{F}_5$ [mol-%]	4- $\text{FC}_6\text{H}_4\text{C}_6\text{F}_5$ [mol-%]	
0.5	58.0	9.2	10.9	11.0	10.9
1.5	37.2	14.3	12.4	13.7	22.4
7	27.2	13.0	14.2	16.0	29.6

^a The total amount (mol-%) of all C_6F_5 compounds was normalized to 100%.

^b Due to superimposition of some C_6F_5 signals the molar percentage was calculated using just the *o*- C_6F_5 signals

The $[\text{B}(\text{CF}_3)_4]^-$ anion slowly reacted (0.5 h = 16%; 1.5 h = 39%; 7 h = 39%) to yield a unidentified borate (^{19}F NMR: $\delta = -59.4$ ppm (m); ^{11}B NMR: $\delta = -16.2$ ppm (m)). Only 42% of $\text{C}_6\text{H}_5\text{F}$ had reacted yielding the biphenyls.

IV.11.3 Reaction of [C₆F₅Xe][BY₄] (Y = F, CF₃, and C₆F₅) and [C₆F₅Xe][AsF₆] with Dried (P₄O₁₀) C₆H₅F (20-Fold Molar Excess) in CH₃CN at RT

The compounds, [C₆F₅Xe][BF₄] (25.77 g; 0.07 mmol) (**a**), [C₆F₅Xe][B(CF₃)₄] (34.88 mg; 0.06 mmol) (**b**), [C₆F₅Xe][B(C₆F₅)₄] (58.31 mg; 0.06 mmol) (**c**), and [C₆F₅Xe][AsF₆] (30.93 mg; 0.06 mmol) (**d**), were each loaded in a 3.5 mm i.d. FEP reaction tube and dissolved in CH₃CN (500 μL). Freshly dried (P₄O₁₀) and distilled fluorobenzene (20 equivalents; **a**): 127.0 μL (130 mg, 1.35 mmol); **b**): 112.3 μL (115 mg, 1.20 mmol); **c**): 112.3 μL (115 mg, 1.20 mmol); **d**): 117.2 μL (120 mg, 1.25 mmol)) was added to the yellow C₆F₅-solutions using a Hamilton syringe. The FEP reaction tubes were periodically shaken and the reaction was monitored periodically by ¹⁹F NMR spectroscopy.

¹⁹F NMR (282.40 MHz) in CH₃CN at 24 °C

C ₆ H ₅ F	δ = -113.2 ppm* (m, F, 1F)
2-FC ₆ H ₄ C ₆ F ₅	δ = -113.2 ppm* (m, 2-F, 1F); -143.5 ppm (m, o-C ₆ F ₅ , 2F); -156.3 ppm (tt, ³ J(¹⁹ F- ¹⁹ F) = 20 Hz, ⁴ J(¹⁹ F- ¹⁹ F) = 1 Hz, p-C ₆ F ₅ , 1F); -163 ppm* (m, m-C ₆ F ₅ , 2F)
3-FC ₆ H ₄ C ₆ F ₅	δ = -112.2 ppm (m, 3-F, 1F); -143.2 ppm (m, o-C ₆ F ₅ , 2F); -155.6 ppm (t, ³ J(¹⁹ F- ¹⁹ F) = 20 Hz, ⁴ J(¹⁹ F- ¹⁹ F) = 1 Hz, p-C ₆ F ₅ , 1F); -163 ppm* (m, m-C ₆ F ₅ , 2F)
4-FC ₆ H ₄ C ₆ F ₅	δ = -111.5 ppm (m, 4-F, 1F); -140.9 ppm (m, o-C ₆ F ₅ , 2F); -154.2 ppm (t, ³ J(¹⁹ F- ¹⁹ F) = 20 Hz, ⁴ J(¹⁹ F- ¹⁹ F) = 2 Hz, p-C ₆ F ₅ , 1F); -163 ppm* (m, m-C ₆ F ₅ , 2F)

* superimposed signals

**Composition of Reactants and Products Resulting from the Reaction of
[C₆F₅Xe][BF₄] with 20 C₆H₅F in CH₃CN at RT**

time [h]	[C ₆ F ₅ Xe] ⁺ ^a [mol-%]	FC ₆ H ₄ C ₆ F ₅ ^a			[BF ₄] ⁻ ^b [mol-%]
		2-FC ₆ H ₄ C ₆ F ₅ [mol-%]	3-FC ₆ H ₄ C ₆ F ₅ [mol-%]	4-FC ₆ H ₄ C ₆ F ₅ [mol-%]	
17 min	100.0	0	0	0	98.0
2.2	100.0	Traces	Traces	Traces	92.1
19.5	76.8	7.2	6.7	9.3	47.9
43.6	68.2	10.2	9.4	12.2	80.9
101.1	55.9	13.9	12.9	17.3	37.2
115.8	48.6	16.5	15.3	19.6	28.4
140.0	40.7	18.9	17.8	22.6	28.8
164.4	34.8	21.5	19.0	24.6	23.3
188.6	28.7	23.2	21.2	26.9	27.0
212.0	23.5	25.1	22.7	28.7	29.9
307.7	9.0	29.9	26.8	34.3	44.1

^a The total amount (mol-%) of all C₆F₅ compounds was normalized to 100%.

^b The amount of the [BF₄]⁻ anion was calculated with regard to the sum of C₆F₅

**Composition of Reactants and Products Resulting from the Reaction of
[C₆F₅Xe][B(CF₃)₄] with 20 C₆H₅F in CH₃CN at RT**

time [h]	[C ₆ F ₅ Xe] ⁺ ^a [mol-%]	FC ₆ H ₄ C ₆ F ₅ ^a			[B(CF ₃) ₄] ⁻ ^b [mol-%]
		2-FC ₆ H ₄ C ₆ F ₅ [mol-%]	3-FC ₆ H ₄ C ₆ F ₅ [mol-%]	4-FC ₆ H ₄ C ₆ F ₅ [mol-%]	
23 min	100	0	0	0 / 0	128.2
2.1	81.9	5.3	5.3	7.4	106.4
19.5	59.0	12.4	12.4	16.2	95.2
43.6	39.1	18.5	17.4	25.0	108.7
101.0	8.5	29.0	26.9	35.5	107.5
115.8	2.5	31.2	28.8	37.5	125.0

^a The total amount (mol-%) of all C₆F₅ compounds was normalized to 100%.

^b The amount of the [B(CF₃)₄]⁻ anion was calculated with regard to the sum of C₆F₅

**Composition of Reactants and Products Resulting from the Reaction of
[C₆F₅Xe][AsF₆] with 20 C₆H₅F in CH₃CN at RT**

time [h]	[C ₆ F ₅ Xe] ⁺ ^a [mol-%]	FC ₆ H ₄ C ₆ F ₅ ^a			[AsF ₆] ⁻ ^b [mol-%]
		2-FC ₆ H ₄ C ₆ F ₅ [mol-%]	3- FC ₆ H ₄ C ₆ F ₅ [mol-%]	4- FC ₆ H ₄ C ₆ F ₅ [mol-%]	
21 min	100	0.0	0.0	0.0	102.0
5.5	87.8	4.0	3.8	4.4	90.8
19.7	33.8	23.9	21.8	27.5	92.6
43.8	0.0	32.6	30.1	37.3	103.8
101.1	0.0	32.7	29.7	37.6	90.7

^a The total amount (mol-%) of all C₆F₅ compounds was normalized to 100%.

^b The amount of the [AsF₆]⁻ anion was calculated with regard to the sum of C₆F₅

IV.11.4 Reaction of [C₆F₅Xe][BY₄] (Y = F, CN) and [C₆F₅Xe][AsF₆] with Dried (P₄O₁₀) C₆H₅F (20-Fold Molar Excess) in CH₃CN at RT

The salts, [C₆F₅Xe][BF₄] (24.31 mg; 0.06 mmol) (**a**), [C₆F₅Xe][B(CN)₄] (21.03 mg; 0.05 mmol) (**b**), and [C₆F₅Xe][AsF₆] (27.03 mg; 0.06 mmol) (**c**), were each loaded into separate 3.5 mm i.d. FEP reaction tubes and dissolved in CH₃CN (500 μL). Freshly dried (P₄O₁₀) and distilled fluorobenzene (20 equivalents; ((**a**): 119 μL (122 mg; 1.27 mmol); (**b**): 96 μL (98 mg; 1.02 mmol); (**c**): 105 μL (107 mg; 1.11 mmol)) was added to the yellow [C₆F₅Xe]⁺ salt solutions using a Hamilton syringe. The FEP reaction tubes were shaken periodically and the reaction monitored by ¹⁹F NMR spectroscopy.

^{19}F NMR (282.40 MHz) in CH_3CN at 24 °C

$\text{C}_6\text{H}_5\text{F}$	$\delta = -113.2$ ppm* (m, ^{13}C -satellites: $^1J(^{13}\text{C}-^{19}\text{F}) = 243.1$ Hz, 1F)
2- $\text{FC}_6\text{H}_4\text{C}_6\text{F}_5$	$\delta = -113.3$ ppm* (m, 2-F, 1F); -143.5 ppm (m, <i>o</i> - C_6F_5 , 2F); -156.3 ppm (tt, $^3J(^{19}\text{F}-^{19}\text{F}) = 20$ Hz, $^4J(^{19}\text{F}-^{19}\text{F}) = 1$ Hz, <i>p</i> - C_6F_5 , 1F); -163.0 ppm (m, <i>m</i> - C_6F_5 , 2F)
3- $\text{FC}_6\text{H}_4\text{C}_6\text{F}_5$	$\delta = -112.3$ ppm (m, 3-F, 1F); -143.2 ppm (m, <i>o</i> - C_6F_5 , 2F); -155.6 ppm (tt, $^3J(^{19}\text{F}-^{19}\text{F}) = 20$ Hz, $^4J(^{19}\text{F}-^{19}\text{F}) = 1$ Hz, <i>p</i> - C_6F_5 , 1F); -162.7 ppm* (m, <i>m</i> - C_6F_5 , 2F)
4- $\text{FC}_6\text{H}_4\text{C}_6\text{F}_5$	$\delta = -111.5$ ppm (m, 4-F, 1F); -140.9 ppm (m, <i>o</i> - C_6F_5 , 2F); -154.9 ppm (tt, $^3J(^{19}\text{F}-^{19}\text{F}) = 20$ Hz, $^4J(^{19}\text{F}-^{19}\text{F}) = 1$ Hz, <i>p</i> - C_6F_5 , 1F); -162.7 ppm* (m, <i>m</i> - C_6F_5 , 2F)

* superimposed signals

Composition of Reactants and Products Resulting from the Reaction of $[\text{C}_6\text{F}_5\text{Xe}][\text{BF}_4]$ with 20 $\text{C}_6\text{H}_5\text{F}$ in CH_3CN at RT

time [h]	$[\text{C}_6\text{F}_5\text{Xe}]^+{}^a$ [mol-%]	$\text{FC}_6\text{H}_4\text{C}_6\text{F}_5$ ^a			$[\text{BF}_4]^-$ ^b [mol-%]
		2- $\text{FC}_6\text{H}_4\text{C}_6\text{F}_5$ [mol-%]	3- $\text{FC}_6\text{H}_4\text{C}_6\text{F}_5$ [mol-%]	4- $\text{FC}_6\text{H}_4\text{C}_6\text{F}_5$ [mol-%]	
10 min	100.0	0.0	0.0	0.0	98.8
30 min	100.0	0.0	0.0	0.0	96.6
1	100.0	0.0	0.0	0.0	99.3
4	85.5	4.5	4.0	6.0	79.1
7	79.3	6.5	5.7	8.5	76.0
24	73.3	8.4	7.5	10.9	54.7
31	70.3	9.2	8.8	11.6	51.1
96	60.4	6.7	14.2	18.6	16.1
120	52.5	15.5	14.1	18.0	20.1
144	42.6	18.5	16.8	22.1	15.5
168	38.2	19.7	18.5	23.6	18.9
192	33.1	21.4	19.9	25.5	17.0
264	19.4	25.9	24.2	30.5	17.1
432	0.0	32.0	29.6	38.4	24.3

^a The total amount (mol-%) of all C_6F_5 compounds was normalized to 100%.

^b The $[\text{BF}_4]^-$ anion was calculated regarding the sum of C_6F_5

**Composition of Reactants and Products Resulting from the Reaction of
[C₆F₅Xe][B(CN)₄] with 20 C₆H₅F in CH₃CN at RT**

time [h]	[C ₆ F ₅ Xe] ⁺ ^a [mol-%]	FC ₆ H ₄ C ₆ F ₅ ^a			C ₆ F ₅ H ^a [mol-%]
		2-FC ₆ H ₄ C ₆ F ₅ [mol-%]	3-FC ₆ H ₄ C ₆ F ₅ [mol-%]	4-FC ₆ H ₄ C ₆ F ₅ [mol-%]	
10 min	100.0	0.0	0.0	0.0	
30 min	100.0	0.0	0.0	0.0	
1	100.0	0.0	0.0	0.0	
4	100.0	0.0	0.0	0.0	
7	87.3	5.0	3.3	4.5	
24	89.0	3.0	2.4	5.5	0.0
31	85.5	4.3	4.6	5.5	
96	26.3	23.7	21.5	28.5	
120	10.2	28.3	26.1	35.4	
144	2.3	31.4	28.9	37.4	
168	0.0	32.7	29.4	37.9	

**Composition of Reactants and Products Resulting from the Reaction of
[C₆F₅Xe][AsF₆] with 20 C₆H₅F in CH₃CN at RT**

time [h]	[C ₆ F ₅ Xe] ⁺ ^a [mol-%]	FC ₆ H ₄ C ₆ F ₅ ^a			[AsF ₆] ⁻ ^b [mol-%]
		2-FC ₆ H ₄ C ₆ F ₅ [mol-%]	3-FC ₆ H ₄ C ₆ F ₅ [mol-%]	4-FC ₆ H ₄ C ₆ F ₅ [mol-%]	
10 min	100.0	0.0	0.0	0.0	73.0
30 min	100.0	0.0	0.0	0.0	83.4
1	100.0	0.0	0.0	0.0	71.7
4	100.0	0.0	0.0	0.0	93.4
7	100.0	0.0	0.0	0.0	88.4
24	83.0	5.6	4.9	6.5	94.4
31	47.2	8.4	7.3	10.1	94.6
96	0.0	32.0	29.5	38.6	102.3

^a The total amount (mol-%) of all C₆F₅ compounds was normalized to 100%.

^b The [AsF₆]⁻ anion was calculated regarding the sum of C₆F₅

IV.11.5 Reaction of $[C_6F_5Xe][BY_4]$ ($Y = F, C_6F_5,$ and CN) with Dried (P_4O_{10}) C_6H_5F (20-Fold Molar Excess) in CH_3CN at RT

The salts, $[C_6F_5Xe][BF_4]$ (25.55 mg; 0.07 mmol) (**a**), $[C_6F_5Xe][B(C_6F_5)_4]$ (61.51 mg; 0.06 mmol) (**b**), and $[C_6F_5Xe][B(CN)_4]$ (28.98 mg; 0.07 mmol) (**c**), were each loaded in 3.5 mm i.d. FEP reaction tubes and dissolved in CH_3CN (500 μ L). Freshly distilled fluorobenzene (20 equivalents; ((**a**): 125 μ L (128 mg; 1.33 mmol); (**b**): 118 μ L (121 mg; 1.26 mmol); (**c**): 130 μ L (133 mg; 1.38 mmol)) was added to the yellow $[C_6F_5Xe]^+$ salt solutions using a Hamilton syringe. The FEP reaction tubes were shaken periodically and the reaction monitored by ^{19}F NMR spectroscopy.

^{19}F NMR (282.40 MHz) in CH_3CN at 24 °C

C_6H_5F	$\delta = -113.2$ ppm (m, ^{13}C -satellites: $^1J(^{13}C-^{19}F) = 243.1$ Hz, 1F)
2- $FC_6H_4C_6F_5$	$\delta = -113.3$ ppm* (m, 2-F, 1F); -143.5 ppm (m, <i>o</i> - C_6F_5 , 2F); -156.3 ppm (tt, $^3J(^{19}F-^{19}F) = 20$ Hz, $^4J(^{19}F-^{19}F) = 1$ Hz, <i>p</i> - C_6F_5 , 1F); -163.0 ppm (m, <i>m</i> - C_6F_5 , 2F)
3- $FC_6H_4C_6F_5$	$\delta = -112.3$ ppm (m, 3-F, 1F); -143.2 ppm (m, <i>o</i> - C_6F_5 , 2F); -155.6 ppm (tt, $^3J(^{19}F-^{19}F) = 20$ Hz, $^4J(^{19}F-^{19}F) = 1$ Hz, <i>p</i> - C_6F_5 , 1F); -162.7 ppm* (m, <i>m</i> - C_6F_5 , 2F)
4- $FC_6H_4C_6F_5$	$\delta = -111.5$ ppm (m, 4-F, 1F); -140.9 ppm (m, <i>o</i> - C_6F_5 , 2F); -154.9 ppm (tt, $^3J(^{19}F-^{19}F) = 20$ Hz, $^4J(^{19}F-^{19}F) = 1$ Hz, <i>p</i> - C_6F_5 , 1F); -162.7 ppm* (m, <i>m</i> - C_6F_5 , 2F)
C_6F_5H	$\delta = -139.1$ ppm (m, <i>o</i> - C_6F_5 , 2F); -155 ppm - -156 ppm* (<i>p</i> - C_6F_5); -165 ppm* (<i>m</i> - C_6F_5)

* superimposed signals

**Composition of Reactants and Products Resulting from the Reaction of
[C₆F₅Xe][BF₄] with 20 C₆H₅F in CH₃CN at RT**

time [h]	[C ₆ F ₅ Xe] ⁺ ^a [mol-%]	FC ₆ H ₄ C ₆ F ₅ ^a			[BF ₄] ⁻ ^b [mol-%]
		2-FC ₆ H ₄ C ₆ F ₅ [mol-%]	3-FC ₆ H ₄ C ₆ F ₅ [mol-%]	4-FC ₆ H ₄ C ₆ F ₅ [mol-%]	
20 min	100	0	0	0	100.2
50 min	96.1	1.3	1.3	1.3	95.2
1.7	94.8	1.6	1.6	2.0	94.4
4.3	92.0	2.4	2.2	3.5	89.6
25.3	92.3	2.4	2.0	3.3	93.0
49.3	70.8	9.6	8.3	11.4	59.6
120.0	50.2	16.1	14.7	19.0	27.1
144.4	41.0	18.9	17.8	22.2	26.2
174	32.8	21.5	20.2	25.5	27.2
192.2	28.5	22.9	21.5	27.1	33.8
217.4	23.6	24.2	23.4	28.7	32.3
292.7	6.8	29.7	28.1	35.4	39.6
313.9	4.0	30.8	28.7	36.5	54.3
342.2	1.6	32.1	29.1	37.2	72.1
361.6	0.0	33.2	29.5	37.4	85.1

^a The total amount (mol-%) of all C₆F₅ compounds was normalized to 100%.

^b The amount of the [BF₄]⁻ anion was calculated with regard to the sum of C₆F₅

**Composition of Reactants and Products Resulting from the Reaction of
[C₆F₅Xe][B(C₆F₅)₄] with 20 C₆H₅F in CH₃CN at RT**

time [h]	[C ₆ F ₅ Xe] ⁺ ^a [mol-%]	FC ₆ H ₄ C ₆ F ₅ ^a			C ₆ F ₅ H ^a [mol-%]
		2-FC ₆ H ₄ C ₆ F ₅ [mol-%]	3-FC ₆ H ₄ C ₆ F ₅ [mol-%]	4-FC ₆ H ₄ C ₆ F ₅ [mol-%]	
20 min	100	0	0	0	0
50 min	100	Traces	Traces	Traces	Traces

Table (continued...)

1.7	100	Traces	Traces	Traces	Traces
4.3	88.7	3.6	3.6	4.1	Traces
25.3	75.4	7.2	6.9	8.7	1.7
49.3	63.0	11.8	11.5	13.7	Traces
120.0	18.1	26.7	24.5	30.7	Traces
144.4	10.9	28.6	27.1	33.4	Traces

^a The total amount (mol-%) of all C₆F₅ compounds excluding [B(C₆F₅)₄]⁻ were normalized to 100%.

Composition of Reactants and Products Resulting from the Reaction of [C₆F₅Xe][B(CN)₄] with 20 C₆H₅F in CH₃CN at RT

time [h]	[C ₆ F ₅ Xe] ⁺ ^a [mol-%]	FC ₆ H ₄ C ₆ F ₅ ^a			C ₆ F ₅ H ^a [mol-%]
		2-FC ₆ H ₄ C ₆ F ₅ [mol-%]	3-FC ₆ H ₄ C ₆ F ₅ [mol-%]	4-FC ₆ H ₄ C ₆ F ₅ [mol-%]	
20 min	100	0	0	0 / 0	0.0
50 min	95.1	1.3	1.3	2.2	
1.7	92.2	2.5	2.5	2.7	
4.3	93.6	2.1	1.8	2.5	
25.3	78.5	7.1	6.4	8.0	
49.3	35.7	21.1	19.3	23.9	
120.0	0.0	32.3	29.8	37.8	
144.4	0.0	32.5	29.7	37.8	

^a The total amount (mol-%) of all C₆F₅ compounds was normalized to 100%.

IV.11.6 Reaction of [C₆F₅Xe][B(C₆F₅)₄] and [C₆F₅Xe][B(CF₃)₄] with Neat C₆H₅F at RT

The salts, [C₆F₅Xe][B(C₆F₅)₄] (45.0 mg; 0.046 mmol) (**a**), [C₆F₅Xe][B(CF₃)₄] (38.7 mg; 0.066 mmol) (**b**), were each loaded in 3.5 mm i.d. FEP reaction tubes and dissolved in freshly dried (P₄O₁₀) and distilled fluorobenzene (400 μL; 4.2 mmol). The solutions were monitored by ¹⁹F NMR spectroscopy.

(a) [C₆F₅Xe][B(C₆F₅)₄]¹⁹F NMR (282.40 MHz) in CH₃CN at 24 °C

C ₆ H ₅ F	δ = -113.2 ppm (m, ¹³ C-satellites: ¹ J(¹³ C- ¹⁹ F) = 243 Hz, 1F)
2-FC ₆ H ₄ C ₆ F ₅	δ = -113.3 ppm* (m, 2-F, 1F); -143.5 ppm (m, <i>o</i> -C ₆ F ₅ , 2F); -156.3 ppm (tt, ³ J(¹⁹ F- ¹⁹ F) = 20 Hz, ⁴ J(¹⁹ F- ¹⁹ F) = 1 Hz, <i>p</i> -C ₆ F ₅ , 1F); -163.0 ppm (m, <i>m</i> -C ₆ F ₅ , 2F)
3-FC ₆ H ₄ C ₆ F ₅	δ = -112.3 ppm (m, 3-F, 1F); -143.2 ppm (m, <i>o</i> -C ₆ F ₅ , 2F); -155.6 ppm (tt, ³ J(¹⁹ F- ¹⁹ F) = 20 Hz, ⁴ J(¹⁹ F- ¹⁹ F) = 1 Hz, <i>p</i> -C ₆ F ₅ , 1F); -162.7 ppm* (m, <i>m</i> -C ₆ F ₅ , 2F)
4-FC ₆ H ₄ C ₆ F ₅	δ = -111.5 ppm (m, 4-F, 1F); -140.9 ppm (m, <i>o</i> -C ₆ F ₅ , 2F); -154.9 ppm (tt, ³ J(¹⁹ F- ¹⁹ F) = 20 Hz, ⁴ J(¹⁹ F- ¹⁹ F) = 1 Hz, <i>p</i> -C ₆ F ₅ , 1F); -162.7 ppm* (m, <i>m</i> -C ₆ F ₅ , 2F)
C ₆ F ₅ H	δ = -139.1 ppm (m, <i>o</i> -C ₆ F ₅ , 2F); -155 ppm - -156 ppm* (<i>p</i> -C ₆ F ₅); -165 ppm* (<i>m</i> -C ₆ F ₅)
C ₆ F ₅ -balance ^a :	C ₆ F ₅ H (8.9%), 2-FC ₆ H ₄ C ₆ F ₅ (2.5%), 3-FC ₆ H ₄ C ₆ F ₅ (2.5%), 4-FC ₆ H ₄ C ₆ F ₅ (3.6%)

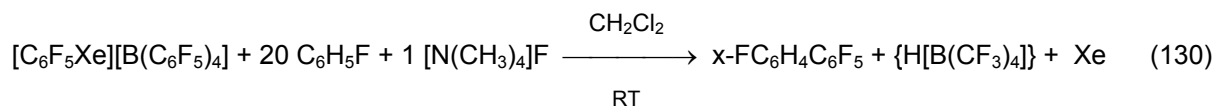
(b) [C₆F₅Xe][B(CF₃)₄]¹⁹F NMR (282.40 MHz) in CH₃CN at 24 °C

C ₆ H ₅ F	δ = -113.2 ppm (m, ¹³ C-satellites: ¹ J(¹³ C- ¹⁹ F) = 243.1 Hz, 1F)
2-FC ₆ H ₄ C ₆ F ₅	δ = -113.3 ppm* (m, 2-F, 1F); -143.5 ppm (m, <i>o</i> -C ₆ F ₅ , 2F); -156.3 ppm (tt, ³ J(¹⁹ F- ¹⁹ F) = 20 Hz, ⁴ J(¹⁹ F- ¹⁹ F) = 1 Hz, <i>p</i> -C ₆ F ₅ , 1F); -163.0 ppm (m, <i>m</i> -C ₆ F ₅ , 2F)
3-FC ₆ H ₄ C ₆ F ₅	δ = -112.3 ppm (m, 3-F, 1F); -143.2 ppm (m, <i>o</i> -C ₆ F ₅ , 2F); -155.6 ppm (tt, ³ J(¹⁹ F- ¹⁹ F) = 20 Hz, ⁴ J(¹⁹ F- ¹⁹ F) = 1.2 Hz, <i>p</i> -C ₆ F ₅ , 1F); -162.7 ppm* (m, <i>m</i> -C ₆ F ₅ , 2F)
4-FC ₆ H ₄ C ₆ F ₅	δ = -111.5 ppm (m, 4-F, 1F); -140.9 ppm (m, <i>o</i> -C ₆ F ₅ , 2F); -154.9 ppm (tt, ³ J(¹⁹ F- ¹⁹ F) = 20 Hz, ⁴ J(¹⁹ F- ¹⁹ F) = 1 Hz, <i>p</i> -C ₆ F ₅ , 1F); -162.7 ppm* (m, <i>m</i> -C ₆ F ₅ , 2F)
C ₆ F ₅ H	δ = -139.1 ppm (m, <i>o</i> -C ₆ F ₅ , 2F); -155 ppm - -156 ppm* (<i>p</i> -C ₆ F ₅); -165 ppm* (<i>m</i> -C ₆ F ₅)
C ₆ F ₅ -balance ^a :	C ₆ F ₅ H (8.9%), 2-FC ₆ H ₄ C ₆ F ₅ (2.5%), 3-FC ₆ H ₄ C ₆ F ₅ (2.5%), 4-FC ₆ H ₄ C ₆ F ₅ (3.6%)

^a The total amount (mol-%) of all C₆F₅ compounds excluding [B(C₆F₅)₄]⁻ was normalized to 100%.

* superimposed signals

IV.11.7 Reaction of [C₆F₅Xe][B(C₆F₅)₄] in the Presence of [N(CH₃)₄]F with C₆H₅F (20-Fold Molar Excess) in CH₂Cl₂ at –55 °C



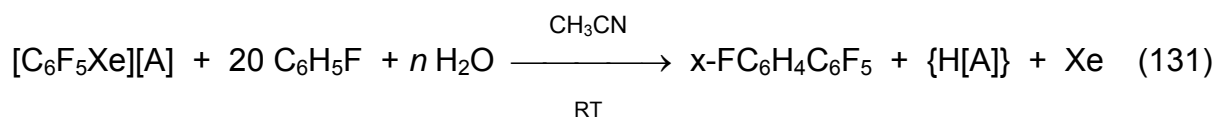
(x = 2, 3, 4)

In the drybox, [C₆F₅Xe][B(C₆F₅)₄] (26.04 mg; 0.03 mmol) was loaded into a 3.5 mm i.d. FEP reaction tube and suspended in cold (–55 °C) CH₂Cl₂ (1000 μL). Freshly dried (P₄O₁₀) and distilled fluorobenzene (20 equivalents; 45 μL; 0.48 mmol) was added to the yellow solution using a Hamilton syringe. The solution was then divided into two equivalent samples (**A** + **B**) and a portion (250 μL = 0.03 mmol) of a solution of [N(CH₃)₄]F (5.72 mg; 0.06 mmol) in cold (–55 °C) CH₂Cl₂ (1000 μL) was added to sample (**A**). Sample (**B**) functioned as reference. The FEP reaction tubes were shaken periodically and the reaction monitored by ¹⁹F NMR spectroscopy.

There was a slow reaction observed between [C₆F₅Xe][B(C₆F₅)₄] and C₆H₅F in the absence of [N(CH₃)₄]F. After 3 h at RT, only small amounts of x-FC₆H₄C₆F₅ and (C₆F₅)₂ were detected. In the case where [N(CH₃)₄]F was present the reaction was complete after 15 min. The main products observed were [B(C₆F₅)₄][–] (116.4%), x-FC₆H₄C₆F₅ (~70.3%), (C₆F₅)₂ (6.5%), C₆F₅H (23.2%), CHF₂Cl and [HF₂][–].

The high mol-% (> 100%) of [B(C₆F₅)₄][–] can be explained by the applied procedure. The sum of C₆F₅ was normalized to 100% and volatile C₆F₅H can penetrate through the FEP walls or leak through the stopper which results in a too low content of C₆F₅H and a too high content of all other compounds.

IV.11.8 Reaction of [C₆F₅Xe][BF₄] and [C₆F₅Xe][AsF₆] with C₆H₅F (20-Fold Molar Excess) in CH₃CN: The Influence of Water (1 and 20 Equivalents) at RT



(x = 2, 3, 4; n = 1, 20; A = BF₄; AsF₆)

The salts, $[\text{C}_6\text{F}_5\text{Xe}][\text{BF}_4]$ (31.66 mg; 0.08 mmol) (**a**), $[\text{C}_6\text{F}_5\text{Xe}][\text{AsF}_6]$ (27.07 mg; 0.06 mmol) (**b**), $[\text{C}_6\text{F}_5\text{Xe}][\text{BF}_4]$ (30.13 mg; 0.08 mmol) (**c**), and $[\text{C}_6\text{F}_5\text{Xe}][\text{AsF}_6]$ (26.86 mg; 0.06 mmol) (**d**), were each loaded into separate 3.5 mm i.d. FEP reaction tubes and dissolved in CH_3CN (500 μL). Freshly dried (P_4O_{10}) and distilled fluorobenzene (20 equivalents; (**a**): 155.0 μL (158.7 mg, 1.66 mmol); (**b**): 110.0 μL (112.6 mg, 1.17 mmol); (**c**): 155.0 μL (158.7 mg, 1.66 mmol); (**d**): 110.0 μL (112.6 mg, 1.17 mmol)) and de-ionized H_2O (1 equivalent: **a**) 1.5 μL ; 0.08 mmol; **b**) 1.0 μL ; 0.06 mmol or 20 equivalents; **c**) 29 μL ; 1.61 mmol; **d**) 20 μL ; 1.11 mmol) were added to the yellow $[\text{C}_6\text{F}_5\text{Xe}]^+$ Salt solutions using a Hamilton syringe. The FEP reaction tubes were periodically shaken and the reaction monitored by ^{19}F NMR spectroscopy. The reaction tubes were stored in the absence of daylight over the entire period.

^{19}F NMR (282.40 MHz) in CH_3CN at 24 °C

$\text{C}_6\text{H}_5\text{F}$	$\delta = -113.2$ ppm* (m, F, 1F)
2- $\text{FC}_6\text{H}_4\text{C}_6\text{F}_5$	$\delta = -113.2$ ppm* (m, 2-F, 1F); -143.5 ppm (m, <i>o</i> - C_6F_5 , 2F); -156.3 ppm (tt, $^3J(^{19}\text{F}-^{19}\text{F}) = 20$ Hz, $^4J(^{19}\text{F}-^{19}\text{F}) = 1$ Hz, <i>p</i> - C_6F_5 , 1F); -163 ppm* (m, <i>m</i> - C_6F_5 , 2F)
3- $\text{FC}_6\text{H}_4\text{C}_6\text{F}_5$	$\delta = -112.2$ ppm (m, 3-F, 1F); -143.2 ppm (m, <i>o</i> - C_6F_5 , 2F); -155.6 ppm (t, $^3J(^{19}\text{F}-^{19}\text{F}) = 20$ Hz, $^4J(^{19}\text{F}-^{19}\text{F}) = 1$ Hz, <i>p</i> - C_6F_5 , 1F); -163 ppm* (m, <i>m</i> - C_6F_5 , 2F)
4- $\text{FC}_6\text{H}_4\text{C}_6\text{F}_5$	$\delta = -111.5$ ppm (m, 4-F, 1F); -140.9 ppm (m, <i>o</i> - C_6F_5 , 2F); -154.2 ppm (t, $^3J(^{19}\text{F}-^{19}\text{F}) = 20$ Hz, $^4J(^{19}\text{F}-^{19}\text{F}) = 2$ Hz, <i>p</i> - C_6F_5 , 1F); -163 ppm* (m, <i>m</i> - C_6F_5 , 2F)

* superimposed signals

a) Composition of Reactants and Products Resulting from the Reaction of $[\text{C}_6\text{F}_5\text{Xe}][\text{BF}_4]$ with 20 $\text{C}_6\text{H}_5\text{F}$ and 1 H_2O in CH_3CN at RT

time [h]	$[\text{C}_6\text{F}_5\text{Xe}]^+$ ^a [mol-%]	$\text{FC}_6\text{H}_4\text{C}_6\text{F}_5$ ^a			$[\text{BF}_4]^-$ ^b [mol-%]
		2- $\text{FC}_6\text{H}_4\text{C}_6\text{F}_5$ [mol-%]	3- $\text{FC}_6\text{H}_4\text{C}_6\text{F}_5$ [mol-%]	4- $\text{FC}_6\text{H}_4\text{C}_6\text{F}_5$ [mol-%]	
25 min	79.9	6.2	5.8	8.1	97.0
1	45.3	17.5	16.2	21.0	95.4

Table (continued...)

2.5	25.1	23.9	22.0	28.9	82.8
4	12.6	28.7	25.6	33.1	89.8
5	6.8	30.2	27.6	35.4	88.9
18.5	0.0	32.5	29.6	37.9	86.2

^a The total amount (mol-%) of all C₆F₅ compounds was normalized to 100%.

^b The amount of the [BF₄]⁻ anion was calculated with regard to the sum of C₆F₅

b) Composition of Reactants and Products Resulting from the Reaction of [C₆F₅Xe][AsF₆] with 20 C₆H₅F and 1 H₂O in CH₃CN at RT

time [h]	[C ₆ F ₅ Xe] ⁺ ^a [mol-%]	FC ₆ H ₄ C ₆ F ₅ ^a			[AsF ₆] ⁻ ^b [mol-%]
		2-FC ₆ H ₄ C ₆ F ₅ [mol-%]	3-FC ₆ H ₄ C ₆ F ₅ [mol-%]	4-FC ₆ H ₄ C ₆ F ₅ [mol-%]	
25 min	79.5	6.8	6.2	7.5	82.7
1	66.9	10.8	9.7	12.6	101.9
2.5	49.1	16.5	15.0	19.4	99.3
4	36.3	20.6	19.0	24.1	98.4
5	31.9	22.0	19.9	26.2	85.5
18.5	4.3	30.9	28.5	36.3	38.1

^a The total amount (mol-%) of all C₆F₅ compounds was normalized to 100%.

^b The amount of the [AsF₆]⁻ anion was calculated with regard to the sum of C₆F₅

a) Composition of Reactants and Products Resulting from the Reaction of [C₆F₅Xe][BF₄] with 20 C₆H₅F and 20 H₂O in CH₃CN at RT

time [h]	[C ₆ F ₅ Xe] ⁺ ^a [mol-%]	FC ₆ H ₄ C ₆ F ₅ ^a			[BF ₄] ⁻ ^b [mol-%]
		2-FC ₆ H ₄ C ₆ F ₅ [mol-%]	3-FC ₆ H ₄ C ₆ F ₅ [mol-%]	4-FC ₆ H ₄ C ₆ F ₅ [mol-%]	
25 min	0.0	32.5	29.7	37.7	106.8

^a The total amount (mol-%) of all C₆F₅ compounds was normalized to 100%.

^b The amount of the [BF₄]⁻ anion was calculated with regard to the sum of C₆F₅

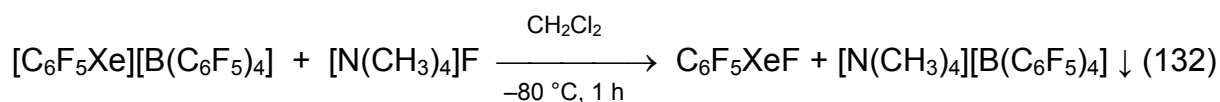
b) Composition of Reactants and Products Resulting from the Reaction of $[\text{C}_6\text{F}_5\text{Xe}][\text{AsF}_6]$ with 20 $\text{C}_6\text{H}_5\text{F}$ and 20 H_2O in CH_3CN at RT

time [h]	$[\text{C}_6\text{F}_5\text{Xe}]^+$ ^a [mol-%]	$\text{FC}_6\text{H}_4\text{C}_6\text{F}_5$ ^a			$[\text{AsF}_6]^-$ ^b [mol-%]
		2- $\text{FC}_6\text{H}_4\text{C}_6\text{F}_5$ [mol-%]	3- $\text{FC}_6\text{H}_4\text{C}_6\text{F}_5$ [mol-%]	4- $\text{FC}_6\text{H}_4\text{C}_6\text{F}_5$ [mol-%]	
25 min	11.6	28.4	26.4	33.6	96.8

^a The total amount (mol-%) of all C_6F_5 compounds was normalized to 100%.

^b The amount of the $[\text{AsF}_6]^-$ anion was calculated with regard to the sum of C_6F_5

IV.11.9 Preparation of $\text{C}_6\text{F}_5\text{XeF}$ from $[\text{C}_6\text{F}_5\text{Xe}][\text{B}(\text{C}_6\text{F}_5)_4]$ and $[\text{N}(\text{CH}_3)_4]\text{F}$ in CH_2Cl_2 at $-80\text{ }^\circ\text{C}$



In the drybox, $[\text{C}_6\text{F}_5\text{Xe}][\text{B}(\text{C}_6\text{F}_5)_4]$ (118.61 mg; 0.12 mmol), was loaded in a 8 mm i.d. FEP reaction tube which contained an adequate stirrbar and was suspended in cold ($-80\text{ }^\circ\text{C}$) CH_2Cl_2 (1000 μL). A solution of cold ($-80\text{ }^\circ\text{C}$) CH_2Cl_2 (500 μL) and $[\text{N}(\text{CH}_3)_4]\text{F}$ (13.59 mg; 0.15 mmol) was added and allowed to react for 1 h. Immediately, a white finely divided suspension of $[\text{N}(\text{CH}_3)_4][\text{B}(\text{C}_6\text{F}_5)_4]$ formed. The suspension was centrifuged at $-80\text{ }^\circ\text{C}$ and the CH_2Cl_2 mother liquor was separated and checked by NMR spectroscopy at $-80\text{ }^\circ\text{C}$. The main product in the mother liquor was $\text{C}_6\text{F}_5\text{XeF}$ (75.1%) in addition to $\text{C}_6\text{F}_5\text{H}$ (4.0%); $\text{C}_6\text{F}_5\text{Cl}$ (0.5%); $[\text{B}(\text{C}_6\text{F}_5)_4]^-$ (9.7%); $(\text{C}_6\text{F}_5)_2$ (2.0%), and several other unidentified C_6F_5 compounds ($\Sigma 8.7\%$). The mother liquor was then removed under vacuum at temperatures below $-50\text{ }^\circ\text{C}$ and the resulting yellow orange solid was dried for several hours at temperatures not exceeding $-50\text{ }^\circ\text{C}$.

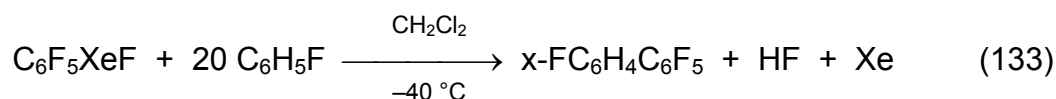
^{19}F NMR (282.40 MHz) in CH_2Cl_2 at $-80\text{ }^\circ\text{C}$

$\text{C}_6\text{F}_5\text{XeF}$ $\delta = -2.8$ ppm (s, $\Delta\nu_{1/2} = 129$ Hz, ^{129}Xe -satellites: $^1J(^{19}\text{F}-^{129}\text{Xe}) = 4016$ Hz, XeF, 1E); -129.6 ppm (m, *o*- C_6F_5 , 2F); -147.0 ppm (t, $^3J(^{19}\text{F}-^{19}\text{F}) = 21$ Hz, *p*- C_6F_5 , 1F); -157.2 ppm (m, *m*- C_6F_5 , 2F)

^{129}Xe NMR (83.02 MHz) in CH_2Cl_2 at $-80\text{ }^\circ\text{C}$

$\text{C}_6\text{F}_5\text{XeF}$ $\delta = -3793.4$ ppm (dtm, $^3J(^{19}\text{F}-^{129}\text{Xe}) = 80$ Hz; ^{129}Xe -satellites: $^1J(^{19}\text{F}-^{129}\text{Xe}) = 4018$ Hz, XeF)

IV.11.10 Reaction of $\text{C}_6\text{F}_5\text{XeF}$ with $\text{C}_6\text{H}_5\text{F}$ (20-Fold Molar Excess) in CH_2Cl_2 at $-40\text{ }^\circ\text{C}$



($x = 2, 3, 4$)

Freshly prepared $\text{C}_6\text{F}_5\text{XeF}$ (16.3 mg; 0.05 mmol) containing $[\text{N}(\text{CH}_3)_4][\text{B}(\text{C}_6\text{F}_5)_4]$ (9%) impurity was dissolved in cold ($-80\text{ }^\circ\text{C}$) CH_2Cl_2 (1200 μL). The yellow solution was divided and transferred into two 3.5 mm i.d. FEP reaction tubes (**A** and **B**). Freshly dried (P_4O_{10}) and distilled $\text{C}_6\text{H}_5\text{F}$ (50 μL ; 51.2 mg; 0.53 mmol) was added at $-80\text{ }^\circ\text{C}$ to portion **A** using a Hamilton syringe. The solution was subsequently allowed to warm to $-40\text{ }^\circ\text{C}$, stirred for 30 min. and monitored periodically by ^{19}F NMR spectroscopy at $-40\text{ }^\circ\text{C}$.

^{19}F NMR (282.40 MHz) in CH_2Cl_2 after 30 min at $-40\text{ }^\circ\text{C}$

C_6F_5 -balance^a: $\text{C}_6\text{F}_5\text{XeF}$ (53.8%)^a, $[\text{B}(\text{C}_6\text{F}_5)_4]^-$ (14.9%)^b, $\text{C}_6\text{F}_5\text{H}$ (8.9%)^a, $\text{C}_6\text{F}_5\text{Cl}$ (9.7%)^a, 2- $\text{FC}_6\text{H}_4\text{C}_6\text{F}_5$ (2.5%)^a, 3- $\text{FC}_6\text{H}_4\text{C}_6\text{F}_5$ (2.5%)^a, 4- $\text{FC}_6\text{H}_4\text{C}_6\text{F}_5$ (3.6%)^a

^a The total amount (mol-%) of all C_6F_5 compounds excluding $[\text{B}(\text{C}_6\text{F}_5)_4]^-$ was normalized to 100%.

^b The amount of the $[\text{B}(\text{C}_6\text{F}_5)_4]^-$ was calculated with regard to the sum of C_6F_5

^{19}F NMR (282.40 MHz) in CH_2Cl_2 after 24 h at $-40\text{ }^\circ\text{C}$

C_6F_5 -balance^a: $\text{C}_6\text{F}_5\text{XeF}$ (33.2%)^a, $[\text{B}(\text{C}_6\text{F}_5)_4]^-$ (55.4%)^b, $\text{C}_6\text{F}_5\text{H}$ (12.2%)^a, $\text{C}_6\text{H}_5\text{Cl}$ (10.4%)^a, 2- $\text{FC}_6\text{H}_4\text{C}_6\text{F}_5$ (7.6%)^a, 3- $\text{FC}_6\text{H}_4\text{C}_6\text{F}_5$ (5.2%)^a, 4- $\text{FC}_6\text{H}_4\text{C}_6\text{F}_5$ (2.9%)^a

^a The total amount (mol-%) of all C_6F_5 containing compounds excluding $[\text{B}(\text{C}_6\text{F}_5)_4]^-$ were calculated to 100%.

^b The amount of the $[\text{B}(\text{C}_6\text{F}_5)_4]^-$ was calculated with regard to the sum of C_6F_5

Portion **B** was mixed with 37 equivalents of cold ($-40\text{ }^{\circ}\text{C}$) CH_3CN (100 μL ; 1.9 mmol), maintained at $-40\text{ }^{\circ}\text{C}$ for 24 h and checked by NMR spectroscopy.

^{19}F NMR (282.40 MHz) in CH_2Cl_2 after 24 h at $-40\text{ }^{\circ}\text{C}$

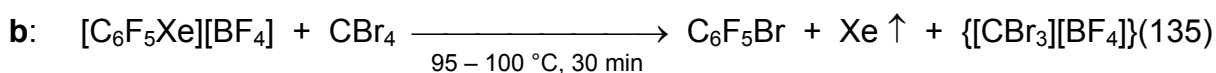
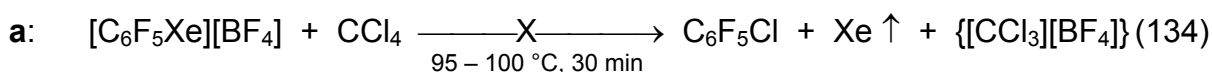
C_6F_5 -balance^a: $\text{C}_6\text{F}_5\text{XeF}$ (49.6%)^a, $[\text{B}(\text{C}_6\text{F}_5)_4]^-$ (53.5%)^b, $\text{C}_6\text{F}_5\text{H}$ (12.8%)^a, $\text{C}_6\text{H}_5\text{Cl}$ (6.0%)^a, $(\text{C}_6\text{F}_5)_2$ (4.6%)^a

^a The total amount (mol-%) of all C_6F_5 compounds excluding $[\text{B}(\text{C}_6\text{F}_5)_4]^-$ was normalized to 100%.

^b The $[\text{B}(\text{C}_6\text{F}_5)_4]^-$ anion was calculated regarding the sum of C_6F_5

IV.12 **Reaction of $[\text{C}_6\text{F}_5\text{Xe}][\text{BY}_4]$ ($Y = \text{F}, \text{C}_6\text{F}_5$) with CX_4 ($X = \text{Cl}, \text{Br}, \text{and I}$) and $\text{C}_6\text{F}_5\text{Z}$ ($Z = \text{Br}, \text{I}$)**

IV.12.1 *Attempts to React $[\text{C}_6\text{F}_5\text{Xe}][\text{BF}_4]$ with CX_4 ($X = \text{Cl}, \text{Br}$) in the Melt ($95 - 100\text{ }^{\circ}\text{C}$)*



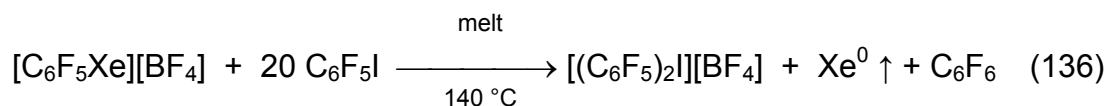
Liquid CCl_4 (**a**: 500 μL) and solid CBr_4 (**b**: 102.30 mg; 0.31 mmol) was added to solid $[\text{C}_6\text{F}_5\text{Xe}][\text{BF}_4]$ (**a**: 26.42 mg; 0.07 mmol; **b**: 21.74 mg; 0.06 mmol) into a 5 mm glass NMR tube (Wilmad 507) at RT. Both samples were heated to $95 - 100\text{ }^{\circ}\text{C}$ using an oil bath, stirred for 30 min. and quenched in liquid nitrogen ($-196\text{ }^{\circ}\text{C}$). The molten mixtures were finally dissolved in CH_3CN (500 μL) and their NMR spectra were recorded.

Sample **a**:

No reaction products such as $\text{C}_6\text{F}_5\text{H}$ or $\text{C}_6\text{F}_5\text{Cl}$ were detected in addition to the characteristic resonances of $[\text{C}_6\text{F}_5\text{Xe}][\text{BF}_4]$.

Sample **b**:¹⁹F NMR (282.40 MHz) in CH₃CN

[C ₆ F ₅ Xe][BF ₄]	δ = −124.5 ppm (m, <i>o</i> -C ₆ F ₅ , 2F); −141.6 ppm (tt, ³ J(¹⁹ F- ¹⁹ F) = 20 Hz, ⁴ J(¹⁹ F- ¹⁹ F) = 5 Hz, <i>p</i> -C ₆ F ₅ , 1F); −148.9 ppm (s, Δ <i>v</i> _{1/2} = 22 Hz, 4F; Δδ (¹⁰ B- ¹¹ B) = 16 Hz); −154.0 ppm (m, <i>m</i> -C ₆ F ₅ , 2F)
C ₆ F ₅ Br	δ = −132.8 ppm (m, <i>o</i> -C ₆ F ₅ , 2F); −154.7 ppm (tt, ³ J(¹⁹ F- ¹⁹ F) = 20 Hz, ⁴ J(¹⁹ F- ¹⁹ F) = 1 Hz, <i>p</i> -C ₆ F ₅ , 1F); −160.4 ppm (m, <i>m</i> -C ₆ F ₅ , 2F)

C₆F₅-balance^a: [C₆F₅Xe]⁺ (85.1%); C₆F₅Br (14.9%)Cation/anion ratio: [C₆F₅Xe]⁺ (89.2%); [BF₄][−] (100%)^a The total amount (mol-%) of all C₆F₅ compounds was normalized to 100%.IV.12.2 Reaction of Molten [C₆F₅Xe][BF₄] with C₆F₅I at 140 °C

Iodopentafluorobenzene (**a**: 61.4 μL; 0.46 mmol, **b**: 64.0 μL; 0.48 mmol, and **c**: 72.0 μL; 0.54 mmol) was added to three samples of solid [C₆F₅Xe][BF₄] (**a**: 8.85 mg; 0.02 mmol; **b**: 9.09 mg; 0.02 mmol, and **c**: 10.33 mg; 0.03 mmol) in separate 5 mm glass NMR tubes (Wilmad 507) at RT. The three samples were warmed to 138 – 146 °C using an oil bath for 30 min. (**a**), 60 min. (**b**), and 120 min. (**c**). All samples were then cooled to 0 °C using an ice bath and quenched with liquid nitrogen (−196 °C) before being dissolved in CH₃CN and monitored by ¹⁹F NMR spectroscopy at RT.

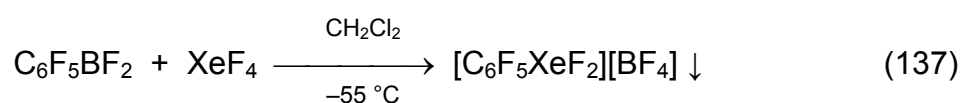
¹⁹F-NMR in CH₃CN after 30, 60 und 120 min. at 140 °C

[C ₆ F ₅ Xe] ⁺	δ = −124.9 ppm (m, <i>o</i> -C ₆ F ₅ , 2F); −141.5 ppm (tt, ³ J(¹⁹ F- ¹⁹ F) = 20 Hz, ⁴ J(¹⁹ F- ¹⁹ F) = 5 Hz, <i>p</i> -C ₆ F ₅ , 1F); −154.4 ppm (m, <i>m</i> -C ₆ F ₅ , 2F)
[BF ₄] [−]	δ = −149.1 ppm (s, 4F)
C ₆ F ₅ I	δ = −120.2 ppm (m, <i>o</i> -C ₆ F ₅ , 2F); −153.5 ppm (tt, ³ J(¹⁹ F- ¹⁹ F) = 20 Hz, ⁴ J(¹⁹ F- ¹⁹ F) = 2 Hz, <i>p</i> -C ₆ F ₅ , 1F); −160.3 ppm (m, <i>m</i> -C ₆ F ₅ , 2F)
[(C ₆ F ₅) ₂ I] ⁺	δ = −120.4 ppm (m, <i>o</i> -C ₆ F ₅ , 4F); −141.2 ppm (tt, ³ J(¹⁹ F- ¹⁹ F) = 20 Hz, ⁴ J(¹⁹ F- ¹⁹ F) = 6 Hz, <i>p</i> -C ₆ F ₅ , 2F); −155.4 ppm (m, <i>m</i> -C ₆ F ₅ , 4F)
C ₆ F ₆	δ = −163.0 ppm (s, Δ <i>v</i> _{1/2} = 1 Hz, 6F)

IV.13 ***Difluoropentafluorophenylxenon(IV) Compounds: Preparation, Characterization, and Physical Properties***

IV.13.1 *Difluoropentafluorophenylxenon(IV)tetrafluoroborate, [C₆F₅XeF₂][BF₄]*

IV.13.1.1 *Preparation of [C₆F₅XeF₂][BF₄]*



In a 23 mm i.d. FEP reaction tube containing an adequate magnetic stir bar, XeF₄ (0.21324 g; 1.03 mmol) was suspended in cold (−80 °C) CH₂Cl₂ (20 mL). The solubility of XeF₄ in CH₂Cl₂ at −55 °C was previously determined to ~20 μmol/mL. Accordingly ~40% of XeF₄ was dissolved. A freshly prepared, cold (−80 °C) C₆F₅BF₂ solution (1950 μL; 1.03 mmol) was transferred onto the XeF₄ suspension at −80 °C. The temperature was raised to −55 °C switching the cold bathes. A pale yellow, fluffy solid precipitated from the solution. The suspension was constantly stirred for 1 h at −55 °C, centrifuged at −80 °C and the CH₂Cl₂ mother liquor was separated. The pale yellow solid was dried under vacuum at temperatures below −55 °C yielding ochre coloured [C₆F₅XeF₂][BF₄] in almost quantitative yield. It was found that pure, dry [C₆F₅XeF₂][BF₄] is very shock sensitive, decomposing explosively to give mostly gaseous decomposition products.

The salt, [C₆F₅XeF₂][BF₄], is very soluble in CH₃CN and aHF. Such solutions have shown that by-products in the magnitude of ~6 mol-% are present in the isolated solid material.

IV.13.1.2 NMR Characterization

In aHF solution at $-80\text{ }^{\circ}\text{C}$

^{19}F NMR (282.40 MHz)

$[\text{C}_6\text{F}_5\text{XeF}_2]^+$ $\delta = -33.1$ ppm (s, ^{129}Xe -satellites: $^1J(^{19}\text{F}-^{129}\text{Xe}) = 3891$ Hz, RXeF_2 , 2F); -123.6 ppm (m, *o*- C_6F_5 , 2F); -129.3 ppm (tt, $^3J(^{19}\text{F}-^{19}\text{F}) = 18$ Hz, $^4J(^{19}\text{F}-^{19}\text{F}) = 9$ Hz, *p*- C_6F_5 , 1F); -150.4 ppm (m, *m*- C_6F_5 , 2F)

$[\text{BF}_4]^-$ $\delta = -148.3$ ppm (q, $^1J(^{11}\text{B}-^{19}\text{F}) = 12$ Hz, 4F)

C_6F_6 $\delta = -162.9$ ppm (s, $\Delta\nu_{1/2} = 4$ Hz, 6F)

aHF $\delta = -189.6$ ppm (s)

XeF_2 $\delta = -194.6$ ppm (s, ^{129}Xe -satellites: $^1J(^{19}\text{F}-^{129}\text{Xe}) = 5665$ Hz, 2F)

C_6F_5 -balance^a: $[\text{C}_6\text{F}_5\text{XeF}_2]^+$ (93.8%); C_6F_6 (6.2%)

xenon-balance^b: XeF_2 (7.2%); $[\text{C}_6\text{F}_5\text{XeF}_2]^+$ (92.8%)

Cation/anion ratio^c: $[\text{C}_6\text{F}_5\text{XeF}_2]^+$ (93.8%) / $[\text{BF}_4]^-$ (100%)

^a The total amount (mol-%) of all C_6F_5 compounds was normalized to 100%.

^b The xenon-balance was calculated from all C_6F_5 signal integrals of xenon containing compounds.

^c The cations, $[\text{C}_6\text{F}_5\text{XeF}_2]^+$ and $[\text{C}_6\text{F}_5\text{Xe}]^+$ were related to the $[\text{BF}_4]^-$ anion which was set to 100%.

^{11}B NMR (96.29 MHz)

$[\text{BF}_4]^-$ $\delta = -1.3$ ppm (qui, $^1J(^{11}\text{B}-^{19}\text{F}) = 11$ Hz)

^{129}Xe NMR (83.02 MHz)

$[\text{C}_6\text{F}_5\text{XeF}_2]^+$ $\delta = -1765.9$ ppm (t, $^1J(^{19}\text{F}-^{129}\text{Xe}) = 3894$ Hz)

XeF_2 $\delta = -1557.1$ ppm (t, $^1J(^{19}\text{F}-^{129}\text{Xe}) = 5665$ Hz)

* $[\text{C}_6\text{F}_5\text{Xe}]^+$ is not listed because it was out of the measuring range (-3814 ppm)

IV.13.1.3 Analysis of the *p*- C_6F_5 Signal of $[\text{C}_6\text{F}_5\text{XeF}_2][\text{BF}_4]$ in aHF at $-80\text{ }^{\circ}\text{C}$ Using 2D NMR Spectroscopy (SERF)

In a 3.5 mm i.d. FEP reaction tube, $[\text{C}_6\text{F}_5\text{XeF}_2][\text{BF}_4]$ was dissolved in cold ($-80\text{ }^{\circ}\text{C}$) aHF (500 μL) and the solution measured by ^{19}F NMR spectroscopy at $-80\text{ }^{\circ}\text{C}$. A homonuclear decoupling 2D NMR experiment (SERF) was performed to determine the coupling constants of the *p*- C_6F_5 signal of the $[\text{C}_6\text{F}_5\text{XeF}_2]^+$ cation. The XeF_2 moiety

was therefore decoupled and the *p*-C₆F₅ signal monitored showing a pseudo-septet structure (tt; ${}^3J(^{19}\text{F}-^{19}\text{F}) = 18$ Hz; ${}^4J(^{19}\text{F}-^{19}\text{F}) = 9$ Hz). The ${}^{19}\text{F}$ - ${}^{19}\text{F}$ coupling between the XeF₂ moiety and the *p*-C₆F₅ fluorines can be determined when comparing this spectrum with the undecoupled spectrum yielding a ${}^6J(^{19}\text{F}-^{19}\text{F})$ coupling constant of 9 Hz.

IV.13.1.4 Thermal Stability of [C₆F₅XeF₂][BF₄] in Solution and Suspension

in aHF at –30 °C

In a 3.5 mm i.d. FEP reaction tube, [C₆F₅XeF₂][BF₄], was dissolved in aHF (500 μL) at –80 °C and allowed to warm to –40 °C. The solution was measured by ${}^{19}\text{F}$ NMR spectroscopy at –80 °C to establish the initial condition. Subsequently, the solution was allowed to warm to –30 °C and maintained at –30 °C in a dryice acetone bath. The sample was monitored by ${}^{19}\text{F}$ NMR spectroscopy at –40 °C .

Initial spectrum for the thermal stability at –30 °C:

${}^{19}\text{F}$ NMR (282.40 MHz) in aHF at –80 °C

[C₆F₅XeF₂]⁺ δ = –33.1 ppm (s, Δ $v_{1/2}$ = 15 Hz, ${}^{129}\text{Xe}$ -satellites: ${}^1J(^{19}\text{F}-{}^{129}\text{Xe}) = 3903$ Hz, 2F); –123.5 ppm (m, *o*-C₆F₅, 2F); –129.2 ppm (tt, ${}^3J(^{19}\text{F}-^{19}\text{F}) = 18$ Hz, ${}^4J(^{19}\text{F}-^{19}\text{F}) = 9$ Hz, *p*-C₆F₅, 1F); –151.8 ppm (m, *m*-C₆F₅, 2F)

[C₆F₅Xe]⁺ δ = –123.7 ppm (m, *o*-C₆F₅, 2F); –138.4 ppm (tt, ${}^3J(^{19}\text{F}-^{19}\text{F}) = 20$ Hz, ${}^4J(^{19}\text{F}-^{19}\text{F}) = 5$ Hz, *p*-C₆F₅, 1F); –151.8 ppm (m, *m*-C₆F₅, 2F)

[BF₄][–] δ = –148.5 ppm (q, ${}^1J(^{11}\text{B}-^{19}\text{F}) = 12$ Hz, 4F)

C₆F₆ δ = –162.8 ppm (s, Δ $v_{1/2}$ = 3 Hz, 6F)

HF δ = –189.7 ppm (s, Δ $v_{1/2}$ = 21 Hz, 1F)

C₆F₅-Bilanz ^a: [C₆F₅XeF₂]⁺ (93.1 %); [C₆F₅Xe]⁺ (6.1 %); C₆F₆ (0.8 %)

Xe-Bilanz ^b: [C₆F₅XeF₂]⁺ (93.8 %); [C₆F₅Xe]⁺ (6.2 %)

Kation/Anion ratio ^c: 1 : 1.1

^a The total amount (mol-%) of all C₆F₅ compounds was normalized to 100%.

^b The xenon-balance was calculated from all C₆F₅ signal integrals of xenon containing compounds.

^c The cations, [C₆F₅XeF₂]⁺ and [C₆F₅Xe]⁺, were related to the [BF₄][–] anion which was set to 100%.

^{11}B -NMR (96.29 MHz) in aHF at $-80\text{ }^\circ\text{C}$

$[\text{BF}_4]^-$ $\delta = -4.4\text{ ppm}$ (qui, $^1J(^{11}\text{B}-^{19}\text{F}) = 12\text{ Hz}$)

Decomposition of $[\text{C}_6\text{F}_5\text{XeF}_2][\text{BF}_4]$ in aHF at $-30\text{ }^\circ\text{C}$

Zeit [d]	$[\text{C}_6\text{F}_5\text{XeF}_2]^+ \text{ a,b}$	$[\text{C}_6\text{F}_5\text{Xe}]^+ \text{ a,b}$	$[\text{C}_6\text{F}_7\text{Xe}]^+ \text{ a}$	$\text{C}_6\text{F}_6 \text{ a}$	$\text{c-C}_6\text{F}_8\text{-1,4} \text{ a}$	$\text{XeF}_2 \text{ b}$
	I) $\text{C}_6\text{F}_5\text{-bal.}$ [mol-%]	I) $\text{C}_6\text{F}_5\text{-bal.}$ [mol-%]	I) $\text{C}_6\text{F}_5\text{-bal.}$ [mol-%]	I) $\text{C}_6\text{F}_5\text{-bal.}$ [mol-%]	I) $\text{C}_6\text{F}_5\text{-bal.}$ [mol-%]	I) $\text{C}_6\text{F}_5\text{-bal.}$ [mol-%]
40 min	I) 79.0	I) 8.4	I) 0	I) 12.6	I) 0	I) 12.6
	II) 78.7	II) 8.4	II) 0			II) 12.9
1	I) 68.0	I) 7.2	I) 0	I) 24.8	I) 0	I) 24.2
	II) 68.4	II) 7.3	II) 0			II) 24.4
2	I) 42.9	I) 8.3	Spuren	I) 46.3	I) 1.2	I) 48.8
	II) 43.0	II) 8.3				II) 48.7
3	I) 28.9	I) 15.2	I) 1.8	I) 0	I) 54.1	I) 0
	II) 62.8	II) 33.1	II) 4.1			II) 0
3*	I) 21.8	I) 20.0	I) 0	I) 0	I) 58.2	I) 0
	II) 52.2	II) 47.8	II) 0			II) 0
4	I) 0	I) 36.8	I) 6.6	I) 0	I) 56.6	I) 0
	II) 0	II) 84.7	II) 15.3			II) 0

^a The total amount (mol-%) of all C_6F_5 compounds was normalized to 100%.

^b The xenon-balance was calculated from all C_6F_5 signal integrals of xenon containing compounds.

* Sample was stored for 13 h at $-80\text{ }^\circ\text{C}$ in a glass trap protected by argon.

Initial spectrum

^{19}F NMR (282.40 MHz) in aHF at $-40\text{ }^\circ\text{C}$

$[\text{C}_6\text{F}_5\text{XeF}_2]^+$ $\delta = -32.6\text{ ppm}$ (s, $\Delta\nu_{1/2} = 15\text{ Hz}$, ^{129}Xe -satellites: $^1J(^{19}\text{F}-^{129}\text{Xe}) = 3891\text{ Hz}$, 2F); -123.4 ppm (m, $o\text{-C}_6\text{F}_5$, 2F); -128.6 ppm (tt, $^3J(^{19}\text{F}-^{19}\text{F}) = 18\text{ Hz}$, $^4J(^{19}\text{F}-^{19}\text{F}) = 9\text{ Hz}$, $p\text{-C}_6\text{F}_5$, 1F); -150.1 ppm (m, $m\text{-C}_6\text{F}_5$, 2F)

$[\text{BF}_4]^-$ $\delta = -148.6\text{ ppm}$ (q, $^1J(^{11}\text{B}-^{19}\text{F}) = 12\text{ Hz}$, $^{11}\text{BF}_4$, 4F)

C_6F_6^* $\delta = -162.9\text{ ppm}$ (s, $\Delta\nu_{1/2} = 4\text{ Hz}$, 6F)

$\text{c-C}_6\text{F}_8\text{-1,4}$ $\delta = -111.3\text{ ppm}$ (tm, $J = 10\text{ Hz}$, 4F); -156.0 ppm (tm, $J = 10\text{ Hz}$, 4F)

aHF $\delta = -191.1\text{ ppm}$ (s)

XeF₂ $\delta = -195.3$ ppm (s, ¹²⁹Xe-satellites: ¹J(¹⁹F-¹²⁹Xe) = 5665 Hz, 2F)

C₆F₅-balance^a: [C₆F₅XeF₂]⁺ (89.4%); c-C₆F₈-1,4 (1.5%); C₆F₆ (9.1%)

xenon-balance^b: XeF₂ (10.7%); [C₆F₅XeF₂]⁺ (89.3%)

Cation/anion ratio^c: [C₆F₅XeF₂]⁺ (80.4%) / [BF₄]⁻ (100%)

^a The total amount (mol-%) of all C₆F₅ compounds was normalized to 100%.

^b The xenon-balance was calculated from all C₆F₅ signal integrals of xenon containing compounds.

^c The cation, [C₆F₅XeF₂]⁺, was related to the [BF₄]⁻ anion which was set to 100%.

* C₆F₆ was taken as internal standard (-192.9 ppm)

in aHF at -40 °C

In a 3.5 mm i.d. FEP reaction tube, [C₆F₅XeF₂][BF₄] was dissolved in aHF at -80 °C and allowed to warm to -40 °C. The yellow solution was maintained at -40 °C in a cryostat inside a glass trap protected by argon gas and was monitored periodically by ¹⁹F NMR spectroscopy at -40 °C. The initial conditions were the same than those in aHF solution at -30 °C.

Decomposition of [C₆F₅XeF₂][BF₄] in aHF at -40 °C

time [d]	[C ₆ F ₅ XeF ₂] ^{+ a,b}	[C ₆ F ₅ Xe] ^{+ a,b}	XeF ₂ ^b	C ₆ F ₆ ^a	c-C ₆ F ₈ -1,4 ^a	c-C ₆ F ₁₀ ^a
	I) C ₆ F ₅ -bal.	I) C ₆ F ₅ -bal.	I) C ₆ F ₅ -bal.	I) C ₆ F ₅ -bal.	I) C ₆ F ₅ -bal.	I) C ₆ F ₅ -bal.
	II) Xe-bal.	II) Xe-bal.	II) Xe-bal.			
	[mol-%]	[mol-%]	[mol-%]	[mol-%]	[mol-%]	[mol-%]
4	I) 50.8	I) 7.6	I) 15.2	I) 17.1	I) 24.5	I) 0.0
	II) 69.1	II) 10.3	II) 20.6			
7	I) 42.5	I) 8.1	I) 14.5	I) 18.7	I) 30.8	I) 0.0
	II) 65.4	II) 12.4	II) 22.2			
14	I) 39.9	I) 7.3	I) 19.6	I) 22.9	I) 29.9	I) 0.0
	II) 59.9	II) 10.9	II) 29.2			
22	I) 35.8	I) 6.6	I) 23.4	I) 28.2	I) 29.4	I) 0.0
	II) 54.5	II) 10.0	II) 35.5			
28	I) 32.3	I) 7.5	I) 26.7	I) 31.6	I) 28.6	I) 0.0
	II) 48.5	II) 11.3	II) 40.2			
42	I) 15.9	I) 6.1	I) 28.3	I) 35.4	I) 39.0	I) 3.6
	II) 31.7	II) 12.1	II) 56.2			

Table (continued...)

45	I) 11.6	I) 5.2	I) 31.8	I) 33.8	I) 45.5	I) 3.9
	II) 24.0	II) 10.7	II) 65.4			
50	I) 11.2	I) 5.9	I) 29.4	I) 37.0	I) 40.8	I) 5.0
	II) 24.1	II) 12.7	II) 63.2			
60	I) 8.1	I) 6.2	I) 26.6	I) 34.8	I) 43.5	I) 7.4
	II) 19.9	II) 15.1	II) 65.0			
67	I) 6.7	I) 6.3	I) 30.6	I) 34.2	I) 43.4	I) 9.4
	II) 15.1	II) 14.5	II) 70.4			
74	I) 5.7	I) 5.7	I) 42.9	I) 33.6	I) 45.6	I) 9.4
	II) 10.5	II) 10.5	II) 79.0			
81	I) 4.8	I) 5.4	I) 19.2	I) 34.8	I) 45.1	I) 9.9
	II) 16.1	II) 18.4	II) 65.5			
88	I) 4.5	I) 6.3	I) 19.0	I) 33.5	I) 44.6	I) 11.1
	II) 14.8	II) 21.2	II) 63.9			

^a The total amount (mol-%) of all C₆F₅ compounds was normalized to 100%.

^b The xenon-balance was calculated from all C₆F₅ signal integrals of xenon containing compounds.

In aHF at –80 °C

In a 3.5 mm i.d. FEP reaction tube, [C₆F₅XeF₂][BF₄] was dissolved in cold (–80 °C) aHF (500 μL). The solution was periodically monitored by ¹⁹F NMR spectroscopy at –80 °C to establish the initial condition. The sample was maintained at –80 °C in a dryice bath inside a glass trap protected by argon gas for 18 d. No significant decomposition was observed.

Initial spectrum

¹⁹F NMR (282.40 MHz) in aHF at –80 °C

[C₆F₅XeF₂]⁺ δ = –33.1 ppm (s, Δ_v^{1/2} = 15 Hz, ¹²⁹Xe-satellites: ¹J(¹⁹F-¹²⁹Xe) = 3891 Hz, 2F); –123.6 ppm (m, *o*-C₆F₅, 2F); –129.3 ppm (tt, ³J(¹⁹F-¹⁹F) = 18 Hz, ⁴J(¹⁹F-¹⁹F) = 9 Hz, *p*-C₆F₅, 1F); –150.4 ppm (m, *m*-C₆F₅, 2F)

[BF₄][–] δ = –148.3 ppm (q, ¹J(¹¹B-¹⁹F) = 12 Hz, ¹¹BF₄, 4F)

C₆F₆^{*} δ = –162.9 ppm (s, Δ_v^{1/2} = 4 Hz, 6F)

aHF δ = –189.6 ppm (s)

XeF₂ $\delta = -194.6$ ppm (s, ¹²⁹Xe-satellites: ¹J(¹⁹F-¹²⁹Xe) = 5665 Hz, 2F)
 C₆F₅-balance^a: [C₆F₅XeF₂]⁺ (93.8%); C₆F₆ (6.2%)
 xenon-balance^b: XeF₂ (7.2%); [C₆F₅XeF₂]⁺ (92.8%)
 Cation/anion ratio^c: [C₆F₅XeF₂]⁺ (93.8%) / [BF₄]⁻ (100%)

¹⁹F NMR (282.40 MHz) after 4 d in aHF at -40 °C

c-C₆F₈-1,4 $\delta = -111.3$ ppm (tm, *J* = 10 Hz, 4F); -156.0 ppm (tm, *J* = 10 Hz, 4F)

C₆F₅-balance^a: [C₆F₅XeF₂]⁺ (89.4%); c-C₆F₈-1,4 (1.5%); C₆F₆ (9.1%)
 xenon-balance^b: XeF₂ (10.7%); [C₆F₅XeF₂]⁺ (89.3%)
 Cation/anion ratio^c: [C₆F₅XeF₂]⁺ (80.4%) / [BF₄]⁻ (100%)

^a The total amount (mol-%) of all C₆F₅ compounds was normalized to 100%.

^b The xenon-balance was calculated from all C₆F₅ signal integrals of xenon containing compounds.

^c The cations, [C₆F₅XeF₂]⁺, was related to the [BF₄]⁻ anion which was set to 100%.

* C₆F₆ was taken as internal standard (-162.9 ppm)

in aHF at ambient temperature

The aHF solution which was maintained for 4 d at -80 °C was subsequently allowed to warm to RT and maintained for 5 min. Strong gas evolution proceeded and white needle shaped crystals precipitated from the solution while cooling the sample to -40 °C. The suspension was checked by NMR spectroscopy at -40 °C.

¹⁹F NMR (282.40 MHz) in aHF bei -40 °C (SR = -1202.04*)

C₆F₅-balance^a: [C₆F₅Xe]⁺ (25.2%); C₆F₆ (8.9%); c-C₆F₈-1,4 (65.9%)
 xenon-balance^b: [C₆F₅Xe]⁺ (100%)

^a The total amount (mol-%) of all C₆F₅ compounds was normalized to 100%.

^b The xenon-balance was calculated from all C₆F₅ signal integrals of xenon containing compounds.

* C₆F₆ was taken as internal standard (-192.9 ppm)

No [BF₄]⁻ signal was observed but unexpectedly, CH₂F₂ ($\delta = -141.3$ ppm (t, ³J(¹⁹F-¹⁹F) = 50 Hz, 2F)) was detected. The sample was allowed to warm to -10 °C to dissolve the white precipitate. The only change in the NMR spectrum was the amount of c-C₆F₈-1,4 which rose from 65.9 to 86.5% supporting the assumption that the precipitate was undissolved c-C₆F₈-1,4.

in CH₂Cl₂ at –80 °C

In a 8 mm i.d. FEP reaction tube, a small amount of [C₆F₅XeF₂][BF₄] was suspended in CH₂Cl₂ (500 μL) at –80 °C. The suspension was allowed to warm to RT whereupon [C₆F₅XeF₂][BF₄] reacted very heavily with CH₂Cl₂ under gas evolution. The clear and colourless solution was then checked by ¹⁹F NMR spectroscopy at –40 °C showing the following product contribution: C₆F₅H (58.3 %), C₆F₅Cl (11.4 %), C₆F₆ (30.3 %), CHF₃ (7.3 %), CH₂ClF (32.6 %), CH₂F₂ (78.3 %), and HF (74.6 %). The sum of C₆F₅ compounds was set to 100 % and non-C₆F₅ compounds were calculated on the base of C₆F₅.

In CH₃CN at –40 °C

In a 3.5 mm i.d. FEP reaction tube, [C₆F₅XeF₂][BF₄], was dissolved in cold (–40 °C) CH₃CN (2000 μL). The solution was divided among three FEP reaction tubes and one sample was checked by ¹⁹F NMR spectroscopy to establish the initial condition. The sample was maintained at –40 °C in a cryostat inside a glass trap protected by argon gas and was periodically monitored by ¹⁹F NMR spectroscopy at –40 °C.

Initial spectrum

¹⁹F NMR (282.40 MHz) in CH₃CN at –40 °C

[C ₆ F ₅ XeF ₂] ⁺	δ = –27.7 ppm (s, ¹²⁹ Xe-satellites: ¹ J(¹⁹ F- ¹²⁹ Xe) = 3910 Hz, 2F); –124.1 ppm (m, <i>o</i> -C ₆ F ₅ , 2F); –133.9 ppm (t, ³ J(¹⁹ F- ¹⁹ F) = 20 Hz, <i>p</i> -C ₆ F ₅ , 1F); –154.3 ppm (m, <i>m</i> -C ₆ F ₅ , 2F)
[C ₆ F ₅ Xe] ⁺	δ = –124.7 ppm (m, <i>o</i> -C ₆ F ₅ , 2F); –141.5 ppm (t, ³ J(¹⁹ F- ¹⁹ F) = 18 Hz, <i>p</i> -C ₆ F ₅ , 1F); –154.3 ppm (m, <i>m</i> -C ₆ F ₅ , 2F)
[BF ₄] [–]	δ = –147.1 ppm (s, Δ <i>v</i> _{1/2} = 4 Hz, ¹¹ BF ₄ , 4F)
C ₆ F ₆	δ = –162.1 ppm (s, Δ <i>v</i> _{1/2} = 5 Hz, 6F)
XeF ₂	δ = –177.5 ppm (s, ¹²⁹ Xe-satellites: ¹ J(¹⁹ F- ¹²⁹ Xe) = 5671 Hz, 2F)
CH ₃ CN·HF	δ = –179.0 ppm (d, ¹ J(¹ H- ¹⁹ F) = 470Hz, 1F)

¹¹B NMR (96.29 MHz) in CH₃CN at –40 °C

[BF ₄] [–]	δ = –0.6 ppm (s, Δ <i>v</i> _{1/2} = 2 Hz)
---------------------------------	--

¹²⁹Xe NMR (83.02 MHz) in CH₃CN at –40 °C

[C ₆ F ₅ XeF ₂] ⁺	δ = –1701.3 ppm (t, ¹ J(¹⁹ F- ¹²⁹ Xe) = 3881 Hz)
XeF ₂	δ = –1557.1 ppm (t, ¹ J(¹⁹ F- ¹²⁹ Xe) = 5670 Hz)

Decomposition of $[\text{C}_6\text{F}_5\text{XeF}_2][\text{BF}_4]$ in CH_3CN at $-40\text{ }^\circ\text{C}$ ^a

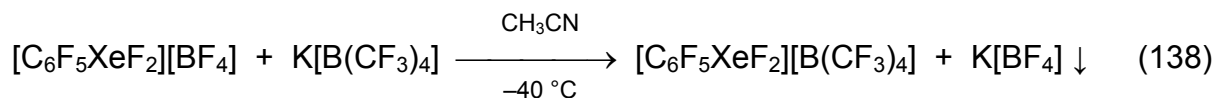
Time [h]	$[\text{C}_6\text{F}_5\text{XeF}_2]^+ \text{ }^{a,b}$	$[\text{C}_6\text{F}_5\text{Xe}]^+ \text{ }^{a,b}$	$\text{XeF}_2 \text{ }^b$	$\text{C}_6\text{F}_6 \text{ }^a$
	I) C_6F_5 -balance II) Xe-balance [mol-%]	I) C_6F_5 -balance II) Xe-balance [mol-%]	I) C_6F_5 -balance II) Xe-balance [mol-%]	I) C_6F_5 -balance [mol-%]
30 min	I) 89.4	I) 6.7	I) 3.0	I) 0.8
	II) 90.2	II) 6.8	II) 3.1	
4	I) 85.3	I) 11.5	I) 4.3	I) 0.8
	II) 84.3	II) 11.4	II) 4.3	
20	I) 75.8	I) 22.2	I) 1.0	I) 1.9
	II) 76.5	II) 22.4	II) 1.1	
44	I) 78.5	I) 19.6	I) 1.8	I) 1.8
	II) 78.6	II) 19.6	II) 1.8	
68	I) 74.4	I) 23.2	I) 3.9	I) 2.4
	II) 73.3	II) 22.9	II) 3.8	
140	I) 59.6	I) 35.4	I) 12.0	I) 4.9
	II) 55.7	II) 33.1	II) 11.2	
168	I) 55.8	I) 38.6	I) 13.7	I) 5.6
	II) 51.6	II) 35.7	II) 12.6	
192	I) 51.1	I) 42.5	I) 16.4	I) 6.3
	II) 46.4	II) 38.6	II) 14.6	
264	I) 44.6	I) 48.0	I) 18.6	I) 7.4
	II) 40.1	II) 43.2	II) 16.7	
336	I) 35.4	I) 55.6	I) 22.6	I) 8.9
	II) 31.2	II) 48.9	II) 19.9	
408	I) 30.1	I) 60.2	I) 24.6	I) 9.6
	II) 26.2	II) 52.4	II) 21.4	
600	I) 13.9	I) 74.2	I) 29.9	I) 11.9
	II) 11.8	II) 62.8	II) 26.8	
1410	I) 0.0	I) 100.0	I) 36.5	I) 0.0
	II) 0.0	II) 73.2	II) 26.8	

^a The total amount (mol-%) of all C_6F_5 compounds was normalized to 100%.

^b The xenon-balance was calculated from all C_6F_5 signal integrals of xenon containing compounds.

IV.13.2 *Difluoropentafluorophenylxenon(IV)*
tetrakis(trifluoromethyl)borate, $[C_6F_5XeF_2][B(CF_3)_4]$

IV.13.2.1 *Metathesis*



In a 3.5 mm i.d. FEP reaction tube, $K[B(CF_3)_4]$ (90.70 mg; 0.28 mmol) was dried under vacuum for 1 h at RT and subsequently dissolved in CH_3CN (500 μ L). This solution was cooled ($-40\text{ }^\circ\text{C}$), added to a freshly prepared cold ($-40\text{ }^\circ\text{C}$) $[C_6F_5XeF_2][BF_4]/CH_3CN$ solution and was maintained at $-40\text{ }^\circ\text{C}$ for 15 min. The ^{19}F NMR spectrum of the resulting suspension was recorded at $-40\text{ }^\circ\text{C}$.

^{19}F -NMR (282.40 MHz) in CH_3CN bei $-40\text{ }^\circ\text{C}$

$[B(CF_3)_4]^-$ $\delta = -61.0$ ppm (q, $^2J(^{11}\text{B}-^{19}\text{F}) = 26$ Hz; sep, $^2J(^{10}\text{B}-^{19}\text{F}) = 9$ Hz, 12F)

$[C_6F_5XeF_2]^+$ $\delta = -23.1$ ppm (s, ^{129}Xe -satellites: $^1J(^{19}\text{F}-^{129}\text{Xe}) = 3877$ Hz, 2F);
 -124.0 ppm (m, *o*- C_6F_5 , 2F); -134.2 ppm (t, *p*- C_6F_5 , 1F); -151.9
 ppm (m, *m*- C_6F_5 , 2F)

$[C_6F_5Xe]^+$ $\delta = -124.6$ ppm (m, *o*- C_6F_5 , 2F); -140.7 ppm (tt, $^3J(^{19}\text{F}-^{19}\text{F}) = 20$ Hz,
 $^4J(^{19}\text{F}-^{19}\text{F}) = 5$ Hz, *p*- C_6F_5 , 1F); -153.6 ppm (m, *m*- C_6F_5 , 2F)

C_6F_5H $\delta = -138.6$ ppm (m, *o*- C_6F_5 , 2F); -154.0 ppm (t, $^3J(^{19}\text{F}-^{19}\text{F}) = 21$ Hz,
p- C_6F_5 , 1F); -161.8 ppm (m, *m*- C_6F_5 , 2F)

C_6F_6 $\delta = -162.2$ ppm (s, 6F)

XeF_2 $\delta = -177.8$ ppm (s, ^{129}Xe -satellites: $^1J(^{19}\text{F}-^{129}\text{Xe}) = 5638$ Hz, 2F)

$CH_3CN \cdot HF$ $\delta = -178.3$ ppm (d, $^1J(^1\text{H}-^{19}\text{F}) = 480$ Hz, 1F)

C_6F_5 -balance^a: $[C_6F_5XeF_2]^+$ (79.9%); $[C_6F_5Xe]^+$ (15.0%); $[C_6F_5BF_3]^-$ (4.1%); C_6F_6
 (1.0%)

xenon-balance^b: XeF_2 (5.1%); $[C_6F_5XeF_2]^+$ (79.9%); $[C_6F_5Xe]^+$ (15.0%)

Cation/anion ratio^c: cations (49.2%) / $[B(CF_3)_4]^-$ (100%)

^a The total amount (mol-%) of all C_6F_5 compounds was normalized to 100%.

^b The xenon-balance was calculated from all C_6F_5 signal integrals of xenon containing compounds.

^c The cations, $[C_6F_5XeF_2]^+$ and $[C_6F_5Xe]^+$, were related to the $[B(CF_3)_4]^-$ anion which was set to 100%. The amount of $[B(CF_3)_4]^-$ belongs not only to the counteranion from $[C_6F_5XeF_2]^+$ and $[C_6F_5Xe]^+$ but also to the excess of $K[B(CF_3)_4]$.

IV.13.2.2 Thermal Stability of $[C_6F_5XeF_2][B(CF_3)_4]$ in Solution

In CH_3CN at $-40\text{ }^\circ\text{C}$

A cold ($-40\text{ }^\circ\text{C}$) CH_3CN solution of $[C_6F_5XeF_2][B(CF_3)_4]$ was transferred into a 8 mm i.d. FEP reaction tube and concentrated under vacuum ($\sim 10^{-2}$ mbar) for 1 h at temperatures below $-35\text{ }^\circ\text{C}$. The residual CH_3CN solution was divided into two equal samples which were transferred into two 3.5 mm i.d. FEP reaction tubes. Both samples were maintained frozen overnight at $-80\text{ }^\circ\text{C}$ inside a glass trap protected by argon until the ^{19}F NMR spectra could be run.

One sample was warmed to $-40\text{ }^\circ\text{C}$ and its thermal stability was periodically monitored by NMR spectroscopy at $-40\text{ }^\circ\text{C}$

^{19}F NMR (282.40 MHz) in CH_3CN at $-40\text{ }^\circ\text{C}$

$C_6F_5CF_3$ $\delta = -139.5$ ppm (m, *o*- C_6F_5 , 2F); -145.7 ppm (t, $^3J(^{19}\text{F}-^{19}\text{F}) = 21$ Hz, *p*- C_6F_5 , 1F); -155.5 ppm (m, *m*- C_6F_5 , 2F)

C_6F_5 -balance^a: $[C_6F_5XeF_2]^+$ (21.1%); $[C_6F_5Xe]^+$ (54.0%); C_6F_5H (10.5%); $C_6F_5CF_3$ (7.7%); C_6F_6 (6.7%)

xenon-balance^b: XeF_2 (24.7%); $[C_6F_5XeF_2]^+$ (21.2%); $[C_6F_5Xe]^+$ (54.1%)

Cation/anion ratio^c: cations (35.9%) / $[B(CF_3)_4]^-$ (100%)

^a The total amount (mol-%) of all C_6F_5 compounds was normalized to 100%.

^b The xenon-balance was calculated from all C_6F_5 signal integrals of xenon containing compounds.

^c The cations, $[C_6F_5XeF_2]^+$ and $[C_6F_5Xe]^+$, were related to the $[B(CF_3)_4]^-$ anion which was set to 100%. The amount of $[B(CF_3)_4]^-$ belongs not only to the counteranion from $[C_6F_5XeF_2]^+$ and $[C_6F_5Xe]^+$ but also to the excess of $K[B(CF_3)_4]$.

^{11}B NMR (96.29 MHz) in CH_3CN at $-40\text{ }^\circ\text{C}$

$[B(CF_3)_4]^-$ $\delta = -18.6$ ppm (tridec, $^2J(^{11}\text{B}-^{19}\text{F}) = 26$ Hz, 1B)

Decomposition of $[\text{C}_6\text{F}_5\text{XeF}_2][\text{B}(\text{CF}_3)_4]$ in CH_3CN at $-40\text{ }^\circ\text{C}$

time [d]	$[\text{C}_6\text{F}_5\text{XeF}_2]^{\text{a,b}}$	$[\text{C}_6\text{F}_5\text{Xe}]^{\text{a,b}}$	$\text{C}_6\text{F}_5\text{H}^{\text{a}}$	$\text{C}_6\text{F}_5\text{CF}_3^{\text{a}}$	$\text{C}_6\text{F}_6^{\text{a}}$	XeF_2^{b}
	I) C_6F_5 -bal. II) Xe-bal.	I) C_6F_5 -bal. II) Xe-bal.	I) C_6F_5 -bal.	I) C_6F_5 -bal.	I) C_6F_5 -bal.	I) C_6F_5 -bal. II) Xe-bal.
	[mol-%]	[mol-%]	[mol-%]	[mol-%]	[mol-%]	[mol-%]
~1.5 h	I) 21.1 II) 21.2	I) 54.0 II) 54.1	I) 10.5	I) 7.7	I) 6.7	I) 24.7 II) 24.7
	I) 15.8 II) 15.6	I) 56.7 II) 55.5	I) 11.1	I) 7.7	I) 8.7	I) 29.3 II) 28.9
1 ^c	I) 11.2 II) 12.3	I) 52.8 II) 57.9	I) 10.8	I) 18.4	I) 6.8	I) 26.4 II) 29.8
	I) 0.0 II) 0.0	I) 69.3 II) 65.8	I) 15.0	I) 7.4	I) 8.3	I) 36.0 II) 34.2

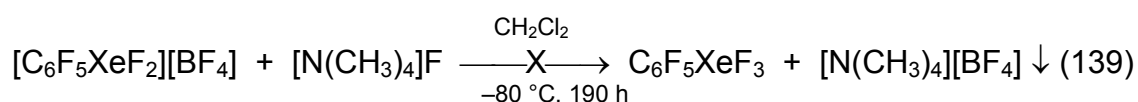
^a The total amount (mol-%) of all C_6F_5 compounds was normalized to 100%.

^b The xenon-balance was calculated from all C_6F_5 signal integrals of xenon containing compounds.

^c The sample was additionally maintained frozen ($-80\text{ }^\circ\text{C}$) for 3 d

^d The sample was additionally maintained frozen ($-80\text{ }^\circ\text{C}$) for 6 d

IV.13.3 Reaction of $[\text{C}_6\text{F}_5\text{XeF}_2][\text{BF}_4]$ with $[\text{N}(\text{CH}_3)_4]\text{F}$ in CH_2Cl_2 at $-80\text{ }^\circ\text{C}$ and $\text{CH}_2\text{Cl}_2/\text{CH}_3\text{CN}$ at $-40\text{ }^\circ\text{C}$



A cold ($-40\text{ }^\circ\text{C}$) CH_3CN solution of $[\text{C}_6\text{F}_5\text{XeF}_2][\text{BF}_4]$ from a former preparation was transferred into a 8 mm i.d. FEP reaction tube and the CH_3CN was removed under dynamic vacuum at temperatures below $-35\text{ }^\circ\text{C}$. The pale ochre coloured solid was subsequently suspended in cold ($-80\text{ }^\circ\text{C}$) CH_2Cl_2 (1000 μL) before a solution of $[\text{N}(\text{CH}_3)_4]\text{F}$ (29.79 mg; 0.32 mmol) in cold ($-80\text{ }^\circ\text{C}$) CH_2Cl_2 (770 μL) was added. The reaction was monitored by NMR spectroscopy at $-80\text{ }^\circ\text{C}$. After 46 h at $-80\text{ }^\circ\text{C}$, $\text{C}_6\text{F}_5\text{H}$ (64%), $\text{C}_6\text{F}_5\text{Y}$ (29%) ($\delta = -129.3$ ppm (m, *o*- C_6F_5 , 2F); -128.6 ppm (tt, $^3J(^{19}\text{F}-^{19}\text{F}) = 18$ Hz, $^4J(^{19}\text{F}-^{19}\text{F}) = 9$ Hz, *p*- C_6F_5 , 1F); -150.1 ppm (m, *m*- C_6F_5 , 2F), C_6F_6 (7%) were detected in addition to a more intense “doublet” at -146.9 ppm. The ^{11}B NMR

spectrum showed no resonances in the range between +50 and –50 ppm. After 190 h at –80 °C cold (–40 °C) CH₃CN (100 μL; 1.91 mmol; 10 equivalents per [C₆F₅XeF₂]⁺) was added. The solution turned deep orange and all solid material dissolved. The solution was checked by NMR spectroscopy gave the following C₆F₅ balance: C₆F₅XeF (54.6%), [C₆F₅Xe]⁺ (7.2%), C₆F₅H (22.4%), C₆F₅Cl (10.3%), and C₆F₆ (5.5%). Beside those compounds XeF₂ (11.6%) and [BF₄][–] (2.3%) were detected.

IV.13.4 Reaction of [C₆F₅XeF₂][BF₄] with KF (3-Fold Molar Excess) in aHF at –30 and –40 °C

In a 23 mm i.d. FEP reaction tube, [C₆F₅XeF₂][BF₄] (~300 mg), was dissolved in cold (–80 °C) aHF (3.5 mL). The solution was divided among three 3.5 mm i.d. FEP reaction tubes (each 500 μL) (**a**, **b** and **c**) and one 7.8 mm i.d. FEP reaction tube (~2000 μL). The 7.8 mm i.d. FEP reaction tube was used for a different experiment. One sample (**a**) was checked by ¹⁹F NMR spectroscopy to establish the initial condition.

Initial spectrum

¹⁹F NMR (282.40 MHz) in aHF at –80 °C

[C₆F₅XeF₂]⁺ δ = –33.1 ppm (s, Δv_{1/2} = 15 Hz, ¹²⁹Xe-satellites: ¹J(¹⁹F-¹²⁹Xe) = 3905 Hz, 2F); –123.5 ppm (m, *o*-C₆F₅, 2F); –129.2 ppm (tt, ³J(¹⁹F-¹⁹F) = 18 Hz, ⁴J(¹⁹F-¹⁹F) = 9 Hz, *p*-C₆F₅, 1F); –151.8 ppm (m, *m*-C₆F₅, 2F)

[C₆F₅Xe]⁺ δ = –123.7 ppm (m, *o*-C₆F₅, 2F); –138.4 ppm (tt, ³J(¹⁹F-¹⁹F) = 21 Hz, ⁴J(¹⁹F-¹⁹F) = 5 Hz, *p*-C₆F₅, 1F); –151.8 ppm (m, *m*-C₆F₅, 2F)

[BF₄][–] δ = –148.5 ppm (q, ¹J(¹¹B-¹⁹F) = 12 Hz, 4F)

C₆F₆ δ = –162.8 ppm (s, Δv_{1/2} = 3 Hz, 6F)

HF δ = –189.7 ppm (s, Δv_{1/2} = 21 Hz, 1F)

C₆F₅-Bilanz ^a: [C₆F₅XeF₂]⁺ (93.1 %); [C₆F₅Xe]⁺ (6.1 %); C₆F₆ (0.8 %)

Xe-Bilanz ^b: [C₆F₅XeF₂]⁺ (93.8 %); [C₆F₅Xe]⁺ (6.2 %)

Cation/anion ratio^c: 1 : 1.1

^a The total amount (mol-%) of all C₆F₅ compounds was normalized to 100%.

^b The xenon-balance was calculated from all C₆F₅ signal integrals of xenon containing compounds.

^c The cations, [C₆F₅XeF₂]⁺ and [C₆F₅Xe]⁺, were related to the [BF₄][–] anion which was set to 100%.

^{11}B -NMR (96.29 MHz) in aHF at $-80\text{ }^\circ\text{C}$

$[\text{BF}_4]^-$ $\delta = -1.4\text{ ppm}$ (qui, $^1J(^{11}\text{B}-^{19}\text{F}) = 12\text{ Hz}$)

In the drybox, spray-dried KF was loaded in two 3.5 mm i.d. FEP reaction tubes (I) 19.77 mg, 0.34 mmol; II) 18.24 mg, 0.31 mmol) and dissolved in cold ($-80\text{ }^\circ\text{C}$) aHF (300 μL). The solutions were transferred to sample **a** and **b** at $-80\text{ }^\circ\text{C}$, respectively. Sample **a** was warmed to $-40\text{ }^\circ\text{C}$ and sample **b** was warmed to $-30\text{ }^\circ\text{C}$. Both samples were periodically monitored by ^{19}F NMR spectroscopy at $-40\text{ }^\circ\text{C}$.

b) Composition of Reactants and Products Resulting from the Reaction of $[\text{C}_6\text{F}_5\text{XeF}_2][\text{BF}_4]$ with KF in aHF at $-30\text{ }^\circ\text{C}$

Zeit [h]	$[\text{C}_6\text{F}_5\text{XeF}_2]^+ \text{ }^{a,b}$	$[\text{C}_6\text{F}_5\text{Xe}]^+ \text{ }^{a,b}$	$\text{C}_6\text{F}_6 \text{ }^a$	c- $\text{C}_6\text{F}_{10} \text{ }^a$	$\text{XeF}_2 \text{ }^b$	$[\text{BF}_4]^- \text{ }^c$
	I) C_6F_5 -bal. II) Xe-bal. [mol-%]	I) C_6F_5 -bal. II) Xe-bal. [mol-%]	I) C_6F_5 -bal. [mol-%]	I) C_6F_5 -bal. [mol-%]	I) C_6F_5 -bal. II) Xe-bal. [mol-%]	I) C_6F_5 -bal. [mol-%]
30 min	I) 70.6	I) 7.9	I) 21.5	I) 0	I) 20.4	I) 102.9
	II) 71.5	II) 7.9			II) 20.6	
1	I) 44.1	I) 8.0	I) 45.3	I) 2.6	I) 41.3	I) 103.3
	II) 47.1	II) 8.6			II) 44.3	
2	I) 18.4	I) 9.3	I) 66.5	I) 5.8	I) 63.3	I) 66.5
	II) 20.2	II) 10.2			II) 69.6	
3	I) 11.3	I) 11.3	I) 72.4	I) 6.8	I) 60.5	I) 111.8
	II) 13.9	II) 11.6			II) 74.5	

^a The total amount (mol-%) of all C_6F_5 compounds was normalized to 100%.

^b The xenon-balance was calculated from all C_6F_5 signal integrals of xenon containing compounds.

^c The $[\text{BF}_4]^-$ anion was calculated on the basis of all C_6F_5 signal integrals

c) Composition of Reactants and Products Resulting from the Reaction of
 $[C_6F_5XeF_2][BF_4]$ with KF in aHF at $-40\text{ }^\circ\text{C}$

Zeit [h]	$[C_6F_5XeF_2]^{+ a,b}$	$[C_6F_5Xe]^{+ a,b}$	$C_6F_6^a$	$c-C_6F_{10}^a$	XeF_2^b	$[BF_4]^-^c$
	I) C_6F_5 -bal. [mol-%]					
30 min	I) 86.0	I) 7.7	I) 6.3	I) 0	I) 3.5	I) 101.5
	II) 88.5	II) 7.9			II) 3.6	
1.5	I) 79.1	I) 7.4	I) 13.5	I) 0	I) 15.1	I) 103.3
	II) 76.4	II) 7.1			II) 14.5	
2	I) 59.5	I) 7.6	I) 28.9	I) 4.0	I) 26.6	I) 101.7
	II) 63.5	II) 8.1			II) 28.4	
3	I) 40.9	I) 9.0	I) 42.7	I) 7.4	I) 30.9	I) 111.6
	II) 50.6	II) 11.1			II) 38.3	
3*	I) 19.3	I) 8.7	I) 56.9	I) 15.1	I) 42.8	I) 51.6
	II) 27.2	II) 12.4			II) 60.4	
4	I) 10.9	I) 10.3	I) 59.4	I) 19.4	I) 41.8	I) 55.7
	II) 17.4	II) 16.3			II) 66.3	
6	I) 0	I) 11.4	I) 59.4	I) 26.4 [#]	I) 37.7	I) 141.5
	II) 0	II) 23.0			II) 77.0	

^a The total amount (mol-%) of all C_6F_5 compounds was normalized to 100%.

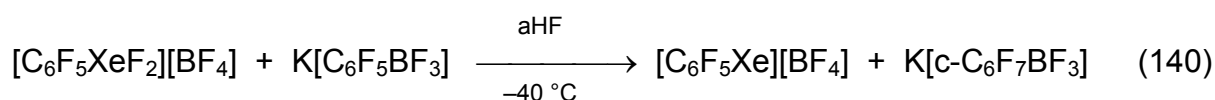
^b The xenon-balance was calculated from all C_6F_5 signal integrals of xenon containing compounds.

^c The $[BF_4]^-$ anion was calculated on the basis of all C_6F_5 signal integrals

* Sample was stored for 13 h at $-80\text{ }^\circ\text{C}$ in a glass trap protected by argon.

[#] + $c-C_6F_8-1,4$ (2.8 %)

IV.13.5 Reaction of $[C_6F_5XeF_2][BF_4]$ with $K[C_6F_5BF_3]$ in aHF at $-40\text{ }^\circ\text{C}$



In a 8 mm i.d. FEP reaction tube, a aHF solution of $[C_6F_5XeF_2][BF_4]$ which was prepared and stored at $-80\text{ }^\circ\text{C}$ for 4 d inside a glass trap under argon protection, was checked by NMR spectroscopy at $-40\text{ }^\circ\text{C}$ to establish its initial condition.

Initial spectrum

^{19}F NMR (282.40 MHz) in aHF at $-40\text{ }^{\circ}\text{C}$

$\text{C}_6\text{F}_5\text{-balance}^{\text{a}}$: $[\text{C}_6\text{F}_5\text{XeF}_2]^+$ (74.4%); $[\text{C}_6\text{F}_5\text{Xe}]^+$ (4.5%); *c*- $\text{C}_6\text{F}_8\text{-1,4}$ (9.0%); C_6F_6 (12.1%)

xenon-balance^b: $[\text{C}_6\text{F}_5\text{XeF}_2]^+$ (82.2%); $[\text{C}_6\text{F}_5\text{Xe}]^+$ (4.9%); XeF_2 (12.9%)

Cation/anion ratio^c: cations (76.3%) / $[\text{BF}_4]^-$ (100%)

^a The total amount (mol-%) of all C_6F_5 compounds was normalized to 100%.

^b The xenon-balance was calculated from all C_6F_5 signal integrals of xenon containing compounds.

^c The cations, $[\text{C}_6\text{F}_5\text{XeF}_2]^+$, was related to the $[\text{BF}_4]^-$ anion which was set to 100%.

In a 3.5 mm i.d. FEP reaction tube, $\text{K}[\text{C}_6\text{F}_5\text{BF}_3]$ (~ 0.1 g; 0.37 mmol) was suspended in cold ($-80\text{ }^{\circ}\text{C}$) aHF (500 μL) and transferred onto the $[\text{C}_6\text{F}_5\text{XeF}_2][\text{BF}_4]/\text{aHF}$ solution. The suspension was stirred for 30 min. at $-40\text{ }^{\circ}\text{C}$ and the ^{19}F and ^{11}B NMR spectra were recorded at $-40\text{ }^{\circ}\text{C}$.

^{19}F NMR (282.40 MHz) in aHF at $-40\text{ }^{\circ}\text{C}$

$[\text{C}_6\text{F}_5\text{Xe}]^+$ $\delta = -123.4$ ppm (m, *o*- C_6F_5 , 2F); -137.7 ppm (tt, $^3J(^{19}\text{F}\text{-}^{19}\text{F}) = 19$ Hz, $^4J(^{19}\text{F}\text{-}^{19}\text{F}) = 6$ Hz, *p*- C_6F_5 , 1F); -151.7 ppm (m, *m*- C_6F_5 , 2F)

$[\text{C}_6\text{F}_5\text{BF}_3]^-$ $\delta = -131.9$ ppm (s, BF_3 , 3F); -136.2 ppm (m, *o*- C_6F_5 , 2F); -155.4 ppm (t, $^3J(^{19}\text{F}\text{-}^{19}\text{F}) = 18$ Hz, *p*- C_6F_5 , 1F); -163.4 ppm (m, *m*- C_6F_5 , 2F)

$[\text{c-C}_6\text{F}_7\text{BF}_3]^-$ $\delta = -99.4$ ppm (s, F(6,6), 2F); -112.5 ppm (s, F(3,3), 2F); -130.8 ppm (s, F(2), 1F); -134.3 ppm (s, 3F); -152.5 ppm (m, F(5), 1F); -159.6 ppm (m, F(4), 1F)

$\text{C}_6\text{F}_5\text{H}$ $\delta = -138.9$ ppm (m, *o*- C_6F_5 , 2F); -154.5 ppm (t, $^3J(^{19}\text{F}\text{-}^{19}\text{F}) = 19$ Hz, *p*- C_6F_5 , 1F); -162.7 ppm (m, *m*- C_6F_5 , 2F)

c- $\text{C}_6\text{F}_8\text{-1,4}$ $\delta = -111.3$ ppm (m, $J = 10$ Hz, 4F); -156.0 ppm (m, $J = 10$ Hz, 4F)

$[\text{BF}_4]^-$ $\delta = -148.8$ ppm (q, $^1J(^{11}\text{B}\text{-}^{19}\text{F}) = 12$ Hz, $^{11}\text{BF}_4$, 4F)

C_6F_6 $\delta = -162.9$ ppm (s, $\Delta\nu_{1/2} = 2$ Hz, 6F)

aHF $\delta = -191.2$ ppm (s)

$\text{C}_6\text{F}_5\text{-balance}^{\text{a}}$: $[\text{C}_6\text{F}_5\text{XeF}_2]^+$ (0%); $[\text{C}_6\text{F}_5\text{Xe}]^+$ (38.4%); $\text{C}_6\text{F}_5\text{H}$ (15.5%); $[\text{c-C}_6\text{F}_7\text{BF}_3]^-$ (23.5%); *c*- $\text{C}_6\text{F}_8\text{-1,4}$ (5.4%); C_6F_6 (17.3%)

$\text{C}_6\text{F}_5\text{-balance}^{\text{b}}$: $[\text{C}_6\text{F}_5\text{XeF}_2]^+$ (0%); $[\text{C}_6\text{F}_5\text{Xe}]^+$ (50.2%); $\text{C}_6\text{F}_5\text{H}$ (20.2%); *c*- $\text{C}_6\text{F}_8\text{-1,4}$ (7.0%); C_6F_6 (22.6%)

- ^a The total amount (mol-%) of all C₆F₅ compounds was normalized to 100%. Due to the fact that K[C₆F₅BF₃] was added undefined and was additionally present as precipitate it was excluded from the C₆F₅ balance
- ^b The total amount (mol-%) of all C₆F₅ compounds was normalized to 100%. K[C-C₆F₇BF₃] can only be formed from K[C₆F₅BF₃] which was added undefined and was additionally present as precipitate. Both compounds were excluded from the C₆F₅ balance.

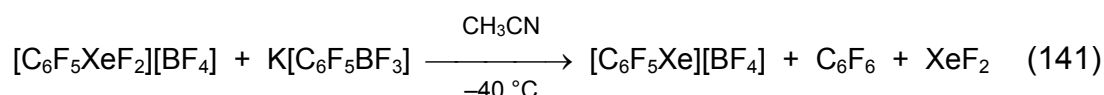
¹¹B-NMR (96.29 MHz) in aHF at -40 °C

[BF₄]⁻ δ = -1.3 ppm (qui, ¹J(¹¹B-¹⁹F) = 12 Hz, ¹¹BF₄)

[c-C₆F₇BF₃]⁻ δ = 2.4 ppm (s)

[C₆F₅BF₃]⁻ δ = 3.5 ppm (s, Δv_{1/2} = 54 Hz)

IV.13.6 Reaction of [C₆F₅XeF₂][BF₄] with K[C₆F₅BF₃] in CH₃CN at -40 °C



In a 3.5 mm i.d. FEP reaction tube, K[C₆F₅BF₃] (25.00 mg; 0.09 mmol) was suspended in CH₃CN (300 μL) and cooled to -40 °C. A cold (-40 °C) CH₃CN solution of [C₆F₅XeF₂][BF₄] was added to the suspension. The suspension was monitored by low-temperature NMR spectroscopy at -40 °C.

¹⁹F NMR (282.40 MHz) in CH₃CN at -40 °C

[C₆F₅XeF₂]⁺ δ = -26.7 ppm (s, ¹²⁹Xe-satellites: ¹J(¹⁹F-¹²⁹Xe) = 3903 Hz, 2F); -123.9 ppm (m, o-C₆F₅, 2F); -130.1 ppm (t, p-C₆F₅, 1F); -151.9 ppm (m, m-C₆F₅, 2F)

[C₆F₅Xe]⁺ δ = -124.6 ppm (m, o-C₆F₅, 2F); -141.3 ppm (tt, ³J(¹⁹F-¹⁹F) = 20 Hz, ⁴J(¹⁹F-¹⁹F) = 5 Hz, p-C₆F₅, 1F); -154.0 ppm (m, m-C₆F₅, 2F)

[C₆F₅BF₃]⁻ δ = -133.8 ppm (br, BF₃, 3F); -134.8 ppm (m, o-C₆F₅, 2F); -159.5 ppm (br, p-C₆F₅, 1F); -164.2 ppm (m, m-C₆F₅, 2F)

[BF₄]⁻ δ = -147.3 ppm (s, ¹¹BF₄, 4F)

C₆F₆ δ = -162.1 ppm (s, Δv_{1/2} = 3 Hz, 6F)

XeF₂ δ = -177.5 ppm (s, ¹²⁹Xe-satellites: ¹J(¹⁹F-¹²⁹Xe) = 5641 Hz, 2F)

CH₃CN·HF δ = -179.0 ppm (d, ¹J(¹H-¹⁹F) = 468Hz)

$[\text{c-C}_6\text{F}_7\text{BF}_3]^-$ $\delta = -101,1$ ppm (s, $\text{c-C}_6\text{F}_7\text{F}(6,6)$); $-111,5$ ppm (s, $\text{c-C}_6\text{F}_7\text{F}(3,3)$); $-130,8$ ppm (s, $\text{c-C}_6\text{F}_7\text{F}(2)$); $-133,5$ ppm (s, BF_3); $-147,9$ ppm (m, $\text{c-C}_6\text{F}_7\text{F}(5)$); $-158,3$ ppm (m, $\text{F}(4)$)

C_6F_5 -balance^a: $[\text{C}_6\text{F}_5\text{XeF}_2]^+$ (85.6%); $[\text{C}_6\text{F}_5\text{Xe}]^+$ (13.2%); C_6F_6 (1.2%); $[\text{c-C}_6\text{F}_7\text{BF}_3]^-$ (traces)

xenon-balance^b: XeF_2 (3.4%); $[\text{C}_6\text{F}_5\text{XeF}_2]^+$ (83.7%); $[\text{C}_6\text{F}_5\text{Xe}]^+$ (12.9%)

Cation/anion ratio^c: cations (97.5%) / anions (100%)

^a The total amount (mol-%) of all C_6F_5 compounds was normalized to 100%.

^b The xenon-balance was calculated from all C_6F_5 signal integrals of xenon containing compounds.

^c The cations, $[\text{C}_6\text{F}_5\text{XeF}_2]^+$ and $[\text{C}_6\text{F}_5\text{Xe}]^+$, were related to the $[\text{BF}_4]^-$ anion which was set to 100%.

Composition of Reactants and Products Resulting from the Reaction of $[\text{C}_6\text{F}_5\text{XeF}_2][\text{BF}_4]$ with $\text{K}[\text{C}_6\text{F}_5\text{BF}_3]$ in CH_3CN at -40 °C^c

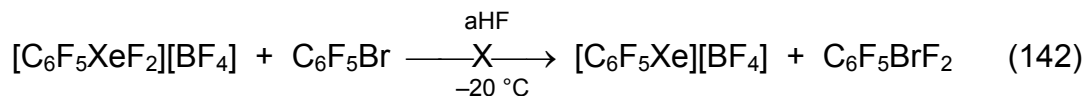
time [h]	$[\text{C}_6\text{F}_5\text{XeF}_2]^+$ ^{a,b}	$[\text{C}_6\text{F}_5\text{Xe}]^+$ ^{a,b}	XeF_2 ^b	$[\text{c-C}_6\text{F}_7\text{BF}_3]^-$ ^a	C_6F_6 ^a
	I) C_6F_5 -balance II) Xe-balance	I) C_6F_5 -balance II) Xe-balance	I) C_6F_5 -balance II) Xe-balance	I) C_6F_5 -balance	I) C_6F_5 -balance
	[mol-%]	[mol-%]	[mol-%]	[mol-%]	[mol-%]
1	I) 85.6	I) 13.2	I) 3.5	I) 0	I) 1.2
	II) 83.7	II) 12.9	II) 3.4		
4	I) 69.8	I) 25.0	I) 4.9	I) 3.4	I) 1.8
	II) 70.0	II) 25.1	II) 4.9		
20	I) 42.2	I) 49.0	I) 12.0	I) 5.0	I) 3.8
	II) 40.9	II) 47.5	II) 11.6		
44	I) 22.5	I) 66.2	I) 17.8	I) 5.5	I) 5.8
	II) 21.2	II) 62.1	II) 16.7		
68	I) 14.4	I) 75.7	I) 21.3	I) 3.5	I) 6.4
	II) 13.0	II) 67.9	II) 19.1		
140	I) 0	I) 86.1	I) 26.6	I) 6.3	I) 7.6
	II) 0	II) 76.4	II) 23.6		

^a The total amount (mol-%) of all C_6F_5 compounds was normalized to 100%. Due to the fact that $\text{K}[\text{C}_6\text{F}_5\text{BF}_3]$ was added undefined and was additionally present as precipitate it was excluded from the C_6F_5 balance

^b The xenon-balance was calculated from all C_6F_5 signal integrals of xenon containing compounds.

^c There were traces of fluorinated C_6F_5 compounds beside the listed products.

IV.13.7 Reaction of $[C_6F_5XeF_2][BF_4]$ with C_6F_5Br in aHF at $-20\text{ }^\circ\text{C}$



In a 8 mm i.d. FEP reaction tube, $[C_6F_5XeF_2][BF_4]$ was dissolved in cold ($-80\text{ }^\circ\text{C}$) aHF (500 μL) and checked by NMR spectroscopy at $-40\text{ }^\circ\text{C}$ to establish the initial condition.

Initial spectrum

^{19}F NMR (282.40 MHz) in aHF at $-40\text{ }^\circ\text{C}$

C_6F_5 -balance^a: $[C_6F_5XeF_2]^+$ (57.1%); $[C_6F_5Xe]^+$ (7.0%); C_6F_6 (12.4%); *c*- C_6F_8 -1,4 (23.5%)

xenon-balance^b: $[C_6F_5XeF_2]^+$ (77.4%); $[C_6F_5Xe]^+$ (13.2%), XeF_2 (13.2%)

Cation/anion ratio^c: cations (70.3%) / $[BF_4]^-$ (100%)

^a The total amount (mol-%) of all C_6F_5 compounds was normalized to 100%.

^b The xenon-balance was calculated from all C_6F_5 signal integrals of xenon containing compounds.

^c The cations, $[C_6F_5XeF_2]^+$ and $[C_6F_5Xe]^+$, were related to the $[BF_4]^-$ anion which was set to 100%.

A small quantity of C_6F_5Br (50 μL ; 0.40 mmol; m.p. $-31\text{ }^\circ\text{C}$) was frozen at $-80\text{ }^\circ\text{C}$ inside a 3.5 mm i.d. FEP reaction tube. The cold ($-80\text{ }^\circ\text{C}$) aHF solution of $[C_6F_5XeF_2][BF_4]$ was transferred onto the frozen C_6F_5Br and allowed to warm to $-20\text{ }^\circ\text{C}$. The sample was maintained at $-20\text{ }^\circ\text{C}$ for 30 min. before the emulsion (C_6F_5Br has a low solubility in aHF) was checked by NMR spectroscopy at $-40\text{ }^\circ\text{C}$.

^{19}F NMR (282.40 MHz) in aHF at $-40\text{ }^\circ\text{C}$

$[C_6F_5XeF_2]^+$ $\delta = -33.2\text{ ppm}$ (s, $\Delta\nu_{1/2} = 15\text{ Hz}$, ^{129}Xe -satellites: $^1J(^{19}\text{F}-^{129}\text{Xe}) = 3894\text{ Hz}$, RXeF_2 , 2F); -123.6 ppm (m, *o*- C_6F_5 , 2F); -129.4 ppm (tt, $^3J(^{19}\text{F}-^{19}\text{F}) = 18\text{ Hz}$, $^4J(^{19}\text{F}-^{19}\text{F}) = 9\text{ Hz}$, *p*- C_6F_5 , 1F); -151.9 ppm (m, *m*- C_6F_5 , 2F)

$[C_6F_5Xe]^+$ $\delta = -123.6\text{ ppm}^*$ (m, *o*- C_6F_5 , 2F); -138.1 ppm (tt, $^3J(^{19}\text{F}-^{19}\text{F}) = 20\text{ Hz}$, $^4J(^{19}\text{F}-^{19}\text{F}) = 6\text{ Hz}$, *p*- C_6F_5 , 1F); -152.9 ppm (m, *m*- C_6F_5 , 2F)

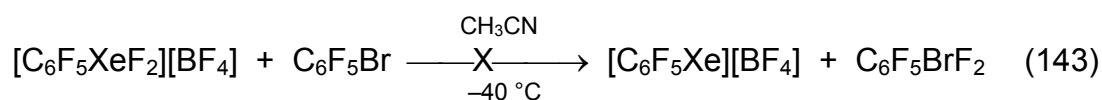
c-C ₆ F ₇ Br	$\delta = -100.4$ ppm (m, c-C ₆ F ₇ F(3,3)); -110.3 ppm* (m, c-C ₆ F ₇ F(6,6)); -118.1 ppm (m, c-C ₆ F ₇ F(2)); -150.9 ppm (m, c-C ₆ F ₇ F(5)), -157.2 ppm (m, c-C ₆ F ₇ F(4))
c-C ₆ F ₈ -1,4	$\delta = -111.6$ ppm (t*, $J = 10$ Hz, 4F); -156.0 ppm (t*, $J = 10$ Hz, 4F)
c-C ₆ F ₁₀	$\delta = -116.8$ ppm (m, F(3,3,6,6), 4F); -136.5 ppm (tt, ${}^3J(^{19}\text{F}-^{19}\text{F}) = 18$ Hz, ${}^4J(^{19}\text{F}-^{19}\text{F}) = 9$ Hz, F(1,2), 2F); -156.1 ppm (m, F(4,4,5,5), 4F)
C ₆ F ₅ Br	$\delta = -132.6$ ppm (m, o-C ₆ F ₅ , 2F); -155.2 ppm (t, ${}^3J(^{19}\text{F}-^{19}\text{F}) = 19$ Hz, p-C ₆ F ₅ , 1F); -161.1 ppm (m, m-C ₆ F ₅ , 2F)
???	$\delta = -131.2$ ppm (m, o-C ₆ F ₅ , 2F); -144.7 ppm (t, ${}^3J(^{19}\text{F}-^{19}\text{F}) = 19$ Hz, p-C ₆ F ₅ , 1F); -158.9 ppm (m, m-C ₆ F ₅ , 2F)
CH ₂ F ₂	$\delta = -141.3$ ppm (t, ${}^1J(^1\text{H}-^{19}\text{F}) = 50$ Hz, 2F)
[BF ₄] ⁻	$\delta = -148.4$ ppm (q, ${}^1J(^{11}\text{B}-^{19}\text{F}) = 12$ Hz, ${}^{11}\text{BF}_4$, 4F)
C ₆ F ₆	$\delta = -162.9$ ppm (s, $\Delta\nu_{1/2} = 3$ Hz, 6F)
aHF	$\delta = -189.7$ ppm (s)
XeF ₂	$\delta = -195.9$ ppm (s, ${}^{129}\text{Xe}$ -satellites: ${}^1J(^{19}\text{F}-^{129}\text{Xe}) = 5671$ Hz, 2F)
C ₆ F ₅ -balance ^a :	[C ₆ F ₅ XeF ₂] ⁺ (3.5%); [C ₆ F ₅ Xe] ⁺ (8.5%); C ₆ F ₅ Br (26.0%); c-C ₆ F ₇ Br (8.2%); c-C ₆ F ₉ Br (7.4%); c-C ₆ F ₈ -1,4 (11.0%); c-C ₆ F ₁₀ (0.9%) ??? (14.6%); C ₆ F ₆ (21.8%)
xenon-balance ^b :	[C ₆ F ₅ XeF ₂] ⁺ (19.7%); [C ₆ F ₅ Xe] ⁺ (47.3%); XeF ₂ (33.0%)

^a The total amount (mol-%) of all C₆F₅ compounds was normalized to 100%.

^b The xenon-balance was calculated from all C₆F₅ signal integrals of xenon containing compounds.

* superimposed signals

IV.13.8 Reaction of [C₆F₅XeF₂][BF₄] with C₆F₅Br in CH₃CN at -40 °C



In a 8 mm i.d. FEP reaction tube, a CH₃CN solution of [C₆F₅XeF₂][BF₄] which was prepared and stored for 1 d at -80 °C inside a glass trap under argon protection, was divided and transferred in two 3.5 mm i.d. FEP reaction tubes. One sample functioned as reference and was checked by ¹⁹F NMR spectroscopy at -40 °C to establish its initial condition. An excess of C₆F₅Br (20 μL ; 0.16 mmol) dissolved in

CH₃CN (100 μL) was added at –40 °C to the second sample. The sample containing C₆F₅Br was periodically monitored by ¹⁹F NMR spectroscopy at –40 °C.

Initial spectrum

¹⁹F NMR (282.40 MHz) in CH₃CN at –40 °C

[C ₆ F ₅ XeF ₂] ⁺	δ = –26.4 ppm (s, ¹²⁹ Xe-satellites: ¹ J(¹⁹ F- ¹²⁹ Xe) = 3893 Hz, 2F); –124.0 ppm (m, <i>o</i> -C ₆ F ₅ , 2F); –134.1 ppm (t, ³ J(¹⁹ F- ¹⁹ F) = 18 Hz, <i>p</i> -C ₆ F ₅ , 1F); –152.0 ppm (m, <i>m</i> -C ₆ F ₅ , 2F)
[C ₆ F ₅ Xe] ⁺	δ = –124.6 ppm (m, <i>o</i> -C ₆ F ₅ , 2F); –141.3 ppm (tt, ³ J(¹⁹ F- ¹⁹ F) = 21 Hz, ⁴ J(¹⁹ F- ¹⁹ F) = 5 Hz, <i>p</i> -C ₆ F ₅ , 1F); –154.1 ppm (m, <i>m</i> -C ₆ F ₅ , 2F)
[C ₆ F ₅ BF ₃] [–]	δ = –130.0 ppm (q, RBF ₃ , 3F); –134.7 ppm (m, <i>o</i> -C ₆ F ₅ , 2F); –159.4 ppm (t, ³ J(¹⁹ F- ¹⁹ F) = 19 Hz, <i>p</i> -C ₆ F ₅ , 1F); –164.1 ppm (m, <i>m</i> -C ₆ F ₅ , 2F)
C ₆ F ₅ H	δ = –138.5 ppm (m, <i>o</i> -C ₆ F ₅ , 2F); <i>p</i> -C ₆ F ₅ *; –161.7 ppm (m, <i>m</i> -C ₆ F ₅ , 2F)
[BF ₄] [–]	δ = –147.3 ppm (s, ¹¹ BF ₄ , 4F)
C ₆ F ₆	δ = –162.1 ppm (s, Δ _v _{1/2} = 3 Hz, 6F)
XeF ₂	δ = –177.6 ppm (s, ¹²⁹ Xe-satellites: ¹ J(¹⁹ F- ¹²⁹ Xe) = 5665 Hz, XeF ₂ , 2F)
HF	δ = –178.7 (s, Δ _v _{1/2} = 753 Hz, 1F)
C ₆ F ₅ -balance ^a :	[C ₆ F ₅ XeF ₂] ⁺ (63.1%); [C ₆ F ₅ Xe] ⁺ (24.4%); C ₆ F ₆ (5.4%); C ₆ F ₅ H (5.4%); [C ₆ F ₅ BF ₃] [–] (1.7%)
Xenon-balance ^b :	[C ₆ F ₅ XeF ₂] ⁺ (62.9%); [C ₆ F ₅ Xe] ⁺ (24.3%); XeF ₂ (12.8%)
Cation/anion ratio ^c :	cations (76.6%) / anions (100%)

¹⁹F NMR (282.40 MHz) in CH₃CN at –40 °C after 15 min.

C ₆ F ₅ -balance ^a :	[C ₆ F ₅ XeF ₂] ⁺ (32.1%); [C ₆ F ₅ Xe] ⁺ (8.1%); C ₆ F ₆ (1.4%); C ₆ F ₅ H (1.5%); [C ₆ F ₅ BF ₃] [–] (1.1%); C ₆ F ₅ Br (55.8%)
Xenon-balance ^b :	[C ₆ F ₅ XeF ₂] ⁺ (73.2%); [C ₆ F ₅ Xe] ⁺ (18.4%) ; XeF ₂ (8.3%)
Cation/anion ratio ^c :	cations (84.9%) / anions (100%)

^a The total amount (mol-%) of all C₆F₅ compounds was normalized to 100%.

^b The Xenon-balance was calculated from all C₆F₅ signal integrals of xenon containing compounds.

^c The cations, [C₆F₅XeF₂]⁺ and [C₆F₅Xe]⁺, were related to the [C₆F₅BF₃][–] and [BF₄][–] anions which were set to 100%.

* superimposed signals

The sample was maintained for ~18 h at -40 to -54 °C and measured again.

^{19}F NMR (282.40 MHz) in CH_3CN at -40 °C to -54 °C after ~18 h

C_6F_5 -balance^a: $[\text{C}_6\text{F}_5\text{XeF}_2]^+$ (29.1%); $[\text{C}_6\text{F}_5\text{Xe}]^+$ (10.6%); C_6F_6 (1.5%); $\text{C}_6\text{F}_5\text{H}$ (0.0%); $[\text{C}_6\text{F}_5\text{BF}_3]^-$ (0.0%); $\text{C}_6\text{F}_5\text{Br}$ (56.8%)

Xenon-balance^b: $[\text{C}_6\text{F}_5\text{XeF}_2]^+$ (69.4%); $[\text{C}_6\text{F}_5\text{Xe}]^+$ (25.3%); XeF_2 (5.4%)

Cation/anion ratio^c: cations (78.7%) / anions (100%)

^a The total amount (mol-%) of all C_6F_5 compounds was normalized to 100%.

^b The Xenon-balance was calculated from all C_6F_5 signal integrals of xenon containing compounds.

^c The cations, $[\text{C}_6\text{F}_5\text{XeF}_2]^+$ and $[\text{C}_6\text{F}_5\text{Xe}]^+$, were related to the $[\text{C}_6\text{F}_5\text{BF}_3]^-$ and $[\text{BF}_4]^-$ anions which were set to 100%.

The sample was allowed to warm to 0 °C and monitored by ^{19}F NMR spectroscopy at -40 °C.

^{19}F NMR (282.40 MHz) in CH_3CN after 30 min. at 0 °C; measured at -40 °C

C_6F_5 -balance^a: $[\text{C}_6\text{F}_5\text{XeF}_2]^+$ (6.5%); $[\text{C}_6\text{F}_5\text{Xe}]^+$ (19.8%); C_6F_6 (5.6%); $\text{C}_6\text{F}_5\text{H}$ (4.0%); $[\text{C}_6\text{F}_5\text{BF}_3]^-$ (0.0%); $\text{C}_6\text{F}_5\text{Br}$ (64.1%)

Xenon-balance^b: XeF_2 (30.9%); $[\text{C}_6\text{F}_5\text{XeF}_2]^+$ (17.0%); $[\text{C}_6\text{F}_5\text{Xe}]^+$ (52.1%)

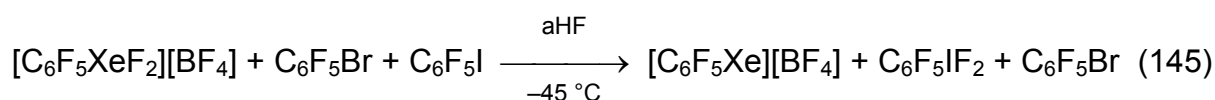
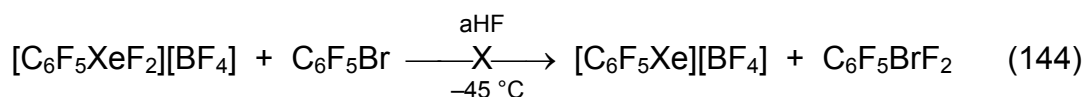
Cation/anion ratio^c: cations (47.8%) / anions (100%)

^a The total amount (mol-%) of all C_6F_5 compounds was normalized to 100%.

^b The Xenon-balance was calculated from all C_6F_5 signal integrals of xenon containing compounds.

^c The cations, $[\text{C}_6\text{F}_5\text{XeF}_2]^+$ and $[\text{C}_6\text{F}_5\text{Xe}]^+$, were related to the $[\text{C}_6\text{F}_5\text{BF}_3]^-$ and $[\text{BF}_4]^-$ anions which were set to 100%.

IV.13.9 Reaction of $[\text{C}_6\text{F}_5\text{XeF}_2][\text{BF}_4]$ with $\text{C}_6\text{F}_5\text{Br}$ and $\text{C}_6\text{F}_5\text{I}$ in aHF at -45 °C



A small quantity of $[\text{C}_6\text{F}_5\text{XeF}_2][\text{BF}_4]$ was dissolved in cold ($-80\text{ }^\circ\text{C}$) aHF (500 μL) and checked by ^{19}F NMR spectroscopy at $-80\text{ }^\circ\text{C}$ to establish its initial condition.

Initial spectrum

^{19}F NMR (282.40 MHz) in aHF bei $-80\text{ }^\circ\text{C}$

$[\text{C}_6\text{F}_5\text{XeF}_2]^+$	$\delta = -33.2\text{ ppm}$ (s, $\Delta\nu_{1/2} = 15\text{ Hz}$, ^{129}Xe -satellites: $^1J(^{19}\text{F}-^{129}\text{Xe}) = 3894\text{ Hz}$, RXeF_2 , 2F); -123.6 ppm (m, $o\text{-C}_6\text{F}_5$, 2F); -129.4 ppm (tt, $^3J(^{19}\text{F}-^{19}\text{F}) = 18\text{ Hz}$, $^4J(^{19}\text{F}-^{19}\text{F}) = 9\text{ Hz}$, $p\text{-C}_6\text{F}_5$, 1F); -151.9 ppm (m, $m\text{-C}_6\text{F}_5$, 2F)
$c\text{-C}_6\text{F}_8\text{-1,4}$	$\delta = -111.6\text{ ppm}$ (t, $J = 10\text{ Hz}$, 4F); -156.0 ppm (t, $J = 10\text{ Hz}$, 4F)
$[\text{BF}_4]^-$	$\delta = -148.4\text{ ppm}$ (q, $^1J(^{11}\text{B}-^{19}\text{F}) = 12\text{ Hz}$, $^{11}\text{BF}_4$, 4F)
C_6F_6	$\delta = -162.9\text{ ppm}$ (s, $\Delta\nu_{1/2} = 3\text{ Hz}$, 6F)
aHF	$\delta = -189.7\text{ ppm}$ (s)
XeF_2	$\delta = -195.1\text{ ppm}$ (s, ^{129}Xe -satellites: $^1J(^{19}\text{F}-^{129}\text{Xe}) = 5671\text{ Hz}$, 2F)
$\text{C}_6\text{F}_5\text{-balance}^{\text{a}}$:	$[\text{C}_6\text{F}_5\text{XeF}_2]^+$ (77.5%); $c\text{-C}_6\text{F}_8\text{-1,4}$ (9.3%); C_6F_6 (13.2%)
Xenon-balance ^b :	XeF_2 (15.6%); $[\text{C}_6\text{F}_5\text{XeF}_2]^+$ (84.4%)
Cation/anion ratio ^c :	$[\text{C}_6\text{F}_5\text{XeF}_2]^+$ (72.7%) / $[\text{BF}_4]^-$ (100%)

^a The total amount (mol-%) of all C_6F_5 compounds was normalized to 100%.

^b The Xenon-balance was calculated from all C_6F_5 signal integrals of xenon containing compounds.

^c The cations, $[\text{C}_6\text{F}_5\text{XeF}_2]^+$ and $[\text{C}_6\text{F}_5\text{Xe}]^+$, were related to the $[\text{BF}_4]^-$ anion which was set to 100%.

* C_6F_6 was taken as internal standard (-162.9 ppm)

A molar excess of $\text{C}_6\text{F}_5\text{Br}$ (15 μL ; 0.12 mmol; m.p. $-31\text{ }^\circ\text{C}$) was added to a $[\text{C}_6\text{F}_5\text{XeF}_2][\text{BF}_4]/\text{aHF}$ solution $-40\text{ }^\circ\text{C}$ using a Hamilton syringe. The aHF mother liquor was separated from the frozen bromopentafluorobenzene and checked by NMR spectroscopy. Dissolved $\text{C}_6\text{F}_5\text{Br}$ was detected in addition to the contents found in the initial spectrum. The solution was stored for 4 d under argon protection inside a glass trap at $-80\text{ }^\circ\text{C}$.

Because no reaction between $[\text{C}_6\text{F}_5\text{XeF}_2][\text{BF}_4]$ and $\text{C}_6\text{F}_5\text{Br}$ in aHF was observed, $\text{C}_6\text{F}_5\text{I}$ (20 μL ; 0.15 mmol) was added at $-80\text{ }^\circ\text{C}$ using a Hamilton syringe. The melting point of dry $\text{C}_6\text{F}_5\text{I}$ was determined to $-35\text{ }^\circ\text{C}$. The suspension was allowed to warm to $-40\text{ }^\circ\text{C}$ and maintained at $-40\text{ }^\circ\text{C}$ for 30 min. The aHF mother liquor was subsequently separated and checked by ^{19}F NMR spectroscopy at $-40\text{ }^\circ\text{C}$. The spectrum showed the following composition:

^{19}F NMR (282.40 MHz) after 30 min. in aHF at $-40\text{ }^{\circ}\text{C}^*$

C_6F_5 -balance^a: $[\text{C}_6\text{F}_5\text{XeF}_2]^+$ (1.3%); $[\text{C}_6\text{F}_5\text{Xe}]^+$ (38.9%); $\text{C}_6\text{F}_5\text{IF}_2$ (41.9%); $\text{C}_6\text{F}_5\text{I}$ (6.5%); $\text{C}_6\text{F}_5\text{Br}$ (2.0%); *c*- $\text{C}_6\text{F}_7\text{X}$ (0.9%); *c*- C_6F_8 -1,4 (1.3%); C_6F_6 (7.2%)

Xenon-balance^b: $[\text{C}_6\text{F}_5\text{XeF}_2]^+$ (3.3%); $[\text{C}_6\text{F}_5\text{Xe}]^+$ (96.7%)

Cation/anion ratio^c: Cations (72.6%) / $[\text{BF}_4]^-$ (100%)

^a The total amount (mol-%) of all C_6F_5 compounds was normalized to 100%.

^b The Xenon-balance was calculated from all C_6F_5 signal integrals of xenon containing compounds.

^c The cations, $[\text{C}_6\text{F}_5\text{XeF}_2]^+$ and $[\text{C}_6\text{F}_5\text{Xe}]^+$, were related to the $[\text{BF}_4]^-$ anion which was set to 100%.

* C_6F_6 was taken as internal standard (-162.9 ppm)

IV.13.10 Analysis of the NMR Signals of $\text{C}_6\text{F}_5\text{IF}_2$ in aHF Using 2D NMR Spectroscopy (SERF)

In a 3.5 mm i.d. FEP reaction tube, $\text{C}_6\text{F}_5\text{IF}_2$ (~50 mg; 0.151 mmol) was dissolved in aHF (500 μL) at $-80\text{ }^{\circ}\text{C}$. The solution was measured by NMR spectroscopy at $-40\text{ }^{\circ}\text{C}$ showing no decomposition of $\text{C}_6\text{F}_5\text{IF}_2$. The iodine bonded fluorine atoms were not detected at $-40\text{ }^{\circ}\text{C}$ but at $-80\text{ }^{\circ}\text{C}$.

^{19}F NMR (282.40 MHz) in aHF bei $-80\text{ }^{\circ}\text{C}$

$\text{C}_6\text{F}_5\text{IF}_2$ $\delta = -119.6$ ppm (m, *o*- C_6F_5 , 2F); -138.3 ppm* (tt, $^3J(^{19}\text{F}-^{19}\text{F}) = 19$ Hz, $^4J(^{19}\text{F}-^{19}\text{F}) = 8$ Hz, *p*- C_6F_5 , 1F); -154.9 ppm (m, *m*- C_6F_5 , 2F); -177.4 ppm (s, $\Delta\nu_{1/2} = 723$ Hz, <2F)

The sample was maintained at $-80\text{ }^{\circ}\text{C}$ for 2 d without decomposition. The sample was allowed to warm to $-15\text{ }^{\circ}\text{C}$ for 1 h whereupon no decomposition was observed. The IF_2 signal was not observed. The following SERF experiments were performed at $-80\text{ }^{\circ}\text{C}$ to show couplings of the IF_2 group to the ring fluorine atoms.

C₆F₅IF₂: *p*-C₆F₅ decoupled; *o*-C₆F₅ measured

The *p*-C₆F₅ fluorine couples with the *o*-C₆F₅ signal giving a pseudo-quartet structure with a coupling constant of 7.2 Hz. The decoupled *o*-C₆F₅ signal splits into a doublet with $J = 16.0$ Hz.

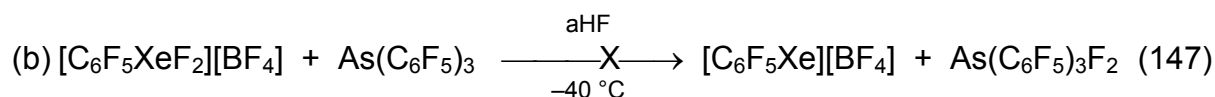
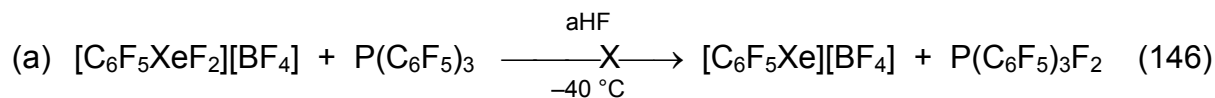
C₆F₅IF₂: IF₂ decoupled; *o*-C₆F₅ measured

The IF₂ group has just a minor effect on the *o*-C₆F₅ signal. It was still obtained as a pseudo-quartet structure but it spread symmetrically in the middle of the signal having a coupling constant of 8.2 Hz for the inner and 7.2 Hz for the outer signals.

C₆F₅IF₂: *o*-C₆F₅ decoupled; *p*-C₆F₅ measured

The *o*-C₆F₅ fluorine couples with the *p*-C₆F₅ signal giving a triplet structure with a coupling constant of 19.2 Hz.

IV.13.11 Reaction of [C₆F₅XeF₂][BF₄] with M(C₆F₅)₃ (M = P, As) in aHF at -40 °C



In two 3.5 mm i.d. FEP reaction tubes, P(C₆F₅)₃ (32.58 mg; 0.06 mmol) (**a**) and As(C₆F₅)₃ (11.09 mg; 0.02 mmol) (**b**), were each suspended in cold (-40 °C) aHF (500 μL). Both suspensions were maintained at -40 °C before being measured by NMR spectroscopy. It has been shown that As(C₆F₅)₃ is insoluble in aHF at -40 °C whereas P(C₆F₅)₃ has a low solubility in aHF at -40 °C.

¹⁹F NMR (282.40 MHz) in aHF at -40 °C

P(C₆F₅)₃ δ = -124.7 ppm (m, *o*-C₆F₅, 2F); -130.9 ppm (m, *p*-C₆F₅, 1F);
-153.4 ppm (m, *m*-C₆F₅, 2F)

³¹P NMR (121.44 MHz) in aHF bei -40 °C

P(C₆F₅)₃ δ = -46.2 ppm (m)

In a 23 mm i.d. FEP reaction tube, $[\text{C}_6\text{F}_5\text{XeF}_2][\text{BF}_4]$ was dissolved in cold (-80 °C) aHF (500 μL), divided into two equivalent samples and transferred into two 7.8 mm FEP reaction tubes. Both solutions were checked by NMR spectroscopy at -40 °C to establish its initial condition.

a) Initial spectrum for the reaction of $[\text{C}_6\text{F}_5\text{XeF}_2][\text{BF}_4]$ with $\text{P}(\text{C}_6\text{F}_5)_3$

^{19}F NMR (282.40 MHz) in aHF at -40 °C

C_6F_5 -balance^a: $[\text{C}_6\text{F}_5\text{XeF}_2]^+$ (74.4%); $[\text{C}_6\text{F}_5\text{Xe}]^+$ (4.5%); C_6F_6 (12.1%); c- C_6F_8 -1,4 (9.0%)

Xenon-balance^b: $[\text{C}_6\text{F}_5\text{XeF}_2]^+$ (82.2%); $[\text{C}_6\text{F}_5\text{Xe}]^+$ (4.9%), XeF_2 (12.9%)

Cation/anion ratio^c: cations (76.3%) / $[\text{BF}_4]^-$ (100%)

b) Initial spectrum for the reaction of $[\text{C}_6\text{F}_5\text{XeF}_2][\text{BF}_4]$ with $\text{As}(\text{C}_6\text{F}_5)_3$

^{19}F NMR (282.40 MHz) in aHF at -40 °C

C_6F_5 -balance^a: $[\text{C}_6\text{F}_5\text{XeF}_2]^+$ (50.8%); $[\text{C}_6\text{F}_5\text{Xe}]^+$ (7.6%); C_6F_6 (17.1%); c- C_6F_8 -1,4 (24.5%)

Xenon-balance^b: $[\text{C}_6\text{F}_5\text{XeF}_2]^+$ (69.1%); $[\text{C}_6\text{F}_5\text{Xe}]^+$ (10.3%), XeF_2 (20.6%)

Cation/anion ratio^c: cations (61.1%) / $[\text{BF}_4]^-$ (100%)

^a The total amount (mol-%) of all C_6F_5 compounds was normalized to 100%.

^b The Xenon-balance was calculated from all C_6F_5 signal integrals of xenon containing compounds.

^c The cations, $[\text{C}_6\text{F}_5\text{XeF}_2]^+$ and $[\text{C}_6\text{F}_5\text{Xe}]^+$, were related to the $[\text{BF}_4]^-$ anion which was set to 100%.

The two aHF solutions of $[\text{C}_6\text{F}_5\text{XeF}_2][\text{BF}_4]$ were each transferred to the $\text{P}(\text{C}_6\text{F}_5)_3$ (a) and $\text{As}(\text{C}_6\text{F}_5)_3$ (b) suspensions and allowed to warm to -40 °C. The solution was stirred for 30 min. at -40 °C and the reaction monitored by NMR spectroscopy at -40 °C.

a) Reaction of $[\text{C}_6\text{F}_5\text{XeF}_2][\text{BF}_4]$ with $\text{P}(\text{C}_6\text{F}_5)_3$

^{19}F NMR (282.40 MHz) in aHF after 30 min. at -40 °C

C_6F_5 -balance^a: $[\text{C}_6\text{F}_5\text{XeF}_2]^+$ (15.6%); $[\text{C}_6\text{F}_5\text{Xe}]^+$ (26.3%); C_6F_6 (40.7%); c- C_6F_8 -1,4 (17.4%), c- C_6F_{10} (traces)

Xenon-balance^b: $[\text{C}_6\text{F}_5\text{XeF}_2]^+$ (18.4%); $[\text{C}_6\text{F}_5\text{Xe}]^+$ (31.0%), XeF_2 (50.6%)

cation/anion ratio^c: cations (33.5%) / $[\text{BF}_4]^-$ (100%)

- ^a The total amount (mol-%) of all C₆F₅ compounds was normalized to 100%.
- ^b The Xenon-balance was calculated from all C₆F₅ signal integrals of xenon containing compounds.
- ^c The cations, [C₆F₅XeF₂]⁺ and [C₆F₅Xe]⁺, were related to the [BF₄]⁻ anion which was set to 100%.

The ³¹P NMR spektrum of this suspenison showed no signals. Suspension **a**) was maintained at -80 °C for 2 d and a ¹⁹F NMR spectrum was recorded at -40 °C.

¹⁹F NMR (282.40 MHz) after 2 d at -80 °C in aHF at -40 °C

C₆F₅-balance^a: [C₆F₅XeF₂]⁺ (6.6%); [C₆F₅Xe]⁺ (29.3%); C₆F₆ (44.7%); c-C₆F_{8-1,4} (17.7%), c-C₆F₁₀ (1.8%)

Xenon-balance^b: [C₆F₅XeF₂]⁺ (8.5%); [C₆F₅Xe]⁺ (37.7%), XeF₂ (53.9%)

Cation/anion ratio^c: cations (27.5%) / [BF₄]⁻ (100%)

b) Reaction of [C₆F₅XeF₂][BF₄] with As(C₆F₅)₃

¹⁹F NMR (282.40 MHz) after 30 min. in aHF at -40 °C

C₆F₅-balance^a: [C₆F₅XeF₂]⁺ (51.1%); [C₆F₅Xe]⁺ (13.1%); C₆F₆ (25.6%); c-C₆F_{8-1,4} (10.2%), c-C₆F₁₀ (traces)

xenon-balance^b: [C₆F₅XeF₂]⁺ (53.4%); [C₆F₅Xe]⁺ (13.7%), XeF₂ (32.9%)

Cation/anion raddio^c: cations (49.2%) / [BF₄]⁻ (100%)

- ^a The total amount (mol-%) of all C₆F₅ compounds was normalized to 100%.
- ^b The Xenon-balance was calculated from all C₆F₅ signal integrals of xenon containing compounds.
- ^c The cations, [C₆F₅XeF₂]⁺ and [C₆F₅Xe]⁺, were related to the [BF₄]⁻ anion which was set to 100%.

The suspension **b**) was maintained for 2 d at -80 °C and checked by NMR spectroscopy at -40 °C.

¹⁹F NMR (282.40 MHz) after 2 d at -80 °C in aHF at -40 °C

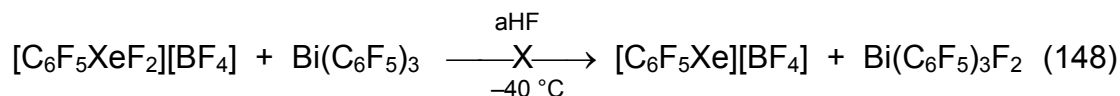
C₆F₅-balance^a: [C₆F₅XeF₂]⁺ (48.8%); [C₆F₅Xe]⁺ (14.1%); C₆F₆ (26.9%); c-C₆F_{8-1,4} (9.0%), c-C₆F₁₀ (1.2%); As(C₆F₅)₃F₂ (?) (1.8%)

xenon-balance^b: [C₆F₅XeF₂]⁺ (8.5%); [C₆F₅Xe]⁺ (37.7%), XeF₂ (53.9%)

Cation/anion ratio^c: cations (27.5%) / [BF₄]⁻ (100%)

- ^a The total amount (mol-%) of all C₆F₅ compounds was normalized to 100%.
- ^b The Xenon-balance was calculated from all C₆F₅ signal integrals of xenon containing compounds.
- ^c The cations, [C₆F₅XeF₂]⁺ and [C₆F₅Xe]⁺, were related to the [BF₄]⁻ anion which was set to 100%.

IV.13.12 Reaction of $[C_6F_5XeF_2][BF_4]$ with $Bi(C_6F_5)_3$ in aHF at $-40\text{ }^\circ\text{C}$



In a 3.5 i.d. FEP reaction tube, $Bi(C_6F_5)_3$ (42.46 mg; 0.06 mmol) was suspended in cold ($-40\text{ }^\circ\text{C}$) aHF (500 μL). The insolubility of $Bi(C_6F_5)_3$ in cold ($-40\text{ }^\circ\text{C}$) aHF (500 μL) was shown by ^{19}F NMR spectroscopy at $-40\text{ }^\circ\text{C}$. A cold ($-80\text{ }^\circ\text{C}$) aHF solution of $[C_6F_5XeF_2][BF_4]$ ($\sim 1000\text{ } \mu\text{L}$) was divided in two equivalent samples. One sample was added to the $Bi(C_6F_5)_3$ suspension at $-80\text{ }^\circ\text{C}$ (b) whereas the other sample functioned as a reference (a). Both samples were periodically monitored by low-temperature ^{19}F NMR spectroscopy. The reference sample was checked by NMR spectroscopy at $-40\text{ }^\circ\text{C}$ to establish its initial condition.

Initial spectrum

^{19}F -NMR (282.40 MHz) in aHF bei $-40\text{ }^\circ\text{C}$

$[C_6F_5XeF_2]^+$	$\delta = -32.4\text{ ppm}$ (s, ^{129}Xe -Satelliten: $^1J(^{19}\text{F}-^{129}\text{Xe}) = 3899\text{ Hz}$, RXeF_2 , 2F); -123.4 ppm (m, <i>o</i> - C_6F_5 , 2F); -128.6 ppm (tt, $^3J(^{19}\text{F}-^{19}\text{F}) = 19\text{ Hz}$, $^4J(^{19}\text{F}-^{19}\text{F}) = 9\text{ Hz}$, <i>p</i> - C_6F_5 , 1F); -150.1 ppm (m, <i>m</i> - C_6F_5 , 2F)
$[C_6F_5Xe]^+$	$\delta = -123.4\text{ ppm}^*$ (m, <i>o</i> - C_6F_5 , 2F); -138.0 ppm (tt, $^3J(^{19}\text{F}-^{19}\text{F}) = 19\text{ Hz}$, $^4J(^{19}\text{F}-^{19}\text{F}) = 6\text{ Hz}$, <i>p</i> - C_6F_5 , 1F); -151.6 ppm (m, <i>m</i> - C_6F_5 , 2F)
$[\text{c-}C_6F_7BF_3]^-$	$\delta = -99.5\text{ ppm}$ (m, F(6,6), 2F); -112.5 ppm (m, F(3,3), 2F); -130.8 ppm (s, F(2), 1F); -134.1 ppm (s, 3F); -152.5 ppm (m, F(5), 1F); -159.7 ppm (m, F(4), 1F)
$[BF_4]^-$	$\delta = -148.6\text{ ppm}$ (q, $^1J(^{11}\text{B}^{19}\text{F}) = 12\text{ Hz}$, 4F)
C_6F_6	$\delta = -162.9\text{ ppm}$ (s, $\Delta\nu_{1/2} = 3\text{ Hz}$, 6F)
aHF	$\delta = -190.8\text{ ppm}$ (s)
XeF_2	$\delta = -195.8\text{ ppm}$ (s, ^{129}Xe -Satelliten: $^1J(^{19}\text{F}-^{129}\text{Xe}) = 5667\text{ Hz}$, 2F)

* superimposed signals

a) Reference sample:

Decomposition of $[\text{C}_6\text{F}_5\text{XeF}_2][\text{BF}_4]$ in aHF at $-40\text{ }^\circ\text{C}$

time [min]	$[\text{C}_6\text{F}_5\text{XeF}_2]^{+ \text{a,b}}$	$[\text{C}_6\text{F}_5\text{Xe}]^{+ \text{a,b}}$	$\text{C}_6\text{F}_6^{\text{a}}$	$[\text{c-C}_6\text{F}_7\text{BF}_3]^{- \text{a}}$	XeF_2^{b}
	I) C_6F_5 -bal. II) Xe-bal.	I) C_6F_5 -bal. II) Xe-bal.	I) C_6F_5 -bal.	I) C_6F_5 -bal.	I) C_6F_5 -bal. II) Xe-bal.
	[mol-%]	[mol-%]	[mol-%]	[mol-%]	[mol-%]
30	I) 76.1 II) 82.5	I) 13.6 II) 14.7	I) 2.4	I) 7.9	I) 2.6 II) 2.8
	I) 60.8 II) 68.6	I) 11.7 II) 13.3	I) 16.2	I) 11.3	I) 16.1 II) 18.2

^a The total amount (mol-%) of all C_6F_5 compounds was normalized to 100%.

^b The xenon-balance was calculated from all C_6F_5 signal integrals of xenon containing compounds.

^c The sample was additionally maintained frozen ($-80\text{ }^\circ\text{C}$) for 3 d

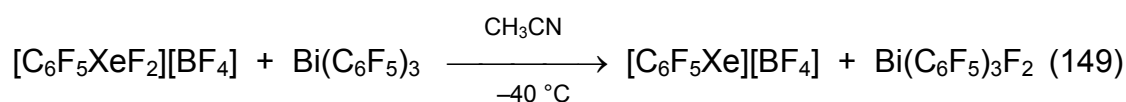
b) Sample with $\text{Bi}(\text{C}_6\text{F}_5)_3$ Composition of Reactants and Products Resulting from the Reaction of $[\text{C}_6\text{F}_5\text{XeF}_2][\text{BF}_4]$ with $\text{Bi}(\text{C}_6\text{F}_5)_3$ in aHF at $-40\text{ }^\circ\text{C}$

time [min]	$[\text{C}_6\text{F}_5\text{XeF}_2]^{+ \text{a,b}}$	$[\text{C}_6\text{F}_5\text{Xe}]^{+ \text{a}}$	$\text{C}_6\text{F}_6^{\text{a}}$	$[\text{c-C}_6\text{F}_7\text{BF}_3]^{- \text{a}}$	XeF_2^{b}	$\text{c-C}_6\text{F}_{10}^{\text{a}}$
	I) C_6F_5 -bal. II) Xe-bal.	I) C_6F_5 -bal. II) Xe-bal.	I) C_6F_5 -bal.	I) C_6F_5 -bal.	I) C_6F_5 -bal. II) Xe-bal.	I) C_6F_5 -bal.
	[mol-%]	[mol-%]	[mol-%]	[mol-%]	[mol-%]	[mol-%]
30	I) 34.8 II) 39.2	I) 15.9 II) 17.9	I) 41.5	I) 7.8	I) 38.1 II) 42.9	I) Traces
	I) 22.0 II) 29.7	I) 19.2 II) 25.9	I) 43.6	I) 7.1	I) 32.9 II) 44.4	I) 8.0

^a The total amount (mol-%) of all C_6F_5 compounds was normalized to 100%.

^b The xenon-balance was calculated from all C_6F_5 signal integrals of xenon containing compounds.

^c Sample was maintained additional 3 d at $-80\text{ }^\circ\text{C}$ in the absence of daylight inside a glass trap protected by argon.

IV.13.13 Reaction of $[\text{C}_6\text{F}_5\text{XeF}_2][\text{BF}_4]$ with $\text{Bi}(\text{C}_6\text{F}_5)_3$ in CH_3CN at $-40\text{ }^\circ\text{C}$ 

In a 3.5 mm i.d. FEP reaction tube, $\text{Bi}(\text{C}_6\text{F}_5)_3$ (95.89 mg; 0.14 mmol), was dissolved in CH_3CN (500 μL) and checked by NMR spectroscopy.

^{19}F -NMR (282,40 MHz) in CH_3CN at 24 °C

$\text{Bi}(\text{C}_6\text{F}_5)_3$ $\delta = -117.1$ ppm (m, *o*- C_6F_5 , 6F); -152.1 ppm (t, $^3J(^{19}\text{F}-^{19}\text{F}) = 19$ Hz
p- C_6F_5 , 3F); -160.1 ppm (m, *m*- C_6F_5 , 6F)

A cold (-40 °C) CH_3CN solution of $[\text{C}_6\text{F}_5\text{XeF}_2][\text{BF}_4]$ (~ 2000 μL) was divided in two equivalent samples. One sample was added to the $\text{Bi}(\text{C}_6\text{F}_5)_3$ solution at -40 °C (b) whereas the other sample functioned as reference. Both samples were monitored by ^{19}F NMR spectroscopy. The reference sample was checked by NMR spectroscopy at -40 °C to establish its initial condition.

Initial spectrum

^{19}F -NMR (282.40 MHz) in CH_3CN at -40 °C

$[\text{C}_6\text{F}_5\text{XeF}_2]^+$ $\delta = -26.5$ ppm (s, ^{129}Xe -satellites: $^1J(^{19}\text{F}-^{129}\text{Xe}) = 3902$ Hz, RXeF_2 , 2F); -124.1 ppm (m, *o*- C_6F_5 , 2F); -134.1 ppm (t, $^3J(^{19}\text{F}-^{19}\text{F}) = 21$ Hz, *p*- C_6F_5 , 1F); -152.0 ppm (m, *m*- C_6F_5 , 2F)

$[\text{C}_6\text{F}_5\text{Xe}]^+$ $\delta = -124.6$ ppm* (m, *o*- C_6F_5 , 2F); -141.4 ppm (t, $^3J(^{19}\text{F}-^{19}\text{F}) = 21$ Hz, *p*- C_6F_5 , 1F); -154.1 ppm (m, *m*- C_6F_5 , 2F)

$[\text{C}_6\text{F}_5\text{BF}_3]^-$ $\delta = -130.2$ ppm (q, BF_3 , 3F); -134.7 (m, *o*- C_6F_5 , 2F); -159.4 ppm (t, $^3J(^{19}\text{F}-^{19}\text{F}) = 20$ Hz, *p*- C_6F_5 , 1F); -164.1 ppm (m, *m*- C_6F_5 , 2F)

$\text{C}_6\text{F}_5\text{H}$ $\delta = -138.5$ ppm (m, *o*- C_6F_5 , 2F); -153.4 ppm (t, $^3J(^{19}\text{F}-^{19}\text{F}) = 21$ Hz, *p*- C_6F_5 , 1F); -161.7 ppm (m, *m*- C_6F_5 , 2F)

$[\text{BF}_4]^-$ $\delta = -147.4$ ppm (q, $^1J(^{11}\text{B}-^{19}\text{F}) = 12$ Hz, $^{11}\text{BF}_4$, 4F)

C_6F_6 $\delta = -162.1$ ppm (s, $\Delta\nu_{1/2} = 4$ Hz, 6F)

XeF_2 $\delta = -177.6$ ppm (s, ^{129}Xe -satellites: $^1J(^{19}\text{F}-^{129}\text{Xe}) = 5650$ Hz, 2F)

HF $\delta = -178.4$ (s, $\Delta\nu_{1/2} = 35$ Hz, 1F)

C_6F_5 -balance^a: $[\text{C}_6\text{F}_5\text{XeF}_2]^+$ (80.1%); $[\text{C}_6\text{F}_5\text{Xe}]^+$ (11.3%); C_6F_6 (0.6%); $\text{C}_6\text{F}_5\text{H}$ (0.8%); $[\text{C}_6\text{F}_5\text{BF}_3]^-$ (7.2%)

Xenon-balance^b: $[\text{C}_6\text{F}_5\text{XeF}_2]^+$ (85.1%); $[\text{C}_6\text{F}_5\text{Xe}]^+$ (12.0%), XeF_2 (2.9%)

Cation/anion ratio^c: cations (93.5%) / anions (100%)

- ^a The total amount (mol-%) of all C₆F₅ compounds was normalized to 100%.
- ^b The xenon-balance was calculated from all C₆F₅ signal integrals of xenon containing compounds.
- ^c The cations, [C₆F₅XeF₂]⁺ and [C₆F₅Xe]⁺, were related to the [C₆F₅BF₃]⁻ and [BF₄]⁻ anions which were set to 100%.
- * superimposed signals

b) Sample with Bi(C₆F₅)₃ after 1 h

¹⁹F-NMR (282.40 MHz) in CH₃CN after 1 h at -40 °C

Same composition than in the initial sample plus the following Bi-compounds:

Bi(C₆F₅)₃ δ = -116.7 ppm (m, *o*-C₆F₅, 6F); -151.4 ppm (t, ³J(¹⁹F-¹⁹F) = 19 Hz
p-C₆F₅, 3F); -159.3 ppm (m, *m*-C₆F₅, 6F)

Bi(C₆F₅)₃F₂ δ = -60.5 ppm (s, Δ*v*_{1/2} = 49 Hz, BiF₂, 2F); -126.3 ppm (m, *o*-C₆F₅,
6F); -142.6 ppm (t, ³J(¹⁹F-¹⁹F) = 21 Hz, *p*-C₆F₅, 3F); -154.4 ppm
(m, *m*-C₆F₅, 6F)

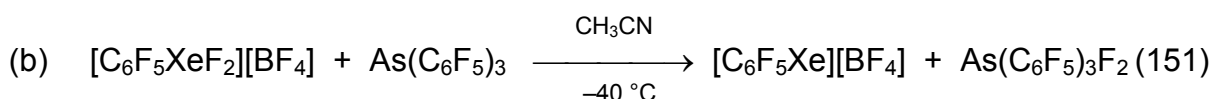
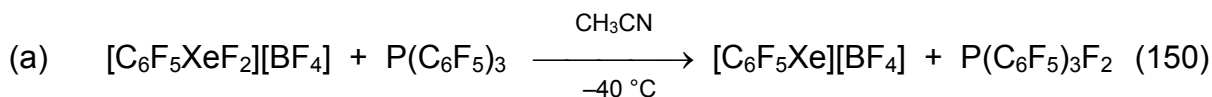
C₆F₅-balance^a: [C₆F₅XeF₂]⁺ (0.0%); [C₆F₅Xe]⁺ (30.8%); C₆F₆ (0.3%); C₆F₅H
(1.4%); [C₆F₅BF₃]⁻ (1.9%); Bi(C₆F₅)₃ (40.2%); Bi(C₆F₅)₃F₂ (25.3%)

xenon-balance^b: XeF₂ (5.6%); [C₆F₅XeF₂]⁺ (0.0%); [C₆F₅Xe]⁺ (94.4%)

Cation/anion ratio^c: cations (93.1%) / anions (100%)

- ^a The total amount (mol-%) of all C₆F₅ compounds was normalized to 100%.
- ^b The xenon-balance was calculated from all C₆F₅ signal integrals of xenon containing compounds.
- ^c The cations, [C₆F₅XeF₂]⁺ and [C₆F₅Xe]⁺, were related to the [C₆F₅BF₃]⁻ and [BF₄]⁻ anions which were set to 100%.

IV.13.14 Reaction of [C₆F₅XeF₂][BF₄] with M(C₆F₅)₃ (M = P, As) in CH₃CN at -40 °C



In separate 3.5 mm i.d. FEP reaction tubes, P(C₆F₅)₃ (133.49 mg; 0.25 mmol) (a) and As(C₆F₅)₃ (143.46 mg; 0.25 mmol) (b) were suspended in CH₃CN (1000 μL), cooled (-40 °C) and a previously prepared cold (-40 °C) [C₆F₅XeF₂][BF₄]/CH₃CN solution was divided in three portions from which two were added to sample a and b

and the third sample functioned as a reference. The reference sample was measured by NMR spectroscopy at $-40\text{ }^{\circ}\text{C}$ to establish its initial condition.

All three samples were maintained 40 min. at $-40\text{ }^{\circ}\text{C}$ before measured by NMR spectroscopy. The yellow solutions **a** and **b** decoloured and a white solid precipitated.

Initial spectrum

^{19}F NMR (282.40 MHz) in CH_3CN at $-40\text{ }^{\circ}\text{C}$

$[\text{C}_6\text{F}_5\text{XeF}_2]^+$	$\delta = -26.4\text{ ppm}$ (s, ^{129}Xe -satellites: $^1J(^{19}\text{F}-^{129}\text{Xe}) = 3894\text{ Hz}$, RXeF_2 , 2F); -124.0 ppm (m, <i>o</i> - C_6F_5 , 2F); -134.1 ppm (t, $^3J(^{19}\text{F}-^{19}\text{F}) = 18\text{ Hz}$, <i>p</i> - C_6F_5 , 1F); -152.0 ppm (m, <i>m</i> - C_6F_5 , 2F)
$[\text{C}_6\text{F}_5\text{Xe}]^+$	$\delta = -124.6\text{ ppm}$ (m, <i>o</i> - C_6F_5 , 2F); -141.3 ppm (t, $^3J(^{19}\text{F}-^{19}\text{F}) = 18\text{ Hz}$, <i>p</i> - C_6F_5 , 1F); -154.1 ppm (m, <i>m</i> - C_6F_5 , 2F)
$[\text{C}_6\text{F}_5\text{BF}_3]^-$	$\delta = -130.0\text{ ppm}$ (q, RBF_3 , 3F); -134.7 ppm (m, <i>o</i> - C_6F_5 , 2F); -159.4 ppm (t, $^3J(^{19}\text{F}-^{19}\text{F}) = 18\text{ Hz}$, <i>p</i> - C_6F_5 , 1F); -164.1 ppm (m, <i>m</i> - C_6F_5 , 2F)
$\text{C}_6\text{F}_5\text{H}$	$\delta = -138.5\text{ ppm}$ (m, <i>o</i> - C_6F_5 , 2F); <i>p</i> - C_6F_5^* ; -161.7 ppm (m, <i>m</i> - C_6F_5 , 2F)
$[\text{BF}_4]^-$	$\delta = -147.3\text{ ppm}$ (s, $^{11}\text{BF}_4$, 4F)
C_6F_6	$\delta = -162.1\text{ ppm}$ (s, $\Delta\nu_{1/2} = 3\text{ Hz}$, 6F)
$\text{CH}_3\text{CN}\cdot\text{HF}$	$\delta = -178.7\text{ ppm}$ (d, $^1J(^1\text{H}-^{19}\text{F}) = 480\text{ Hz}$, 1F)
C_6F_5 -balance ^a :	$[\text{C}_6\text{F}_5\text{XeF}_2]^+$ (86.8%); $[\text{C}_6\text{F}_5\text{Xe}]^+$ (8.4%); C_6F_6 (0.8%); $\text{C}_6\text{F}_5\text{H}$ (0.6%); $[\text{C}_6\text{F}_5\text{BF}_3]^-$ (3.4%)
xenon-balance ^b :	$[\text{C}_6\text{F}_5\text{XeF}_2]^+$ (88.7%); $[\text{C}_6\text{F}_5\text{Xe}]^+$ (8.6%) XeF_2 (2.7%)
Cation/anion ratio ^c :	cations (97.0%) / anions (100%)

a) Reaction of $[\text{C}_6\text{F}_5\text{XeF}_2][\text{BF}_4]$ with $\text{P}(\text{C}_6\text{F}_5)_3$ (suspension)

Same composition than in the initial sample plus the following P-compounds:

$\text{P}(\text{C}_6\text{F}_5)_3\text{F}_2$	$\delta = -2.0\text{ ppm}$ (d, $^1J(^{19}\text{F}-^{35}\text{P}) = 681\text{ Hz}$, 2F); -132.6 ppm (m, <i>o</i> - C_6F_5 , 6F); -145.3 ppm (t, $^3J(^{19}\text{F}-^{19}\text{F}) = 20\text{ Hz}$, <i>p</i> - C_6F_5 , 3F); -158.1 ppm (m, <i>m</i> - C_6F_5 , 6F)
$\text{P}(\text{C}_6\text{F}_5)_3$	$\delta = -131.5\text{ ppm}$ (m, <i>o</i> - C_6F_5 , 6F); -148.1 ppm (t, $^3J(^{19}\text{F}-^{19}\text{F}) = 18\text{ Hz}$, <i>p</i> - C_6F_5 , 1F); -158.1 ppm (m, <i>m</i> - C_6F_5 , 6F)
C_6F_5 -balance ^a :	$[\text{C}_6\text{F}_5\text{XeF}_2]^+$ (0.0%); $[\text{C}_6\text{F}_5\text{Xe}]^+$ (83.7%); C_6F_6 (0.7%); $\text{C}_6\text{F}_5\text{H}$ (2.5%); $[\text{C}_6\text{F}_5\text{BF}_3]^-$ (3.6%); $\text{P}(\text{C}_6\text{F}_5)_3\text{F}_2$ (4.1%); $\text{P}(\text{C}_6\text{F}_5)_3$ (5.3%)
xenon-balance ^b :	XeF_2 (4.5%); $[\text{C}_6\text{F}_5\text{XeF}_2]^+$ (0.0%); $[\text{C}_6\text{F}_5\text{Xe}]^+$ (95.5%)

Cation/anion ratio^c: cations (90.2%) / anions (100%)

^a The total amount (mol-%) of all C₆F₅ compounds was normalized to 100%.

^b The xenon-balance was calculated from all C₆F₅ signal integrals of xenon containing compounds.

^c The cations, [C₆F₅XeF₂]⁺ and [C₆F₅Xe]⁺, were related to the [C₆F₅BF₃]⁻ and [BF₄]⁻ anions which were set to 100%.

* superimposed signals

b) Reaction of [C₆F₅XeF₂][BF₄] with As(C₆F₅)₃ (suspension)

Same composition than in the initial sample plus the following As-compounds:

As(C₆F₅)₃F₂ δ = -23.6 ppm (m, 2F); -132.6 ppm (m, *o*-C₆F₅, 6F); -145.3 ppm (t, ³J(¹⁹F-¹⁹F) = 20 Hz, *p*-C₆F₅, 3F); -158.1 ppm (m, *m*-C₆F₅, 6F)

As(C₆F₅)₃ δ = -131.5 ppm (m, *o*-C₆F₅, 6F); -148.1 ppm (t, ³J(¹⁹F-¹⁹F) = 20 Hz, *p*-C₆F₅, 1F); -158.1 ppm (m, *m*-C₆F₅, 6F)

C₆F₅-balance^a: [C₆F₅XeF₂]⁺ (0.0%); [C₆F₅Xe]⁺ (81.8%); C₆F₆ (0.6%); C₆F₅H (1.9%); [C₆F₅BF₃]⁻ (3.4%); As(C₆F₅)₃F₂ (7.2%); As(C₆F₅)₃ (5.1%)

xenon-balance^b: [C₆F₅XeF₂]⁺ (0.0%); [C₆F₅Xe]⁺ (95.1%); XeF₂ (4.9%)

Cation/anion ratio^c: cations (94.3%) / anions (100%)

^a The total amount (mol-%) of all C₆F₅ compounds was normalized to 100%.

^b The xenon-balance was calculated from all C₆F₅ signal integrals of xenon containing compounds.

^c The cations, [C₆F₅XeF₂]⁺ and [C₆F₅Xe]⁺, were related to the [C₆F₅BF₃]⁻ and [BF₄]⁻ anions which were set to 100%.

To dissolve the precipitate, more CH₃CN (500 μL) was added to both samples (**a** and **b**) at RT. The solutions were measured again by NMR spectroscopy at RT, showing that the precipitate was only a mixture of M(C₆F₅)₃/ M(C₆F₅)₃F₂.

b) Reaction of [C₆F₅XeF₂][BF₄] with P(C₆F₅)₃ (solution)

C₆F₅-balance^a: [C₆F₅XeF₂]⁺ (0.0%); [C₆F₅Xe]⁺ (12.3%); C₆F₆ (0.3%); C₆F₅H (9.8%); [C₆F₅BF₃]⁻ (0.0%); P(C₆F₅)₃F₂ (39.3%); P(C₆F₅)₃ (34.4%)

xenon-balance^b: [C₆F₅XeF₂]⁺ (0.0%); [C₆F₅Xe]⁺ (100.0%); XeF₂ (0.0%)

Cation/anion ratio^c: no [BF₄]⁻ signal intensity measurable

^a The total amount (mol-%) of all C₆F₅ compounds was normalized to 100%.

^b The xenon-balance was calculated from all C₆F₅ signal integrals of xenon containing compounds.

^c The cations, [C₆F₅XeF₂]⁺ and [C₆F₅Xe]⁺ and were related to the anionic species [C₆F₅BF₃]⁻ and [BF₄]⁻ which were set to 100%.

c) Reaction of $[\text{C}_6\text{F}_5\text{XeF}_2][\text{BF}_4]$ with $\text{P}(\text{C}_6\text{F}_5)_3$ (solution)

C_6F_5 -balance^a: $[\text{C}_6\text{F}_5\text{XeF}_2]^+$ (0.0%); $[\text{C}_6\text{F}_5\text{Xe}]^+$ (29.1%); C_6F_6 (0.3%); $\text{C}_6\text{F}_5\text{H}$ (3.3%); $[\text{C}_6\text{F}_5\text{BF}_3]^-$ (0.0%); $\text{As}(\text{C}_6\text{F}_5)_3\text{F}_2$ (38.3%); $\text{As}(\text{C}_6\text{F}_5)_3$ (29.0%)

xenon-balance^b: $[\text{C}_6\text{F}_5\text{XeF}_2]^+$ (0.0%); $[\text{C}_6\text{F}_5\text{Xe}]^+$ (100.0%); XeF_2 (0.0%)

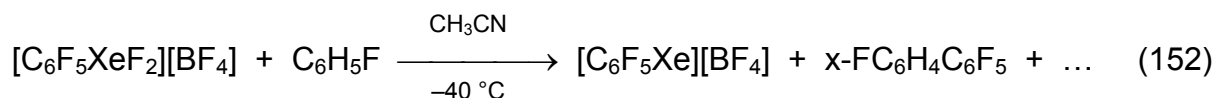
Cation/anion ratio^c: cations (100 %) / anions (100%)

^a The total amount (mol-%) of all C_6F_5 compounds was normalized to 100%.

^b The xenon-balance was calculated from all C_6F_5 signal integrals of xenon containing compounds.

^c The cations, $[\text{C}_6\text{F}_5\text{XeF}_2]^+$ and $[\text{C}_6\text{F}_5\text{Xe}]^+$, were related to the $[\text{C}_6\text{F}_5\text{BF}_3]^-$ and $[\text{BF}_4]^-$ anions which were set to 100%.

IV.13.15 Reaction of $[\text{C}_6\text{F}_5\text{XeF}_2][\text{BF}_4]$ and $\text{C}_6\text{H}_5\text{F}$ in CH_3CN at $-40\text{ }^\circ\text{C}$



In a 3.5 mm i.d. FEP reaction tube, $[\text{C}_6\text{F}_5\text{XeF}_2][\text{BF}_4]$, was dissolved in cold ($-40\text{ }^\circ\text{C}$) CH_3CN (500 μL) and checked by ^{19}F NMR spectroscopy at $-40\text{ }^\circ\text{C}$ to establish its initial condition. To this solution, $\text{C}_6\text{H}_5\text{F}$ (40 μL ; 0.43 mmol) was added, and the solution was periodically shaken before monitored by ^{19}F NMR spectroscopy.

^{19}F NMR (282.40 MHz) in CH_3CN at $-40\text{ }^\circ\text{C}$

$[\text{C}_6\text{F}_5\text{XeF}_2]^+$ $\delta = -27.4$ ppm (s, ^{129}Xe -satellites: $^1J(^{19}\text{F}-^{129}\text{Xe}) = 3894$ Hz, RXeF_2 , 2F); -124.0 ppm (m, *o*- C_6F_5 , 2F); -133.9 ppm (t, $^3J(^{19}\text{F}-^{19}\text{F}) = 20$ Hz, *p*- C_6F_5 , 1F); -152.0 ppm (m, *m*- C_6F_5 , 2F)

$[\text{C}_6\text{F}_5\text{Xe}]^+$ $\delta = -124.7$ ppm (m, *o*- C_6F_5 , 2F); -141.5 ppm (t, $^3J(^{19}\text{F}-^{19}\text{F}) = 20$ Hz, *p*- C_6F_5 , 1F); -154.2 ppm (m, *m*- C_6F_5 , 2F)

$[\text{C}_6\text{F}_5\text{BF}_3]^-$ $\delta = -129.9$ ppm (q, RBF_3 , 3F); -134.8 ppm (m, *o*- C_6F_5 , 2F); -159.4 ppm (t, $^3J(^{19}\text{F}-^{19}\text{F}) = 18$ Hz, *p*- C_6F_5 , 1F); -164.2 ppm (m, *m*- C_6F_5 , 2F)

2- $\text{FC}_6\text{H}_4\text{C}_6\text{F}_5$ $\delta = -113.2$ ppm (m, 2-F, 1F); -143.3 ppm (m, *o*- C_6F_5 , 2F); -156.3 ppm (tt, $^3J(^{19}\text{F}-^{19}\text{F}) = 20$ Hz, $^4J(^{19}\text{F}-^{19}\text{F}) = 1$ Hz, *p*- C_6F_5 , 1F); -163 ppm (m, *m*- C_6F_5 , 2F)

3- $\text{FC}_6\text{H}_4\text{C}_6\text{F}_5$ $\delta = -112.2$ ppm (m, 3-F, 1F); -142.9 ppm (m, *o*- C_6F_5 , 2F); -155.6 ppm (t, $^3J(^{19}\text{F}-^{19}\text{F}) = 20$ Hz, $^4J(^{19}\text{F}-^{19}\text{F}) = 1$ Hz, *p*- C_6F_5 , 1F); -163 ppm (m, *m*- C_6F_5 , 2F)

$4\text{-FC}_6\text{H}_4\text{C}_6\text{F}_5$	$\delta = -111.5$ ppm (m, 4-F, 1F); -140.6 ppm (m, <i>o</i> -C ₆ F ₅ , 2F); -154.9 ppm (t, $^3J(^{19}\text{F}-^{19}\text{F}) = 20$ Hz, $^4J(^{19}\text{F}-^{19}\text{F}) = 2$ Hz, <i>p</i> -C ₆ F ₅ , 1F); -163 ppm (m, <i>m</i> -C ₆ F ₅ , 2F)
$[\text{BF}_4]^-$	$\delta = -147.2$ ppm (s, $^{11}\text{BF}_4$, 4F)
C_6F_6	$\delta = -162.1$ ppm (s, $\Delta\nu_{1/2} = 3$ Hz, 6F)
XeF_2	$\delta = -177.2$ ppm (s, ^{129}Xe -satellites: $^1J(^{19}\text{F}-^{129}\text{Xe}) = 5671$ Hz, 2F)
$\text{CH}_3\text{CN}\cdot\text{HF}$	$\delta = -179.0$ ppm (d, $^1J(^1\text{H}-^{19}\text{F}) = 469$ Hz)

^{11}B -NMR (96.29 MHz) in CH₃CN at -40 °C

$[\text{BF}_4]^-$	$\delta = -0.6$ ppm (s, $\Delta\nu_{1/2} = 2$ Hz)
-------------------	---

^{129}Xe -NMR (83.02 MHz) in CH₃CN at -40 °C

$[\text{C}_6\text{F}_5\text{XeF}_2]^+$	$\delta = -1701.3$ ppm (t, $^1J(^{19}\text{F}-^{129}\text{Xe}) = 3881$ Hz)
--	--

**Composition of Reactants and Products Resulting from the Reaction of
[C₆F₅XeF₂][BF₄] with 20 C₆H₅F in CH₃CN at -40 °C**

time [h]	[C ₆ F ₅ Xe] ^{+ a,b}		FC ₆ H ₄ C ₆ F ₅ ^a			[C ₆ F ₅ BF ₃] ^{- a}	C ₆ F ₆ ^a	XeF ₂ ^b
	I) C ₆ F ₅ -bal.	I) C ₆ F ₅ -bal.	I) C ₆ F ₅ -bal.			I) C ₆ F ₅ -bal.	I) C ₆ F ₅ -bal.	I) C ₆ F ₅ -bal.
	II) Xe-bal. [mol-%]	II) Xe-bal. [mol-%]	2- FC ₆ H ₄ C ₆ F ₅ [mol-%]	3- FC ₆ H ₄ C ₆ F ₅ [mol-%]	4- FC ₆ H ₄ C ₆ F ₅ [mol-%]	[mol-%]	[mol-%]	II) Xe-bal. [mol-%]
1.5	I) 14.8	I) 78.1	I) 0.5	I) 0.7	I) 0.7	I) 3.6	I) 1.6	I) 3.0
	II) 15.4	II) 81.4						II) 3.2
4	I) 26.7	I) 63.5	I) 1.2	I) 1.2	I) 1.7	I) 2.9	I) 2.9	I) 2.8
	II) 28.7	II) 68.2						II) 3.0
20	I) 43.5	I) 44.3	I) 2.0	I) 1.9	I) 2.0	I) 2.4	I) 3.9	I) 3.6
	II) 47.6	II) 48.5						II) 3.9
44	I) 53.0	I) 31.5	I) 2.7	I) 3.0	I) 3.4	I) 1.5	I) 4.9	I) 6.7
	II) 58.1	II) 34.6						II) 7.4
68	I) 68.0	I) 11.1	I) 4.2	I) 4.5	I) 4.7	I) 1.2	I) 6.3	I) 10.2
	II) 76.1	II) 12.5						II) 11.5
192	I) 74.8	I) 0.0	I) 5.5	I) 5.6	I) 6.0	I) 1.1	I) 7.0	I) 10.0
	II) 88.2	II) 0.0						II) 11.8

V Summary

Four new $[\text{C}_6\text{F}_5\text{Xe}]^+$ salts, namely $[\text{C}_6\text{F}_5\text{Xe}][\text{B}(\text{CN})_4]$, $[\text{C}_6\text{F}_5\text{Xe}][\text{B}(\text{CF}_3)_4]$, $[\text{C}_6\text{F}_5\text{Xe}][\text{B}(\text{OTeF}_5)_4]$, and $[\text{C}_6\text{F}_5\text{Xe}][\text{B}(\text{C}_6\text{F}_5)_4]$ were prepared by metathesis reactions of $[\text{C}_6\text{F}_5\text{Xe}][\text{BF}_4]$ and the corresponding salts, $\text{M}[\text{BY}_4]$ ($\text{Y} = \text{CN}, \text{CF}_3, \text{OTeF}_5,$ and C_6F_5 ; $\text{M} = \text{K}, \text{Cs}$), in CH_3CN at ambient temperature and isolated as pale yellow solids. Complete characterizations of the salts, $[\text{C}_6\text{F}_5\text{Xe}][\text{BY}_4]$ ($\text{Y} = \text{F}, \text{CN}, \text{CF}_3, \text{OTeF}_5,$ and C_6F_5), were accomplished by multi-NMR and Raman spectroscopy, X-ray crystallography, thermo-analytical measurements, and by computational studies.

The characterization in CH_3CN solution or, in so far as was possible, in CH_2Cl_2 solution was performed by multi-NMR spectroscopy. In CH_3CN solution, the anions, $[\text{BY}_4]^-$ ($\text{Y} = \text{CN}, \text{CF}_3, \text{OTeF}_5,$ and C_6F_5), were all found to be less coordinating than CH_3CN resulting in the formation of the $[\text{C}_6\text{F}_5\text{Xe}\cdot\text{NCCH}_3]^+$ cation-base adduct, in which the C_6F_5 groups have identical chemical shift values. A similar trend was observed for the $^3J(^{19}\text{F}-^{129}\text{Xe})$ spin-spin coupling constant, which was also independent of the counteranion for all leading to the salts $[\text{C}_6\text{F}_5\text{Xe}\cdot\text{NCCH}_3]^+$ cation-base adduct. The chemical shifts of the counteranions were found not to be affected by the base-buffered $[\text{C}_6\text{F}_5\text{Xe}\cdot\text{NCCH}_3]^+$ cation and are comparable to those previously reported. For the first time, it was possible to obtain fully resolved NMR spectra of the $[\text{C}_6\text{F}_5\text{Xe}\cdot\text{NCCH}_3]^+$ adduct-cation at 7.0463 T showing all of the expected $^{19}\text{F}-^{129}\text{Xe}$ spin-spin couplings in the ^{129}Xe NMR spectra and all of the expected $^{19}\text{F}-^{19}\text{F}$ spin-spin couplings of the *p*- C_6F_5 fluorine atom in the ^{19}F NMR spectra.

Access to the CH_2Cl_2 -soluble salts, $[\text{C}_6\text{F}_5\text{Xe}][\text{BY}_4]$ ($\text{Y} = \text{OTeF}_5, \text{CF}_3,$ and C_6F_5), opened up the possibility to examine the properties of the weakly coordinated $[\text{C}_6\text{F}_5\text{Xe}]^+$ cation. It appears that only salts containing very weakly coordinating anions such as $[\text{B}(\text{CF}_3)_4]^-$, $[\text{B}(\text{OTeF}_5)_4]^-$, and $[\text{B}(\text{C}_6\text{F}_5)_4]^-$ are soluble in weakly coordinating solvents such as CH_2Cl_2 , SO_2ClF , and $\text{CF}_3\text{CH}_2\text{CF}_2\text{CH}_3$, whereas $[\text{BF}_4]^-$ and $[\text{B}(\text{CN})_4]^-$ salts are insoluble. It was found that only solutions of $[\text{C}_6\text{F}_5\text{Xe}][\text{B}(\text{CF}_3)_4]$ in CH_2Cl_2 and $\text{CF}_3\text{CH}_2\text{CF}_2\text{CH}_3$ are stable at ambient temperature for more than 3 and 5 days, respectively, contrasting with CH_2Cl_2 solutions of $[\text{C}_6\text{F}_5\text{Xe}][\text{B}(\text{C}_6\text{F}_5)_4]$ and $[\text{C}_6\text{F}_5\text{Xe}][\text{B}(\text{OTeF}_5)_4]$, which must be maintained at temperatures below -40°C to avoid rapid decomposition. A comparison of the ^{19}F NMR chemical shifts was

undertaken using $[\text{C}_6\text{F}_5\text{Xe}][\text{B}(\text{CF}_3)_4]$ in CH_3CN , $\text{CF}_3\text{CH}_2\text{CF}_2\text{CH}_3$, and CH_2Cl_2 at 24 °C. In CH_2Cl_2 , it was found that the C_6F_5 fluorine resonances were shifted to higher frequencies (~5 ppm; *m*- and *p*- C_6F_5), indicative of a more weakly coordinated $[\text{C}_6\text{F}_5\text{Xe}]^+$ cation.

A very interesting question was how CH_3CN coordination affects changes in the geometry and bonding of the *ipso*-C-Xe bond. The fully assigned vibrational spectra of $[\text{C}_6\text{F}_5\text{Xe}][\text{BY}_4]$ ($\text{Y} = \text{CN}$, CF_3 , and C_6F_5) and the X-ray crystal structures of $[\text{C}_6\text{F}_5\text{Xe}][\text{B}(\text{CN})_4]$, $[\text{C}_6\text{F}_5\text{Xe}][\text{B}(\text{CF}_3)_4]$, $[\text{C}_6\text{F}_5\text{Xe}\cdot\text{NCCH}_3][\text{B}(\text{CF}_3)_4]$, and $[\text{C}_6\text{F}_5\text{Xe}\cdot\text{NCCH}_3][\text{B}(\text{C}_6\text{F}_5)_4]$, clearly show the astonishing insensitivity of the geometry and bond lengths upon coordination of CH_3CN . The vibrational assignments for $[\text{C}_6\text{F}_5\text{Xe}]^+$, $[\text{C}_6\text{F}_5\text{Xe}\cdot\text{NCCH}_3]^+$, $\text{C}_6\text{F}_5\text{I}$, CH_3CN were made with the assistance of quantum mechanical calculations carried out at the HF and DFT ((SDB-)cc-pVTZ) levels of theory and allowed valid comparisons to be made. The characteristic $\nu(\text{C-Xe})$ stretch was the most intense resonance in the Raman spectra of $[\text{C}_6\text{F}_5\text{Xe}][\text{B}(\text{CN})_4]$ and $[\text{C}_6\text{F}_5\text{Xe}][\text{BF}_4]$ at 201 and 205 cm^{-1} , respectively, and are comparable to the intense mode of $\text{C}_6\text{F}_5\text{I}$ at 204 cm^{-1} . The $\nu(\text{C-Xe})$ mode in the $[\text{C}_6\text{F}_5\text{Xe}\cdot\text{NCCH}_3]^+$ adduct-cation is predicted to shift to lower frequency by 14 cm^{-1} upon coordination, but, in practice, it is observed at ca. 200 cm^{-1} in both the non- CH_3CN -coordinated cation and in the CH_3CN -coordinated adduct-cation. The $\nu(\text{C-N})$ stretch is expected to shift by 10 cm^{-1} to higher frequency upon coordination, which is in good agreement with the observed shift at -150 °C ($\text{CH}_3\text{CN} = 2267 \text{ cm}^{-1}$; $[\text{C}_6\text{F}_5\text{Xe}\cdot\text{NCCH}_3]^+ = 2278$ and 2273 cm^{-1}).

The structural data for both the $[\text{C}_6\text{F}_5\text{Xe}]^+$ cation and the $[\text{C}_6\text{F}_5\text{Xe}\cdot\text{NCCH}_3]^+$ adduct-cation obtained from the crystal structures of $[\text{C}_6\text{F}_5\text{Xe}][\text{B}(\text{CN})_4]$, $[\text{C}_6\text{F}_5\text{Xe}\cdot\text{NCCH}_3][\text{B}(\text{CF}_3)_4]$, $[\text{C}_6\text{F}_5\text{Xe}\cdot\text{NCCH}_3][\text{B}(\text{C}_6\text{F}_5)_4]$, and $[\text{C}_6\text{F}_5\text{Xe}][\text{B}(\text{CF}_3)_4]$ are not affected, within $\pm 3\sigma$, and are in good agreement with the calculated values for the gas phase. The C-Xe bond length of $[\text{C}_6\text{F}_5\text{Xe}]^+$ of 2.104(6) Å and $[\text{C}_6\text{F}_5\text{Xe}\cdot\text{NCCH}_3]^+$ of 2.099(6) Å are also found to be equal within $\pm 3\sigma$. A significant cation-anion interaction was thereby obtained in the crystal structure of $[\text{C}_6\text{F}_5\text{Xe}][\text{B}(\text{CN})_4]$ (2.716(3) Å) whereas well separated cations and anions were obtained in the crystal structures of $[\text{C}_6\text{F}_5\text{Xe}\cdot\text{NCCH}_3][\text{B}(\text{CF}_3)_4]$ (3.317(7) Å) and $[\text{C}_6\text{F}_5\text{Xe}\cdot\text{NCCH}_3][\text{B}(\text{C}_6\text{F}_5)_4]$ (3.202(18) Å). The very weak cation-anion interaction of the $[\text{C}_6\text{F}_5\text{Xe}]^+$ and $[\text{B}(\text{CF}_3)_4]^-$ determined from the NMR data was confirmed in the crystal structure, with the closest Xe-F contact at 2.913(4) Å, which is 0.197 Å longer than the closest Xe-N contact in $[\text{C}_6\text{F}_5\text{Xe}][\text{B}(\text{CN})_4]$.

Thermal stability studies of the new $[\text{C}_6\text{F}_5\text{Xe}]^+$ salts were performed in solution and the solid state. Thermo-analytical DSC measurements of the solids have confirmed that $[\text{C}_6\text{F}_5\text{Xe}][\text{AsF}_6]$ and $[\text{C}_6\text{F}_5\text{Xe}][\text{BF}_4]$ have melting points of 80.9 and 110.0 °C, respectively. The reversibility of the melting process was proved experimentally and occurred without decomposition. In contrast, the salts, $[\text{C}_6\text{F}_5\text{Xe}][\text{B}(\text{CN})_4]$, $[\text{C}_6\text{F}_5\text{Xe}][\text{B}(\text{CF}_3)_4]$, and $[\text{C}_6\text{F}_5\text{Xe}][\text{B}(\text{C}_6\text{F}_5)_4]$, decompose exothermally without melting at 85.2, 117.2, and 152.2 °C, respectively.

The stability in solution was examined with respect to the different counteranions in CH_3CN and CH_2Cl_2 at ambient temperature. The high stability of the $[\text{C}_6\text{F}_5\text{Xe}][\text{BF}_4]$ salt in aHF (only 15% conversion to C_6F_6 within 54 d) was shown. The dominating effect of solvation of the counteranions in aHF and the very slow decomposition rate was not suitable for comparison in the series of $[\text{C}_6\text{F}_5\text{Xe}][\text{BY}_4]$ salts. The decomposition pathway in CH_3CN was shown to be initiated by coordination of CH_3CN to the Xe(II) center followed by a homolytic cleavage of the C-Xe bond. The resulting $\text{C}_6\text{F}_5\cdot$ radical attacks the solvent and forms mainly, and in some cases only, $\text{C}_6\text{F}_5\text{H}$. The decomposition rates (total decomposition times) were $[\text{C}_6\text{F}_5\text{Xe}][\text{BF}_4]$ (67 d) < $[\text{C}_6\text{F}_5\text{Xe}][\text{B}(\text{CN})_4]$ (60 d) < $[\text{C}_6\text{F}_5\text{Xe}][\text{B}(\text{CF}_3)_4]$ (43 d) < $[\text{C}_6\text{F}_5\text{Xe}][\text{B}(\text{OTeF}_5)_4]$ (>24 d) < $[\text{C}_6\text{F}_5\text{Xe}][\text{B}(\text{C}_6\text{F}_5)_4]$ (11 d). Decomposition in CH_2Cl_2 was examined for $[\text{C}_6\text{F}_5\text{Xe}][\text{B}(\text{CF}_3)_4]$ and $[\text{C}_6\text{F}_5\text{Xe}][\text{B}(\text{C}_6\text{F}_5)_4]$, and showed decomposition rates comparable to those obtained in CH_3CN . The pathway is likely initiated by coordination of CH_2Cl_2 to the positively charged xenon center of the $[\text{C}_6\text{F}_5\text{Xe}]^+$ cation. The following decomposition is assumed to occur by a pathway analogous to that described for CH_3CN but results in $\text{C}_6\text{F}_5\text{H}$ and $\text{C}_6\text{F}_5\text{Cl}$ as the main decomposition products.

It had been previously shown that $[\text{C}_6\text{F}_5\text{Xe}][\text{AsF}_6]$ reacts with aromatic compounds, such as $\text{C}_6\text{H}_5\text{R}$ ($\text{R} = \text{CH}_3, \text{F}, \text{CF}_3, \text{NO}_2, \text{and CN}$) in CH_3CN at ambient temperature and formed isomeric mixtures of polyfluorobiphenyls, $x\text{-RC}_6\text{H}_4\text{C}_6\text{F}_5$ ($x = 2, 3, 4, \text{R} = \text{CH}_3, \text{F}, \text{CN}, \text{CF}_3, \text{NO}_2$).^[83] These preliminary experiments have demonstrated that electron-rich aromatics react faster than electron-poor aromatics. In this Thesis, the reaction pathways as well as the major parameters influencing reactivity were investigated in detail. Five borate salts, $[\text{C}_6\text{F}_5\text{Xe}][\text{BY}_4]$ ($\text{Y} = \text{F}, \text{CN}, \text{CF}_3, \text{OTeF}_5, \text{and C}_6\text{F}_5$), were reacted with different amounts (1.2, 20, 200, neat) of $\text{C}_6\text{H}_5\text{F}$ in different solvents ($\text{CH}_3\text{CN}, \text{CH}_2\text{Cl}_2$). All reactions yielded mainly polyfluorobiphenyl isomers, $x\text{-FC}_6\text{H}_4\text{C}_6\text{F}_5$ ($x = 2, 3, \text{and } 4$). The only significant

difference was the rate of reaction which was as follows for CH₃CN solutions and 20-molar amounts of C₆H₅F: [C₆F₅Xe][B(CF₃)₄] (5 d) > [C₆F₅Xe][B(C₆F₅)₄] (>6 d) ≈ [C₆F₅Xe][B(CN)₄] (7 d) > [C₆F₅Xe][BF₄] (17 d). The initial step of the reaction, the coordination of a nucleophile to the positively charged Xe(II) center can occur with basic solvent molecules, the counteranion of the [C₆F₅Xe]⁺ cation or with fluorobenzene. However, it was found that in the presence of C₆H₅F, a much faster rate of biphenyl formation was observed in cases of nucleophilic anions. Differences in the reaction rate were mainly dependent on the nucleophilicity of the counteranion. More strongly coordinating anions inhibit the reaction because of competing anions in the inner coordination sphere of Xe(II), whereas in cases of weakly coordinating anions more basic solvent molecules and fluorobenzene dominate the inner coordination sphere. The fastest reaction was found for reactions of [C₆F₅Xe]⁺ salts which were soluble in neat fluorobenzene. Only salts having weakly coordinating anions, [C₆F₅Xe][B(CF₃)₄] and [C₆F₅Xe][B(C₆F₅)₄], were soluble in C₆H₅F at ambient temperatures, whereas [C₆F₅Xe][BF₄] and [C₆F₅Xe][B(CN)₄] were insoluble.

There was, up to now, only one example of an organoxenon(IV) compound, difluoropentafluorophenylxenon(IV) tetrafluoroborate, [C₆F₅XeF₂][BF₄]. In the framework of this Thesis, its preparation was analyzed and the parameters influencing the synthesis were optimized. It is now possible to prepare pure [C₆F₅XeF₂][BF₄] in almost quantitative yield. It was found that the ochre yellow solid was shock sensitive and decomposed explosively without any residue at -80 °C.

It was possible to prepare a second example of an organoxenon(IV) compound, [C₆F₅XeF₂][B(CF₃)₄] by the metathesis reaction of [C₆F₅XeF₂][BF₄] with M[B(CF₃)₄] (M = K, Cs) in CH₃CN at -40 °C. Rapid decomposition of the [C₆F₅XeF₂]⁺ cation occurred in CH₃CN even at -40 °C so that it was, unfortunately, not possible to isolate the new salt as a solid.

The salt, [C₆F₅XeF₂][BF₄], was characterized in CH₃CN and aHF by multi-NMR spectroscopy. The results obtained in aHF exhibit a less coordinated [C₆F₅XeF₂]⁺ cation compared with the CH₃CN solution, where the [C₆F₅XeF₂·(NCCH₃)_n]⁺ adduct is formed. Two-dimensional selective decoupling NMR experiments were used to analyse all expected spin-spin couplings, showing that the pseudo-nonet pattern of the *para* fluorine atom in the ¹⁹F spectrum consists of a triplet of triplets of triplets attributed to 3-bond, 4-bond, and 6-bond ¹⁹F-¹⁹F spin couplings. In contrast to [C₆F₅Xe]⁺ no ¹⁹F-¹²⁹Xe spin coupling was obtained.

Prior to this work there was a complete lack of solid state information on $[\text{C}_6\text{F}_5\text{XeF}_2]^+$ either by way of X-ray crystal structure or vibrational studies. The X-ray crystal structure of $[\text{C}_6\text{F}_5\text{XeF}_2][\text{BF}_4]$ represents the first crystallographic characterization of a C-Xe(IV) compound. The structure allowed “uncoordinated” $[\text{C}_6\text{F}_5\text{XeF}_2]^+$ cation and $[\text{C}_6\text{F}_5\text{XeF}_2 \cdot (\text{NCCH}_3)_n]^+$ adduct-cations with one and two CH_3CN molecules coordinated to the xenon(IV) center to be obtained. The structural investigations have shown comparable fluoride donor and acceptor abilities towards neighbour molecules as previously shown in the crystal structure of isoelectronic $\text{C}_6\text{F}_5\text{IF}_2$.

Vibrational spectra of $[\text{C}_6\text{F}_5\text{XeF}_2][\text{BF}_4]$ were recorded and completely assigned and were also compared with that of isoelectronic $\text{C}_6\text{F}_5\text{IF}_2$, which was also completely assigned for the first time. The vibrational assignments for $[\text{C}_6\text{F}_5\text{XeF}_2]^+$ and $\text{C}_6\text{F}_5\text{IF}_2$, were made with the assistance of quantum mechanical calculations carried out at the HF and DFT ((SDB-)cc-pVTZ) levels of theory. The electronic structures of the $[\text{C}_6\text{F}_5\text{XeF}_2]^+$ cation, the $[\text{C}_6\text{F}_5\text{XeF}_2 \cdot \text{NCCH}_3]^+$, $[\text{C}_6\text{F}_5\text{XeF}_2 \cdot (\text{NCCH}_3)_2]^+$ solvent-adduct cation, and $\text{C}_6\text{F}_5\text{IF}_2$ were additionally calculated using Hartree-Fock (HF) and density function theory (DFT) with the Stuttgart and (SDB-)cc-pVTZ basis sets.

Thermal stability studies of the $[\text{C}_6\text{F}_5\text{XeF}_2][\text{BY}_4]$ ($\text{Y} = \text{F}, \text{CF}_3$) salts were performed in solutions and in suspensions. The pale ochre solid, $[\text{C}_6\text{F}_5\text{XeF}_2][\text{BF}_4]$, was insoluble in weakly coordinating solvents such as CH_2Cl_2 , SO_2ClF , and $\text{CF}_3\text{CH}_2\text{CF}_2\text{CH}_3$, consistent with the assumption of a strong cation-anion interaction in the solid state, but were very soluble in aHF and CH_3CN .

The rate of decomposition in CH_3CN and aHF was studied and showed that decomposition in CH_3CN at $-40\text{ }^\circ\text{C}$ proceeded faster (58 d) than in aHF solution (88 d) at $-40\text{ }^\circ\text{C}$. The decomposition pathways were analyzed and the factor that influenced the decomposition were studied and led to a proposal for the main decomposition pathway. The main decomposition product in CH_3CN at $-40\text{ }^\circ\text{C}$ is $[\text{C}_6\text{F}_5\text{Xe}][\text{BF}_4]$ (83%) besides significant amounts of XeF_2 (36%) and HF (46%). Only small amounts of C_6F_6 (13%) and its fluorinated product, c- C_6F_8 -1,4 (4%), and no c- C_6F_{10} were detected. The decomposition likely occurred in three steps: approach of CH_3CN , coordination of CH_3CN and subsequent electron transfer under formation of $[\text{C}_6\text{F}_5\text{Xe}]^+$, 2 F^- , and $2\text{ CH}_3\text{CN}^{\bullet+}$.

The main decomposition products in aHF are different which is indicative of the higher oxidation potential of the $[\text{C}_6\text{F}_5\text{XeF}_2]^+$ cation in aHF solution. The main decomposition products were mainly XeF_2 and C_6F_6 from solvolysis of the C-Xe bond. Further interactions of XeF_2 with C_6F_6 yields the oxidation products of C_6F_6 , namely *c*- C_6F_8 -1,4 and *c*- C_6F_{10} . The influence of bases on the stability of $[\text{C}_6\text{F}_5\text{XeF}_2][\text{BF}_4]$ were also examined in both CH_3CN and aHF solution. It was found that the decomposition rate in aHF in the presence of KF or $\text{K}[\text{C}_6\text{F}_5\text{BF}_3]$ was 400 and 4250 times faster than without basic additives. The rate of consumption of the $[\text{C}_6\text{F}_5\text{XeF}_2]^+$ cation in CH_3CN and in the presence of $\text{K}[\text{C}_6\text{F}_5\text{BF}_3]$ was roughly 10 times faster than without addition of $\text{K}[\text{C}_6\text{F}_5\text{BF}_3]$.

The reactivity of the $[\text{C}_6\text{F}_5\text{XeF}_2]^+$ cation was previously limited to reactions with I_2 , $\text{C}_6\text{F}_5\text{I}$ and $\text{P}(\text{C}_6\text{F}_5)_3$.^[72] The evaluation of the oxidation strength of $[\text{C}_6\text{F}_5\text{XeF}_2]^+$ was extended in systematic studies with $\text{Pn}(\text{C}_6\text{F}_5)_3$ compounds (Pn = P, As, Bi) and $\text{C}_6\text{F}_5\text{Hal}$ (Hal = Br, I) in CH_3CN and aHF solution. The salt, $[\text{C}_6\text{F}_5\text{XeF}_2][\text{BF}_4]$, was reacted with $\text{C}_6\text{F}_5\text{I}$ and $\text{C}_6\text{F}_5\text{Br}$ in CH_3CN and aHF at $-40\text{ }^\circ\text{C}$. The reaction of $[\text{C}_6\text{F}_5\text{XeF}_2][\text{BF}_4]$ with excess $\text{C}_6\text{F}_5\text{I}$ quantitatively yielded, in a rapid reaction (15 – 30 minutes) at $-40\text{ }^\circ\text{C}$, and independent of the solvent, CH_3CN or aHF, $\text{C}_6\text{F}_5\text{IF}_2$. No formation of $\text{C}_6\text{F}_5\text{BrF}_2$ was obtained in CH_3CN and aHF at $-40\text{ }^\circ\text{C}$. Fluorination of the C_6F_5 group of $\text{C}_6\text{F}_5\text{Br}$ was detected at elevated temperatures ($-20\text{ }^\circ\text{C}$) in aHF but $\text{C}_6\text{F}_5\text{BrF}_2$ was not formed. Rapid reactions of $[\text{C}_6\text{F}_5\text{XeF}_2][\text{BF}_4]$ with $\text{Pn}(\text{C}_6\text{F}_5)_3$ (Pn = P, As, Bi) (15 minutes) occurred at $-40\text{ }^\circ\text{C}$ even under moderate conditions (coordinating solvent CH_3CN) and yielded in all cases examined the corresponding Pn(V) compound, $(\text{C}_6\text{F}_5)_3\text{PnF}_2$ (Pn = P, As, Bi). The main co-product detected was the $[\text{C}_6\text{F}_5\text{Xe}][\text{BF}_4]$. The successful fluorination of $\text{Bi}(\text{C}_6\text{F}_5)_3$ illustrates the strongly oxidative fluorination ability of the $[\text{C}_6\text{F}_5\text{XeF}_2]^+$ cation.

References

- [1] G. J. Schrobilgen, in *Synthetic Fluorine Chemistry*, Vol. 29 (Eds.: G. A. Olah, G. K. S. Prakash, R. D. Chambers), New York, **1982**, pp. 167.
- [2] G. J. Schrobilgen, M. D. Moran, *Kirk Oth Ect.* **2003**, 1.
- [3] G. J. Schrobilgen, in *The Encyclopedia of Nuclear Magnetic Resonance* (Eds.: D. M. Grant, R. K. Harris), John Wiley & Sons, Inc., New York, **1996**, p. 3251.
- [4] H. Selig, J. H. Holloway, in *Top. Curr. Chem.*, Vol. 124 (Ed.: F. L. Boschke), Springer Verlag, Berlin, **1984**, pp. 33.
- [5] J. H. Holloway, in *Noble Gas Chemistry*, Methuen & Co., Bungay, Suffolk, **1968**.
- [6] H. H. Claassen, *The Noble Gases*, D.C. Heath & Co., Boston, **1966**.
- [7] H. H. Hyman, *Noble Gas Compounds*, University of Chicago Press, Chicago, **1963**.
- [8] G. J. Schrobilgen, in *NMR and the Periodic Table*, Vol. Chapt. 14 (Ed.: R. K. Mann), Academic Press, London, **1974**, pp. 439.
- [9] R. J. Gillespie, B. Landa, G. J. Schrobilgen, *J. Inorg. Nucl. Chem.* **1976**, 179.
- [10] M. Gerken, G. J. Schrobilgen, *Coord. Chem. Rev.* **2000**, 197, 335.
- [11] N. Bartlett, F. O. Sladky, in *Comprehensive Inorganic Chemistry*, Vol. Vol. 1, Chapt. 6 (Eds.: J. C. Bailar, H. J. Emeleus, R. Nyholm, A. F. Trotman-Dickenson), Pergamon Press, New York, **1973**.
- [12] K. O. Christe, *Angew. Chem.* **2001**, 113, 1465.
- [13] P. Lazlo, G. J. Schrobilgen, *Angew. Chem.* **1988**, 100, 495.
- [14] J. F. Liebman, C. A. Deakyne, *J. Fluorine Chem.* **2003**, 121, 1.
- [15] N. Bartlett, *Proc. Chem. Soc.* **1962**, 218.
- [16] L. Graham, O. Graudejus, N. K. Jha, N. Bartlett, *Coord. Chem. Rev.* **2000**, 197, 321.
- [17] H. H. Claassen, H. Selig, J. G. Malm, *J. Am. Chem. Soc.* **1962**, 84, 3593.
- [18] R. Hoppe, W. Dähne, H. Mattauch, K. Rödder, *Angew. Chem. Int. Ed. Engl.* **1962**, 1, 599.
- [19] S. Reichman, F. Schreiner, *J. Chem. Phys.* **1969**, 51, 2355.
- [20] J. H. Burns, P. A. Agron, H. A. Levy, *Science* **1963**, 139, 1208.
- [21] H. H. Rupp, K. Seppelt, *Angew. Chem. Int. Ed. Engl.* **1974**, 13, 612.
- [22] H. Meinert, *Z. Chem.* **1966**, 6, 71.

- [23] W. F. Howard, L. Andrews, *J. Am. Chem. Soc.* **1974**, *96*, 7864.
- [24] G. J. Perlow, M. R. Perlow, *J. Chem. Phys.* **1964**, *41*, 1157.
- [25] G. J. Perlow, M. R. Perlow, *J. Chem. Phys.* **1968**, *48*, 955.
- [26] G. J. Perlow, H. Yoshida, *J. Chem. Phys.* **1968**, *49*, 1474.
- [27] P. Boldrini, R. J. Gillespie, P. R. Ireland, G. J. Schrobilgen, *Inorg. Chem.* **1974**, *13*, 1690.
- [28] J. H. Holloway, G. J. Schrobilgen, *Inorg. Chem.* **1980**, *19*, 2632.
- [29] J. H. Holloway, G. J. Schrobilgen, *Inorg. Chem.* **1981**, *20*, 3363.
- [30] R. J. Gillespie, G. J. Schrobilgen, *Inorg. Chem.* **1974**, *13*, 1694.
- [31] G. Frlec, J. H. Holloway, *J. Chem. Soc., Dalton. Trans.* **1975**, 535.
- [32] N. Vasdev, B. E. Pointner, R. Chirakal, G. J. Schrobilgen, *J. Am. Chem. Soc.* **2002**, *124*, 12863.
- [33] R. Hagiwara, F. Hollander, C. Maines, N. Bartlett, *Eur. J. Solid State Inorg. Chem.* **1991**, *28*, 855.
- [34] K. Matsumoto, R. Hagiwara, Y. Ito, O. Tamada, *Solid State Sci.* **2002**, *4*, 1465.
- [35] M. Tramšec, P. Benkic, A. Turicnik, G. Tavcar, B. Žemva, *J. Fluorine Chem.* **2002**, *114*, 143.
- [36] M. Tramšec, E. Lork, R. Mews, B. Žemva, *J. Solid State Chem.* **2001**, *162*, 243.
- [37] M. Tramšec, P. Benkic, B. Žemva, *Solid State Sci.* **2002**, *4*, 9.
- [38] G. Tavcar, P. Benkic, B. Žemva, *Inorg. Chem.* **2004**, *43*, 1452.
- [39] G. Tavcar, B. Žemva, *Inorg. Chem.* **2005**, *in press*.
- [40] P. Benkic, M. Tramšec, B. Žemva, *Solid State Sci.* **2002**, *4*, 1425.
- [41] M. Tramšec, P. Benkic, B. Žemva, *Inorg. Chem.* **2004**, *43*, 699.
- [42] A. Turicnik, P. Benkic, B. Žemva, *Inorg. Chem.* **2002**, *41*, 5521.
- [43] P. Boldrini, R. J. Gillespie, P. R. Ireland, G. J. Schrobilgen, *Inorg. Chem.* **1974**, *13*, 1690.
- [44] D. E. McKee, A. Zalkin, N. Bartlett, *Inorg. Chem.* **1973**, *12*, 1713.
- [45] R. J. Gillespie, D. Martin, G. J. Schrobilgen, D. R. Slim, *J. Chem. Soc., Chem. Commun.* **1977**, 2234.
- [46] K. O. Christe, E. C. Curtis, D. A. Dixon, H. P. A. Mercier, J. C. P. Sanders, G. J. Schrobilgen, *J. Am. Chem. Soc.* **1991**, *113*, 3351.
- [47] N. Maggiorosa, Dissertation thesis, Universität zu Köln (Köln, Nordrhein-Westfalen, Germany), **1999**.

- [48] K. O. Christe, W. W. Wilson, G. W. Drake, D. A. Dixon, J. A. Boatz, R. Z. Gnann, *J. Am. Chem. Soc.* **1998**, *120*, 4711.
- [49] B. Žemva, *Croat. Chem. Acta.* **1988**, *61*, 163.
- [50] A. F. Hollemann, E. Wiberg, *Lehrbuch der anorganischen Chemie*, de Gruyter, Berlin, **1985**.
- [51] J. Berkowitz, W. A. Chupka, *Chem. Phys. Lett.* **1970**, *7*, 447.
- [52] G. Frenking, W. Koch, C. A. Deakyne, J. F. Liebman, N. Bartlett, *J. Am. Chem. Soc.* **1989**, *111*, 31.
- [53] M. W. Wong, L. Radom, *J. Chem. Soc., Chem. Commun.* **1989**, 719.
- [54] L. Khriachtchev, M. Pettersson, N. Runeberg, J. Lundell, M. Räsänen, *Nature* **2000**, *406*, 874.
- [55] M. W. Wong, *J. Am. Chem. Soc.* **2000**, *122*, 6289.
- [56] L. J. Turbini, R. E. Aikman, R. J. Lagow, *J. Am. Chem. Soc.* **1979**, *101*, 5833.
- [57] M. Schmeißer, R. Walter, D. Naumann, *Z. Anorg. Allg. Chem.* **1980**, *464*, 233.
- [58] D. Naumann, W. Tyrra, *J. Chem. Soc., Chem. Commun.* **1989**, 47.
- [59] H.-J. Frohn, S. Jakobs, G. Henkel, *Angew. Chem.* **1989**, *101*, 1534.
- [60] H.-J. Frohn, S. Jakobs, *J. Chem. Soc., Chem. Commun.* **1989**, 625.
- [61] D. Naumann, H. Butler, R. Gnann, W. Tyrra, *Inorg. Chem.* **1993**, *32*, 861.
- [62] H.-J. Frohn, C. Rossbach, *Z. Anorg. Allg. Chem.* **1993**, *619*, 1672.
- [63] H.-J. Frohn, S. Jakobs, C. Rossbach, *Eur. J. Solid State Inorg. Chem.* **1992**, *29*, 729.
- [64] Y. L. Yagupolskii, W. Tyrra, R. Gnann, N. Maggiasosa, D. Naumann, *J. Fluorine Chem.* **2002**, *113*, 143.
- [65] H. Butler, D. Naumann, W. Tyrra, *Eur. J. Solid State Inorg. Chem.* **1992**, *29*, 739.
- [66] D. Naumann, W. Tyrra, D. Pfolk, *Z. Anorg. Allg. Chem.* **1994**, *620*, 987.
- [67] H.-J. Frohn, V. V. Bardin, *Z. Anorg. Allg. Chem.* **2003**, *629*, 2465.
- [68] H.-J. Frohn, V. V. Bardin, *Chem. Comm.* **1999**, 919.
- [69] H.-J. Frohn, N. Y. Adonin, V. V. Bardin, *Z. Anorg. Allg. Chem.* **2003**, *629*, 2499.
- [70] H.-J. Frohn, V. V. Bardin, *Chem. Comm.* **2003**, 2352.
- [71] V. V. Zhdankin, P. J. Stang, N. S. Zefirov, *J. Chem. Soc., Chem. Commun.* **1992**, 578.
- [72] H.-J. Frohn, N. LeBlond, K. Lutar, B. Žemva, *Angew. Chem.* **2000**, *112*, 405.

- [73] M. H. Becher, G. J. Schrobilgen, 4GO6 thesis, McMaster University (Hamilton, Canada), **2000**.
- [74] H.-J. Frohn, A. Klose, G. Henkel, *Angew. Chem. Int. Ed. Engl.* **1993**, *32*, 99.
- [75] H.-J. Frohn, T. Schroer, G. Henkel, *Angew. Chem.* **1999**, *111*, 2751.
- [76] H.-J. Frohn, M. Theißen, *Angew. Chem.* **2000**, *112*, 4762.
- [77] H.-J. Frohn, M. Theißen, *J. Fluorine Chem.* **2004**, *125*, 981.
- [78] N. Maggiorosa, D. Naumann, W. Tyrra, *Angew. Chem.* **2000**, *112*, 4759.
- [79] H. Schmidt, H. Scherer, W. Tyrra, J. Hahn, D. Naumann, *Inorg. Chem.* **2004**, *43*, 1837.
- [80] N. Maggiorosa, D. Naumann, W. Tyrra, *Angew. Chem.* **2000**, *39*, 4588.
- [81] H. B. Bock, D. Hinz-Hübner, U. Ruschewitz, D. Naumann, *Angew. Chem.* **2002**, *114*, 465.
- [82] H.-J. Frohn, M. Theißen, *J. Fluorine Chem.* **2004**, *125*, 981.
- [83] H.-J. Frohn, A. Klose, V. V. Bardin, *J. Fluorine Chem.* **1993**, *64*, 201.
- [84] R. D. Chambers, T. Chivers, *Proc. Chem.* **1963**, 208.
- [85] R. D. Chambers, T. Chivers, *J. Chem. Soc.* **1965**, 3933.
- [86] R. D. Chambers, T. Chivers, *Organomet. Chem. Rev.* **1966**, *1*, 279.
- [87] H.-J. Frohn, H. Franke, P. Fritzen, V. V. Bardin, *J. Organometal. Chem.* **2000**, *598*, 127.
- [88] K. Koppe, P. Fritzen, *unpublished results*.
- [89] H.-J. Frohn, T. Schroer, *J. Fluorine Chem.* **2001**, *112*, 259.
- [90] H. Franke, Dissertation thesis, Gerhard-Mercator Universität (Duisburg, Nordrhein-Westfalen, Germany), **2000**.
- [91] T. Scholten, Dissertation thesis, Gerhard-Mercator Universität (Duisburg, Nordrhein-Westfalen, Germany), **1996**.
- [92] H.-J. Frohn, T. Scholten, in *11th European Symposium on Fluorine Chemistry*, Bled, Slovenia, **17.-22. Sept. 1995**, p. 80.
- [93] H.-J. Frohn, A. Klose, T. Schroer, G. Henkel, V. Buss, D. Opitz, R. Vahrenhorst, *Inorg. Chem.* **1998**, *37*, 4884.
- [94] S. Jakobs, Dissertation thesis, Gerhard-Mercator Universität **1991**.
- [95] K. Koppe, *this study*.
- [96] T. Schroer, Dissertation thesis, Gerhard-Mercator Universität (Duisburg, Nordrhein-Westfalen, Germany), **1996**.

- [97] E. Bernhardt, G. Henkel, H. Willner, G. Pawelke, H. Bürger, *Chem. Eur. J.* **2001**, 7, 4696.
- [98] E. Bernhardt, G. Henkel, H. Willner, *Z. Anorg. Allg. Chem.* **2000**, 626, 560.
- [99] E. Bernhardt, M. Berkei, H. Willner, M. Schürmann, *Z. Anorg. Allg. Chem.* **2003**, 629, 677.
- [100] A. Bondi, *J. Phys. Chem.* **1964**, 68, 441.
- [101] H.-J. Frohn, A. Klose, G. Henkel, *GIT Fachz. Lab.* **1993**, 752.
- [102] H.-J. Frohn, S. Görg, G. Henkel, M. Läge, *Z. Anorg. Allg. Chem.* **1995**, 621, 1251.
- [103] I. J. Hyams, E. R. Lipincott, R. T. Bailey, *Spectrochim. Acta* **1966**, 22, 695.
- [104] D. A. Long, D. Steele, *Spectrochim. Acta* **1963**, 19, 1955.
- [105] D. A. Long, D. Steele, *Spectrochim. Acta* **1963**, 19, 1947.
- [106] W. W. Wilson, A. Vij, V. Vij, E. Bernhard, K. O. Christe, *Chem. Eur. J.* **2003**, 9, 2840.
- [107] F. Bailly, P. Barthen, W. Breuer, H.-J. Frohn, M. Giesen, J. Helber, G. Henkel, A. Priewitzer, *Z. Anorg. Allg. Chem.* **2000**, 626, 1406.
- [108] G. J. Schrobilgen, *J. Chem. Soc., Chem. Commun.* **1988**, 1506.
- [109] B. A. Fir, H. Mercier, J. P. Sanders, D. A. Dixon, G. J. Schrobilgen, *J. Fluorine Chem.* **2001**, 110, 89.
- [110] H.-J. Frohn, A. Klose, G. Henkel, *Angew. Chem.* **1993**, 105, 114.
- [111] A. A. A. Emara, Ph.D. thesis, McMaster University (Hamilton, Ontario, Canada), **1991**.
- [112] A. A. A. Emara, G. J. Schrobilgen, *J. Chem. Soc., Chem. Commun.* **1987**, 1644.
- [113] A. A. A. Emara, G. J. Schrobilgen, *J. Chem. Soc., Chem. Commun.* **1988**, 257.
- [114] A. A. A. Emara, G. J. Schrobilgen, *Inorg. Chem.* **1992**, 31, 1323.
- [115] B. Fir, M.Sc. thesis, McMaster University (Hamilton, Ontario, Canada), **1999**.
- [116] C. Eickes, Vordiploma thesis, McMaster University (Hamilton, Ontario, Canada), **1995**.
- [117] K. Koppe, Vordiploma thesis, McMaster University (Hamilton, Ontario, Canada), **1999**.
- [118] K. Koppe, C. Eickes, G. J. Schrobilgen, H. P. A. Mercier, *unpublished results*.
- [119] A. Zalkin, D. L. Ward, R. N. Biagioni, D. H. Templeton, N. Bartlett, *Inorg. Chem.* **1978**, 17, 1318.

- [120] H.-J. Frohn, A. Klose, V. V. Bardin, A. J. Kruppa, T. V. Leshina, *J. Fluorine Chem.* **1995**, *70*, 147.
- [121] A. Terheiden, E. Bernhardt, H. Willner, F. Aubke, *Angew. Chem.* **2002**, *114*, 823.
- [122] M. Finze, E. Bernhard, M. Zähres, H. Willner, *2004* **2004**, *43*, 490.
- [123] H. Kropshofer, O. Leitzke, P. Peringer, F. Sladky, *Chem. Ber.* **1981**, *114*, 2644.
- [124] D. M. V. Seggen, P. K. Hurlburt, M. D. Noiro, O. P. Anderson, S. H. Strauss, *Inorg. Chem.* **1992**, *31*, 1423.
- [125] P. Biagini, G. Luigi, L. Abis, P. A. (Enichem), US Patent 5602269, **1997**.
- [126] M. Bochmann, M. J. Sarsfield, *Organometallics* **1998**, *17*, 5908.
- [127] D. A. Walker, T. J. Woodman, D. L. Hughes, M. Bochmann, *Organometallics* **2001**, *20*, 3772.
- [128] N. Maggiorosa, D. Naumann, W. Tyrra, *Angew. Chem. Int. Ed. Engl.* **2000**, *39*, 4588.
- [129] M. Theissen, Dissertation thesis, Universität Duisburg-Essen (Standort Duisburg) (Duisburg, Nordrhein-Westfalen, Germany), **2000**.
- [130] H.-J. Frohn, H. Franke, V. V. Bardin, *Z. Naturforsch.* **1999**, *54b*, 1495.
- [131] S. H. Strauss, *Chem. Rev.* **1993**, *93*, 927.
- [132] H. P. A. Mercier, M. D. Moran, J. C. P. Sanders, G. J. Schrobilgen, R. J. Suontamo, *Inorg. Chem.* **2005**, *44*, 49.
- [133] A. Klose, Dissertation thesis, Gerhard-Mercator Universität (Duisburg, Nordrhein-Westfalen, Germany), **1993**.
- [134] D. E. McKee, A. Zalkin, N. Bartlett, *Inorg. Chem.* **1973**, *12*, 1713.
- [135] K. Koppe, H.-J. Frohn, G. J. Schrobilgen, H. P. A. Mercier, *unpublished results*.
- [136] H. A. Levy, P. A. Argon, *J. Am. Chem. Soc.* **1963**, *85*, 241.
- [137] D. Naumann, E. Renk, E. Lehmann, *J. Fluorine Chem.* **1977**, *10*, 395.
- [138] S. Hoyer, K. Seppelt, *Angew. Chem.* **2000**, *112*, 1512.
- [139] J. A. Obaleye, L. C. Sams, *Inorg. Nucl. Chem. Letters* **1980**, *16*, 343.
- [140] W. Breuer, H.-J. Frohn, *J. Fluorine Chem.* **1987**, *34*, 443.
- [141] J. A. Berry, G. Oates, J. M. Winfield, *J. Chem. Soc., Dalton. Trans.* **1974**, 509.
- [142] H.-J. Frohn, H. Maurer, *J. Fluorine Chem.* **1986**, *34*, 73.
- [143] J. A. Gibson, R. K. Marat, A. F. Janzen, *Can. J. Chem.* **1975**, *53*, 3044.

- [144] H.-J. Frohn, H. Maurer, *J. Fluorine Chem.* **1986**, *34*, 129.
- [145] R. Kasemann, D. Naumann, *J. Fluorine Chem.* **1988**, *41*, 321.
- [146] T. Lewe, D. Naumann, G. Nowicki, H. Schneider, W. Tyrra, *Z. Anorg. Allg. Chem.* **1997**, *623*, 122.
- [147] W. Tyrra, D. Naumann, *Can. J. Chem.* **1989**, *67*, 1949.
- [148] D. Naumann, W. Tyrra, T. Lewe, *J. Fluorine Chem.* **1997**, *84*, 69.
- [149] W. Tyrra, Dissertation thesis, Universität Dortmund (Dortmund, Nordrhein-Westfalen, Germany), **1989**.
- [150] R. E. Banks, B. E. Smart, J. C. Tatlow, in *Organofluorine Chemistry - Principles and Commercial Applications*, Plenum Press, New York and London, **1994**, pp. 339.
- [151] Bruker, Version 4.0.24 ed., Bruker Optik GmbH, **2002**.
- [152] SMART, Version 5.6.11 ed., Siemens Energy and Automotive Analytical Instrumentation, Madison, WI, **1999**.
- [153] SAINT+, Version 6.02 ed., Siemens Energy and Automotive Analytical Instrumentation, Madison, WI, **1999**.
- [154] G. M. Sheldrick, *SADABS (Siemens Area Detector Adsorption Corrections)*, Version 2.03 ed., Bruker AXS Inc., Madison, WI, **1999**.
- [155] G. M. Sheldrick, *SHELXTL*, Version 5.1 ed., Siemens Analytical X-Ray Instruments, Inc., Madison, WI, **1998**.
- [156] NETZSCH, Proteus, *Messung*, Version 4.2.1 ed., Netzsch Gerätebau GmbH, Selb, Germany, **2002**.
- [157] M. J. Frisch, G. W. Trucks, H. B. Schlegel, G. E. Scuseria, M. A. Robb, J. R. Cheeseman, V. G. Zakrzewski, J. A. Montgomery, R. E. Stratmann, J. C. Burant, S. Dapprich, J. M. Milliam, A. D. Daniels, K. N. Kudin, M. C. Strain, O. Farkas, J. Tomasi, V. Barone, M. Cossi, R. Cammi, B. Mennucci, C. Pomelli, C. Adamo, S. Clifford, J. Ochterski, G. A. Petterson, P. Y. Ayala, Q. Cui, K. Morokuma, P. Salvador, J. J. Dannenberg, D. K. Malick, A. D. Rabuck, K. Raghavachari, J. B. Foresman, J. Cioslowski, J. V. Ortiz, A. G. Baboul, B. B. Stefanov, G. Lui, A. Liashenko, P. Piskorz, I. Komaromi, R. Gomperts, R. L. Martin, D. J. Fox, T. Keith, M. A. Al-Laham, C. Y. Peng, A. Nanayakkara, C. Gonzalez, M. Challacombe, P. M. W. Gill, B. Johnson, W. Chen, M. W. Wong, J. L. Andres, C. Gonzalez, M. Head-Gordon, E. S. Replogle, J. A. Pople, Gaussian 98, revision A.11 ed., Gaussian Inc., Pittsburgh, PA, **2001**.

- [158] G. J. Schrobilgen, J. H. Holloway, P. Granger, C. Brevard, *Inorg. Chem.* **1978**, *17*, 980.
- [159] N. Ignat'ev, P. Sartori, *J. Fluorine Chem.* **2000**, *103*, 57.
- [160] R. Bau, K. O. Christe, J. Feng, R. D. Wilson, W. W. Wilson, *J. Am. Chem. Soc.* **1990**, *112*, 7619.
- [161] H. P. A. Mercier, J. C. P. Sanders, G. J. Schrobilgen, S. S. Tsai, *Inorg. Chem.* **1993**, *32*, 386.
- [162] J. G. Malm, C. L. Chernick, *Inorg. Synth.* **1966**, *43*, 254.
- [163] I. Sheft, M. Splittler, F. H. Martin, *Science* **1964**, *145*, 701.
- [164] H.-J. Frohn, N. Y. Adonin, V. V. Bardin, V. F. Starichenko, *Z. Anorg. Allg. Chem.* **2002**, *628*, 2827.
- [165] H.-J. Frohn, S. Jakobs, G. Henkel, *Angew. Chem. Int. Ed. Engl.* **1989**, *28*, 1506.

VI Appendix

List of Figures

Figure 1	Typical o- and m-C ₆ F ₅ fluorine resonances of the [C ₆ F ₅ Xe] ⁺ cation (in [C ₆ F ₅ Xe][B(CN) ₄] salt) in CH ₃ CN at 24 °C. Asterisks denote ¹²⁹ Xe satellites.....	18
Figure 2	A typical p-C ₆ F ₅ fluorine resonance of the [C ₆ F ₅ Xe] ⁺ cation (in [C ₆ F ₅ Xe][B(CN) ₄] salt) in CH ₃ CN solvent at 24 °C	19
Figure 3	The ¹²⁹ Xe NMR spectrum of [C ₆ F ₅ Xe---NCCH ₃] ⁺ (in [C ₆ F ₅ Xe][B(CF ₃) ₄]), in CH ₃ CN at 24 °C.....	20
Figure 4	Crystal structure of [C ₆ F ₅ Xe·NCCH ₃][B(CF ₃) ₄]. Thermal ellipsoids are shown at the 50% probability level.	25
Figure 5	Crystal structure of [C ₆ F ₅ Xe][B(CF ₃) ₄]. Thermal ellipsoids are shown at the 50% probability level.....	25
Figure 6	Crystal structure of [C ₆ F ₅ Xe·NCCH ₃][B(C ₆ F ₅) ₄]. Thermal ellipsoids are shown at the 50% probability level.	26
Figure 7	Crystal structure of [C ₆ F ₅ Xe][B(CN) ₄]. Thermal ellipsoids are shown at the 50% probability level.....	26
Figure 8	Comparison of the crystal structures of [C ₆ F ₅ Xe] ⁺ , [C ₆ F ₅ Xe·NCCH ₃] ⁺ (both in [C ₆ F ₅ Xe][B(CF ₃) ₄]), and C ₆ F ₅ I. ^[102] Thermal ellipsoids are shown at the 50% probability level.....	30
Figure 9	Raman spectrum of solid [C ₆ F ₅ Xe][B(CN) ₄] at -150 °C	35
Figure 10	Raman spectrum of solid [C ₆ F ₅ Xe][BF ₄] at -150 °C	36
Figure 11	Raman spectrum of solid [C ₆ F ₅ Xe][B(CF ₃) ₄] at -150 °C	40
Figure 12	Raman spectrum of solid [C ₆ F ₅ Xe][B(C ₆ F ₅) ₄] at -150 °C.....	41
Figure 13	Raman spectrum of solid Cs[B(C ₆ F ₅) ₄] at -150 °C	43
Figure 14	Decomposition of the [C ₆ F ₅ Xe] ⁺ cation in CH ₃ CN solutions of [C ₆ F ₅ Xe][BY ₄] salts (Y = F, CN, CF ₃ , OTeF ₅ , C ₆ F ₅) at ambient temperatures.	51
Figure 15	The crystal structure of [C ₆ F ₅ XeF ₂][BF ₄]. Thermal ellipsoids are shown at the 50 % probability level.	87

Figure 16	The crystal structure of $[\text{C}_6\text{F}_5\text{XeF}_2 \cdot (\text{NCCH}_3)_{1.5}][\text{BF}_4]$. Thermal ellipsoids are shown at the 50 % probability level.....	87
Figure 17	Geometry of the $[\text{C}_6\text{F}_5\text{XeF}_2]^+$ cation (in $[\text{C}_6\text{F}_5\text{XeF}_2][\text{BF}_4]$). Thermal ellipsoids are shown at the 50 % probability level.....	90
Figure 18	Pentagonal planar arrangement of the formal $[\text{C}_6\text{F}_5\text{XeF}_2\text{F}_2]^-$ anion. Thermal ellipsoids are shown at the 50 % probability level.....	91
Figure 19	Dimer of $[\text{C}_6\text{F}_5\text{XeF}_2]_2$. Thermal ellipsoids are shown at the 50 % probability level.....	92
Figure 20	Crystal packing of $[\text{C}_6\text{F}_5\text{XeF}_2][\text{BF}_4]$ along the a-axis.....	93
Figure 21	Crystal packing of $[\text{C}_6\text{F}_5\text{XeF}_2][\text{BF}_4]$ along the c-axis.....	94
Figure 22	Two of the three non-equivalent molecules of the asymmetric cell of the crystal structure $[\text{C}_6\text{F}_5\text{XeF}_2 \cdot (\text{NCCH}_3)_{1.5}][\text{BF}_4]$. Thermal ellipsoids are shown at the 50 % probability level.	95
Figure 23	Pentagonal planar arrangement of the formal $\text{C}_6\text{F}_5\text{XeF}_2\text{N}_2$ arrangement. Thermal ellipsoids are shown at the 50 % probability level.	95
Figure 24	The third of the three non-equivalent molecules of the asymmetric cell of the crystal structure $[\text{C}_6\text{F}_5\text{XeF}_2 \cdot (\text{NCCH}_3)_{1.5}][\text{BF}_4]$. Thermal ellipsoids are shown at the 50 % probability level.....	96
Figure 25	Raman spectrum of solid $[\text{C}_6\text{F}_5\text{XeF}_2][\text{BF}_4]$ at $-150\text{ }^\circ\text{C}$	101
Figure 26	Decomposition trend of $[\text{C}_6\text{F}_5\text{XeF}_2][\text{BF}_4]$ in CH_3CN at $-40\text{ }^\circ\text{C}$	116
Figure 27	Decomposition trend of $[\text{C}_6\text{F}_5\text{XeF}_2][\text{BF}_4]$ in the presence of $\text{K}[\text{C}_6\text{F}_5\text{BF}_3]$ in CH_3CN at $-40\text{ }^\circ\text{C}$	124
Figure 28	Comparison of the consumption rates of the $[\text{C}_6\text{F}_5\text{XeF}_2]^+$ cation in the presence and absence of $\text{K}[\text{C}_6\text{F}_5\text{BF}_3]$	124
Figure 29	Transfer equipment for solutions and/or suspensions.....	132
Figure 30	Double pierced Teflon plugs used in the transfer equipment.....	133
Figure 31	$\frac{1}{4}$ inch o.d. h- and T-shaped FEP reaction tubes equipped with a Kel-F valve.....	138
Figure 32	HOTeF_5 glass-apparatus.....	159
Figure 33	Crystalline $\text{B}(\text{OTeF}_5)_3$	162
Figure 34	The crystal structure of $[\text{C}_6\text{F}_5\text{XeF}_2][\text{BF}_4]$. Thermal ellipsoids are shown at the 50 % probability level.	267
Figure 35	Crystal packing of $[\text{C}_6\text{F}_5\text{XeF}_2][\text{BF}_4]$ along the a-axis.....	267

Figure 36	Crystal packing of $[\text{C}_6\text{F}_5\text{XeF}_2][\text{BF}_4]$ along the c-axis.	268
Figure 37	The crystal structure of $[\text{C}_6\text{F}_5\text{XeF}_2 \cdot (\text{NCCH}_3)_{1.5}][\text{BF}_4]$. Thermal ellipsoids are shown at the 50 % probability level.	270
Figure 38	Crystal packing of $[\text{C}_6\text{F}_5\text{XeF}_2 \cdot (\text{NCCH}_3)_{1.5}][\text{BF}_4]$ along the b-axis.	270
Figure 39	Crystal packing of $[\text{C}_6\text{F}_5\text{XeF}_2 \cdot (\text{NCCH}_3)_{1.5}][\text{BF}_4]$ along the a-axis.	271
Figure 40	Crystal structure of $[\text{C}_6\text{F}_5\text{Xe} \cdot \text{NCCH}_3][\text{B}(\text{CF}_3)_4]$. Thermal ellipsoids are shown at the 50% probability level.	277
Figure 41	Crystal packing of $[\text{C}_6\text{F}_5\text{Xe} \cdot \text{NCCH}_3][\text{B}(\text{CF}_3)_4]$ along the a-axis.	278
Figure 42	Crystal structure of $[\text{C}_6\text{F}_5\text{Xe}][\text{B}(\text{CF}_3)_4]$. Thermal ellipsoids are shown at the 50% probability level.	280
Figure 43	Crystal packing of $[\text{C}_6\text{F}_5\text{Xe}][\text{B}(\text{CF}_3)_4]$ along the a-axis.	281
Figure 44	Crystal packing of $[\text{C}_6\text{F}_5\text{Xe}][\text{B}(\text{CF}_3)_4]$ along the c-axis.	281
Figure 45	Crystal structure of $[\text{C}_6\text{F}_5\text{Xe} \cdot \text{NCCH}_3][\text{B}(\text{C}_6\text{F}_5)_4]$. Thermal ellipsoids are shown at the 50% probability level.	284
Figure 46	Crystal packing of $[\text{C}_6\text{F}_5\text{Xe} \cdot \text{NCCH}_3][\text{B}(\text{C}_6\text{F}_5)_4]$ along the a-axis.	285
Figure 47	Crystal packing of $[\text{C}_6\text{F}_5\text{Xe} \cdot \text{NCCH}_3][\text{B}(\text{C}_6\text{F}_5)_4]$ along the c-axis.	285
Figure 48	Crystal structure of $[\text{C}_6\text{F}_5\text{Xe}][\text{B}(\text{CN})_4]$. Thermal ellipsoids are shown at the 50% probability level.	289
Figure 49	Crystal packing of $[\text{C}_6\text{F}_5\text{Xe}][\text{B}(\text{CN})_4]$ along the a-axis.	290
Figure 50	Crystal packing of $[\text{C}_6\text{F}_5\text{Xe}][\text{B}(\text{CN})_4]$ along the c-axis.	290
Figure 51	Raman spectrum of solid CH_2Cl_2 at -150°C	295
Figure 52	Raman spectrum of solid CH_3CN at -150°C	296
Figure 53	Raman spectrum of solid CH_3CN at -150°C	297

List of Tables

Table 1	^{19}F NMR Data for Selected $[\text{C}_6\text{F}_5\text{Xe}]^+$ Salts in CH_3CN Solution.....	16
Table 2	The ^{19}F -NMR chemical shifts of $[\text{C}_6\text{F}_5\text{Xe}][\text{B}(\text{CF}_3)_4]$ in different solvents recorded at 24 °C	22
Table 3	Crystallographic Data for $[\text{C}_6\text{F}_5\text{Xe}\cdot\text{NCCH}_3][\text{B}(\text{CF}_3)_4]$, $[\text{C}_6\text{F}_5\text{Xe}][\text{B}(\text{CF}_3)_4]$, $[\text{C}_6\text{F}_5\text{Xe}\cdot\text{NCCH}_3][\text{B}(\text{C}_6\text{F}_5)_4]$, and $[\text{C}_6\text{F}_5\text{Xe}][\text{B}(\text{CN})_4]$	24
Table 4	Experimental Geometrical Parameters for $[\text{C}_6\text{F}_5\text{Xe}][\text{B}(\text{CF}_3)_4]$, $[\text{C}_6\text{F}_5\text{Xe}\cdot\text{NCCH}_3][\text{B}(\text{CF}_3)_4]$, $[\text{C}_6\text{F}_5\text{Xe}\cdot\text{NCCH}_3][\text{B}(\text{C}_6\text{F}_5)_4]$, $[\text{C}_6\text{F}_5\text{Xe}][\text{B}(\text{CN})_4]$, and Calculated Geometrical Parameters for $[\text{C}_6\text{F}_5\text{Xe}]^+$, $[\text{C}_6\text{F}_5\text{Xe}\cdot\text{NCCH}_3]^+$, $[\text{B}(\text{C}_6\text{F}_5)_4]^-$, $[\text{B}(\text{CF}_3)_4]^-$, and $[\text{B}(\text{CN})_4]^-$	27
Table 5	Experimental ^a Raman Vibrational Frequencies and Intensities for $[\text{C}_6\text{F}_5\text{Xe}][\text{B}(\text{CN})_4]$ and $[\text{C}_6\text{F}_5\text{Xe}][\text{BF}_4]$ and Calculated Vibrational Frequencies and Infrared Intensities for $[\text{C}_6\text{F}_5\text{Xe}]^+$	33
Table 6	Observed Raman Frequencies for $[\text{C}_6\text{F}_5\text{Xe}\cdot\text{NCCH}_3]^+$ in $[\text{C}_6\text{F}_5\text{Xe}\cdot\text{NCCH}_3][\text{B}(\text{CF}_3)_4]$ and $[\text{C}_6\text{F}_5\text{Xe}\cdot\text{NCCH}_3][\text{B}(\text{C}_6\text{F}_5)_4]$ and Calculated Frequencies for $[\text{C}_6\text{F}_5\text{Xe}\cdot\text{NCCH}_3]^+$ and CH_3CN	37
Table 7	Observed Raman Frequencies for $[\text{B}(\text{C}_6\text{F}_5)_4]^-$ in $\text{Cs}[\text{B}(\text{C}_6\text{F}_5)_4]$ and $[\text{C}_6\text{F}_5\text{Xe}\cdot\text{NCCH}_3][\text{B}(\text{C}_6\text{F}_5)_4]$	42
Table 8	Calculated ^a Natural Atomic Charges, Mayer Bond Orders, and Mayer Natural Atomic Orbital Valencies for $[\text{C}_6\text{F}_5\text{Xe}]^+$ and $[\text{C}_6\text{F}_5\text{Xe}\cdot\text{NCCH}_3]^+$...	47
Table 9	Experimental and Calculated (C_s) Infrared Frequencies and Intensities for $\text{C}_6\text{F}_5\text{I}$	48
Table 10	Thermo-analytical properties of solid $[\text{C}_6\text{F}_5\text{Xe}][\text{Y}]$ ($\text{Y} = \text{BF}_4$, AsF_6 , $\text{B}(\text{CN})_4$, $\text{B}(\text{C}_6\text{F}_5)_4$, and $\text{B}(\text{CF}_3)_4$)	67
Table 11	Comparison of the decomposition of $[\text{C}_6\text{F}_5\text{Xe}][\text{BY}_4]$ ($\text{Y} = \text{F}$, CN , C_6F_5 , and CF_3) versus their reaction with 20 molar excess $\text{C}_6\text{H}_5\text{F}$ in CH_3CN at ambient temperature.....	72
Table 12	NMR chemical shifts of $[\text{C}_6\text{F}_5\text{XeF}_2][\text{BF}_4]$, $[\text{C}_6\text{F}_5\text{Xe}][\text{BF}_4]$, and $\text{C}_6\text{F}_5\text{IF}_2$ in CH_3CN and aHF at -40 °C, respectively.	84
Table 13	Crystallographic Data for $[\text{C}_6\text{F}_5\text{XeF}_2][\text{BF}_4]$ and $[\text{C}_6\text{F}_5\text{XeF}_2\cdot(\text{NCCH}_3)_{1.5}][\text{BF}_4]$	86
Table 14	Experimental Geometrical Parameters for $[\text{C}_6\text{F}_5\text{XeF}_2][\text{BF}_4]$ and $[\text{C}_6\text{F}_5\text{XeF}_2\cdot(\text{NCCH}_3)_{1.5}][\text{BF}_4]$	88

Table 15	Experimental and Calculated Vibrational Frequencies for $[\text{C}_6\text{F}_5\text{XeF}_2][\text{BF}_4]$ and $\text{C}_6\text{F}_5\text{IF}_2$	98
Table 16	Calculated ^a (C_1) Geometrical Parameters for $[\text{C}_6\text{F}_5\text{XeF}_2]^+$, $[\text{C}_6\text{F}_5\text{XeF}_2 \cdot \text{NCCH}_3]^+$, $[\text{C}_6\text{F}_5\text{XeF}_2 \cdot (\text{NCCH}_3)_2]^+$ and $\text{C}_6\text{F}_5\text{IF}_2$	105
Table 17	Extended Crystallographic Data for $[\text{C}_6\text{F}_5\text{XeF}_2][\text{BF}_4]$, and $[\text{C}_6\text{F}_5\text{XeF}_2 \cdot (\text{NCCH}_3)_{1.5}][\text{BF}_4]$	266
Table 18	Anisotropic Displacement Parameters [\AA^2]	268
Table 19	Atomic Coordinates and Equivalent Isotropic Displacement Coefficients (\AA^2)	269
Table 20	Anisotropic Displacement Parameters [\AA^2]	271
Table 21	Atomic Coordinates and Equivalent Isotropic Displacement Coefficients (\AA^2)	272
Table 22	Extended Crystallographic Data for $[\text{C}_6\text{F}_5\text{Xe} \cdot \text{NCCH}_3][\text{B}(\text{CF}_3)_4]$, $[\text{C}_6\text{F}_5\text{Xe}][\text{B}(\text{CF}_3)_4]$, $[\text{C}_6\text{F}_5\text{Xe} \cdot \text{NCCH}_3][\text{B}(\text{C}_6\text{F}_5)_4]$ and $[\text{C}_6\text{F}_5\text{Xe}][\text{B}(\text{CN})_4]$...	275
Table 23	Anisotropic Displacement Parameters [\AA^2]	278
Table 24	Atomic Coordinates and Equivalent Isotropic Displacement Coefficients (\AA^2)	279
Table 25	Anisotropic Displacement Parameters [\AA^2]	282
Table 26	Atomic Coordinates and Equivalent Isotropic Displacement Coefficients (\AA^2)	283
Table 27	Anisotropic Displacement Parameters [\AA^2]	286
Table 28	Atomic Coordinates and Equivalent Isotropic Displacement Coefficients (\AA^2)	287
Table 29	Anisotropic Displacement Parameters [\AA^2]	291
Table 30	Atomic Coordinates and Equivalent Isotropic Displacement Coefficients (\AA^2)	291
Table 31	Calculated Natural Atomic Charges, for $[\text{C}_6\text{F}_5\text{XeF}_2]^+$, $[\text{C}_6\text{F}_5\text{XeF}_2 \cdot \text{NCCH}_3]^+$, $[\text{C}_6\text{F}_5\text{XeF}_2 \cdot (\text{NCCH}_3)_2]^+$, and $\text{C}_6\text{F}_5\text{IF}_2$	293

VI.1 Extended Crystallographic Information

Table 17 Extended Crystallographic Data for $[\text{C}_6\text{F}_5\text{XeF}_2][\text{BF}_4]$, and $[\text{C}_6\text{F}_5\text{XeF}_2 \cdot (\text{NCCH}_3)_{1.5}][\text{BF}_4]$

	$[\text{C}_6\text{F}_5\text{XeF}_2][\text{BF}_4]$	$[\text{C}_6\text{F}_5\text{XeF}_2 \cdot (\text{NCCH}_3)_{1.5}][\text{BF}_4]$
Chem. formula	C6F11BXe	C9H4.5F11BN1.5Xe
Crystal System	Monoclinic	Monoclinic
space group	P21/n	C2/c
a (Å)	7.4740(7)	12.803(5)
b (Å)	19.195(2)	23.549(8)
c (Å)	7.7611(8)	19.439(6)
α (°)	90	90
β (°)	109.320(7)	103.08(3)
γ (°)	90	90
V (Å³)	1050.8	5708.6
molecules/unit cell	4	16
mol wt (g·mol⁻¹)	1692	7756
Calcd. density (g·cm⁻³)	2.675	2.256
F(000)	776.0	3808.0
Crystal size (mm³)	0.15 × 0.15 × 0.1	0.15 × 0.15 × 0.1
Max. 2θ range	57.66	58.54
Index ranges	-9 ≤ h ≤ 9 -24 ≤ k ≤ 20 -10 ≤ l ≤ 9	-17 ≤ h ≤ 17 -31 ≤ k ≤ 31 -26 ≤ l ≤ 26
Reflections collected	7677	26193
Independent reflections	2523 [R(int) = 0.0877]	6918 [R(int) = 0.2371]
Data/restraints/parameter	2523 / 0 / 173	6918 / 0 / 429
Refinement method	Full-matrix least-squares on F2	Full-matrix least-squares on F2
Largest difference peak and hole (e·Å⁻³)	1.59 and -1.14	1.12 and -1.10
Goodness-of-fit on F2	1.061	0.950
T (°C)	-173	-173
μ (mm⁻¹)	3.42	2.54
Extinction coefficient	0.0000(6)	0.000178
R indices (all data)	0.1427	0.2429
R₁^a	0.0791	0.0818
wR₂^b	0.1539	0.1807

$${}^a R_1 = \frac{\sum ||F_0| - |F_c||}{\sum |F_0|} \text{ for } I > 2\sigma(I); \quad {}^b wR_2 = \sqrt{\frac{\sum w \cdot (|F_0|^2 - |F_c|^2)^2}{\sum w \cdot (|F_0|^2)^2}} \text{ for } I > 2\sigma(I)$$

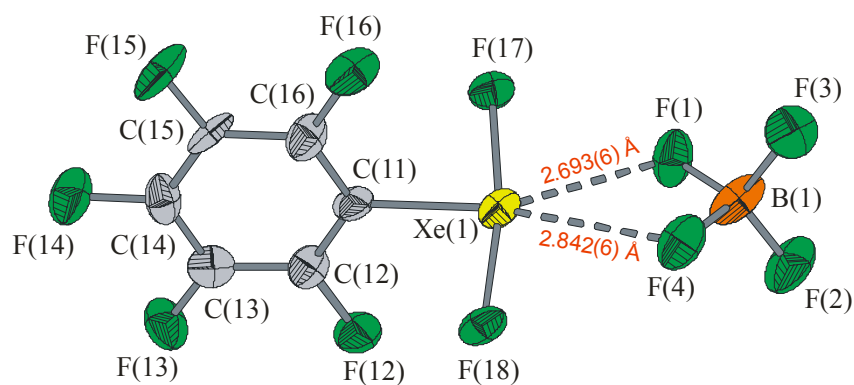
VI.1.1 $[C_6F_5XeF_2][BF_4]$ 

Figure 34 The crystal structure of $[C_6F_5XeF_2][BF_4]$. Thermal ellipsoids are shown at the 50 % probability level.

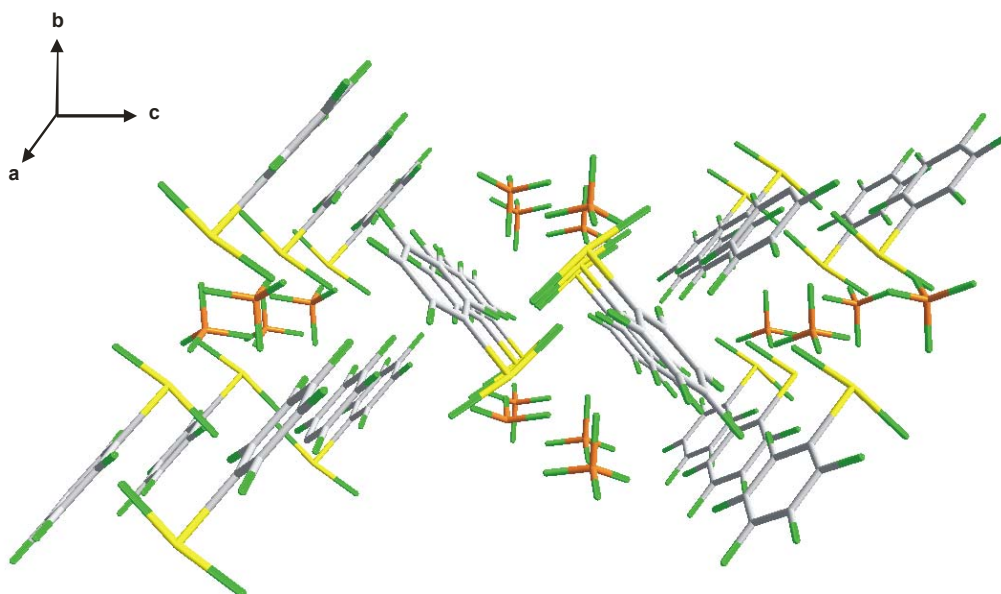


Figure 35 Crystal packing of $[C_6F_5XeF_2][BF_4]$ along the a-axis.

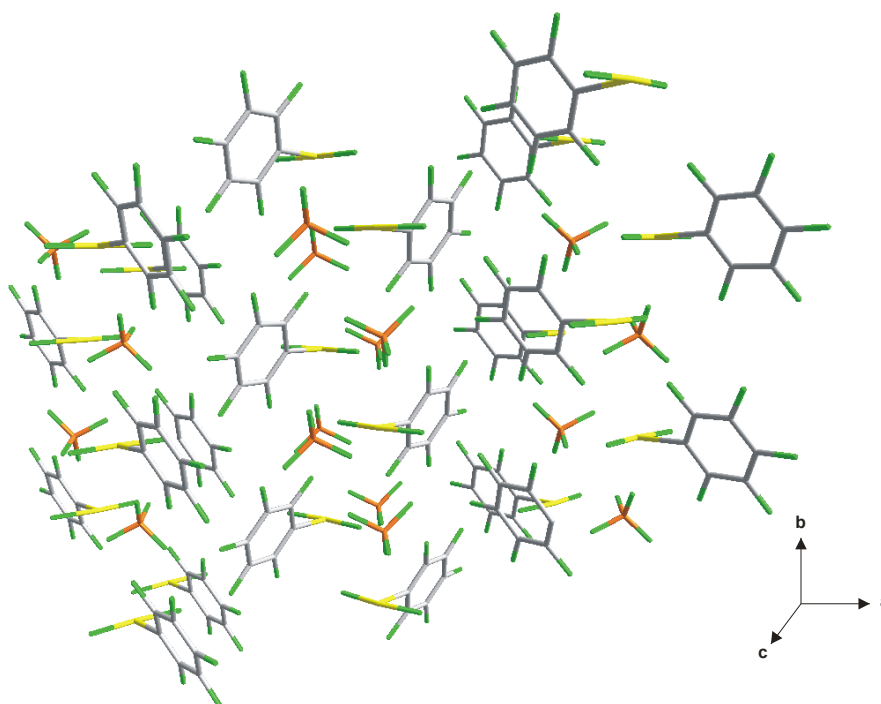


Figure 36 Crystal packing of $[\text{C}_6\text{F}_5\text{XeF}_2][\text{BF}_4]$ along the *c*-axis.

Table 18 Anisotropic Displacement Parameters [\AA^2]

	U_{11}	U_{22}	U_{33}	U_{23}	U_{13}	U_{12}
Xe1	0.0289(4)	0.0486(5)	0.0288(4)	0.0027(4)	0.0111(3)	0.0022(4)
F8	0.048(4)	0.076(6)	0.038(4)	0.001(4)	0.012(3)	0.011(4)
F7	0.041(4)	0.045(4)	0.035(3)	0.008(3)	0.014(3)	-0.001(3)
F6	0.047(4)	0.047(4)	0.035(3)	0.016(3)	0.018(3)	0.011(3)
F5	0.033(4)	0.056(5)	0.057(4)	0.000(4)	0.027(3)	-0.002(3)
F10	0.036(4)	0.069(5)	0.046(4)	-0.002(4)	0.006(3)	-0.006(3)
F1	0.026(4)	0.087(6)	0.037(4)	-0.001(4)	0.010(3)	-0.012(3)
F2	0.035(4)	0.110(6)	0.032(3)	-0.003(4)	0.021(3)	0.004(4)
F11	0.039(4)	0.112(7)	0.057(5)	-0.021(4)	0.030(4)	-0.016(4)
C1	0.028(6)	0.040(7)	0.041(6)	0.006(5)	0.024(5)	0.006(5)
F3	0.049(5)	0.078(6)	0.052(4)	-0.015(4)	0.022(4)	0.006(4)
F9	0.061(5)	0.066(5)	0.028(3)	-0.003(3)	0.006(3)	0.016(4)
F4	0.040(4)	0.050(5)	0.064(5)	-0.019(4)	0.020(4)	-0.012(3)
C2	0.027(6)	0.056(8)	0.029(6)	-0.003(5)	0.006(5)	-0.006(5)
C6	0.031(6)	0.042(7)	0.033(6)	0.000(5)	0.012(5)	0.000(5)
C3	0.023(6)	0.063(8)	0.021(5)	0.009(5)	0.011(5)	0.015(5)

Table 18 (continued...)

B1	0.014(6)	0.104(14)	0.027(6)	0.013(8)	0.002(5)	0.009(7)
C5	0.034(7)	0.047(8)	0.035(6)	0.009(6)	0.010(6)	0.003(6)
C4	0.041(7)	0.038(7)	0.025(6)	-0.004(5)	0.000(6)	0.007(5)

Table 19 Atomic Coordinates and Equivalent Isotropic Displacement Coefficients (\AA^2)

	X	Y	Z	U(eq)
Xe1		0.28530(10)	0.05380(4)	0.76991(9)
F8	0.1655(10)	0.0004(4)	0.4077(9)	0.0549(19)
F7	0.3096(9)	-0.0183(3)	0.9521(8)	0.0403(15)
F6	0.2655(9)	0.1365(3)	0.6243(8)	0.0422(16)
F5	0.5973(8)	0.1590(4)	0.9768(9)	0.0456(17)
F10	0.1161(9)	-0.1160(4)	0.3786(9)	0.0521(19)
F1	0.0081(9)	0.0795(4)	0.9943(9)	0.0500(19)
F2	0.0327(9)	0.1715(4)	1.2698(9)	0.056(2)
F11	0.3876(10)	-0.0693(4)	0.3570(10)	0.066(2)
C1	0.3014(15)	0.1209(6)	0.9857(15)	0.033(3)
F3	0.3452(10)	0.2511(4)	1.4059(10)	0.058(2)
F9	0.3361(10)	-0.0698(4)	0.6306(8)	0.054(2)
F4	0.6290(9)	0.2447(4)	1.2672(10)	0.0501(18)
C2	0.1596(15)	0.1222(6)	1.0577(15)	0.038(3)
C6	0.4610(15)	0.1615(6)	1.0510(15)	0.035(3)
C3	0.1709(14)	0.1660(7)	1.1983(13)	0.035(3)
B1	0.2543(17)	-0.0651(9)	0.4373(18)	0.050(4)
C5	0.4764(16)	0.2070(6)	1.1940(15)	0.039(3)
C4	0.3311(16)	0.2081(6)	1.2665(14)	0.037(3)

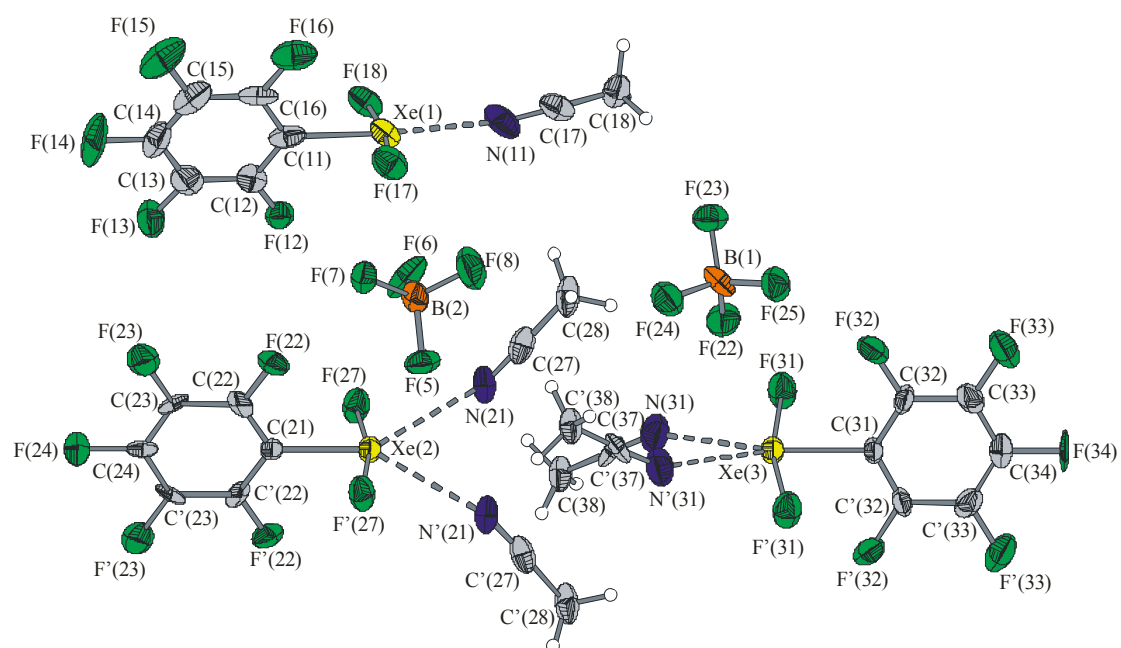
VI.1.2 $[C_6F_5XeF_2 \cdot (NCCH_3)_{1.5}][BF_4]$ 

Figure 37 The crystal structure of $[C_6F_5XeF_2 \cdot (NCCH_3)_{1.5}][BF_4]$. Thermal ellipsoids are shown at the 50 % probability level.

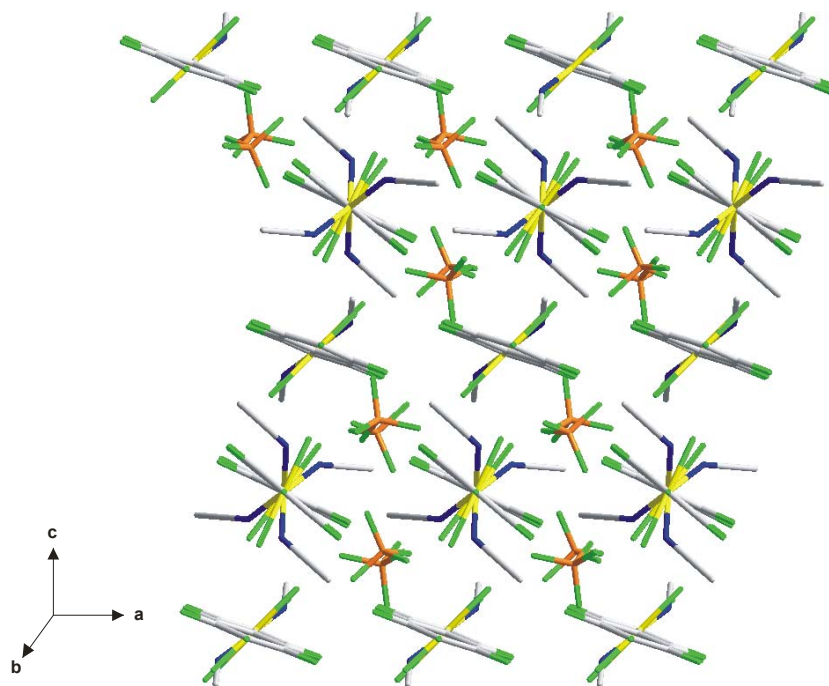


Figure 38 Crystal packing of $[C_6F_5XeF_2 \cdot (NCCH_3)_{1.5}][BF_4]$ along the b-axis.

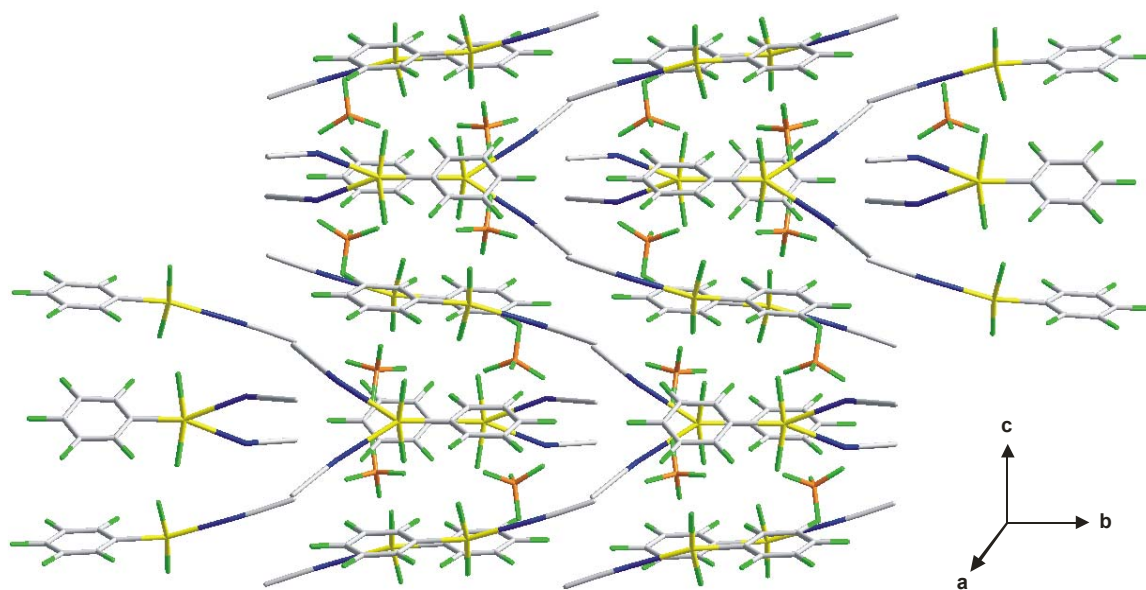


Figure 39 Crystal packing of $[\text{C}_6\text{F}_5\text{XeF}_2 \cdot (\text{NCCH}_3)_{1.5}][\text{BF}_4]$ along the a-axis.

Table 20 Anisotropic Displacement Parameters [\AA^2]

	U_{11}	U_{22}	U_{33}	U_{23}	U_{13}	U_{12}
Xe1	0.0410(8)	0.0235(7)	0.0277(7)	0.000	0.0097(6)	0.000
Xe2	0.0407(8)	0.0234(7)	0.0294(7)	0.000	0.0099(6)	0.000
F1	0.035(5)	0.046(5)	0.038(5)	-0.009(4)	-0.003(4)	-0.010(4)
F3	0.065(8)	0.031(7)	0.054(8)	0.000	0.008(6)	0.000
F6	0.065(6)	0.032(4)	0.040(5)	-0.001(4)	0.025(4)	0.007(4)
F10	0.151(12)	0.006(6)	0.042(8)	0.000	0.037(8)	0.000
F2	0.062(6)	0.047(5)	0.044(5)	-0.011(4)	0.010(5)	0.008(4)
C1	0.054(15)	0.025(11)	0.016(11)	0.000	0.000(10)	0.000
F25	0.068(6)	0.039(5)	0.046(5)	0.000(4)	0.016(5)	-0.011(4)
F8	0.049(5)	0.045(5)	0.041(5)	-0.013(4)	-0.001(4)	-0.002(4)
F13	0.078(6)	0.037(5)	0.043(5)	0.002(4)	0.028(5)	0.002(4)
C2	0.044(10)	0.030(8)	0.028(8)	-0.024(7)	0.007(7)	0.009(7)
F9	0.094(7)	0.043(5)	0.048(6)	-0.013(4)	0.023(5)	-0.025(5)
C9	0.029(12)	0.015(10)	0.051(14)	0.000	-0.008(11)	0.000
F24	0.064(6)	0.048(5)	0.054(6)	-0.009(4)	0.011(5)	-0.005(4)

Table 20 (continued...)

F23	0.044(5)	0.056(5)	0.037(5)	0.007(4)	0.002(4)	-0.007(4)
F22	0.036(5)	0.050(5)	0.085(7)	0.007(5)	-0.015(5)	0.003(4)
C4	0.026(12)	0.048(13)	0.013(10)	0.000	-0.001(9)	0.000
C11	0.075(13)	0.032(9)	0.024(9)	-0.007(7)	0.014(8)	-0.015(8)
N2	0.059(9)	0.035(8)	0.074(10)	0.008(7)	0.009(8)	0.014(6)
C3	0.023(9)	0.042(9)	0.029(9)	0.014(7)	-0.008(7)	0.018(7)
C10	0.046(10)	0.017(7)	0.035(9)	0.004(6)	0.009(8)	0.005(7)
C13	0.056(11)	0.036(8)	0.036(9)	0.020(8)	0.008(8)	0.033(8)
C12	0.049(15)	0.019(11)	0.045(14)	0.000	0.030(12)	0.000
B1	0.045(11)	0.040(11)	0.046(12)	-0.025(9)	0.011(9)	-0.013(9)
C14	0.027(8)	0.017(7)	0.063(10)	0.001(7)	0.011(7)	-0.014(6)
Xe3	0.0384(6)	0.0414(6)	0.0328(6)	-0.0103(4)	0.0096(4)	-0.0110(4)
F17	0.126(9)	0.029(5)	0.101(8)	0.010(5)	0.053(7)	0.037(5)
F15	0.034(5)	0.039(5)	0.036(5)	0.005(4)	0.004(4)	-0.004(4)
F20	0.037(5)	0.054(5)	0.045(5)	-0.016(4)	0.011(4)	-0.014(4)
F16	0.062(6)	0.035(5)	0.067(6)	0.000(4)	0.014(5)	-0.009(4)
F19	0.035(6)	0.095(7)	0.046(6)	0.001(5)	0.005(5)	0.012(5)
C22	0.030(9)	0.071(12)	0.023(8)	-0.002(8)	-0.003(7)	0.005(9)
C21	0.055(12)	0.065(12)	0.052(11)	0.015(9)	0.010(10)	0.026(10)
F29	0.048(5)	0.032(4)	0.041(5)	0.002(3)	0.015(4)	0.000(4)
F28	0.092(7)	0.066(6)	0.054(6)	0.032(5)	0.041(5)	0.049(5)
F27	0.033(5)	0.062(5)	0.036(5)	0.011(4)	-0.007(4)	-0.003(4)
F26	0.067(7)	0.039(5)	0.122(9)	-0.013(5)	-0.010(6)	-0.009(5)
B2	0.059(12)	0.031(10)	0.037(11)	-0.010(8)	0.022(10)	0.008(9)
N3	0.028(8)	0.068(10)	0.069(10)	-0.028(8)	0.001(7)	-0.010(6)
C24	0.069(11)	0.019(7)	0.047(9)	-0.007(7)	0.023(8)	0.006(7)
C23	0.028(9)	0.083(13)	0.029(9)	-0.001(9)	0.001(7)	-0.017(8)
N1	0.077(10)	0.022(7)	0.065(10)	-0.002(6)	0.014(8)	0.003(7)
C7	0.026(8)	0.024(7)	0.093(13)	0.001(8)	0.011(8)	-0.014(6)
C8	0.055(11)	0.034(9)	0.063(12)	0.013(8)	0.029(10)	0.029(8)

Table 21 Atomic Coordinates and Equivalent Isotropic Displacement Coefficients (\AA^2).

	X	Y	Z	U(eq)
Xe1	0.0000	0.19645(5)	0.2500	0.0304(3)
Xe2	0.0000	0.83955(5)	0.2500	0.0309(3)

Table 21 (continued...)

F1	-0.1849(6)	0.2844(3)	0.1972(4)	0.042(2)
F3	0.0000	0.4559(5)	0.2500	0.051(3)
F6	0.0624(6)	0.2059(3)	0.1689(4)	0.044(2)
F10	0.0000	0.5810(4)	0.2500	0.064(4)
F2	-0.1815(6)	0.3995(3)	0.1921(4)	0.051(2)
C1	0.0000	0.2831(7)	0.2500	0.033(5)
F25	-0.3468(6)	0.8413(3)	0.1447(4)	0.051(2)
F8	-0.1700(6)	0.7521(3)	0.1723(4)	0.047(2)
F13	0.0329(6)	0.8285(3)	0.1575(4)	0.050(2)
C2	-0.0949(11)	0.3118(6)	0.2221(7)	0.034(3)
F9	-0.1682(7)	0.6361(3)	0.1705(4)	0.061(3)
C9	0.0000	0.7502(7)	0.2500	0.035(5)
F24	-0.3287(6)	0.9370(3)	0.1587(4)	0.056(2)
F23	-0.3362(6)	0.8978(3)	0.0512(4)	0.047(2)
F22	-0.1889(6)	0.8848(3)	0.1382(5)	0.061(2)
C4	0.0000	0.3982(8)	0.2500	0.030(4)
C11	-0.0855(12)	0.6653(6)	0.2092(7)	0.043(4)
N2	0.0759(10)	0.9417(5)	0.2018(7)	0.057(4)
C3	-0.0907(10)	0.3719(5)	0.2209(7)	0.034(3)
C10	-0.0874(11)	0.7237(5)	0.2107(7)	0.033(3)
C13	0.1393(12)	0.9812(6)	0.2055(7)	0.043(4)
C12	0.0000	0.6374(8)	0.2500	0.035(5)
B1	-0.2986(14)	0.8901(7)	0.1231(9)	0.043(4)
C14	0.2122(9)	1.0247(5)	0.2092(7)	0.035(3)
Xe3	0.99030(7)	0.31247(4)	0.00857(5)	0.0373(3)
F17	1.0093(8)	0.0544(3)	-0.0080(5)	0.081(3)
F15	0.8101(6)	0.2218(3)	-0.0399(4)	0.0368(19)
F20	0.9089(6)	0.2975(3)	0.0795(4)	0.045(2)
F16	0.8184(7)	0.1075(3)	-0.0480(4)	0.054(2)
F19	1.1851(6)	0.2290(4)	0.0459(4)	0.059(2)
F21	1.0764(6)	0.3138(3)	-0.0620(4)	0.052(2)
C18	0.9003(11)	0.1958(6)	-0.0225(7)	0.035(3)
C17	0.9943(11)	0.2256(6)	0.0018(6)	0.039(4)
F18	1.1907(7)	0.1126(4)	0.0397(5)	0.073(3)
C20	1.0068(13)	0.1100(6)	-0.0067(8)	0.048(4)
C19	0.9058(13)	0.1376(6)	-0.0267(7)	0.045(4)
C22	1.0968(11)	0.1981(7)	0.0216(7)	0.043(4)
C21	1.0991(14)	0.1406(8)	0.0184(9)	0.058(5)
F29	0.6379(6)	0.2062(3)	0.1422(4)	0.0396(19)

Table 21 (continued...)

F28	0.7673(7)	0.1655(3)	0.0972(4)	0.067(3)
F27	0.7704(6)	0.1532(3)	0.2117(4)	0.046(2)
F26	0.6397(7)	0.1113(3)	0.1292(5)	0.081(3)
B2	0.7055(14)	0.1598(7)	0.1456(9)	0.040(4)
N3	0.9295(9)	0.4180(6)	0.0461(7)	0.057(4)
C24	0.9377(11)	0.5223(5)	0.0873(7)	0.043(4)
C23	0.9334(10)	0.4686(7)	0.0647(7)	0.048(4)
N1	-0.0214(11)	0.0942(5)	0.1689(7)	0.055(4)
C7	-0.1675(10)	1.0204(5)	0.0963(8)	0.048(4)
C8	0.9141(12)	0.0607(6)	0.1367(8)	0.048(4)

Table 22 Extended Crystallographic Data for $[\text{C}_6\text{F}_5\text{Xe}\cdot\text{NCCH}_3][\text{B}(\text{CF}_3)_4]$, $[\text{C}_6\text{F}_5\text{Xe}][\text{B}(\text{CF}_3)_4]$, $[\text{C}_6\text{F}_5\text{Xe}\cdot\text{NCCH}_3][\text{B}(\text{C}_6\text{F}_5)_4]$ and $[\text{C}_6\text{F}_5\text{Xe}][\text{B}(\text{CN})_4]$

	$[\text{C}_6\text{F}_5\text{Xe}\cdot\text{NCCH}_3][\text{B}(\text{CF}_3)_4]$	$[\text{C}_6\text{F}_5\text{Xe}][\text{B}(\text{CF}_3)_4]$	$[\text{C}_6\text{F}_5\text{Xe}\cdot\text{NCCH}_3][\text{B}(\text{C}_6\text{F}_5)_4]$	$[\text{C}_6\text{F}_5\text{Xe}][\text{B}(\text{CN})_4]$
Chem. formula	$\text{C}_{12}\text{H}_3\text{F}_{17}\text{BNXe}$	$\text{C}_{10}\text{F}_{17}\text{BXe}$	$\text{C}_{32}\text{F}_{25}\text{H}_3\text{BNXe}$	$\text{C}_{10}\text{F}_5\text{BN}_4\text{Xe}$
Crystal System	Orthorhombic	Monoclinic	Monoclinic	Orthorhombic
space group	$Pca2_1$	$P2_1/c$	$P2_1/c$	$Pbca$
a (Å)	18.903(8)	6.751(2)	10.606(2)	9.919(2)
b (Å)	7.472(4)	15.950(5)	22.458(4)	16.269(4)
c (Å)	12.801(6)	14.715(4)	13.835(2)	16.783(4)
α (°)	90	90	90	90
β (°)	90	99.740(5)	94.775(5)	90
γ (°)	90	90	90	90
V (Å ³)	1808.14	1561.52	3284.07	2708.12
molecules/unit cell	4	4	4	8
Mol. wt. (g·mol ⁻¹)	2505.06	2340.84	4073.86	3306.00
Calc.density(g·cm ⁻³)	2.284	2.489	2.060	2.027
F(000)	1176.0	1088.0	1944.0	1536.0
Crystal size (mm ³)	0.04 × 0.04 × 0.08	0.26 × 0.16 × 0.04	0.2 × 0.1 × 0.02	0.22 × 0.22 × 0.05
Max. 2θ range	58.16	57.84	43.93	59.99

Table 22 (continued...)

	$-24 \leq h \leq 25$	$-9 \leq h \leq 9$	$-11 \leq h \leq 11$	$-13 \leq h \leq 13$
Index ranges	$-10 \leq k \leq 10$	$-21 \leq k \leq 21$	$-23 \leq k \leq 23$	$-22 \leq k \leq 19$
	$-16 \leq l \leq 17$	$-19 \leq l \leq 19$	$-14 \leq l \leq 14$	$-22 \leq l \leq 23$
Reflections collected	17109	13790	35408	60958
Independent reflections	4124	3736	4006	3946
Data/restraints/ Parameter	4124 / 1 / 285	3736 / 0 / 263	4006 / 0 / 538	3946 / 0 / 191
Refinement method	Full-matrix least-squares on F^2	Full-matrix least-squares on F^2	Full-matrix least-squares on F^2	Full-matrix least-squares on F^2
Largest difference peak and hole ($e \cdot \text{\AA}^{-3}$)	1.03 and -1.55	1.98 and -1.25	1.38 and -1.24	0.74 and -0.75
Goodness-of-fit F^2	0.814	0.967	0.886	0.974
T ($^{\circ}\text{C}$)	-173	-173	-173	-173
μ (mm^{-1})	2.08	2.39	1.22	2.60
Extinction coefficient	0.0019(4)	0.0022(4)	0.0043(5)	0.0007(1)
R indices (all data)	0.1119	0.1036	0.1178	0.0821
R_1^a	0.0354	0.0445	0.0594	0.0363
wR_2^b	0.0531	0.1131	0.1776	0.0543

$${}^a R_1 = \frac{\sum \left(|F_0| - |F_c| \right)}{\sum |F_0|} \text{ for } I > 2\sigma(I); \quad {}^b wR_2 = \sqrt{\frac{\sum w \cdot \left(|F_0|^2 - |F_c|^2 \right)^2}{\sum w \cdot \left(|F_0|^2 \right)^2}} \text{ for } I > 2\sigma(I)$$

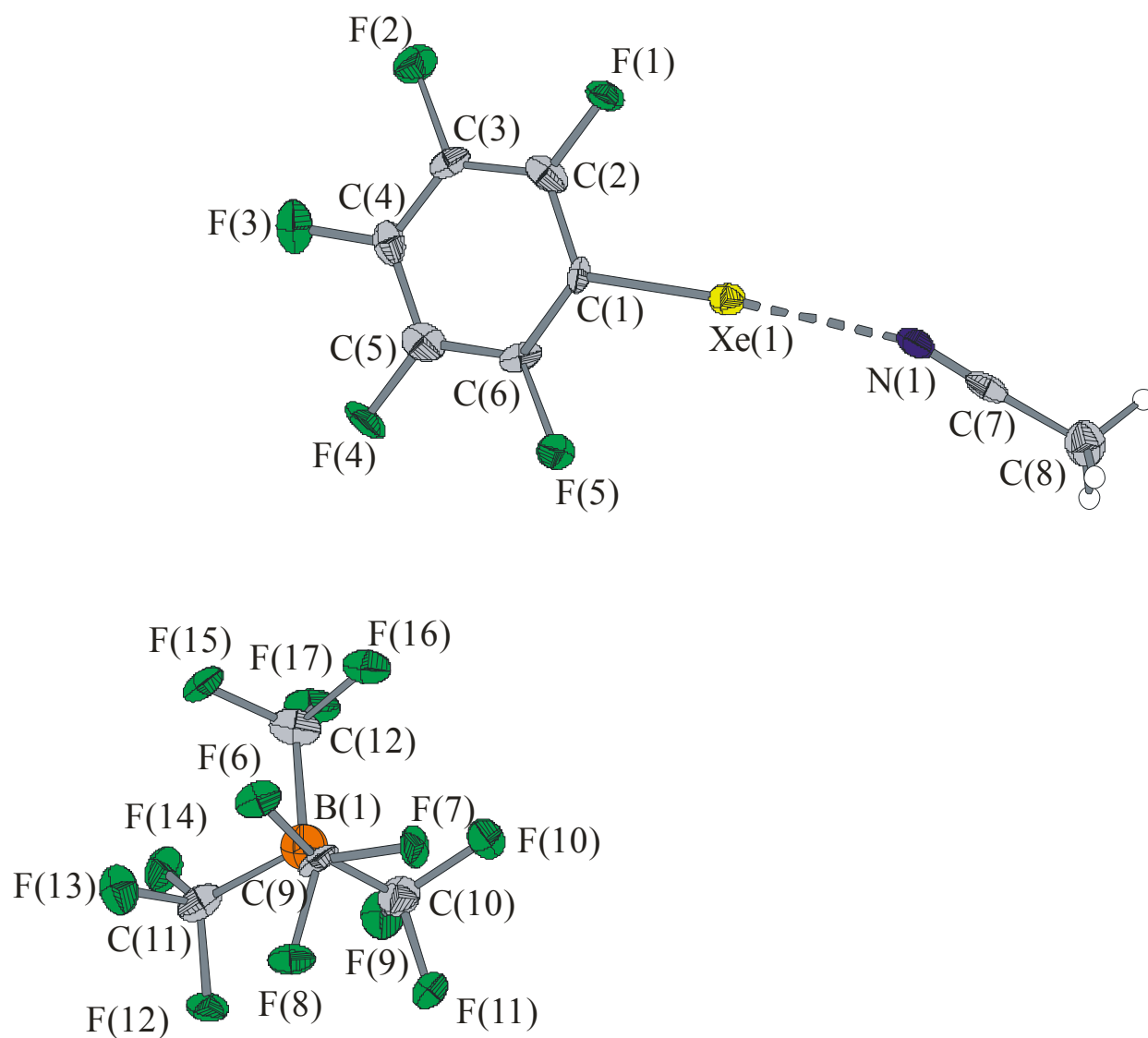
VI.1.3 $[C_6F_5Xe \cdot NCCH_3][B(CF_3)_4]$ 

Figure 40 Crystal structure of $[C_6F_5Xe \cdot NCCH_3][B(CF_3)_4]$. Thermal ellipsoids are shown at the 50% probability level.

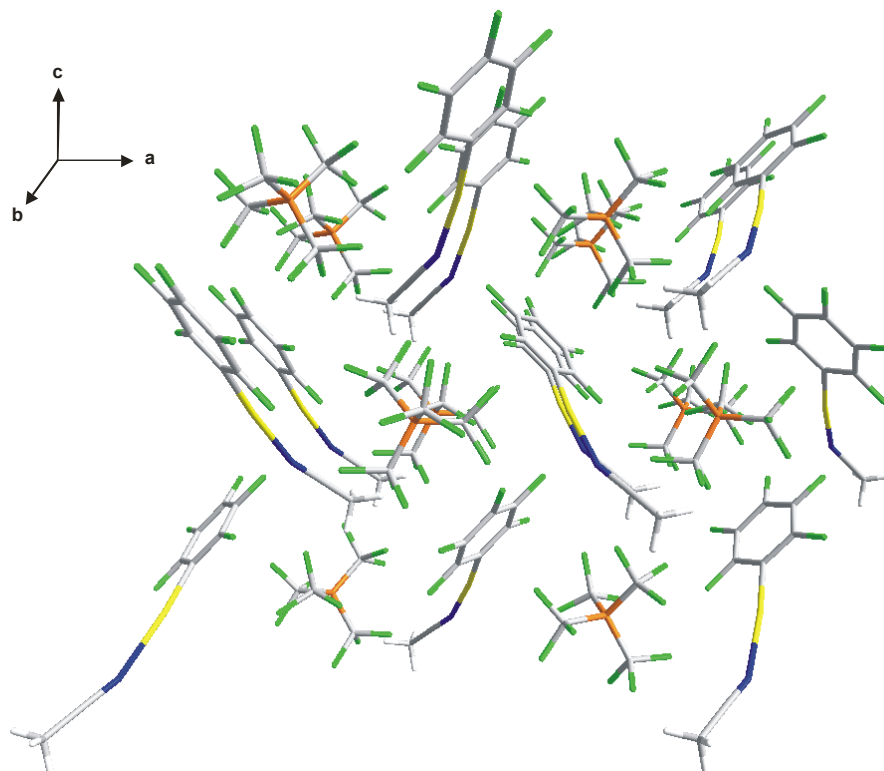


Figure 41 Crystal packing of $[\text{C}_6\text{F}_5\text{Xe}\cdot\text{NCCH}_3][\text{B}(\text{CF}_3)_4]$ along the a-axis.

Table 23 Anisotropic Displacement Parameters [\AA^2]

	U_{11}	U_{22}	U_{33}	U_{23}	U_{13}	U_{12}
Xe1	0.01727(18)	0.0229(2)	0.02220(18)	0.0031(5)	0.0003(4)	0.0010(2)
F11	0.030(3)	0.027(3)	0.031(3)	-0.004(3)	-0.012(2)	-0.003(3)
F1	0.031(4)	0.020(4)	0.025(3)	-0.003(3)	-0.006(2)	0.012(3)
F17	0.028(3)	0.047(4)	0.021(3)	0.022(2)	0.005(2)	0.003(3)
F4	0.030(3)	0.015(3)	0.047(3)	0.004(3)	0.002(2)	0.012(3)
F3	0.044(4)	0.027(4)	0.031(3)	-0.005(3)	0.008(3)	-0.009(3)
F16	0.025(3)	0.036(3)	0.033(3)	0.008(2)	-0.0016(18)	0.007(2)
F6	0.018(3)	0.040(4)	0.018(3)	0.002(2)	0.004(2)	0.000(3)
F10	0.032(2)	0.023(2)	0.036(4)	0.001(2)	-0.001(3)	0.001(2)
F15	0.022(3)	0.038(4)	0.023(3)	0.000(3)	-0.009(2)	-0.006(3)
F14	0.029(2)	0.033(3)	0.026(2)	-0.012(2)	0.0022(19)	-0.002(2)
F13	0.028(2)	0.027(2)	0.042(3)	-0.003(3)	0.011(3)	-0.0036(18)
F7	0.024(3)	0.017(3)	0.037(3)	-0.013(2)	0.001(2)	0.003(2)

Table 23 (continued...)

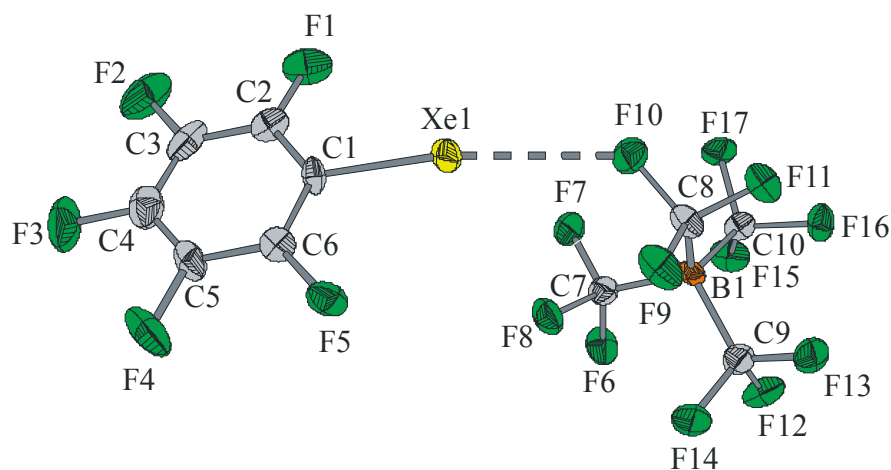
C3	0.014(3)	0.033(4)	0.013(4)	0.005(3)	-0.001(3)	-0.005(3)
F12	0.023(3)	0.027(3)	0.036(3)	-0.0051(19)	-0.0081(18)	0.015(2)
C12	0.022(4)	0.040(6)	0.019(4)	0.011(5)	0.011(3)	0.007(5)
C9	0.024(5)	0.037(6)	0.019(5)	-0.003(4)	-0.014(4)	-0.004(4)
C10	0.019(4)	0.034(5)	0.037(8)	-0.005(4)	0.000(4)	0.003(4)
C11	0.022(4)	0.042(5)	0.010(5)	-0.006(5)	0.001(4)	0.000(4)
C4	0.024(4)	0.018(5)	0.031(4)	0.001(4)	0.009(3)	-0.006(5)
C1	0.017(4)	0.014(4)	0.020(4)	-0.006(3)	0.000(3)	-0.005(3)
C5	0.013(3)	0.030(4)	0.034(4)	0.001(4)	0.011(4)	0.006(5)
F9	0.024(2)	0.035(3)	0.032(2)	-0.003(3)	0.013(2)	-0.003(3)
F5	0.026(2)	0.024(2)	0.032(3)	0.004(2)	-0.005(2)	-0.0008(17)
F8	0.024(2)	0.037(3)	0.018(2)	0.008(2)	-0.0019(16)	0.005(2)
F2	0.029(3)	0.038(3)	0.023(3)	-0.004(2)	-0.0045(19)	0.002(2)
C7	0.021(4)	0.020(5)	0.020(4)	0.004(4)	0.008(3)	0.013(5)
C2	0.019(4)	0.022(5)	0.031(4)	0.007(4)	0.012(3)	0.007(4)
C6	0.005(4)	0.035(5)	0.015(4)	0.009(4)	0.005(3)	-0.004(3)
N1	0.033(5)	0.019(5)	0.028(4)	0.001(3)	-0.007(3)	0.009(4)
C8	0.039(5)	0.028(5)	0.028(4)	-0.002(4)	0.002(3)	-0.002(4)

Table 24 Atomic Coordinates and Equivalent Isotropic Displacement Coefficients (\AA^2)

	X	Y	Z	U(eq)
Xe1	0.589337(18)	0.82812(5)	0.54080(4)	0.02079(11)
F11	0.9562(2)	-0.1607(7)	0.6541(3)	0.0293(11)
F1	0.4785(3)	0.7920(7)	0.3580(4)	0.0253(15)
F17	0.8312(2)	-0.1265(7)	0.3800(3)	0.0321(14)
F4	0.6247(2)	0.1703(6)	0.3882(3)	0.0310(12)
F3	0.5224(3)	0.2062(8)	0.2418(4)	0.0340(17)
F16	0.76081(19)	-0.0146(6)	0.4985(2)	0.0316(12)
F6	0.7364(3)	-0.2902(7)	0.6673(3)	0.0253(15)
F10	0.90749(19)	0.0443(4)	0.5609(4)	0.0302(12)
F15	0.7439(3)	-0.2838(7)	0.4370(4)	0.0274(15)
F14	0.87772(19)	-0.4844(5)	0.4277(3)	0.0296(10)
F13	0.81190(17)	-0.5733(4)	0.5542(5)	0.0322(11)
F7	0.8068(2)	-0.0799(7)	0.7166(4)	0.0263(13)
C3	0.5024(6)	0.498(2)	0.2976(8)	0.0199(15)

Table 24 (continued...)

F12	0.92350(18)	-0.5219(5)	0.5796(3)	0.0287(11)
B1	0.8463(3)	-0.2487(9)	0.5576(8)	0.0156(19)
C12	0.7952(4)	-0.1720(12)	0.4697(5)	0.0270(19)
C9	0.8053(4)	-0.2405(11)	0.6695(6)	0.027(2)
C10	0.9181(4)	-0.1363(10)	0.5632(7)	0.030(3)
C11	0.8653(3)	-0.4548(10)	0.5289(7)	0.0246(19)
C4	0.5386(3)	0.3426(12)	0.3047(6)	0.0243(17)
C1	0.5664(3)	0.6145(9)	0.4398(5)	0.0172(17)
C5	0.5895(4)	0.3208(11)	0.3814(5)	0.0258(15)
F9	0.9647(2)	-0.1737(7)	0.4880(3)	0.0304(12)
F5	0.65215(18)	0.4443(4)	0.5231(4)	0.0274(12)
F8	0.83524(18)	-0.3589(5)	0.7416(3)	0.0261(11)
F2	0.45121(19)	0.5186(6)	0.2230(3)	0.0298(11)
C7	0.6688(4)	1.1677(12)	0.7102(5)	0.0206(17)
C2	0.5146(4)	0.6413(10)	0.3637(5)	0.0240(19)
C6	0.6036(3)	0.4612(10)	0.4478(5)	0.0182(17)
N1	0.6304(4)	1.0891(9)	0.6655(5)	0.0266(18)
C8	0.7189(4)	1.2785(9)	0.7710(5)	0.032(2)
H3H	0.7686	1.2458	0.7589	0.038
H3A	0.7098	1.2657	0.8461	0.038
H3H	0.7134	1.4048	0.7567	0.038

VI.1.4 $[C_6F_5Xe][B(CF_3)_4]$ **Figure 42** Crystal structure of $[C_6F_5Xe][B(CF_3)_4]$. Thermal ellipsoids are shown at the 50% probability level.

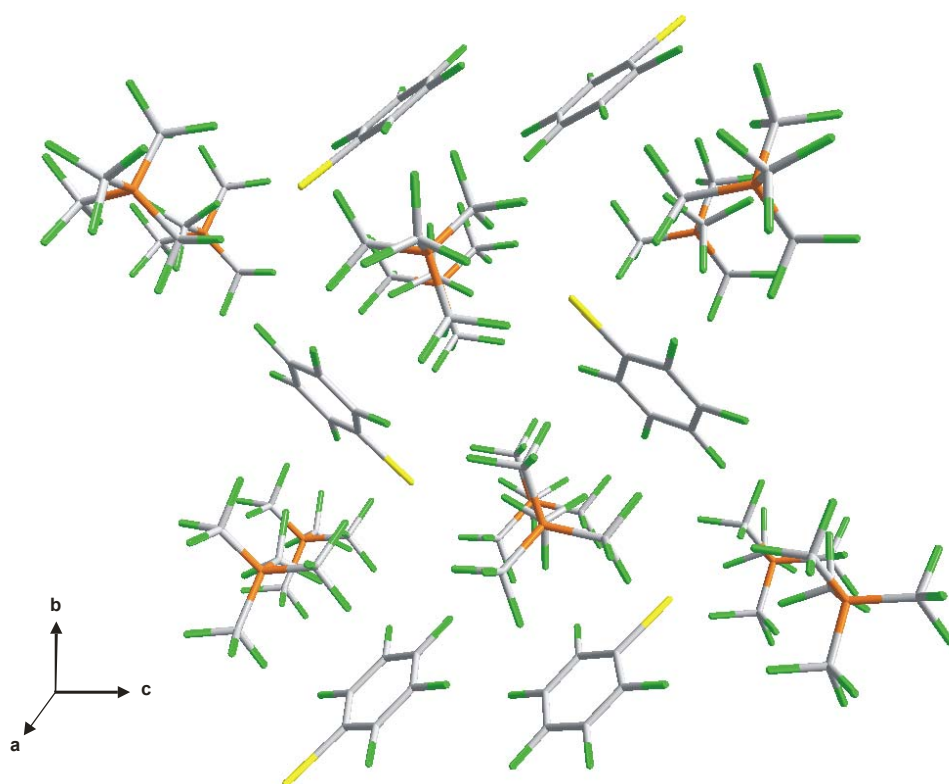


Figure 43 Crystal packing of [C₆F₅Xe][B(CF₃)₄] along the a-axis.

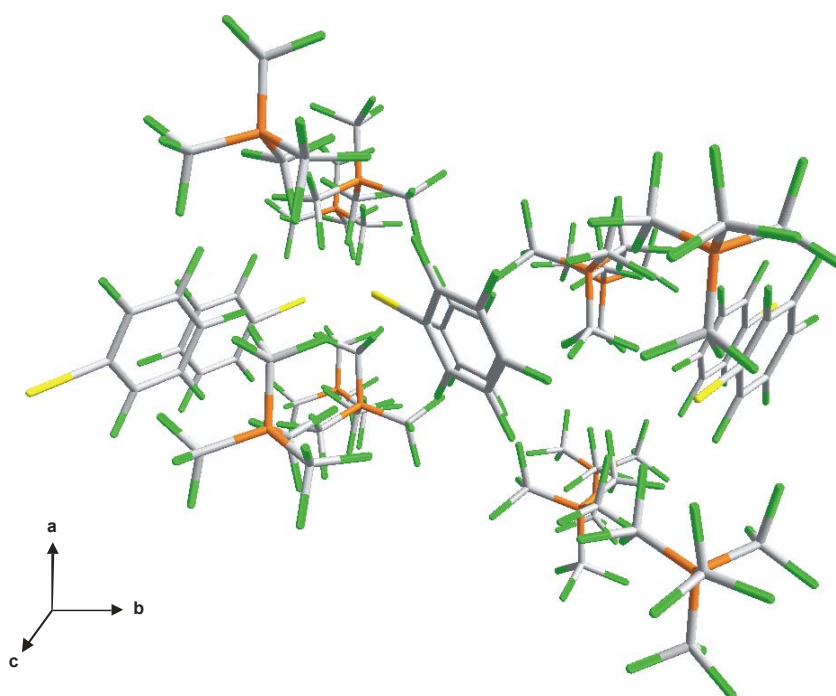


Figure 44 Crystal packing of [C₆F₅Xe][B(CF₃)₄] along the c-axis.

Table 25 Anisotropic Displacement Parameters [\AA^2]

	U_{11}	U_{22}	U_{33}	U_{23}	U_{13}	U_{12}
Xe1	0.0339(2)	0.0342(3)	0.0167(2)	0.0035(2)	0.00150(14)	-0.0048(2)
F17	0.0216(15)	0.044(2)	0.033(2)	0.0021(17)	0.0156(15)	0.0014(15)
F7	0.0286(17)	0.035(2)	0.047(3)	0.0064(18)	0.0102(17)	0.0103(16)
F11	0.047(2)	0.024(2)	0.026(2)	-0.0004(16)	0.0106(16)	-0.0008(16)
F16	0.0370(18)	0.040(2)	0.0208(19)	0.0092(16)	0.0096(15)	0.0137(17)
F15	0.0429(19)	0.046(2)	0.0215(19)	-0.0112(18)	0.0130(16)	-0.0084(18)
F13	0.0223(16)	0.058(3)	0.040(2)	-0.009(2)	0.0043(16)	-0.0030(17)
F6	0.049(2)	0.021(2)	0.037(2)	-0.0032(17)	-0.0055(18)	-0.0066(17)
F5	0.0347(18)	0.035(2)	0.038(2)	0.0022(17)	0.0186(17)	-0.0001(17)
F10	0.0333(18)	0.036(2)	0.034(2)	0.0000(18)	-0.0050(16)	-0.0035(17)
F12	0.0288(17)	0.042(2)	0.040(2)	0.0065(18)	0.0170(16)	0.0126(17)
F9	0.064(2)	0.040(2)	0.018(2)	-0.0027(17)	0.0178(18)	-0.0069(19)
F2	0.036(2)	0.050(3)	0.096(4)	-0.014(3)	-0.009(2)	0.018(2)
F8	0.0437(19)	0.037(2)	0.025(2)	0.0091(17)	0.0045(17)	-0.0037(17)
F1	0.0363(19)	0.056(3)	0.052(3)	-0.016(2)	0.0248(19)	-0.0018(19)
F14	0.0323(18)	0.059(3)	0.040(2)	0.013(2)	0.0205(17)	0.0039(18)
F4	0.086(3)	0.049(3)	0.034(3)	0.010(2)	0.020(2)	-0.017(2)
F3	0.080(3)	0.042(3)	0.058(3)	0.024(2)	-0.023(2)	0.000(2)
C10	0.022(3)	0.030(4)	0.017(3)	-0.005(3)	0.007(2)	0.002(3)
B1	0.022(3)	0.023(4)	0.016(4)	0.003(3)	0.009(3)	-0.002(3)
C9	0.025(3)	0.040(4)	0.025(4)	0.006(3)	0.006(3)	0.002(3)
C2	0.025(3)	0.037(4)	0.028(4)	-0.010(3)	0.007(3)	0.002(3)
C8	0.036(3)	0.027(4)	0.012(3)	0.000(3)	0.012(3)	-0.002(3)
C1	0.033(3)	0.020(3)	0.013(3)	0.001(2)	0.004(2)	0.009(3)
C7	0.024(3)	0.029(4)	0.024(4)	0.000(3)	0.002(3)	-0.003(3)
C5	0.052(4)	0.031(4)	0.012(3)	-0.002(3)	0.002(3)	-0.011(3)
C3	0.027(3)	0.036(4)	0.049(5)	-0.012(4)	-0.012(3)	0.007(3)
C6	0.030(3)	0.024(3)	0.023(3)	-0.007(3)	0.009(3)	0.002(3)
C4	0.049(4)	0.031(4)	0.034(4)	-0.001(3)	-0.007(3)	-0.002(3)

Table 26 Atomic Coordinates and Equivalent Isotropic Displacement Coefficients (\AA^2).

	X	Y	Z	U(eq)
Xe1	0.68770(6)	-0.15725(3)	0.85394(3)	0.02859(16)
F17	1.0501(4)	0.2334(2)	0.7962(2)	0.0319(9)
F7	1.0660(5)	0.0923(2)	0.9230(3)	0.0364(9)
F11	0.8852(5)	0.3523(2)	0.9356(2)	0.0317(8)
F16	0.7570(5)	0.2847(2)	0.7510(2)	0.0321(8)
F15	0.8095(5)	0.1512(2)	0.7394(2)	0.0358(9)
F13	0.4541(5)	0.1678(2)	0.8150(3)	0.0402(10)
F6	0.7626(5)	0.0463(2)	0.8946(3)	0.0370(9)
F5	0.8752(5)	-0.0860(2)	0.6908(3)	0.0343(9)
F10	1.1040(5)	0.2613(2)	0.9972(3)	0.0360(9)
F12	0.4828(5)	0.2864(2)	0.8844(3)	0.0356(9)
F9	0.8262(6)	0.2769(2)	1.0494(2)	0.0394(9)
F2	0.1549(5)	0.0657(3)	0.6882(4)	0.0629(14)
F8	0.8787(5)	0.0998(2)	1.0272(2)	0.0353(9)
F1	0.2881(5)	-0.0514(3)	0.8191(3)	0.0461(11)
F14	0.4877(5)	0.1723(2)	0.9635(3)	0.0421(10)
F4	0.7423(6)	0.0314(3)	0.5608(3)	0.0548(12)
F3	0.3859(7)	0.1081(3)	0.5619(3)	0.0640(14)
C10	0.8528(8)	0.2176(4)	0.7967(4)	0.0226(13)
B1	0.7996(9)	0.2029(4)	0.8986(5)	0.0198(14)
C9	0.5580(8)	0.2070(4)	0.8899(4)	0.0297(15)
C2	0.3947(8)	-0.0318(4)	0.7539(4)	0.0299(15)
C8	0.9010(8)	0.2726(4)	0.9688(4)	0.0239(13)
C1	0.5777(8)	-0.0694(4)	0.7510(4)	0.0217(12)
C7	0.8758(8)	0.1107(4)	0.9345(4)	0.0259(14)
C5	0.6294(10)	0.0105(4)	0.6237(4)	0.0319(15)
C3	0.3306(9)	0.0270(4)	0.6881(5)	0.0396(18)
C6	0.6967(8)	-0.0493(4)	0.6880(4)	0.0251(13)
C4	0.4469(11)	0.0483(4)	0.6236(5)	0.0397(17)

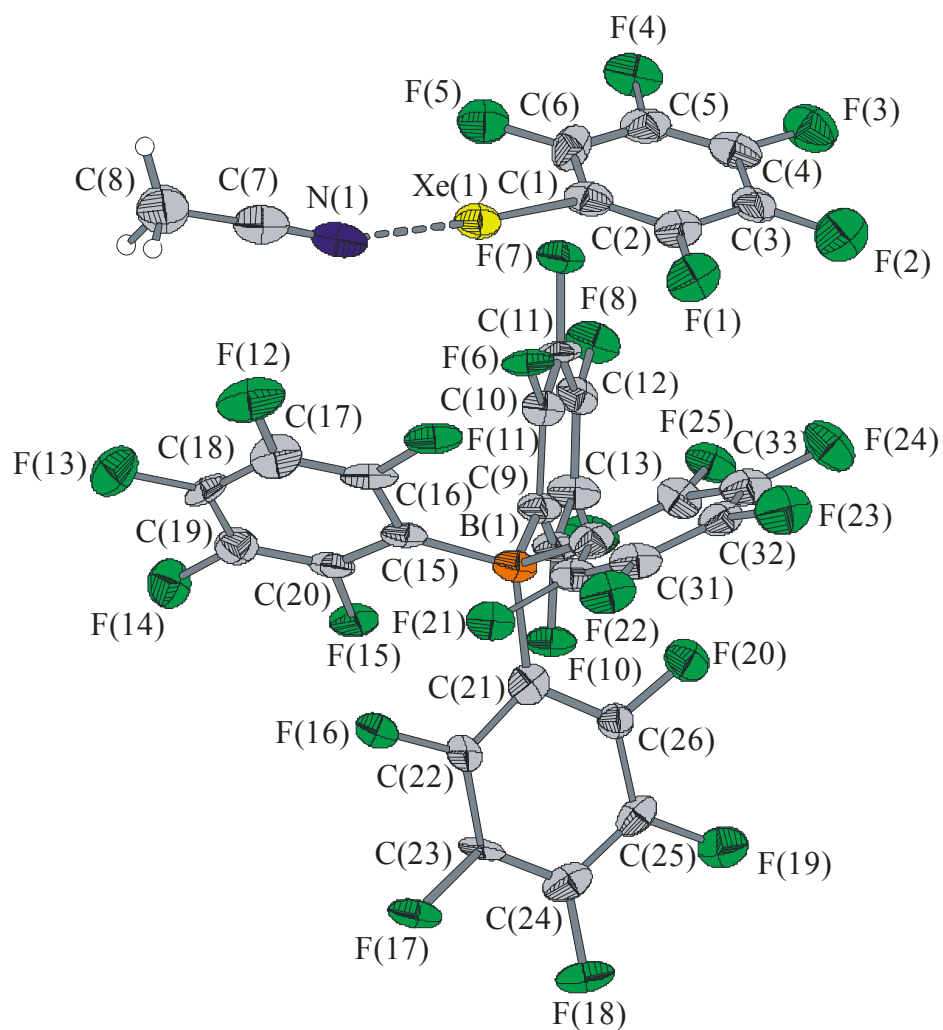
VI.1.5 $[C_6F_5Xe \cdot NCCH_3][B(C_6F_5)_4]$ 

Figure 45 Crystal structure of $[C_6F_5Xe \cdot NCCH_3][B(C_6F_5)_4]$. Thermal ellipsoids are shown at the 50% probability level.

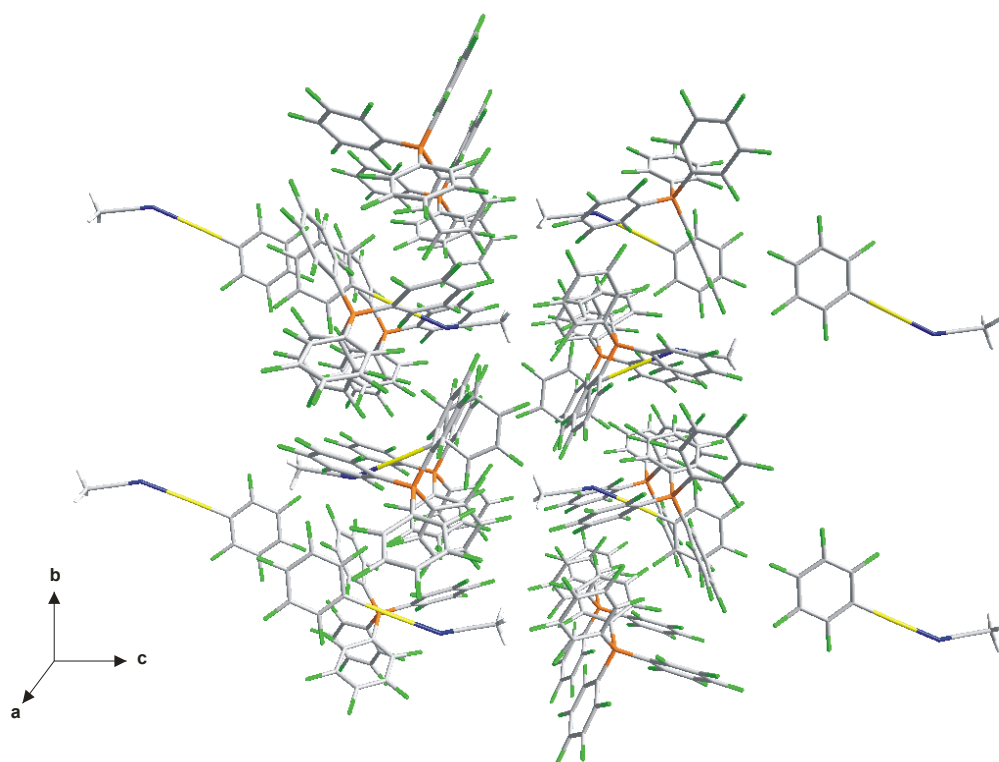


Figure 46 Crystal packing of $[\text{C}_6\text{F}_5\text{Xe}\cdot\text{NCCH}_3][\text{B}(\text{C}_6\text{F}_5)_4]$ along the a-axis.

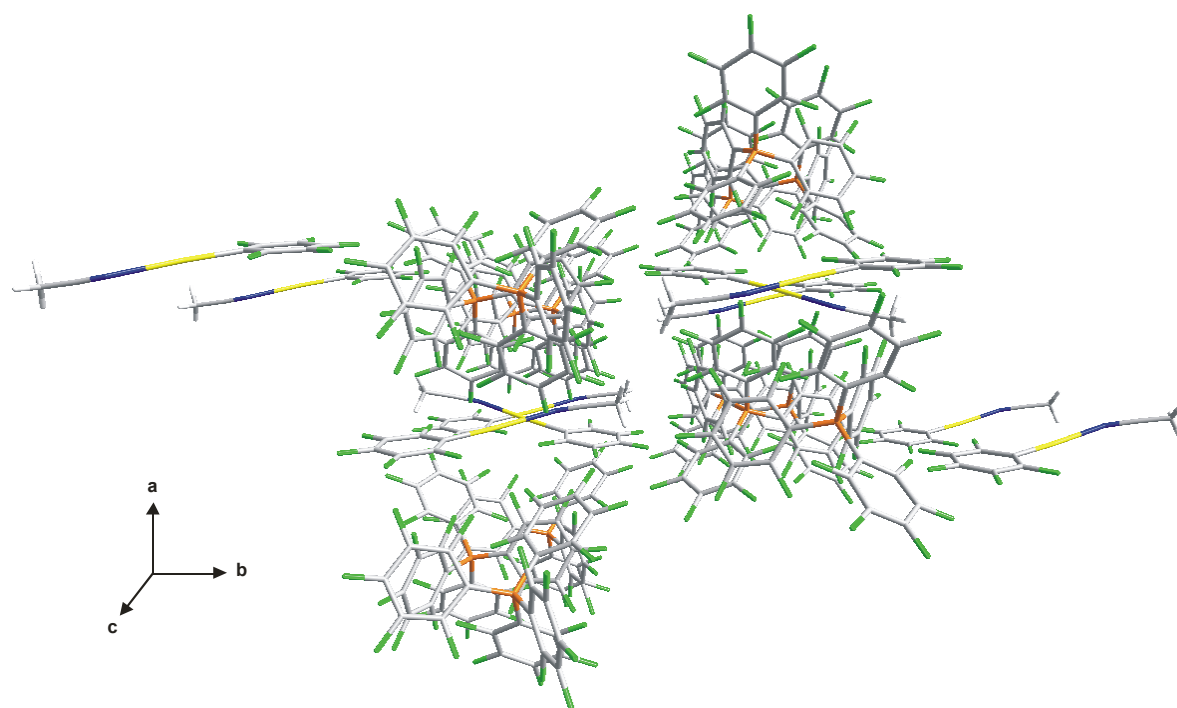


Figure 47 Crystal packing of $[\text{C}_6\text{F}_5\text{Xe}\cdot\text{NCCH}_3][\text{B}(\text{C}_6\text{F}_5)_4]$ along the c-axis.

Table 27 Anisotropic Displacement Parameters [\AA^2]

	U_{11}	U_{22}	U_{33}	U_{23}	U_{13}	U_{12}
Xe1	0.0197(5)	0.0443(6)	0.0344(5)	0.0010(5)	0.0023(3)	-0.0015(5)
F16	0.027(4)	0.038(5)	0.035(4)	0.004(4)	0.006(3)	-0.005(4)
F17	0.020(4)	0.062(6)	0.032(4)	0.006(4)	0.008(3)	-0.007(4)
F7	0.026(4)	0.051(5)	0.031(4)	0.001(4)	0.008(4)	-0.007(4)
F10	0.018(4)	0.052(5)	0.029(4)	0.006(4)	0.006(3)	0.003(4)
F22	0.026(4)	0.069(6)	0.029(4)	-0.003(4)	-0.006(4)	0.005(4)
F15	0.009(4)	0.052(5)	0.035(4)	-0.003(4)	0.001(3)	0.003(4)
F5	0.029(5)	0.054(6)	0.044(5)	0.003(4)	-0.001(4)	0.003(4)
F25	0.022(4)	0.052(5)	0.035(4)	0.007(4)	-0.004(3)	-0.006(4)
F2	0.055(6)	0.060(6)	0.048(5)	-0.003(5)	-0.001(4)	0.003(5)
F12	0.032(5)	0.085(7)	0.051(5)	0.014(5)	0.005(4)	0.032(5)
F8	0.032(4)	0.058(5)	0.027(4)	0.012(4)	-0.004(3)	-0.004(4)
F11	0.018(4)	0.070(5)	0.035(4)	0.005(4)	0.007(3)	0.007(4)
F23	0.033(5)	0.077(7)	0.043(5)	-0.013(5)	-0.008(4)	-0.009(5)
F21	0.029(4)	0.049(5)	0.029(4)	0.005(4)	0.001(3)	0.001(4)
F20	0.029(4)	0.042(5)	0.037(4)	0.001(4)	-0.001(4)	-0.005(4)
F6	0.012(4)	0.056(5)	0.028(4)	0.006(4)	0.007(3)	0.010(4)
F1	0.042(5)	0.060(6)	0.031(5)	-0.002(4)	-0.008(4)	0.006(4)
F18	0.029(4)	0.069(6)	0.039(5)	0.002(4)	0.015(4)	0.011(4)
F14	0.038(5)	0.044(5)	0.037(4)	-0.006(4)	-0.007(4)	-0.004(4)
F3	0.038(5)	0.055(6)	0.063(6)	0.013(5)	0.006(4)	0.001(4)
F19	0.039(5)	0.052(6)	0.047(5)	0.000(4)	0.011(4)	0.004(4)
F24	0.035(5)	0.054(6)	0.050(5)	0.007(4)	-0.010(4)	-0.018(4)
F4	0.033(5)	0.071(6)	0.031(5)	0.011(4)	-0.004(4)	-0.003(4)
F9	0.014(4)	0.067(6)	0.045(5)	0.014(4)	-0.003(4)	0.004(4)
F13	0.052(6)	0.043(6)	0.051(5)	-0.002(4)	0.004(4)	0.018(4)
C27	0.018(7)	0.044(10)	0.038(9)	-0.006(7)	0.002(6)	0.002(7)
C22	0.010(6)	0.031(9)	0.025(7)	-0.004(7)	-0.009(6)	-0.007(7)
C23	0.005(6)	0.053(11)	0.015(6)	-0.001(6)	-0.001(5)	-0.014(7)
C14	0.010(8)	0.044(9)	0.034(8)	-0.003(7)	0.004(6)	-0.002(6)
N1	0.038(8)	0.063(10)	0.047(8)	0.009(7)	0.018(6)	-0.004(7)
C5	0.018(8)	0.057(12)	0.047(10)	-0.005(9)	0.008(7)	-0.002(7)
C25	0.020(8)	0.035(9)	0.030(8)	-0.008(7)	-0.006(6)	0.014(7)
C12	0.027(8)	0.040(9)	0.025(8)	-0.001(6)	-0.002(7)	-0.010(7)

Table 27 (continued...)

C15	0.018(7)	0.050(9)	0.008(6)	0.000(6)	0.001(5)	-0.007(7)
C11	0.017(8)	0.046(9)	0.030(8)	-0.008(7)	0.015(7)	-0.005(6)
C32	0.017(7)	0.038(9)	0.034(8)	0.009(7)	-0.007(6)	0.002(7)
C20	0.022(8)	0.038(10)	0.037(8)	0.012(7)	0.016(7)	0.003(7)
C21	0.017(7)	0.040(9)	0.026(7)	-0.004(7)	-0.011(6)	0.001(7)
C30	0.019(8)	0.053(11)	0.038(9)	-0.021(8)	0.006(7)	-0.009(7)
C19	0.037(9)	0.042(10)	0.024(8)	-0.003(7)	0.005(7)	-0.006(8)
C9	0.015(7)	0.044(9)	0.026(7)	-0.003(6)	0.003(6)	-0.006(6)
C10	0.022(8)	0.039(9)	0.018(7)	0.002(6)	-0.004(6)	-0.002(6)
C29	0.014(7)	0.060(11)	0.026(8)	0.000(7)	-0.005(6)	0.002(7)
C31	0.017(8)	0.061(11)	0.032(8)	-0.007(8)	-0.001(7)	-0.001(8)
C7	0.034(9)	0.063(13)	0.039(9)	0.005(9)	0.008(7)	0.002(9)
C17	0.020(8)	0.047(10)	0.041(9)	0.008(7)	-0.009(7)	0.016(8)
C28	0.030(8)	0.044(10)	0.025(8)	0.009(7)	0.008(7)	0.003(7)
C24	0.018(8)	0.055(11)	0.030(8)	-0.011(8)	-0.003(7)	0.007(8)
C18	0.025(9)	0.034(9)	0.033(8)	-0.004(7)	0.011(7)	0.016(7)
C3	0.017(8)	0.041(10)	0.054(10)	0.002(8)	0.009(7)	-0.004(7)
C1	0.019(8)	0.044(10)	0.040(9)	0.012(7)	0.006(7)	0.006(7)
C16	0.018(8)	0.067(11)	0.019(7)	0.012(7)	0.006(6)	0.004(8)
C4	0.020(8)	0.049(11)	0.041(9)	0.016(8)	0.002(7)	0.004(7)
C2	0.020(8)	0.051(11)	0.027(8)	-0.002(8)	-0.003(6)	0.000(7)
C6	0.029(8)	0.040(10)	0.039(9)	-0.016(8)	-0.005(7)	0.000(7)
C8	0.043(10)	0.056(12)	0.076(12)	-0.003(9)	0.014(9)	0.001(9)
B1	0.021(8)	0.046(11)	0.015(8)	0.001(7)	-0.001(7)	-0.006(8)
C13	0.010(7)	0.060(10)	0.028(8)	0.004(7)	-0.006(6)	-0.002(7)

Table 28 Atomic Coordinates and Equivalent Isotropic Displacement Coefficients (\AA^2)

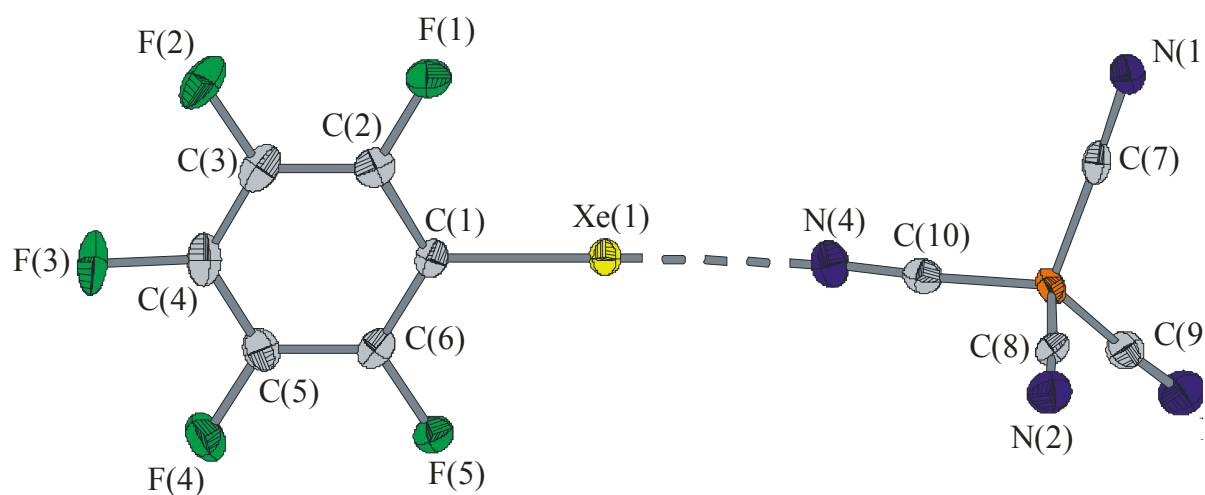
	X	Y	Z	U(eq)
Xe1	0.78479(8)	0.23756(4)	0.84312(6)	0.0328(4)
F16	1.4394(6)	0.2903(4)	0.6659(5)	0.0330(19)
F17	1.6177(6)	0.2726(4)	0.5477(5)	0.037(2)
F7	1.1481(7)	0.1255(3)	1.0883(5)	0.0354(19)
F10	1.5514(6)	0.1399(3)	0.8720(5)	0.0328(18)
F22	0.9996(7)	0.1947(4)	0.4758(5)	0.042(2)
F15	1.4857(6)	0.2728(3)	0.8653(5)	0.0324(18)

Table 28 (continued...)

F5	0.8716(7)	0.1967(4)	1.0588(5)	0.043(2)
F25	1.1708(6)	0.0701(3)	0.7969(5)	0.0366(19)
F2	0.8289(8)	0.0012(4)	0.8276(6)	0.055(2)
F12	1.0251(7)	0.3755(4)	0.8076(6)	0.056(2)
F8	1.3797(7)	0.0805(3)	1.1564(5)	0.039(2)
F11	1.0499(6)	0.2633(4)	0.7562(5)	0.0405(19)
F23	0.9137(7)	0.0815(4)	0.5067(6)	0.052(2)
F21	1.1810(6)	0.2418(4)	0.5968(5)	0.0358(19)
F20	1.4163(7)	0.0826(3)	0.7193(5)	0.0364(19)
F6	1.1169(6)	0.1746(3)	0.9127(5)	0.0317(18)
F1	0.7921(7)	0.1110(4)	0.7483(5)	0.045(2)
F18	1.7033(7)	0.1620(4)	0.5133(5)	0.045(2)
F14	1.4575(7)	0.3873(3)	0.9114(5)	0.040(2)
F3	0.8755(7)	-0.0106(4)	1.0225(6)	0.052(2)
F19	1.5974(7)	0.0664(4)	0.5989(6)	0.046(2)
F24	1.0030(7)	0.0221(4)	0.6699(6)	0.047(2)
F4	0.9017(7)	0.0857(4)	1.1374(5)	0.045(2)
F9	1.5777(6)	0.0881(4)	1.0435(5)	0.042(2)
F13	1.2270(8)	0.4404(4)	0.8858(6)	0.048(2)
C27	1.1830(12)	0.1602(6)	0.7055(10)	0.033(3)
C22	1.4739(10)	0.2334(6)	0.6540(8)	0.022(3)
C23	1.5673(11)	0.2257(6)	0.5926(8)	0.024(3)
C14	1.4472(11)	0.1362(6)	0.9207(9)	0.029(3)
N1	0.7173(12)	0.3417(7)	0.7722(9)	0.048(3)
C5	0.8762(12)	0.0934(8)	1.0420(11)	0.040(4)
C25	1.5574(12)	0.1217(6)	0.6184(9)	0.029(3)
C12	1.3632(12)	0.1052(6)	1.0669(9)	0.031(3)
C15	1.2714(11)	0.2621(6)	0.8044(8)	0.025(3)
C11	1.2453(12)	0.1283(6)	1.0326(9)	0.031(3)
C32	1.1345(12)	0.1041(6)	0.7182(9)	0.030(3)
C26	1.4653(12)	0.1318(6)	0.6796(9)	0.026(3)
C20	1.3673(12)	0.2969(6)	0.8477(10)	0.031(3)
C21	1.4193(12)	0.1874(6)	0.7020(9)	0.028(3)
C30	0.9990(12)	0.1072(7)	0.5711(10)	0.037(4)
C19	1.3558(13)	0.3554(7)	0.8743(9)	0.034(4)
C9	1.3311(11)	0.1591(6)	0.8809(9)	0.028(3)
C10	1.2342(12)	0.1532(6)	0.9436(9)	0.027(3)
C29	1.0439(12)	0.1621(7)	0.5553(9)	0.034(4)
C31	1.0454(12)	0.0762(7)	0.6528(10)	0.037(4)

Table 28 (continued...)

C7	0.6972(14)	0.3916(9)	0.7847(11)	0.045(4)
C17	1.1399(13)	0.3507(7)	0.8196(10)	0.036(4)
C28	1.1363(13)	0.1872(7)	0.6180(9)	0.033(3)
C24	1.6128(12)	0.1697(7)	0.5750(10)	0.035(4)
C18	1.2393(12)	0.3838(6)	0.8601(9)	0.031(3)
C3	0.8364(12)	0.0487(7)	0.8852(11)	0.037(4)
C1	0.8302(12)	0.1537(6)	0.9033(10)	0.034(4)
C16	1.1570(12)	0.2928(7)	0.7961(9)	0.034(4)
C4	0.8620(12)	0.0443(7)	0.9858(10)	0.037(4)
C2	0.8215(12)	0.1050(7)	0.8443(9)	0.033(4)
C6	0.8584(13)	0.1486(7)	1.0017(10)	0.037(4)
C8	0.6785(15)	0.4543(8)	0.7996(13)	0.058(5)
H3	0.6156	0.4641	0.8391	0.069
H2	0.6655	0.4711	0.7337	0.069
H1	0.7626	0.4695	0.8224	0.069
B1	1.3014(14)	0.1927(7)	0.7748(10)	0.027(4)
C13	1.4608(12)	0.1100(6)	1.0092(9)	0.033(4)

VI.1.6 $[C_6F_5Xe][B(CN)_4]$ **Figure 48** Crystal structure of $[C_6F_5Xe][B(CN)_4]$. Thermal ellipsoids are shown at the 50% probability level.

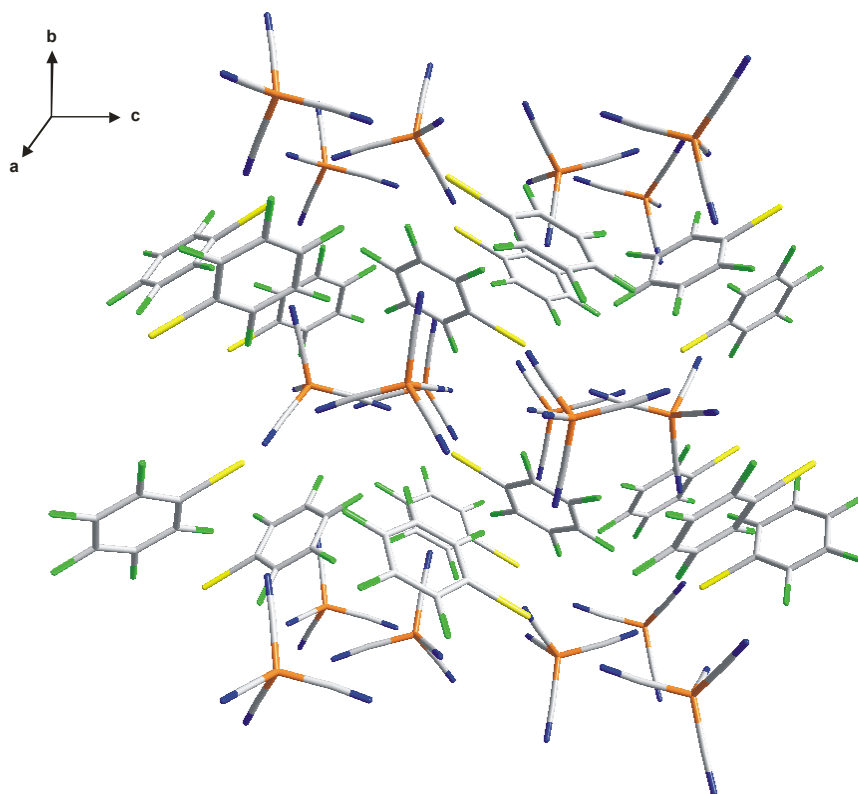


Figure 49 Crystal packing of [C₆F₅Xe][B(CN)₄] along the a-axis.

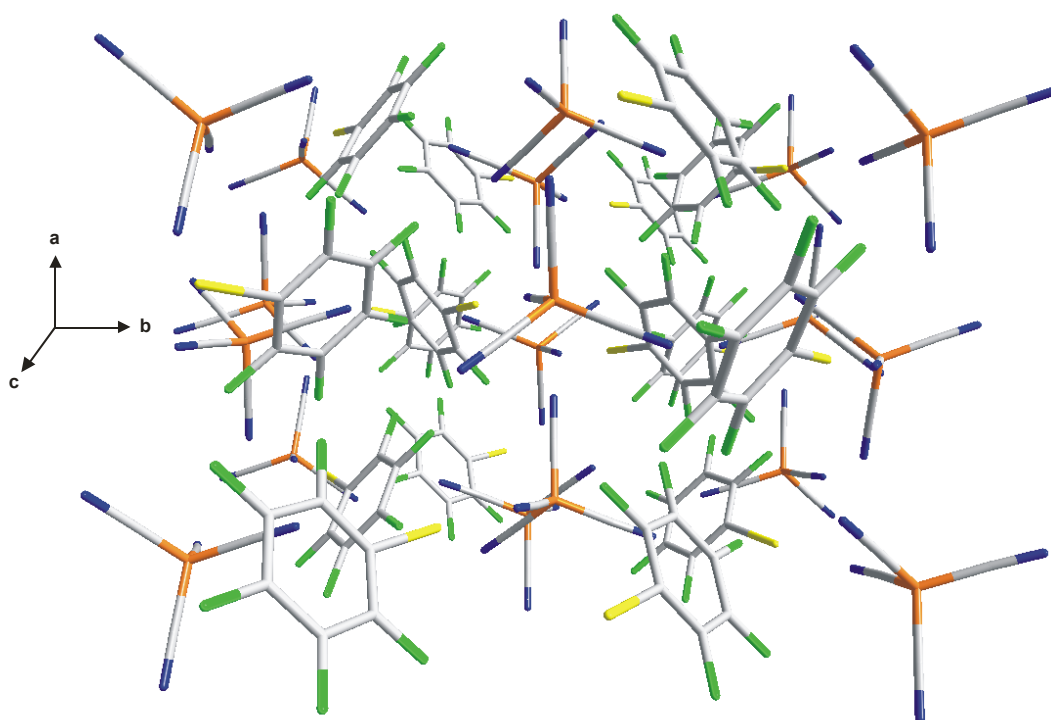


Figure 50 Crystal packing of [C₆F₅Xe][B(CN)₄] along the c-axis.

Table 29 Anisotropic Displacement Parameters [\AA^2]

	U_{11}	U_{22}	U_{33}	U_{23}	U_{13}	U_{12}
Xe	0.02058(10)	0.01689(9)	0.01546(9)	0.00018(10)	0.00061(11)	-0.00123(11)
F5	0.0225(10)	0.0283(11)	0.0250(9)	-0.0025(11)	-0.0002(10)	0.0057(9)
F3	0.0657(16)	0.0291(12)	0.0207(11)	-0.0111(10)	-0.0015(10)	0.0030(12)
C6	0.0238(19)	0.0145(15)	0.0215(16)	0.0008(12)	0.0068(16)	-0.0007(17)
F4	0.0356(13)	0.0392(14)	0.0254(11)	-0.0039(9)	-0.0104(10)	-0.0001(10)
F1	0.0244(12)	0.0300(12)	0.0315(11)	0.0000(9)	-0.0020(9)	0.0066(10)
B	0.021(2)	0.0172(18)	0.0155(16)	-0.0020(13)	-0.0068(19)	0.0012(19)
N3	0.032(2)	0.0270(18)	0.0366(18)	-0.0008(14)	-0.0014(16)	0.0063(16)
N2	0.0263(17)	0.0341(18)	0.0311(16)	-0.0029(16)	0.0042(16)	-0.0032(13)
C1	0.022(2)	0.0123(16)	0.0175(14)	0.0002(11)	0.0027(15)	-0.0020(15)
C4	0.044(3)	0.020(2)	0.0196(16)	-0.0026(14)	0.0002(18)	-0.0040(17)
C10	0.0188(18)	0.0166(16)	0.0241(17)	0.0010(13)	-0.0012(17)	-0.0012(17)
C5	0.027(2)	0.0225(18)	0.0184(16)	0.0027(13)	-0.0030(16)	-0.0013(16)
C2	0.0232(19)	0.0174(17)	0.0203(18)	0.0061(14)	0.0024(16)	-0.0011(14)
C9	0.0221(17)	0.025(2)	0.0196(16)	0.0018(16)	-0.0012(14)	0.0020(17)
N4	0.0334(19)	0.0278(16)	0.0208(14)	0.0006(12)	-0.0025(15)	-0.0026(16)
C8	0.017(2)	0.026(2)	0.0237(17)	-0.0089(15)	0.0002(15)	0.0065(16)
C7	0.028(2)	0.0127(17)	0.0144(16)	-0.0023(12)	0.0017(15)	-0.0017(15)
N1	0.0240(17)	0.0242(16)	0.0224(16)	-0.0045(12)	-0.0028(13)	0.0003(14)
F2	0.0476(15)	0.0257(11)	0.0370(12)	-0.0046(10)	0.0107(11)	0.0150(11)
C3	0.035(2)	0.0131(18)	0.0251(18)	0.0031(14)	0.0090(17)	0.0022(16)

Table 30 Atomic Coordinates and Equivalent Isotropic Displacement Coefficients (\AA^2).

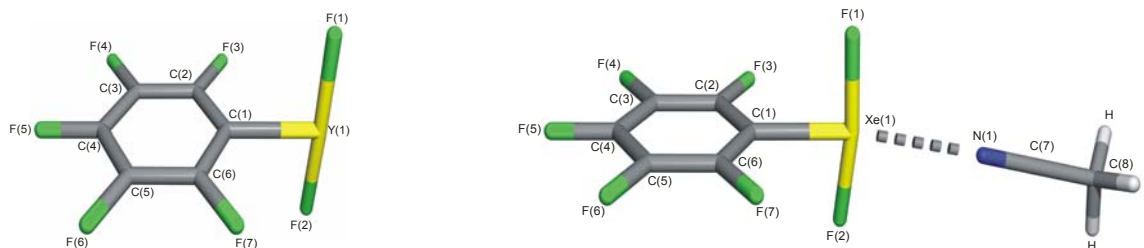
	X	Y	Z	U(eq)
Xe	0.94182(2)	0.112689(12)	0.431750(11)	0.01764(6)
F5	1.15745(18)	0.10503(11)	0.56698(11)	0.0253(4)
F3	0.9952(2)	0.30376(12)	0.74653(12)	0.0385(6)
C6	1.0657(4)	0.16155(19)	0.58772(17)	0.0199(7)
F4	1.1811(2)	0.18877(13)	0.70778(11)	0.0334(5)
F1	0.7555(2)	0.24855(12)	0.51147(11)	0.0286(5)
B	0.9428(4)	-0.0297(2)	0.1420(2)	0.0179(7)

Table 30 (continued...)

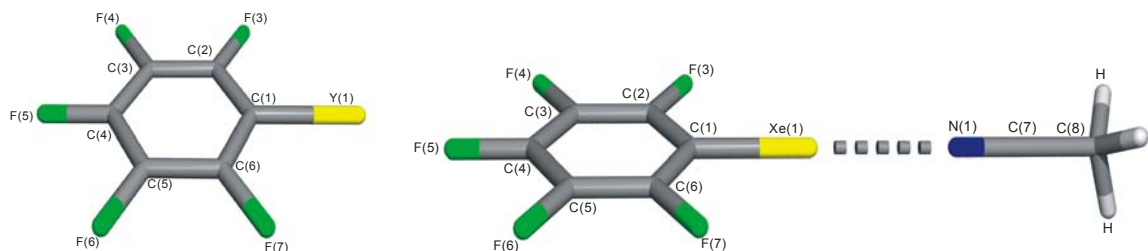
N3	1.0359(3)	-0.18592(19)	0.11579(18)	0.0319(8)
N2	1.1016(3)	0.08636(19)	0.07062(19)	0.0305(7)
C1	0.9593(3)	0.17854(19)	0.53763(18)	0.0173(7)
C4	0.9810(4)	0.2609(2)	0.6788(2)	0.0276(9)
C10	0.9363(4)	-0.00552(19)	0.23491(18)	0.0198(7)
C5	1.0775(4)	0.2035(2)	0.65875(18)	0.0228(8)
C2	0.8616(3)	0.23458(19)	0.55838(19)	0.0203(7)
C9	0.9994(3)	-0.1209(2)	0.12849(19)	0.0221(7)
N4	0.9274(3)	0.01742(17)	0.29912(16)	0.0273(7)
C8	1.0361(4)	0.0369(2)	0.0989(2)	0.0225(8)
C7	0.7926(4)	-0.0246(2)	0.10875(18)	0.0184(7)
N1	0.6847(3)	-0.02161(18)	0.08695(15)	0.0235(7)
F2	0.7807(2)	0.33228(13)	0.65048(12)	0.0368(6)
C3	0.8723(4)	0.2759(2)	0.6297(2)	0.0243(8)

VI.2 Extended Calculated Natural Atomic Charges

Table 31 Calculated Natural Atomic Charges, for $[\text{C}_6\text{F}_5\text{XeF}_2]^+$, $[\text{C}_6\text{F}_5\text{XeF}_2\cdot\text{NCCH}_3]^+$, $[\text{C}_6\text{F}_5\text{XeF}_2\cdot(\text{NCCH}_3)_2]^+$, and $\text{C}_6\text{F}_5\text{IF}_2$



Atoms	$[\text{C}_6\text{F}_5\text{XeF}_2]^+$	$[\text{C}_6\text{F}_5\text{XeF}_2\cdot\text{NCCH}_3]^+$	$[\text{C}_6\text{F}_5\text{XeF}_2\cdot(\text{NCCH}_3)_2]^+$	$\text{C}_6\text{F}_5\text{IF}_2$
I(1)/Xe(1)	1.22	1.18	1.54	0.78
F(1)	-0.33	-0.35	-0.48	-0.44
F(2)	-0.33	-0.35	-0.48	-0.44
C(1)	-0.36	-0.33	-0.28	-0.33
F(3)	-0.04	-0.06	-0.16	-0.08
C(2)	0.26	0.14	0.36	0.08
F(4)	-0.02	-0.04	-0.15	-0.08
C(3)	0.15	0.11	0.21	0.12
F(5)	-0.01	-0.02	-0.13	-0.07
C(4)	0.12	0.14	0.22	0.24
F(6)	-0.02	-0.04	-0.15	-0.08
C(5)	0.15	0.14	0.21	0.12
F(7)	-0.04	-0.05	-0.16	-0.08
C(6)	0.26	0.14	0.36	0.24
N(1)		-0.18 x 2	-0.18	
C(7)		0.01 x 2	0.01	
C(8)		-0.23 x 2	-0.23	
H x 3		0.14 x 2	0.14	

Table 32 Calculated Natural Atomic Charges, Mayer Bond Orders, and Mayer Natural Atomic Orbital Valencies for $[\text{C}_6\text{F}_5\text{Xe}]^+$ and $[\text{C}_6\text{F}_5\text{Xe}\cdot\text{NCCH}_3]^+$ 

		$[\text{C}_6\text{F}_5\text{Xe}]^+$	$[\text{C}_6\text{F}_5\text{Xe}\cdot\text{NCCH}_3]^+$	NCCH_3
charge	Xe(1)	0.90	0.94	
	C(1)	-0.25	-0.31	
	F(3)	-0.24	-0.26	
	C(2)	0.29	0.30	
	F(4)	-0.22	-0.23	
	C(3)	0.30	0.29	
	F(5)	-0.22	-0.23	
	C(4)	0.32	0.31	
	F(6)	-0.22	-0.23	
	C(5)	0.30	0.29	
	F(7)	-0.24	-0.26	
	C(6)	0.29	0.30	
	N(1)		-0.46	-0.31
	C(7)		0.45	0.27
	C(8)		-0.80	-0.79
	H(1-3)			0.28 x 3
	valency	Xe(1)	0.71	0.78
C(1)		3.10	3.05	
F(3)		0.83	0.81	
C(2)		3.13	3.13	
F(4)		0.74	0.73	
C(3)		3.02	3.02	
F(5)		0.74	0.73	
C(4)		3.03	3.03	
F(6)		0.74	0.73	
C(5)		3.02	3.02	
F(7)		0.83	0.81	
C(6)		3.13	3.13	
N(1)			2.04	1.96
C(7)			3.01	3.01
C(8)			3.32	3.30
H(1-3)			0.79 x 3	0.79 x 3
bond order		Xe(1)–C(1)	0.72	0.68
	C(1)–C(2)	1.15	1.16	
	C(2)–F(3)	0.85	0.84	
	C(2)–C(3)	1.11	1.12	
	C(3)–F(4)	0.77	0.76	
	C(3)–C(4)	1.11	1.11	
	C(4)–F(5)	0.77	0.76	
	C(4)–C(5)	1.11	1.11	
	C(5)–F(6)	0.77	0.76	
	C(5)–C(6)	1.11	1.12	
	C(6)–F(7)	0.85	0.84	
	C(6)–C(1)	1.15	1.16	
	Xe(1)–N(1)		0.11	
	N(1)–C(7)		1.91	1.95
	C(7)–C(8)		1.04	1.01

VI.3 Raman Spectra of Selected Materials

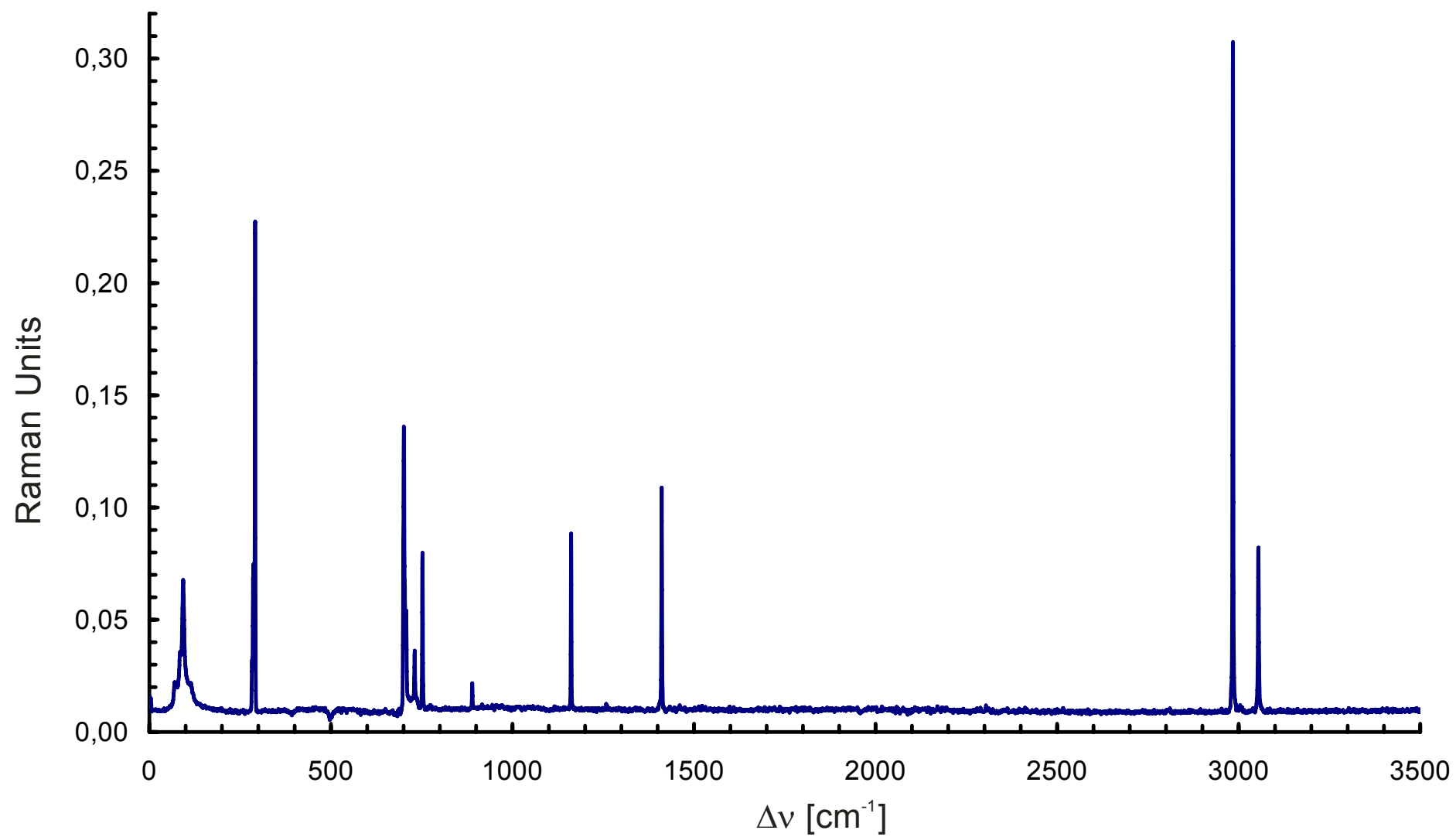


Figure 51 Raman spectrum of solid CH_2Cl_2 at $-150\text{ }^\circ\text{C}$

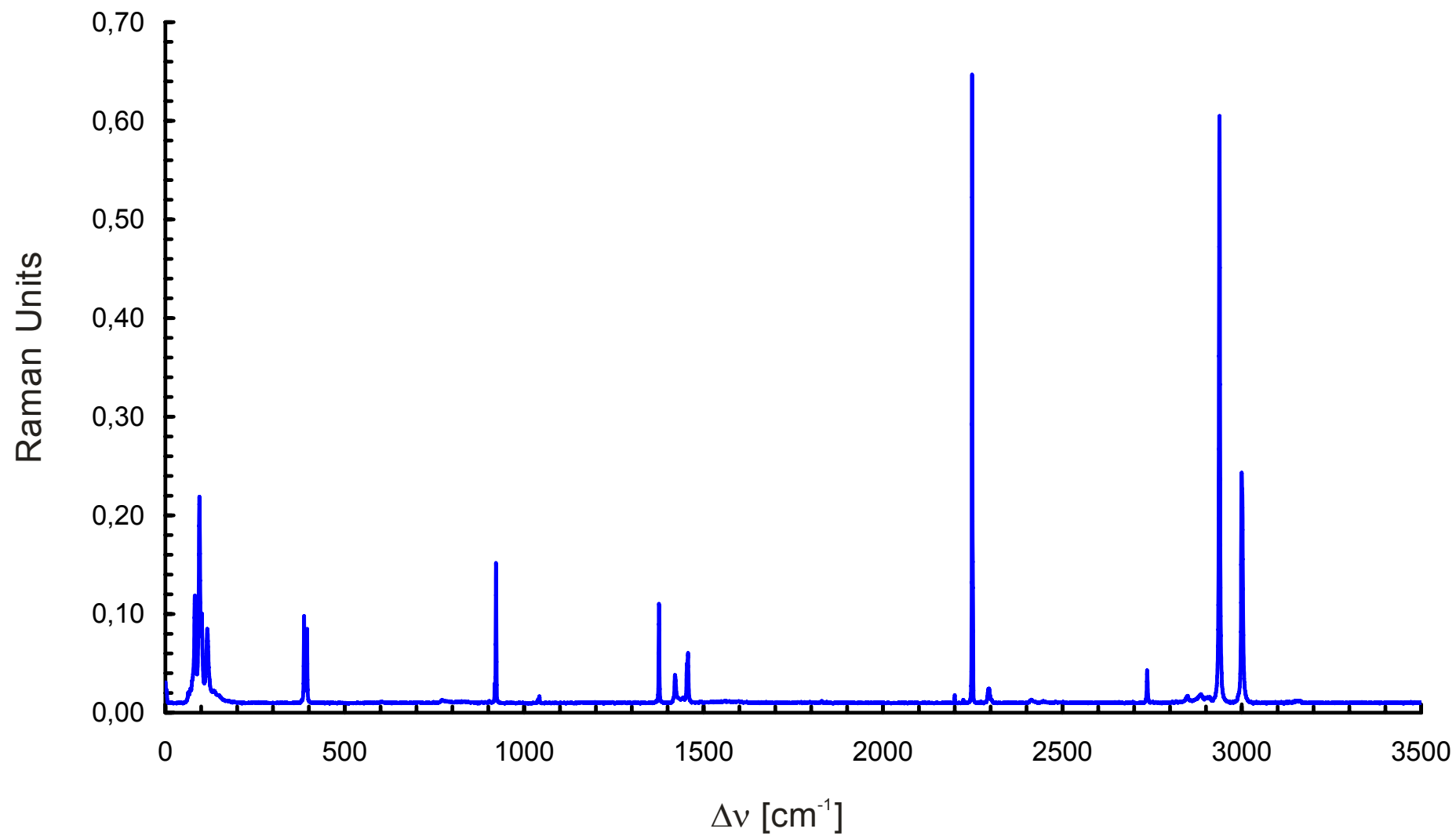


Figure 52 Raman spectrum of solid CH_3CN at $-150\text{ }^\circ\text{C}$

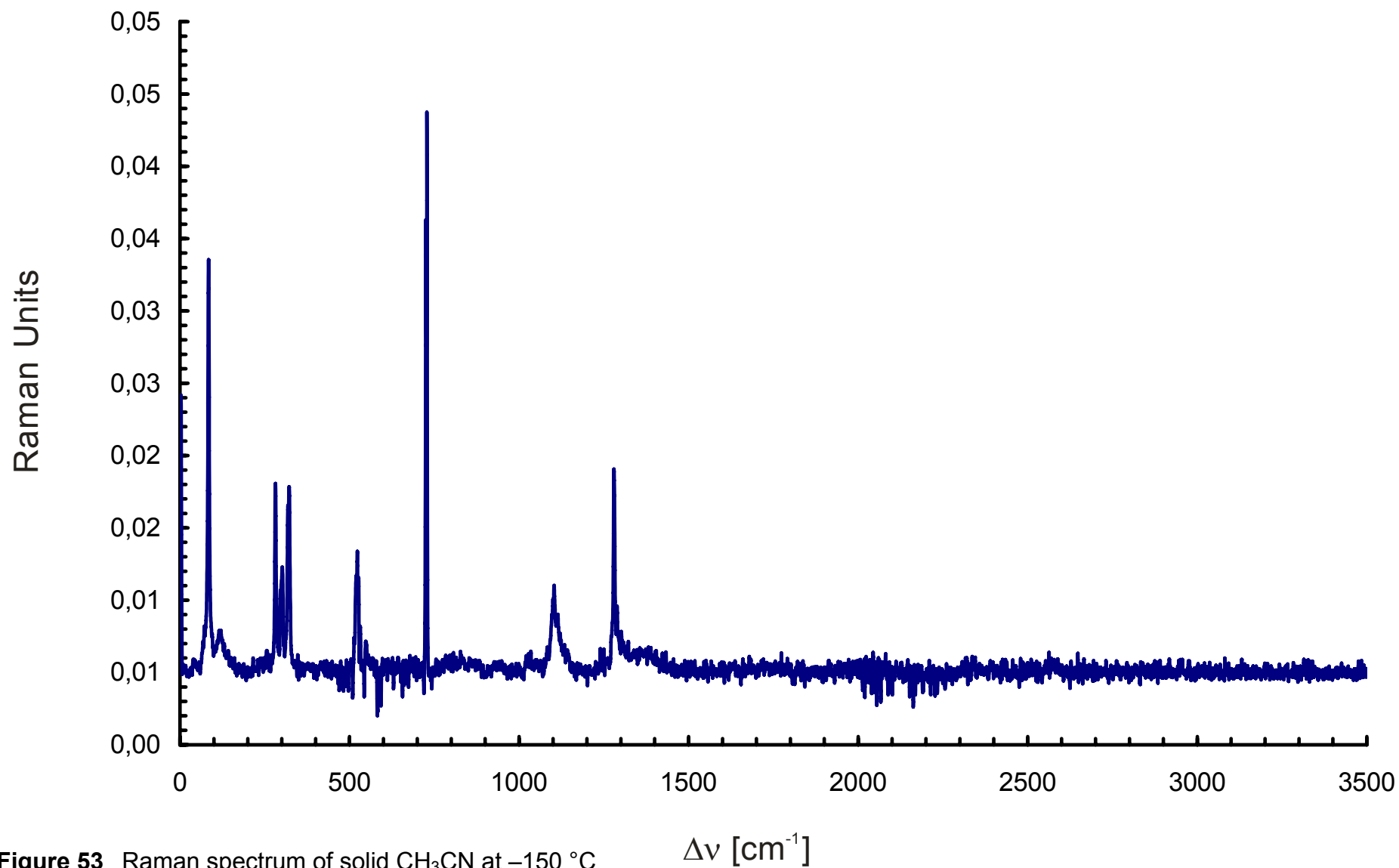


Figure 53 Raman spectrum of solid CH_3CN at $-150\text{ }^\circ\text{C}$

Curriculum Vitae

Name	Karsten Koppe
Adresse	Von-Schwind-Str. 8 45768 Marl
e-Mail	karstenkoppe@gmx.de
Geboren	05.12.1974 in Marl
Familienstand	verheiratet
Staatsangehörigkeit	Deutsch



Schulischer Werdegang

1985 – 1991	Ernst - Immel - Realschule der Stadt Marl Abschluss: Sekundarstufe II mit Qualifikation
1991 – 1994	Hans - Böckler - Kollegschule der Stadt Marl Abschluss: Chemisch-technischer Assistent Fachhochschulreife mit der Gesamtnote 2,2 (gut)
1996 – 2001	Diplom II (Chemie) Gerhard-Mercator Universität Thema: Die regiospezifische Fluorierung bei β -Dicarbonyl-verbindungen und verwandten α -CH-aciden Verbindungen mit Pentafluorphenyliod(III)difluorid unter der Leitung von Prof. Dr. Dr.(h.c.) Hermann-Josef Frohn Abschluss: Diplom Chemiker mit der Gesamtnote 1,4 (sehr gut)
1999 – 2000	Auslandsstudium McMaster University (Ontario, Kanada) Thema: Synthesis and Characterization of Xe(II)-N Bonded Compounds by X-Ray Crystallography and Raman Spectroscopy unter der Leitung von Prof. Dr. Gary J. Schrobilgen
2002 – 2005	Promotion an der Universität Duisburg-Essen und McMaster Universität in Kanada. Thema: Synthesis, Reactivity, Structural and Computational Studies of $[\text{C}_6\text{F}_5\text{Xe}]^+$ and $[\text{C}_6\text{F}_5\text{XeF}_2]^+$ Salts unter der Leitung von Prof. Dr. Dr.(h.c.) Hermann-Josef Frohn und Prof. Dr. Gary J. Schrobilgen Abschluss: Dr. rer. nat. 19. Oktober 2005

Zivildienst

1995 – 1996	Städtische Kinderklinik Gelsenkirchen Betreuung hypersensibler und hyperaktiver Kinder
-------------	--

Berufliche Erfahrungen

06.1991 – 06.1994

Hans - Böckler - Kollegschule

Abschluss: Chemisch-technischer Assistent

06.1994 – 08.1994

10.1994 – 12.1994

02.1996 – 05.1996

07.1996 – 08.1996

03.1997 – 04.1997

03.1998 – 04.1998

02.1999 – 03.1999

Gelsenwasser AG

Abteilung: Informatik und Rechnungsprüfung

Abteilung: Zentrallabor Chemie (Leitung: Dr. Claus Schlett)

04.1999 – 07.1999

01.2000 – 03.2000

Studentische Hilfskraft in der Elektrochemie

(Forschungsbereich optoelektronische Materialien und spektroelektrochemische Methoden) unter Leitung von Prof. Dr. Josef Salbeck.

07.1999 – 01.2000

06.2001 – 12.2001

01.2002 – 03.2002

Studentische Hilfskraft in der Anorganischen Chemie

Leitung: Prof. Dr. Helge Willner.

03.2002 – 12.2005

Wissenschaftlicher Angestellter in der Anorganischen Chemie

Leitung: Prof. Dr. Dr.(h.c.) Hermann-Josef Frohn.

02.2005 –

Wissenschaftlicher Angestellter in Kooperation mit der Firma Merck KGaA

Bereich: Forschung und Applikation auf dem Themengebiet Ionische Flüssigkeiten unter Leitung von Prof. Dr. Dr.(h.c.) Hermann-Josef Frohn und Prof. Dr. Nicolay Ignat'ev

End